LIPIDS, LIPID-RELATED BIOMOLECULES AND LIPID-PROTEIN INTERACTIONS INVOLVEMENT IN PHOTOSYNTHESIS

EDITED BY: Yoshitaka Nishiyama and Przemysław Malec

PUBLISHED IN: Frontiers in Plant Science

frontiers Research Topics

frontiers

Frontiers eBook Copyright Statement

The copyright in the text of individual articles in this eBook is the property of their respective authors or their respective institutions or funders. The copyright in graphics and images within each article may be subject to copyright of other parties. In both cases this is subject to a license granted to Frontiers.

The compilation of articles constituting this eBook is the property of Frontiers.

Each article within this eBook, and the eBook itself, are published under the most recent version of the Creative Commons CC-BY licence. The version current at the date of publication of this eBook is CC-BY 4.0. If the CC-BY licence is updated, the licence granted by Frontiers is automatically updated to the new version.

When exercising any right under the CC-BY licence, Frontiers must be attributed as the original publisher of the article or eBook, as applicable.

Authors have the responsibility of ensuring that any graphics or other materials which are the property of others may be included in the CC-BY licence, but this should be checked before relying on the CC-BY licence to reproduce those materials. Any copyright notices relating to those materials must be complied with.

Copyright and source acknowledgement notices may not be removed and must be displayed in any copy, derivative work or partial copy which includes the elements in question.

All copyright, and all rights therein, are protected by national and international copyright laws. The above represents a summary only. For further information please read Frontiers' Conditions for Website Use and Copyright Statement, and the applicable CC-BY licence.

ISSN 1664-8714
ISBN 978-2-88971-246-5
DOI 10.3389/978-2-88971-246-5

About Frontiers

Frontiers is more than just an open-access publisher of scholarly articles: it is a pioneering approach to the world of academia, radically improving the way scholarly research is managed. The grand vision of Frontiers is a world where all people have an equal opportunity to seek, share and generate knowledge. Frontiers provides immediate and permanent online open access to all its publications, but this alone is not enough to realize our grand goals.

Frontiers Journal Series

The Frontiers Journal Series is a multi-tier and interdisciplinary set of open-access, online journals, promising a paradigm shift from the current review, selection and dissemination processes in academic publishing. All Frontiers journals are driven by researchers for researchers; therefore, they constitute a service to the scholarly community. At the same time, the Frontiers Journal Series operates on a revolutionary invention, the tiered publishing system, initially addressing specific communities of scholars, and gradually climbing up to broader public understanding, thus serving the interests of the lay society, too.

Dedication to Quality

Each Frontiers article is a landmark of the highest quality, thanks to genuinely collaborative interactions between authors and review editors, who include some of the world's best academicians. Research must be certified by peers before entering a stream of knowledge that may eventually reach the public - and shape society; therefore, Frontiers only applies the most rigorous and unbiased reviews.
Frontiers revolutionizes research publishing by freely delivering the most outstanding research, evaluated with no bias from both the academic and social point of view. By applying the most advanced information technologies, Frontiers is catapulting scholarly publishing into a new generation.

What are Frontiers Research Topics?

Frontiers Research Topics are very popular trademarks of the Frontiers Journals Series: they are collections of at least ten articles, all centered on a particular subject. With their unique mix of varied contributions from Original Research to Review Articles, Frontiers Research Topics unify the most influential researchers, the latest key findings and historical advances in a hot research area! Find out more on how to host your own Frontiers Research Topic or contribute to one as an author by contacting the Frontiers Editorial Office: frontiersin.org/about/contact

LIPIDS, LIPID-RELATED BIOMOLECULES AND LIPID-PROTEIN INTERACTIONS INVOLVEMENT IN PHOTOSYNTHESIS

Topic Editors:
Yoshitaka Nishiyama, Saitama University, Japan
Przemysław Malec, Jagiellonian University, Poland

Citation: Nishiyama, Y., Malec, P., eds. (2021). Lipids, Lipid-Related Biomolecules and Lipid-Protein Interactions Involvement in Photosynthesis. Lausanne: Frontiers Media SA. doi: 10.3389/978-2-88971-246-5

Table of Contents

frontiers in Plant Science

ORIGINAL RESEARCH
published: 25 March 2020
doi: 10.3389/fpls.2020.00337

Mutation of the Atypical Kinase ABC1K3 Partially Rescues the PROTON GRADIENT REGULATION 6 Phenotype in *Arabidopsis thaliana*

Thibaut Pralon[1], Joy Collombat[1], Rosa Pipitone[1], Brigitte Ksas[2], Venkatasalam Shanmugabalaji[1], Michel Havaux[2], Giovanni Finazzi[3], Paolo Longoni[1] and Felix Kessler[1]**

[1] Laboratory of Plant Physiology, Institute Biology, University of Neuchâtel, Neuchâtel, Switzerland, [2] Aix Marseille University, Centre National de la Recherche Scientifique (CNRS), Commissariat à l'Énergie Atomique et aux Énergies Alternatives (CEA), UMR 7265, Biosciences et Biotechnologies Institute of Aix-Marseille, Saint-Paul-lez-Durance, France, [3] Université Grenoble Alpes, Centre National de la Recherche Scientifique (CNRS), Commissariat à l'Énergie Atomique et aux Énergies Alternatives (CEA), Institut National de la Recherche Agromique (INRA), Interdisciplinary Research Institute of Grenoble - Cell and Plant Physiology Laboratory (IRIG-LPCV), Grenoble, France

OPEN ACCESS

Edited by:
Przemysław Malec, Jagiellonian University, Poland

Reviewed by:
Claire Remacle, University of Liège, Belgium
Peter J. Gollan, University of Turku, Finland

***Correspondence:**
Paolo Longoni
paolo.longoni@unine.ch
Felix Kessler
felix.kessler@unine.ch

Specialty section:
This article was submitted to Plant Physiology, a section of the journal Frontiers in Plant Science

Received: *27 November 2019*
Accepted: *06 March 2020*
Published: *25 March 2020*

Citation:
Pralon T, Collombat J, Pipitone R, Ksas B, Shanmugabalaji V, Havaux M, Finazzi G, Longoni P and Kessler F (2020) Mutation of the Atypical Kinase ABC1K3 Partially Rescues the PROTON GRADIENT REGULATION 6 Phenotype in Arabidopsis thaliana. Front. Plant Sci. 11:337. doi: 10.3389/fpls.2020.00337

Photosynthesis is an essential pathway providing the chemical energy and reducing equivalents that sustain higher plant metabolism. It relies on sunlight, which is an inconstant source of energy that fluctuates in both intensity and spectrum. The fine and rapid tuning of the photosynthetic apparatus is essential to cope with changing light conditions and increase plant fitness. Recently PROTON GRADIENT REGULATION 6 (PGR6-ABC1K1), an atypical plastoglobule-associated kinase, was shown to regulate a new mechanism of light response by controlling the homeostasis of photoactive plastoquinone (PQ). PQ is a crucial electron carrier existing as a free neutral lipid in the photosynthetic thylakoid membrane. Perturbed homeostasis of PQ impairs photosynthesis and plant acclimation to high light. Here we show that a homologous kinase, ABC1K3, which like PGR6-ABC1K1 is associated with plastoglobules, also contributes to the homeostasis of the photoactive PQ pool. Contrary to PGR6-ABC1K1, ABC1K3 disfavors PQ availability for photosynthetic electron transport. In fact, in the *abc1k1/abc1k3* double mutant the *pgr6*(*abc1k1*) the photosynthetic defect seen in the *abc1k1* mutant is mitigated. However, the PQ concentration in the photoactive pool of the double mutant is comparable to that of *abc1k1* mutant. An increase of the PQ mobility, inferred from the kinetics of its oxidation in dark, contributes to the mitigation of the *pgr6*(*abc1k1*) photosynthetic defect. Our results also demonstrate that ABC1K3 contributes to the regulation of other mechanisms involved in the adaptation of the photosynthetic apparatus to changes in light quality and intensity such as the induction of thermal dissipation and state transitions. Overall, we suggests that, besides the absolute concentration of PQ, its mobility and exchange between storage and active pools are critical for light acclimation in plants.

Keywords: photosynthetic electron transport, plastoquinone pool, plastoglobule, high light acclimation, NPQ

INTRODUCTION

The photosynthetic conversion of light energy into chemical energy occurs via a series of redox reactions resulting in electron transport along the thylakoid membrane. The linear electron transport begins with water splitting at the level of photosystem II (PSII) and ends at photosystem I (PSI) with the reduction of $NADP^+$ by ferredoxin. Both PSII and PSI utilize photonic energy to fuel the redox reactions. Electrons are transferred from PSII to PSI via the cytochrome *b6f* complex (cyt *b6f*). At the Q_B site of PSII, a molecule of plastoquinone (PQ) is reduced twice and protonated to form plastoquinol (PQH_2). The PQH_2 can then diffuse within the thylakoid membrane to reach the Q_O site of cyt *b6f*. Oxidation of PQH_2 at cyt *b6f* occurs through the Q-cycle that releases protons into the thylakoid lumen contributing to the formation of the trans-thylakoid proton gradient. In addition, two electrons are released, one of which returns to PQ pool, while the other is transferred via the plastocyanin to PSI (Tikhonov, 2014). The proportion of PQ that participates in electron transport in the thylakoid membrane is considered as the photoactive PQ pool; whereas the remaining proportion, which is approximately 60–70% of the total PQ, constitutes the non-photoactive pool and is largely stored inside thylakoid-associated lipid droplets known as plastoglobules (PG) (Kruk and Karpinski, 2006; Block et al., 2013; Ksas et al., 2018).

To shuttle electrons, PQ has to rapidly navigate in the thylakoid lipid bilayer (Blackwell et al., 1994). However, the thylakoid membrane is crowded with integral proteins, covering up to 70% of the surface in the grana stacks, which drastically restrict PQ diffusion, especially at the long-range (Kirchhoff et al., 2000). Thylakoid membranes are close to the percolation threshold, therefore it has been suggested that the organization of the protein supercomplexes creates lipid microdomains that facilitate PQ mobility and thus electron shuttling between PSII and cyt *b6f* (Lavergne and Joliot, 1991; Kirchhoff et al., 2000; Kirchhoff, 2014). On the other hand, long-range mobility of the PQ is also important, for instance to mobilize the non-photoactive pool when damaged PQ molecules have to be replaced as it was proposed to occur during high light stress (Ksas et al., 2018). Therefore, the mobility of plastoquinone/ol molecules within the thylakoid lipid bilayer is a critical parameter to ensure electron transport and maintain the photosynthetic electron transport chain (ETC).

Apart from the role of PQ as electron carrier, its redox state is an important signal in the regulation of many physiological processes within the chloroplast such as state transitions (as described below), gene expression, carotenoid biosynthesis, and antioxidant activity (Karpinski et al., 1999; Li et al., 2009; Suzuki et al., 2012). A rapid readout of the PQ redox state allows photosynthetic adaptation to changes in environmental conditions and therefore increases plant fitness in the natural environment. The adaptation to such varying light conditions is essential for plants to maintain the highest photosynthetic efficiency while avoiding photo-induced damage. To alleviate the negative effects of an imbalance between the activity of the two photosystems, plants have developed a short-term adaptive mechanism: the state transitions. This process allows the re-equilibration of the light energy input between the two photosystems on a time scale of a few minutes by re-allocating part of the mobile light-harvesting complexes II (LHCII) (Allen et al., 1981; Rochaix, 2007, 2013). Phosphorylation of LHCII by the STN7 kinase, the activity of which is dependent on the PQ redox state, allows its movement from PSII to PSI (state 2) (Bellafiore et al., 2005; Shapiguzov et al., 2016; Dumas et al., 2017). The process is reverted by the dephosphorylation of LHCII, operated by the PPH1/TAP38 phosphatase (state 1) (Pesaresi et al., 2010, 2011; Shapiguzov et al., 2010; Trotta et al., 2016). To prevent harmful effects of excess light, plants can dissipate the energy excess as heat by a set of regulated mechanisms summarily referred to as non-photochemical quenching (NPQ). These mechanisms include the rapid rearrangement to a "quenched" state of the LHCII antenna dependent on the PSBS protein and the conversion of the xanthophylls associated to LHCII from violaxanthin to zeaxanthin. The sum of all components creates a system with differential kinetics activated within a few seconds to hours (Dall'Osto et al., 2005; Joliot and Finazzi, 2010; Nilkens et al., 2010; Sylak-Glassman et al., 2014; Ruban, 2016, 2018). Nonetheless, upon continuous light stress, ROS can be produced at the PSII reaction center leading to loss of the PSII activity by damaging the core protein D1 (PsbA). Loss of PSII activity, known as photoinhibition (qI), contributes to the dissipation of excess light (Gong and Ohad, 1991; Miyao, 1994; Vasilikiotis and Melis, 1994). To restore PSII activity after inhibition there is an efficient repair cycle (Aro et al., 1993; Rintamaki et al., 1996, 1997; Theis and Schroda, 2016). The replacement of damaged D1 (PsbA) is facilitated by the phosphorylation of the core proteins of the PSII reaction center by STN8 kinase and requires PSII to migrate from the grana to the stroma lamellae (Aro et al., 1993; Bonardi et al., 2005; Tikkanen et al., 2008; Theis and Schroda, 2016; Li et al., 2018). Photo oxidative stress also triggers other responses allowing the chloroplast to alleviate the damage. These responses involve regulation of gene expression (Pfannschmidt et al., 1999; Pfannschmidt, 2003), structural changes of the thylakoids (Moejes et al., 2017) and synthesis of antioxidant molecules (Munné-Bosch and Alegre, 2002; Kanwischer et al., 2005; Gruszka et al., 2008; Nowicka and Kruk, 2012; Block et al., 2013; Martinis et al., 2014; Ksas et al., 2015, 2018; Spicher et al., 2016; Ferretti et al., 2018).

An important player in the plant stress response is the plastoglobule (PG). PGs are small lipid droplets, attached to the outer lipid leaflet of the thylakoid membrane, delimited by a membrane lipid monolayer consisting mostly of galactolipids and coated with proteins (Austin et al., 2006). Several neutral lipids including prenylquinones, carotenoids, triacylglycerols, phytolesters fill the plastoglobule (Lichtenthaler and Peveling, 1966; Steinmuller and Tevini, 1985; Gaude et al., 2007; Zbierzak et al., 2010; Lippold et al., 2012; Lundquist et al., 2013; Rottet et al., 2016; van Wijk and Kessler, 2017). In response to various stresses PGs increase in size and number (Taylor and Craig, 1971; Hall et al., 1972; Gaude et al., 2007; Martinis et al., 2014; Zechmann, 2019). Physical connections between PG and the thylakoid membranes suggest bidirectional lipid

trafficking between these two compartments (Austin et al., 2006). Besides being a lipid storage site, the PG proteome revealed the presence of specific proteins, several of which are involved in prenylquinone metabolism (Vidi et al., 2006; Ytterberg et al., 2006; Lundquist et al., 2012).

After fibrillins (Lundquist et al., 2012), the second most abundant protein family in PG is composed of homologs of the ABC1 (Activity of BC1 complex) atypical kinases (Lundquist et al., 2012). The ABC1 domain has been conserved through evolution, suggesting that it has a crucial role (Lohscheider and Rio Bartulos, 2016). In microorganisms as well as in human cells, ABC1 proteins were shown to be essential in ubiquinone synthesis and in mitochondrial electron transport (Bousquet et al., 1991; Brasseur et al., 1997; Poon et al., 2000; Mollet et al., 2008). Six members of the ABC1-like kinase family are found in the PG proteome. A member of this family, ABC1K1 (At4g31390), was identified as *PGR6* in a genetic screen to identify mutants affected in proton gradient formation (PGR) (Shikanai et al., 1999). PGR mutants are characterized by high chlorophyll fluorescence and reduced NPQ under different light conditions (from 50 to 500 μmol of photons m^{-2} s^{-1}) (Shikanai et al., 1999; Martinis et al., 2014; Yamori and Shikanai, 2016). In the *abc1k1* mutant, the electron transport rate as well as NPQ are constitutively limited in a light fluency dependent manner when compared to the wild type. Under prolonged exposure to high light, *abc1k1* adult plants exhibited almost complete photoinhibition during the early days of treatment and after several days PSII maximum efficiency recovered despite the plants still being still exposed to high light (Martinis et al., 2014). Nonetheless, the metabolic profile of *abc1k1* was profoundly altered. In particular, plants displayed a decrease in tocopherol accumulation and a shift from starch production to soluble sugars (Martinis et al., 2014).

ABC1K1 was identified as BDR1 (Bleached dwarf under red light) (Huang et al., 2015; Yang et al., 2016). During early seedling development under continuous red light, the mutant is severely stunted and has white cotyledons. Since the bleaching phenotype was accompanied by a specific diminishment of the photosystem D1 (PsbA) protein but not that of other photosynthetic proteins tested [D2 (PsbD); PsbC; PsbB] the pale phenotype was attributed to photobleaching (Huang et al., 2015; Yang et al., 2016). A repressor of the *bdr1* mutation, RBD1 (repressor of *bdr1*) was also identified as the ABC1K1 homolog ABC1K3. As the *abc1k3* mutation repressed the *bdr1*(*abc1k1*) phenotype, it led to the hypothesis that the two homologs have opposing functions (Huang et al., 2015). Furthermore, *abc1k3* adult plants are not severely affected by prolonged high light and they showed a decreased plastochromanol accumulation (Martinis et al., 2013). However, previous investigations on adult plants reported that the double *abc1k1/abc1k3* mutation results in an additive, senescence-like phenotype characterized by conditional degreening, including the loss of chlorophyll and photosystem proteins, and recruitment of the jasmonate pathway to PG under prolonged high light treatment (Lundquist et al., 2013). Furthermore, ABC1K1 and ABC1K3 may interact and form a complex that may be involved in the stabilization of plastoglobule proteins (Lundquist et al., 2013; Martinis et al., 2013).

Recently, a molecular mechanism explaining the *pgr6*(*abc1k1*) defect was proposed: ABC1K1 would be required for the homeostasis of photoactive PQ. Indeed, upon high light, the photoactive PQ pool in *abc1k1* mutant becomes limiting and this can explain the diminished linear electron transport and NPQ, the dephosphorylation of the LHCII antenna and perturbation of the state transitions; all these leading to an overall decrease in the photosynthetic efficiency (Pralon et al., 2019).

In this study, we investigated the impact of the *abc1k3* mutation in the *pgr6(abc1k1)* mutant background. In particular we focused on the capacity of a double mutant, lacking both *ABC1K1* and *ABC1K3*, to acclimate to a short high light treatment (3 h, 500 $\mu mol \cdot m^{-2} \cdot s^{-1}$). We found that the *abc1k3* mutant has no photosynthetic defect compared to the wild type under the tested conditions. However, by stacking this mutation with *abc1k1* we observe a partial alleviation of all the photosynthetic defects previously reported in *abc1k1* (Shikanai et al., 1999; Martinis et al., 2014; Pralon et al., 2019). Surprisingly, the phenotype complementation does not originate from an effect on the size of the photoactive PQ pool but rather from an effect on PQ mobility in the thylakoid membrane. This evidence suggests that there is a push-pull relationship of ABC1K1 and ABC1K3 with regard to the mobility of PQ, and that this regulated process is fundamental to ensure the photosynthetic efficiency under high light.

MATERIALS AND METHODS

Plants Material and Treatments

The wild type *Arabidopsis thaliana* refers to var. Columbia-0 (Col-0). *abc1k1.1* (Salk_068628), *abc1k1.2* (Salk_130499C) *abc1k3.1* (Salk_128696), or with *abc1k3.2* (Sail_918_E10) T-DNA insertion lines were purchased at Nottingham Arabidopsis Stock Centre (NASC)[1]. The double mutant lines *abc1k1/akc1k3.1* and *abc1k1/akc1k3.2* were produced by crossing *abc1k1.1* mutant with *abc1k3.1* and *abc1k3.2*, respectively. TDNA insertion was verified by PCR, and primers were listed in **Supplementary Table 1**. The mutant lines *stn7/stn8* (Fristedt et al., 2009) and *sps2* (Block et al., 2013) were kindly provided by the respective research groups. The *ptox* mutant was obtained from NASC, and corresponds to the previously characterized immutans variegation mutant (Wetzel et al., 1994).

Plants were grown in pots on soil pre-treated with solbac (Andermatt) with standard light conditions (120 $\mu mol\ m^{-2}\ s^{-1}$, 8 h light/16 h dark) in a controlled environment room maintaining a daily temperature of 22 ± 1°C. For high light treatment, 4–5 weeks old plants were exposed for 3 h to 500 $\mu mol\ m^{-2}\ s^{-1}$ of white light (FutureLED), always at 22 ± 1°C.

Leaf samples were collected directly under the light in the growth chamber, and immediately snap frozen in liquid nitrogen, and stored at −20°C.

[1]http://arabidopsis.info

Photosynthetic Parameters

Before measuring the photosynthetic performance, the plants were kept in the dark for at least 10 min. The measurements were performed using a Fluorcam (Photon System Instrument, Czech Republic)[2] with a modified light curve protocol. Briefly, after measuring the minimal fluorescence (F_0) and the maximal fluorescence during a saturating pulse (F_M) in dark, the plants were exposed to increasing blue light (470 nm) intensities for 1 min following this scheme: 2.5–95–347–610–876–1145 μmol m^{-2} s^{-1}. At the end of every light period, a saturating flash was used to measure the maximal fluorescence in light (F_M'). The fluorescence recorded before the peak were used as F_S (steady-state chlorophyll fluorescence in the light). Three parameters were calculated from the above values: Maximum quantum yield of photosystem II $\Phi_{MAX} = (F_V/F_M)$; quantum yield of photosystem II $\Phi_{PSII} = (F_M' - F_S)/F_M'$ and Non-Photochemical Quenching $NPQ = (F_M - F_M')/F_M'$. To assess the extent of the "state transitions" the plants were exposed to 10 min red light (50 μmol m^{-2} s^{-1} 660 nm peak measured as PPFD) supplemented with far-red (17 μmol m^{-2} s^{-1} calculated from the 733 nm peak area considering values between 500 and 800 nm) followed by 10 min of the red light only. The maximal fluorescence in the light was measured at the end of both 10 min periods to obtain F_MST1 when far-red was supplemented and "state I" promoted and F_MST2 after 10 min of pure red, which promotes the transition toward "state II." The extent of the quenching related to state transition (qT) was calculated as $qT = (F_M ST1 - F_M ST2)/F_M$.

P_{700} Oxidation

The photooxidation of the photosystem I reaction center (P_{700}) was assessed by the increase in absorption at 810 nm after deconvolution of the plastocyanin absorption as previously described (Joliot and Joliot, 2006). The measurement was performed with a JTS-10 LED spectrometer (BioLogic Science Instruments) in absorbance mode equipped with a Far-red (FAR) LED peaking at 735 nm filtered through three Wratten filters 55 to block the wavelengths shorter than 700 nm, a red LED, peaking at 640 nm, was used for the actinic light. To estimate maximum extent of P_{700}^+ a saturating white light flash was superimposed on the top of the FAR. The measurement of the maximum number of electrons contained in the electron transport chain (ETC) per PSI was performed as follows. The plants were pre-incubated 2 min under a strong white light (500 μmol m^{-2} s^{-1}) to activate CO_2 assimilation in the leaves and thus reduce the contribution of the cyclic electron flow (Joliot and Joliot, 2006), which can only be reactivated after prolonged dark incubation (Joliot and Joliot, 2006; Trouillard et al., 2012). This allows only electrons from the linear ETC, including the photoactive PQ pool, to be available for PSI reduction. Detached leaves were put inside the holder and subjected to 2 min of FAR to oxidize the ETC followed by 2 s of dark allowing the reduction of P_{700}. The kinetic of the subsequent reoxidation induced by FAR were followed with a saturating flash of actinic light (1000 μmol m^{-2} s^{-1} for 100 μs) to fully reduce the ETC or without so that the ETC was fully oxidized. The ratio between the lag times between the FAR onset and the beginning of the P_{700} oxidation in these two conditions is used as a proxy for the number of available electrons per PSI (Pralon et al., 2019).

[2]http://www.psi.cz

Chlorophyll *a* Fluorescence Curve Kinetics (OJIP, JIP-Test)

Plants were dark-adapted for at least 10 min before measurements and then a single leaf detached in dark and put in a clip holder for the Plant Efficiency Analyzer (M-PEA 2; Hansatech Ltd.). The chlorophyll *a* fluorescence induction curve was recorded and the JIP-parameters recovered with M-PEA software Hansatech Ltd. The measurement was automatically repeated after increasing intervals of dark (4, 8, 12, 16, 20, 24 s) and far-red light (0.05, 0.1, 0.2, 0.4, 0.8, 1.6 s). The parameters extracted from the first pulse after the dark incubation were used to assess the steady state of the ETC after moderate light or 3 h of high light (Stirbet et al., 2018). The yield of the electron transport from Q_A to Q_B ($\Phi ET2o$) and the yield of the transport to final PSI acceptors ($\Phi RE1o$) were calculated according to the JIP-Model described in Strasser et al. (2010) and Kalaji et al. (2014a,b). The variable fluorescence at 3 ms ($V_J = F_J/F_M$) value was used as a proxy of the redox state of the photoactive plastoquinone (Tóth et al., 2007). The data points of V_J over time were interpolated with a logarithmic function with RStudio (RStudio, Inc.).

Plastoquinone Analysis

The analysis of the photoactive PQ pool, and of the total pool were performed as previously described (Pralon et al., 2019). Briefly, leaf disks of 0.8 cm of diameter were collected from 5 weeks old plants. The disks were exposed either to 15 s of saturating light (2000 μmol m^{-2} s^{-1}) or to 2 min of far-red light (735 nm, 5.5 μmol m^{-2} s^{-1}). The samples were flash frozen and used for total lipid analysis as described in Kruk and Karpinski (2006) and Ksas et al. (2015, 2018). The photoactive PQ pool was determined from the difference between the reduced PQ after high light (maximal reduction of the photoactive PQ pool) and the amount measured after far-red light (maximal oxidation of the photoactive PQ pool).

Immunoblot Analysis

Fully expanded leaves of adult plants (at least 4 weeks old) were collected under the relevant light condition and flash frozen in liquid nitrogen. The leaves were ground to a fine powder in a 1.5 mL microtube with a micro-pestle. Four hundred mircroliter of lysis buffer [100 mM Tris-HCl pH 8.5, 2% SDS, 10 mM NaF, 0.05% of protease inhibitor cocktail for plant (Sigma)] was add to the powder and the material incubated at 37°C for 30 min, debris were removed by centrifugation (5 min at 16,000 g) at room temperature. The chlorophyll concentration of the sample was determined according to Arnon (1949). Proteins were precipitated in chloroform-methanol and the pellet solubilized directly in the gel loading buffer (50 mM Tris-HCl pH 6.8, 100 mM Dithiothreitol, 2% SDS, 0.1% Bromophenol Blue, 10% Glycerol) to a concentration of 0.5 μg chlorophyll/μL.

Following denaturation at 65°C for 10 min, 4 μL of each sample were loaded into a 12% Acrylamide SDS gel. After separation by electrophoresis the proteins were transferred to a nitrocellulose membrane. The membrane was decorated using the following antibodies: anti-Actin (Sigma, A 0480) at 1/3000 dilution in 5% fat free milk/PBS, anti-Lhcb2 (Agrisera, AS01 003), anti-D1 (PsbA) (Agrisera, AS05 084), anti-PetC (Agrisera, AS08 330); anti-PsaD (Agrisera, AS09 461), anti-PsaC (Agrisera, AS04 042P), anti-AtpC (Agrisera, AS08 312); at 1/5000 dilution in 5% fat free milk/TBS, and anti-Phosphothreonine (Cell Signaling Technology, #9381) at 1/10,000 in 3% BSA/TBS Tween20 0.1%; anti-PTOX (Agrisera, AS16 3692) at 1/2000 in 6% BSA/TBS Tween20 0.05%. Secondary antibodies (anti-rabbit (Merck, AP132P) or anti-mouse (Sigma, A5278) at 1/3000) conjugated with HRP allow the detection of proteins of interest with 1 mL of enhanced chemiluminescence and 3.3 μL of H_2O_2 3% using an imager for chemiluminescence (Amersham Imager 600, Amersham Biosciences, Inc.).

RESULTS

Isolation and Selection of abc1k1/abc1k3 Double Mutants

ABC1K1 and ABC1K3 are two homologous, atypical kinases located at plastoglobules and share 31.6% identity at the level of the global amino acid sequence (**Supplementary Figure 1**). To analyze potential interactions between ABC1K1 and ABC1K3 in the regulation of photosynthesis, two double mutant *abc1k1/abc1k3* lines were produced by crossing *abc1k1.1* (Salk_068628) with *abc1k3.1* (Salk_128696) or with *abc1k3.2* (Sail_918_E10). Double *abc1k1/abc1k3* mutant lines were selected and verified by PCR. The genotyping confirmed the presence of TDNA insertions in both genes (**Figure 1**).

Thermal Dissipation and Electron Transport Capacities Are Partially Recovered in abc1k1/abc1k3

Independent studies indicate that *abc1k1* is impaired in NPQ as well as electron transport (Shikanai et al., 1999; Martinis et al., 2014; Pralon et al., 2019), while the *abc1k3* mutant did not show defects in those parameters even after prolonged high light exposure (Martinis et al., 2013). To further characterize the *abc1k1/abc1k3* double mutant, we measured photosynthetic parameters such as PSII maximum efficiency [φ_{MAX} (= F_V/F_M)], NPQ as well as electron capacity of the ETC in 4–5 weeks old plants grown under moderate light (120 μmol m^{-2} s^{-1}) (ML) and after 3 h of high light (500 μmol m^{-2} s^{-1}).

The maximum quantum yield of the PSII (φ_{MAX}) in wild type (WT), *abc1k1*, *abc1k3,* and *abc1k1/abc1k3* slightly decreased after 3 h of high light but without any significant difference between the lines (**Figure 2A**). Furthermore, after 3 h of high light, there was no major impact on the PSII yield, and this allowed the measurement of the efficiency of the ETC avoiding potential bias caused by PSII photodamage.

Short-term high light treatment affected NPQ induction, which decreased in all the tested genotypes compared to moderate light conditions. Nonetheless, the NPQ in WT and in *abc1k3* was always higher than the one measured in *abc1k1* lines. Intriguingly, both under moderate light and after high light, the double mutants showed greater NPQ compared to *abc1k1* lines but still less than the WT level (**Figure 2B**), suggesting a partial rescue of the *pgr6*(*abc1k1*) phenotype in the double mutant.

Starting from P_{700} oxidation kinetics (Joliot and Joliot, 2006) and the JIP-test (Strasser et al., 2010; Kalaji et al., 2014a,b), we evaluated the ETC capacity at the PSI and PSII sides under moderate light and after exposure to high light to determine whether the rescued NPQ in *abc1k1/abc1k3* correlated with an increase in the electron capacity of the ETC.

P_{700} oxidation kinetics were analyzed after full reduction of the ETC by a saturating flash and its full oxidation by far-red illumination (**Figure 3A**; Joliot and Joliot, 2006; Pralon et al., 2019). The maximum number of electrons (e^-) present in the electron transport chain per PSI was assessed from P_{700} oxidation kinetic curves: by dividing the lag time after a strong light pulse (time required to oxidize P_{700} when ETC is fully reduced) by the lag time after far-red exposure (oxidation time of a single electron present in P_{700} reaction center) (Joliot and Joliot, 2006). When sampled under moderate light, *abc1k3* and WT ETC had the same electron capacity per PSI (20 ± 3 and 20 ± 4 electrons respectively), whereas the *abc1k1* ETC carried fewer electrons per PSI (8 ± 1 electrons) (**Figure 3B**). In the *abc1k1/abc1k3* mutant grown under moderate light the number of electrons carried by the ETC per PSI (16 ± 5) was intermediate between *abc1k1* and the WT. The measure was repeated on plants kept 3 h under high light. After high light treatment, in the WT the number of electrons carried by the ETC per PSI was 13 ± 3, thus it decreased in comparison to the same genotype sampled under moderate light. Similarly, in *abc1k1* as well as *abc1k1/abc1k3* the number of electrons per PSI dropped after high light treatment to 4 ± 2 and 8 ± 1 respectively. The measured electron transport capacity in *abc1k1/abc1k3* was double than that in *abc1k1*, indicating partial rescue of the ETC capacity. The *abc1k3* mutant displayed only a very slight decrease in the number of the ETC carriers per PSI (18 ± 4) upon shifting from moderate light to high light for 3 h, thus more ETC carriers than WT in this condition (**Figure 3B**).

The ETC capacity, before and after the high light treatment, was also estimated using fast chlorophyll *a* fluorescence (JIP-test) by normalizing the area above curve over variable fluorescence [Area/(F_M-F_O)] (Strasser et al., 2010; Kalaji et al., 2014a,b). This area positively correlates with the number of turnovers of the Q_A site of PSII before being fully closed. Since each turnover corresponds to a single electron injected in the ETC, the area offers a proxy of the number of available electron acceptors per PSII. These acceptors are internal to PSII, pheophytin and Q_A, or external, PQ molecules of the photoactive plastoquinone pool, the cyt *b6f* complex and plastocyanin. Under moderate light, the electron capacity estimated by the normalized area, was bigger in *abc1k3* than in WT (17 ± 2), while it was smaller in both *abc1k1* lines (15 ± 1; 14 ± 1). In the two

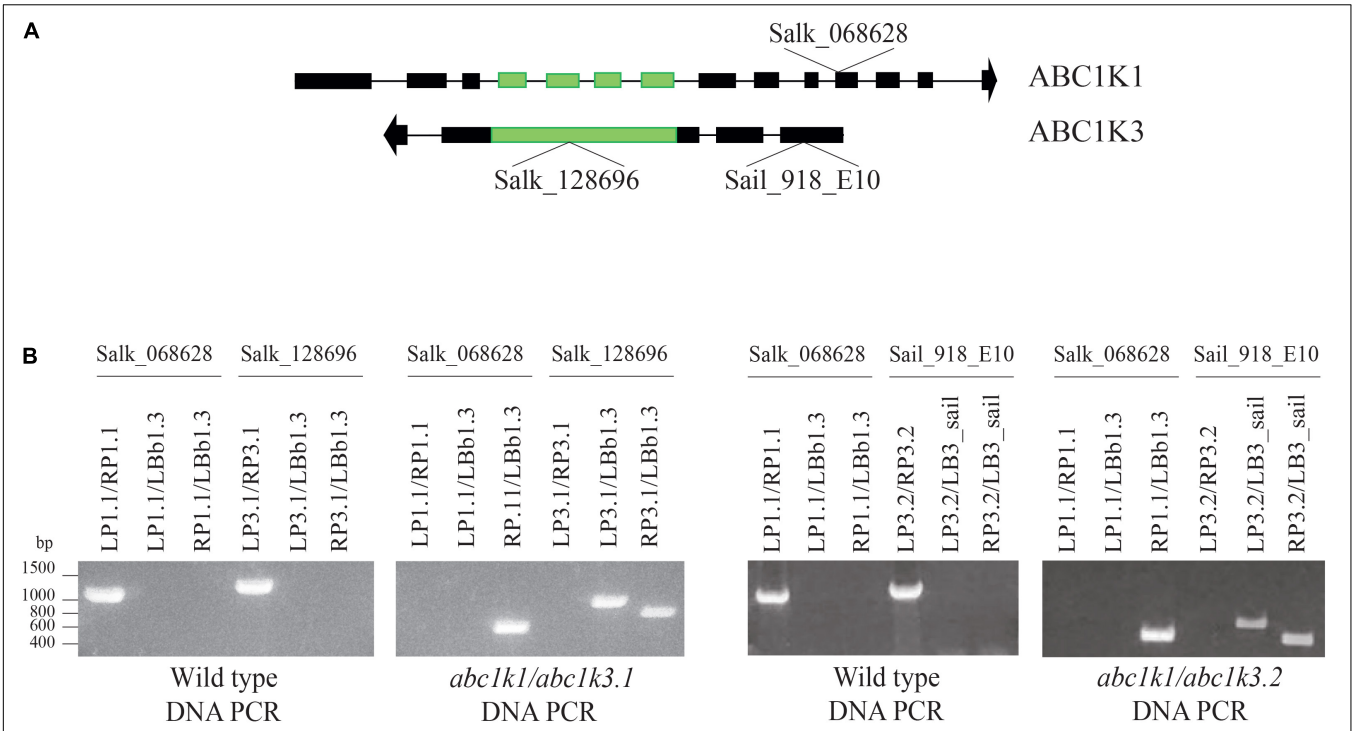

FIGURE 1 | Selection and isolation of *abc1k1/abc1k3* double mutant lines. **(A)** Schematic representation of the position of the T-DNA insertions in *ABC1K1* (At4g31390) and *ABC1K3* (At1g79600) gene sequences. **(B)** Electrophoresis of the amplification products obtained from genomic DNA extracted from Wild type, *abc1k1/abc1k3.1* and *abc1k1/abc1k3.2* confirm the homozygous mutation of both loci. The double mutant *abc1k1/abc1k3.1* was obtained from the crossing between *abc1k1.1* (SALK_068628) and *abc1k3.1* (SALK_128696), while *abc1k1/abc1k3.2* is the result of the crossing between *abc1k1.1* (SALK_068628) and *abc1k3.2* (SAIL_918_E10). The primer used for the amplification are listed in **Supplementary Table 1**.

abc1k1/abc1k3 lines the estimated electron capacity (18 ± 2; 20 ± 3) was comparable to WT (**Figure 4A**). A second measurement was performed on leaves sampled after 3 h of high light, in this sample, compared to the moderate light condition, the availability of the electron acceptors per PSII remained essentially unchanged in WT (19 ± 2) and in both *abc1k1/abc1k3* lines (19 ± 2; 18 ± 3). In the two *abc1k1* lines, after high light treatment, the electron transport capacity was diminished (13 ± 1; 11 ± 2) compared to the moderate light conditions. In contrast, both *abc1k3* lines showed a tendency toward an increase in electron carriers (22 ± 2; 24 ± 3) when comparing leaves sampled after 3 h of high light with those harvested in moderate light condition (**Figure 4A**).

To obtain an indication of the impact of the mutations on different components of the electron transport chain, we calculated the quantum yields of the electron transport flux from Q_A^- to PQ (ΦET2o) and to the PSI electron acceptors (ΦRE1o) by analyzing chlorophyll fluorescence inductions of JIP-curves at 3 ms (F_J) and 30 ms (F_I).

In leaves collected under moderate light, ΦET2o was lower in *abc1k1/abc1k3* and *abc1k1* compared to WT and *abc1k3*. After challenging the plants with 3 h of high light, the measurement revealed that ΦET2o dropped in all lines, with the most severe decrease in *abc1k1* lines followed by *abc1k1/abc1k3* (**Figure 4B**).

The quantum yield of electron transport to PSI final acceptors (ΦRE1o), in plants maintained under moderate light, was similar in WT and *abc1k1/abc1k3*, lower in *abc1k1* and higher in *abc1k3*. After 3 h of high light, ΦRE1o in *abc1k1*diminished even further, while it remained essentially unchanged in *abc1k1/abc1k3* when compared to moderate light. Therefore, *abc1k1/abc1k3* quantum yield was comparable to the WT in both light condition. For this parameter, the double mutation appears to partially attenuate the photosynthetic defects due to the *abc1k1* mutation. Finally, after high light, ΦRE1o in *abc1k3* did not change compared to moderate light, thus being always higher than in the WT (**Figure 4C**).

To verify whether the recovery of photosynthetic parameters in *abc1k1/abc1k3* as well as the higher photosynthetic capacities measured in *abc1k3*, were due to an increased cytochrome *b6f* activity, the turnover rate was measured (Finazzi et al., 2002). The measurement showed that there was no negative impact on the level of activity among all the tested lines (**Supplementary Figure 2**).

Together, these results indicate that the mutation of *abc1k3* has no negative impact the electron transport between the photosynthetic complexes, since the transport efficiency in this mutant line was elevated also after exposure to high light. Conversely, the electron transport in *abc1k1* was impaired in the moderate light condition and worsened upon exposure of the plants to 3 h of high light. The double mutation of *abc1k1* and

A

Maximum PSII Quantum Yield (ΦMAX)

	WT	*abc1k1.1*	*abc1k1.2*	*abc1k3.1*	*abc1k3.2*	*abc1k1/abc1k3.1*	*abc1k1/abc1k3.2*
ML	0.830 ± 0.010 [a]	0.817 ± 0.023 [a]	0.823 ± 0.006 [a]	0.830 ± 0.000 [a]	0.827 ± 0.015 [a]	0.817 ± 0.023 [a]	0.830 ± 0.000 [a]
HL 3h	0.773 ± 0.006 [b]	0.743 ± 0.031 [b]	0.723 ± 0.031 [b]	0.727 ± 0.012 [b]	0.763 ± 0.006 [b]	0.767 ± 0.017 [b]	0.740 ± 0.017 [b]

B

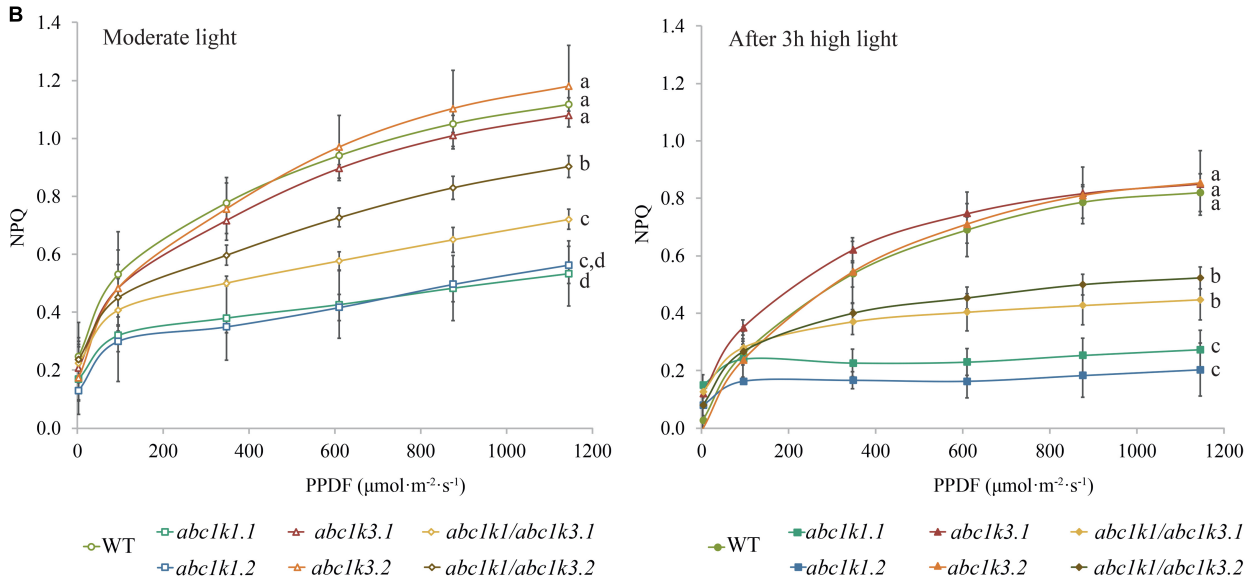

FIGURE 2 | Non-photochemical quenching is partially recovered in *abc1k1/abc1k3* lines compared to *abc1k1*. **(A)** PSII maximum quantum efficiency (ΦPSII = (FM – FO)/FM) and **(B)** non-photochemical quenching (NPQ) of 4–5 weeks old plants of wild type (WT), *abc1k1.1, -2, abc1k3.1, -2* and *abc1k1/abc1k3.1, -2* under moderate light and after 3 h of high light. Plants were dark-adapted 10 min before measurement. Non-photochemical quenching (NPQ = (FM – FM')/FM') was calculated from the maximal fluorescence at room temperature recorded after 1 min of exposure at increasing blue light intensities (470 nm). These measures were performed with a Fluorcam (MF800 – PSI). Each value represents the average of a pot containing 2–3 plants. Superscript letters are used to indicate statistically different groups ($p < 0.05$) by paired Student's *t*-test. Error bars indicate ± SD between different pots ($n = 3$).

abc1k3 resulted in a partial recovery of the electron transport and NPQ to WT levels when compared to *abc1k1*.

Mutation of abc1k3 Has No Effect on the Photoactive PQ Pool Size

The level of NPQ and the electron acceptor capacity of the ETC may be related to the size of the photoactive PQ pool (Block et al., 2013; Pralon et al., 2019). Therefore, we examined whether the partial rescue of the electron transport and NPQ capacities in *abc1k1/abc1k3* compared to *abc1k1* can be attributed to the size of the photoactive plastoquinone pool (i.e., the number of PQ molecules readily available per PSII). For this, we measured the total PQ (nmol cm^{-2}) and the relative photoactive PQ pool (in% of total PQ pool) in 4–5 weeks old plants under moderate light and after 3 h of high light exposure. The photoactive PQ pool is defined as the fraction of total PQ that is rapidly reduced during a saturating light pulse and oxidized when the sample is exposed to far-red light. To measure this fraction, PQH_2 and PQ amounts were analyzed by HPLC-MS on leaves illuminated either with a strong light flash in order to completely reduce the photoactive PQ pool, or with far-red to obtain its complete oxidation (Kruk and Karpinski, 2006; Block et al., 2013; Ksas et al., 2018; Pralon et al., 2019). The difference between the amount of reduced PQ after the saturating flash and that measured after far-red illumination determines the photoactive PQ pool.

Total plastoquinone levels (photoactive PQ pool + non-photoactive PQ pool) in *abc1k1* and in *abc1k1/abc1k3* lines were similar when compared to WT and decreased only slightly after 3 h of high light exposure. Conversely, the total PQ level was lower in *abc1k3* compared to WT (**Figure 5A**). The photoactive PQ pool (photoactive PQ/total PQ) measured in *abc1k3* was larger under moderate light condition and identical to the WT after 3 h of high light (**Figure 5B**). Whereas, in *abc1k1* after 3 h of high light, the photoactive PQ pool was strongly diminished compared to WT. Although the double mutant was not severely impaired in either ETC capacity or NPQ (**Figures 2**, **4**), the relative photoactive PQ pool, measured in plants grown under moderate light, in *abc1k1/abc1k3* was unexpectedly small and similar to the one of *abc1k1*. High light had no negative effect on the size of the photoactive PQ pool in the *abc1k1/abc1k3* double mutant. However, after 3 h of high light, its photoactive PQ pool size was smaller than that of the WT or *abc1k3*, and comparable to *abc1k1* (**Figure 5B**).

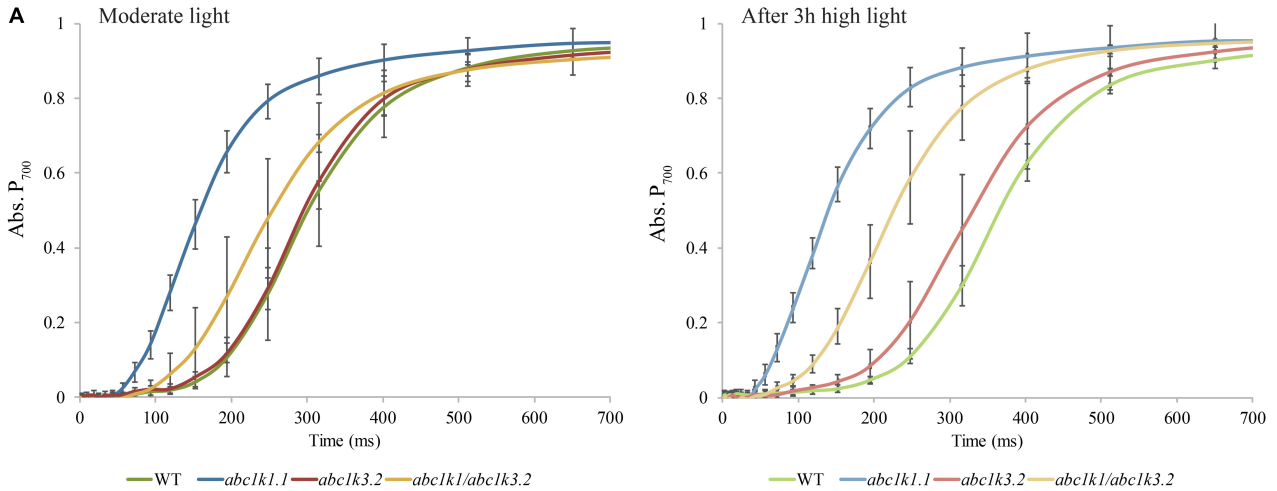

B

Moderate light				
	WT	***abc1k1.1***	***abc1k3.2***	***abc1k1/abc1k3.2***
Lag time after FAR (ms)	8.68	10.07	8.79	9.49
Lag time after pulse (ms)	173.68	75.22*	170.44	139.90*
Calculated pulse e^- number	20 ± 1	**8 ± 2***	20 ± 3	**16 ± 5***

After 3h high light				
	WT	***abc1k1.1***	***abc1k3.2***	***abc1k1/abc1k3.2***
Lag time after FAR (ms)	17.87	15.92	11.68	14.47
Lag time after pulse (ms)	215.14	49.85*	200.60	109.84*
Calculated pulse e^- number	13 ± 4	**4 ± 2***	18 ± 4	**8 ± 1***

FIGURE 3 | The shortage of electron carriers per photosystem I of *abc1k1* is partially recovered in *abc1k1/abc1k3*. **(A)** Kinetics of P_{700} re-oxidation induced by far-red light were recorded after a saturating light pulse (Time 0 = far-red ON) in wild type, *abc1k1.1, abc1k3.2,* and *abc1k1/abc1k3.2* kept under moderate light and after 3 h of high light. The P_{700} oxidation status was measured by the increase in absorption at 810 nm on fully expanded leaves of each genotype. **(B)** Electron (e^-) carried by the electron transport chain per photosystem I calculated from the lag time of P_{700} oxidation after a saturating pulse divided by the lag time of the oxidation after dark. Asterisk are used to indicate statistically different groups by Student's *t*-test ($p < 0.05$) ($n = 4$ biologically independent samples).

The analysis of the photoactive PQ pool suggests that the complementation of the *pgr6*(*abc1k1*) photosynthetic phenotype, induced by the *abc1k3* mutation, does not simply arise from a change of the amount of PQ readily available at PSII.

Mutation of ABC1K1 and ABC1K3 Impacts the Kinetics of PQ Re-oxidation in the Dark

The redox state of PQ in the light is dependent on the activity of the PSII, which will reduce the photoactive pool, and on that of the cytochrome *b6f*, which oxidizes the PQ pool transferring electrons along the ETC toward PSI. However, the photosynthetic complexes are inactive in the dark and therefore the redox state of PQ is mostly dependent on light-independent electron routes alternative to the cytochrome *b6f*. In the transition from light to dark the photoactive PQ pool will tend to start in a reduced form and be re-oxidized. The principal actor of this re-oxidation is PTOX. This enzyme, in Arabidopsis, is mostly located in the stroma lamellae fraction of the thylakoid membrane (Joet et al., 2002; Lennon et al., 2003; Houyoux et al., 2011). PSII being more abundant in the grana stacks, and considering the timescale of the mobility of PQ (Kirchhoff, 2014), we may assume that a large portion of the photoactive PQ pool is located within the grana stacks. Therefore, in order to be oxidized by PTOX the photoactive PQ has to migrate from the grana stacks to the stroma lamellae and then return to the grana stacks. Considering this, the kinetics of the oxidation of the photoactive PQ pool represents a proxy of the mobility of the PQ across the different portions of the thylakoid membrane. To estimate the redox state of the photoactive PQ pool we used the rapid chlorophyll *a* fluorescence induction, we based the analysis on the relative fluorescence at 3 ms (VJ). It has been shown that the fluorescence recorded at this time interval correlates with the redox state of the photoactive PQ pool (Strasser et al., 2010; Kalaji et al.,

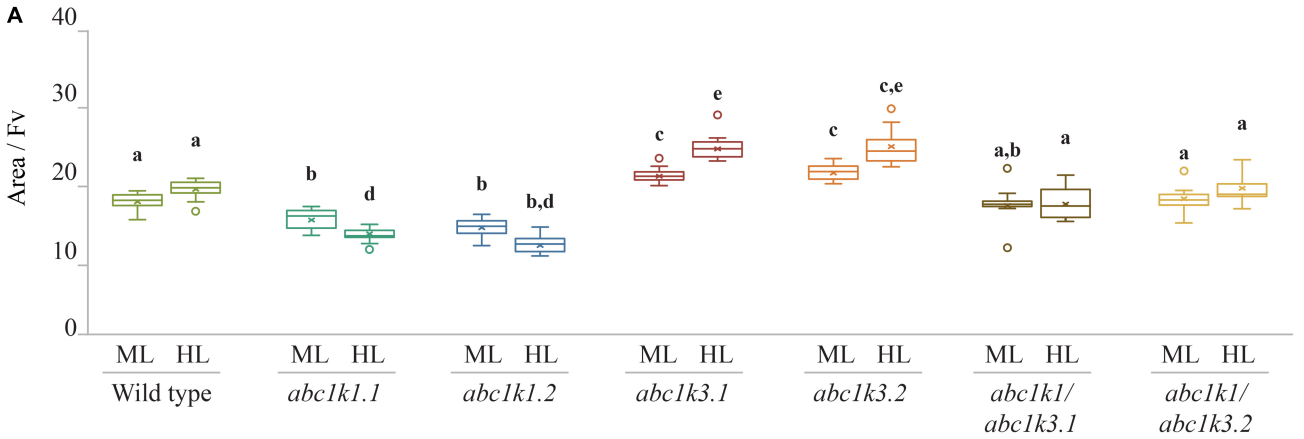

B

φET2o

	WT	*abc1k1.1*	*abc1k1.2*	*abc1k3.1*	*abc1k3.2*	*abc1k1/abc1k3.1*	*abc1k1/abc1k3.2*
ML	0.48 ± 0.02 ^{a}	**0.42 ± 0.03** ^{b}	**0.38 ± 0.04** ^{c}	0.48 ± 0.01 ^{a}	0.49 ± 0.01 ^{a}	**0.44 ± 0.02** ^{b}	**0.43 ± 0.03** ^{b}
HL 3h	0.42 ± 0.04 ^{b,c}	**0.31 ± 0.04** ^{d,e}	**0.26 ± 0.07** ^{e}	0.40 ± 0.03 ^{b,c}	0.40 ± 0.03 ^{b,c}	**0.32 ± 0.02** ^{d}	**0.33 ± 0.03** ^{d}

C

φRE1o

	WT	*abc1k1.1*	*abc1k1.2*	*abc1k3.1*	*abc1k3.2*	*abc1k1/abc1k3.1*	*abc1k1/abc1k3.2*
ML	0.14 ± 0.03 ^{a}	**0.11 ± 0.02** ^{b}	**0.10 ± 0.02** ^{b}	**0.18 ± 0.01** ^{c}	**0.18 ± 0.02** ^{c}	0.14 ± 0.02 ^{a}	0.13 ± 0.03 ^{a}
HL 3h	0.15 ± 0.02 ^{a}	**0.08 ± 0.01** ^{d}	**0.06 ± 0.02** ^{d}	**0.18 ± 0.02** ^{c}	**0.17 ± 0.02** ^{c}	0.11 ± 0.02 ^{a,b}	0.12 ± 0.02 ^{a,b}

FIGURE 4 | High light as a moderate impact on photosynthetic electron transport fluxes in *abc1k1/abc1k3*. Fully expanded leaves from Wild type (WT), *abc1k1.1, -2, abc1k3.1, -2,* and *abc1k1/abc1k3.1, -2* plants were collected under moderate light conditions (120 μmol of photons m^{-2} s^{-1}) (ML) and after 3 h of high light (500 μmol of photons m^{-2} s^{-1}) (HL). **(A)** Normalized area (Area/Fv) above the chlorophyll fluorescence induction curve measured after 15 min of dark incubation. This value estimates the number of available electron carriers per PSII reaction center. **(B)** Quantum electron transport yield from Q_A to PQ pool (ΦET2o), and **(C)** until the PSI electron acceptors (ΦRE1o). These measures were performed with Handy-PEA (Hansatech Instruments). Whiskers and box plot shows the minimum, first quartile, median, average, third quartile, and maximum of each data set (n = 12 biologically independent samples). Superscript letters are used to indicate statistically different groups by paired Student's t-test ($p < 0.05$).

2014a). A high V_J value is recorded in samples where the photoactive PQ pool is mostly reduced, and it decreases with its oxidation (Tóth et al., 2007). The chlorophyll *a* fluorescence induction was measured at increasing time intervals of dark incubation after a saturating light pulse. The results show that the measured oxidation, which appears to be almost completely PTOX dependent, is faster in the *abc1k3* mutants, while severely impaired in *abc1k1* (**Figure 6A**).

A limitation of total PQ, as in the *sps2* mutant (Block et al., 2013; Pralon et al., 2019), resulted in a slower oxidation in the dark as well. The PQ oxidation in the *abc1k1/abc1k3* double mutant progressed more rapidly than in the *abc1k1* single mutant (**Figure 6A**). The dark re-oxidation of the photoactive PQ pool is independent on the photosynthetic ETC. In fact, all the tested mutant lines displayed the same kinetics when the PQ oxidation was performed by the cytochrome *b6f*, as observed when PSI was excited with far-red light (**Figure 6B**). The kinetics of PQ oxidation in the dark may be influenced by the level of accumulation of the PTOX protein (Ivanov et al., 2012). We therefore used immunodetection to test the PTOX accumulation in total protein samples from the different mutants. The result showed no differences at the protein level, which appeared to be uniform among the lines (**Supplementary Figure 3**). After 3 h under high light the dark re-oxidation of the photoactive PQ in the *abc1k1* mutant is almost completely blocked, and it is slower overall in all lines analyzed. Once again, the defect was milder in the *abc1k1/abc1k3* double mutant (**Supplementary Figure 4**). It is worth noting that after 3 h of high light the oxidation kinetics under far-red light were also affected in *abc1k1*, suggesting that 3 h of high light exposure induce a perturbation of the ETC, consistently with the previous report (Pralon et al., 2019).

This experiment shows that *abc1k1* is impaired in the regulation of the photoactive PQ redox state independently of the activity of the ETC. Considering the specific localization and identical protein levels of PTOX, this supports a model

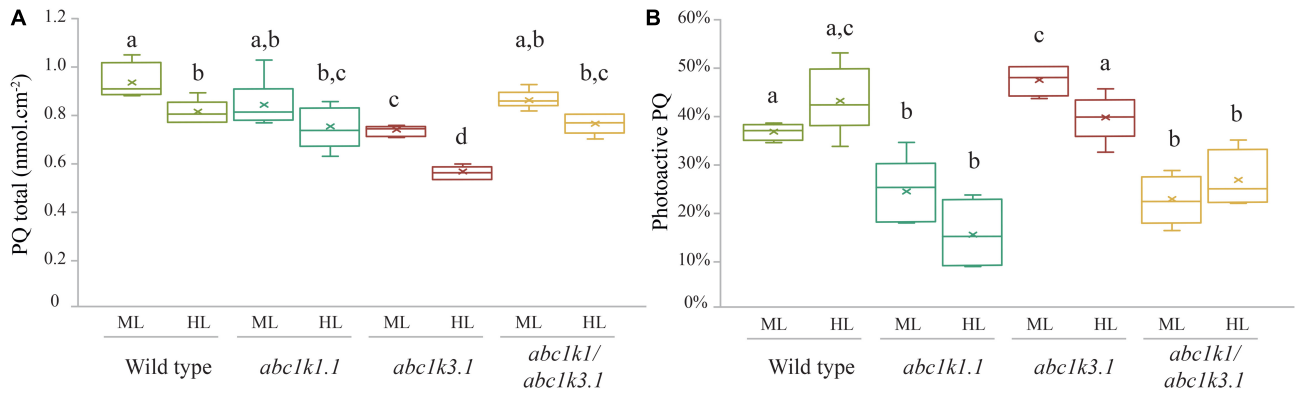

FIGURE 5 | Photoactive PQ pool is smaller in all the lines containing the *abc1k1* mutation. **(A)** Total plastoquinone content (nmol cm^{-2}) and **(B)** photoactive plastoquinone pool (as% of total PQ) were analyzed from leaves of Wild type, *abc1k1.1*, *abc1k3.2,* and *abc1k1/abc1k3.2* under moderate light and after 3 h high light. The photoactive plastoquinone pool was determined by the difference of the plastoquinol (PQH_2) amount measured when the PQ pool is maximally reduced by strong white light pulse (15 s at 2,000 m^{-2} s^{-1}), and the amount of PQH_2 measured when the PQ pool is fully oxidized after far-red illumination (2 min at 5.5 μmol of photons m^{-2} s^{-1}). Whiskers and box plot shows the minimum, first quartile, median, average, third quartile, and maximum of each data set (n = 4 biologically independent samples). Superscript letters are used to indicate statistically different groups by paired Student's t-test ($p < 0.05$).

of limited mobility of PQ. Interestingly, said defect is partially complemented by *abc1k3* mutation.

Major Thylakoid Membrane Protein Phosphorylation and State Transitions Are Partially Restored in abc1k1/abc1k3

A smaller photoactive PQ pool (**Figure 5B**) should be prone to over-reduction or at least to "mimic" a condition of over-reduction as fewer PQ molecules are available (**Figure 4B**). This would be expected to perturb state transitions (Bellafiore et al., 2005; Shapiguzov et al., 2010, 2016; Tikkanen et al., 2012; Trotta et al., 2016; Pralon et al., 2019). Cytochrome *b6f* activity is dependent on the redox state of PQ and regulates the activation of STN7, the principal kinase involved in LHCII phosphorylation. Therefore, we evaluated the phosphorylation status of the major thylakoid membrane proteins by immunodetection. Moreover, we measured the re-allocation of the mobile light harvesting complex II (LHCII) between the two photosystems by room temperature chlorophyll fluorescence in *abc1k1/abc1k3* during state 1 to state 2 transition induced by changes in the light spectrum. Both approaches were used as proxies to assess the redox state of the PQ pool *in vivo*.

The phosphorylation status of the thylakoid protein was assessed by anti-phosphothreonine immunoblotting on total protein extracts from leaves collected under moderate light and after 3 h high light exposure. Under moderate light, the thylakoid phosphoprotein pattern was similar among all the lines tested (**Figure 7A**). Compared to the moderate light, after 3 h of high light exposure PSII core proteins D1 (PsbA) and D2 (PsbD) were only slightly more phosphorylated in *abc1k1*, while their phosphorylation increased markedly in WT, *abc1k3* as well as in *abc1k1/abc1k3*. Similarly, after the high light stress, the LHCII proteins were highly phosphorylated in *abc1k3, abc1k1/abc1k3,* and WT, while the LHCII phosphorylation was clearly lower in *abc1k1* (**Figure 7A**). This suggests that, despite the shortage of photoactive PQ in *abc1k1/abc1k3* (**Figure 5B**), the STN7 kinase maintains its activity toward LHCII even after exposure to high light. Furthermore, neither the change in total PQ nor in the photoactive fraction had an impact on the abundance of selected photosynthetic proteins after 3 h of high light (**Figure 7B**).

To determine whether thylakoid protein phosphorylation observed in *abc1k1/abc1k3* correlated with the ability to perform state transitions we followed and measured room temperature chlorophyll *a* fluorescence kinetics on dark-adapted plants by switching red light supplemented with far-red light (State 1) to red light only (State 2). The quenching (fluorescence decline) caused by state transitions (qT), was calculated as the difference between the maximal fluorescence (Fm) after "State 1" illumination (Fm_ST1) and the one after "State 2" light (Fm_ST2) normalized on maximal fluorescence (Fm) (qT = (Fm_ST1 – Fm_ST2)/Fm), which reflects the dissociation of antenna from PSII and its association with PSI.

Under moderate light, the qT in all genotypes was comparable to the WT, indicating their ability to perform transition from State 1 to State 2 and only *abc1k1* lines appeared to be slightly impaired (**Figure 7C**). *stn7/stn8*, which is completely unable to perform state transitions, was used as a negative control. After 3 h of high light exposure, *abc1k3* and WT maintained their capacity to perform state transitions, while *abc1k1* lines were defective in state transitions. After 3 h of high light, state transitions in *abc1k1/abc1k3* lines exhibited a level of quenching comparable to WT and *abc1k3* (**Figure 7C**). This shows that LHCII phosphorylation, and thus the activity of the STN7 kinase, which is maintained in *abc1k1/abc1k3* mutants, allows the state transitions after high light exposure.

DISCUSSION

The photosynthetic apparatus has to adapt to photo-oxidative stress induced by excess light in order to prevent thylakoid

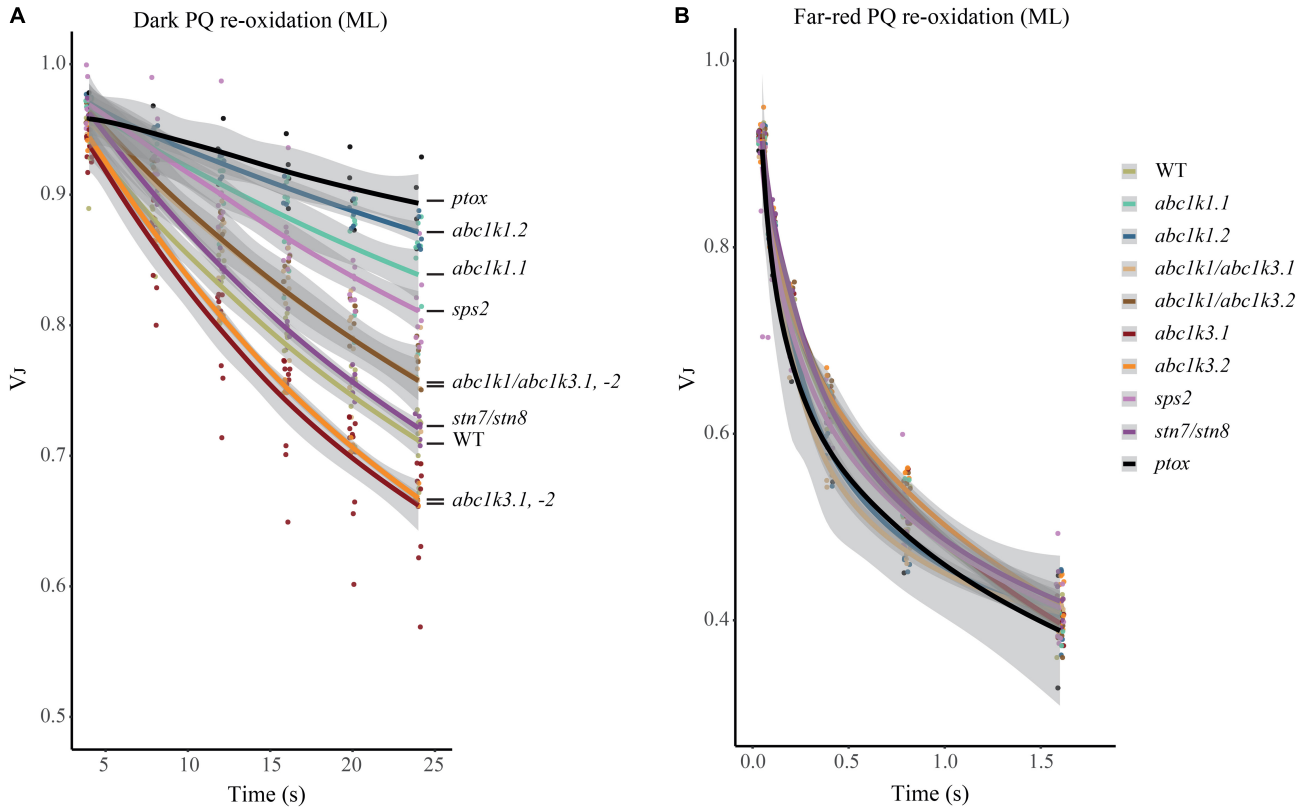

FIGURE 6 | Mutations of ABC1K1 and ABC1K3 influence the dark re-oxidation kinetic of the photoactive plastoquinone. The relative fluorescence after 3 ms (VJ) is plotted over the time from the previous saturating pulse. The sample was incubated in dark **(A)** or with far-red light **(B)**. Kinetics of the re-oxidation are shown by interpolation of the data points with a logarithmic curve with the deviation of the model in gray (R-Studio) for wild type (WT) *abc1k1.1, -2, abc1k3.1, -2,* and *abc1k1/abc1k3.1, -2, sps2, stn7/stn8, ptox* plants grown under moderate light (ML). These measures were performed with Handy-PEA (Hansatech Instruments) on detached leaves incubated for 10 min in dark.

membrane damage and maintain photosynthetic efficiency. Photo-protective strategies comprise adjustment of electron transport capacity (ETC) (Rochaix, 2011), equilibration of energy between photosystems (state transitions) (Rochaix, 2007) and induction of NPQ (Müller et al., 2001; Ruban, 2016). All three mechanisms are directly or indirectly related to the activity of the plastoquinone as an electron carrier. Recently, it has been demonstrated that ABC1K1 is implicated in photosynthesis regulation by homeostasis of photoactive PQ under high light (Pralon et al., 2019). In this study, we describe the involvement of ABC1K3 (Lundquist et al., 2013; Martinis et al., 2013; Huang et al., 2015), a close homolog of ABC1K1, in the same process.

We tested two *abc1k3* mutant lines for their ability to induce NPQ under increasing light intensities. Contrary to *abc1k1,* this mutation did not cause any perturbation in NPQ induction when compared with the WT (**Figure 2**). A previous report shows that, during several days of exposure to high light (500 µmol of photons m^{-2} s^{-1}), *abc1k3* had a tendency to induce slightly less NPQ compared to WT, however this difference was not statistically significant nor constant over the time course (Martinis et al., 2013). This suggests that the NPQ parameter alone is not sufficient to discriminate the photosynthetic adaptation of *abc1k3* from WT. In fact, the differences between WT and *abc1k3* are significant only when the photosynthetic ETC capacity is analyzed in detail (**Figures 3**, **4**). To further address the role of *abc1k3* in the photosynthetic regulation, we crossed this mutant with *abc1k1* to obtain *abc1k1/abc1k3* double mutant plants (**Figure 1**). The *abc1k3* mutation was capable to partially alleviate the NPQ defect observed in *abc1k1*; while the NPQ level in *abc1k1/abc1k3* was higher than in the single *abc1k1* mutant, it remained lower than in the WT (**Figure 2**).

In order to confirm that the NPQ perturbation is due to a lack of transport through the ETC, we measured the number of electrons transported per PSI after a saturating light pulse by analyzing the lag time of PSI oxidation. As expected from previous reports (Shikanai et al., 1999; Martinis et al., 2014; Pralon et al., 2019), *abc1k1* transfers less electrons to PSI, and the difference compared to the WT increases after exposure to 3 h high light. On the contrary, *abc1k3* was not impaired and appeared capable of maintaining a high level of electron transfer after 3 h of high light (**Figure 3**). In *abc1k1/abc1k3*, the electron transport capacity was still lower than the WT, however, more electrons were transferred per PSI compared to *abc1k1* and the decrease after 3 h of high light was comparable to the one observed in the WT (**Figure 3**). This finding suggests that the defect in the photosynthetic electron carriers of *abc1k1* was

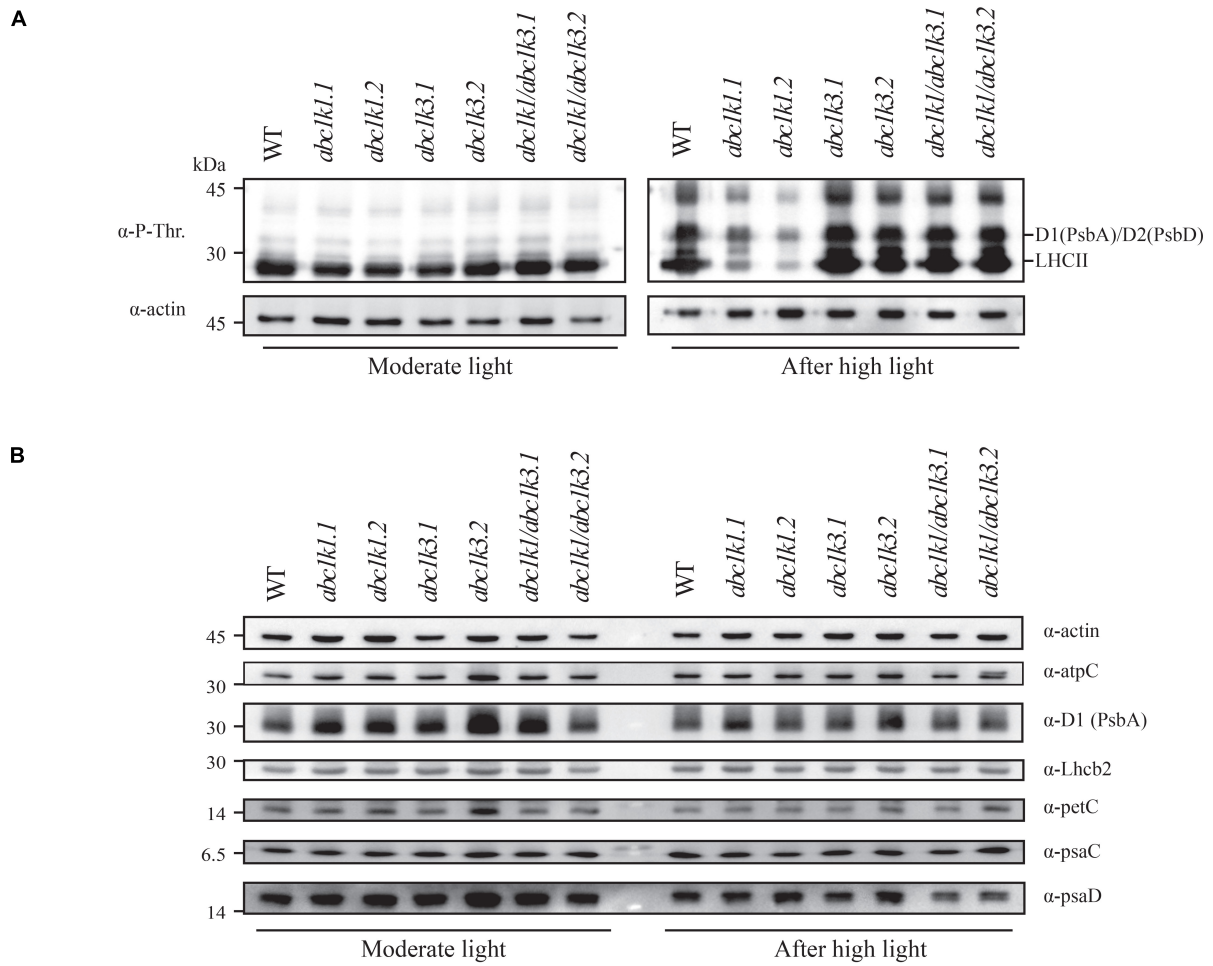

C

State transition quenching (qT)

	WT	*abc1k1.1*	*abc1k1.2*	*abc1k3.1*	*abc1k3.2*	*abc1k1/abc1k3.1*	*abc1k1/abc1k3.2*	*stn7/stn8*
ML	6,1 ± 1,2 [a]	3,8 ± 1,7 [b]	3,2 ± 2,4 [b]	6,1 ± 1,0 [a]	5,9 ± 1,3 [a]	6,0 ± 1,0 [a]	5,7 ± 0.9 [a]	**-3,8 ± 1,7** [c]
HL 3h	3,0 ± 1,2 [b]	**-2,1 ± 2,4** [c]	**-3,1 ± 1,9** [c]	2,4 ± 1,4 [b]	2,3 ± 1,0 [b]	3.0 ± 1.6 [a,b]	1.7 ± 2.6 [a,b,c]	**-11,0 ± 0,5** [d]

FIGURE 7 | Double mutant maintains thylakoid protein phosphorylation and state transitions after high light. **(A)** Total protein extracts of wild type (WT), *abc1k1.1, -2, abc1k3.1, -2,* and *abc1k1/abc1k3.1, -2* light-exposed leaves were separated by SDS PAGE, transferred on nitrocellulose membrane and decorated with anti-phosphothreonine antibody. The main thylakoid phospho-proteins are indicated on the right according to their size. Core photosystem II proteins D1 (PsbA) and D2 (PsbD) are indicated together due their poor resolution. **(B)** The accumulation of the principal photosynthetic complexes was assessed using antibodies against specific subunits of each complex: anti-Lhcb2 for the major LHCII, anti-D1 (PsbA) for PSII, anti-PetC for cytochrome *b6f*, anti-PsaD and anti-PsaC for PSI, and anti-AtpC for ATP synthase. Actin signal is shown as a loading control. **(C)** Fluorescence quenching related to the state transitions (qT) of wild type (WT), *abc1k1.1, -2, abc1k3.1, -2,* and *abc1k1/abc1k3.1, -2* under moderate light (120 μmol of photons m^{-2} s^{-1}) (ML) and after 3 h of high light (500 μmol of photons m^{-2} s^{-1}) (HL). qT was calculated from the maximal chlorophyll fluorescence measured after 10 min exposure to red light (660 nm) supplemented with far-red illumination (720 nm) "State 1" (FMST1) or to pure red light "State 2" (FMST2). Quenching related to state transition was calculated as qT = (FMST1 – FMST2)/FM. Each value represents the average of a pot containing 2–3 plants. Superscript letters are used to indicate statistically different groups ($p < 0.05$) by paired Student's *t*-test.

partially rescued in *abc1k1/abc1k3,* presumably by increasing the efficiency of the electron transfer in the ETC. In a previous report, the limitation of the electron transport capacity observed in *abc1k1* was linked to a depletion of the photoactive PQ pool (Pralon et al., 2019). However, the decrease in the number of electrons transported to PSI appeared to be more severe than the measured decrease in the size of the photoactive PQ pool. Therefore, it was hypothesized that the PQ mobility in the ETC plays an additional role in limiting the electron transport capacity. To investigate this hypothesis the energy fluxes along the ETC were analyzed by rapid fluorescence induction curves. The estimation of the number of electrons present in the ETC

before saturation, expressed as the Area/Fv (**Figure 4A**), was consistent with the P_{700} oxidation analysis (**Figure 3**). In fact, already under moderate light the normalized area was smaller in *abc1k1* mutant and larger in *abc1k3* in comparison to WT, consistent with *abc1k1* having limited electron transport and *abc1k3* having more carriers than the WT. In this condition, the *abc1k1/abc1k3* double mutant had an Area/Fv value in between those of the two single mutants, suggesting once again, a partial recovery of the photosynthetic electron transport. Upon exposure to high light only the *abc1k1* mutant showed a decrease in the number of available carriers; while all the other lines had a tendency to increase the Area/Fv value, compared to moderate light, indicating a better, or at least unchanged, electron transport capacity (**Figure 4A**). By analyzing the induction curve's principal steps, we can obtain hints regarding the different components that may be affected in the ETC. The first step, at 3 ms from the start of the saturating flash, was reported to be dependent of the Q_B redox state at the PSII and therefore linked to the redox state of the photoactive PQ pool (Tóth et al., 2007), which is also affected by the size of the photoactive PQ pool (Pralon et al., 2019). From the fluorescence value at 3 ms (F_J) it is possible to calculate the ΦET2o, the efficiency of the electron transport between Q_A and Q_B (which depends on the status of the photoactive PQ pool) (Strasser et al., 2010; Kalaji et al., 2014a,b). We observed that the ΦET2o is lower both in *abc1k1* and in *abc1k1/abc1k3*, suggesting a similar defect in the photoactive PQ pool. However, the defect appears to be somewhat milder in the double mutant compared to *abc1k1* (**Figure 4B**). The second step in the fluorescence rise occurs at 30 ms (F_I), and the level of the fluorescence recorded at this step is linked to the electron transport to the PSI final acceptors in the OJIP model (Strasser et al., 2010; Kalaji et al., 2014a,b). From the F_I value is also possible to calculate the electron transport efficiency, defined as ΦRE1o. Comparison of this efficiency revealed that *abc1k1* has a lower efficiency compared to the WT but that was not the case for *abc1k1/abc1k3*. In the latter, the ΦRE1o was the same as in the WT in moderate light, and was less affected upon the exposure to 3 h high light compared to *abc1k1* (**Figure 4C**). The *abc1k3* single mutation did not create any measurable defect in electron transport. On the contrary, the efficiency of the transport to PSI acceptors appeared to be even higher than in the WT, both under moderate light and after exposure to high light (**Figure 4C**). This suggests that the mutation of the *ABC1K3* gene leads to an increased efficiency in the electron mobility between PSII and PSI.

To support the fluorescence induction results we biochemically measured the size of the photoactive pool in the mutants exposed to moderate light and to high light. Consistent with the biophysical observations, the photoactive PQ pool was smaller in both *abc1k1* and *abc1k1/abc1k3* compared to the WT in moderate light condition (**Figure 5B**). Exposure to 3 h of high light had a limited effect on the size of the photoactive PQ pool in the four tested lines (**Figure 5B**). However, while the WT and the double *abc1k1/abc1k3* mutant display a tendency toward the increase of the photoactive PQ after 3 h of high light, we detected a slight decrease of the photoactive PQ pool in *abc1k1* as previously reported (Pralon et al., 2019). The depletion observed in this report was not significant as it was in the previous report, this may suggest that the photoactive PQ pool homeostasis relies on multiple factors (e.g., thylakoid organization, lipid distribution) and that ABC1K1, despite its prominent role, is not the only factor regulating the photoactive PQ pool size. A similar depletion of the photoactive PQ pool after 3 h of high light, was observed in *abc1k3* even though the relative photoactive PQ pool size was still larger than in *abc1k1*, and comparable to the WT (**Figure 5B**). On the contrary, the *abc1k1/abc1k3* double mutant constitutively displayed a small photoactive PQ pool that was not depleted by the exposure to high light (**Figure 5B**). This leads to the conclusion that the photoactive PQ pool size *per se* has a limited influence on photosynthetic efficiency, and that the photosynthetic defect becomes symptomatic only when PQ limitation is associated with an additional impairment in its mobility. Impaired PQ mobility may be the cause affecting the reoxidation of the photoactive PQ by PTOX, since it may require an exchange between grana stacks and stroma lamellae (**Figure 6A**; Stepien and Johnson, 2018). Furthermore, it would affect the exchange between the photoactive pool and the reservoir stored in the PGs necessary to maintain the photoactive PQ pool size (Pralon et al., 2019). We cannot exclude that the defect in the mobility and exchange between the different PQ pools stems from a defect in the thylakoid membrane composition. In fact, it has been previously reported that the mutation of *abc1k1* results in a lower amount of several prenyl lipids (Martinis et al., 2014) compared to the WT under control growth conditions (150 μmol of photons m^{-2} s^{-1}) as well as after several days of growth in high light (500 μmol of photons m^{-2} s^{-1}). However, the *abc1k3* mutant has a similar defect in the level of accumulation of these lipophilic compounds (Martinis et al., 2013). Therefore, no obvious correlation between the photosynthetic defect and the amount of the principal chloroplast lipids can be drawn at this stage.

A lower amount of total PQ, which decreased after 3 h of high light, was observed in *abc1k3* (**Figure 5A**). This decrease may be an indirect effect of the increased photosynthetic electron transport observed in *abc1k3* compared to WT. A possible explanation is that the amount or the redox state of PQ in the photoactive pool act as a signal to regulate PQ biosynthesis. This is supported also by previous reports showing a correlation between PQ biosynthesis and increase in light intensity (Zbierzak et al., 2010; Ksas et al., 2015). Consistent with this hypothesis, the increased relative PQ accumulation in the photoactive pool, observed in the *abc1k3* mutant under moderate light (**Figure 5B**), would alter this signal and therefore limit the biosynthesis resulting in a lower amount of total PQ (**Figures 5A**, **8**).

A crosstalk between photoactive PQ pool and biosynthesis would ensure the coupling of the photosynthetic electron transport efficiency with the production of a PQ reserve in the non-photoactive pool allowing fast adaptation to changing environmental conditions. It is necessary to point out that the decrease of total PQ after 3 h of high light was likely to be transitory since, under permissive light intensity, *abc1k3* was capable of restoring the total PQ amount to WT levels as previously shown (Martinis et al., 2013). We cannot exclude that ABC1K1 and ABC1K3 play an active role in this

signaling pathway, through still unidentified targets, therefore the mutation of these two kinases would result in a combined effect on the source of the signal, the photoactive PQ pool, as well as on the transmission of said signal.

Another feature linked to the *abc1k1* mutation was the loss of thylakoid protein phosphorylation. These phosphorylation events are mostly dependent on STN7 and STN8 kinases, activities of which depend on the redox status of the PQ pool (Aro and Ohad, 2003; Pesaresi et al., 2010; Puthiyaveetil, 2011; Puthiyaveetil et al., 2012). The mutation of *abc1k3* in the *abc1k1* background was sufficient to re-establish the phosphorylation of the thylakoid proteins to WT level after 3 h of high light. This observation has an important implication to understand the factors regulating the redox state of the photoactive PQ pool. In fact, the PQ pool redox state appears to be dependent also on the exchanges between the photoactive pool and storage sites and not only on the size of the photoactive pool and the activity of the ETC. We cannot exclude that protein phosphorylation has a positive feedback loop effect; in fact, the phosphorylation of the thylakoid proteins may favor their mobility in the membrane and by doing so increase also the mobility of the PQ between different portions of the thylakoid membrane (Kirchhoff et al., 2000; Fristedt et al., 2009; Kirchhoff, 2014). We also cannot exclude the involvement of the phosphorylation of other, less evident, targets such as CURT1b, the phosphorylation of which is also dependent on STN8 kinase (Trotta et al., 2019). By their phosphorylation level, the proteins imbedded in the thylakoid membrane may change the overall conformation of the membrane system and by this also the mobility and exchange of the PQ, and other lipids, between the photoactive pool and the reservoir (Armbruster et al., 2013). Moreover, ABC1K1 and ABC1K3 are also predicted to function as kinases; therefore, they may phosphorylate yet unknown target proteins leading to the regulation of the photosynthetic activity and potentially influencing membrane fluidity and/or thylakoid protein organization (Yokoyama et al., 2016).

The results lead us to propose the following model for the action of ABC1K1 and ABC1K3, being two kinases located at the plastoglobule (Vidi et al., 2006; Lundquist et al., 2012; Martinis et al., 2013, 2014). The role of ABC1K1 would be to promote the release, or the exchange of the PQ between the storage and the photoactive pool, while ABC1K3 would act in limiting such diffusion blocking this PQ flux (**Figure 8**). This model would explain the slightly bigger size of the photoactive pool in *abc1k3* and also the difference between *abc1k1* and *abc1k1/abc1k3*, the latter having a better photosynthetic performance since it is missing the ABC1K3 protein that would otherwise act as a "brake" to the PQ supply to the photoactive pool (**Figure 8**). To fully explain the observed results, we also have to assume that, without the activity of ABC1K1, the PQ tends to over-accumulate in the non-photoactive pool thus leading to a depletion of the photoactive pool. In this regard, the role of ABC1K1 is crucial to maintaining the photosynthetic efficiency by promoting the movement and accumulation of the PQ against its "passive" distribution. In contrast ABC1K3, acting as a brake to the mobilization of the non-photoactive pool, may have a more important role in other processes and phases of plant development when lipids need to be efficiently accumulated in the reserve compartments (e.g., senescence, fruit maturation). Previous reports describe a direct interaction between ABC1K1 and ABC1K3 (Lundquist et al., 2013). It is possible to hypothesize that this interaction allows a reciprocal regulation of the two kinases. For instance, a negative regulation of ABC1K3, mediated by ABC1K1, could partially explain the results of this report. In this scenario, the *abc1k1* mutation would cause a deregulation, or over activation, of the ABC1K3 kinase and this would then cause the photosynthetic defect. Following this model, the removal of ABC1K3, as in the double *abc1k1/abc1k3* mutant, would partially rescue the defect caused by the first mutation. It has

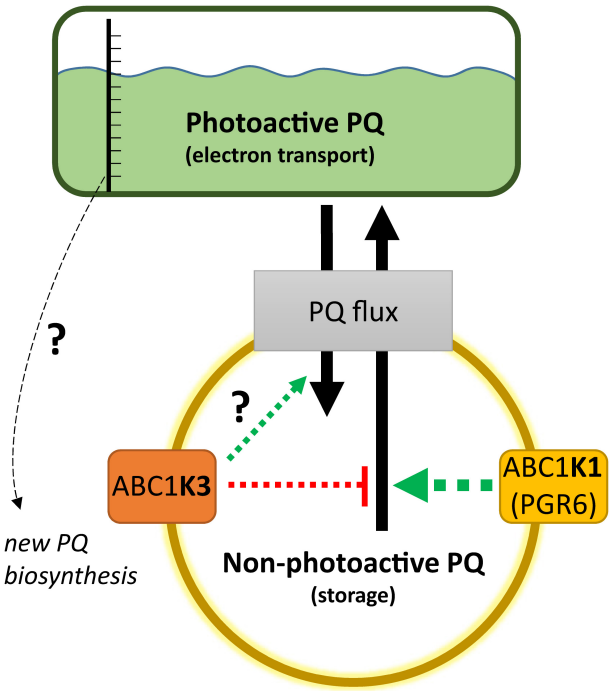

FIGURE 8 | Working model on the activity of ABC1K1 and ABC1K3 on the plastoquinone (PQ) redistribution. The two atypical kinases are enriched in the plastoglobule proteome, therefore presumably in the proximity of the non-photoactive PQ pool. The activity of the ABC1K1 promotes the mobilization of PQ toward the photoactive pool, while ABC1K3 counteracts this mobilization thus favoring the accumulation of PQ in the non-photoactive pool. In the absence of both kinases the PQ tends to accumulate in the non-photoactive pool, therefore a positive regulation of ABC1K3 on the flux from the photoactive to the non-photoactive pool is not essential, as highlighted by the question mark, but cannot be excluded in this model. The observation that in absence of both kinases PQ tends to accumulate in the non-photoactive pool suggests a prominent role of ABC1K1 in the PQ flux regulation (larger arrow). A not yet identified sensor of the size and/or the redox state of the photoactive PQ pool may serve to regulate the level of PQ biosynthesis. When the relative size of the photoactive pool is larger, and the electron transport more efficient as in the *abc1k3* mutant, the signal promoting PQ biosynthesis may be dimmed resulting in a lower amount of total PQ. The dashed arrows represent that the regulation of the PQ fluxes, mediated by the two atypical kinases, is likely to be indirect. Although the effect on PQ flux is opposite, the presented working model cannot exclude that the two atypical kinases act via separate mechanisms and that the impact observed on PQ mobility is a consequence of the alteration of their primary targets.

to be underlined that the physiological state of the double mutant *abc1k1/abc1k3* is still not optimal and that the absence of ABC1K3 only partially rescues the photosynthetic phenotype. This observation is thus consistent with previous reports showing that the double mutant, lacking both kinases, displays a stunted phenotype under prolonged stress conditions to which is unable to adapt (Lundquist et al., 2013).

CONCLUSION

In conclusion, we show that the *abc1k3* mutation allows a partial recovery of the *pgr6/abc1k1* phenotype. Consequently, ABC1K1 and ABC1K3 act in an opposite manner in order to cope with short-term high light. Therefore, we suggest that the system of the atypical kinases ABC1K1 and ABC1K3 allows a dynamic regulation of the PQ pool mobility and availability, which is fundamental for the plant to cope with variations in environmental conditions. In the working model ABC1K3 would act by limiting the distribution of PQ to the photoactive pool, while ABC1K1 acts in the opposite way. The role of ABC1K1 would be prominent considering that, without any regulation, the relative amount of PQ in the photoactive pool is lower, as is the case for the double *abc1k1/abc1k3* mutant. The opposing activities of these two atypical kinases would allow to equilibrate the amount of PQ, and potentially other lipids, between the storage compartments and the thylakoid membrane. Finally, a hypothetical signaling mechanism from the photoactive PQ pool to the PQ biosynthesis could explain the decreased amount of total PQ observed in *abc1k3* (**Figure 8**). Overall, the ABC1K1/ABC1K3 mechanism, by regulating lipid partitioning, could be important to allow plastid plasticity that is essential for the progression into different developmental stages of the plant life.

DATA AVAILABILITY STATEMENT

The raw data supporting the conclusions of this article will be made available by the authors, without undue reservation, to any qualified researcher.

AUTHOR CONTRIBUTIONS

TP, VS, PL, and FK designed the experiments. TP, JC, RP, BK, VS, PL, MH, and GF performed all the experiments. TP, VS, PL, MH, GF, and FK contributed to the analysis and the interpretation of the results. TP, PL, MH, GF, and FK wrote the manuscript.

FUNDING

This work was supported by the Swiss National Science Foundation (SNSF) grants 31003A_156998, 31003A_179417, and 31003A_176191. GF acknowledges support from the LabEX GRAL, ANR-10-LABX-49-01 financed within the University Grenoble Alpes graduate school (Ecoles Universitaires de Recherche) CBH-EUR-GS (ANR-17-EURE-0003).

ACKNOWLEDGMENTS

The Laboratory of Plant Physiology thanks Véronique Douet for her technical support during the project.

SUPPLEMENTARY MATERIAL

The Supplementary Material for this article can be found online at: https://www.frontiersin.org/articles/10.3389/fpls.2020.00337/full#supplementary-material

REFERENCES

Allen, J. F., Bennett, J., Steinback, K. E., and Arntzen, C. J. (1981). Chloroplast protein phosphorylation couples plastoquinone redox state to distribution of excitation energy between photosystems. *Nature* 291, 25–29. doi: 10.1038/291025a0

Armbruster, U., Labs, M., Pribil, M., Viola, S., Xu, W., Scharfenberg, M., et al. (2013). *Arabidopsis* CURVATURE THYLAKOID1 proteins modify thylakoid architecture by inducing membrane curvature. *Plant Cell* 25, 2661–2678. doi: 10.1105/tpc.113.113118

Aro, E. M., and Ohad, I. (2003). Redox regulation of thylakoid protein phosphorylation. *Antioxid. Redox Signal.* 5, 55–67. doi: 10.1089/152308603321223540

Aro, E. M., Virgin, I., and Andersson, B. (1993). Photoinhibition of photosystem II. Inactivation, protein damage and turnover. *Biochim. Biophys. Acta* 1143, 113–134. doi: 10.1016/0005-2728(93)90134-2

Austin, J. R. II, Frost, E., Vidi, P. A., Kessler, F., and Staehelin, L. A. (2006). Plastoglobules are lipoprotein subcompartments of the chloroplast that are permanently coupled to thylakoid membranes and contain biosynthetic enzymes. *Plant Cell* 18, 1693–1703. doi: 10.1105/tpc.105.039859

Bellafiore, S., Barneche, F., Peltier, G., and Rochaix, J. D. (2005). State transitions and light adaptation require chloroplast thylakoid protein kinase STN7. *Nature* 433, 892–895. doi: 10.1038/nature03286

Blackwell, M., Gibas, C., Gygax, S., Roman, D., and Wagner, B. (1994). The plastoquinone diffusion coefficient in chloroplasts and its mechanistic implications. *Biochim. Biophys. Acta Bioenerg.* 1183, 533–543. doi: 10.1016/0005-2728(94)90081-7

Block, A., Fristedt, R., Rogers, S., Kumar, J., Barnes, B., Barnes, J., et al. (2013). Functional modeling identifies paralogous solanesyl-diphosphate synthases that assemble the side chain of plastoquinone-9 in plastids. *J. Biol. Chem.* 288, 27594–27606. doi: 10.1074/jbc.M113.492769

Bonardi, V., Pesaresi, P., Becker, T., Schleiff, E., Wagner, R., Pfannschmidt, T., et al. (2005). Photosystem II core phosphorylation and photosynthetic acclimation require two different protein kinases. *Nature* 437, 1179–1182. doi: 10.1038/nature04016

Bousquet, I., Dujardin, G., and Slonimski, P. P. (1991). ABC1, a novel yeast nuclear gene has a dual function in mitochondria: it suppresses a cytochrome b mRNA translation defect and is essential for the electron transfer in the bc 1 complex. *EMBO J.* 10, 2023–2031. doi: 10.1002/j.1460-2075.1991.tb07732.x

Brasseur, G., Tron, P., Dujardin, G., Slonimski, P. P., and Brivet-Chevillotte, P. (1997). The nuclear ABC1 gene is essential for the correct conformation and functioning of the cytochrome bc1 complex and the neighbouring complexes II and IV in the mitochondrial respiratory chain. *Eur. J. Biochem.* 246, 103–111. doi: 10.1111/j.1432-1033.1997.t01-1-00103.x

Dall'Osto, L., Caffarri, S., and Bassi, R. (2005). A mechanism of nonphotochemical energy dissipation, independent from PsbS, revealed by a conformational

change in the antenna protein CP26. *Plant Cell* 17, 1217–1232. doi: 10.1105/tpc.104.030601

Dumas, L., Zito, F., Blangy, S., Auroy, P., Johnson, X., Peltier, G., et al. (2017). A stromal region of cytochrome b6f subunit IV is involved in the activation of the Stt7 kinase in *Chlamydomonas*. *Proc. Natl. Acad. Sci. U.S.A.* 114, 12063–12068. doi: 10.1073/pnas.1713343114

Ferretti, U., Ciura, J., Ksas, B., Rac, M., Sedlarova, M., Kruk, J., et al. (2018). Chemical quenching of singlet oxygen by plastoquinols and their oxidation products in *Arabidopsis*. *Plant J.* 95, 848–861. doi: 10.1111/tpj.13993

Finazzi, G., Rappaport, F., Furia, A., Fleischmann, M., Rochaix, J. D., Zito, F., et al. (2002). Involvement of state transitions in the switch between linear and cyclic electron flow in Chlamydomonas reinhardtii. *EMBO Rep.* 3, 280–285. doi: 10.1093/embo-reports/kvf047

Fristedt, R., Willig, A., Granath, P., Crèvecoeur, M., Rochaix, J. D., and Vener, A. V. (2009). Phosphorylation of photosystem II controls functional macroscopic folding of photosynthetic membranes in *Arabidopsis*. *Plant Cell* 21, 3950–3964. doi: 10.1105/tpc.109.069435

Gaude, N., Bréhélin, C., Tischendorf, G., Kessler, F., and Dormann, P. (2007). Nitrogen deficiency in *Arabidopsis* affects galactolipid composition and gene expression and results in accumulation of fatty acid phytyl esters. *Plant J.* 49, 729–739. doi: 10.1111/j.1365-313x.2006.02992.x

Gong, H. S., and Ohad, I. (1991). The PQ/PQH2 ratio and occupancy of photosystem II-QB site by plastoquinone control the degradation of D1 protein during photoinhibition in vivo. *J. Biol. Chem.* 266, 21293–21299.

Gruszka, J., Pawlak, A., and Kruk, J. (2008). Tocochromanols, plastoquinol, and other biological prenyllipids as singlet oxygen quenchers-determination of singlet oxygen quenching rate constants and oxidation products. *Free Radic. Biol. Med.* 45, 920–928. doi: 10.1016/j.freeradbiomed.2008.06.025

Hall, J. D., Barr, R., Al-Abbas, A. H., and Crane, F. L. (1972). The Ultrastructure of chloroplasts in mineral-deficient maize leaves. *Plant Physiol.* 50, 404–409. doi: 10.1104/pp.50.3.404

Houyoux, P.-A., Ghysels, B., Lecler, R., and Franck, F. (2011). Interplay between non-photochemical plastoquinone reduction and re-oxidation in pre-illuminated *Chlamydomonas reinhardtii*: a chlorophyll fluorescence study. *Photosynth. Res.* 110:13. doi: 10.1007/s11120-011-9686-5

Huang, H., Yang, M., Su, Y., Qu, L., and Deng, X. W. (2015). *Arabidopsis* atypical kinases ABC1K1 and ABC1K3 act oppositely to cope with photodamage under red light. *Mol Plant* 8, 1122–1124. doi: 10.1016/j.molp.2015.04.003

Ivanov, A. G., Rosso, D., Savitch, L. V., Stachula, P., Rosembert, M., Oquist, G., et al. (2012). Implications of alternative electron sinks in increased resistance of PSII and PSI photochemistry to high light stress in cold-acclimated *Arabidopsis thaliana*. *Photosynth. Res.* 113, 191–206. doi: 10.1007/s11120-012-9769-y

Joet, T., Genty, B., Josse, E. M., Kuntz, M., Cournac, L., and Peltier, G. (2002). Involvement of a plastid terminal oxidase in plastoquinone oxidation as evidenced by expression of the *Arabidopsis thaliana* enzyme in tobacco. *J. Biol. Chem.* 277, 31623–31630. doi: 10.1074/jbc.m203538200

Joliot, P., and Finazzi, G. (2010). Proton equilibration in the chloroplast modulates multiphasic kinetics of nonphotochemical quenching of fluorescence in plants. *Proc. Natl. Acad. Sci. U.S.A.* 107, 12728–12733. doi: 10.1073/pnas.1006399107

Joliot, P., and Joliot, A. (2006). Cyclic electron flow in C3 plants. *Biochim. Biophys. Acta* 1757, 362–368. doi: 10.1016/j.bbabio.2006.02.018

Kalaji, H. M., Oukarroum, A., Alexandrov, V., Kouzmanova, M., Brestic, M., Zivcak, M., et al. (2014a). Identification of nutrient deficiency in maize and tomato plants by *in vivo* chlorophyll *a* fluorescence measurements. *Plant Physiol. Biochem.* 81, 16–25. doi: 10.1016/j.plaphy.2014.03.029

Kalaji, H. M., Schansker, G., Ladle, R. J., Goltsev, V., Bosa, K., Allakhverdiev, S. I., et al. (2014b). Frequently asked questions about in vivo chlorophyll fluorescence: practical issues. *Photosynth. Res.* 122, 121–158. doi: 10.1007/s11120-014-0024-6

Kanwischer, M., Porfirova, S., Bergmüller, E., and Dörmann, P. (2005). Alterations in tocopherol cyclase activity in transgenic and mutant plants of *Arabidopsis* affect tocopherol content, tocopherol composition, and oxidative stress. *Plant Physiol.* 137, 713–723. doi: 10.1104/pp.104.054908

Karpinski, S., Reynolds, H., Karpinska, B., Wingsle, G., Creissen, G., and Mullineaux, P. (1999). Systemic signaling and acclimation in response to excess excitation energy in *Arabidopsis*. *Science* 284, 654–657. doi: 10.1126/science.284.5414.654

Kirchhoff, H. (2014). Diffusion of molecules and macromolecules in thylakoid membranes. *Biochim. Biophys. Acta Bioenerg.* 1837, 495–502. doi: 10.1016/j.bbabio.2013.11.003

Kirchhoff, H., Horstmann, S., and Weis, E. (2000). Control of the photosynthetic electron transport by PQ diffusion microdomains in thylakoids of higher plants. *Biochim. Biophys. Acta Bioenerg.* 1459, 148–168. doi: 10.1016/s0005-2728(00)00143-2

Kruk, J., and Karpinski, S. (2006). An HPLC-based method of estimation of the total redox state of plastoquinone in chloroplasts, the size of the photochemically active plastoquinone-pool and its redox state in thylakoids of *Arabidopsis*. *Biochim. Biophys. Acta* 1757, 1669–1675. doi: 10.1016/j.bbabio.2006.08.004

Ksas, B., Becuwe, N., Chevalier, A., and Havaux, M. (2015). Plant tolerance to excess light energy and photooxidative damage relies on plastoquinone biosynthesis. *Sci. Rep.* 5:10919. doi: 10.1038/srep10919

Ksas, B., Legeret, B., Ferretti, U., Chevalier, A., Pospisil, P., Alric, J., et al. (2018). The plastoquinone pool outside the thylakoid membrane serves in plant photoprotection as a reservoir of singlet oxygen scavengers. *Plant Cell Environ.* 41, 2277–2287. doi: 10.1111/pce.13202

Lavergne, J., and Joliot, P. (1991). Restricted diffusion in photosynthetic membranes. *Trends Biochem. Sci.* 16, 129–134. doi: 10.1016/0968-0004(91)90054-y

Lennon, A. M., Prommeenate, P., and Nixon, P. J. (2003). Location, expression and orientation of the putative chlororespiratory enzymes, Ndh and IMMUTANS, in higher-plant plastids. *Planta* 218, 254–260. doi: 10.1007/s00425-003-1111-7

Li, L., Aro, E. M., and Millar, A. H. (2018). Mechanisms of photodamage and protein turnover in photoinhibition. *Trends Plant Sci.* 23, 667–676. doi: 10.1016/j.tplants.2018.05.004

Li, Z., Wakao, S., Fischer, B. B., and Niyogi, K. K. (2009). Sensing and responding to excess light. *Annu. Rev. Plant Biol.* 60, 239–260. doi: 10.1146/annurev.arplant.58.032806.103844

Lichtenthaler, H. K., and Peveling, E. (1966). Plastoglobuli in different types of plastids from *Allium cepa* L. *Planta* 72, 1–13. doi: 10.1007/BF00388140

Lippold, F., vom Dorp, K., Abraham, M., Holzl, G., Wewer, V., Yilmaz, J. L., et al. (2012). Fatty acid phytyl ester synthesis in chloroplasts of *Arabidopsis*. *Plant Cell* 24, 2001–2014. doi: 10.1105/tpc.112.095588

Lohscheider, J. N., and Rio Bartulos, C. (2016). Plastoglobules in algae: a comprehensive comparative study of the presence of major structural and functional components in complex plastids. *Mar. Genomics* 28, 127–136. doi: 10.1016/j.margen.2016.06.005

Lundquist, P. K., Poliakov, A., Bhuiyan, N. H., Zybailov, B., Sun, Q., and van Wijk, K. J. (2012). The functional network of the *Arabidopsis* plastoglobule proteome based on quantitative proteomics and genome-wide coexpression analysis. *Plant Physiol.* 158, 1172–1192. doi: 10.1104/pp.111.193144

Lundquist, P. K., Poliakov, A., Giacomelli, L., Friso, G., Appel, M., McQuinn, R. P., et al. (2013). Loss of plastoglobule kinases ABC1K1 and ABC1K3 causes conditional degreening, modified prenyl-lipids, and recruitment of the jasmonic acid pathway. *Plant Cell* 25, 1818–1839. doi: 10.1105/tpc.113.111120

Martinis, J., Glauser, G., Valimareanu, S., and Kessler, F. (2013). A chloroplast ABC1-like kinase regulates vitamin E metabolism in *Arabidopsis*. *Plant Physiol.* 162, 652–662. doi: 10.1104/pp.113.218644

Martinis, J., Glauser, G., Valimareanu, S., Stettler, M., Zeeman, S. C., Yamamoto, H., et al. (2014). ABC1K1/PGR6 kinase: a regulatory link between photosynthetic activity and chloroplast metabolism. *Plant J.* 77, 269–283. doi: 10.1111/tpj.12385

Miyao, M. (1994). Involvement of active oxygen species in degradation of the D1 protein under strong illumination in isolated subcomplexes of photosystem II. *Biochemistry* 33, 9722–9730. doi: 10.1021/bi00198a043

Moejes, F. W., Matuszynska, A., Adhikari, K., Bassi, R., Cariti, F., Cogne, G., et al. (2017). A systems-wide understanding of photosynthetic acclimation in algae and higher plants. *J. Exp. Bot.* 68, 2667–2681. doi: 10.1093/jxb/erx137

Mollet, J., Delahodde, A., Serre, V., Chretien, D., Schlemmer, D., Lombes, A., et al. (2008). CABC1 gene mutations cause ubiquinone deficiency with cerebellar ataxia and seizures. *Am. J. Hum. Genet.* 82, 623–630. doi: 10.1016/j.ajhg.2007.12.022

Müller, P., Li, X. P., and Niyogi, K. K. (2001). Non-photochemical quenching. A response to excess light energy. *Plant Physiol.* 125, 1558–1566. doi: 10.1104/pp.125.4.1558

Munné-Bosch, S., and Alegre, L. (2002). Plant aging increases oxidative stress in chloroplasts. *Planta* 214, 608–615. doi: 10.1007/s004250100646

Nilkens, M., Kress, E., Lambrev, P., Miloslavina, Y., Müller, M., Holzwarth, A. R., et al. (2010). Identification of a slowly inducible zeaxanthin-dependent component of non-photochemical quenching of chlorophyll fluorescence generated under steady-state conditions in *Arabidopsis*. *Biochim. Biophys. Acta Bioenerg.* 1797, 466–475. doi: 10.1016/j.bbabio.2010.01.001

Nowicka, B., and Kruk, J. (2012). Plastoquinol is more active than alpha-tocopherol in singlet oxygen scavenging during high light stress of *Chlamydomonas reinhardtii*. *Biochim. Biophys. Acta* 1817, 389–394. doi: 10.1016/j.bbabio.2011.12.002

Pesaresi, P., Hertle, A., Pribil, M., Schneider, A., Kleine, T., and Leister, D. (2010). Optimizing photosynthesis under fluctuating light. *Plant Signal. Behav.* 5, 21–25. doi: 10.4161/psb.5.1.10198

Pesaresi, P., Pribil, M., Wunder, T., and Leister, D. (2011). Dynamics of reversible protein phosphorylation in thylakoids of flowering plants: the roles of STN7, STN8 and TAP38. *Biochim. Biophys. Acta* 1807, 887–896. doi: 10.1016/j.bbabio.2010.08.002

Pfannschmidt, T. (2003). Chloroplast redox signals: how photosynthesis controls its own genes. *Trends Plant Sci.* 8, 33–41. doi: 10.1016/s1360-1385(02)00005-5

Pfannschmidt, T., Nilsson, A., and Allen, J. F. (1999). Photosynthetic control of chloroplast gene expression. *Nature* 397:625. doi: 10.1038/17624

Poon, W. W., Davis, D. E., Ha, H. T., Jonassen, T., Rather, P. N., and Clarke, C. F. (2000). Identification of *Escherichia coli* ubiB, a gene required for the first monooxygenase step in ubiquinone biosynthesis. *J. Bacteriol.* 182, 5139–5146. doi: 10.1128/jb.182.18.5139-5146.2000

Pralon, T., Shanmugabalaji, V., Longoni, P., Glauser, G., Ksas, B., Collombat, J., et al. (2019). Plastoquinone homoeostasis by *Arabidopsis* proton gradient regulation 6 is essential for photosynthetic efficiency. *Commun. Biol.* 2:220. doi: 10.1038/s42003-019-0477-4

Puthiyaveetil, S. (2011). A mechanism for regulation of chloroplast LHC II kinase by plastoquinol and thioredoxin. *FEBS Lett.* 585, 1717–1721. doi: 10.1016/j.febslet.2011.04.076

Puthiyaveetil, S., Ibrahim, I. M., and Allen, J. F. (2012). Oxidation-reduction signalling components in regulatory pathways of state transitions and photosystem stoichiometry adjustment in chloroplasts. *Plant Cell Environ.* 35, 347–359. doi: 10.1111/j.1365-3040.2011.02349.x

Rintamaki, E., Kettunen, R., and Aro, E. M. (1996). Differential D1 dephosphorylation in functional and photodamaged photosystem II centers. Dephosphorylation is a prerequisite for degradation of damaged D1. *J. Biol. Chem.* 271, 14870–14875. doi: 10.1074/jbc.271.25.14870

Rintamaki, E., Salonen, M., Suoranta, U. M., Carlberg, I., Andersson, B., and Aro, E. M. (1997). Phosphorylation of light-harvesting complex II and photosystem II core proteins shows different irradiance-dependent regulation in vivo. Application of phosphothreonine antibodies to analysis of thylakoid phosphoproteins. *J. Biol. Chem.* 272, 30476–30482. doi: 10.1074/jbc.272.48.30476

Rochaix, J. D. (2007). Role of thylakoid protein kinases in photosynthetic acclimation. *FEBS Lett.* 581, 2768–2775. doi: 10.1016/j.febslet.2007.04.038

Rochaix, J. D. (2011). Regulation of photosynthetic electron transport. *Biochim. Biophys. Acta* 1807, 375–383. doi: 10.1016/j.bbabio.2010.11.010

Rochaix, J. D. (2013). Redox regulation of thylakoid protein kinases and photosynthetic gene expression. *Antioxid. Redox Signal.* 18, 2184–2201. doi: 10.1089/ars.2012.5110

Rottet, S., Devillers, J., Glauser, G., Douet, V., Besagni, C., and Kessler, F. (2016). Identification of plastoglobules as a site of carotenoid cleavage. *Front. Plant Sci.* 7:1855. doi: 10.3389/fpls.2016.01855

Ruban, A. V. (2016). Nonphotochemical chlorophyll fluorescence quenching: mechanism and effectiveness in protecting plants from photodamage. *Plant Physiol.* 170, 1903–1916. doi: 10.1104/pp.15.01935

Ruban, A. V. (2018). Light harvesting control in plants. *FEBS Lett.* 592, 3030–3039. doi: 10.1002/1873-3468.13111

Shapiguzov, A., Chai, X., Fucile, G., Longoni, P., Zhang, L., and Rochaix, J. D. (2016). Activation of the Stt7/STN7 Kinase through dynamic interactions with the cytochrome b6f complex. *Plant Physiol.* 171, 82–92. doi: 10.1104/pp.15.01893

Shapiguzov, A., Ingelsson, B., Samol, I., Andres, C., Kessler, F., Rochaix, J. D., et al. (2010). The PPH1 phosphatase is specifically involved in LHCII dephosphorylation and state transitions in *Arabidopsis*. *Proc. Natl. Acad. Sci. U.S.A.* 107, 4782–4787. doi: 10.1073/pnas.0913810107

Shikanai, T., Munekage, Y., Shimizu, K., Endo, T., and Hashimoto, T. (1999). Identification and characterization of *Arabidopsis* mutants with reduced quenching of chlorophyll fluorescence. *Plant Cell Physiol.* 40, 1134–1142. doi: 10.1093/oxfordjournals.pcp.a029498

Spicher, L., Glauser, G., and Kessler, F. (2016). Lipid antioxidant and galactolipid remodeling under temperature stress in tomato plants. *Front. Plant Sci.* 7:167. doi: 10.3389/fpls.2016.00167

Steinmuller, D., and Tevini, M. (1985). Composition and function of plastoglobuli : 1. Isolation and purification from chloroplasts and chromoplasts. *Planta* 163, 201–207. doi: 10.1007/BF00393507

Stepien, P., and Johnson, G. N. (2018). Plastid terminal oxidase requires translocation to the grana stacks to act as a sink for electron transport. *Proc. Natl. Acad. Sci. U.S.A.* 115, 9634–9639. doi: 10.1073/pnas.1719070115

Stirbet, A., Lazár, D., Kromdijk, J., and Govindjee (2018). Chlorophyll *a* fluorescence induction: can just a one-second measurement be used to quantify abiotic stress responses? *Photosynthetica* 56, 86–104. doi: 10.1007/s11099-018-0770-3

Strasser, R. J., Tsimilli-Michael, M., Qiang, S., and Goltsev, V. (2010). Simultaneous in vivo recording of prompt and delayed fluorescence and 820-nm reflection changes during drying and after rehydration of the resurrection plant *Haberlea rhodopensis*. *Biochim. Biophys. Acta* 1797, 1313–1326. doi: 10.1016/j.bbabio.2010.03.008

Suzuki, N., Koussevitzky, S., Mittler, R., and Miller, G. (2012). ROS and redox signalling in the response of plants to abiotic stress. *Plant Cell Environ.* 35, 259–270. doi: 10.1111/j.1365-3040.2011.02336.x

Sylak-Glassman, E. J., Malnoe, A., De Re, E., Brooks, M. D., Fischer, A. L., Niyogi, K. K., et al. (2014). Distinct roles of the photosystem II protein PsbS and zeaxanthin in the regulation of light harvesting in plants revealed by fluorescence lifetime snapshots. *Proc. Natl. Acad. Sci. U.S.A.* 111, 17498–17503. doi: 10.1073/pnas.1418317111

Taylor, A. O., and Craig, A. S. (1971). Plants under climatic stress: II. Low temperature, high light effects on chloroplast ultrastructure. *Plant Physiol.* 47, 719–725. doi: 10.1104/pp.47.5.719

Theis, J., and Schroda, M. (2016). Revisiting the photosystem II repair cycle. *Plant Signal. Behav.* 11:e1218587. doi: 10.1080/15592324.2016.1218587

Tikhonov, A. N. (2014). The cytochrome b6f complex at the crossroad of photosynthetic electron transport pathways. *Plant Physiol. Biochem.* 81, 163–183. doi: 10.1016/j.plaphy.2013.12.011

Tikkanen, M., Gollan, P. J., Suorsa, M., Kangasjarvi, S., and Aro, E. M. (2012). STN7 operates in retrograde signaling through controlling redox balance in the electron transfer chain. *Front. Plant Sci.* 3:277. doi: 10.3389/fpls.2012.00277

Tikkanen, M., Nurmi, M., Kangasjarvi, S., and Aro, E. M. (2008). Core protein phosphorylation facilitates the repair of photodamaged photosystem II at high light. *Biochim. Biophys. Acta* 1777, 1432–1437. doi: 10.1016/j.bbabio.2008.08.004

Tóth, S. Z., Schansker, G., and Strasser, R. J. (2007). A non-invasive assay of the plastoquinone pool redox state based on the OJIP-transient. *Photosynth. Res.* 93, 193. doi: 10.1007/s11120-007-9179-8

Trotta, A., Bajwa, A. A., Mancini, I., Paakkarinen, V., Pribil, M., and Aro, E. M. (2019). The role of phosphorylation dynamics of CURVATURE THYLAKOID 1B in plant thylakoid membranes. *Plant Physiol.* 181, 1615–1631. doi: 10.1104/pp.19.00942

Trotta, A., Suorsa, M., Rantala, M., Lundin, B., and Aro, E. M. (2016). Serine and threonine residues of plant STN7 kinase are differentially phosphorylated upon changing light conditions and specifically influence the activity and stability of the kinase. *Plant J.* 87, 484–494. doi: 10.1111/tpj.13213

Trouillard, M., Shahbazi, M., Moyet, L., Rappaport, F., Joliot, P., Kuntz, M., et al. (2012). Kinetic properties and physiological role of the plastoquinone terminal oxidase (PTOX) in a vascular plant. *Biochim. Biophys. Acta* 1817, 2140–2148. doi: 10.1016/j.bbabio.2012.08.006

van Wijk, K. J., and Kessler, F. (2017). Plastoglobuli: plastid microcompartments with integrated functions in metabolism, plastid developmental transitions, and environmental adaptation. *Annu. Rev. Plant Biol.* 68, 253–289. doi: 10.1146/annurev-arplant-043015-111737

Vasilikiotis, C., and Melis, A. (1994). Photosystem II reaction center damage and repair cycle: chloroplast acclimation strategy to irradiance stress. *Proc. Natl. Acad. Sci. U.S.A.* 91, 7222–7226. doi: 10.1073/pnas.91.15.7222

Vidi, P. A., Kanwischer, M., Baginsky, S., Austin, J. R., Csucs, G., Dormann, P., et al. (2006). Tocopherol cyclase (VTE1) localization and vitamin E accumulation in chloroplast plastoglobule lipoprotein particles. *J. Biol. Chem.* 281, 11225–11234. doi: 10.1074/jbc.m511939200

Wetzel, C. M., Jiang, C. Z., Meehan, L. J., Voytas, D. F., and Rodermel, S. R. (1994). Nuclear-organelle interactions: the immutans variegation mutant of *Arabidopsis* is plastid autonomous and impaired in carotenoid biosynthesis. *Plant J.* 6, 161–175. doi: 10.1046/j.1365-313x.1994.6020161.x

Yamori, W., and Shikanai, T. (2016). Physiological functions of cyclic electron transport around photosystem I in sustaining photosynthesis and plant growth. *Annu. Rev. Plant Biol.* 67, 81–106. doi: 10.1146/annurev-arplant-043015-112002

Yang, M., Huang, H., Zhang, C., Wang, Z., Su, Y., Zhu, P., et al. (2016). *Arabidopsis* atypical kinase ABC1K1 is involved in red light-mediated development. *Plant Cell Rep.* 35, 1213–1220. doi: 10.1007/s00299-016-1953-7

Yokoyama, R., Yamamoto, H., Kondo, M., Takeda, S., Ifuku, K., Fukao, Y., et al. (2016). Grana-localized proteins, RIQ1 and RIQ2, affect the organization of light-harvesting complex II and grana stacking in *Arabidopsis*. *Plant Cell* 28, 2261–2275. doi: 10.1105/tpc.16.00296

Ytterberg, A. J., Peltier, J. B., and van Wijk, K. J. (2006). Protein profiling of plastoglobules in chloroplasts and chromoplasts. A surprising site for differential accumulation of metabolic enzymes. *Plant Physiol.* 140, 984–997. doi: 10.1104/pp.105.076083

Zbierzak, A. M., Kanwischer, M., Wille, C., Vidi, P. A., Giavalisco, P., Lohmann, A., et al. (2010). Intersection of the tocopherol and plastoquinol metabolic pathways at the plastoglobule. *Biochem. J.* 425, 389–399. doi: 10.1042/BJ20090704

Zechmann, B. (2019). Ultrastructure of plastids serves as reliable abiotic and biotic stress marker. *PLoS One* 14:e0214811. doi: 10.1371/journal.pone.0214811

Conflict of Interest: The authors declare that the research was conducted in the absence of any commercial or financial relationships that could be construed as a potential conflict of interest.

Copyright © 2020 Pralon, Collombat, Pipitone, Ksas, Shanmugabalaji, Havaux, Finazzi, Longoni and Kessler. This is an open-access article distributed under the terms of the Creative Commons Attribution License (CC BY). The use, distribution or reproduction in other forums is permitted, provided the original author(s) and the copyright owner(s) are credited and that the original publication in this journal is cited, in accordance with accepted academic practice. No use, distribution or reproduction is permitted which does not comply with these terms.

frontiers in Plant Science

REVIEW
published: 21 April 2020
doi: 10.3389/fpls.2020.00455

Lipid Dependence of Xanthophyll Cycling in Higher Plants and Algae

Reimund Goss[1] and Dariusz Latowski[2]*

[1] Department of Plant Physiology, Institute of Biology, Leipzig University, Leipzig, Germany, [2] Department of Plant Physiology and Biochemistry, Faculty of Biochemistry, Biophysics and Biotechnology, Jagiellonian University, Kraków, Poland

The xanthophyll cycles of higher plants and algae represent an important photoprotection mechanism. Two main xanthophyll cycles are known, the violaxanthin cycle of higher plants, green and brown algae and the diadinoxanthin cycle of Bacillariophyceae, Xanthophyceae, Haptophyceae, and Dinophyceae. The forward reaction of the xanthophyll cycles consists of the enzymatic de-epoxidation of violaxanthin to antheraxanthin and zeaxanthin or diadinoxanthin to diatoxanthin during periods of high light illumination. It is catalyzed by the enzymes violaxanthin or diadinoxanthin de-epoxidase. During low light or darkness the back reaction of the cycle, which is catalyzed by the enzymes zeaxanthin or diatoxanthin epoxidase, restores the epoxidized xanthophylls by a re-introduction of the epoxy groups. The de-epoxidation reaction takes place in the lipid phase of the thylakoid membrane and thus, depends on the nature, three dimensional structure and function of the thylakoid lipids. As the xanthophyll cycle pigments are usually associated with the photosynthetic light-harvesting proteins, structural re-arrangements of the proteins and changes in the protein-lipid interactions play an additional role for the operation of the xanthophyll cycles. In the present review we give an introduction to the lipid and fatty acid composition of thylakoid membranes of higher plants and algae. We introduce the readers to the reaction sequences, enzymes and function of the different xanthophyll cycles. The main focus of the review lies on the lipid dependence of xanthophyll cycling. We summarize the current knowledge about the role of lipids in the solubilization of xanthophyll cycle pigments. We address the importance of the three-dimensional lipid structures for the enzymatic xanthophyll conversion, with a special focus on non-bilayer lipid phases which are formed by the main thylakoid membrane lipid monogalactosyldiacylglycerol. We additionally describe how lipids and light-harvesting complexes interact in the thylakoid membrane and how these interactions can affect the structure of the thylakoids. In a dedicated chapter we offer a short overview of current membrane models, including the concept of membrane domains. We then use these concepts to present a model of the operative xanthophyll cycle as a transient thylakoid membrane domain which is formed during high light illumination of plants or algal cells.

Keywords: fatty acid, lipid, MGDG, thylakoid membrane domain, violaxanthin de-epoxidase, xanthophyll cycle

OPEN ACCESS

Edited by:
Yoshitaka Nishiyama, Saitama University, Japan

Reviewed by:
Koichi Kobayashi, Osaka Prefecture University, Japan
Alexei E. Solovchenko, Lomonosov Moscow State University, Russia

****Correspondence:***
Reimund Goss
rgoss@rz.uni-leipzig.de

Specialty section:
This article was submitted to Plant Physiology, a section of the journal Frontiers in Plant Science

Received: *25 February 2020*
Accepted: *27 March 2020*
Published: *21 April 2020*

Citation:
Goss R and Latowski D (2020) Lipid Dependence of Xanthophyll Cycling in Higher Plants and Algae. Front. Plant Sci. 11:455. doi: 10.3389/fpls.2020.00455

INTRODUCTION

Xanthophyll cycles, which consist of the de-epoxidation of epoxy-xanthophylls during high light and the epoxidation of epoxy-free xanthophylls during low light or darkness, are found in all eukaryotic photoautotrophs (for reviews see Goss and Jakob, 2010; Niyogi and Truong, 2013; Goss and Lepetit, 2015). The xanthophyll cycles act as an important protection mechanism against damage of the photosynthetic apparatus by supersaturating light conditions (for reviews see Horton, 2014; Ruban, 2016). The main part of photoprotection provided by the xanthophyll cycles operates on the time-scale of minutes and thus allows the plants to react to short-term changes of the light intensities in their natural environment (Demmig-Adams and Adams, 2006; Demmig-Adams et al., 2014). For higher plants fast fluctuations of the light intensity can be induced by clouds or by rapid changes of the leaf coverage in shaded environments such as the tropical rainforests. For algae even moderate water mixing can result in a rapid change of the light intensity from full sunlight to almost complete darkness. In addition, tidal changes affect the light exposure of those species inhabiting the coastal regions. Besides the fast photoprotection the xanthophyll cycles provide long-term protection which lasts for days, weeks or even months (Demmig-Adams and Adams, 2006; Demmig-Adams et al., 2014). These long-lasting photoprotection components can be observed in evergreen plant species which are exposed to prolonged environmental stress like the combination of cold temperatures and high light intensities during the winter months.

The observation that changes in the light intensities lead to inter-conversions of specific leaf xanthophylls dates back to the late 1950s/early 1960s (Hager, 1957; Saphozhnikov et al., 1957; Yamamoto et al., 1962). These first experiments revealed that the xanthophyll violaxanthin (Vx) is converted to the intermediate xanthophyll antheraxanthin (Ax) and then finally to zeaxanthin (Zx) during high light illumination. Later, it was demonstrated that darkness or low light lead to the reversal of the light-driven xanthophyll inter-conversions (Hager, 1967a) and the term Vx cycle was introduced (section Types of Xanthophyll Cycles). In addition, the existence of a second xanthophyll cycle, namely the diadinoxanthin (Ddx) cycle, in several groups of algae was reported (Hager and Stransky, 1970; Stransky and Hager, 1970). Newer measurements have shown that, besides the dominant Vx- and Ddx cycles, further less common light-driven cyclic inter-conversions of xanthophylls exist (Rabinowitch et al., 1975; Goss et al., 1998; Bungard et al., 1999). The following investigations were concerned with the characteristics of the enzymes which carry out the de-epoxidation and epoxidation reactions such as pH-optimum and co-substrate requirements (Hager, 1967a,b; section Reaction Sequences and Xanthophyll Cycle Enzymes). With regard to the function of the xanthophyll cycles it took until the late 1980s that a connection between the conversion of Vx to Zx and the quenching of chlorophyll a fluorescence, which indicates a thermal dissipation of excitation energy, could be obtained and described (Demmig et al., 1987, 1988, section Function of Xanthophyll Cycles). Since then numerous studies have dealt with this process which was called NPQ (reviewed in Horton, 2014; Ruban, 2016) and even today work on the molecular mechanism of NPQ in higher plants and algae represents an important research topic. With respect to the localization of the xanthophyll cycle pigments it was clear from the beginning that the pigments are located within the chloroplast. Later studies have presented evidence that within the plastidic thylakoid membranes the xanthophyll cycle pigments are associated with the light-harvesting complexes of the photosystems (Bassi et al., 1993; Ruban et al., 1994, section Localization of Xanthophyll Cycle Pigments in the Thylakoid Membrane). Regarding the main topic of the present review, i.e., the influence of lipids on the operation of the xanthophyll cycles, first evidence that the main thylakoid membrane monogalactosyldiacylglycerol (MGDG) plays an important role in the conversion of Vx to Ax and Zx dates back to the 1970s (Yamamoto and Higashi, 1978, sections Lipid Classes and Lipids as Solvents for Xanthophyll Cycle Pigments). Later measurements demonstrated that the thylakoid membrane lipids, and especially MGDG, act as solvents of the xanthophyll cycle pigments (Latowski et al., 2004; Goss et al., 2005, section Lipids as Solvents for Xanthophyll Cycle Pigments) and that special three-dimensional lipid structures or phases, i.e., non-bilayer lipid phases, are needed for the efficient operation of the xanthophyll cycles of higher plants and algae (Latowski et al., 2002, 2004; Goss et al., 2005, 2007, sections Three Dimensional Structures of Lipids and Role of Non-bilayer Lipid Phases for Xanthophyll Cycling). Additional investigations could show that the xanthophyll cycle pigments are not only associated with the light-harvesting proteins via special protein binding sites but also exist in lipid shields surrounding the complexes (Lepetit et al., 2010; Schaller et al., 2010; section Localization of Non-bilayer Lipid Phases in the Thylakoid Membrane). Recent research on the lipid dependence of xanthophyll cycling has focused on the localization of the non-bilayer lipid phases within the thylakoid membrane (Garab et al., 2017, section Localization of Non-bilayer Phases Involved in Xanthophyll Cycling) and how these structures are formed during high light illumination (Goss et al., 2007; Jahns et al., 2009, section Formation of Non-bilayer Lipid Phases by Structural Changes of Light-Harvesting Proteins). Models describing the operation of the xanthophyll cycle within the thylakoid membrane have also included information from the newest concepts on the structure and function of biological membranes (Goni, 2014; Nicholson, 2014, section The Xanthophyll Cycle Membrane Domain in the Light of Recent Membrane Models).

LIPID COMPOSITION OF THYLAKOID MEMBRANES OF HIGHER PLANTS AND ALGAE

Lipid Classes

One of the most important biological functions of lipids is the formation of membranes within the cell and the cell organelles. In plant cells the largest membrane system is the thylakoid membrane within the chloroplast. Thylakoid membranes, like the inner membranes of mitochondria, are characterized by a

high protein per lipid ratio which already indicates that the thylakoid lipids play an important role not only as membrane building blocks, but also as regulators of the structure and function of both integral and peripheral membrane proteins, including the photosynthetic complexes or the xanthophyll cycle enzymes (Krauss, 2001; Kirchhoff et al., 2002; Kobayashi et al., 2016, see also section Xanthophyll Cycles of Higher Plants and Algae). In the thylakoid membranes representatives of the following three lipid classes are present: glycosylglycerol lipids (GGLs), glycerophospholipids (GPs), and prenol lipids (PRs). Both GGL and GP molecules are characterized by the presence of two fatty acyl residues and one trihydric alcohol, namely glycerol. The main difference between these two lipid groups is the presence of a phosphate residue attached to glycerol in GPs, whereas in GGL molecules one or more sugar residues are directly associated with glycerol through glycosidic bonds (Li-Beisson et al., 2016). PRs also represent an important group of thylakoid lipids. They include, among others, quinones such as plastoquinone, phylloquinone (vitamin K_1) or tocopherols, as well as isoprenoids such as the carotenoids or the phytol chains of the chlorophyll molecules (Li-Beisson et al., 2016). PRs, and especially carotenoids, play an important role for the variability of the thylakoid lipid composition and can be used for the classification of various groups of algae.

While the thylakoid membranes of different photoautotrophs may differ in the nature of their prenol lipids, the other lipid classes appear to be comparable for different types of thylakoids. Differences are not observed in the general structure of the different lipid classes but rather in their fatty acid (FA) composition and their contribution to the total thylakoid membrane lipid. The most common lipids of thylakoid membranes are three types of GGLs and one representative of the GPs (**Figure 1**). Among the lipids belonging to the GGLs two lipids, namely digalactosyldiacylglycerol (DGDG) and monogalactosyldiacylglycerol (MGDG), contain a galactopyranosyl residue, whereas the sulfolipid sulfoquinovosyldiacylglycerol (SQDG) carries a glucopyranosyl residue with a sulfonic group at the C6 position of the glucose residue. The first galactose residues of MGDG and DGDG are β-anomeric forms, while the second galactose of DGDG, as well as the glucose residue of SQDG are α-sugars (Hölzl and Dörmann, 2019). In addition to MGDG, DGDG, and SQDG phosphatidylglycerol (PG), a lipid belonging to the class of GPs, is present in the thylakoid membrane (Harwood and Guschina, 2009; **Figure 1**). While DGDG and MGDG are neutral lipids, SQDG and PG are negatively charged due to the presence of the sulfate and phosphate residues, respectively (Boudiere et al., 2014). The presence of three other representatives of the GPs, namely phosphatidylinositol (PI), phosphatidylcholine (PC), and in the case of the green alga *Chlamydomonas reinhardii* phosphatidylethanolamine (PE), in thylakoid membranes has been proposed. However, it is still under discussion if these lipids really represent specific components of the inner thylakoid membrane. While in all thylakoids isolated from both plants and algae PI was commonly detected with concentrations up to 5% of the total membrane lipid, it is not clear whether PC and PE simply represent contaminations of thylakoid preparations with lipids from membranes rich in GPs, such as cellular or mitochondrial membranes. In addition, nothing is known so far about the putative role of these three GPs in photosynthesis (Boudiere et al., 2014).

Whereas the presence of PI, and especially that of PC or PE, in thylakoid membranes still needs verification, MGDG, DGDG, SQDG, and PG unequivocally represent the typical lipids of all oxygenic photosynthetic membranes, ranging from cyanobacteria to thylakoids of algae and plants (Boudiere et al., 2014; Kobayashi et al., 2016). Among these four thylakoid lipids, MGDG contributes up to 50% to the total higher

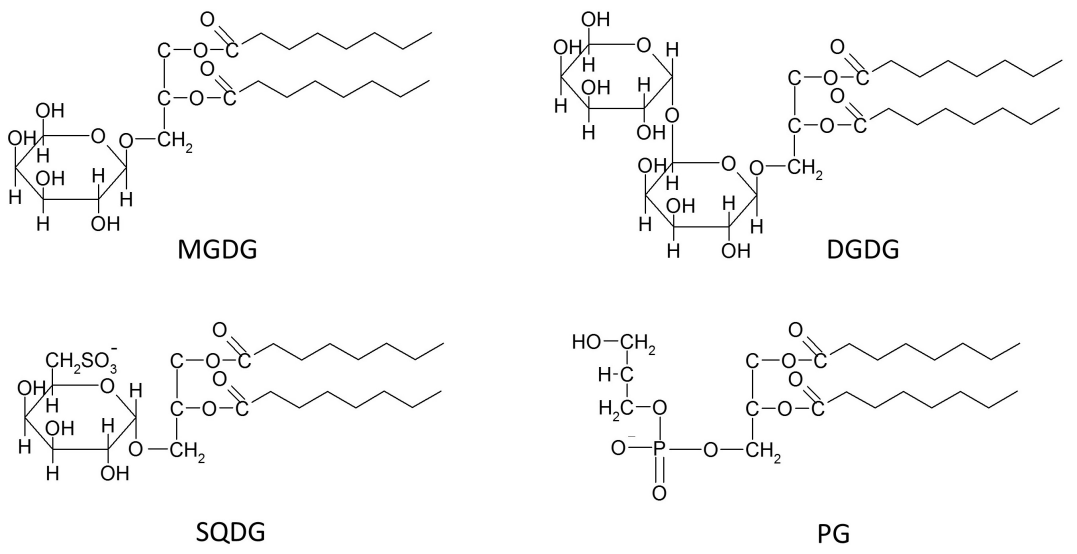

FIGURE 1 | Schematic structures of the four main thylakoid membrane lipids, i.e., the three glycosylglycerol lipids (GGLs) monogalactosyldiacylglycerol (MGDG), digalactosyldiacylglycerol (DGDG) and sulfoquinovosyldiacylglycerol (SQDG), and the one glycerophospholipid (GP) phosphatidylglycerol (PG).

plant membrane lipid, DGDG contributes approximately 25%, whereas the content of PG reaches up to 10% and SQDG oscillates in the range from about 2 to 20%. Despite the fact that SQDG is widely considered as the least concentrated of the four main thylakoid lipids, many results have shown that especially the SQDG levels are highly variable in response to different environmental conditions. Thylakoid membranes of higher plants or marine cyanobacteria under phosphate depletion can show maximum levels of SQDG of up to 50 or even 70%, respectively. Additionally, under conditions of phosphate limitation, PG seems to be the only representative of the GP lipids with a content of solely 2% of the total membrane lipid of marine cyanobacteria (van Mooy et al., 2006; Shimojima, 2011; Boudiere et al., 2014). A replacement of PG by SQDG is commonly observed and is considered to be a ubiquitous phenomenon in photosynthetic organisms. Keeping constant the concentrations of the negatively charged lipids most likely ensures the stability of an anionic lipid environment within the photosynthetic membranes under phosphate limitation (Boudiere et al., 2014). With respect to function, SQDG appears to be important for the protection of PSII in halophytes. In general, the level of SQDG was found to be considerably higher in many salt treated halophytes, e.g., in *Aster tripolium*, *Sesuvium portulacastrum,* or *Crithmum maritimum*, although no changes in the sulfolipid contents were observed in glycophytes which were treated with different salt concentration (Ben Hamed et al., 2005; Ramani et al., 2006). In the light of these results it is possible that the high levels of SQDQ reported for various marine photoautotrophs represent an adaptation to the high salt concentration in their natural environment. In 2013 a small amount of a new negatively charged glycolipid was detected in several plant species under phosphorus depletion. The lipid was identified as glucuronosyldiacylglycerol (GlcADG), which contains a glucuronic acid instead of the glucose residue (Okazaki et al., 2013). GlcADG is synthesized by sulfoquinovosyltransferase SQD2, the same glycosyltransferase which is located in the inner envelope membrane of the chloroplast and is responsible for SQDG synthesis in plants and eukaryotic algae (Yu et al., 2002).

In general, the level of SQDG is significantly higher in cyanobacteria and algae than in plants. Within the algae diatoms, brown and red algae seem to be characterized by higher SQDG contents compared with the green algae. High concentrations of SQDG have been reported for the pennate diatom *Phaeodactylum tricornutum* and the centric diatoms *Cyclotella meneghiniana* and *Skeletonema* sp. (Goss et al., 2009; Yan et al., 2011; Lepetit et al., 2012). The high SQDG contents were especially obvious in thylakoid membranes isolated from cultures of *P. tricornutum* or *C. meneghiniana* which were grown under high light intensities (Lepetit et al., 2012). In these membranes SQDG represented the most abundant lipid and SQDG and PG contributed to more than 50% to the total membrane lipid. The ratio of neutral to negatively charged lipids was in the range between 1 and 2 whereas in higher plants and green algae values between 3 and 4 are typically observed. The data suggest a significantly higher negative charge of diatom thylakoid membranes compared to the thylakoids of higher plants or green algae. The significance of these extremely charged membranes for the diatom physiology is, however, still unknown (Vieler et al., 2007; Goss and Wilhelm, 2009).

Whereas SQDG and MGDG are almost undetectable in extraplastidic membranes of algae and plant cells, DGDG was shown to be able to substitute phospholipids in non-photosynthetic membranes, like the tonoplast (Andersson et al., 2005), the mitochondrial (Jouhet et al., 2004) or other plasma membranes (Andersson et al., 2003). Replacement of phospholipids by DGDG usually takes place under phosphate-deficient conditions (Härtel and Benning, 2000; Li et al., 2006). Under these limitations DGDG can amount to high concentrations and DGDG concentrations of up to 25% of the total membrane lipid were found in the plasma membranes and tonoplasts of oat root cells (Andersson et al., 2005). DGDG together with MGDG, seems to play a key role in the stabilization of chloroplast membranes under various kinds of environmental stresses such as drought, exposure to ozone, cold or heat stress, which generally result in an increase of the DGDG to MGDG ratio in the photosynthetic membrane (van Besouw and Wintermans, 1978; Heinz and Roughan, 1983; Heemskerk et al., 1986; Chen et al., 2006; Moellering et al., 2010; Moellering and Benning, 2011). This is not surprising, considering that MGDG is a substrate for DGDG synthases which belong to the glycosyltransferases and are upregulated by environmental stress like e.g., phosphate limitation. With respect to the role of MGDG, reduction of the MGDG concentrations of the thylakoid membrane by a down-regulation of MGDG synthases led to an impairment of the photosynthetic performance and photoautotrophic growth (Kobayashi et al., 2007). Moreover, in one of two MGDG-deficient mutants of *Arabidopsis thaliana*, *mgd1-1*, with about 40% less MGDG compared to the wild-type plant, a limitation of the Vx de-epoxidation to Ax and Zx was observed (see section Xanthophyll Cycles of Higher Plants and Algae). The reason for this limitation is an almost 40% reduction of the proton conductivity of the thylakoid membrane of the *mgd1-1* mutant under light stress (more than 1000 μmol photons m^{-2} s^{-1}, Aronsson et al., 2008). The lower MGDG concentrations of the *mgd1-1* mutant thylakoid membrane led to an increased permeability of the membrane for protons and thus a decreased lumen acidification, resulting in a decreased pH-dependent activation of the xanthophyll cycle enzyme Vx de-epoxidase (VDE, see section Xanthophyll Cycles of Higher Plants and Algae).

Besides the lipids described above, two further lipids were identified in the thylakoid membranes of the green alga *C. reinhardtii*. One of them, acylsulfoquinovosyldiacylglycerol belongs to the GGLs whereas the other lipid, diacylgyceryl-N-trimethylhomoserine (DGTS), is a representative of the betaine lipids. DGTS was also detected in several other species of green algae as well as in ferns and mosses, but it is unknown if this lipid really represents a genuine thylakoid membrane lipid (Goss and Wilhelm, 2009). Similarly, other exotic lipids, which are often characteristic for only one algal species, such as the betaine lipids DGTA (diacylglycerylhydroxymethyl-N,N,N-trimethyl-β-alanine) and DGCC (diacylglycerylcarboxyhydroxymethylcholine) are found

in brown algae or diatoms (Guschina and Harwood, 2006; Goss and Wilhelm, 2009).

However, in the case of *C. reinhardtii* it was not only demonstrated that DGTS represents a thylakoid lipid, but also that thylakoid DGTS is richer in trienes and C20 FAs than DGTS of other cellular membranes, which contains equal amounts of saturated and tetraene FAs (Janero and Barrnett, 1982). Interestingly, not only the composition of *C. reinhardtii* thylakoid membranes involves untypical lipids, but also the VDE of this algae seems to be unique (see also section Xanthophyll Cycles of Higher Plants and Algae). The enzyme is located at the stromal side of the thylakoid membrane and is related to a lycopene cyclase of photosynthetic bacteria but not to the typical VDE of plants or other algae (Li et al., 2016). Interestingly, the unique lipid and VDE composition of *C. reinhardtii* may be seen as one of the indicators of a strong relationship between the xanthophyll de-epoxidases and the lipid composition of the thylakoid membrane.

Fatty Acids

Both the cross-species acclimation and the species-specific adaptation of biological membranes to various environmental conditions are based not only on changes of the stoichiometry of the individual lipid classes but also on changes of the respective FA residues of the lipids.

In plant cells, plastids, including chloroplasts, play the most important role in these adaptation processes since they represent the organelles where about 95% of the total plant FAs are produced (Ohlrogge et al., 1979). The fundamental importance of FAs was shown by null mutations in many single locus genes of FA synthesis which resulted in plant death during gamete or embryo development. Mutations in genes responsible for the later steps of the GP lipid synthesis seem to be not as deleterious for the establishment of photosynthetically active chloroplasts like mutations in the genes for FA synthesis (Hölzl and Dörmann, 2019).

The first products of phosphatidic acid (PA) acylation in chloroplasts are mainly PAs with residues of oleic acid (18:1) at the sn-1 and palmitic acid (16:0) at the sn-2 position, because the plastidic acyltransferases are specific for 16:0 and 18:1 acyl groups (Frentzen et al., 1983). Subsequently, after dephosphorylation of PA to diacylglycerol (DAG), FA specific desaturases (FADs) form double bonds in the acyl groups. This results in the transformation of 18:1 into linoleic (18:2) and α-linolenic (18:3) acid and the conversion of 16:0 into hexadecenoic (16:1) and hexadecatrienoic (16:3) FA residues. These FAs are commonly found in thylakoid PG (especially 16:1) and MGDG (especially 16:3), as a result of the so-called prokaryotic pathway of FA incorporation into glycerolipids (Higashi and Saito, 2019). On this pathway FAs are directly integrated into the glycerol backbones within the thylakoid membranes. Another way to combine FAs with PA, the so-called eukaryotic pathway, takes place in the membranes of the endoplasmic reticulum (ER). DAGs synthesized within the ER are subsequently transported to the chloroplast to be converted into GGLs. Recently it was determined that under physiological conditions in *A. thaliana* approximately one half of the plastidic GGLs is formed via the prokaryotic pathway and the other half is synthesized within the eukaryotic pathway. However, the main representative of the thylakoid GPs, namely PG, is predominantly derived from the prokaryotic pathway. Moreover, *A. thaliana*, like about 12% of the Angiosperm species, belongs to the so-called 16:3 plants, i.e., plants, which under physiological growth conditions, contain more than 10% of the total MGDG pool with 16:3 and 18:3 FA residues (Higashi and Saito, 2019). Plant mutants, with decreased levels of 16:3 or 16:3 and 18:3 FAs, appeared to be more sensitive to low temperatures and expressed growth inhibition and leaf chlorosis at 6 but not at 22°C (Hölzl and Dörmann, 2019). Numerous plant species, including wheat and turf grasses, in which the prokaryotic pathway is not used for the synthesis of GGLs, are termed 18:3 plants. In the thylakoids of these plants GGLs are synthesized via the eukaryotic pathway and thus contain 18:3 at the sn-2 position, while GGLs with 16:3 FAs can only be found in trace amounts (Roughan and Slack, 1984; Mongrand et al., 1998; Higashi and Saito, 2019). Additionally, nowadays 468 plant species are known, whose leaf FA profile suggests a loss of the prokaryotic pathway during evolution (Mongrand et al., 1998). Moreover, in plants possessing both active pathways of PA acylation, the temperature was shown to play an important role in the balance between the prokaryotic and eukaryotic pathways. Decreases of the expression of important genes of the prokaryotic pathway during heat stress lead to reduced levels of 16:3 FAs in MGDG and DGDG at the sn-2 position (Higashi et al., 2015; Li et al., 2015). In addition, FAD8, which introduces double bonds at the ω-3 position of the saturated acyl chains of the MGDG molecule, is degraded under high temperatures (Matsuda et al., 2005). Heat-stress also leads to a hydrolization of the 18:3 FAs of MGDG by a chloroplast heat-inducible lipase (HIL1), which in this way initiates and contributes to the MGDG degradation under high temperatures. The concerted action of these mechanisms explains the decreased levels of MGDG and DGDG-bound polyunsaturated FAs (PUFAs) during heat stress (Higashi et al., 2018). Interestingly, in chloroplasts, the decrease of 18:3 FAs is accompanied by an increased concentration 18:2 acyl chains in the GGLs (Higashi and Saito, 2019).

Temperature is not the sole environmental factor resulting in modification of the FA composition of the thylakoid lipids. Thylakoid membrane lipids and the FAs bound to the lipids are involved in the protection against a great number of biotic and abiotic stresses generated by various environmental factors (Wang et al., 2014). Among the thylakoid lipids, MGDG plays a central role in these protection mechanisms. MGDG is highly enriched in 18:3 and 16:3 PUFAs whereas the other membrane lipids DGDG, SQDG, and PG also contain saturated FAs in the form of 16:0. MGDG seems to be involved in the protection against reactive oxygen species (ROS) and it has been suggested that MGDG molecules surrounding photosystem (PS) I and II act as efficient scavengers of $^1O_2$ as well as hydroxyl radicals which are mainly created within PSII (Schmid-Siegert et al., 2016). MGDG is furthermore engaged in a cyclic mechanism with antioxidative function. In this process lipid peroxidation products such as malondialdehyde (MDA) are formed within the GGL molecules, which, after self-regeneration, can again

be fragmented into MDA. This way, the PUFAs bound to the thylakoid membrane GGLs act as a sink for various types of ROS (Mène-Saffrané et al., 2009; Schmid-Siegert et al., 2016). Moreover, 18:3 FAs are postulated to act as direct non-enzymatic scavengers of ROS (Mène-Saffrané et al., 2009).

Besides the formation of MDA, oxidative stresses, including heat and high light stress, lead to a conversion of the lipid-bound PUFAs to lipid peroxides (LOOHs). This lipid peroxidation generates different types of harmful chemical components such as the secondary products of lipid peroxidation and ROS. Lipid peroxidation products subsequently cause protein cleavage, protein oxidation or crosslinking between proteins, lipids and proteins with lipids. The numerous molecules which provide protection against or are formed by the action of ROS and lipid peroxidation products within the thylakoid membrane include (i) large complexes, like the central PSII dimers which dissociate from the surrounding LHCs, (ii) smaller molecules, like the photodamaged D1 protein together with degraded zexanthin expoxidase (ZEP, see section Xanthophyll Cycles of Higher Plants and Algae), and finally (iii) small molecules, like the de-epoxidized xanthophylls of the xanthophyll cycle (see section Xanthophyll Cycles of Higher Plants and Algae). All of these molecules and processes require a free movement in the thylakoid membrane to exert their protective function (Jahns et al., 2009; Kirchhoff, 2014; Yamamoto, 2016). Free movement in the thylakoid membrane depends on the fluidity of the membrane which itself is determined by the structure and composition of the FAs bound to the thylakoid membrane lipids. Highly unsaturated FAs lead to a membrane in a more fluid state whereas a high concentration of saturated FAs increases the rigidity of the thylakoids. Thus, changes of the FA composition of thylakoid membrane lipids in response to various environmental stresses seem to play an important role in the remodeling and functional stabilization of the membranes and the integrated protection mechanisms. With regard to the FA composition it has become clear that photoautotrophs inhabiting different ecosystems show pronounced differences in the FA profiles of both MGDG and the other thylakoid lipids. While in general the FA composition of the thylakoid lipids of the majority of freshwater green algae is comparable to that of 16:3 plants, the algal lipids seem to be enriched in 16C PUFAs while the C18 PUFAs exhibit lower concentrations. On the other hand, marine green algae are rich in C18 PUFAs, whereas red algae show high contents of C20 PUFAs, such as the 20:5 eicosapentaenoic acid (EPA) or the 20:4 arachidonic acid (AA). High levels of both C18 and C20 PUFAs are also typical for brown algae (Goss and Wilhelm, 2009; Kumari et al., 2013).

In diatoms MGDG contains the main long-chain FA of diatoms, i.e., eicosapentaenoic acid (EPA, 20:5, Yongmanitchai and Ward, 1993; Yan et al., 2011; Dodson et al., 2013; Dodson et al., 2014). EPA is preferentially bound to the sn-1 position of the glycerol backbone whereas the sn-2 position is usually occupied by C16 FAs with varying degrees of unsaturation (16:1, 16:2, 16:3, 16:4). MGDG with C20:5 and C16:3 seems to represent the most abundant form of the diatom GGL. Besides the C20/C16 forms of MGDG, MGDG molecules with C16 FAs at both the sn-1 and sn-2 position can be observed. DGDG exhibits a comparable FA composition to MGDG and is also enriched in EPA (Yongmanitchai and Ward, 1993; Yan et al., 2011; Dodson et al., 2013, 2014). Like in the MGDG molecule EPA usually occupies the sn-1 position of DGDG while at the sn-2 position C16 FAs are observed. As it has been demonstrated for MGDG, DGDG forms with C16 FAs at both the sn-1 and sn-2 positions can be found and DGDG with C20:5 and C16:3 seems to represent the most abundant diatom DGDG molecule. Earlier studies have reported that a difference exists in the FA composition of centric and pennate diatoms and that in the pennate diatoms EPA is replaced by C18 FAs in the MGDG and DGDG molecules (Dodson et al., 2013). However, more recent studies have indicated that the differences in the FA composition of MGDG and DGDG of centric and pennate diatoms may be related to differences in their reaction to environmental temperatures and that EPA is present at lower temperatures and may be replaced by C18 FAs at higher temperatures (Dodson et al., 2014). The anionic membrane lipid SQDG of diatoms seems to be enriched in FAs with a shorter chain length and C14 and C16 FAs are usually observed in both the sn-1 and sn-2 positions (Yongmanitchai and Ward, 1993; Yan et al., 2011). The second anionic lipid PG, on the other hand, seems to contain C18:1 FAs as the main molecular species (Yan et al., 2011).

The FA composition of MGDG also influences the three-dimensional structure of the MGDG molecule (see section Three Dimensional Structures of Lipids). Among the thylakoid lipids, MGDG represents the sole non-bilayer lipid and forms the so-called inverted hexagonal phases (H_{II}-phases) in aqueous solutions. The ability of MGDG to form H_{II}-phases as well as the properties of the H_{II}-phase, such as the flexibility, strongly depend both on the proportion of MGDG in a lipid mixture and the FA composition of the MGDG molecule. High concentrations of MGDG-bound PUFAs seem to facilitate the H_{II} formation (Kobayashi et al., 2016).

Three Dimensional Structures of Lipids

All lipids can be divided into two groups depending on the type of lipid phases they create in aqueous systems. These groups are the bilayer-forming and the non-bilayer-forming lipids. Lipids of the first group aggregate to bilayers, which form lamellar phases in one of the two main states: (i) "fluid" lamellar liquid crystalline (L_α) phases, also referred to as liquid-disordered (L_d, $L_{l/d}$) phases, or (ii) "solid" lamellar gel (L_β) phases, which are also designated as ordered solid (S_o) phases. The second group of lipids includes non-bilayer-forming lipids which can aggregate to normal or inverted (reversed) phases which are denoted with subscripts I and II, respectively. Normal phases, which are commonly observed in neutral lipid/water systems, are micellas (L_1), normal discontinuous cubic phases (I_I), normal hexagonal phases (H_I) and the normal bicontinuous cubic phases (Q_I). The reversed phases include inverted micellas (L_2), reversed bicontinuous cubic phases (Q_{II}), the reversed discontinuous cubic phases (Q_{III}), and the inverted hexagonal phases (H_{II}) (Huang and Gui, 2018). Types of aggregates, as well as types of phases created by the lipids, are determined both by geometry of the lipid molecule and several physicochemical parameters of its surroundings. The chemical geometry of the

lipid molecule is described by the critical packing parameter (CPP) which denotes the ratio of the maximum volume, which can be occupied by the FA residues (V), and the product of the length of these residues (l) and the cross-sectional area of the hydrophilic lipid headgroups (a) (**Table 1**; Yamashita, 2018). The relatively small polar headgroup of the MGDG molecule, accompanied by the large area occupied by the expanded PUFA tails, results in a cone-like geometry of the molecule. This structure enables MGDG to spontaneously form H_{II}-phases in both aqueous systems and model or natural lipid membranes (Shipley et al., 1973). H_{II}-phases consist of a great number of tightly packed cylindrical micelles with a diameter between 1–2 nm and contain 30–60 weight percent of water. DGDG, SQDG and PG possess a cylindrical shape due to the large headgroup areas and the lower content of longer-chain PUFAs and thus belong to the bilayer-forming lipids (Jouhet, 2013). Besides the influence of the inherent chemical structures of the lipid molecules, the formation of lipid phases is strongly affected by the neighboring molecules like proteins, pigments, other lipids or even ions. Divalent cations, for example, facilitate the formation of H_{II}-phases. With respect to the lipid phases formed by MGDG it has been demonstrated that the proteins involved in the phototransformation of protochlorophylls support the formation of a cubic phase (Selstam, 1998). For the function of the thylakoid membrane it is of high importance that the LHCII strongly interacts with MGDG and forces the MGDG molecules into a membrane bilayer structure (Simidjiev et al., 2000). In thylakoid membranes, MGDG seems to play a key role in providing the membrane fluidity which is essential for the efficient diffusion of the xanthophll cycle pigments (see section Xanthophyll Cycles of Higher Plants and Algae), LHC proteins or proteins involved in the turnover and repair of PSII and ZEP. Thus, MGDG and the H_{II}-phases created by MGDG are not only important for chlorophyll biosynthesis during chloroplast development (Jarvis et al., 2000), but also play significant role in the proper functioning of the photosynthetic machinery in differentiated chloroplasts (Zhou et al., 2009; Schaller et al., 2011). On a molecular level MGDG molecules have been shown to be integral parts of the PSI and PSII core complexes (van Eerden et al., 2017) where they promote the PSII dimerization or form a cavity for the docking of plastoquinone Q_B (Guskov et al., 2009; Kansy et al., 2014). However, the importance of the three-dimensional structures formed by MGDG for the function of the MGDG molecules located within the PSI and PSII core complexes remains to be clarified.

Recently, the results of an *in silico* study using the PSII x-ray structure of the thermophilic cyanobacterium *Thermosynechococcus vulcanus* showed that lipid domains surrounding the PSII core complex may be also enriched in SQDG. Like it was discussed above for MGDG, it is not clear if and how the three-dimensional phases formed by SQDG influence the PSII structure and function (van Eerden et al., 2017).

With respect to the H_{II}-phases formed by MGDG it was demonstrated that physical factors, like a high temperature or dehydration, can also induce the formation of non-lamellar phases. Low pH-values, as they are typical for the thylakoid lumen during high light illumination have also been shown to promote the formation of H_{II}-phases by MGDG (Garab et al., 2017, see also section Localization of Non-bilayer Lipid Phases in the Thylakoid Membrane).

TABLE 1 | Dependence of the lipid self-assembly structures on the value of the critical packing parameter (CPP).

Critical packing parameter value (CPP) $CPP = V/a*l$ (a, v, l)	Type of structure
≤1/3	Normal micelle (L_1), (I_1)
[1/3 – 1/2]	Normal hexagonal phase (H_I)
[1/2 – 1]	Normal bicontinuous cubic phase (Q_I)
≈ 1	Lamellar phases (L_α, L_d, L_β)
≥1	Reversed bicontinuous cubic phase (Q_{II})
>1	Reversed micelle (L_2) Reversed discontinuous cubic (Q_{III}) Reversed hexagonal phase (H_{II})

V, volume, which can be occupied by the FA residues; l, length of the FA residues; a, the cross-sectional area of the hydrophilic lipid headgroups. For further detail see Yamashita (2018).

XANTHOPHYLL CYCLES OF HIGHER PLANTS AND ALGAE

Types of Xanthophyll Cycles

The main xanthophyll cycles that are known today are the violaxanthin (Vx) cycle of higher plants, green and brown algae and the diadinoxanthin (Ddx) cycle of diatoms, haptophytes and dinophytes (**Figure 2**, for a review see Goss and Jakob, 2010). Algae containing the Ddx cycle also contain the pigments of the Vx cycle because Vx is a precursor in the biosynthesis pathway of the Ddx cycle pigments (Lohr and Wilhelm, 1998, 2001). The presence of Vx cycle pigments in Ddx cycle containing algae is especially visible during longer periods of high light exposure when a pronounced *de novo* synthesis of Ddx cycle pigments is taking place. In addition to these two xanthophyll cycles, the existence of a lutein epoxide (Lx) cycle has been shown which is, however, restricted to some families of higher plants (Esteban and Garcia-Plazaola, 2014). Some members of the Prasinophyceae, which represent a class of unicellular green algae, or some species within the genus *Gracilaria* belonging to the Rodophyta are characterized by a modified Vx cycle (Goss et al., 1998; Bertrand and Schoefs, 1999; Cardol et al., 2008).

Reaction Sequences and Xanthophyll Cycle Enzymes

The xanthophyll cycles consist of forward reactions which take place during illumination of plants or algae with high light illumination and back reactions which revert the forward reaction during periods of low light exposure or darkness.

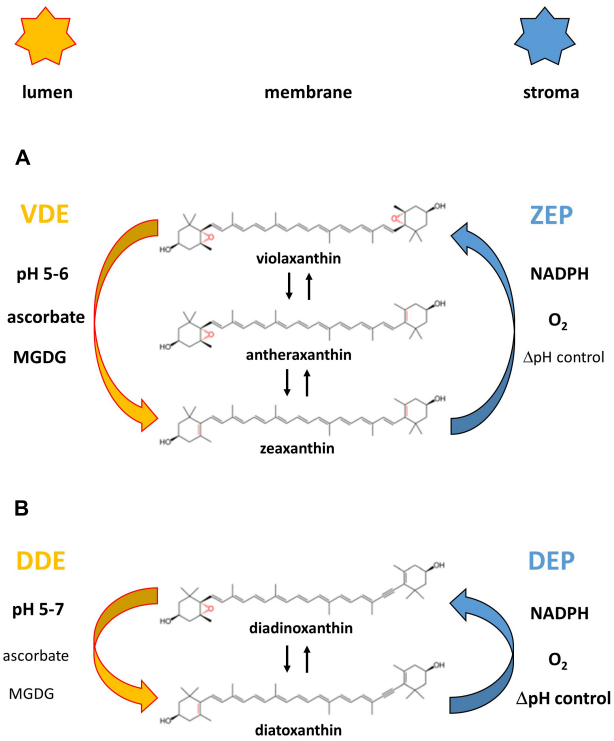

FIGURE 2 | Reaction sequences and enzymes of the violaxanthin **(A)** and diadinoxanthin **(B)** cycle. The violaxanthin cycle is present in higher plants and green and brown algae, the diadinoxanthin cycle is found in diatoms, haptophytes and dinophytes. **Figure 2** also shows the cofactor requirements of the enzymes catalyzing the de-epoxidation reaction (violaxanthin de-epoxidase, VDE and diadinoxanthin de-epoxidase, DDE) and the epoxidation reaction (zeaxanthin epoxidase, ZEP and diatoxanthin epoxidase, DEP), respectively. Representation of the cofactors in bold or normal type indicates whether high or low concentrations of the respective cofactors are needed for high enzyme activity. The establishment of a proton gradient inhibits diatoxanthin epoxidation (high ΔpH control) and is thus presented in bold type whereas zeaxanthin epoxidation is unaffected by the presence of the transmembrane ΔpH (ΔpH control depicted in normal type). The pH value of the thylakoid lumen which leads to VDE and DDE activation (possibly by VDE or DDE dimerization) and membrane binding is also indicated for the two xanthophyll cycles.

In the Vx cycle the forward reaction consists of a two-step de-epoxidation of the di-epoxy xanthophyll Vx to the mono-epoxide Ax and finally to the epoxy-free Zx (Yamamoto et al., 1962; Hager, 1967a). The back reaction re-introduces the two epoxy groups into the Zx molecule and regenerates Vx via the intermediate reaction product Ax (Hager, 1967a). The Vx cycle of the Prasinophyceae and of some species of the genus *Gracilaria* is incomplete and during high light illumination an accumulation of the intermediate de-epoxidation product Ax is observed in Prasinophycean cells (Goss et al., 1998; Cardol et al., 2008). In the red algae *Graciliaria gracilis* or *G. multipartite* an absence of Vx was detected and Ax seems to be the only substrate which can be converted to Zx (Bertrand and Schoefs, 1999). Despite the ongoing uncertainties about the presence of a xanthophyll cycle in Rodophyta, a recent study has presented clear evidence that at least a Zx epoxidase, which is able to convert Zx to Ax, is present in the red algae (Dautermann and Lohr, 2017).

Thus, these two modifications of the Vx cycle, like the Ddx and the Lx cycles, consist of only one de-epoxidation and one epoxidation step. In the Vx cycle of the Prasinophyceae the xanthophyll di-epoxide Vx is converted to the mono-epoxide Ax whereas in all other one-step xanthophyll cycles mono-epoxides such as Ax, Ddx and Lx are converted to the epoxy-free xanthophylls such as Zx, diatoxanthin (Dtx), and lutein (L), respectively (Hager and Stransky, 1970; Stransky and Hager, 1970; Rabinowitch et al., 1975; Bungard et al., 1999; Bertrand and Schoefs, 1999). In the back reaction one epoxy-group is re-introduced into the epoxy-free xanthophylls Dtx or L and Ddx or Lx are regenerated. The forward reaction of the Vx cycle is catalyzed by the enzyme Vx de-epoxidase (VDE), the back reaction by the enzyme Zx epoxidase (ZEP). Both the VDE and the ZEP belong to a family of diverse proteins, the so-called lipocalins (Hieber et al., 2000; Grzyb et al., 2006). Lipocalins usually bind hydrophobic molecules and act as carrier proteins for their substrates. VDE is localized in the thylakoid lumen and has a pH-optimum of around pH 5.2 (Hager, 1969; Pfündel et al., 1994). During high light illumination the light-driven proton gradient leads to a decrease of the pH-value of the thylakoid lumen, thereby activating the VDE. Activation of VDE is probably driven by a dimerization of the water-soluble monomeric VDE, followed by the binding of the active, dimeric VDE to the lumen side of the thylakoid membrane (Hager and Holocher, 1994; Arnoux et al., 2009; Saga et al., 2010). With regard to the dimerization it has been proposed that the C-terminus of the VDE plays a role in the interaction of the VDE monomers (Hallin et al., 2016) and that four specific amino acid residues are important for the pH-dependent activation (Fufezan et al., 2012). In addition, it has been suggested that the conserved cysteine residues and the disulfide bridges formed by the cysteines are sensitive to redox changes of the thylakoid membrane induced by the photosynthetic electron transport (Hallin et al., 2015; Simionato et al., 2015). Changes of the thylakoid redox potential may play a role in the regulation and activation of the VDE via dithiol/disulfide exchange reactions. Reduced ascorbate has been identified as the co-substrate of the de-epoxidation reaction and is important for the reduction of the epoxy group and the subsequent abstraction as H_2O (Hager, 1969). Interestingly, a recent study has reported that the atypical VDE of the green algae *Chlamydomonas reinhardtii* (Li et al., 2016) does not require the presence of ascorbate (Vidal-Meireles et al., 2020). In contrast to the VDE the ZEP seems to be permanently associated with the stromal side of the thylakoid membrane as a peripheral membrane protein (Schaller et al., 2012b). ZEP uses O_2 and NADPH + H^+ as co-substrates to re-introduce the epoxy group into the Zx and Ax molecule, respectively (Hager, 1967a). The VDE of higher plants and green algae is characterized by a higher substrate affinity for Ax compared with Vx which results in faster kinetics of the second de-epoxidation step from Ax to Zx compared with the first de-epoxidation step from Vx to Ax (Frommolt et al., 2001; Goss, 2003). However, the VDE of the Prasinophyceae differs from

the VDE of higher plants and other green algae and exhibits a higher substrate affinity for Vx compared with Ax (Goss, 2003). This results in a very slow second de-epoxidation step from Ax to Zx and together with the simultaneous epoxidation reaction results in the accumulation of Ax during high light illumination in these green algae (Frommolt et al., 2001). Interestingly, the decreased substrate affinity of the VDE of the Prasinophyceae is not restricted to the mono-epoxide Ax but the enzyme is characterized by a generally low substrate affinity for xanthophyll mono-epoxides whereas xanthophyll di-epoxides like Vx are converted with high efficiency. For the Lx cycle which occurs in some families of higher plants it has been suggested that the VDE and ZEP also carry out the additional de-epoxidation of Lx to L and from L back to Lx (Esteban et al., 2009). The enzymes of the Ddx cycle in diatoms show some differences to the respective enzymes in higher plants and green algae. VDEs in diatoms and some other groups of algae, like dinophytes, haptophytes or phaeophytes, are also denoted as diadinoxanthin de-epoxidases (DDEs). Before 2007 the presence of different VDE genes and thus the presence of different VDEs/DDEs in organisms containing the Ddx cycle was not known and the measurements dealing with the properties of the DDE were ascribed to one single enzyme. It was shown that the DDE is characterized by a pH-optimum which is shifted toward higher pH-values (Jakob et al., 2001). In addition, it has been reported that DDE activity and thus the de-epoxidation of Ddx to Dtx can take place at neutral pH-values. In addition, DDE is able to operate efficiently with lower concentrations of the co-substrate ascorbate compared with the VDE of higher plants (Grouneva et al., 2006).

It might be possible that a relationship exists between the higher SQDG and lower MGDG concentrations of the diatom thylakoid membrane (see section Lipid Classes) and the broad pH-optimum of the diatom DDE. Taking into account that the thylakoid membranes of the *A. thaliana mgd1-1* mutant, which are strongly reduced in their MGDG content, are impaired in their ability to build-up a strong proton gradient during illumination (Aronsson et al., 2008, see also section Lipid Classes), a comparable situation might occur in the diatom thylakoids with their low MGDG concentration. The possible inability of the diatom thylakoid membranes to generate a very strong ΔpH would then require the onset of DDE activity at a weaker pH-gradient across the membrane and thus at higher luminal pH-values. Such a behavior, i.e., DDE activity at almost neutral pH-values, has been observed in *in vitro* experiments where the pH-activity and pH-optimum of the DDE were determined (Jakob et al., 2001).

Today, it is clear that the diatom genome codes for more than one de-epoxidase. Two DDE-encoding genes were shown to be present in the centric diatom *Thalassiosira pseudonana* (Montsant et al., 2007). One of these genes (labeled as *TpVDE*) is similar to the genes encoding the typical plant VDEs while the other (designated as violaxanthin de-epoxidase-like; *TpVDL*) is more distantly related. Later, it was demonstrated that the genome of the pennate diatom *Phaeodactylum tricornutum* contains one gene similar to the genes of "typical VDEs" (termed *PtVDE*) and two VDE-like genes, designated as *PtVDL1* and *PtVDL2* (Coesel et al., 2008). Important differences can also be observed for the epoxidation reaction of the Ddx cycle. Here it has been demonstrated that the Dtx epoxidase (DEP) shows significantly higher Dtx epoxidation rates than the ZEP of higher plants and green algae (Mewes and Richter, 2002; Goss et al., 2006). The kinetics of the conversion of Dtx to Ddx are almost comparable to the very fast de-epoxidation of Ddx to Dtx by the DDE. To avoid a futile cycle and to enable a fast accumulation of Dtx during illumination with high light intensities the DEP underlies a strict light-dependent control (Mewes and Richter, 2002; Goss et al., 2006). DEP activity is completely suppressed during high light illumination by the build-up of the light-driven proton gradient. During low light illumination or during periods of darkness when no or only a weak trans-membrane proton gradient is present, DEP is fully activated and Dtx is rapidly converted back to Ddx.

Localization of Xanthophyll Cycle Pigments in the Thylakoid Membrane

With respect to the localization of the xanthophyll cycle pigments in the thylakoid membrane two main pools can be differentiated. The first pool consists of xanthophyll cycle pigments which are bound to the light-harvesting proteins. In higher plants and green algae the majority of the protein-bound Vx cycle pigments is associated with the light-harvesting complex of photosystem II (LHCII), which represents the main thylakoid membrane protein (Ruban et al., 1999), although proteins of the light-harvesting complex of photosystem I (LHCI) also bind Vx, as well as L and β-carotene (Croce et al., 2002, 2007). Interestingly, recent data have shown that the binding of the xanthophyll cycle pigments can have an impact on the supramolecular structure of LHCII (Zhou et al., 2020). LHCII contains a special binding site for Vx which has been termed V1. V1 is located at the periphery of each LHCII apoprotein and contains a loosely bound Vx molecule (Morosinotto et al., 2003). In the minor PSII antenna proteins CP29, CP26, and CP24, which contain higher concentrations of Vx cycle pigments compared to the LHCII, Vx seems to occupy the L2 binding site (Morosinotto et al., 2003). This binding site is usually responsible for the association of one of the two lutein molecules in the LHCII. In contrast to the V1 site the L2 site is not located at the periphery but represents an internal pigment binding site. Experiments with recombinant LHCII and minor PSII antenna proteins have shown that only Vx, which is associated with the peripheral V1 binding site, can be efficiently converted to Ax and Zx (Jahns et al., 2001; Wehner et al., 2006). Vx bound to the internal L2 binding site is not easily accessible by the VDE and no or only a very limited de-epoxidation can be observed. The loose association of Vx with the LHCII apoprotein at the peripheral binding site is thought to enable the efficient detachment of Vx from the protein during high light illumination followed by the diffusion into the lipid phase of the thylakoid membrane where the actual enzymatic conversion to Ax and Zx by the enzyme VDE is taking place (Latowski et al., 2002; Goss et al., 2007). Recently, it has been shown that the binding of neoxanthin (Nx) to the LHCII affects the binding affinity of Vx (Wang et al., 2017). In the presence of Nx Vx is only weakly

bound to the LHCII, easily dissociates into the lipid phase of the membrane, thereby enhancing the first step of the de-epoxidation reaction. In contrast to the general assumption that Zx rebinds to the Vx binding sites at the LHCII and the minor PSII antenna proteins after the de-epoxidation of Vx, Xu et al. (2015) provided evidence that Zx does not necessarily exchange for Vx in the internal binding sites. It may be located in the periphery of the complexes and exert its quenching capacity in a position between the LHCs.

In diatoms the protein bound Ddx cycle pigments are located in the different fucoxanthin chlorophyll protein (FCP) complexes. The recent elucidation of the molecular structure of an FCP complex composed of Lhcf3 and Lhcf4 by x-ray crystallography (Wang et al., 2019) showed that, like Vx in the LHCII, Ddx is located at the periphery of the apoprotein and thus most likely also loosely bound. Like the easy detachment of Vx from the LHCII followed by the rebinding of Zx, the peripheral binding of Ddx is thought to facilitate the exchange with Dtx during the operation of the Ddx cycle. Interestingly, the binding site of the Ddx molecule seems to be located at the opposite side of the apoprotein compared with the Vx binding site in the LHCII. Besides the Lhcf proteins which build-up the peripheral antenna system of diatoms, but may also be more closely associated with the PSII core complex, the Lhcr proteins which form the PSI-specific antenna of diatoms, bind Ddx cycle pigments. According to Lepetit et al. (2008) the concentration of Ddx and Dtx seems to be even slightly higher in the PSI antenna compared to the peripheral FCP complex. Like higher plants and green algae diatoms show an increase of the xanthophyll cycle pigment pool upon cultivation with higher light intensities (Lavaud et al., 2003; Schumann et al., 2007; Gundermann and Büchel, 2008; Lepetit et al., 2010; Gundermann et al., 2019). The increase of the Ddx cycle pigment pool size is significantly more pronounced compared with the increase of the Vx cycle pigment concentrations. With respect to the additional Ddx and Dtx synthesized during exposure to high light intensities it has been proposed that a part of these additional Ddx cycle pigments is bound by the photoprotective Lhcx proteins which also show a stronger expression under high light conditions (Lepetit et al., 2013). In the centric diatoms which are characterized by a more complicated antenna system than the pennate diatoms, it could be shown that both the FCPa and FCPb complexes bind Ddx cycle pigments (Gundermann and Büchel, 2008). In the FCPa complex increased Ddx binding during high light cultivation was accompanied by an increased content of the Fcp6 and Fcp7 proteins. Interestingly, Dtx-induced decreases of the FCP fluorescence emission could only be observed in the FCPa.

It is noteworthy that the differences in the main thylakoid membrane proteins, i.e., the light-harvesting complexes (LHCs), go together with differences in the lipid and FA composition of the thylakoids (see sections Lipid Classes and Fatty Acids). In higher plants and green algae, which contain the LHCII and LHCI, the thylakoid lipids are rich in C16 and C18 FAs. Diatoms and brown algae, which are characterized by the presence of Fx, contain MGDG and DGDG molecules with a high concentration of C18 and C20 FAs. It may be possible that the differences in the FA composition of MGDG and DGDG between the green lineage and diatoms/brown algae are related to differences in the structures of LHCs and FCPs. Furthermore, these differences may represent an optimal harmonization of the thylakoid membranes to allow the best possible LHC/FCP structure and function, i.e., light-harvesting or non-photochemical quenching of Chl a fluorescence (NPQ, see section Function of Xanthophyll Cycles). With respect to the different xanthophyll cycles in higher plants/green algae and diatoms the differences in the lipid and FA composition may even influence the interplay between the LHCs/FCPs and the xanthophyll cycle enzymes. In this regard, it is interesting that the Vx cycle enzymes of brown algae, which contain FCP complexes and are enriched in C18 and C20 FAs, show some of the typical features of the Ddx cycle enzymes of diatoms, like e.g., a fast epoxidation reaction (Garcia-Mendoza and Colombo-Pallotta, 2007).

The second main pool of xanthophyll cycle pigments consists of Vx or Ddx cycle pigments which are not protein bound but localized as free pigments in the lipid phase of the thylakoid membrane. First evidence for the existence of free Zx molecules was obtained from studies on the fluidity of thylakoid membranes which showed that the conversion of Vx to Zx leads to a rigidification of the membrane (Gruszecki and Strzalka, 1991, 2005; Tardy and Havaux, 1997, see also section Function of Xanthophyll Cycles). Isolation of LHCII with different preparation methods led to the purification of LHCII with different concentrations of native lipids and Vx cycle pigments (Schaller et al., 2010). Further analysis of the LHCII preparations demonstrated that the concentration of LHCII-associated Vx was correlated with the amount of MGDG which was isolated with the complexes. Decreases of the MGDG content led to a decrease of the Vx concentration, indicating that a part of the Vx cycle pigment pool was protein-bound whereas another part was localized within an MGDG-shield surrounding the LHCII. Comparable results were obtained for the Prasinophyceae *Mantoniella squamata* where LHC could be isolated which contained high concentrations of MGDG and Vx (Schaller et al., 2012a). In diatoms which are characterized by a strong increase of the Ddx cycle pigment pool during high light exposure a comparable separation between a protein bound and lipid dissolved Ddx cycle pigments could be observed. The first indication for a pool of Ddx cycle pigments, which are not bound to FCP complexes, was obtained from measurements of NPQ of high light cultivated diatoms (Schumann et al., 2007). These measurements indicated that additional Dtx synthesized during high light treatment is not able to enhance NPQ and thus cannot be bound to the respective binding sites of the FCP complexes. Additional experiments with isolated FCP complexes from low and high light cultivated diatom cells demonstrated that the additional Ddx cycle pigments show the same absorption spectrum as purified Ddx which is dissolved in MGDG (Lepetit et al., 2010). The enrichment of MGDG in the isolated FCP complexes led to the conclusion that, like in higher plants, the diatom antenna complexes are surrounded by an MGDG shield which incorporates a part of the Ddx cycle pigments. Also like in higher plants the free Ddx cycle pigments have been shown to play a role in the modulation of the thylakoid

membrane fluidity (Bojko et al., 2019, see section Function of Xanthophyll Cycles).

Function of Xanthophyll Cycles

The xanthophyll cycles of plants and algae are important protection mechanisms against damage to the photosynthetic apparatus induced by high light intensities. The function of the xanthophyll cycles as photoprotective mechanisms is trifold: (i) they play an important role in the dissipation of excessive excitation energy as heat in the process of NPQ (Goss and Lepetit, 2015; Ruban, 2016), (ii) they are able to directly scavenge ROS within the thylakoid membrane (Havaux, 1998; Triantaphylidès and Havaux, 2009) and (iii) they serve as stabilizers of the lipid phase of the thylakoid membrane (Gruszecki and Strzalka, 2005; Bojko et al., 2019).

With respect to the process of NPQ the de-epoxidized xanthophylls Zx and Dtx have been shown to induce a structural change of the light-harvesting complexes of higher plants (Ruban et al., 1992, 1997; Holzwarth et al., 2009) and diatoms (Gundermann and Büchel, 2008; Miloslavina et al., 2009; Schaller-Laudel et al., 2015). This structural change leads to the transformation of excessive excitation energy into heat followed by the harmless dissipation of thermal energy. In higher plants protonation of the LHCII and the presence of the PsbS protein (Li et al., 2000) are further essential factors which regulate NPQ and thus the structural change of the PSII antenna. In this respect, Welc et al. (2016) have shown that Vx cycle pigments which are not bound to the LHCII can nonetheless modulate the structure of the LHCII. Vx seems to promote the formation of LHCII supramolecular structures whereas free Zx induced an LHCII structure suitable for the dissipation of excessive excitation energy. Recently, an interaction between Zx and the PsbS protein has been described which leads to a preferential association of PsbS with the minor PSII antenna proteins (Sacharz et al., 2017). PsbS itself seems to form clusters and may act as initiator for LHCII aggregation. LHCII aggregation can also be induced *in vitro* by the addition of Mg^{2+} ions (Schaller et al., 2014) which in the chloroplast act as counter-ions to the light-induced proton influx from the stroma to the thylakoid lumen during the build-up of the transmembrane proton gradient. In green algae comparable LHCII aggregation has been observed during the induction of NPQ, the role of the PsbS protein in the establishment of NPQ has, however, been replaced by the LHCSR proteins (Peers et al., 2009; Bonente et al., 2011; Gerotto and Morosinotto, 2013). Like PsbS the LHCSR3 protein has been proposed to sense the decrease of the pH in the thylakoid lumen during illumination (Ballottari et al., 2016). Nawrocki et al. (2019) have shown that LHCSR proteins are responsible for NPQ in *Chlamydomonas reinhardtii* but that PsbS proteins also play a role in photoprotection. LHCII aggregation is characterized by a shift of the chlorophyll a fluorescence emission to longer wavelengths (Holzwarth et al., 2009) which, interestingly, can also be observed upon the aggregation of FCP complexes in diatoms (Miloslavina et al., 2009; Lavaud and Lepetit, 2013). In diatoms the Lhcx proteins have been demonstrated to adopt the role of the PsbS protein (Bailleul et al., 2010; Zhu and Green, 2010; Taddei et al., 2016, 2018). Recently, it was demonstrated that NPQ depends on the concerted action of the Ddx cycle and the Lhcx proteins and that Lhcx proteins provide photoprotection via the thermal dissipation of excitation energy (Buck et al., 2019). For both higher plants (Holzwarth et al., 2009; Jahns and Holzwarth, 2012) and diatoms (Goss and Lepetit, 2015; Taddei et al., 2018) models for the localization and function of NPQ have been established. These models predict the formation of two quenching sites where the transformation of excitation energy into heat is taking place. Quenching site Q1 is composed of detached LHCII and FCP complexes, respectively, which after their dissociation from the PSII core complex undergo a structural change and form aggregates. NPQ at quenching site Q1 seems to be independent of the de-epoxidation of Vx to Zx. For the formation of quenching site Q2, however, the presence of Zx is important. Quenching site Q2 is located in the vicinity of the PSII core complex and most likely involves the minor PSII antenna proteins in higher plants and green algae and special FCP proteins which are more closely associated with the PSII core in diatoms. Newer data indicates that NPQ in trimeric LHCIIs does depend on Zx but not on lutein whereas NPQ in the monomeric LHC proteins requires Zx and L and involves the formation of a radical pair (Dall'Osto et al., 2017). Recently, it has been demonstrated that PsbS-dependent NPQ occurs mainly in the LHCII whereas another quenching site operates within the PSII core complex (Nicol et al., 2019). For plants containing the Lx cycle and green algae exhibiting the shortened Vx/Ax cycle it was demonstrated that L or Ax can play a similar role in NPQ induction and enhancement as it is normally observed for Zx (Goss et al., 1998; Garcia-Plazaola et al., 2003; Leonelli et al., 2017).

While the xanthophyll cycle-dependent induction of NPQ is linked to Zx or Dtx bound to the antenna proteins of higher plants and algae, the anti-oxidative function of Zx or Dtx is related to those molecules which are localized as free pigment in the lipid phase of the membrane. For both Zx and Dtx it has been shown that these xanthophylls are able to detoxify ROS which are generated by alternative electron pathways or via the triplet excited state of Chl a under supersaturating light conditions (Havaux and Niyogi, 1999; Havaux et al., 2007; Lepetit et al., 2010). Deactivation of ROS by Zx or Dtx minimizes the damaging effects of ROS on membrane lipids, the embedded photosynthetic membrane proteins and the photosynthetic pigments. The antioxidant function of Zx may be located at the interface between LHCII and the membrane lipids because it was shown that Zx associated with oligomeric LHCII is active in the detoxification of ROS (Johnson et al., 2007).

Recently, a further function of de-epoxidized xanthophyll cycle pigments has been proposed. From former studies it was known that the conversion of Vx to Zx increases the membrane rigidity of thylakoids (Gruszecki and Strzalka, 1991, 2005). The membrane stabilizing effect of Zx was attributed to the fact that Zx spans the complete thylakoid membrane and that the polar head groups of the xanthophyll molecule are anchored within the hydrophilic part of the membrane where the lipid head groups are located (Gruszecki and Strzalka, 2005, see also Grudzinski et al., 2017). Furthermore, it was proposed

that the xanthophyll molecules play a comparable role in the modulation of the physical membrane properties as cholesterol in animal or human membranes. The recent analysis of the effect of Dtx on membrane properties provided additional information on the action of the de-epoxidized xanthophylls (Bojko et al., 2019). Based on EPR measurements with the 5-SASL and 16-SASL spin probes it was shown that during the conversion of Ddx to Dtx a dynamic effect takes place whereas the high Dtx concentrations after de-epoxidation exert a stable effect on the properties of the diatom thylakoid membrane. The combined action of both effects results in a temporary increase of the rigidity of both peripheral and central parts of the membrane bilayer whereas the stable effect leads to a more permanent increase of the rigidity of the hydrophobic core of the membrane. Both effects are supposed to play a role in the short-term adaptation of diatom thylakoid membranes to changing temperatures.

LIPID DEPENDENCE OF XANTHOPHYLL CYCLING IN HIGHER PLANTS AND ALGAE

Lipids as Solvents for Xanthophyll Cycle Pigments

First evidence for the role of lipids in the process of Vx de-epoxidation was obtained by Yamamoto et al. (1974) and Yamamoto and Higashi (1978) who isolated VDE which contained MGDG as single lipid component and VDE without attached MGDG. In *in vitro* enzyme assays with the isolated VDEs it became clear that MGDG is needed for the de-epoxidation of Vx to Ax and Zx and that a ratio of MGDG to Vx of about 30 is ideal for the efficient conversion. The authors concluded that one of the functions of MGDG is the solubilization of the hydrophobic pigment, thereby presenting the substrate in a form that meets the requirements of the active site of the VDE. More recent experiments with single lipids have shown that membrane lipids which form inverted hexagonal structures, i.e., MGDG and phosphatidylethanolamine (PE), have a high capacity to solubilize the xanthophyll cycle pigments Vx and Ddx (Latowski et al., 2004; Goss et al., 2005). Membrane lipids like DGDG, SQDG or PC, which form bilayers in aqueous solutions, are also able to solubilize Vx or Ddx but significantly higher concentrations are needed to achieve complete solubilization. Solubilization converts aggregates of the hydrophobic pigments Vx or Ddx into lipid dissolved single molecules which can then be de-epoxidized by the enzyme VDE. The higher capacity of the non-bilayer lipids MGDG and PE to solubilize the xanthophyll cycle pigments can also be seen in artificial membranes which are composed of a non-bilayer and bilayer lipid (Goss et al., 2007). Liposomes constructed with equal amounts of PC/PE, PC/MGDG or DGDG/MGDG show a strong enrichment of Vx or Ddx in non-bilayer lipids. The preferential localization of the xanthophyll cycle pigments in the liposome non-bilayer phase is in line with the presence of Vx or Ddx in the MGDG shield surrounding the higher plant or diatom antenna complexes (Lepetit et al., 2010; Schaller et al., 2010). Taken together this indicates that in the native membrane the xanthophyll cycle pigments are enriched in non-bilayer lipid phases. With respect to the comparison of the two main xanthophyll cycle pigments Vx and Ddx the experiments demonstrated that higher concentrations of inverted hexagonal phase forming lipids are needed for the complete solubilization of Vx compared with Ddx (Goss et al., 2005). The increased solubility of Ddx in MGDG is in line with the decreased concentration of MGDG and the increased amount of Ddx cycle pigments in the diatom thylakoid membrane compared with the thylakoids of higher plants and green algae (Lavaud et al., 2003; Gundermann and Büchel, 2008; Lepetit et al., 2010, 2012). Complete solubilization of Ddx and Dtx under these conditions can only be achieved if a low lipid per pigment ratio is sufficient for solubilization. While in the studies detailed above no or only a very slow conversion of Vx or Ddx to Zx or Dtx was observed upon the complete solubilization of the substrates in bilayer lipids, comparable experiments performed by Yamamoto (2006) yielded slightly different results. These results indicated that MGDG or DGDG support Vx de-epoxidation in different ways. While the presence of MGDG leads to a fast and complete conversion of Vx to Zx, the de-epoxidation is slow but nevertheless complete when DGDG is added to the enzyme assay. Based on the results it was concluded that the solubilization of aggregated Vx by DGDG proceeds during the time course of the de-epoxidation reaction thereby circumventing the negative effects of the decreased solubilization capacity of the bilayer forming lipid.

Role of Non-bilayer Lipid Phases for Xanthophyll Cycling

The first results on the role of inverted hexagonal phases for xanthophyll de-epoxidation were reported by Latowski et al. (2000, 2002, 2004). The authors used unilamellar liposomes composed of PC, which were supplemented with different concentrations of the non-bilayer lipid MGDG, to study the conversion of Vx to Ax and Zx. In the liposome systems an increase in the de-epoxidation efficiency was observed with increasing ratios of MGDG to PC. In addition, through the use of ^{31}P-NMR spectroscopy, the presence of inverted hexagonal phases formed by MGDG was detected. Based on the results it was concluded that Vx diffuses into the inverted hexagonal phase where the actual conversion to Ax and Zx by the enzyme VDE is taking place. The importance of inverted hexagonal phases for Vx de-epoxidation was demonstrated in a subsequent study where different non-bilayer and bilayer lipids where tested for their ability to enhance the de-epoxidation reaction (Latowski et al., 2004). The non-bilayer lipids MGDG and PE induced a fast and efficient conversion of Vx whereas in the presence of the bilayer lipids DGDG and PC no or only a very slow Vx de-epoxidation could be observed. The use of either GGLs or GPs demonstrated that not the nature of the lipid but the three-dimensional structures formed by the lipids are responsible for the stimulation of Vx de-epoxidation. Later it

could be shown that the bilayer lipids DGDG or PC are able to completely solubilize either Vx or Ddx (Goss et al., 2005). However, no or only a very slow conversion of Vx to Ax and Zx or Ddx to Dtx was observed in the single bilayer lipid systems. In liposome systems composed of only bilayer lipids, i.e., DGDG or PC, a complete solubilization of Vx or Ddx could be achieved as well, but Vx or Ddx de-epoxidation could only be detected when the liposomes where supplemented with a certain concentration of the inverted hexagonal phase forming lipids MGDG or PE (Goss et al., 2007). Later it was demonstrated that the main lipid of diatom thylakoid membranes, the negatively charged SQDG has a pronounced inhibitory effect on Ddx de-epoxidation (Goss et al., 2009). A comparable inhibition of the DDE could be demonstrated for the anionic GP PG. The results from the solubilization and de-epoxidation experiments in single lipid systems and liposomes composed of different lipids implied that the solubilization of the lipids represents an important factor for the de-epoxidation of Vx or Ddx but that, despite efficient solubilization, the three-dimensional structures of the lipids are mandatory for an efficient conversion of the xanthophyll cycle pigments. Based on these results it was suggested that the inverted hexagonal structure and not the bilayer structure enables the access of the enzymes VDE or DDE to their respective solubilized substrates. The penetration of the VDE or DDE into the hydrophobic interior of the lipid phase has to be deep enough to allow the interaction of the catalytic site of the enzymes with the substrates Vx or Ddx. Penetration of the β-barrel structure, which forms the catalytic site of the lipocalins to which both VDE and DDE belong (Hieber et al., 2000), may be facilitated by a decreased surface tension of the inverted hexagonal phase compared with the bilayer phase (van den Brink-van der Laan et al., 2004). The decreased surface tension is most probably caused by the conical shape of the non-bilayer lipids like MGDG molecules which are characterized by a small headgroup and long unsaturated FAs which cover a significantly larger area than the mono-galactose headgroup (Garab et al., 2000, see section Three Dimensional Structures of Lipids). Bilayer lipids like DGDG, on the other hand, have a cylindrical shape because the larger headgroups and FA chains cover a comparable area. Lipid phases composed of bilayer lipids are thus rather tightly sealed, show a high surface tension and do not enable the penetration of VDE or DDE into the hydrophobic membrane interior. Yamamoto (2006) proposed a different concept of Vx de-epoxidation in the thylakoid membrane. Based on the observation that Vx could be completely converted to Zx in the presence of the bilayer lipid DGDG, albeit with a significantly lower Vx de-epoxidation rate compared to MGDG, it was proposed that Vx de-epoxidation is not restricted to MGDG reverse micelles and that the VDE is able to operate throughout the lipid phase of the single bilayer thylakoid membrane.

Localization of Non-bilayer Lipid Phases in the Thylakoid Membrane

The existence of non-bilayer lipid phases in thylakoid membranes has been studied by freeze-fracture electron microscopy. It was demonstrated that exposure of higher plant thylakoid membranes to increasing temperatures in the range from 35 to 45°C leads to a destacking of grana membranes (Gounaris et al., 1984). Further increases of the temperature up to 45–55°C induces a pronounced lipid phase separation and the formation of large areas of inverted hexagonal lipid phases. Lipid phase separation and irreversible induction of inverted hexagonal phases can also be triggered by exposure of thylakoid membranes to pH-values lower than pH 4.5 or treatment with phospholipase A_2 (Thomas et al., 1985). In addition, incubation of isolated thylakoids in reaction buffers complemented with high concentrations of compatible solutes, such as sucrose, trehalose, sorbitol or betaine, induces the phase separation of non-bilayer forming lipids, followed by the establishment of large areas of inverted hexagonal lipid phases (Williams et al., 1992). Later, first measurements of isolated wheat thylakoid membranes with ^{31}P-NMR spectroscopy supported the formation of inverted hexagonal lipid phases when the thylakoids were exposed to high temperatures between 55 and 60°C (Haranczyk et al., 1995). Krumova et al. (2008) used PG as an intrinsic bulk label lipid for ^{31}P-NMR studies to analyze the lipid phases of the thylakoid membrane. The data showed that besides the lamellar phase a non-bilayer isotropic phase exists which becomes predominant at higher temperatures. In addition, it was demonstrated that the phospholipid was not restricted to the lamellar phase of the membrane. Using molecular dynamics simulations for the characterization of the thylakoid membranes of higher plants and cyanobacteria differences between these membranes could be detected (van Eerden et al., 2015). The simulations revealed that the thylakoid membrane is in a state close to the formation of the inverted hexagonal phase. Furthermore, the molecular dynamic simulations showed that the higher plant thylakoid membrane more readily undergoes the transition to the inverted hexagonal phase compared with the cyanobacterial membrane which is most likely caused by the higher degree of unsaturation of the FA moieties of the plant lipids. It is interesting to note that the simulations of van Eerden et al. (2015) did not present evidence for an enrichment of MGDG molecules in the inverted hexagonal phase. Instead, a well-mixed system of lipids could be observed in both the lamellar and the inverted hexagonal phase. Recent studies employing ^{31}P-NMR measurements and time-resolved fluorescence spectroscopy of the fluorescent, lipophilic dye MC_{540} revealed the presence of not only one but three inverted hexagonal phases which coexist with one bilayer phase in the thylakoid membrane of higher plants (Garab et al., 2017). According to the data the three inverted hexagonal phases are located at the luminal and stromal sides of the thykakoid membrane, accompanied by a lipid phases in the junction region of the grana and stroma membranes. Garab et al. (2017) showed that the non-bilayer lipid phases were sensitive to the osmolarity and the ionic strength of the medium which was later confirmed by the results of Kotakis et al. (2018) who used high concentrations of the compatible solute sucrose to induce the formation of the inverted hexagonal phases. Besides the presence of osmolytes low pH-values led to a pronounced increase of the non-bilayer thylakoid lipid phases which could

additionally be modulated by the degree of unsaturation of the lipid FAs.

Localization of Non-bilayer Phases Involved in Xanthophyll Cycling

It has been proposed that the non-bilayer lipid phases involved in xanthophyll cycling are localized in the vicinity of the LHCII in higher plants and green algae or the FCP complexes in diatoms. This proposal is based on the purification of LHCII and FCP complexes which, under mild solubilization conditions, leads to the isolation of LHCII and FCP complexes with a shield of MGDG molecules incorporating the Vx or Ddx cycle pigments (see section Localization of Xanthophyll Cycle Pigments in the Thylakoid Membrane and references therein). In addition, a fast and efficient rebinding of the de-epoxidized xanthophyll cycle pigments Zx or Dtx to the light-harvesting complexes has to take place in order to establish rapid xanthophyll-dependent photoprotection via NPQ (section Function of Xanthophyll Cycles and references). With respect to the binding of the pigment molecules to the LHC apoproteins it is interesting to note that the de-epoxidized Ddx cycle pigment Dtx shows a decreased solubility in MGDG compared with the epoxidized Ddx which possibly accelerates the rebinding of Dtx to the FCP complex (Goss et al., 2007). Since in higher plants and green algae the majority of the Vx cycle pigments are bound to the LHCII (section Localization of Xanthophyll Cycle Pigments in the Thylakoid Membrane and references) it is reasonable to believe that most of the non-bilayer lipid phases are located in the vicinity of LHCII and thus in the grana regions of the thylakoid membrane. On the other hand, Vx de-epoxidation is not restricted to the LHCII but also occurs in the LHCI (Lee and Thornber, 1995; Arvidsson et al., 1997; Zhu et al., 1997) which would require the presence of inverted hexagonal phases in the stroma thylakoids in the vicinity of LHCI. However, based on the observation that Vx de-epoxidation in the LHCI is less efficient than that in LHCII (Wehner et al., 2004) the non-bilayer lipid phases in the stroma thylakoid membranes may be less well-defined as the non-bilayer lipid phases in the grana membranes. The idea of a tight association of the non-bilayer lipid phase and the light-harvesting complexes is supported by the analysis of the molecular structure of the LHCII at 3.2 Å resolution which revealed the presence of a putative binding site for the enzyme VDE (Liu et al., 2004). It is thus possible that the local non-bilayer lipid phase enables the direct interaction between the VDE and the LHCII. A close association between the LHCII and the VDE is furthermore corroborated by the recent direct isolation of a functional Vx cycle membrane domain from thylakoid membranes of higher plants (Goss et al., 2017). With the use of the very mild detergent α-dodecylmaltoside and a preparation at pH5, which ensured the binding of VDE to the luminal side of the thylakoid membrane, the authors were able to isolate a membrane domain consisting of LHCII, VDE and MGDG. The domain was in functional state as evidenced by the de-epoxidation of Vx to Ax and Zx by the domain-associated VDE. However, the studies of Arvidsson et al. (1997) and Macko et al. (2002) are in favor of a greater distance between the LHCII and the lipid phase of the membrane where the actual Vx de-epoxidation is taking place. In both studies the activity of isolated, exogenous VDE was analyzed. VDE was added to the stromal side of thylakoid membranes where the activity of the endogenous VDE at the luminal site of the membrane was inhibited by DTT (Arvidsson et al., 1997) or to the stromal side of thylakoids isolated from *Arabidopsis thaliana* mutants that did not contain VDE (Macko et al., 2002). Both studies show that the de-epoxidation efficiency of VDE located at the stromal side of the membrane is comparable to the activity of native VDE at the luminal side of the thylakoid membrane. Since in these experiments the VDE located at the stromal membrane site had no accession to the grana stacks it was concluded that the lipid phase where de-epoxidation is taking place is located at a certain distance to the central part of the grana membranes and located at the surface of the grana stacks. This notion was supported by the lower VDE activity at reduced temperatures which the authors interpreted in such a way that Vx cycle pigments, which have detached from the LHCII, have to diffuse a certain distance in the membrane until they reach the lipid phase for de-epoxidation.

With respect to the possible localization of the non-bilayer lipid phase in diatom thylakoids it has to be taken into account that the diatom thylakoid membranes show a different architecture compared with the thylakoids of higher plants. The diatom thylakoids are not separated into grana and stroma thylakoids but are characterized by regular stacks of three membranes (Gibbs, 1962, 1970). Based on the observations that MGDG forms a lipid shield around the FCP complexes which incorporates the lipid-dissolved Ddx cycle pigments (Lepetit et al., 2010) and that the negatively charged lipid SQDG, which is present in high concentration in the diatom membranes, inhibits the de-epoxidation of Ddx (Goss et al., 2009) a model for the lipid and protein arrangement in the diatom thylakoid membranes was established (Lepetit et al., 2012). This model predicts that PSII with its tightly associated FCP complexes and its peripheral antenna complexes is located in the inner membranes of the stacks of three membranes. In addition, the inner core membranes are enriched in the PSII-associated MGDG. The outer membranes of the regular stacks contain the PSI complexes with their PSI-specific FCP complexes and the ATP synthase. According to the model, the lipid composition of the outer membranes is dominated by the anionic SQDG. Recently, the model of Lepetit et al. (2012) was supported by new data which show that the thylakoid membranes of the pennate diatom *P. tricornutum* contain large areas which are exclusively occupied by PSI supercomplexes, consisting of PSI core complexes with their specific antenna complexes (Bina et al., 2016). Flori et al. (2017) also obtained evidence for a compartmentalization of the two photosystems. Like the model of Lepetit et al. (2012) they propose that PSII is located in the core membranes whereas PSI is enriched in the peripheral membranes which are exposed to the chloroplast stroma. Since the FCP complexes associated with PSII are surrounded by an MGDG phase, MGDG is most probably also enriched in the inner membranes. The enrichment of MGDG in the core membranes may lead to the formation of non-bilayer structures which then represent attraction sites for the diatom DDE and support the

efficient conversion of Ddx to Dtx. The confinement of SQDG to the outer, peripheral membranes is most likely needed in order to prevent the interaction with the DDE in the non-bilayer phases in the core membranes which would result in a pronounced inhibition of Ddx de-epoxidation.

Formation of Non-bilayer Lipid Phases by Structural Changes of Light-Harvesting Proteins

The high concentration of MGDG in thylakoid membranes of higher plants and green algae poses the risk of the formation of inverted hexagonal phases and the segregation of MGDG out of the membrane bilayer in an aqueous environment. In the native thylakoids the formation of extensive non-bilayer lipid phases is restricted by the high protein content of the membranes and extensive lipid phase separation can only be observed when thylakoids are exposed to various abiotic stresses. For the thylakoids of higher plants it has been demonstrated that the interaction of the main membrane protein LHCII and MGDG plays a crucial role in establishing and maintaining the lipid bilayer structure (Simidjiev et al., 1998, 2000). *In vitro* studies with isolated LHCII and MGDG showed that in the presence of MGDG large, ordered lamellar structures of protein and lipid are formed. In addition, the presence of LHCII disturbs the inverted hexagonal phase of MGDG and forces the MGDG molecules into a bilayer structure. Based on these results it was proposed that in thylakoid membranes the spatial limitation caused by the high concentration of membrane proteins inhibits the formation of non-bilayer lipid phases. Additional studies demonstrated that MGDG stabilizes the oligomeric states of LHCII (Schaller et al., 2011), FCP complexes and the LHC of the Prasinophyceae *M. squamata* (Schaller-Laudel et al., 2017). Furthermore, MGDG increases the mechanical stability of the LHCII (Seiwert et al., 2017), thereby preventing the unfolding of trimeric LHCII. Stabilization of LHCII by MGDG was attributed to a steric matching of the conically shaped MGDG and the hourglass shape of trimeric LHCII (Seiwert et al., 2017). Several studies have shown that LHCII in its lipid environment is structurally flexible and can undergo molecular rearrangements (see section Function of Xanthophyll Cycles and references therein). During high light illumination of plants or algae, which triggers the process of NPQ, aggregation of LHCII is taking place. With respect to the formation of non-bilayer lipid phases in the thylakoid membrane the aggregation of LHCII or FCP complexes is thought to play an important role. Protein aggregation, in general, leads to a segregation of lipid molecules which are otherwise associated with the non-aggregated protein complexes. It is thought that in the case of the LHCII and FCP complexes aggregation leads to the liberation of a significant part of the MGDG molecules associated with the light-harvesting proteins followed by a separation from the lipid bilayer phase of the thylakoid membrane and finally the formation of inverted hexagonal phases. Although it is still a matter of debate if the non-bilayer phases are formed within the lipid bilayer (Jahns et al., 2009) or are associated with the outside of the membrane (Garab et al., 2016 see **Figure 3**), recent results have implicated that non-bilayer lipid phases are located at the luminal and stromal sides of the thylakoid membrane (Garab et al., 2017).

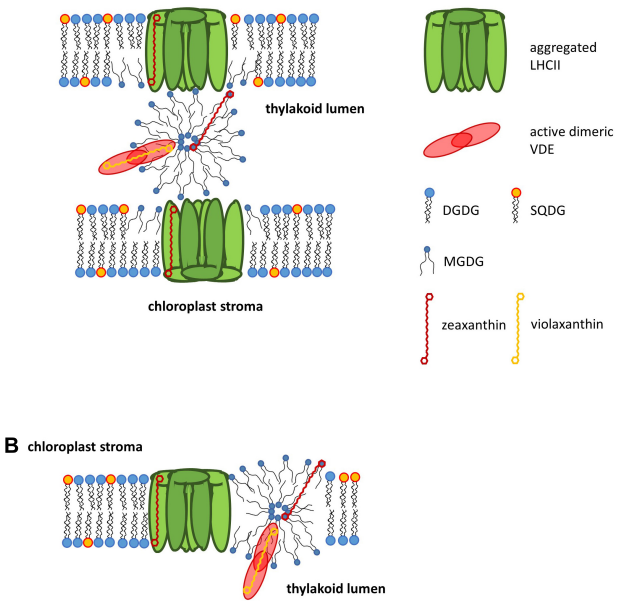

FIGURE 3 | Model for the violaxanthin cycle domain in thylakoid membranes of higher plants. High light illumination leads to a disconnection of the main light-harvesting complex of photosystem II, LHCII from the photosystem II core complex followed by protein aggregation. MGDG molecules, which during low light illumination surround the LHCII, dissociate, segregate and form a non-bilayer lipid phase. This non-bilayer lipid phase may be located outside of the membrane bilayer, i.e., within the thylakoid lumen **(A)**, or within the plane of the thylakoid membrane **(B)**. During high light illumination violaxanthin disconnects from its binding site at the LHCII apoproteins and diffuses into the non-bilayer lipid phase. The non-bilayer lipid phase represents an attraction site for the enzyme violaxanthin de-epoxidase (VDE), which, after its pH-dependent activation and dimerization, binds to the non-bilayer lipid phase. The non-bilayer lipid phase is characterized by a reduced surface tension and thus allows the penetration of the enzyme's hydrophobic catalytic site into the hydrophobic core of the non-bilayer lipid phase where it gains access to the hydrophobic pigment violaxanthin. After the conversion of violaxanthin to zeaxanthin, zeaxanthin rebinds to the LHCII and participates in photoprotection via NPQ. Since the violaxanthin cycle domain, consisting of LHCII, MGDG, VDE and xanthophyll cycle pigments, is only established during high light illumination of plants, the domain can be described as a transient membrane domain.

The Xanthophyll Cycle Membrane Domain in the Light of Recent Membrane Models

More than 40 years ago the fluid mosaic model of biomembranes was introduced by Singer and Nicholson (1972). The first main feature of this model is the amphiphilic nature of the membrane lipids which means that the lipids contain a hydrophilic head group and a hydrophobic area covered by the FA moieties (see section Three Dimensional Structures of Lipids). The amphiphilic character of the lipids leads to the formation of a lipid bilayer in aqueous surroundings. A second important feature concerns the proteins which can

be associated with the hydrophilic head groups of the lipids as peripheral proteins or with the hydrophobic core of the membrane as trans-membrane proteins. A third important aspect lies in the fluidity of the membrane which means that both lipids and proteins are in constant motion. Protein and lipid motion can occur in lateral direction, i.e., in the plane of the membrane. In addition, rotation of proteins and lipids along their long axis is possible. Since the first presentation of the fluid mosaic model a wealth of information about the structure of biomembranes has been gathered (for recent reviews see Bagotelli and Mouritsen, 2013; Goni, 2014; Nicholson, 2014). Although these data do not question the general assumptions of the fluid mosaic model they have refined the model in several important ways. The first important aspect concerns the high concentration of membrane proteins. While in the original model only few proteins span the membrane bilayer it is known today that the membrane is densely packed with membrane and peripheral proteins (for a review see Engelmann, 2005). Especially in membranes like the thylakoid membrane or the inner mitochondrial membrane the protein density is so high that bilayer phases composed solely of lipids are hardly observed (for a recent review on the thylakoid architecture see Kirchhoff, 2018). A second new finding, which is also critical for the understanding of the xanthophyll cycle function, is the observation that proteins exist which only transiently bind to biomembranes (reviewed by Goni, 2002). This class of proteins can exist in water-soluble form in an aqueous environment but can also bind to the membrane after certain requirements have been met. The transient proteins supplement the proteins which are permanently associated with the membrane and the water-soluble proteins which never come into contact with the lipid bilayer. A further important extension of the original fluid mosaic model, which is also of fundamental importance for the operation of the xanthophyll cycle, is the finding that non-bilayer phases can co-exist with the lipid bilayer (for the presence of inverted hexagonal phases in thylakoid membranes see section Localization of Non-bilayer Lipid Phases in the Thylakoid Membrane and references therein). Another feature which separates the new membrane models from the original fluid mosaic model concerns the observation that biomembranes are characterized by a pronounced lateral heterogeneity. It has become clear that the membrane bilayer consists of heterogeneous domains (for reviews on domains and lipid rafts in plant membranes see Mongrand et al., 2010; Simon-Plas et al., 2011). These membrane domains contain a specific lipid and protein composition and perform a special function. Other important aspects of the new generation of membrane models describe the membrane not as a flat surface but as a curved structure. In this regard the observation of a hydrophobic mismatch is interesting (for a review see Killian, 1998). Hydrophobic mismatch describes the situation when the hydrophobic thickness of the transmembrane region of a membrane protein does not match the hydrophobic thickness of the membrane in which it is localized. Here it has been shown that both membrane proteins, by re-arrangements of the protein structure, and membrane lipids, by stretching or tilting of the FA chains, can adapt to this situation. According to the results outlined in the preceding chapters (see references therein) the part of the thylakoid membrane where the Vx cycle, and most likely the Ddx cycle, too, takes place can be described as a special membrane domain (**Figure 3**). The Vx cycle domain contains a specific protein composition, namely the LHCII, a membrane protein which is permanently associated with the membrane, and the VDE, a water-soluble protein which, after its pH-dependent activation, transiently binds to the membrane. The Vx cycle domain is characterized by a specific lipid composition because it is enriched in the non-bilayer lipid MGDG which likely forms an inverted hexagonal structure within the domain. The enrichment of MGDG is driven by the structural re-arrangement, i.e., the aggregation, of the LHCII which leads to a local enrichment of free MGDG molecules. The Vx cycle domain carries out a special function, i.e., the conversion of the di-epoxy xanthophyll Vx to Ax and Zx. The Vx cycle domain can be characterized as a transient domain which is only established during high light illumination when Vx de-epoxidation is needed for photoprotection via NPQ. A transition from high light illumination back to low light conditions or darkness reverses the domain formation by a detachment of the VDE from the membrane and a disaggregation of LHCII. Disaggregation of the LHCII re-enables the tight interaction of the membrane protein with MGDG, thereby re-enforcing the membrane bilayer structure.

OUTLOOK

Although recent measurements have begun to shed light on the existence and localization of inverted hexagonal phases in the thylakoid membrane of higher plants (Garab et al., 2017), and the isolation of a putative, functional Vx cycle membrane domain has been reported (Goss et al., 2017), there is still a wealth of open questions with respect to the lipid dependence of xanthophyll cycling. Future measurements have to show where the inverted hexagonal phase responsible for Vx de-epoxidation is located, i.e., whether it is located within the plane of the thylakoid membrane or whether it is attached to the luminal side of the membrane. With respect to the localization of the non-bilayer lipid phase it has to be clarified if the lipid phase is located in the direct vicinity of the LHCII or at a greater distance, possibly in the grana margins. A greater distance between the xanthophyll cycle pigment binding proteins and the lipid phase, where the actual enzymatic reaction is taking place, would require significantly longer diffusion times of Vx and Zx. Future measurements have to provide a way to determine the size of the inverted hexagonal phases to answer the question if fewer but larger non-bilayer lipid phases exist or if the xanthophyll cycle pigments are converted in a larger number of smaller sized inverted hexagonal phases. In this respect it has to be demonstrated if the VDE, which seems to be present in only very low concentrations in the thylakoid lumen (Arvidsson et al., 1996), stays attached to a larger non-bilayer phase or if it detaches and rebinds to a higher number of smaller phases. With regard to the conversion of Vx to Ax and Zx in the LHCI (Croce et al., 2002, 2007) it has to be elucidated if non-bilayer phases or even xanthophyll cycle domains exist in

the vicinity of PSI and thus the stroma membranes. According to our knowledge it is also unclear if the back reaction of the xanthophyll cycle, which is carried out by the peripheral membrane protein ZEP (Schaller et al., 2012b), requires the presence of special membrane lipid structures, like e.g., the inverted hexagonal phase, and where this hypothetical phase or domain is located. Finally, scientists working with algae may concentrate on the question if similar xanthophyll cycle domains exist in the different algal classes and, taking into account the different thylakoid structures (Lepetit et al., 2012; Flori et al., 2017), where these domains are localized.

AUTHOR CONTRIBUTIONS

RG and DL wrote and corrected the text and constructed the figures.

ACKNOWLEDGMENTS

We thank our collaborators, co-workers, and students who have contributed with their work to our research in the field of lipids and xanthophyll cycles.

REFERENCES

Andersson, M. X., Larsson, K. E., Tjellström, H., Liljenberg, C., and Sandelius, A. S. (2005). Phosphate limited oat. The plasma membrane and the tonoplast as major targets for phospholipid-to-glycolipid replacement and stimulation of phospholipases in the plasma membrane. *J. Biol. Chem.* 280, 27578–27586. doi: 10.1074/jbc.M503273200

Andersson, M. X., Stridh, M. H., and Larsson, K. E., (2003). Phosphate deficient oat replaces a major portion of the plasma membrane phospholipids with the galactolipid digalactosyldiacylglycerol. *FEBS Lett.* 537, 128–132. doi: 10.1016/S0014-5793(03)00109-1

Arnoux, P., Morosinotto, T., Saga, G., Bassi, R., and Pignol, D. (2009). A structural basis for the pH-dependent xanthophyll cycle in *Arabidopsis thaliana*. *Plant Cell* 21, 2036–2044. doi: 10.1105/tpc.109.068007

Aronsson, H., Schüttler, M. A., Kelly, A. A., Sundqvist, C., Dörmann, P., Karim, S., et al. (2008). Monogalactosyldiacylglycerol deficiency in *Arabidopsis thaliana* affects pigment composition in the prolamellar body and impairs thylakoid membrane energization and photoprotection in leaves. *Plant Physiol.* 148, 580–592. doi: 10.1104/pp.108.123372

Arvidsson, P.-O., Bratt, C. E., Carlsson, M., and Akerlund, H.-E. (1996). Purification and identification of the violaxanthin deepoxidase as a 43 kDa protein. *Photosynth. Res.* 49, 119–129. doi: 10.1007/bf00117662

Arvidsson, P.-O., Carlsson, M., Stefansson, H., Albertsson, P. A., and Akerlund, H.-E. (1997). Violaxanthin accessibility and temperature dependency for de-epoxidation in spinach thylakoid membranes. *Photosynth. Res.* 52, 39–48.

Bagotelli, L. A., and Mouritsen, O. G. (2013). Is the fluid mosaic (and the accompanying raft hypothesis) a suitable model to describe fundamental features of biological membranes? What may be missing? *Front. Plant Sci.* 4:457. doi: 10.3389/fpls.2013.00457

Bailleul, B., Rogato, A., de Martino, A., Coesel, S., Cardol, P., Bowler, C., et al. (2010). An atypical member of the light-harvesting complex stress-related protein family modulates diatom responses to light. *Proc. Natl. Acad. Sci. U.S.A.* 107, 18214–18219. doi: 10.1073/pnas.1007703107

Ballottari, M., Truong, T. B., De Re, E., Erickson, E., Stella, G. R., Fleming, G. R., et al. (2016). Identification of pH-sensing sites in the light-harvesting complex stress-related 3 protein essential for triggering non-photochemical quenching in *Chlamydomonas reinhardtii*. *J. Biol. Chem.* 291, 7334–7346. doi: 10.1074/jbc.m115.704601

Bassi, R., Pineau, B., Dainese, P., and Marquardt, J. (1993). Carotenoid-binding proteins of photosystem II. *Eur. J. Biochem.* 212, 297–303. doi: 10.1111/j.1432-1033.1993.tb17662.x

Ben Hamed, K., Ben Youssef, N., Ranieri, A., Zarrouk, M., and Abdelly, C. (2005). Changes in content and fatty acid profiles of total lipids and sulfolipids in the halophyte *Crithmum maritimum* under salt stress. *J. Plant Physiol.* 162, 599–602. doi: 10.1016/j.jplph.2004.11.010

Bertrand, M., and Schoefs, B. (1999). "Photosynthetic pigment metabolism in plants during stress," in *Handbook of Plant And Crop Stress*, 2nd Edn, ed. M. Pessarakli (New York, NY: Marcel Dekker), 527–541.

Bina, D., Herbstova, M., Gardian, Z., Vacha, F., and Litvin, R. (2016). Novel structural aspect of the diatom thylakoid membrane: lateral segregation of photosystem I under red-enhanced illumination. *Sci. Rep.* 6:25583.

Bojko, M., Olchawa-Pajor, M., Goss, R., Schaller-Laudel, S., Strzalka, K., and Latowski, D. (2019). Diadinoxanthin de-epoxidation as important factor in the short-term stabilization of diatom photosynthetic membranes exposed to different temperatures. *Plant Cell Environ.* 42, 1270–1286. doi: 10.1111/pce.13469

Bonente, G., Ballotari, M., Truong, T. B., Morosinotto, T., Ahn, T. K., Fleming, G. R., et al. (2011). Analysis of LhcSR3, a protein essential for feedback de-excitation in the green alga *Chlamydomonas reinhardtii*. *PLoS Biol.* 9:e1000577. doi: 10.1371/journal.pbio.1000577

Boudiere, L., Michaud, M., Petroutsos, D., Rébeillé, F., Falconet, D., Bastien, O., et al. (2014). Glycerolipids in photosynthesis: composition, synthesis and trafficking. *Biochim. Biophys. Acta* 1837, 470–480. doi: 10.1016/j.bbabio.2013.09.007

Buck, J. M., Sherman, J., Bartulos, C. R., Serif, M., Halder, M., Henkel, J., et al. (2019). Lhcx proteins provide photoprotection via thermal dissipation of absorbed light in the diatom *Phaeodactylum tricornutum*. *Nat. Commun.* 10:4167.

Bungard, R. A., Ruban, A. V., Hibberd, J. M., Press, M. C., Horton, P., and Scholes, J. D. (1999). Unusual carotenoid composition and a new type of xanthophyll cycle in plants. *Proc. Natl. Acad. Sci. U.S.A.* 96, 1135–1139. doi: 10.1073/pnas.96.3.1135

Cardol, P., Bailleul, B., Rappaport, F., Derelle, E., Béal, D., Breyton, C., et al. (2008). An original adaptation of photosynthesis in the marine green alga *Ostreococcus*. *Proc. Natl. Acad. Sci. U.S.A.* 105, 7881–7886. doi: 10.1073/pnas.0802762105

Chen, J., Burke, J. J., Xin, Z., Xu, C., and Velten, J. (2006). Characterization of the Arabidopsis thermosensitive mutant atts02 reveals an important role for galactolipids in thermotolerance. *Plant Cell Environm.* 29, 1437–1448. doi: 10.1111/j.1365-3040.2006.01527.x

Coesel, S., Obornik, M., Varela, J., Falciatore, A., and Bowler, C. (2008). Evolutionary origins and functions of the carotenoid biosynthetic pathway in marine diatoms. *PLoS One* 3:e2896. doi: 10.1371/journal.pone.0002896

Croce, R., Morosinotto, T., Castelletti, S., Breton, J., and Bassi, R. (2002). The Lhca antenna complexes of higher plants photosystem I. *Biochim. Biophys. Acta* 1556, 29–40. doi: 10.1016/s0005-2728(02)00304-3

Croce, R., Mozzo, M., Morosinotto, T., Romeo, A., Hienerwadel, R., and Bassi, R. (2007). Singlet and triplet state transitions of carotenoids in the antenna complexes of higher-plant Photosystem I. *Biochemistry* 46, 3846–3855. doi: 10.1021/bi602531k

Dall'Osto, L., Cazzaniga, S., Bressan, M., Palecek, D., Zidek, K., Niyogi, K. K., et al. (2017). Two mechanisms for dissipation of excess light in monomeric and trimeric light-harvesting complexes. *Nat. Plants* 3:17033.

Dautermann, O., and Lohr, M. (2017). A functional zeaxanthin epoxidase from red algae shedding light on the evolution of light-harvesting carotenoids and the xanthophyll cycle in photosynthetic eukaryotes. *Plant J.* 92, 879–892.

Demmig, B., Winter, K., Krüger, A., and Czygan, F.-C. (1987). Photoinhibition and zeaxanthin formation in intact leaves. A possible role for the xanthophyll cycle in the dissipation of excess light. *Plant Physiol.* 84, 218–224. doi: 10.1104/pp.84.2.218

Demmig, B., Winter, K., Krüger, A., and Czygan, F.-C. (1988). Zeaxanthin and the heat dissipation of excess light energy in *Nerium oleander* exposed to a combination of high light and water stress. *Plant Physiol.* 87, 17–24. doi: 10.1104/pp.87.1.17

Demmig-Adams, B., and Adams, W. W. III (2006). Photoprotection in an ecological context: the remarkable complexity of thermal energy dissipation. *New Phytol.* 172, 11–21. doi: 10.1111/j.1469-8137.2006.01835.x

Demmig-Adams, B., Koh, S.-C., Cohu, C. M., Muller, O., Stewart, J. J., and Adams, W. W. III (2014). "Non-photochemical fluorescence quenching in contrasting plant species and environments," in *Non-Photochemical Quenching And Energy Dissipation In Plants, Algae And Cyanobacteria*, eds B. Demmig-Adams, G. Garab, W. W. Adams, and M. Govindjee (Dordrecht: Springer), 531–552. doi: 10.1007/978-94-017-9032-1_24

Dodson, V. J., Dahmen, J. L., Mouget, J.-L., and Leblond, J. D. (2013). Mono- and digalactosyldiacylglycerol composition of the marennine-producing diatom, *Haslea ostrearia*: comparison to a selection of pennate and centric diatoms. *Phycol. Res.* 61, 199–207. doi: 10.1111/pre.12015

Dodson, V. J., Mouget, J.-L., Dahmen, J. L., and Leblond, J. D. (2014). The long and short of it: temperature-dependent modifications of fatty acid chain length and unsaturation in the galactolipid profiles of the diatoms *Haslea ostrearia* and *Phaeodactylum tricornutum*. *Hydrobiologia* 727, 95–107. doi: 10.1007/s10750-013-1790-4

Engelmann, D. M. (2005). Membranes are more mosaic than fluid. *Nature* 438, 578–580. doi: 10.1038/nature04394

Esteban, R., Becerril, J. M., and Garcia-Plazaola, J. I. (2009). Lutein epoxide cycle-more than a just a forest tale. *Plant Signal. Behav.* 4, 342–344. doi: 10.4161/psb.4.4.8197

Esteban, R., and Garcia-Plazaola, J. I. (2014). "Involvement of a second xanthophyll cycle in non-photochemical quenching of chlorophyll fluorescence: the lutein epoxide story," in *Non-Photochemical Quenching And Energy Dissipation In Plants, Algae And Cyanobacteria*, eds B. Demmig-Adams, G. Garab, and W. W. Adams (Dordrecht: Springer), 277–295. doi: 10.1007/978-94-017-9032-1_12

Flori, S., Jouneau, P., Bailleul, B., Gallet, B., Estrozi, L. F., Moriscot, C., et al. (2017). Plastid thylakoid architecture optimizes photosynthesis in diatoms. *Nat. Commun.* 18:15885.

Frentzen, M., Heinz, E., McKeon, T. A., and Stumpf, P. K. (1983). Specificities and selectivities of glycerol-3- phosphate acyltransferase and monoacylglycerol-3-phosphate acyltransferase from pea and spinach chloroplasts. *Eur. J. Biochem.* 129, 629–636. doi: 10.1111/j.1432-1033.1983.tb07096.x

Frommolt, R., Goss, R., and Wilhelm, C. (2001). The de-epoxidase and epoxidase reactions of *Mantoniella squamata* (Prasinophyceae) exhibit different substrate-specific reaction kinetics compared to spinach. *Planta* 213, 446–456. doi: 10.1007/s004250100589

Fufezan, C., Simionato, D., and Morosinotto, T. (2012). Identification of key residues for pH dependent activation of violaxanthin de-epoxidase from *Arabidopsis thaliana*. *PLoS One* 7:e35669. doi: 10.1371/journal.pone.0035669

Garab, G., Lohner, K., Laggner, P., and Farkas, T. (2000). Self-regulation of the lipid content of membranes by non-bilayer lipids: a hypothesis. *Trends Plant Sci.* 5, 489–494. doi: 10.1016/s1360-1385(00)01767-2

Garab, G., Ughy, B., de Waard, P., Akhtar, P., Javornik, U., Kotakis, C., et al. (2017). Lipid polymorphism in chloroplast thylakoid membranes - as revealed by ^{31}P-NMR and time resolved merocyanine fluorescence spectroscopy. *Sci. Rep.* 7:13343.

Garab, G., Ughy, B., and Goss, R. (2016). "Role of MGDG and non-bilayer lipid phases in the structure and dynamics of chloroplast thylakoid membranes," in *Lipids in Plant and Algae Development*, eds Y. Nakamura and Y. Li-Beisson (Dordrecht: Springer), 127–157.

Garcia-Mendoza, E., and Colombo-Pallotta, M. F. (2007). The giant kelp *Macrocystis pyrifera* presents a different nonphotochemical quenching control than higher plants. *New Phytol.* 173, 526–536. doi: 10.1111/j.1469-8137.2006.01951.x

Garcia-Plazaola, J. I., Hernandez, A., Olano, J. M., and Becerril, J. M. (2003). The operation of the lutein epoxide cycle correlates with energy dissipation. *Funct. Plant Biol.* 30, 319–324.

Gerotto, C., and Morosinotto, T. (2013). Evolution of photoprotection mechanisms upon land colonization: evidence of PSBS-dependent NPQ in late Streptophyte algae. *Physiol. Plant.* 149, 583–598. doi: 10.1111/ppl.12070

Gibbs, S. P. (1962). The ultrastructure of the chloroplasts of algae. *J. Ultrastruct. Res.* 7, 418–435. doi: 10.1016/s0022-5320(62)90038-2

Gibbs, S. P. (1970). The comparative ultrastructure of the algal chloroplast. *Ann. N. Y. Acad. Sci.* 175, 454–473. doi: 10.1111/j.1749-6632.1970.tb45167.x

Goni, F. M. (2002). Non-permanent proteins in membranes: when proteins come as visitors. *Mol. Membr. Biol.* 19, 237–245. doi: 10.1080/09687680210003 5078

Goni, F. M. (2014). The basic structure and dynamics of cell membranes: an update of the singer-nicholson model. *Biochim. Biophys. Acta* 1838, 1467–1476. doi: 10.1016/j.bbamem.2014.01.006

Goss, R. (2003). Substrate specificity of the violaxanthin de-epoxidase of the primitive green alga *Mantoniella squamata* (Prasinophyceae). *Planta* 217, 801–812. doi: 10.1007/s00425-003-1044-1

Goss, R., Böhme, K., and Wilhelm, C. (1998). The xanthophyll cycle of *Mantoniella squamata* converts violaxanthin into antheraxanthin but not to zeaxanthin: consequences for the mechanism of enhanced non-photochemical energy dissipation. *Planta* 205, 613–621. doi: 10.1007/s004250050364

Goss, R., Greifenhagen, A., Bergner, J., Volke, D., Hoffmann, R., Wilhelm, C., et al. (2017). Direct isolation of a functional violaxanthin cycle domain from thylakoid membranes of higher plants. *Planta* 245, 793–806. doi: 10.1007/s00425-016-2645-9

Goss, R., and Jakob, T. (2010). Regulation and function of xanthophyll cycle-dependent photoprotection in algae. *Photosynth. Res.* 106, 103–122. doi: 10.1007/s11120-010-9536-x

Goss, R., Latowski, D., Grzyb, J., Vieler, A., Lohr, M., Wilhelm, C., et al. (2007). Lipid dependence of diadinoxanthin solubilization and de-epoxidation in artificial membrane systems resembling the lipid composition of the natural thylakoid membrane. *Biochim. Biophys. Acta* 1768, 67–75. doi: 10.1016/j.bbamem.2006.06.006

Goss, R., and Lepetit, B. (2015). Biodiversity of NPQ. *J. Plant Physiol.* 172, 13–32. doi: 10.1016/j.jplph.2014.03.004

Goss, R., Lohr, M., Latowski, D., Grzyb, J., Vieler, A., Wilhelm, C., et al. (2005). Role of hexagonal structure-forming lipids in diadinoxanthin and violaxanthin solubilization and de-epoxidation. *Biochemistry* 44, 4028–4036. doi: 10.1021/bi047464k

Goss, R., Nerlich, J., Lepetit, B., Schaller, S., Vieler, A., and Wilhelm, C. (2009). The lipid dependence of diadinoxanthin de-epoxidation presents new evidence for a macrodomain organization of the diatom thylakoid membrane. *J. Plant Physiol.* 166, 1839–1854. doi: 10.1016/j.jplph.2009.05.017

Goss, R., Pinto, E. A., Wilhelm, C., and Richter, M. (2006). The importance of a highly active and ΔpH-regulated diatoxanthin epoxidase for the regulation of the PS II antenna function in diadinoxanthin cycle containing algae. *J. Plant Physiol.* 163, 1008–1021. doi: 10.1016/j.jplph.2005.09.008

Goss, R., and Wilhelm, C. (2009). "Lipids in algae, lichens and mosses," in *Lipids in Photosynthesis: Essential and Regulatory Functions*, eds H. Wada, N. Murata, and M. Govindjee (Berlin: Springer), 119–120.

Gounaris, K., Brain, A. P. R., Quinn, P. J., and Williams, W. P. (1984). Structural reorganization of chloroplast thylakoid membranes in response to heat stress. *Biochim. Biophys. Acta* 766, 198–208. doi: 10.1016/0005-2728(84)90232-9

Grouneva, I., Jakob, T., Wilhelm, C., and Goss, R. (2006). Influence of ascorbate and pH on the activity of the diatom xanthophyll cycle-enzyme diadinoxanthin de-epoxidase. *Physiol. Plant.* 126, 205–211. doi: 10.1111/j.1399-3054.2006.00613.x

Grudzinski, W., Nierzwicki, L., Welc, R., Reszczynska, E., Luchowski, R., Czub, J., et al. (2017). Localization and orientation of xanthophylls in a lipid bilayer. *Sci. Rep.* 7:9619.

Gruszecki, W. I., and Strzalka, K. (1991). Does the xanthophyll cycle take part in the regulation of fluidity of the thylakoid membrane? *Biochim. Biophys. Acta* 1060, 310–314. doi: 10.1016/s0005-2728(05)80322-6

Gruszecki, W. I., and Strzalka, K. (2005). Carotenoids as modulators of lipid membrane physical properties. *Biochim. Biophys. Acta* 1740, 108–115. doi: 10.1016/j.bbadis.2004.11.015

Grzyb, J., Latowski, D., and Strzalka, K. (2006). Lipocalins - a family portrait. *J. Plant Physiol.* 163, 895–915. doi: 10.1016/j.jplph.2005.12.007

Gundermann, K., and Büchel, C. (2008). The fluorescence yield of the trimeric fucoxanthin-chlorophyll-protein FCPa in the diatom *Cyclotella meneghiniana* is dependent on the amount of bound diatoxanthin. *Photosynth. Res.* 95, 229–235. doi: 10.1007/s11120-007-9262-1

Gundermann, K., Wagner, V., Mittag, M., and Büchel, C. (2019). Fucoxanthin-chlorophyll protein complexes of the centric diatom *Cyclotella meneghiniana* differ in Lhcx1 and Lhcx6_1 content. *Plant Physiol.* 179, 1779–1795. doi: 10.1104/pp.18.01363

Guschina, I. A., and Harwood, J. L. (2006). Lipids and lipid metabolism in eukaryotic algae. *Prog. Lipid Res.* 45, 160–186. doi: 10.1016/j.plipres.2006.01.001

Guskov, A., Kern, J., and Saenger, W. (2009). Cyanobacterial photosystem II at 2.9-A resolution and the role of quinones, lipids, channels and chloride. *Nat. Struct. Mol. Biol.* 16, 334–342. doi: 10.1038/nsmb.1559

Hager, A. (1957). Über den Einfluss klimatischer Faktoren auf den Blattfarbstoffgehalt höherer Pflanzen. *Planta* 49, 524–560. doi: 10.1007/bf01917726

Hager, A. (1967a). Untersuchungen über die lichtinduzierten, reversiblen Xanthophyllumwandlungen an *Chlorella* und *Spinacia oleracea*. *Planta* 74, 148–172. doi: 10.1007/bf00388326

Hager, A. (1967b). Untersuchungen üben die Rückreaktionen im Xanthophyll-Cyclus bei *Chlorella*, *Spinacia* und *Taxus*. *Planta* 76, 138–148. doi: 10.1007/BF00385460

Hager, A. (1969). Lichtbedingte pH-Erniedrigung in einem *Chloroplasten-Kompartiment* als Ursache der enzymatischen Violaxanthin-Zeaxanthin-Umwandlung: Beziehungen zur Photophosphorylierung. *Planta* 89, 224–243. doi: 10.1007/bf00385028

Hager, A., and Holocher, K. (1994). Localization of the xanthophyll-cycle enzyme violaxanthin de-epoxidase within the thylakoid lumen and abolition of its mobility by a (light-dependent) pH decrease. *Planta* 192, 581–589.

Hager, A., and Stransky, H. (1970). Das Carotinoidmuster und die Verbreitung des lichtinduzierten Xanthophyllcyclus in verschiedenen Algenklassen. *Arch. Mikrobiol.* 73, 77–89. doi: 10.1007/bf00409954

Hallin, E. I., Guo, K., and Akerlund, H. E. (2015). Violaxanthin de-epoxidase disulphides and their role in activity and thermal stability. *Photosynth Res.* 124, 191–198. doi: 10.1007/s11120-015-0118-119

Hallin, E. I., Hasan, M., Guo, K., and Akerlund, H.-E. (2016). Molecular studies on structural changes and oligomerisation of violaxanthin deepoxidase associated with the pH-dependent activation. *Photosynth. Res.* 129, 29–41. doi: 10.1007/s11120-016-0261-y

Haranczyk, H., Strzalka, K., Dietrich, W., and Blicharski, J. S. (1995). ^{13}P-NMR observation of the temperature and glycerol induced non-lamellar phase formation in wheat thylakoid membranes. *J. Biol. Phys.* 21, 125–139. doi: 10.1007/bf00705595

Härtel, H., and Benning, C. (2000). Can digalactosyldiacylglycerol substitute for phosphatidylcholine upon phosphate deprivation in leaves and roots of Arabidopsis? *Biochem. Soc. Trans.* 28, 729–732. doi: 10.1042/bst0280729

Harwood, J. L., and Guschina, I. A. (2009). The versatility of algae and their lipid metabolism. *Biochimie* 91, 679–684. doi: 10.1016/j.biochi.2008.11.004

Havaux, M. (1998). Carotenoids as membrane stabilizers in chloroplasts. *Trends Plant Sci.* 3, 147–151. doi: 10.1016/s1360-1385(98)01200-x

Havaux, M., Dall'Osto, L., and Bassi, R. (2007). Zeaxanthin has enhanced antioxidant capacity with respect to all other xanthophylls in *Arabidopsis* leaves and functions independent of binding to PSII antennae. *Plant Physiol.* 145, 1506–1520. doi: 10.1104/pp.107.108480

Havaux, M., and Niyogi, K. K. (1999). The violaxanthin cycle protects plants from photooxidative damage by more than one mechanism. *Proc. Natl. Acad. Sci. U.S.A.* 96, 8762–8767. doi: 10.1073/pnas.96.15.8762

Heemskerk, J. W. M., Wintermans, J. F. G. M., Joyard, J., Block, M. A., Dorne, A. J., and Douce, R. (1986). Localization of galactolipid–galactolipid galactosyltransferase and acyltransferase in outer envelope membrane of spinach chloroplasts. *Biochim. Biophys. Acta* 877, 281–289. doi: 10.1016/0005-2760(86)90305-x

Heinz, E., and Roughan, P. G. (1983). Similarities and differences in lipid metabolism of chloroplasts isolated from 18:3 and 16:3 plants. *Plant Physiol.* 72, 273–279. doi: 10.1104/pp.72.2.273

Hieber, A. D., Bugos, R. C., and Yamamoto, H. Y. (2000). Plant lipocalins: violaxanthin de-epoxidase and zeaxanthin epoxidase. *Biochim. Biophys. Acta* 1482, 84–91. doi: 10.1016/s0167-4838(00)00141-2

Higashi, Y., Okazaki, Y., Myouga, F., Shinozaki, K., and Saito, K. (2015). Landscape of the lipidome and transcriptome under heat stress in *Arabidopsis thaliana*. *Sci. Rep.* 5:10533.

Higashi, Y., Okazaki, Y., Takano, K., Myouga, F., Shinozaki, K., Knoch, E., et al. (2018). A lipase gene, HEAT INDUCIBLE LIPASE1, is involved in remodeling chloroplastic monogalactosyldiacylglycerol by liberatingα-linolenic acid in *Arabidopsis* leaves under heat stress. *Plant Cell* 30, 1887–1905. doi: 10.1105/tpc.18.00347

Higashi, Y., and Saito, K. (2019). Lipidomic studies of membrane glycerolipids in plant leaves under heat stress. *Prog. Lipid Res.* 75:100990. doi: 10.1016/j.plipres.2019.100990

Hölzl, G., and Dörmann, P. (2019). Chloroplast lipids and their biosynthesis. *Annu. Rev. Plant Biol.* 70, 51–81. doi: 10.1146/annurev-arplant-050718-100202

Holzwarth, A. R., Miloslavina, Y., Nilkens, M., and Jahns, P. (2009). Identification of two quenching sites active in the regulation of photosynthetic light-harvesting studied by time-resolved fluorescence. *Chem. Phys. Lett.* 483, 262–267. doi: 10.1016/j.cplett.2009.10.085

Horton, P. (2014). "Developments in research on non-photochemical fluorescence quenching: emergence of key ideas, theories and experimental approaches," in *Non-Photochemical Quenching And Energy Dissipation In Plants, Algae And Cyanobacteria*, eds B. Demmig-Adams, G. Garab, and W. W. Adams (Dordrecht: Springer), 73–95. doi: 10.1007/978-94-017-9032-1_3

Huang, Y., and Gui, S. (2018). Factors affecting the structure of lyotropic liquid crystals and the correlation between structure and drug diffusion. *RSC Adv.* 8, 6978–6987. doi: 10.1039/c7ra12008g

Jahns, P., and Holzwarth, A. R. (2012). The role of the xanthophyll cycle and of lutein in photoprotection of photosystem II. *Biochim. Biophys. Acta* 1817, 182–193. doi: 10.1016/j.bbabio.2011.04.012

Jahns, P., Latowski, D., and Strzalka, K. (2009). Mechanism and regulation of the violaxanthin cycle: the role of antenna proteins and membrane lipids. *Biochim. Biophys. Acta* 1787, 3–14. doi: 10.1016/j.bbabio.2008.09.013

Jahns, P., Wehner, A., Paulsen, H., and Hobe, S. (2001). De-epoxidation of violaxanthin after reconstitution into different carotenoid binding sites of light-harvesting complex II. *J. Biol. Chem.* 276, 22154–22159. doi: 10.1074/jbc.m102147200

Jakob, T., Goss, R., and Wilhelm, C. (2001). Unusual pH-dependence of diadinoxanthin de-epoxidase activation causes chlororespiratory induced accumulation of diatoxanthin in the diatom *Phaeodactylum tricornutum*. *J. Plant Physiol.* 158, 383–390. doi: 10.1078/0176-1617-00288

Janero, D. R., and Barrnett, R. (1982). Isolation and characterization of an ether-linked homoserine lipid from the thylakoid membrane of *Chlamydomonas reinhardtii* 137+. *J. Lipid Res.* 23, 307–316.

Jarvis, P., Dörmann, P., and Chory, J. (2000). Galactolipid deficiency and abnormal chloroplast development in the *Arabidopsis* MGD synthase 1 mutant. *Proc. Natl. Acad. Sci. U.S.A.* 97, 8175–8179. doi: 10.1073/pnas.100132197

Johnson, M. P., Havaux, M., Triantaphylides, C., Ksas, B., Pascal, A. A., Robert, B., et al. (2007). Elevated zeaxanthin bound to oligomeric LHCII enhances the resistance of Arabidopsis to photooxidative stress by a lipid-protective, antioxidant mechanism. *J. Biol. Chem.* 282, 22605–22618. doi: 10.1074/jbc.m702831200

Jouhet, J. (2013). Importance of the hexagonal lipid phase in biological membrane organization. *Front. Plant Sci.* 4:494. doi: 10.3389/fpls.2013.00494

Jouhet, J., Maréchal, E., Baldan, B., Bligny, R., Joyard, J., and Block, M. A. (2004). Phosphate deprivation induces transfer of DGDG galactolipid from chloroplast to mitochondria. *J. Cell. Biol.* 167, 863–874. doi: 10.1083/jcb.200407022

Kansy, M., Wilhelm, C., and Goss, R. (2014). Influence of thylakoid membrane lipids on the structure and function of the plant photosystem II core complex. *Planta* 240, 781–796. doi: 10.1007/s00425-014-2130-2

Killian, J. A. (1998). Hydrophobic mismatch between proteins and lipids in membranes. *Biochim. Biophys. Acta* 1376, 401–416. doi: 10.1016/s0304-4157(98)00017-3

Kirchhoff, H. (2014). Diffusion of molecules and macromolecules in thylakoid membranes. *Biochim. Biophys. Acta* 1837, 495–502. doi: 10.1016/j.bbabio.2013.11.003

Kirchhoff, H. (2018). Structure-function relationships in photosynthetic membranes: challenges and emerging fields. *Plant Sci.* 266, 76–82. doi: 10.1016/j.plantsci.2017.09.021

Kirchhoff, H., Mukherjee, U., and Galla, H.-J. (2002). Molecular architecture of the thylakoid membrane: lipid diffusion space for plastoquinone. *Biochemistry* 41, 4872–4882. doi: 10.1021/bi011650y

Kobayashi, K., Endo, K., and Wada, H. (2016). "Roles of lipids in photosynthesis," in *Lipids in Plant and Algae Development*, eds Y. Nakamura and Y. Li-Beisson (Berlin: Springer), 21–49. doi: 10.1007/978-3-319-25979-6_2

Kobayashi, K., Kondo, M., Fukuda, H., Nishimura, M., and Ohta, H. (2007). Galactolipid synthesis in chloroplast inner envelope is essential for proper thylakoid biogenesis, photosynthesis, and embryogenesis. *Proc. Natl. Acad. Sci. U.S.A.* 104, 17216–17221. doi: 10.1073/pnas.0704680104

Kotakis, C., Akhtar, P., Zsiros, O., Garab, G., and Lambrev, P. H. (2018). Increased thermal stability of photosystem II and the macro-organization of thylakoid membranes, induced by co-solutes, associated with changes in the lipid-phase behaviour of thylakoid membranes. *Photosynthetica* 56, 254–264. doi: 10.1007/s11099-018-0782-z

Krauss, S. (2001). "Mitochondria: structure and role in respiration," in *Encyclopedia of Life Sciences*, (New York, NY: Nature Publishing Group), 1–6.

Krumova, S. B., Dijkema, C., de Waard, P., van As, H., Garab, G., and van Amerongen, H. (2008). Phase behavior of phosphatidylglycerol in spinach thylakoid membranes as revealed by ^{31}P-NMR. *Biochim. Biophys. Acta* 1778, 997–1003. doi: 10.1016/j.bbamem.2008.01.004

Kumari, P., Kumar, M., Reddy, C. R. K., and Jha, B. (2013). "Algal lipids, fatty acids and sterols," in *Functional Ingredients From Algae For Foods And Nutraceuticals*, ed. H. Dominguez (Sawston: Woodhead Publishing Ltd), 87–134. doi: 10.1533/9780857098689.1.87

Latowski, D., Akerlund, H.-E., and Strzalka, K. (2004). Violaxanthin de-epoxidase, the xanthophyll cycle enzyme, requires lipid inverted hexagonal structures for its activity. *Biochemistry* 43, 4417–4420. doi: 10.1021/bi049652g

Latowski, D., Kostecka, A., and Strzalka, K. (2000). Effect of monogalactosyldiacylglycerol and other thylakoid lipids on violaxanthin de-epoxidation in liposomes. *Biochem. Soc. Trans.* 28, 810–812. doi: 10.1042/bst0280810

Latowski, D., Kruk, J., Burda, K., Skrzynecka-Jaskier, M., Kostecka-Gugala, A., and Strzalka, K. (2002). Kinetics of violaxanthin de-epoxidation by violaxanthin de-epoxidase, a xanthophyll cycle enzyme, is regulated by membrane fluidity in model lipid bilayers. *Eur. J. Biochem.* 269, 4656–4665. doi: 10.1046/j.1432-1033.2002.03166.x

Lavaud, J., and Lepetit, B. (2013). An explanation for the inter-species variability of the photo-protective non-photochemical chlorophyll fluorescence quenching in diatoms. *Biochim. Biophys. Acta* 1827, 294–302. doi: 10.1016/j.bbabio.2012.11.012

Lavaud, J., Rousseau, B., and Etienne, A. (2003). Enrichment of the light-harvesting complex in diadinoxanthin and implications for the nonphotochemical fluorescence quenching in diatoms. *Biochemistry* 42, 5802–5808. doi: 10.1021/bi027112i

Lee, A. L.-C., and Thornber, J. P. (1995). Analysis of the pigment stoichiometry of pigment-protein complexes from barley (*Hordeum vulgare*). *Plant Physiol.* 107, 565–574. doi: 10.1104/pp.107.2.565

Leonelli, L., Brooks, M. D., and Niyogi, K. K. (2017). Engineering the lutein epoxide cycle into *Arabidopsis thaliana*. *Proc. Natl. Acad. Sci. U.S.A.* 114, E7002–E7008. doi: 10.1073/pnas.1704373114

Lepetit, B., Goss, R., Jakob, T., and Wilhelm, C. (2012). Molecular dynamics of the diatom thylakoid membrane under different light conditions. *Photosynth. Res.* 111, 245–257. doi: 10.1007/s11120-011-9633-5

Lepetit, B., Sturm, S., Rogato, A., Gruber, A., Sachse, M., Falciatore, A., et al. (2013). High light acclimation in the secondary plastids containing diatom *Phaeodactylum tricornutum* is triggered by the redox state of the plastoquinone pool. *Plant Physiol.* 161, 853–865. doi: 10.1104/pp.112.207811

Lepetit, B., Volke, D., Gilbert, M., Wilhelm, C., and Goss, R. (2010). Evidence for the existence of one antenna-associated, lipid-dissolved, and two protein-bound pools of diadinoxanthin cycle pigments in diatoms. *Plant Physiol.* 154, 1905–1920. doi: 10.1104/pp.110.166454

Lepetit, B., Volke, D., Szabo, M., Hoffmann, R., Garab, G., Wilhelm, C., et al. (2008). "The oligomeric antenna of the diatom *P. tricornutum* - localization of diadinoxanthin cycle pigments," in *Photosynthesis. Energy from the sun*, eds J. F. Allen, E. Gantt, J. H. Golbeck, and B. Osmond (Berlin: Springer), 277–280.

Li, M., Welti, R., and Wang, X. (2006). Quantitative profiling of Arabidopsis polar glycerolipids in response to phosphorus starvation. Roles of phospholipases D zeta1 and D zeta 2 in phosphatidylcholine hydrolysis and digalactosyldiacylglycerol accumulation in phosphorus-starved plants. *Plant Physiol.* 142, 750–761. doi: 10.1104/pp.106.085647

Li, Q., Zheng, Q., Shen, W., Cram, D., Fowler, D. B., Wei, Y., et al. (2015). Understanding the biochemical basis of temperature induced lipid pathway adjustments in plants. *Plant Cell* 27, 86–103. doi: 10.1105/tpc.114.134338

Li, X., Björkman, O., Shih, C., Grossman, A. R., Rosenquist, M., Jansson, S., et al. (2000). A pigment-binding protein essential for regulation of photosynthetic light harvesting. *Nature* 403, 391–395. doi: 10.1038/35000131

Li, Z., Peers, G., Dent, R. M., Bai, Y., Yang, S. Y., Apel, W., et al. (2016). Evolution of an atypical de-epoxidase for photoprotection in the green lineage. *Nat. Plants* 2:16140.

Li-Beisson, Y., Nakamura, Y., and Harwood, J. (2016). Lipids: from chemical structures, biosynthesis, and analyses to industrial applications. *Subcell. Biochem.* 86, 1–21.

Liu, Z., Yan, H., Wang, K., Kuang, T., Zhang, J., Gui, L., et al. (2004) crystal structure of spinach major light-harvesting complex at 2.72 A resolution. *Nature* 428, 287–292. doi: 10.1038/nature02373

Lohr, M., and Wilhelm, C. (1998). Algae displaying the diadinoxanthin cycle also possess the violaxanthin cycle. *Proc. Natl. Acad. Sci. U.S.A.* 96, 8784–8789. doi: 10.1073/pnas.96.15.8784

Lohr, M., and Wilhelm, C. (2001). Xanthophyll synthesis in diatoms: quantification of putative intermediates and comparison of pigment conversion kinetics with rate constants derived from a model. *Planta* 212, 382–391. doi: 10.1007/s004250000403

Macko, S., Wehner, A., and Jahns, P. (2002). Comparison of violaxanthin de-epoxidation from the stroma and lumen sides of isolated thylakoid membranes from Arabidopsis: Implications for the mechanism of de-epoxidation. *Planta* 216, 309–314. doi: 10.1007/s00425-002-0848-8

Matsuda, O., Sakamoto, H., Hashimoto, T., and Iba, K. (2005). A temperature-sensitive mechanism that regulates post-translational stability of a plastidial omega-3 fatty acid desaturase (FAD8) in Arabidopsis leaf tissues. *J. Biol. Chem.* 280, 3597–3604. doi: 10.1074/jbc.m407226200

Mewes, H., and Richter, M. (2002). Supplementary Ultraviolet-B radiation induces a rapid reversal of the diadinoxanthin cycle in the strong light-exposed diatom *Phaeodactylum tricornutum*. *Plant Physiol.* 130, 1527–1535. doi: 10.1104/pp.006775

Miloslavina, Y., Grouneva, I., Lambrev, P. H., Lepetit, B., Goss, R., Wilhelm, C., et al. (2009). Ultra-fast fluorescence study on the location and mechanism of non-photochemical quenching in diatoms. *Biochim. Biophys. Acta* 1787, 1189–1197. doi: 10.1016/j.bbabio.2009.05.012

Moellering, E. R., and Benning, C. (2011). Galactoglycerolipid metabolism under stress: a time for remodeling. *Trends Plant Sci.* 16, 98–107. doi: 10.1016/j.tplants.2010.11.004

Moellering, E. R., Muthan, B., and Benning, C. (2010). Freezing tolerance in plants requires lipid remodeling at the outer chloroplast membrane. *Science* 330, 226–228. doi: 10.1126/science.1191803

Mongrand, S., Bessoule, J.-J., Cabantous, F., and Cassagne, C. (1998). The C16:3/C18:3 fatty acid balance in photosynthetic tissues from 468 plant species. *Phytochemistry* 49, 1049–1064. doi: 10.1016/s0031-9422(98)00243-x

Mongrand, S., Stanislas, T., Bayer, E. M. F., Lherminier, J., and Simon-Plas, F. (2010). Membrane rafts in plant cells. *Trends Plant Sci.* 15, 656–663. doi: 10.1016/j.tplants.2010.09.003

Montsant, A., Allen, A. E., Coesel, S., De Martino, A., Falciatore, A., Mangogna, M., et al. (2007). Identification and comparative genomic analysis of signaling and regulatory components in the diatom *Thalassiosira pseudonana*. *J. Phycol.* 43, 585–604.

Morosinotto, T., Caffarri, S., Dall'Osto, L., and Bassi, R. (2003). Mechanistic aspects of the xanthophyll dynamics in higher plant thylakoids. *Physiol. Plant.* 119, 347–354. doi: 10.1034/j.1399-3054.2003.00213.x

Mène-Saffrané, L., Dubugnon, L., Chételat, A., Stolz, S., Gouhier-Darimont, C., and Farmer, E. (2009). Nonenzymatic oxidation of trienoic fatty acids contributes to reactive oxygen species management in *Arabidopsis*. *J. Biol. Chem.* 284, 1702–1708. doi: 10.1074/jbc.m807114200

Nawrocki, W. J., Liu, X., and Croce, R. (2019). *Chlamydomonas reinhardtii* exhibits de facto constitutive NPQ capacity in physiologically relevant conditions. *Plant Physiol.* 182, 472–479. doi: 10.1104/pp.19.00658

Nicholson, G. L. (2014). The fluid-mosaic model of membrane structure: Still relevant to understanding the structure, function and dynamics of biological membranes after more than 40 years. *Biochim. Biophys. Acta* 1838, 1451–1466. doi: 10.1016/j.bbamem.2013.10.019

Nicol, L., Nawrocki, W. J., and Croce, R. (2019). Disentangling the sites of non-photochemical quenching in vascular plants. *Nature Plants* 5, 1177–1183. doi: 10.1038/s41477-019-0526-5

Niyogi, K. K., and Truong, T. B. (2013). Evolution of flexible non-photochemical quenching mechanisms that regulate light harvesting in oxygenic photosynthesis. *Curr. Opin. Plant Biol.* 16, 307–314. doi: 10.1016/j.pbi.2013.03.011

Ohlrogge, J. B., Kuhn, D. N., and Stumpf, P. K. (1979). Subcellular localization of acyl carrier protein in leaf protoplasts of *Spinacia oleracea*. *Proc. Natl. Acad. Sci. U.S.A.* 76, 1194–1198. doi: 10.1073/pnas.76.3.1194

Okazaki, Y., Otsuki, H., Narisawa, T., Kobayashi, M., Sawai, S., Kamide, Y., et al. (2013). A new class of plant lipid is essential for protection against phosphorus depletion. *Nat. Commun.* 4:1510.

Peers, G., Truong, T. B., Ostendorf, E., Busch, A., Elrad, D., Grossman, A. R., et al. (2009). An ancient light-harvesting protein is critical for the regulation of algal photosynthesis. *Nature* 462, 518–521. doi: 10.1038/nature08587

Pfündel, E. E., Renganathan, M., Gilmore, A. M., Yamamoto, H. Y., and Dilley, R. A. (1994). Intrathylakoid pH in isolated Pea chloroplasts as probed by violaxanthin deepoxidation. *Plant Physiol.* 106, 1647–1658. doi: 10.1104/pp.106.4.1647

Rabinowitch, H. D., Budowski, P., and Kedar, N. (1975). Carotenoids and epoxide cycles in mature-green tomatoes. *Planta* 122, 91–97. doi: 10.1007/bf00385408

Ramani, B., Reeck, T., Debez, A., Stelzer, R., Huchzermeyer, B., Schmidt, A., et al. (2006). *Aster tripolium* L. and *Sesuvium portulacastrum* L.: two halophytes, two strategies to survive in saline habitats. *Plant Physiol. Biochem.* 44, 395–408. doi: 10.1016/j.plaphy.2006.06.007

Roughan, G., and Slack, R. (1984). Glycerolipid synthesis in leaves. *Trends Biochem. Sci.* 9, 383–386. doi: 10.1016/0968-0004(84)90220-2

Ruban, A. V. (2016). Nonphotochemical fluorescence quenching: mechanism and effectiveness in protecting plants from photodamage. *Plant Physiol.* 170, 1903–1916. doi: 10.1104/pp.15.01935

Ruban, A. V., Lee, P. J., Wentworth, M., Young, A. J., and Horton, P. (1999). Determination of the stoichiometry and strength of binding of xanthophylls to the photosystem II light harvesting complexes. *J. Biol. Chem.* 274, 10458–10465. doi: 10.1074/jbc.274.15.10458

Ruban, A. V., Phillip, D., Young, A. J., and Horton, P. (1997). Carotenoid-dependent oligomerization of the major chlorophyll a/b light harvesting complex of photosystem II of plants. *Biochemistry* 36, 7855–7859. doi: 10.1021/bi9630725

Ruban, A. V., Rees, D., Pascal, A. A., and Horton, P. (1992). Mechanism of ΔpH dependent dissipation of absorbed excitation energy by photosynthetic membranes. II. The relation-ship between LHCII aggregation in vitro and qE in isolated thylakoids. *Biochim. Biophys. Acta* 1102, 39–44. doi: 10.1016/0005-2728(92)90062-7

Ruban, A. V., Young, A. J., Pascal, A. A., and Horton, P. (1994). The effects of illumination on the xanthophyll composition of the photosystem II light-harvesting complexes of spinach thylakoid membranes. *Plant Physiol.* 104, 227–234. doi: 10.1104/pp.104.1.227

Sacharz, J., Giovagnetti, V., Ungerer, P., Mastroianni, G., and Ruban, A. V. (2017). The xanthophyll cycle affects reversible interactions between PsbS and light-harvesting complex II to control non-photochemical quenching. *Nature Plants* 3:16225.

Saga, G., Giorgetti, A., Fufezan, C., Giacometti, G. M., Bassi, R., and Morosinotto, T. (2010). Mutation analysis of violaxanthin de-epoxidase identifies substrate-binding sites and residues involved in catalysis. *J. Biol. Chem.* 285, 23763–23770. doi: 10.1074/jbc.m110.115097

Saphozhnikov, D. J., Krasovskaya, T. A., and Mayevskaya, A. N. (1957). Changes observed in the relation between the main carotenoids in the plastids of green leaves exposed to light. *Dokl. Akad. Nauk. SSSR 1* 13, 465–467.

Schaller, S., Latowski, D., Jemiola-Rzeminska, M., Quaas, T., Wilhelm, C., Strzalka, K., et al. (2012a). The investigation of violaxanthin de-epoxidation in the primitive green alga *Mantoniella squamata* (Prasinophyceae) indicates mechanistic differences in xanthophyll conversion to higher plants. *Phycologia* 51, 359–370. doi: 10.2216/11-127.1

Schaller, S., Wilhelm, C., Strzalka, K., and Goss, R. (2012b). Investigating the interaction between the violaxanthin cycle enzyme zeaxanthin epoxidase and the thylakoid membrane. *J. Photochem. Photobiol. B: Biol.* 2012, 119–125. doi: 10.1016/j.jphotobiol.2012.05.019

Schaller, S., Latowski, D., Jemiola-Rzeminska, M., Wilhelm, C., Strzalka, K., and Goss, R. (2010). The main thylakoid membrane lipid monogalactosyldiacylglycerol (MGDG) promotes the de-epoxidation of violaxanthin associated with the light-harvesting complex of photosystem II (LHCII). *Biochim. Biophys. Acta* 2, 414–424. doi: 10.1016/j.bbabio.2009.12.011

Schaller, S., Latowski, D., Jemioła-Rzemioska, M., Dawood, A., Wilhelm, C., Strzałka, K., et al. (2011). Regulation of LHCII aggregation by different thylakoid membrane lipids. *Biochim. Biophys. Acta* 1807, 326–335. doi: 10.1016/j.bbabio.2010.12.017

Schaller, S., Richter, K., Wilhelm, C., and Goss, R. (2014). Influence of pH, Mg^{2+}, and lipid composition on the aggregation state of the diatom FCP in comparison to the LHCII of vascular plants. *Photosynth. Res.* 119, 305–317. doi: 10.1007/s11120-013-9951-x

Schaller-Laudel, S., Latowski, D., Jemioła-Rzeminska, M., Strzałka, K., Daum, S., Bacia, K., et al. (2017). Influence of thylakoid membrane lipids on the structure of aggregated light-harvesting complexes of the diatom *Thalassiosira pseudonana* and the green alga *Mantoniella squamata*. *Physiol. Plant.* 160, 339–358. doi: 10.1111/ppl.12565

Schaller-Laudel, S., Volke, D., Redlich, M., Kansy, M., Hoffmann, R., Wilhelm, C., et al. (2015). The diadinoxanthin diatoxanthin cycle induces structural rearrangements of the isolated FCP antenna complexes of the pennate diatom *Phaeodactylum tricornutum*. *Plant Physiol. Biochem.* 96, 364–376. doi: 10.1016/j.plaphy.2015.09.002

Schmid-Siegert, E., Stepushenko, O., Glauser, G., and Farmer, E. (2016). Membranes as structural antioxidants - recycling of malondialdehyde to its source in oxidation-sensitive chloroplast fatty acids. *J. Biol. Chem.* 291, 13005–13013. doi: 10.1074/jbc.m116.729921

Schumann, A., Goss, R., Jakob, T., and Wilhelm, C. (2007). Investigation of the quenching efficiency of diatoxanthin in cells of *Phaeodactylum tricornutum* (Bacillariophyceae) with different pool sizes of xanthophyll cycle pigments. *Phycologia* 46, 113–117. doi: 10.2216/06-30.1

Seiwert, D., Witt, H., Janshoff, A., and Paulsen, H. (2017). The non-bilayer lipid MGDG stabilizes the major light-harvesting complex (LHCII) against unfolding. *Sci. Rep.* 7:5158.

Selstam, E. (1998). "Development of thylakoid membranes with respect to lipids," in *Lipids in Photosynthesis: Structure, Function And Genetics*, eds P. A. Siegenthaler and N. Murata (Dordrecht: Kluwer Academic Publishers), 209–224. doi: 10.1007/0-306-48087-5_11

Shimojima, M. (2011). Biosynthesis and functions of the plant sulfolipid. *Progr. Lipid Res.* 50, 234–239. doi: 10.1016/j.plipres.2011.02.003

Shipley, G. G., Green, J. P., and Nichols, B. W. (1973). The phase behaviour of monogalactosyl, digalactosyl, and sulphoquinovosyl diglycerides. *Biochim. Biophys. Acta* 311, 531–544. doi: 10.1016/0005-2736(73)90128-4

Simidjiev, I., Barzda, V., Mustardy, L., and Garab, G. (1998). Role of thylakoid lipids in the structural flexibility of lamellar aggregates of the isolated light-harvesting chlorophyll a/b complex of photosystem II. *Biochemistry* 37, 4169–4173. doi: 10.1021/bi972726m

Simidjiev, I., Stoylova, S., Amenitsch, H., Javorfi, T., Mustardy, L., Laggner, P., et al. (2000). Self-assembly of large, ordered lamellae from non-bilayer lipids and integral membrane proteins in vitro. *Proc. Natl. Acad. Sci. U.S.A.* 97, 1473–1476. doi: 10.1073/pnas.97.4.1473

Simionato, D., Basso, S., Zaffagnini, M., Lana, T., Marzotto, F., Trost, P., et al. (2015). Protein redox regulation in the thylakoid lumen: the importance of disulfide bonds for violaxanthin deepoxidase. *FEBS Lett.* 589, 919–923. doi: 10.1016/j.febslet.2015.02.033

Simon-Plas, F., Perraki, A., Bayer, E., Gerbot-Pissot, P., and Mongrand, S. (2011). An update on plant membrane rafts. *Curr. Opin. Plant Biol.* 14, 642–649. doi: 10.1016/j.pbi.2011.08.003

Singer, S. J., and Nicholson, G. L. (1972). The fluid mosaic model of the structure of cell membranes. *Science* 175, 720–731. doi: 10.1126/science.175.4023.720

Stransky, H., and Hager, A. (1970). Das Carotinoidmuster und die Verbreitung des lichtinduzierten Xanthophyllzyklus in verschiedenen Algenklassen. II: Xanthophyceae. *Arch. Mikrobiol.* 71, 164–190. doi: 10.1007/bf00417740

Taddei, L., Chukhutsina, V. U., Lepetit, B., Stella, G. R., Bassi, R., van Amerongen, H., et al. (2018). Dynamic changes between two LHCX-related energy

quenching sites control diatom photoacclimation. *Plant Physiol.* 177, 953–965. doi: 10.1104/pp.18.00448

Taddei, L., Stella, G. R., Rogato, A., Bailleul, B., Fortunato, A. E., Annunziata, R., et al. (2016). Multisignal control of expression of the LHCX protein family in the marine diatom *Phaeodactylum tricornutum*. *J. Exp. Bot.* 67, 3939–3951. doi: 10.1093/jxb/erw198

Tardy, F., and Havaux, M. (1997). Thylakoid membrane fluidity and thermostability during the operation of the xanthophyll cycle in higher plant chloroplasts. *Biochim. Biophys. Acta* 1330, 179–193. doi: 10.1016/s0005-2736(97)00168-5

Thomas, P. G., Brain, A. P. R., Quinn, P. J., and Williams, W. P. (1985). Low pH and phospholipase A2 treatment induce the phase separation of non-bilayer lipids within pea chloroplast membranes. *FEBS Letts.* 183, 161–166. doi: 10.1016/0014-5793(85)80976-5

Triantaphylidès, C., and Havaux, M. (2009). Singlet oxygen in plants: production, detoxification and signaling. *Trends Plant Sci.* 14, 219–228. doi: 10.1016/j.tplants.2009.01.008

van Besouw, A., and Wintermans, J. F. (1978). Galactolipid formation in chloroplast envelopes. I. Evidence for two mechanisms in galactosylation. *Biochim. Biophys. Acta* 529, 44–53. doi: 10.1016/0005-2760(78)90102-9

van den Brink-van der Laan, E., Killian, J. A., and de Kruijff, B. (2004). Non-bilayer lipids affect peripheral and integral membrane proteins via changes in the lateral pressure profile. *Biochim. Biophys. Acta* 1666, 275–288. doi: 10.1016/j.bbamem.2004.06.010

van Eerden, F. J., de Jong, D. H., de Vries, A. H., Wassenaar, T. A., and Marrink, S. J. (2015). Characterization of thylakoid lipid membranes from cyanobacteria and higher plants by molecular dynamics simulations. *Biochim. Biophys. Acta* 1848, 1319–1330. doi: 10.1016/j.bbamem.2015.02.025

van Eerden, F. J., Melo, M. N., Frederix, P. W. J. M., and Marrink, S. J. (2017). Prediction of thylakoid lipid binding sites on Photosystem II. *Biophys. J.* 113, 2669–2681. doi: 10.1016/j.bpj.2017.09.039

van Mooy, B. A. S., Rocap, G., Fredricks, H. F., Evans, C. T., and Devol, A. H. (2006). Sulfolipids dramatically decrease phosphorus demand by picocyanobacteria in oligotrophic marine environments. *Proc. Natl. Acad. Sci. U.S.A.* 103, 8607–8612. doi: 10.1073/pnas.0600540103

Vidal-Meireles, A., Toth, D., Kovacz, L., Neupert, J., and Toth, S. Z. (2020). Ascorbate deficiency does not limit non-photochemical quenching in *Chlamydomonas reinhardtii*. *Plant Physiol.* 182:E00916.2019. doi: 10.1104/pp.19.00916

Vieler, A., Wilhelm, C., Goss, R., Süss, R., and Schiller, J. (2007). The lipid composition of the unicellular green alga *Chlamydomonas reinhardtii* and the diatom *Cyclotella menghiniana* investigated by MALDI-TOF MS and TLC. *Chem. Phys. Lipids* 150, 143–155. doi: 10.1016/j.chemphyslip.2007.06.224

Wang, K., Tu, W., Liu, C., Rao, Y., Gao, Z., and Yang, C. (2017). 9-cis-neoxanthin in light harvesting complexes of photosystem II regulates the binding of violaxanthin and the xanthophyll cycle. *Plant Physiol.* 174, 86–96. doi: 10.1104/pp.17.00029

Wang, S., Uddin, M. I., Tanaka, K., Yin, L., Shi, Z., Qi, Y., et al. (2014). Maintenance of chloroplast structure and function by overexpression of the OsMGD gene leads to enhanced salt tolerance in tobacco. *Plant Physiol.* 165, 1144–1155. doi: 10.1104/pp.114.238899

Wang, W., Yu, L.-J., Xu, C., Tomizaki, T., Zhao, S., Umena, Y., et al. (2019). Structrual basis for blue-green light harvesting and energy dissipation in diatoms. *Science* 363:eaav0365. doi: 10.1126/science.aav0365

Wehner, A., Grasses, T., and Jahns, P. (2006). De-epoxidation of violaxanthin in the minor antenna proteins of photosystem II, LHCB4, LHCB5, and LHCB6. *J. Biol. Chem.* 281, 21924–21933. doi: 10.1074/jbc.m602915200

Wehner, A., Storf, S., Jahns, P., and Schmid, V. H. (2004). De-epoxidation of violaxanthin in light-harvesting complex I proteins. *J. Biol. Chem.* 279, 26823–26829. doi: 10.1074/jbc.m402399200

Welc, R., Luchowski, R., Grudzinski, W., Puzio, M., Sowinski, K., and Gruszecki, W. I. (2016). A key role of xanthophylls that are not embedded in proteins in regulation of the photosynthetic antenna function in plants, revealed by monomolecular layer studies. *J. Phys. Chem. B* 120, 13056–13064. doi: 10.1021/acs.jpcb.6b10393

Williams, W. P., Brain, A. P. R., and Dominy, P. J. (1992). Induction of non-bilayer lipid phase separations in chloroplast thylakoid membranes by compatible co-solutes and its relation to the thermal stability of Photosystem II. *Biochim. Biophys. Acta* 1099, 137–144. doi: 10.1016/0304-4173(92)90019-b

Xu, P., Tian, L., Kloz, M., and Croce, R. (2015). Molecular insights into zeaxanthin-dependent quenching in higher plants. *Sci. Rep.* 5:13679.

Yamamoto, H., Nakayama, T., and Chichester, C. (1962). Studies on the light and dark interconversions of leaf xanthophylls. *Arch. Biochem. Biophys.* 97, 168–173. doi: 10.1016/0003-9861(62)90060-7

Yamamoto, H. Y. (2006). Functional roles of the major chloroplast lipids in the violaxanthin cycle. *Planta* 224, 719–724. doi: 10.1007/s00425-006-0257-5

Yamamoto, H. Y., Chenchin, E. E., and Yamada, D. K. (1974). "Effect of chloroplast lipids on violaxanthin de-epoxidase activity," in *Proceedings of the Third International Congress on Photosynthesis*, ed. M. Avron (Amsterdam: Elsevier), 1999–2006.

Yamamoto, H. Y., and Higashi, R. M. (1978). Violaxanthin de-epoxidase. Lipid composition and substrate specificity. *Arch. Biochem. Biophys.* 190, 514–522.

Yamamoto, Y. (2016). Quality control of Photosystem II: The mechanisms for avoidance and tolerance of light and heat stresses are closely linked to membrane fluidity of the thylakoids. *Front. Plant Sci.* 7:1136. doi: 10.3389/fpls.2016.01136

Yamashita, Y. (2018). "Recent dispersion technology using liquid crystal," in *Liquid Crystals-Recent Advancements in Fundamental and Device Technologies*, ed. P. K. Choudhury (London: IntechOpen), doi: 10.5772/intechopen.74156

Yan, X., Chen, D., Xu, J., and Zhou, C. (2011). Profiles of photosynthetic glycerolipids in three strains of *Skeletonema* determined by UPLC-Q-TOF-MS. *J. Appl. Phycol.* 23, 271–282. doi: 10.1007/s10811-010-9553-3

Yongmanitchai, W., and Ward, O. P. (1993). Positional distribution of fatty acids, and molecular species of polar lipids, in the diatom *Phaeodactylum tricornutum*. *J. Gen. Microbiol.* 139, 465–472. doi: 10.1099/00221287-139-3-465

Yu, B., Xu, C., and Benning, C. (2002). Arabidopsis disrupted in SQD2 encoding sulfolipid synthase is impaired in phosphate-limited growth. *Proc. Natl. Acad. Sci. U.S.A.* 99, 5732–5737. doi: 10.1073/pnas.082696499

Zhou, F., Liu, S., and Yang, C. (2009). Effect of monogalactosyldiacylglycerol on the interaction between photosystem II core complex and its antenna complexes in liposomes of thylakoid lipids. *Photosynth. Res.* 99, 185–193. doi: 10.1007/s11120-008-9388-9

Zhou, J., Sekatskii, S., Welc, R., Dietler, G., and Gruszecki, W. I. (2020). The role of xanthophylls in the supramolecular organization of the photosynthetic complex LHCII in lipid membranes studied by high-resolution imaging and nanospectroscopy. *Biochim. Biophys. Acta* 1861, 148117. doi: 10.1016/j.bbabio.2019.148117

Zhu, J., Gomez, S. M., Mawson, B. T., Jin, X., and Zeiger, E. (1997). The coleoptile chloroplast: distinct distribution of xanthophyll cycle pigments, and enrichment in photosystem II. *Photosynth. Res.* 51, 137–147.

Zhu, S. H., and Green, B. R. (2010). Photoprotection in the diatom *Thalassiosira pseudonana*: role of LI818-like proteins in response to high light stress. *Biochim. Biophys. Acta* 1797, 1449–1457. doi: 10.1016/j.bbabio.2010.04.003

Conflict of Interest: The authors declare that the research was conducted in the absence of any commercial or financial relationships that could be construed as a potential conflict of interest.

Copyright © 2020 Goss and Latowski. This is an open-access article distributed under the terms of the Creative Commons Attribution License (CC BY). The use, distribution or reproduction in other forums is permitted, provided the original author(s) and the copyright owner(s) are credited and that the original publication in this journal is cited, in accordance with accepted academic practice. No use, distribution or reproduction is permitted which does not comply with these terms.

frontiers in Plant Science

ORIGINAL RESEARCH
published: 04 June 2020
doi: 10.3389/fpls.2020.00745

Growth Temperature Influence on Lipids and Photosynthesis in *Lepidium sativum*

*Hamed Sattari Vayghan[1], Shahrzad Tavalaei[1], Armand Grillon[1], Léa Meyer[1], Gent Ballabani[1], Gaëtan Glauser[2] and Paolo Longoni[1]**

[1] *Laboratory of Plant Physiology, Faculty of Sciences, Institute of Biology, University of Neuchâtel, Neuchâtel, Switzerland,*
[2] *Neuchâtel Platform of Analytical Chemistry, Faculty of Sciences, University of Neuchâtel, Neuchâtel, Switzerland*

Temperature has a major impact on plant development and growth. In temperate climates, the seasonal temperature displays large variations that can affect the early stages of plant growth and development. Sessile organisms need to be capable of responding to these conditions, so that growth temperature induces morphological and physiological changes in the plant. Besides development, there are also important molecular and ultrastructural modifications allowing to cope with different temperatures. The chloroplast plays a crucial role in plant energetic metabolism and harbors the photosynthetic apparatus. The photosynthetic light reactions are at the interface between external physical conditions (light, temperature) and the cell biochemistry. Therefore, photosynthesis requires structural flexibility to be able to optimize its efficiency according to the changes of the external conditions. To investigate the effect of growth temperature on the photosynthetic apparatus, we followed the photosynthetic performances and analyzed the protein and lipid profiles of *Lepidium sativum* (cress) grown at three different temperatures. This revealed that plants developing at temperatures above the optimum have a lower photosynthetic efficiency. Moreover, plants grown under elevated and low temperatures showed a different galactolipid profile, especially the amount of saturated galactolipids decreased at low temperature and increased at high temperature. From the analysis of the chlorophyll *a* fluorescence induction, we assessed the impact of growth temperature on the re-oxidation of plastoquinone, which is the lipidic electron carrier of the photosynthetic electron transport chain. We show that, at low temperature, along with an increase of unsaturated structural lipids and plastochromanol, there is an increase of the plastoquinone oxidation rate in the dark. These results emphasize the importance of the thylakoid membrane composition in preserving the photosynthetic apparatus under non-optimal temperatures.

Keywords: photosynthesis, thylakoid membrane, membrane lipids, plastoquinone, temperature stress, electron transport

OPEN ACCESS

Edited by:
Yoshitaka Nishiyama, Saitama University, Japan

Reviewed by:
Koichi Kobayashi, Osaka Prefecture University, Japan
Esa Tyystjärvi, University of Turku, Finland

****Correspondence:***
Paolo Longoni
paolo.longoni@unine.ch

Specialty section:
This article was submitted to Plant Physiology, a section of the journal Frontiers in Plant Science

Received: *26 November 2019*
Accepted: *11 May 2020*
Published: *04 June 2020*

Citation:
Sattari Vayghan H, Tavalaei S, Grillon A, Meyer L, Ballabani G, Glauser G and Longoni P (2020) Growth Temperature Influence on Lipids and Photosynthesis in Lepidium sativum. Front. Plant Sci. 11:745. doi: 10.3389/fpls.2020.00745

INTRODUCTION

Plant metabolism must respond to daily and seasonal temperature variations. Photosynthesis, which is the main energetic process allowing plants to produce organic carbon, chemical energy, and reducing power, is no exception. Furthermore, the photosynthetic process is peculiar in the fact that uses light as the energy source of the primary photosynthetic reactions. As temperature differences affect the biochemical reactions but not the pigment excitation, the conversion of light energy into chemical energy needs to be finely tuned to be adapted to different temperatures (Yamori et al., 2014).

Light energy conversion requires a series of pigment–protein complexes, namely photosystem II (PSII), cytochrome b_6f (Cytb_6f), and photosystem I (PSI). These complexes are functionally connected constituting an electron transport chain (Rochaix, 2011). The electrons obtained from the water-splitting reaction at PSII are transferred to plastoquinone (PQ), which is reduced to plastoquinol (reduced PQ). Reduced PQ diffuses into the membrane until Cytb_6f. This complex oxidizes the reduced PQ, splitting the two electrons obtained from the oxidation, one toward the plastocyanin and the other to a second PQ molecule. The electrons from plastocyanin are then transferred to PSI and from this complex to the final acceptor NADP via ferredoxin. The water-splitting and the cycle of the PQ during the electron transport increase the proton concentration in the thylakoid lumen generating a pH gradient across the membrane (ΔpH). ΔpH is used by the ATP synthase complex to produce ATP. The light absorption capacity of PSI and PSII reaction centers is extended by the light harvesting complex II (LHCII), a complex of trimeric and monomeric proteins binding chlorophylls and carotenoids that are capable to capture photons converting them into excitation energy. LHCII proteins can also act as dissipators of excess light energy by releasing part of the excitation energy as heat. Fine regulation of this energy dissipation has an important impact on plant growth and productivity (Kromdijk et al., 2016; Ware et al., 2016). The transmembrane ΔpH is the trigger of the thermal dissipation (Wraight and Crofts, 1970), the presence and abundance of the protein PsbS promote its induction (Li et al., 2000), while the xanthophylls, primarily lutein and zeaxanthin, are the main pigments acting as dissipators (Dall'Osto et al., 2010; Leuenberger et al., 2017). The processes allowing the dissipation of light excess as heat take collectively the name of non-photochemical quenching (NPQ).

The photosynthetic proteins involved in the electron transport chain are sensitive to changes in temperature. Prolonged low temperature results in the increase of the trimeric LHCII over monomeric LHCII in maize (Caffarri et al., 2005), and high temperature induces a change in the phosphorylation of the thylakoid proteins and by this also their localization in the thylakoid membrane subdomains (Rokka et al., 2000). Furthermore, the electron flux toward alternative pathways increases at suboptimal temperatures resulting in a lower efficiency of photosynthetic electron transport (Ivanov et al., 2012). These alternative electron routes, such as chlororespiration through the plastidic terminal oxidase (PTOX), water–water cycle, cyclic electron flow, and mitochondrial oxidative electron transport, may act collectively in reducing the excitation pressure on the photosystems and thus protecting the photosynthetic proteins from photodamage (Ivanov et al., 2012; Sunil et al., 2019).

Light reactions of the photosynthesis depend also on the lipids constituting the membrane in which the protein complexes are embedded. The membrane lipid composition influences PQ diffusion, and this may affect its functionality as electron transporter (Kirchhoff et al., 2002). The structural lipids of the thylakoid membrane are mostly galactolipids: Monogalactosyldiacylglycerols (MGDGs), representing around 50% of the total thylakoid lipids by weight, and digalactosyldiacylglycerols (DGDGs), constituting about 26%. Anionic lipids phosphatidylglycerol (PG) and sulfoquinovosyldiacylglycerol (SQDG) constitute most of the remaining lipid fraction of the thylakoid membrane (Dörmann, 2013). The temperature influences thylakoid membrane composition as well. At high temperature, the thylakoid membrane accumulates structural lipids with a higher degree of saturation (Falcone et al., 2004; Higashi et al., 2015). In addition to the structural lipids, the thylakoid membrane also contains antioxidant molecules such as tocopherols and plastochromanol (Mène-Saffrané et al., 2010; Spicher et al., 2016). These antioxidants have been shown to have an important role in the preservation of the photosynthetic apparatus during stress conditions such as high light (Rastogi et al., 2014), high temperature (Spicher et al., 2016), and their combination (Spicher et al., 2017). Furthermore, the chloroplast ultrastructure was also reported to change in response to temperature, for instance, following a temperature increase, the *Arabidopsis thaliana* chloroplast was reported to swell and the number and size of the internal lipid droplets, known as plastoglobules, was reported to increase (Zhang et al., 2010).

Here we investigate the impact of two growth temperatures, one above (30°C) and one below (10°C) the optimal growth temperature (22°C), on the photosynthetic apparatus of *Lepidium sativum* (cress). Cress is a fast-growing species belonging to the *Brassicaceae* family. We will focus on the differences in thylakoid membrane lipids and on the alternative pathways for the photosynthetic electrons as an adaptive strategy to reduce the excitation pressure and thus the damage of the photosynthetic apparatus.

MATERIALS AND METHODS

Plant Growth and Stress Condition

Seeds of *L. sativum* were obtained from a local supplier. The seeds were put on soil and kept overnight at 6–8°C in the dark for stratification. The seeded pots were then transferred at 22°C under long day illumination (16 h L/8 h D, photosynthetic photon flux density in photoactive radiation PAR spectrum 86 μmol photons m^{-2} s^{-1}) and allowed to germinate for 48 h. After germination, the plants were moved to 10°C or 30°C under the same light conditions, or maintained at 22°C, and grown for 5 additional days. Warm and cold conditions were produced within a FitoClima 600 (Aralab) climatic chamber. The length

of the hypocotyl was measured manually for each plant. The leaf area per plant was calculated with ImageJ (NIH) measuring the green area of each plant from a top view picture using a scale for reference as previously described (Longoni et al., 2019). Five samples constituting the epigeal part of three plants were collected at the end of the growth to measure the average plant dry weight. For that, the samples were lyophilized for 120 h (FreeZone 2.5, Labconco, Kansas City, MO, United States) before weighing. To calculate the dry weight percentage over fresh weight, five samples per temperature, containing only the leaves collected from three plants, were weighted before and after 120 h of lyophilization.

Photosynthetic Parameters

Each batch of plants was kept in the dark for at least 10 min before the measurements. Room temperature chlorophyll fluorescence was measured with a MF800 Fluorcam (Photon System Instrument, Czechia)[1] employing a personalized light protocol (Pralon et al., 2020). The protocol is composed of blue light (470 nm) steps of 1 min with increasing intensity (35, 125, 315, 500, 690, and 875 μmol photons m^{-2} s^{-1} of PAR intensity). F_M' for each light intensity was measured with a saturating pulse at the end of the corresponding light step. After every light step, the actinic light was turned off for 10 s. During the first 2 s, far-red light was turned on to oxidize the photosynthetic electron transport chain. F_0' for each step was measured during the remaining part of the dark period. F_S is the steady-state fluorescence recorded at each light condition before the saturating light pulse. PSII quantum yield under light (ΦPSII) was calculated as ΦPSII = $(F_M'-F_S)/F_M'$. The fraction of the open PSII centers (qL) was calculated with the following formula: $qL = [(F_M'-F_S)/(F_M'-F_0')]^*(F_0'/F_S)$ (Kramer et al., 2004). The non-photochemical energy dissipation was measured as $NPQ = (F_M-F_M')/F_M'$. The average fluorescence signal of each plant was used for the calculation of the photosynthetic parameters. Rapid chlorophyll fluorescence induction of PSII was measured on detached leaves with Plant Efficiency Analyser (M-PEA 2; Hansatech Ltd). The following protocol was used: after an initial saturating pulse (3000 μmol photons m^{-2} s^{-1}, 700 ms, red light, dominant λ625 nm), the saturating light pulse was repeated after sequentially longer dark intervals (0.05, 4, 8, 12, 16, 20, and 24 s) for a total of eight pulses. After the eighth pulse, far-red light (20%) was turned on, and the leaf sample was submitted to a second series of saturating pulses separated by increasing time intervals (0.05, 0.1, 0.2, 0.4, 0.8, and 1.6 s) with continuous far-red light in between the pulses. For each saturating pulse, the parameters of the fast chlorophyll fluorescence curve were extrapolated by the M-PEA 2 software (Hansatech Ltd). The variable fluorescence at 3 ms (V_J) and the Fo normalized over the maximal fluorescence (F_O/F_M) were analyzed by plotting them over the time interval between the pulses.

Protein Analysis

Plant samples were ground to a fine powder in a 1.5 ml plastic tube with glass beads in an Ivoclar Vivadent shaker (Silamat). The proteins were extracted adding 10 μl per mg FW of lysis buffer [100 mM Tris–HCl, pH 8.5, 2% SDS, 10 mM NaF, 0.05% of protease inhibitor cocktail for plants (Sigma)], vortexing and incubating the sample at 37°C for 30 min. Plant debris was removed by centrifugation (5 min at 16,000 × *g*) at room temperature. The samples were diluted four times in water and supplemented with gel loading buffer (50 mM Tris–HCl, pH 6.8, 100 mM dithiothreitol, 2% SDS, 0.1% bromophenol blue, 10% glycerol). After denaturation at 75°C for 10 min, an aliquot of 10 μl of the diluted sample was loaded in the gel. The protein separation was performed following the standard SDS-PAGE protocol in a 12% acrylamide bis acrylamide (37.5:1) gel (Laemmli, 1970). The proteins were transferred on a nitrocellulose membrane, stained for 30 s with amido black solution (15% isopropanol, 10% acetic acid, 0.1% w/v amido black), and destained with a destaining solution (40% ethanol, 10% acetic acid). An image of the stained membrane was taken for the quantification of the total proteins in each lane. The membrane was blocked with 5% milk in TBS-0.05% Tween and then decorated with the following antibodies: anti-Lhcb2 (Agrisera, AS01 003), anti-Lhcb1 (Agrisera, AS01 004), anti-D1 (PsbA) (Agrisera, AS05 084), anti-PetC (Agrisera, AS08 330); anti-PsaD (Agrisera, AS09 461), anti-RbcL (Agrisera, AS03 037A); a secondary antibody anti-rabbit conjugated with HRP (Merk) was used to allow the detection of the protein by chemioluminescence (ECL). The ECL signal was recorded with a CCD camera (Amersham Imager 600 Amersham Biosciences, Inc.), set on automatic detection time. Band intensity was measured with ImageQuant TL 8.1 Software (GE Healthcare Life Sciences). The obtained values were normalized over the sum of the amido black band intensities measured with the same software using a minimum profile subtraction method. The protein extraction was performed on leaf samples harvested during at least two independent biological replicates (9 total samples for PsbA and PsaD, 6 samples for RbcL and PetC, 5 for Lhcb2 and 4 for Lhcb1). For PTOX detection (Agrisera, AS16 3692), the membrane was blocked in 6% BSA in TBS-0.05% Tween; the same solution was used for the preparation of the primary and secondary antibody dilutions.

Pigments and Lipid Profiling

The sample used for chlorophyll quantification and lipidomic profiling is constituted of at least two leaves collected from two different plants grown at the same temperature. Chlorophyll extraction was performed in 80% acetone by adding 10 μl of solvent per mg of FW of leaf sample. The sample was further diluted twofold in 80% acetone before measuring the absorbance at multiple wavelengths (470, 646, 663 nm). The quantification of chlorophyll *a* and *b* was performed according to Lichtenthaler and Wellburn (1983). The measured chlorophyll concentration was adjusted to the dry weight based on the average leaf water content measured for each growth temperature. The measure was repeated on 15 samples from different plants obtained from five independent experiments. Extraction of the lipid fraction was performed on 12 samples from different plants obtained from three independent experiments. In brief, after grinding, the lipids were extracted in 10 μl of tetrahydrofuran:methanol

[1] http://www.psi.cz

50:50 (v/v) per mg of FW, plant debris was separated by centrifugation (3 min, 14,000 × *g*), and the supernatant was carefully transferred to an HPLC vial. The lipids were separated by ultra-high pressure liquid chromatography and identified by a coupled atmospheric pressure chemical ionization-quadrupole time-of-flight mass spectrometry (UHPLC-APCI-QTOF-MS) as previously described (Spicher et al., 2016). Lipids were separated on a reverse-phase Acquity BEH C18 column (50 × 2.1 mm, 1.7 μm) maintained at 60°C. The elution was as follows: solvent A = water; solvent B = methanol; 80–100% B in 3 min, 100% B for 2 min, re-equilibration at 80% B for 2.0 min. The flow rate was 0.8 ml min^{-1} and the injection volume was 2.5 μl. Data were acquired using MassLynx version 4.1 (Waters) and further processed with QuanLynx (Waters). Compound identity was determined based on reference standards that were also used for the quantification curve (Spicher et al., 2016). Violaxanthin and neoxanthin could be resolved neither in the chromatographic nor in the mass dimensions under the conditions employed; therefore, the measured peak corresponds to the sum of these compounds. The same applies for lutein and zeaxanthin. MGDG 36:6, 36:5, 36:4, 34:6, 34:5, 34:4 and DGDG 36:6, 36:5, 36:4, 36:3, 34:6, 34:3, 34:2, 34:1 identities were confirmed comparing the peak of the extract with a standard plant MGDG mix and DGDG mix (Avanti Polar Lipids). The calibration curves of MGDG 36:6, MGDG 34:6, DGDG 36:6, and DGDG 34:6 were used for the quantification of all MGDG 36:x, MGDG 34:x, DGDG 36:x and DGDG 34:x, respectively (**Supplementary Figure S1**). To avoid any bias due to signal saturation in the quantification of the most abundant DGDGs, the samples were measured a second time following a tenfold dilution in tetrahydrofuran:methanol 50:50 (v/v). The values obtained by the calibration curves were corrected by the percentage of each molecule composing the standard mix, as reported by the manufacturer (Avanti Polar Lipids). The molecules not detected in the standard mix were tentatively characterized based on m/z and retention time characteristics, which vary proportionally to the degree of acyl chain length and saturation (Li et al., 2008).

Statistical Analysis

The normal distribution of the residuals of each data set was tested before any other statistical analysis. If this assumption was met, an ANOVA model was utilized; otherwise, a Kruskal–Wallis rank sum test was performed. If the results were significant, we used *post hoc* Tukey's HSD test for multiple comparisons. The reported *p*-values were obtained with the latter. The calculations were performed with RStudio (Version 1.2.5019 RStudio Inc).

RESULTS

Growth Temperature Affects Photosynthetic Efficiency

The plants of *L. sativum* grown at different temperatures had a slightly different morphology. The leaf area was smaller in the plants grown at 10°C and 30°C compared with the control condition. The hypocotyl was longer in the plants grown at 30°C, while there was no significant difference in the other two conditions. However, both the plants grown at 10°C and 30°C produced less dry biomass per plant (**Supplementary Figure S2**). The entire pot, containing 24 plants, was analyzed by chlorophyll fluorescence to determine the impact of the different growth temperatures on the overall functionality of the photosynthetic electron transport chain. The first parameter observed was the maximal quantum yield of the photosystem II (F_V/F_M), a decrease in this value would suggest the presence of persistent damage on PSII. The maximum quantum yield was slightly lower in the plants grown at 10°C ($p < 0.0001$) compared to the other two growth temperatures (**Figure 1**). However, the average value of 0.83 measured at 10°C, which is PSII efficiency reported for healthy plants, suggests that there was no major damage during the growth at this suboptimal temperature (Maxwell and Johnson, 2000). The negligible effect on the maximum yield of PSII allowed investigating further the photosynthetic activity and adaptation under increasing actinic light intensity. Chlorophyll *a* fluorescence was measured at 22°C by red flashes while stepwise increasing the actinic light intensity. The use of a saturating pulse at the end of each light step allowed the calculation of the fraction of the energy dissipated as heat (NPQ) at each light intensity (Caffarri et al., 2005). Plants

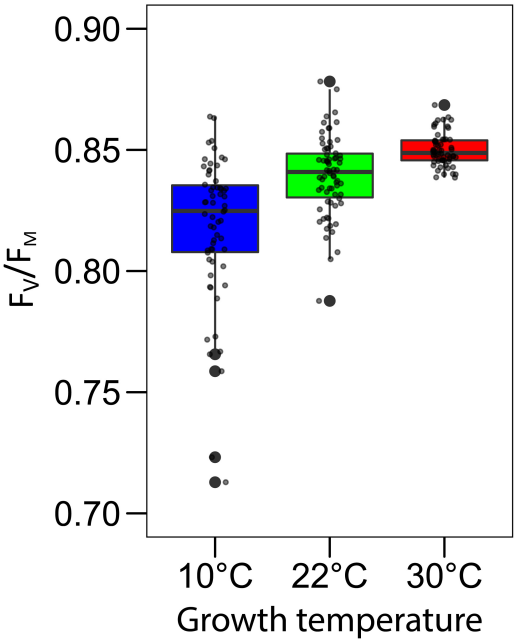

FIGURE 1 | Growth temperature has a minimal impact on the Photosystem II maximum efficiency. The maximum PSII quantum yield was measured in trays containing 20–24 plants, grown at three different temperatures (10, 22, and 30°C) for 5 days. Before measuring, the plants were incubated 10 min in the dark at room temperature. Gray points represent the average value for each single plant. In the box plots, the lower and upper hinges correspond to the first and third quartiles (the 25th and 75th percentiles). The whiskers extend from the hinge to the farthest value no further than 1.5 times the distance between the first and third quartiles from the hinge. Farther points are considered as "outliers" and plotted individually as solid black points.

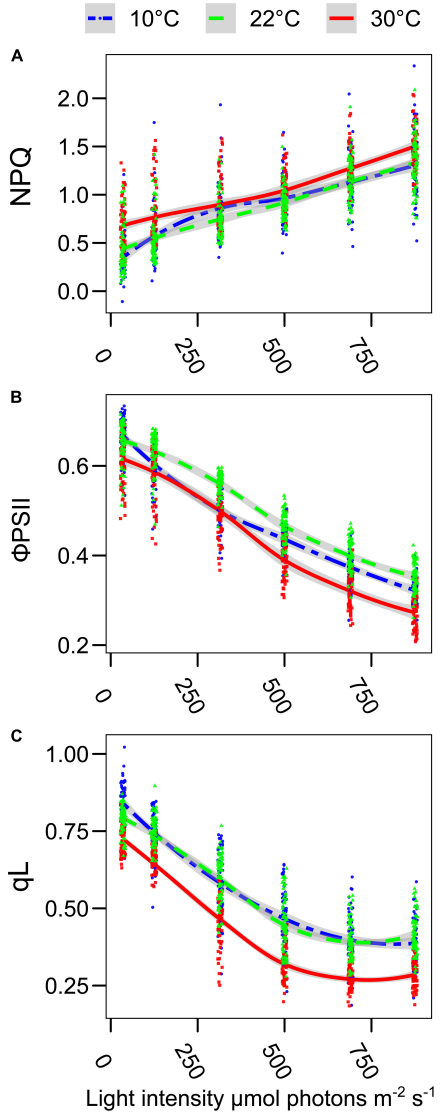

FIGURE 2 | Growth temperature affects the photosynthetic electron transport chain in *Lepidium sativum*. The room temperature fluorescence was measured on trays with 20–24 plants, grown at the three different temperatures (10°C blue, 22°C green, and 30°C red). Prior to the measurement, the plants were incubated 10 min in the dark at room temperature and directly used for the measure of the chlorophyll *a* fluorescence kinetic. **(A)** Level of thermal dissipation measured as NPQ for the three growth conditions after 1 min of exposure to increasing light intensity. **(B)** Photosystem II quantum yield (ΦPSII) measured at the end of each 1-min light intensity step. **(C)** Fraction of the open PSII reaction centers (qL) after 1 min of exposure to increasing light intensities. The light intensities are expressed as µmol photons m^{-2} s^{-1} of blue light (470 nm), and the same scale is used for the three graphs. The points were fitted with a local regression algorithm based on a polynomial quadratic function to visually represent the data distribution in function of the light intensities with a continuous error estimate. The fit is shown for the three growth conditions (10°C, blue double dashed line, 22°C green dashed line, and 30°C red continuous line). The standard error of the interpolation is shown as a gray area around the curve. All the data points from the 30°C growth are statistically different from the 22°C control conditions (*Post Hoc* analysis, $p < 0.0001$). The three parameters were measured simultaneously, and they originated from two independent experimental replicates (30°C, $n = 60$; 22°C, $n = 70$; 10°C, $n = 62$).

grown at 30°C had a higher NPQ value compared to those grown under control temperature (**Figure 2A**). This effect was evident already at the lower light intensity tested (35 µmol photons m^{-2} s^{-1}) ($p < 0.0001$ compared to both 10°C and 22°C), a condition in which the NPQ of the plants grown at 10°C was statistically lower than the control ($p = 0.0005$). Only at 315 µmol photons m^{-2} s^{-1}, the plants grown at 10°C appear to have a slightly higher NPQ compared with the control condition ($p = 0.11$); otherwise, there was no statistically significant difference between these two conditions. The changes in the NPQ are symmetrically reflected in the quantum yield of photosystem II photochemistry (ΦPSII, **Figure 2B**). The plants grown at 30°C had constantly a lower yield of PSII compared to the control growth temperature. ΦPSII of those grown at 10°C was also lower, especially at 125 and 315 µmol photons m^{-2} s^{-1} ($p < 0.0001$). While at higher light intensities, ΦPSII difference between the plants grown at 10°C and those at 22°C became smaller. Therefore, at the higher light intensities tested, the plants grown at 10°C had a higher ΦPSII compared to the plants grown at 30°C. Analysis of the fraction of open PSII centers (qL) revealed that the plants grown at 30°C had a steady increase in the fraction of closed PSII as measured by the qL parameter (Baker, 2008). Surprisingly, this is not the case for the plants grown at 10°C, which have a similar qL level compared to the control temperature (22°C) (**Figure 2C**). Since these differences may underlay a change in the organization of the electron transport chain, we further analyzed the protein and the lipid composition of the plants grown at the different temperatures.

Effect of Growth Temperature on Major Thylakoid Pigments and Proteins

The stoichiometry of the different photosynthetic complexes of the thylakoid membrane, namely the two photosystems (PSI and PSII), the cytochrome b_6f (Cytb_6f), and the light harvesting complex II (LHCII), may vary upon acclimation of the photosynthetic machinery to the environment. To test the impact of the growth temperature on the organization of the major thylakoid proteins, the total chlorophyll content was measured along with the chlorophyll *a* to *b* ratio. This gives an indication of the ratio between the LHCII antenna complex, enriched in chlorophyll *b*, and the two photosystems, which have a higher chlorophyll *a*/*b* ratio. The chlorophyll concentration was adjusted to the average calculated dry mass of the sample, which corresponds to 7% at 22°C and 8% both at 30 and 10°C of the respective fresh weight ($n = 5$). The chlorophyll concentrations of the plants grown at the three temperatures differed a little. Plants grown at 10°C had a slightly lower chlorophyll concentration compared to those grown at 30°C ($p = 0.0626$, $n = 15$) and at 22°C ($p = 0.1338$, $n = 15$) (**Figure 3A**). A clear difference was instead observed by comparing the chlorophyll *a*/*b* ratio. In both the plants grown at 30°C and at 10°C, the a/b ratio was significantly lower than the one observed at control temperature (22°C–30°C, $p = 0.0004$, $n = 15$; 10°C–22°C, $p = 0.0343$, $n = 15$) (**Figure 3B**). This suggests that the relative amount of

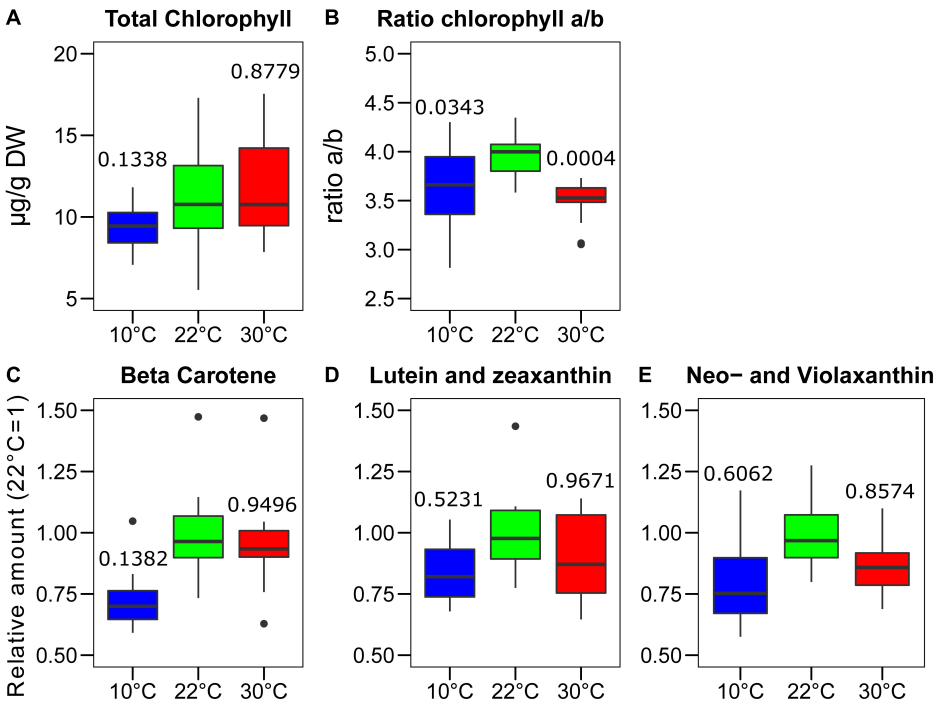

FIGURE 3 | Changes in pigments content after the growth of *Lepidium sativum* at different temperatures. The chlorophyll content was measured in a sample constituted of two leaves collected from different plants grown in the same condition. **(A)** Content in total chlorophyll measured after the growth at three different temperatures normalized on the leaf dry weight. **(B)** Chlorophyll *a*/*b* ratio measured in the same samples shown in **(A)** (n = 15). Carotenoids analysis was performed by chromatography coupled with mass spectrometry (n = 11). The values are reported in terms of differences from the average value at 22°C for **(C)** Beta-carotene, **(D)** Lutein and zeaxanthin, and **(E)** neoxanthin and violaxanthin. The carotenoids in the blots **(D)** and **(E)** were indistinguishable in time or *m*/*z* and therefore are plotted as the sum of the two. In the box plots, the lower and upper hinges correspond to the first and third quartiles (the 25th and 75th percentiles). The whiskers extend from the hinge to the farthest value no further than 1.5 times the distance between the first and third quartiles from the hinge. Farther points are considered as "outliers" and plotted individually. The *p*-value derived from a *post hoc* test comparing the data with the value at 22°C is shown above each box.

chlorophyll *b* rich proteins, such as LHCII, increased in the plants grown in both non-optimal temperatures. The carotenoids were quantified by mass spectrometry (UHPLC-APCI-QTOF-MS). For the carotenoids analyzed, we observed a general trend toward lower accumulation at 10°C compared to the other two growth temperatures. However, these differences appeared not to be statistically significant. β-carotene was the compound showing the most consistent difference among biological replicates when comparing plants grown at 10°C with those grown at the control temperature of 22°C (p = 0.1382, n = 11) (**Figure 3C**). Other carotenoids associated with the photosynthetic proteins, instead, do not show a differential level of accumulation at the different temperatures; this is the case for lutein and zeaxanthin and for the combination of neoxanthin and violaxanthin (**Figures 3D,E**).

The changes in the accumulation of the major photosynthetic complex were estimated by immunodetection of the subunits of each complex in total protein extracts. Interestingly, it appeared that growth at 10°C, compared to the control at 22°C, results in a lower accumulation, on a total protein basis, of PSII (PsbA/D1) (p < 0.0001, n = 9), PSI (PsaD) (p = 0.0001, n = 9), Cytb_6f (PetC) (p = 0.02, n = 6). For the trimeric LHCII (Lhcb2 and Lhcb1), the reduction was milder so that we did not observe a significant difference in the detected protein compared to the 22°C condition (Lhcb1 p = 0.29, n = 4; Lhcb2 p = 0.82, n = 5) (**Figure 4**). At 30°C, the only significant difference observed by immunodetection was for PetC of the Cytb_6f, which was reduced similarly to the 10°C condition (10°C–30°C, p = 0.76; 22°C–30°C, p = 0.1) (**Figure 4**).

Temperature-Dependent Changes in the Lipids of the Thylakoid Membrane

Alpha-tocopherol and plastochromanol, major antioxidants present in the thylakoid membrane, were measured by mass spectrometry following chromatographic separation (Mène-Saffrané et al., 2010; Spicher et al., 2017; **Figure 5**). The amount of α-tocopherol, on a dry weight basis, was higher in both non-optimal temperatures compared to the plants grown at 22°C (10°C–22°C, p = 0.0001; 30°C–22°C, p = 0.0077; n = 11). The difference between 10 and 30°C was not statistically significant for this compound (p = 0.4834) (**Figure 5A**). Similarly, plastochromanol concentration was higher, 1.5-fold to twofold, in both temperature conditions (10°C–22°C, p < 0.0001; 30°C–22°C, p = 0.0046), with a tendency toward a greater amount at 10°C compared to 30°C (p = 0.1061) (**Figure 5C**). The accumulation of the two precursors of these molecules, γ-tocopherol and PQ, was measured as well. Despite a large difference between replicates, the concentration of

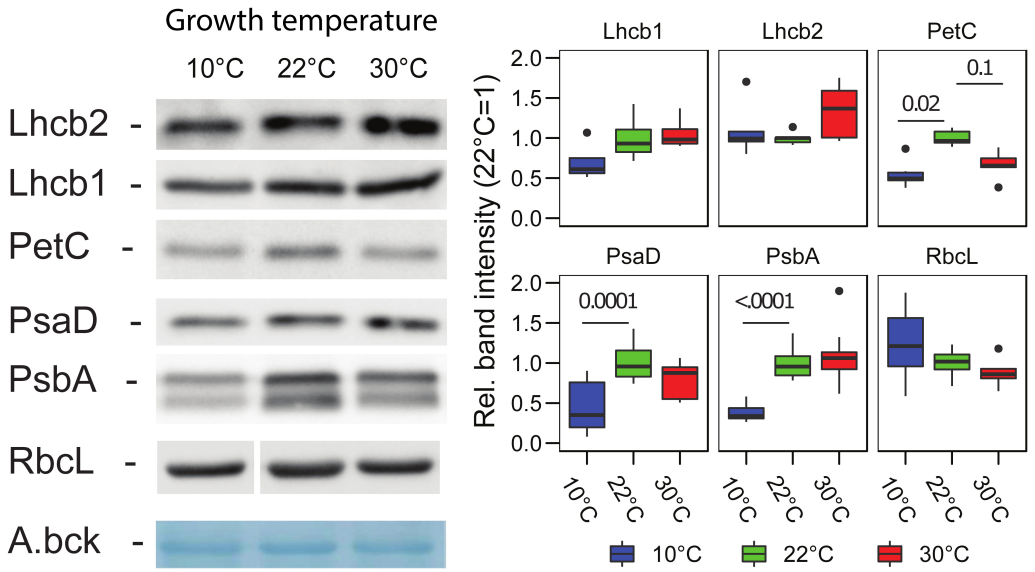

FIGURE 4 | Photosynthetic protein accumulation in *Lepidium sativum* at different growth temperatures. Representative proteins for the complexes of the electron transport chain, PSII (PsbA), PSI (PsaD), Cytb$_6$f (PetC), and LHCII (Lhcb1, Lhcb2) were analyzed by immunodetection in samples normalized on fresh weight. A representative blot is shown for each protein along with a representative band of the total transferred proteins stained with amido black (A.bck) as a protein loading control. The box plots show the band intensity, normalized over the total amido black lane staining, compared to the control condition (22°C) (average intensity 22°C = 1). PSII (PsbA/D1) (n = 9), PSI (PsaD) (n = 9), Cytb$_6$f (PetC) (n = 6), LHCII (Lhcb2) (n = 5), Lhcb1 (n = 4), and RbcL (n = 6). In the box plots, the lower and upper hinges correspond to the first and third quartiles (the 25th and 75th percentiles). The whiskers extend from the hinge to the farthest value no further than 1.5 times the distance between the first and third quartiles from the hinge. Farther points are considered as "outliers" and plotted individually.

γ-tocopherol was found to be higher at 10°C and slightly lower at 30°C compared to the control temperature (10°C, $p < 0.0001$; 30°C, $p = 0.0924$) (**Figure 5B**). This may suggest that at 10°C there could be an incomplete conversion of γ-tocopherol into α-tocopherol as vegetative tissues do not normally accumulate γ-tocopherol (Abbasi et al., 2007). This conversion may be possibly faster at 30°C, and this leading to the lower accumulation was observed. On the contrary, the amount of PQ was not significantly different in the three temperatures tested, even if a tendency toward higher PQ concentrations was observed in the plants grown at 30°C and toward lower concentrations in those grown at 10°C creating a significant difference between the two conditions (10°C–30°C, $p = 0.0564$) (**Figure 5D**).

The saturation degree of the lipids composing the biological membrane is known to change depending on temperature (Falcone et al., 2004). This is also the case for the major structural lipids of the thylakoid membrane that are monogalactosyldiacylglycerols (MGDG) and digalactosyldiacylglycerols (DGDG) (Block et al., 1983). The growth temperature had a wide impact on the profile of the galactolipids (**Figure 5E**). At 10°C, long-chained unsaturated mono- and digalactolipids (36:6) were relatively more abundant compared to the control temperature. The effect was opposite for the plants grown at 30°C in which there was a higher proportion of galactolipids with 34 carbons and particularly of those which are more saturated (34:3, 34:2), compared to the control condition at 22°C (**Figure 5E**). A specific difference was observed for MGDG 34:6, which is the most abundant galactolipid; its level was maximal in the plants grown at 22°C but lower at both 10 and 30°C (**Figure 5E**). Also, the MGDG/DGDG ratio was different in the plants grown at non-optimal temperatures. In fact, over the total of the measured galactolipids, the MGDG fraction was 72 ± 4% in the control condition (22°C) but it decreased to 67 ± 4% and 63 ± 3% at 10 and 30°C, respectively (10°C–22°C, $p = 0.0184$; 30°C–22°C, $p < 0.0001$; $n = 11$). Furthermore, there was also a different accumulation of the galactolipids originating from the endoplasmic reticulum (ER), containing two 18 carbon acyl chains (C18/C18), and those of plastid origin containing one 18 carbon chain and the second with 16 carbons (C18/C16) (Boudière et al., 2014). Considering the molar fraction of the measured galactolipids, in control condition (22°C), 32 ± 5% had two acyl chains of 18 carbons. In the cress plants grown at 10°C, the fraction of the C18/C18 galactolipids increased to 43 ± 5%, significantly higher than in the control condition ($p < 0.0001$, $n = 11$). An intermediate state was observed at 30°C with C18/C18 galactolipids representing 38 ± 3% of the total, differing from the cress grown at 22°C ($p = 0.0092$, $n = 11$) and at 10°C ($p = 0.0214$, $n = 11$). The average number of desaturations per molecule of the measured galactolipids was significantly lower ($p < 0.0001$, $n = 11$) in the plants grown at 30°C (5.1 ± 0.2) compared to the control condition (5.5 ± 0.1) and to the 10°C temperature (5.7 ± 0.1). The difference in the average number of desaturations per molecule was bigger considering only DGDGs, and the average number of desaturations per molecule at 22°C was 5.09 ± 0.2, significantly higher at 10°C (5.44 ± 0.2; 10°C–22°C, $p = 0.0123$) and lower at 30°C (4.62 ± 0.4; 30°C–22°C, $p = 0.0009$).

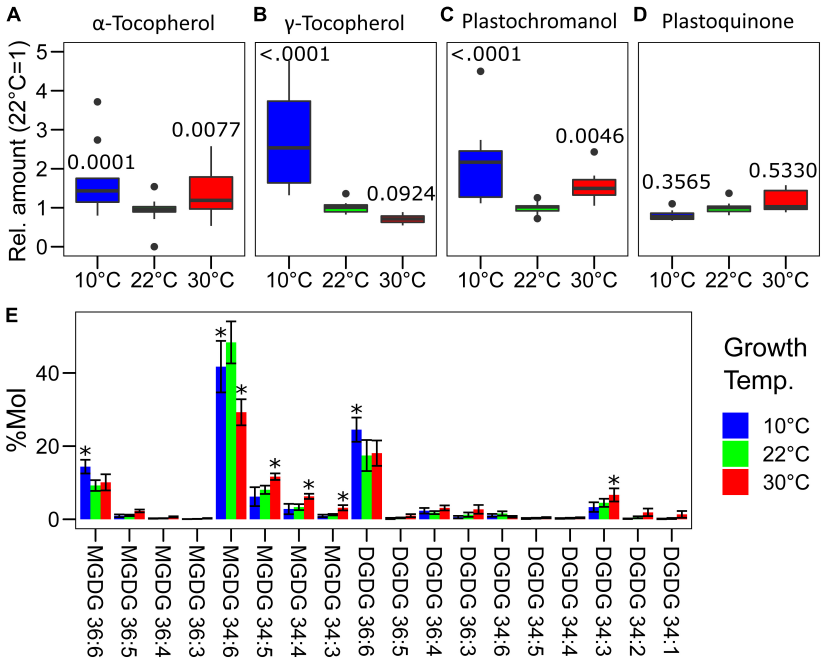

FIGURE 5 | Profile of the galacto- and prenyl-lipids in *Lepidium sativum* grown at different temperatures. Total lipids were extracted from pooled leaf samples, separated by liquid chromatography and identified by mass spectrometry. Eleven leaf samples from three independent growth replicates were used. Relative concentration of the principal antioxidants of the thylakoid membrane **(A)** α-tocopherol, **(B)** γ-tocopherol, **(C)** plastochromanol, and its precursors **(D)** plastoquinone, the latter also serves as an electron carrier in the electron transport chain. In the box plots, the lower and upper hinges correspond to the first and third quartiles (the 25th and 75th percentiles). The whiskers extend from the hinge to the farthest value no further than 1.5 times the distance between the first and third quartiles from the hinge. Farther points are considered as "outliers" and plotted individually. The *p*-value derived from a *post hoc* test comparing the data with the value at 22°C is shown above each box. **(E)** Profile of the monogalactosyldiacylglycerols (MGDG) and digalactosyldiacylglycerols (DGDG) expressed as % molecules over the total of the measured galactolipids. The compounds are listed by the length and degree of saturation of the acyl chains, and significant differences from the control temperature 22°C ($p < 0.05$) are highlighted with an asterisk ($n = 11$).

Plastoquinone Oxidation Is Altered at Low Temperature

The alteration of the lipid composition may have a functional impact on electron transport and on the PQ dynamics. We therefore assessed the re-oxidation kinetics of the photoactive PQ pool using an indirect method based on PSII fluorescence induction curve. It has been shown that the fluorescence level at 3 ms (Fj) correlates with the redox state of the Q_B site of photosystem II, and the latter is in equilibrium with the photoactive PQ pool (Tóth et al., 2007). Therefore, the relative fluorescence at 3 ms (V_J) and its kinetics after a dark or far red-light period of increasing length were taken as a proxy of the PQ oxidation over time. In the dark, the PQ oxidation is performed by electron pathways alternative to the photosynthetic electron transport chain, mostly via the plastid terminal oxidase (PTOX) (Pralon et al., 2020). Conversely, far-red will activate PSI allowing a photochemical oxidation of PQ (Rochaix, 2011). As expected, PQ oxidation under far-red light was faster than the oxidation observed in the dark, PTOX being a much slower oxidizer than PSI (Tóth et al., 2007). The PQ oxidation in the dark, as inferred by the V_J parameter, was faster in the plants grown at 10°C compared to both other conditions ($p < 0.001$), which, on the contrary, did not differ significantly (**Figure 6A**). When the oxidation of the photoactive PQ pool was performed by the electron transport chain, exciting PSI with far-red light, the plants grown at 30°C showed a faster initial re-oxidation, up to 0.4 s ($p = 0.0513$), while further followed the same kinetics as the plants grown at 22°C. For the plants grown at 10°C, the effect was reversed; in fact, the kinetics up to 0.2 s were identical to the plants grown at 22°C, while the following re-oxidation kinetics appeared to be slower, so that the V_J was significantly higher at the 0.4 and 0.8 s time points ($p = 0.0005$ and $p = 0.0015$, respectively; **Figure 6B**). The fluorescence in the dark, before the saturating pulse (F_O) calculated by the M-PEA instrument, does also decline with increasing time intervals between the pulses. However, the F_O value normalized over the F_M does not show the same difference between the samples as observed for V_J (**Supplementary Figure S3**), suggesting that the two parameters are partially independent.

DISCUSSION

Temperature is a challenge for the photosynthetic apparatus, affecting enzymatic kinetics, as well as membrane dynamics and organization (Yamori et al., 2014). It is therefore essential for the plant to adopt strategies to protect its photosynthetic apparatus while maximizing light utilization at the non-optimal

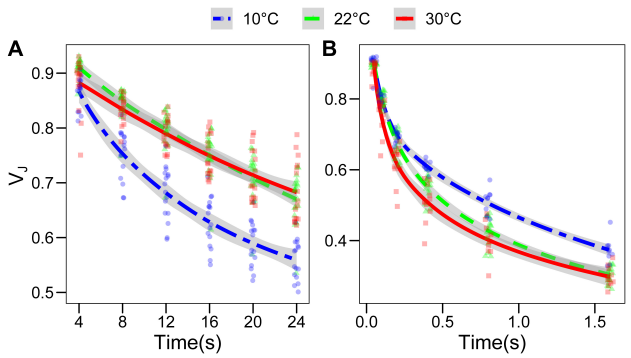

FIGURE 6 | Fluorescence relaxation in the dark is faster in *Lepidium sativum* grown at low temperature. The fluorescence value measured at 3 ms during a 700 ms saturating pulse was normalized over the maximal fluorescence to obtain the V_J parameter. This parameter was used as a proxy of the redox state of the photoactive plastoquinone pool. **(A)** Evolution of the V_J parameter upon sequential incubations of the sample in the dark, for the three growth conditions. The points were fitted with a local regression algorithm based on a logarithmic function to visually represent the data distribution in function of the time with a continuous error estimate (10°C, blue double dashed line, 22°C green dashed line, 30°C red continuous line). The standard error of the interpolation is shown as a gray area around the curve. **(B)** Evolution of the V_J parameter upon sequential incubation with far-red light exciting preferentially the photosystem I. The statistical significance of the difference between non-overlapping error areas of the interpolation was confirmed by a *post hoc* test ($p < 0.001$) (10°C, $n = 10$; 30°C, $n = 11$; 22°C, $n = 16$). Different *X* and *Y* axes are used in **(A)** and **(B)** to highlight the differences between the growth temperatures.

temperature condition. Here we explored the response on the early growth of a fast-developing species: *L. sativum*, which belongs to the same family, *Brassicaceae*, as model organism *A. thaliana* and important crop species.

The total chlorophyll concentration displayed minor differences compared with those previously reported using other plant species that were exposed to high and low temperature (Grimaud et al., 2013; Spicher et al., 2016). This is possibly because the temperatures employed in this experiment were milder, and therefore, a strong detrimental stress to the photosynthetic apparatus was avoided. This is in line with the limited effect on the maximum quantum yield of PSII observed in the plants grown at 10°C (**Figure 1**). However, both the plants grown at 10 and 30°C showed an alteration in the measured photosynthetic parameters compared to the control temperature (**Figure 2**). It has to be underlined that all the photosynthetic measurements were performed at 22°C, i.e., the temperature at which the control plants were grown, and it is therefore not surprising that plants grown at the same temperature are the best performers at this temperature. The average PSII redox state under light was inferred from the qL parameter, representing the probability of a photon to be transferred to an open PSII reaction center in an interconnected lake model (Kramer et al., 2004). Surprisingly, for the plants grown at 30°C, the qL was smaller compared to the plant grown at the two other temperatures (**Figure 2**). This result is consistent with the protein amount, as the plants grown at 30°C appear to have a lower level of the Cytb_6f complex (PetC), which is the rate limiting step of the electron transport chain under moderate light condition and in the presence of CO_2 (Rochaix, 2011). This downregulation has been hypothesized to serve as a protective mechanism for the photosystems (Krieger-Liszkay et al., 2000). In this regard, the specific relative loss of Cytb_6f at 30°C may be part of the regulation mechanism to protect PSI challenged by the high temperature, by slowing down the electron flow toward PSI, while PSII repair cycle and the higher constitutive NPQ maintain PSII efficiency (Yamane et al., 1997). At 10°C, all the three complexes involved in the electron transport appear to be diminished to a similar extent compared to the control temperature. Therefore, there should be no effect on the relative electron transport capacity per PSII. Consistently, the fraction of open PSII reaction centers (qL) in 35 to 875 µmol photons m^{-2} s^{-1} of PAR intensity range is comparable to the control (**Figure 2C**). Another protective mechanism of PSII is the thermal dissipation of the light excess (NPQ), which also appears to be induced in the plants grown at 30°C that display a stronger thermal dissipation component already at the lowest light intensity used in the fluorescence measurement (**Figure 2A**). The growth at lower temperature results in a minor change of the thermal dissipation at moderately high intensity; however, the NPQ at higher light intensities (above 500 µmol photons m^{-2} s^{-1}) was similar to the NPQ of the plants grown at control temperature (22°C). As NPQ induction is dependent on the transmembrane ΔpH (Wraight and Crofts, 1970), this observation suggests that plants grown at higher temperature could be less efficient in the dissipation of the ΔpH, or alternatively that the components of the NPQ machinery are over-accumulated in these plants. However, PsbS, which is the protein responsible for the fast NPQ component (Li et al., 2000), was reported not to respond to temperature as it is not induced in low temperature (Rorat et al., 2001; Norén et al., 2003). Furthermore, the *PSBS* gene expression was not altered upon changes in the growth temperature, neither by increasing nor by lowering it, in *A. thaliana* (Kilian et al., 2007). In the plants grown at the higher temperature, there was no increase in the concentration of the two xanthophylls, lutein and zeaxanthin, which are directly involved in the dissipation of the chlorophyll excitation energy, compared with the control (**Figure 3**; Leuenberger et al., 2017). Therefore, a tentative explanation for the higher NPQ observed in the plants grown at 30°C is the aggregation of LHCII (Tang et al., 2007); this effect should produce a constitutive energy dissipation that would explain the quenching detected already at low light intensity. A relative increase of LHCII over the photosystems would also explain the lower chlorophyll *a*/*b* ratio (**Figure 3B**). A tendency over a higher Lhcb2 accumulation was observed at 30°C ($p = 0.14$, **Figure 4**). The lack of a quantitative confirmation of this increased accumulation by immunodetection may be explained by an interference of the N-terminal phosphorylation of the antenna on the protein recognition by the antibodies (Longoni et al., 2015). Indeed, the Lhcb2 protein tends to be more phosphorylated when plants were grown at 30°C (**Supplementary Figure S4**). The level of NPQ affects also directly the quantum yield of PSII (ΦPSII). The plants grown at 30°C induced the most NPQ and had a lower ΦPSII in all

the light conditions tested (**Figure 2B**). The factor limiting ΦPSII in cress grown at low temperature, on the contrary, does not appear to be the NPQ. Most likely in this case unrepaired damage on PSII is responsible for the lower efficiency (Grimaud et al., 2013). This hypothesis would be consistent with the slightly lower F_V/F_M value measured in the plants grown at lower temperature (**Figure 1**). This shows that, despite both un-optimal temperatures affecting photosynthesis, the response to the temperature change is different, and not necessarily symmetrical, between lower and higher temperatures.

Membrane lipid composition, including galactolipids of the thylakoid membrane, varies in response to temperature (Falcone et al., 2004; Spicher et al., 2016). As expected, we observed a tendency toward the accumulation of long-chained unsaturated galactolipids (36:6) at 10°C, while the opposite (i.e., accumulation of 34 acyl-carbons and more saturated lipids) was true at higher temperature. This change is most likely necessary to have a similar level of membrane fluidity at different temperatures (Barber et al., 1984). The average number of desaturations per acyl chain in the measured galactolipids was significantly higher at 30°C and lower at 10°C compared to 22°C. The mode by which galactolipid desaturation influences the thylakoid membrane fluidity is not yet defined unambiguously. However, the level of galactolipid saturation does change in different plant species in response to a temperature shift (Falcone et al., 2004). Consistently, modification of the level of lipid saturation by knocking down or overexpressing individual fatty acid desaturases results in an altered resistance of the plants to extreme temperatures (Penfield, 2008). This suggests that the differences observed in the acyl chain saturation are part of cress acclimation to growth temperature. At both non-optimal temperatures, the cress accumulated a larger proportion of MGDG and DGDG originating from the ER (i.e., containing two acyl chains at 18 carbons (C18/C18)] over the galactolipids of plastid origin (i.e., containing one acyl chain of 18 carbons and one of 16 carbons (C18/C16)] (**Figure 5**; Boudière et al., 2014). The induction of the ER-derived eukaryotic pathway for chloroplast galactolipids upon heat stress has been reported in several species (Higashi and Saito, 2019). Furthermore, a previous report showed an increase of the ER-derived galactolipids and the key role of the ACYL-LIPID DESATURASE2 located in the ER in the acclimation to low temperature in *A. thaliana* (Chen and Thelen, 2013). The reported difference in the relative abundance of the galactolipid acyl chains supports the hypothesis that a shift from the plastid to the ER pathway for membrane lipid biosynthesis is part of the plant response to non-optimal temperatures. Considering the MGDG/DGDG ratio observed at 10°C, the relative DGDG content was higher than at 22°C. This is consistent with previous reports showing that, during acclimation to prolonged cold periods, the MGDG/DGDG ratio became smaller, while minor changes were observed in the concentration of the other major thylakoid membrane components PG and SQDG (Hendrickson et al., 2006). However, PG and SQDG may also have an impact on thylakoid membrane structure and dynamics depending on the desaturation of the acyl chains. In fact, PG accumulation and desaturation may be critical for photosynthetic acclimation to low temperature (Gao et al., 2015).

The differences in the galactolipid levels may affect the thylakoid organization. For instance, a larger DGDG fraction may strengthen the stacking of the thylakoid membranes by the interactions between facing headgroups of these galactolipids (Demé et al., 2014; Kanduè et al., 2017). However, a lower MGDG/DGDG ratio could also affect the stacking of the LHCII-rich portions of the thylakoid membranes (Seiwert et al., 2018). As the relative level of DGDG was higher at 30°C than in the other two growth temperature, it is plausible that the increased proportion of DGDG strengthens the membrane interactions. This, along with the lower average number of desaturations per molecule, may increase the thermal stability of the thylakoid membrane and may also have a direct effect on the NPQ component acting on the aggregation of LHCII (Krumova et al., 2010).

High temperature may directly affect the photosystem II electron transport efficiency and its structure causing the production of ROS (Pospíšil, 2016). Low temperature hampers PSII repair cycle, leading to photoinhibition and activation of ROS signaling pathways (Grimaud et al., 2013). Consistently, previous reports have shown that temperature changes lead to an increase in the concentration of antioxidant compounds embedded in the thylakoid membrane (Mène-Saffrané et al., 2010; Spicher et al., 2016). In a previous report on tomato, α-tocopherol and plastochromanol were shown to accumulate following a temperature increase, while minor to no change was observed in plants grown at low temperature (Spicher et al., 2016). This study, conversely, found a similar increase in α-tocopherol and plastochromanol concentrations in the plants grown at 10 and 30°C compared to the control condition at 22°C (**Figure 5**). It is interesting to note that PQ re-oxidation in the dark was faster in the plants grown at 10°C compared to the other two growth temperatures, as inferred by the chlorophyll *a* fluorescence parameter V_J. In the absence of light, the oxidation of PQ is mostly dependent on the activity of the plastid terminal oxidase PTOX (Carol and Kuntz, 2001). In *A. thaliana* an accumulation of the PTOX protein was reported in plants acclimated to low temperature (Ivanov et al., 2012). However, the commercial antibody against PTOX detects multiple bands even on cress protein sample obtained from purified thylakoid (**Supplementary Figure S5**). Lacking any genomic data of *L. sativum,* it is not possible to exclude that different forms of PTOX exist in this species, although the majority of the sequenced higher plants contain a single PTOX gene (Nawrocki et al., 2015). These uncertainties do not allow drawing a conclusion on the accumulation of PTOX in cress at different temperatures. High level of PTOX protein was hypothesized to be responsible for an increase in the non-photochemical oxidation of PQ in the high mountain plant species *Ranunculus glacialis* as a strategy allowing a better acclimation to low temperatures combined with high irradiation (Streb et al., 2005). However, in this species low temperature alone was not sufficient to induce PTOX protein accumulation (Laureau et al., 2013). Furthermore, considering studies where an ectopic overexpression of the PTOX protein was achieved, it appears that the PTOX protein level is not the unique determinant of the non-photochemical PQ oxidation rate (Johnson and Stepien, 2016).

The crowded thylakoid membrane poses major limitations to the mobility of PQ and therefore may physically hamper its oxidation in the dark (Tremmel et al., 2003). Considering this, the differences in the galactolipid profile (**Figure 5**) and the change in the photosynthetic protein accumulation (**Figure 4**) observed at 10°C may be functional in facilitating PQ mobility and therefore its oxidation by PTOX (Pralon et al., 2020). Furthermore, the accumulation of plastochromanol, which appears to be tendentially higher at 10°C than at 30°C, would allow to contrast more efficiently membrane lipid peroxidation (**Figure 5**; Nowicka et al., 2013). Accumulation of lipid peroxides, in fact, would reduce the membrane fluidity and therefore the mobility of PQ (Niki, 2009). Accumulation of α-tocopherol, necessary to protect from ROS in both temperature condition, would, on the contrary, stabilize the membrane (Arora et al., 2000). The accumulation of γ-tocopherol, observed at 10°C (**Figure 5A**), may be a hint of a downregulation of α-tocopherol biosynthesis, functional to control its concentration and thus preserve the membrane fluidity. Membrane fluidity, and the mobility of PQ, may also explain the difference in qL observed between the plants grown at 10°C and those at 30°C (**Figure 2**). Lipid circulation would facilitate the access of oxidized PQ to PSII. The difference in the V_J kinetics in the dark between these two temperatures is consistent with a difference in long-distance PQ mobility (**Figure 6**). Increased fluidity may also facilitate the movement of PTOX to the grana stacks, as in *Eutrema salsugineum* under salt stress (Stepien and Johnson, 2018).

The presumed higher thylakoid membrane fluidity of the plants developed at 10°C compared to the other growth temperatures had, if any, a negative impact on PQ oxidation under far-red. Plants developed at 10°C displayed a slower photochemical PQ oxidation compared to 22°C. While in the plants grown at 30°C, PQ oxidation under far-red appears to be slightly faster than in those grown at 22°C (**Figure 5B**). This difference may be rationalized assuming that the accumulation of more saturated galactolipids and α-tocopherol observed at 30°C results in the stabilization of the thylakoid membrane structure and grana stacking (Arora et al., 2000; Krumova et al., 2010). In this scenario, the photochemical oxidation of PQ would be accelerated by the stabilization of PQ microdomains inside the grana allowing a more efficient circulation of PQ between PSII and $Cytb_6f$ (Kirchhoff et al., 2002). Conversely, the stabilization of the membrane may reduce PQ exchange between microdomains and between different portions of the thylakoid membrane, thus limiting the total PQ pool available per PSII and resulting in the lower ΦPSII and qL observed in the plants grown at 30°C (**Figure 2**). A hypothetic destabilization of the membrane domains, possibly due to the lower degree of galactolipid saturation, could explain the opposite effect on PQ mobility at 10°C compared to the 30°C scenario.

The dark re-oxidation rate, inferred from the V_J parameter, appears to be two order of magnitude slower than the one under far-red. In this scenario, the contribution of PTOX as an efficient alternative sink of electrons to protect the photosystems appears doubtful. Nevertheless, it has been shown that *Arabidopsis* plants lacking PTOX had a more severe variegation phenotype at lower temperature, suggesting that PTOX contribution is more critical at low temperature (Rosso et al., 2009). The increased non-photochemical oxidation of PQ may then serve to sustain the biosynthesis of carotenoids allowing to compensate for the enzymatic activity limitation imposed by the lower temperature (Norris et al., 1995). Consistently with this hypothesis, the accumulation of the most abundant carotenoids, on a dry weight basis, was only slightly lower in the plants grown at 10°C compared to the other conditions tested (**Figure 3**).

The differences observed in plants grown at higher and lower temperature are not symmetrical, but show some common differences, such as the higher level of the membrane antioxidants and a lower MGDG/DGDG ratio. However, at lower temperature, the acclimation is a trade-off between membrane fluidity and protection from ROS, which results in a detectable damage to PSII, while at higher temperature, membrane fluidity is not a constraint allowing to a more efficient protection. Furthermore, in the plants grown at lower temperature, the non-photochemical oxidation of PQ was faster compared to those at 22 and 30°C. This supports the model in which the activation of alternative electron pathways is an important strategy to protect the photosynthetic apparatus under cold stress.

DATA AVAILABILITY STATEMENT

The datasets generated for this study can be found in the Zenodo repository https://doi.org/10.5281/zenodo.3839245.

AUTHOR CONTRIBUTIONS

HS, ST, AG, LM, and PL designed the experimental plan. HS, ST, AG, LM, GB, and PL performed the experiments. GG performed the lipid profile analysis. ST and PL performed the statistical analysis of the data. PL wrote the manuscript. All authors read and approved the manuscript.

FUNDING

This work was supported by the University of Neuchâtel and the Swiss National Science Foundation (31003A_179417).

ACKNOWLEDGMENTS

The authors would like to acknowledge Felix Kessler, for hosting the research in his laboratory, Michel Goldschmidt Clermont for his critical reading of the manuscript, and Veronique Douet, Gautier Pizzolon, and Jenny Pego Morales for their technical assistance.

SUPPLEMENTARY MATERIAL

The Supplementary Material for this article can be found online at: https://www.frontiersin.org/articles/10.3389/fpls.2020.00745/full#supplementary-material

REFERENCES

Abbasi, A.-R., Hajirezaei, M., Hofius, D., Sonnewald, U., and Voll, L. M. (2007). Specific Roles of α- and γ-tocopherol in abiotic stress responses of transgenic tobacco. *Plant Phys.* 143, 1720–1738. doi: 10.1104/pp.106.094771

Arora, A., Byrem, T. M., Nair, M. G., and Strasburg, G. M. (2000). Modulation of liposomal membrane fluidity by flavonoids and isoflavonoids. *Arch. Biochem. Biophys.* 373, 102–109. doi: 10.1006/abbi.1999.1525

Baker, N. R. (2008). Chlorophyll fluorescence: a probe of photosynthesis in vivo. *Annu. Rev. Plant Biol.* 59, 89–113. doi: 10.1146/annurev.arplant.59.032607.092759

Barber, J., Ford, R. C., Mitchell, R. A., and Millner, P. A. (1984). Chloroplast thylakoid membrane fluidity and its sensitivity to temperature. *Planta* 161, 375–380. doi: 10.1007/bf00398729

Block, M. A., Dorne, A. J., Joyard, J., and Douce, R. (1983). Preparation and characterization of membrane fractions enriched in outer and inner envelope membranes from spinach chloroplasts. II. Biochemical characterization. *J. Biol. Chem.* 258, 13281–13286.

Boudière, L., Michaud, M., Petroutsos, D., Rébeillé, F., Falconet, D., Bastien, O., et al. (2014). Glycerolipids in photosynthesis: composition, synthesis and trafficking. *Biochim. Biophys. Acta* 1837, 470–480. doi: 10.1016/j.bbabio.2013.09.007

Caffarri, S., Frigerio, S., Olivieri, E., Righetti, P. G., and Bassi, R. (2005). Differential accumulation of Lhcb gene products in thylakoid membranes of Zea mays plants grown under contrasting light and temperature conditions. *Proteomics* 5, 758–768. doi: 10.1002/pmic.200402008

Carol, P., and Kuntz, M. (2001). A plastid terminal oxidase comes to light: implications for carotenoid biosynthesis and chlororespiration. *Trends Plant Sci.* 6, 31–36. doi: 10.1016/s1360-1385(00)01811-2

Chen, M., and Thelen, J. J. (2013). ACYL-LIPID DESATURASE2 is required for chilling and freezing tolerance in *Arabidopsis*. *Plant Cell* 25, 1430–1444. doi: 10.1105/tpc.113.111179

Dall'Osto, L., Cazzaniga, S., Havaux, M., and Bassi, R. (2010). Enhanced Photoprotection by protein-bound vs free xanthophyll pools: a comparative analysis of chlorophyll b and xanthophyll biosynthesis mutants. *Mol. Plant* 3, 576–593. doi: 10.1093/mp/ssp117

Demé, B., Cataye, C., Block, M. A., Maréchal, E., and Jouhet, J. (2014). Contribution of galactoglycerolipids to the 3-dimensional architecture of thylakoids. *FASEB J.* 28, 3373–3383. doi: 10.1096/fj.13-247395

Dörmann, P. (2013). "Galactolipids in plant membranes," in *eLS* (Chichester: John Wiley & Sons, Ltd.). doi: 10.1002/9780470015902.a0020100.pub2

Falcone, D. L., Ogas, J. P., and Somerville, C. R. (2004). Regulation of membrane fatty acid composition by temperature in mutants of *Arabidopsis* with alterations in membrane lipid composition. *BMC Plant Biol.* 4:17. doi: 10.1186/1471-2229-4-17

Gao, J., Wallis, J. G., and Browse, J. (2015). Mutations in the prokaryotic pathway rescue the fatty acid biosynthesis1 mutant in the cold. *Plant Physiol.* 169, 442–452. doi: 10.1104/pp.15.00931

Grimaud, F., Renaut, J., Dumont, E., Sergeant, K., Lucau-Danila, A., Blervacq, A.-S., et al. (2013). Exploring chloroplastic changes related to chilling and freezing tolerance during cold acclimation of pea (*Pisum sativum* L.). *J. Proteomics* 80, 145–159. doi: 10.1016/j.jprot.2012.12.030

Hendrickson, L., Vlèková, A., Selstam, E., Huner, N., Öquist, G., and Hurry, V. (2006). Cold acclimation of the *Arabidopsis* dgd1 mutant results in recovery from photosystem I-limited photosynthesis. *FEBS Lett.* 580, 4959–4968. doi: 10.1016/j.febslet.2006.07.081

Higashi, Y., Okazaki, Y., Myouga, F., Shinozaki, K., and Saito, K. (2015). Landscape of the lipidome and transcriptome under heat stress in *Arabidopsis thaliana*. *Sci. Rep.* 5, 1–11. doi: 10.1038/srep10533

Higashi, Y., and Saito, K. (2019). Lipidomic studies of membrane glycerolipids in plant leaves under heat stress. *Prog. Lipid Res.* 75:100990. doi: 10.1016/j.plipres.2019.100990

Ivanov, A. G., Rosso, D., Savitch, L. V., Stachula, P., Rosembert, M., Oquist, G., et al. (2012). Implications of alternative electron sinks in increased resistance of PSII and PSI photochemistry to high light stress in cold-acclimated *Arabidopsis thaliana*. *Photosyn. Res.* 113, 191–206. doi: 10.1007/s11120-012-9769-y

Johnson, G. N., and Stepien, P. (2016). Plastid terminal oxidase as a route to improving plant stress tolerance: known knowns and known unknowns. *Plant Cell Physiol.* 57, 1387–1396.

Kanduè, M., Schlaich, A., de Vries, A. H., Jouhet, J., Maréchal, E., Demé, B., et al. (2017). Tight cohesion between glycolipid membranes results from balanced water-headgroup interactions. *Nat. Commun.* 8:14899. doi: 10.1038/ncomms14899

Kilian, J., Whitehead, D., Horak, J., Wanke, D., Weinl, S., Batistic, O., et al. (2007). The AtGenExpress global stress expression data set: protocols, evaluation and model data analysis of UV-B light, drought and cold stress responses. *Plant J.* 50, 347–363.

Kirchhoff, H., Mukherjee, U., and Galla, H.-J. (2002). Molecular architecture of the thylakoid membrane: lipid diffusion space for plastoquinone. *Biochemistry* 41, 4872–4882.

Kramer, D. M., Johnson, G., Kiirats, O., and Edwards, G. E. (2004). New fluorescence parameters for the determination of QA redox state and excitation energy fluxes. *Photosyn. Res.* 79:209. doi: 10.1023/B:PRES.0000015391.99477.0d

Krieger-Liszkay, A., Kienzler, K., and Johnson, G. N. (2000). Inhibition of electron transport at the cytochrome b6f complex protects photosystem II from photoinhibition. *FEBS Lett.* 486, 191–194.

Kromdijk, J., Głowacka, K., Leonelli, L., Gabilly, S. T., Iwai, M., Niyogi, K. K., et al. (2016). Improving photosynthesis and crop productivity by accelerating recovery from photoprotection. *Science* 354, 857–861.

Krumova, S. B., Laptenok, S. P., Kovács, L., Tóth, T., van Hoek, A., Garab, G., et al. (2010). Digalactosyl-diacylglycerol-deficiency lowers the thermal stability of thylakoid membranes. *Photosyn. Res.* 105, 229–242. doi: 10.1007/s11120-010-9581-5

Laemmli, U. K. (1970). Cleavage of structural proteins during the assembly of the head of bacteriophage T4. *Nature* 227, 680–685.

Laureau, C., Paepe, R. D., Latouche, G., Moreno−Chacón, M., Finazzi, G., Kuntz, M., et al. (2013). Plastid terminal oxidase (PTOX) has the potential to act as a safety valve for excess excitation energy in the alpine plant species Ranunculus glacialis L. *Plant Cell Environ.* 36, 1296–1310. doi: 10.1111/pce.12059

Leuenberger, M., Morris, J. M., Chan, A. M., Leonelli, L., Niyogi, K. K., and Fleming, G. R. (2017). Dissecting and modeling zeaxanthin- and lutein-dependent nonphotochemical quenching in *Arabidopsis thaliana*. *Proc. Natl. Acad. Sci. U.S.A.* 114, E7009–E7017. doi: 10.1073/pnas.1704502114

Li, H., Yan, X., Xu, J., and Zhou, C. (2008). Precise identification of photosynthetic glycerolipids in microalga Tetraselmis chuii by UPLC-ESI-Q-TOF-MS. *Sci. China C Life Sci.* 51, 1101–1107. doi: 10.1007/s11427-008-0138-1

Li, X.-P., Björkman, O., Shih, C., Grossman, A. R., Rosenquist, M., Jansson, S., et al. (2000). A pigment-binding protein essential for regulation of photosynthetic light harvesting. *Nature* 403, 391–395.

Lichtenthaler, H. K., and Wellburn, A. R. (1983). Determinations of total carotenoids and chlorophylls a and b of leaf extracts in different solvents. *Biochem. Soc. Trans.* 11, 591–592.

Longoni, P., Douchi, D., Cariti, F., Fucile, G., and Goldschmidt-Clermont, M. (2015). Phosphorylation of the light-harvesting complex II Isoform Lhcb2 Is central to state transitions. *Plant Physiol.* 169, 2874–2883. doi: 10.1104/pp.15.01498

Longoni, P., Samol, I., and Goldschmidt-Clermont, M. (2019). The kinase STATE TRANSITION 8 phosphorylates light harvesting complex II and contributes to light acclimation in *Arabidopsis thaliana*. *Front. Plant Sci.* 10:1156. doi: 10.3389/fpls.2019.01156

Maxwell, K., and Johnson, G. N. (2000). Chlorophyll fluorescence—a practical guide. *J. Exp. Bot.* 51, 659–668.

Mène-Saffrané, L., Jones, A. D., and DellaPenna, D. (2010). Plastochromanol-8 and tocopherols are essential lipid-soluble antioxidants during seed desiccation and quiescence in Arabidopsis. *Proc. Natl. Acad. Sci. U.S.A.* 107, 17815–17820. doi: 10.1073/pnas.1006971107

Nawrocki, W. J., Tourasse, N. J., Taly, A., Rappaport, F., and Wollman, F.-A. (2015). The plastid terminal oxidase: its elusive function points to multiple contributions to plastid physiology. *Annu. Rev. Plant. Biol.* 66, 49–74. doi: 10.1146/annurev-arplant-043014-114744

Niki, E. (2009). Lipid peroxidation: physiological levels and dual biological effects. *Free Radic. Biol. Med.* 47, 469–484. doi: 10.1016/j.freeradbiomed.2009.05.032

Norén, H., Svensson, P., Stegmark, R., Funk, C., Adamska, I., and Andersson, B. (2003). Expression of the early light-induced protein but not the PsbS protein is influenced by low temperature and depends on the developmental stage of the plant in field-grown pea cultivars. *Plant Cell Environ.* 26, 245–253.

Norris, S. R., Barrette, T. R., and DellaPenna, D. (1995). Genetic dissection of carotenoid synthesis in *Arabidopsis* defines plastoquinone as an essential component of phytoene desaturation. *Plant Cell* 7, 2139–2149.

Nowicka, B., Gruszka, J., and Kruk, J. (2013). Function of plastochromanol and other biological prenyllipids in the inhibition of lipid peroxidation—a comparative study in model systems. *Biochim. Biophys. Acta* 1828, 233–240. doi: 10.1016/j.bbamem.2012.08.018

Penfield, S. (2008). Temperature perception and signal transduction in plants. *New Phytol.* 179, 615–628. doi: 10.1111/j.1469-8137.2008.02478.x

Pospíšil, P. (2016). Production of reactive oxygen species by photosystem II as a response to light and temperature stress. *Front. Plant Sci.* 7:1950. doi: 10.3389/fpls.2016.01950

Pralon, T., Collombat, J., Pipitone, R., Ksas, B., Shanmugabalaji, V., Havaux, M., et al. (2020). Mutation of the atypical kinase ABC1K3 partially rescues the proton gradient regulation 6 Phenotype in *Arabidopsis thaliana*. *Front. Plant Sci.* 11:337. doi: 10.3389/fpls.2020.00337

Rastogi, A., Yadav, D. K., Szymańska, R., Kruk, J., Sedláøová, M., and Pospíšil, P. (2014). Singlet oxygen scavenging activity of tocopherol and plastochromanol in *Arabidopsis thaliana*: relevance to photooxidative stress. *Plant Cell Environ.* 37, 392–401. doi: 10.1111/pce.12161

Rochaix, J.-D. (2011). Regulation of photosynthetic electron transport. *Biochim. Biophys. Acta* 1807, 375–383. doi: 10.1016/j.bbabio.2010.11.010

Rokka, A., Aro, E.-M., Herrmann, R. G., Andersson, B., and Vener, A. V. (2000). Dephosphorylation of photosystem II reaction center proteins in plant photosynthetic membranes as an immediate response to abrupt elevation of temperature. *Plant Physiol.* 123, 1525–1536.

Rorat, T., Havaux, M., Irzykowski, W., Cuiné, S., Becuwe, N., and Rey, P. (2001). PSII-S gene expression, photosynthetic activity and abundance of plastid thioredoxin-related and lipid-associated proteins during chilling stress in *Solanum species* differing in freezing resistance. *Physiol. Plant* 113, 72–78.

Rosso, D., Bode, R., Li, W., Krol, M., Saccon, D., Wang, S., et al. (2009). Photosynthetic redox imbalance governs leaf sectoring in the *Arabidopsis thaliana* variegation mutants immutans, spotty, var1, and var2. *Plant Cell* 21, 3473–3492. doi: 10.1105/tpc.108.062752

Seiwert, D., Witt, H., Ritz, S., Janshoff, A., and Paulsen, H. (2018). The nonbilayer lipid MGDG and the major light-harvesting complex (LHCII) promote membrane stacking in supported lipid bilayers. *Biochemistry* 57, 2278–2288. doi: 10.1021/acs.biochem.8b00118

Spicher, L., Almeida, J., Gutbrod, K., Pipitone, R., Dörmann, P., Glauser, G., et al. (2017). Essential role for phytol kinase and tocopherol in tolerance to combined light and temperature stress in tomato. *J. Exp. Bot.* 68, 5845–5856. doi: 10.1093/jxb/erx356

Spicher, L., Glauser, G., and Kessler, F. (2016). Lipid antioxidant and galactolipid remodeling under temperature stress in tomato plants. *Front. Plant Sci.* 7:167. doi: 10.3389/fpls.2016.00167

Stepien, P., and Johnson, G. N. (2018). Plastid terminal oxidase requires translocation to the grana stacks to act as a sink for electron transport. *Proc. Natl. Acad. Sci. U.S.A.* 115, 9634–9639. doi: 10.1073/pnas.1719070115

Streb, P., Josse, E.-M., Gallouët, E., Baptist, F., Kuntz, M., and Cornic, G. (2005). Evidence for alternative electron sinks to photosynthetic carbon assimilation in the high mountain plant species Ranunculus glacialis. *Plant Cell Environ.* 28, 1123–1135.

Sunil, B., Saini, D., Bapatla, R. B., Aswani, V., and Raghavendra, A. S. (2019). Photorespiration is complemented by cyclic electron flow and the alternative oxidase pathway to optimize photosynthesis and protect against abiotic stress. *Photosyn. Res.* 139, 67–79. doi: 10.1007/s11120-018-0577-x

Tang, Y., Wen, X., Lu, Q., Yang, Z., Cheng, Z., and Lu, C. (2007). Heat stress induces an aggregation of the light-harvesting complex of photosystem II in spinach plants. *Plant Physiol.* 143, 629–638.

Tóth, S. Z., Schansker, G., and Strasser, R. J. (2007). A non-invasive assay of the plastoquinone pool redox state based on the OJIP-transient. *Photosyn. Res.* 93, 193–203.

Tremmel, I. G., Kirchhoff, H., Weis, E., and Farquhar, G. D. (2003). Dependence of plastoquinol diffusion on the shape, size, and density of integral thylakoid proteins. *Biochim. Biophys. Acta* 1607, 97–109.

Ware, M. A., Dall'Osto, L., and Ruban, A. V. (2016). An in vivo quantitative comparison of photoprotection in *Arabidopsis* xanthophyll mutants. *Front. Plant Sci.* 7:841. doi: 10.3389/fpls.2016.00841

Wraight, C. A., and Crofts, A. R. (1970). Energy-dependent quenching of chlorophyll a fluorescence in isolated chloroplasts. *Eur. J. Biochem.* 17, 319–327.

Yamane, Y., Kashino, Y., Koike, H., and Satoh, K. (1997). Increases in the fluorescence Fo level and reversible inhibition of Photosystem II reaction center by high-temperature treatments in higher plants. *Photosyn. Res.* 52, 57–64.

Yamori, W., Hikosaka, K., and Way, D. A. (2014). Temperature response of photosynthesis in C3, C4, and CAM plants: temperature acclimation and temperature adaptation. *Photosyn. Res.* 119, 101–117. doi: 10.1007/s11120-013-9874-6

Zhang, R., Wise, R. R., Struck, K. R., and Sharkey, T. D. (2010). Moderate heat stress of *Arabidopsis thaliana* leaves causes chloroplast swelling and plastoglobule formation. *Photosyn. Res.* 105, 123–134. doi: 10.1007/s11120-010-9572-6

Conflict of Interest: The authors declare that the research was conducted in the absence of any commercial or financial relationships that could be construed as a potential conflict of interest.

Copyright © 2020 Sattari Vayghan, Tavalaei, Grillon, Meyer, Ballabani, Glauser and Longoni. This is an open-access article distributed under the terms of the Creative Commons Attribution License (CC BY). The use, distribution or reproduction in other forums is permitted, provided the original author(s) and the copyright owner(s) are credited and that the original publication in this journal is cited, in accordance with accepted academic practice. No use, distribution or reproduction is permitted which does not comply with these terms.

frontiers in Plant Science

ORIGINAL RESEARCH
published: 05 June 2020
doi: 10.3389/fpls.2020.00723

Specific Composition of Lipid Phases Allows Retaining an Optimal Thylakoid Membrane Fluidity in Plant Response to Low-Temperature Treatment

Radosław Mazur[1†], Katarzyna Gieczewska[2†], Łucja Kowalewska[2], Anna Kuta[1‡], Małgorzata Proboszcz[1‡], Wieslaw I. Gruszecki[3], Agnieszka Mostowska[2] and Maciej Garstka[1*]*

[1] Department of Metabolic Regulation, Faculty of Biology, Institute of Biochemistry, University of Warsaw, Warsaw, Poland, [2] Department of Plant Anatomy and Cytology, Faculty of Biology, Institute of Plant Experimental Biology and Biotechnology, University of Warsaw, Warsaw, Poland, [3] Department of Biophysics, Institute of Physics, Maria Curie-Skłodowska University, Lublin, Poland

OPEN ACCESS

Edited by:
Yoshitaka Nishiyama, Saitama University, Japan

Reviewed by:
Gyozo Garab, Biological Research Centre, Hungarian Academy of Sciences (MTA), Hungary
Andrea Trotta, University of Turku, Finland
Juliette Jouhet, UMR 5168 Laboratoire de Physiologie Cellulaire Vegetale (LPCV), France

***Correspondence:**
Radosław Mazur
rmazur@biol.uw.edu.pl
Maciej Garstka
garstka@biol.uw.edu.pl

[†] These authors have contributed equally to this work

[‡] **Present address:**
Anna Kuta, ImmuNext Inc., Lebanon, NH, United States
Małgorzata Proboszcz, Department of Internal Medicine, Pulmonary Diseases and Allergy, Medical University of Warsaw, Warsaw, Poland

Specialty section:
This article was submitted to Plant Physiology, a section of the journal Frontiers in Plant Science

Received: 24 February 2020
Accepted: 06 May 2020
Published: 05 June 2020

Citation:
Mazur R, Gieczewska K, Kowalewska Ł, Kuta A, Proboszcz M, Gruszecki WI, Mostowska A and Garstka M (2020) Specific Composition of Lipid Phases Allows Retaining an Optimal Thylakoid Membrane Fluidity in Plant Response to Low-Temperature Treatment. Front. Plant Sci. 11:723. doi: 10.3389/fpls.2020.00723

Thylakoid membranes isolated from leaves of two plant species, the chilling tolerant (CT) pea and chilling sensitive (CS) runner bean, were assessed for the composition of lipids, carotenoids as well as for the arrangement of photosynthetic complexes. The response to stress conditions was investigated in dark-chilled and subsequently photo-activated detached leaves of pea and bean. Thylakoids of both species have a similar level of monogalactosyldiacylglycerol (MGDG) and digalactosyldiacylglycerol (DGDG), but different sulfoquinovosyldiacylglycerol to phosphatidylglycerol (PG) ratio. In pea thylakoid fraction, the MGDG, DGDG and PG, have a higher double bond index (DBI), whereas bean thylakoids contain higher levels of high melting point PG. Furthermore, the lutein to the β-carotene ratio is higher in bean thylakoids. Smaller protein/lipid ratio in pea than in bean thylakoids suggests different lipid-protein interactions in both species. The differences between species are also reflected by the course of temperature-dependent plots of chlorophyll fluorescence pointing various temperatures of the lipid phase transitions of pea and bean thylakoids. Our results showed higher fluidity of the thylakoid membrane network in pea than in bean in optimal temperature conditions. Dark-chilling decreases the photochemical activity and induces significant degradation of MGDG in bean but not in pea leaves. Similarly, substantial changes in the arrangement of photosynthetic complexes with increase in LHCII phosphorylation and disturbances of the thylakoid structure take place in bean thylakoids only. Changes in the physical properties of bean thylakoids are manifested by the conversion of a three-phase temperature-dependent plot to a one-phase plot. Subsequent photo-activation of chilled bean leaves caused a partial restoration of the photochemistry and of membrane physical properties, but not of the photosynthetic complexes arrangement nor the thylakoid network structure. Summarizing, the composition of the thylakoid lipid

matrix of CT pea allows retaining the optimal fluidity of its chloroplast membranes under low temperatures. In contrast, the fluidity of CS bean thylakoids is drastically changed, leading to the reorganization of the supramolecular structure of the photosynthetic complexes and finally results in structural remodeling of the CS bean thylakoid network.

Keywords: photosynthesis, chilling stress, thylakoid membranes, membrane fluidity, lipid composition, pea, bean, LHCII phosphorylation

INTRODUCTION

Thylakoid membranes in chloroplasts of higher plants are assemblies of chlorophyll-protein (CP) complexes and lipids, organized into two distinct domains: stacked membranes called grana and unstacked stroma thylakoids (Ruban and Johnson, 2015). CP complexes are organized hierarchically in supercomplexes and megacomplexes, and are spatially segregated (Kouřil et al., 2012). Photosystem II (PSII) with light-harvesting complexes (LHCII) is organized in LHCII-PSII supercomplexes and localized in the grana, whereas the LHCI-PSI supercomplexes consist of Photosystem I (PSI) and its antenna (LHCI), which are localized in unstacked thylakoids (Danielsson et al., 2004, 2006; Daum et al., 2010; Koochak et al., 2019). Dynamic changes in the arrangement of CP complexes and grana structure play a crucial role in the regulation of photosynthesis in response to environmental conditions (Wood et al., 2018; Johnson and Wientjes, 2019).

The lipid phase of thylakoids is formed by monogalactosyldiacylglycerol (MGDG) that accounts for about 50% of the total lipid content, digalactosyldiacylglycerol (DGDG) (∼30%), sulfoquinovosyldiacylglycerol (SQDG) (∼5–12%), and phosphatidylglycerol (PG) (∼5–12%) (Pali et al., 2003). The MGDG, the lipid forming inverted hexagonal phase, is linked with the dynamic polymorphism of lipids in thylakoid membranes, where the main bilayer phase coexists with minor non-bilayer domains (Garab et al., 2017). The formation of large lamellar structures is related to the presence of integral membrane proteins, mainly LHCII, which inhibits the formation of a non-bilayer structure (Simidjiev et al., 2000; Janik et al., 2013; Kowalewska et al., 2016). On the other hand, the MGDG protects the LHCII against unfolding (Seiwert et al., 2017). Furthermore, specific lipids bound inside the PSI, PSII or LHCII enable the functional conformation and photochemical activity of CP complexes (Jones, 2007; Domonkos et al., 2008; Mizusawa and Wada, 2012; Kobayashi et al., 2017). Membrane fluidity increases with the degree of desaturation of lipid acyl chains and with the content of β-carotene, whereas the presence of xanthophylls and α-tocopherol incorporated into bilayer leads to an increase of membrane rigidity (Pali et al., 2003; Gruszecki and Strzalka, 2005; Szilagyi et al., 2008). The ratio of lipids to proteins in thylakoids is estimated to be roughly 0.3 (Koochak et al., 2019); therefore, the membrane dynamics might be substantially modulated by lipid-protein interactions (Pali et al., 2003).

The lipid composition of thylakoids is an important factor determining the stabilization of the photosynthetic complexes under low temperature. An increase of the level of desaturated lipids is correlated with the increase of plant resistance to chilling conditions, as was described for many cold-adapted plants (Zheng et al., 2016; Kenchanmane Raju et al., 2018), as well as for plants with elevated (Orlova et al., 2003; Khodakovskaya et al., 2006) or decreased (Ivanov et al., 2012; Chen and Thelen, 2013) acyl-lipid desaturases. A decrease of MGDG/DGDG ratio and the level of PG induced by low temperature is generally present but varies depending on the plant species (Zheng et al., 2016; Skupien et al., 2017; Kenchanmane Raju et al., 2018).

The response of plant species to low temperature is also related to their evolutionary background. The chilling-sensitive plants (CS), susceptible to temperatures below 12°C, mostly originated from subtropical areas, whereas the chilling-tolerant (CT) ones, resistant to low but non-freezing temperatures, evolved in temperate climate (Garstka et al., 2005, 2007). In many cases, the chilling-stress is studied using the dark-chilling model in which observed effects are due mainly to the low temperature alone; chilling in the light may cause photo-inhibition of both photosystems and strong oxidative stress (Garstka et al., 2007; Mazur et al., 2018).

Low temperature induces up-regulation of genes involved in PG and galactolipid synthesis and their remodeling both in CT and CS plants (Gu et al., 2017; Marla et al., 2017; Kenchanmane Raju et al., 2018). The expression of *type 2* plastid-localized lipoxygenase, an enzyme catalyzing oxygenation of polyunsaturated fatty acids, is noted in CS plants (Mazur et al., 2018). In many CS plants, dark-chilling leads to the accumulation of free fatty acids (FFA) due to the high activity of galactolipase under these conditions (Kaniuga, 2008). Furthermore, a higher proportion of motionally restricted lipids, localized in the boundary phase of CP complexes, is registered in CS compared with CT plants, indicating the role of lipid-protein interaction in chilling response (Li et al., 1990).

Apart from the lipid phases composition, plant response to low temperature is also considered in the context of CP complexes arrangement. A decrease in PSII activity in detached leaves of CS plants chilled in the dark is associated with the release of manganese from the oxygen-evolving complex of PSII (Kaniuga, 2008) and with the destabilization of PSII extrinsic proteins (Shen et al., 1990; Garstka and Kaniuga, 1991; Higuchi et al., 2003). Dark-chilling induces rearrangements of CP supercomplexes – LHCI-PSI and LHCII trimers leading to the disturbance of thylakoids structure in CS bean and tomato (Garstka et al., 2005, 2007).

In the present paper, we studied the effect of low temperature on chloroplasts and thylakoids isolated from dark-chilled and subsequently photo-activated detached leaves of CT garden pea and CS runner bean. We investigated whether the

differences in the composition of lipid phases, arrangement of CP complexes and their phosphorylation determine the response of these species to low temperature. Complex analyses of lipid and carotenoid compositions of pea and bean thylakoids were performed. Moreover, the structural arrangements of CP complexes were examined by time-resolved, temperature-dependent and low-temperature chlorophyll *a* (Chl *a*) fluorescence, as well as by Fourier-transform infrared spectroscopy (FTIR). Data were complemented by imaging the chloroplast structure by confocal laser scanning (CLSM) and transmission electron microscopy (TEM). The protein phosphorylation was studied using the electrophoretic technique. The relations between microscopic, biochemical and biophysical data were discussed in detail regarding lipid-protein interactions and reversible protein phosphorylation.

We found that the pea and bean thylakoid membranes differ in lipid and carotenoid composition, lipid desaturation level, protein/lipid ratio and arrangement of CP complexes. These features significantly influence the physical properties of thylakoid membranes. The dark-chilling treatment does not influence the physical properties of pea thylakoids and high fluidity of their membranes is preserved at low temperatures. On the contrary, more rigid bean thylakoid membranes change significantly under dark-chilling conditions leading to the reorganization of the supramolecular structure of photosynthetic complexes and structural remodeling of the CS bean thylakoid network.

MATERIALS AND METHODS

Plant Growth and Chilling Treatment

Runner bean (*Phaseolus coccineus* L. cv. Eureka) and garden pea (*Pisum sativum* L. cv. Demon) plants (both from PlantiCo Zielonki, 05-082 Babice Stare, Poland) were grown in 3 L perlite-containing pots in a climate-controlled room (21°C day/18°C night) at a photosynthetic active radiation (PAR) of 200 μmol photons m^{-2} s^{-1} during a 16 h photoperiod and relative humidity of 60–70%. Fully expanded primary leaves of 10 day-old bean and 3rd–4th leaves of 20 day-old pea were harvested 30 min after the light was switched on. For the control samples the thylakoids were immediately isolated from harvested leaves or intact leaves were used for *in vivo* fluorescence measurements. For dark-chilling treatment, the detached leaves of bean and green parts of pea were placed in Dewar flasks (4°C, 100% relative humidity) for 5 days. For photo-activation, dark-chilled leaves/green parts were placed on a water layer in a transparent plastic dish at 21°C with PAR of 200 μmol of photons m^{-2} s^{-1} and optimal humidity for 3 h.

Preparation of Chloroplasts and Thylakoid Membranes

Intact chloroplasts and thylakoid membranes were isolated by homogenization of pea and bean leaves in a buffered isotonic medium and subsequent centrifugation as described previously (Rumak et al., 2012). The concentration of chlorophyll was quantified spectrophotometrically after extraction with 80% (v:v) acetone (Rumak et al., 2012).

In vivo Chlorophyll *a* Fluorescence and P700 Measurements

Chlorophyll *a* fluorescence and P700 absorption changes were measured *in vivo* by the Pulse-Amplitude-Modulation approach using the Dual-PAM 100 (Heinz Walz GmbH, Effeltrich, Germany). Before all measurements, plants were dark-adapted for 30 min. Minimal (F_0) and maximal (F_M) fluorescence were measured by applying red light pulse with intensity below 1 μmol photons m^{-2} s^{-1} and 90 ms red light saturation pulse with 20,000 μmol photons m^{-2} s^{-1}, respectively. Simultaneously fast kinetics curves were measured during 160 ms and 10 μs data collection intervals.

Kinetics of P700 oxidation were measured with the help of far-red illumination. Dark-adapted leaves were pre-illuminated for 5 min with far-red light of intensity ∼250 μmol photons m^{-2} s^{-1}. Next, the single turnover (ST) flash (50 μs, 10,000 μmol photons m^{-2} s^{-1}) and after 10 s the multiple turnover (MT) flash (300 ms, 10,000 μmol photons m^{-2} s^{-1}) were applied. The first 4 s after MT flash of P700 signals were analyzed; the amplitude of the P700 signals was normalized to 1.

The capacity of intersystem electron carrier pool P700 was measured by a similar approach, as described above. The dark-adapted leaves were illuminated with far-red light of intensity ∼50 μmol photons m^{-2} s^{-1} during 60 s. Next, the ST (50 μs) and MT (50 ms) flashes were applied with 10 s between them, and the P700 signal was recorded 120 s after applying MT. The P700 reduction areas induced by ST and MT were used for calculation of the capacity of the intersystem electron carrier pool, basing on the assumption that MT flash fills up the intersystem carriers pool (Asada et al., 1992).

Non-photochemical plastoquinone (PQ) reduction was measured according to (Shikanai et al., 1998) with some modifications. Dark-adapted leaves were illuminated by red actinic light of the intensity of 750 μmol photons m^{-2} s^{-1} for 5 min, followed by 3 min in darkness. The fluorescence signal was measured by weak modulated blue light with a 5 ms interval.

Determination of Temperature-Dependent Chl *a* Fluorescence of Thylakoid Membranes

The temperature-dependent changes in Chl *a* fluorescence were analyzed according to Gruszecki et al. (1999) with some modifications. The intensity of fluorescence emission was determined with the Shimadzu RF-5301PC spectrofluorimeter with 3 and 10 nm spectral resolution for excitation and emission, respectively. The thylakoid suspension (12 μg Chl mL^{-1}) placed in a sealed quartz cuvette (10 mm optical path length) was magnetically stirred to prevent settling. The sample was initially cooled to 1°C and then the temperature was increased gradually from 1 to 40°C with 1°C interval. During sample stabilization at particular temperature the sample was kept in darkness for 1 min, and then the shutter of the spectrofluorimeter was opened for 20 s only. The intensities of exctitation light were 40 and 100

μmol photons m^{-2} s^{-1} for 412 and 470 nm, respectively. The fluorescence intensity at two excitation/emission wavelengths (412/680 nm; 470/680 nm) was recorded simultaneously, 40 points for each degree at 0.5 s interval, but average values were calculated only for the last 20 points, where the fluorescence level was stable.

Low-Temperature Fluorescence Measurements

Steady-state fluorescence emission spectra of chlorophyll at low temperature (77 K) were recorded using the modified Shimadzu RF-5301PC spectrofluorimeter with the emission and excitation beams guided through the light pipes. Thylakoid membranes diluted to chlorophyll concentration of 10 μg/mL were placed in a polytetrafluoroethylene cuvette and submerged in liquid nitrogen. The excitation wavelength was set at 412 and 470 nm, excitation and emission slits at 5 nm, and scans were taken in the range of 600–800 nm through the LP600 emission filter.

Fourier-Transform Infrared Spectroscopy (FTIR) Measurements

Thylakoid membranes isolated from control, chilled, and photoactivated plants were resuspended in a ^2H_2O-based 20 mM Hepes–NaOH (pH 7.0) buffer containing 330 mM sorbitol, 15 mM NaCl and 4 mM $MgCl_2$ and then centrifuged at 5000 *g* for 5 min at 4°C. This step was repeated three times to replace the H_2O based buffers with the ^2H_2O ones. Fourier-transform infrared (FTIR) spectra were recorded with a Bruker Vector 33 spectrometer equipped with a horizontal attenuated total reflection (ATR) crystal as described previously (Rumak et al., 2010).

Extraction and Analysis of Polar Lipids

Thylakoid membranes containing 0.8 mg of chlorophyll were dissolved in 6 mL of chloroform: methanol 2:1 (v:v) mixture. Total polar lipid extraction was performed as described in Skupien et al. (2017). Extracted lipids were separated using the Waters 600 HPLC system connected with ZQ 2000 mass spectrometer (Waters). The samples were injected (20 μL) into a Discovery™ RP Amide C16 (5.0 μm, 180 Å, 2.1 × 150 mm) column equilibrated in 20% of solvent A (water) and 80% of solvent B (methanol: acetonitrile 7:3 (v:v). Elution was carried out with a constant flow rate of 0.3 mL/min with linearly increasing solvent B to 90% for 20 min. Next, a stepped linear gradient of solvents B and C (2-propanol) was distributed as follows: 90–100% B in the 20–70 min; 100% B in 71–80 min; 100–30% B and 0–70% C in 80–100 min. The column was re-equilibrated in 30% of A and 70% of B for 20 min before the next injection. The quality of sample separation was monitored by an absorption detector at 210 and 436 nm. Mass spectra between 500 and 1000 m/z were recorded in a positive and negative mode using the ZQ 2000 single quadrupole mass spectrometer with an electrospray ion source. The capillary and cone voltages were the same for the positive and negative ionization and were set at 4 kV and 30 V, respectively. Specific lipids were assigned to molecular masses by a comparison of the collected mass spectra with the standards and with the literature data (Skupien et al., 2017). Up to 35 molecular species of four classes of lipids (MGDG, DGDG, SQDG, and PG) were identified. Quantitative analysis was performed on the basis of areas under the spectrum calculated using the MassLynx v3.5 software (Waters) and results were presented as a relative composition of lipid classes. The double-bond index (DBI) and acyl chain length (ACL) were calculated as a sum of percentage participation of the total number of double bonds (N) or the total number of carbons (n) in the two fatty acid chains of each lipid molecular species or of all identified lipids, according to equation $DBI(ACL) = \Sigma[N(n) \times \%\ lipid])/100$ (Zheng et al., 2016).

Extraction and Analysis of Carotenoids

Pigments, including carotenoids, were extracted as described earlier (Szalonek et al., 2015). Extracted pigments were separated using Waters 600 HPLC system (Waters). The samples were injected (20 μL) into an Atlantis™ dC18 (3 μm, 100 Å, 3.0 × 150 mm) analytical column equilibrated in 100% of solvent A (water : methanol 1:9, v:v). The column was eluted at 25°C at a constant flow rate of 0.225 mL/min with 100% of solvent A for 10 min. Next the stepped linear gradient of buffer B (methanol : 2-propanol : hexane 2:1:1, v:v:v) was distributed as follows: 0–20% of B in the 10–42 min (flow rate 0.225–0.32 mL/min); 20–70% of B in 42–92 min and 70–100% of B in 92–120 min (flow rate 0.32 mL/min); and held for 10 min more at 100% of B with increasing flow rate to 0.5 mL/min. In the next 5 min the concentration of solvent B was decreased to 0% and the column was equilibrated for 15 more min (flow rate 0.5 mL/min) before the next injection. The separation of samples was monitored by an absorption detector at 436 and 652 nm. For quantification of carotenoids, chromatogram at 436 nm was integrated using MassLynx 3.5 software (Waters) and results were presented as a relative contribution of specific carotenoids in the total carotenoid fraction.

Electrophoretic Techniques

Thylakoid membrane proteins were separated by the standard SDS-PAGE technique using 14% polyacrylamide (with no addition of urea) resolving gels. Phospho-protein and protein staining were performed using the ProQ®-Diamond and SYPRO® Ruby according to the manufacturer (Invitrogen™, cat. no MPM33305) protocol. Briefly, after fixation in 50% methanol, 10% acetic acid gels were washed (3 × 10 min) in ultrapure water and stained in the ProQ®-Diamond during 90 min in the dark. Stained gels were placed in a destaining solution (20% acetonitrile, 50 mM sodium acetate pH 4.0) for 3 × 30 min in the dark. After washing (2 × 5 min, ultrapure water) gels were scanned using the Typhoon FLA9000 laser scanner (Amersham Biosciences). The excitation source was set to 532 nm and fluorescence was detected through a 560 nm long-pass emission filter. Scanned gels were washed in 50% methanol, 10% acetic acid during 30 min and stained in the SYPRO® Ruby overnight. Then, gels were washed in 10% methanol, 7% acetic acid during 30 min following 2 × 5 min in ultrapure water. The SYPRO® Ruby fluorescence was detected using the Typhoon FLA9000 scanner with a 473 nm laser source

and a 560 nm longpass emission filter. The other parameters were the same as for the Pro-Q® Diamond. Relative band intensities were quantified using the Quantity One software (Bio-Rad, United States). Bands of selected phosphoproteins were analyzed by densitometry; selected band pixel intensities of ProQ® Diamond signal were divided by corresponding bands intensities of SYPRO® Ruby signal to eliminate possible unequal protein content.

Microscopy Techniques

For Transmission Electron Microscopy (TEM) samples of ca. 3 mm^2 were cut from middle parts of the leaves and prepared as described previously (Kowalewska et al., 2016). The 70 nm thick sections were examined with a JEM 1400 electron microscope (Jeol, Japan).

For Confocal Laser Scanning Microscopy (CLSM) isolated intact chloroplasts were suspended in 20 mM HEPES-NaOH buffer (pH 7.5) containing 330 mM sorbitol, 6% (v/v) glycerol, 15 mM NaCl, 4 mM $MgCl_2$, and 30 μM DCMU to a final chlorophyll concentration of 30 μg mL^{-1}. After 10 min of incubation in the dark and on ice, the suspension was immobilized on a microscope glass covered with poly-L-lysine. Chloroplast images were taken using the Zeiss LSM 510 confocal laser scanning fluorescence microscope as described previously (Rumak et al., 2012). The collected data sets were deconvolved using the AutoQuant X3 software (Media Cybernetics Inc., United States).

Statistical Analysis

The statistical significance of differences between species and experimental conditions was verified by one-way ANOVA with *post hoc* Tukey test at $p = 0.05$. The number of repetitions of specific experiments are given in the figure legends and table footnotes.

RESULTS

Modification of Photochemical Activity by Dark-Chilling Conditions

Detailed analysis of photochemical parameters related to the photochemical activity of both photosystems of pea and bean is presented in **Figure 1**. In pea, the maximal quantum yield of PSII (F_V/F_M) was stable in all experimental conditions (**Figure 1A**), while in bean, after a dark-chilling high decrease of F_V/F_M value was observed with partial recovery after photo-activation (**Figure 1A**). The fast fluorescence induction curves (**Figures 1B,C**) showed that in pea there was some decrease of fluorescence intensity after dark-chilling comparing to control leaves, however, subsequent photo-activation led to almost complete recovery (**Figure 1B**). In bean, a decrease of fluorescence in dark-chilling leaves was much more pronounced and photo-activation resulted in weaker recovery comparing to pea (**Figure 1C**).

In order to determine photochemical efficiency downstream PSII, we examined the P700 oxidation kinetics and capacity of the intersystem electron carrier pool (**Figures 1D–F**). In pea, the P700 oxidation was slightly slower after dark-chilling and after subsequent photo-activation this effect was even more visible (**Figure 1D**). In contrast, in bean the dark-chilling caused an acceleration of the P700 oxidation kinetics comparing to control conditions (**Figure 1E**), however, after photo-activation, the P700 oxidation slowed down compared to the dark-chilled and control conditions (**Figure 1E**). Estimation of the intersystem electron carrier pool showed a substantial increase in the carrier pool in pea after photo-activation of dark-chilled samples (**Figure 1F**). In contrast, in bean, the carrier pool decreased after dark-chilling, while photo-activation induced recovery to the values observed in control leaves (**Figure 1F**).

To determine the activity of alternative electron routes, we measured non-photochemical reduction of PQ by changes in Chl *a* fluorescence in the presence of actinic light and the dark (Shikanai et al., 1998). The detection of reduced PQ in the darkness indicates the activity of Ndh and PGR5/PGRL1 dependent electron transport in thylakoids. The non-photochemical PQ reduction in control conditions was more effective in pea than in bean (**Figures 1G,H**). In pea, the dark-chilling induce a decrease of non-photochemical PQ reduction and after photo-activation the full recovery was observed (**Figure 1G**). In bean, the dark-chilling caused complete inactivation of PQ reduction in the dark, while photo-activation, similarly to pea, led to full recovery (**Figure 1G**).

Analysis of Physical Properties of Thylakoid Membranes

We estimated the relationship between supramolecular membrane arrangement and the photochemical activity, via the analysis of temperature dependence of the steady-state Chl *a* fluorescence emission of thylakoids isolated from control, chilled and photo-activated leaves. The fluorescence emission at 680 nm was recorded simultaneously at two excitation (ex) wavelengths, allowing preferential excitation of Chl *a* (412 nm) and Chl *b* (470 nm). Fluorescence emission patterns recorded at both excitations (**Figure 2** and **Supplementary Figure 1**), indicated that both core (ex 412 nm) and antenna (ex 470 nm) complexes revealed similar responses under the applied experimental conditions.

The intensity of fluorescence decreases with the increase of the temperature. In the case of control pea thylakoids, the linear regression analysis of the plots revealed, that the decrease of Chl *a* fluorescence, excited at 470 nm, exhibited two distinct linear phases (**Figure 2A**), in which the breakpoint between these phases was estimated to be roughly 30°C. The gradient of the temperature-dependent plot below this temperature was 40% smaller than for the phase between 30 and 40°C (**Supplementary Table 1**). The temperature-dependent plot of control bean thylakoids was more complex; three independent phases with two breakpoints were noted (**Figure 2D**). In the first phase, up to about 18°C, the rate of fluorescence decrease was almost temperature independent. The slope of the next phase, between 18 and 30°C was three times larger as compared to the first phase. The gradient in 18–30°C phase was similar to

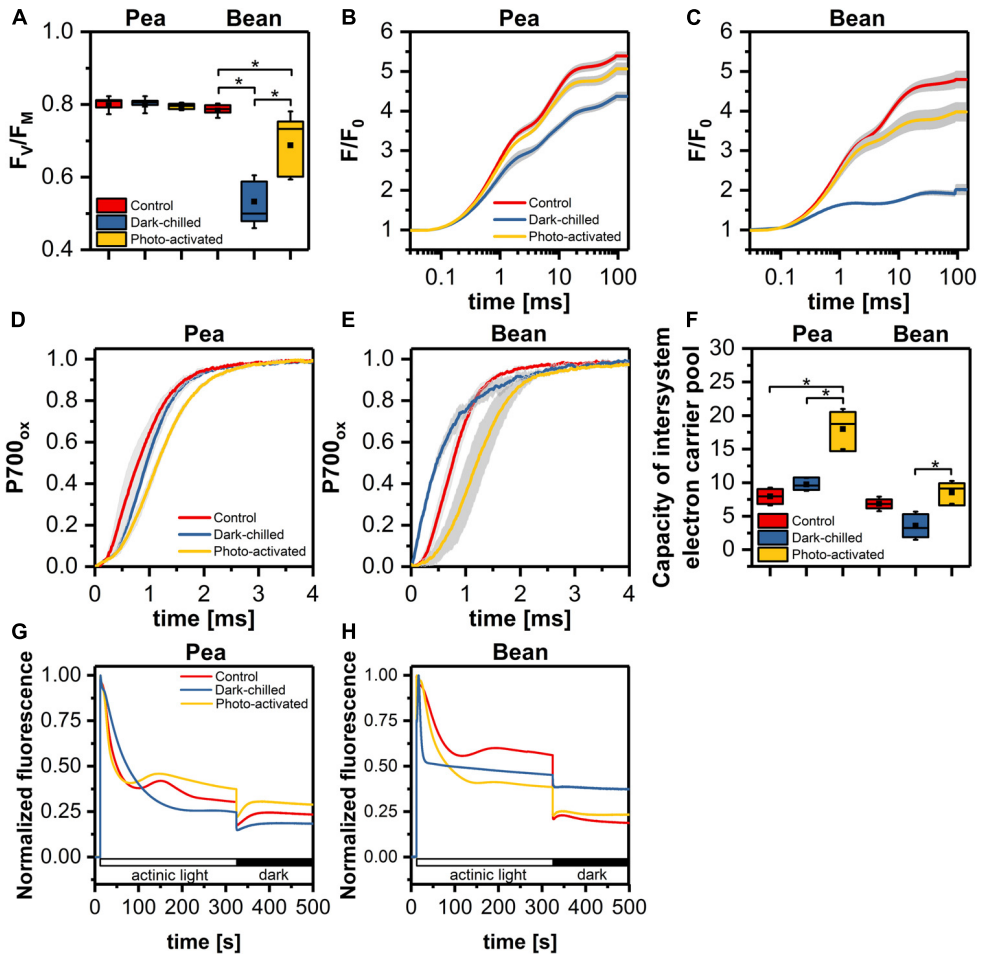

FIGURE 1 | The efficiency of photosynthetic light reactions of pea and bean plants in control, dark-chilled, and photo-activated conditions **(A)** maximal quantum yield of PSII (F_V/F_M); **(B,C)** Chlorophyll *a* fluorescence fast induction curves of pea **(B)** and bean **(C)** leaves; **(D,E)** kinetics of P700 oxidation in pea **(D)** and bean **(E)** leaves; **(F)** capacity of intersystem electron carrier pool; **(G,H)** analysis of non-photochemical reduction of plastoquinone pool in pea **(G)** and bean **(H)**. The data are mean values ± SD from three independent experiments; pairs of results marked with an asterisk differ significantly at $p = 0.05$.

the 1–30°C phase in pea thylakoids (**Supplementary Table 1**). The third phase for control bean thylakoids, above 30°C, revealed a more rapid decrease of the Chl *a* fluorescence, with a 7-fold higher slope than in the first phase in bean, and noticeably higher than for the 30–40°C phase in pea thylakoids (**Supplementary Table 1**).

The temperature-dependent plots of fluorescence decrease for thylakoids isolated from dark-chilled and subsequently photo-activated pea revealed similar behavior to the control (**Figures 2B,C**), except for a small increase of slopes in second phases (**Supplementary Table 1**). These observations suggest a stable interaction between CP complexes in pea thylakoids despite applied temperature conditions. On the contrary, the temperature-dependent plot for thylakoids isolated from dark-chilled bean leaves were significantly different from the control ones, and had a single-phase dependence on the incubation temperature (**Figure 2E**); the slope was similar to that of the 1–30°C and 18–30°C phase registered in control pea and bean thylakoids, respectively (**Supplementary Table 1**). Lack of breakpoint indicated an increase of uniform interactions between CP complexes inside thylakoids, which allow the quench of the Chl *a* fluorescence at the same activation energy (Wentworth et al., 2003). Subsequent photo-activation of bean leaves restored a three-phase behavior of the temperature-dependent plot (**Figure 2F**) with similar breakpoints and the appropriate rate of fluorescence decrease (**Supplementary Table 1**), suggesting reconstruction of the initial interactions between CP complexes.

Analysis of Photosynthetic Complexes Arrangement by Low-Temperature Fluorescence

The relative contribution of specific complexes to the normalized fluorescence emission spectra at 77 K was investigated in thylakoids isolated from control and stressed leaves. The typical spectrum consists of three main bands: (i) at around 683 nm, corresponding to emission from both trimers and monomers of

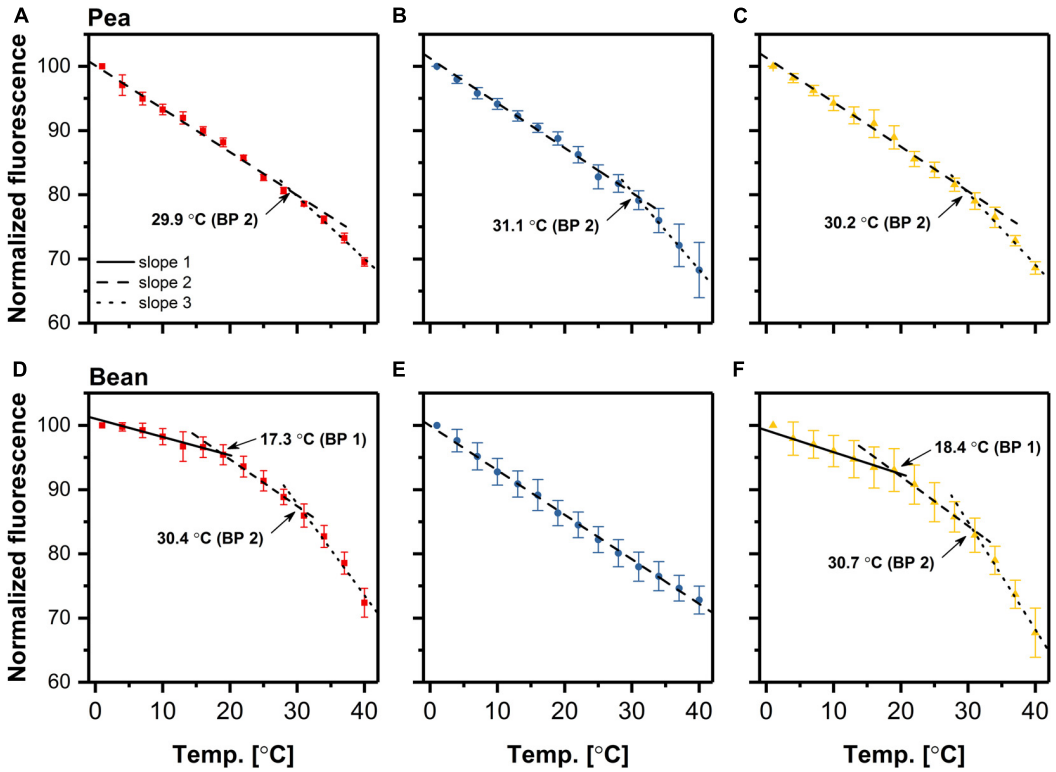

FIGURE 2 | Temperature-dependent plots of the rate of chlorophyll fluorescence decrease in pea **(A–C)** and bean **(D–F)** thylakoids isolated from control **(A,D)**, dark-chilled **(B,E)** and subsequent photo-activated **(C,F)** leaves. Fluorescence emission at 680 nm was excited at 470 nm. The data are mean values ± SD for 3–5 independent experiments. The values for breakpoints (BP) were calculated by linear regression independently for each experiment. For a clear presentation of plots, two out of every three consecutive points were omitted.

LHCII, (ii) at around 693 nm originated from PSII core, (iii) at 734 nm related mainly to the PSI-LHCI.

The chlorophyll fluorescence was excited at 412 nm (Chl *a*) (**Supplementary Figure 2**) and 470 nm (Chl *b*) (**Figure 3**), and difference spectra revealed similar shapes independent on the excitation wavelength. The ratio of fluorescence at 683–693 nm was estimated to 1.3 and 1.0 in pea and bean thylakoids, respectively. These data indicated a larger abundance of LHCII connected with PSII in pea compared with bean thylakoids.

The difference spectrum for thylakoids from dark-chilling pea leaves – minus – control showed a slight increase in the emission at around 698 and 715 nm accompanied by a simultaneous decrease of fluorescence around 739 nm. The subsequent photo-activation of leaves led to a partial recovery to the values observed in control conditions (**Figure 3C**).

Dark-chilling of bean leaves led to a decrease of emission at 686 and 698 nm related to the fluorescence emission from LHCII and PSII core complexes (**Figure 3D**). Furthermore, the difference spectrum exhibited a positive band at around 742 nm due to the emission from LHCI/PSI complexes. The intensities of these bands decreased upon photo-activation, which suggested a partial recovery of CP complexes organization during photo-activation. However, the difference spectrum calculated from the emission spectra for thylakoids isolated from the photo-activated and dark-chilled leaves revealed a positive band around 704 nm, indicating the formation of LHCII aggregates (**Figure 3D**).

The Structural Relationship Between Lipids and Proteins in Pea and Bean Thylakoid Membranes

The FTIR spectroscopy is a useful method to analyze the relationships between lipids and proteins, as well as the changes in the protein secondary structure. The band between 1760 and 1710 cm^{-1} is related to a ester C=O vibration; a bond originating exclusively from lipids, whereas Amide I region (1700–1580 cm^{-1}) corresponds to the vibration of the peptide bond carbonyl group. The relative ratio of these band intensities, in spectrum normalized at 1650 cm^{-1}, reflects the relative lipid to protein ratio (Szalontai et al., 2000; Rumak et al., 2010; Kovacs et al., 2019). In the case of our study, the calculated protein/lipid ratios (**Figures 4A,B**) for control pea and bean thylakoids were estimated to 9.46 ± 0.57 and 25.89 ± 1.96, respectively.

The pea – minus – bean FTIR difference spectrum revealed a positive band in the C=O vibration region, and additionally, bands related to the protein structure (**Figure 4C**). The Amide I region can be divided into several individual components attributed to different secondary structures of proteins – the region around 1650 cm^{-1} representing a

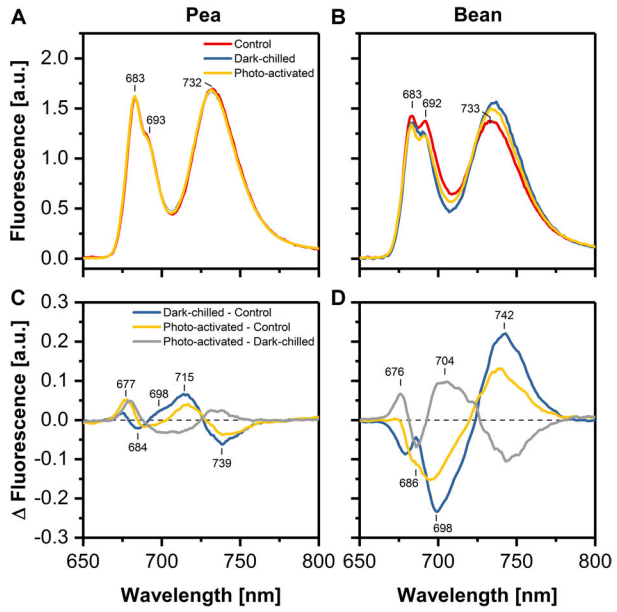

FIGURE 3 | Effect of dark-chilling and subsequent photo-activation on fluorescence emission spectra (Ex 470 nm) at 77 K of isolated thylakoids from control (red), dark-chilled (blue) and subsequently photo-activated (orange) leaves of pea **(A)** and bean **(B)**, respectively. Lower panels present the corresponding difference fluorescence spectra for pea **(C)** and bean **(D)**. The spectra **(A,B)** were normalized to the area of 100 under the spectrum, and the arithmetic differences **(C,D)** between them were calculated. The presented spectra are representative of 3–5 independent experiments.

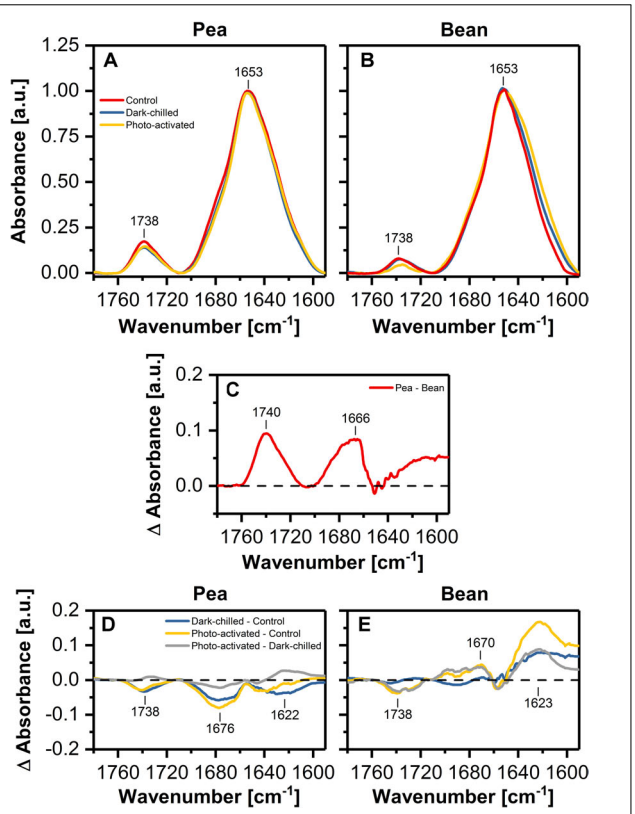

FIGURE 4 | Normalized (at 1650 cm^{-1} to one) infrared absorption spectra in the Amide I and ester C=O regions recorded from pea **(A)** and bean **(B)** thylakoids isolated from control (red), dark-chilled (blue) and subsequently photo-activated (orange) leaves. **(C)** Presents the difference spectrum between pea and bean control spectra. Lower panels show the difference spectra between control and stressed thylakoids for pea **(D)** and bean **(E)**, respectively. The presented spectra are representative of 3 independent experiments.

protein α-helical structure and the region around 1690 cm^{-1} attributed to antiparallel β-sheet structures, probably formed by hydrogen bonds between the polar loops of thylakoid proteins localized outside the membrane. Additionally, the region around 1620 cm^{-1} can be assigned to a parallel β-structure associated with the formation of hydrogen bonds between α-helices of neighboring proteins in the lateral planes of membranes (Rumak et al., 2010; Janik et al., 2013). The pea – minus – bean thylakoid difference spectrum of Amid I region revealed noticeable differences in the regions attributed to the formation of both pseudo-β-structures formed between neighboring proteins in both planes of membranes (**Figure 4C**), suggesting higher interactions between proteins in pea than in bean thylakoids.

The difference FTIR spectrum for thylakoids of dark-chilled pea leaves (dark-chilled – minus – control) showed a slight decrease in the band assigned to lipids and in the band corresponding to the interactions between neighboring membrane proteins. Subsequent photo-activation of leaves did not change the pattern of the difference spectra (photo-activated – minus – control) (**Figure 4D**).

The difference FTIR spectra (**Figure 4E**) for bean thylakoids revealed more evident changes than in pea. The positive band around 1620 cm^{-1} was observed for both thylakoids isolated from chilled and subsequent photo-activated leaves (**Figure 4E**), suggesting noticeable changes in lamellar interactions between proteins.

Composition of Lipids Phase of Bean and Pea Thylakoids Under Control and Stress Conditions

The influence of lipid composition on pea and bean response to chilling conditions was analyzed by the comparison of the main four classes of thylakoid lipids (MGDG, DGDG, SQDG, and PG) (**Figure 5**). The control percentage contribution of main galactolipids MGDG and DGDG and their ratio were similar in both species (**Figures 5A,B** and **Supplementary Table 2**), but the abundance of anionic lipids, SQDG and PG significantly differed. The content of SQDG in pea control thylakoids was two-times larger, while the PG level was about three-times smaller than in bean (**Figures 5A,B**). The overall content of SQDG and PG constituted roughly 17% of the analyzed lipid fraction of the thylakoids of both species, but the SQDG to PG ratio was over two times higher in pea than in bean thylakoids (**Supplementary Table 2**).

The double-bond index (DBI) indicates the average number of double bonds in the fatty acid chains of a lipid molecular species; higher values of DBI correspond to the increase in

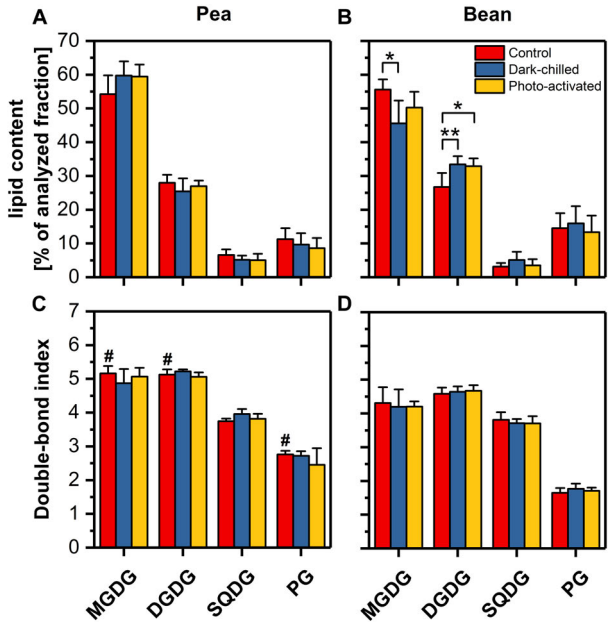

FIGURE 5 | Profiles of the main four classes of lipids extracted from thylakoids isolated from pea **(A)** and bean **(B)** control (red), dark-chilled (blue) and subsequent photo-activation (orange) leaves. Lower panels present the double bond index (DBI) for corresponding lipid classes of pea **(C)** and bean **(D)** thylakoids. The data are mean values ± SD for 4–5 independent experiments. The indicating pairs of bars marked with an asterisk differ significantly at $p = 0.05$ (**) or 0.1 (*). Values marked with a hash indicate a significant difference ($p = 0.05$) between species in control samples.

membrane fluidity (Zheng et al., 2016). The average DBI of the control thylakoid lipids of pea was around 20% higher than for bean thylakoid lipids (**Supplementary Table 2**), which resulted from the higher DBI of only three pea lipid classes – MGDG, DGDG and PG in particular (**Figures 5C,D**). Furthermore, the relative content of the high melting point PG (32:0 and 32:1 molecular species) was almost five times higher in bean than in pea thylakoids (**Supplementary Table 2**). The DBI values for SQDG were almost equal in both species (**Figures 5C,D**).

The average acyl chain length (ACL) is the second indicator of the physical properties of the membrane – longer chains of fatty acids are related to lower fluidity of membrane (Zheng et al., 2016). The average ACL and ACL for MGDG and DGDG lipid classes only slightly differed between species (**Supplementary Table 2**).

After the dark-chilling treatment, the relative content of galactolipids and the ratio of lipid classes changed significantly in bean thylakoids only (**Figures 5A,B**). The MGDG to DGDG ratio decreased to 65% of the value estimated for the control bean samples (**Supplementary Table 2**), and the relative MGDG level decreased by 10% (**Figure 5B**). Simultaneously, the slight increase of SQDG to PG was noted in dark-chilled bean thylakoids (**Supplementary Table 2**). However, both in pea and bean thylakoids, the DBI and ACL did not change under dark-chilling conditions (**Figures 5C,D** and **Supplementary Table 2**). The photo-activation did not significantly influence the lipid composition of both species thylakoid membranes compared with dark-chilling conditions (**Figures 5A,B**). Similarly, the DBI and ACL parameters remained unchanged (**Figures 5C,D** and **Supplementary Table 2**).

Carotenoid Composition of Pea and Bean Thylakoids in Control, Under the Dark-Chilling Treatment, and After Photo-Activation

Carotenoids play different roles in the thylakoid membranes they can (i) participate in photochemical reactions and dissipate the excess of light energy, (ii) effectively quench the free radicals and (iii) modify the fluidity of the lipid phase (Domonkos et al., 2013). Therefore, the determination of the carotenoid composition is important in assessing the physical properties of thylakoid membranes.

The content of the main carotenoids in control samples was significantly different in thylakoids from pea and bean leaves. In pea thylakoids, the lutein and β-carotene reached 45 and 2l% of the total carotenoid pool, respectively, making the lutein to β-carotene ratio equal 2. Bean thylakoids contained about 53% of lutein and 15% of β-carotene in the total carotenoid pool; the lutein/carotene ratio reached the value of almost 4 and the ratio of α- to β-carotene was estimated to 0.22 (**Figures 6A,B** and **Supplementary Table 3**). The relative content of neoxanthin was similar in both species, whereas the violaxanthin was slightly more abundant in pea thylakoids. The content of zeaxanthin and antheraxanthin did not exceed 0.2 and 1.7%, respectively (**Figures 6A,B**). The ratio of lutein to the sum of β-xanthophylls indicated noticeably higher value for bean thylakoids. Furthermore, the presence of α-carotene was noted in bean thylakoids only (**Supplementary Table 3**).

The exposure of leaves to dark-chilling conditions did not significantly affect the carotenoid compositions in both species except for a decrease of one-third of the β-carotene relative content in pea thylakoids (**Figures 6A,B**). The photo-activation of leaves of both species did not change the proportion of carotenoids in comparison with data obtained for dark-chilled leaves (**Figures 6A,B**).

The Influence of Dark-Chilling on Pea and Bean Thylakoid Protein Patterns

The protein patterns of the thylakoid membrane fractions isolated from control, dark-chilled and photo-activated pea and bean leaves were analyzed using SDS-PAGE and fluorescence staining. In pea, there were no significant qualitative and quantitative changes in protein abundance in dark-chilled and photo-activated samples (**Figure 7A**, left panel). In contrast, in bean, dark-chilling induced multiple changes in the protein pattern of the thylakoid membranes (**Figure 7B**, left panel, arrowheads). Some of the proteins: lipoxygenase PCLOXA (96 kDa), Rubisco (55 and 15 kDa), and PsbQ (18 kDa) were identified in our previous study (Mazur et al., 2018).

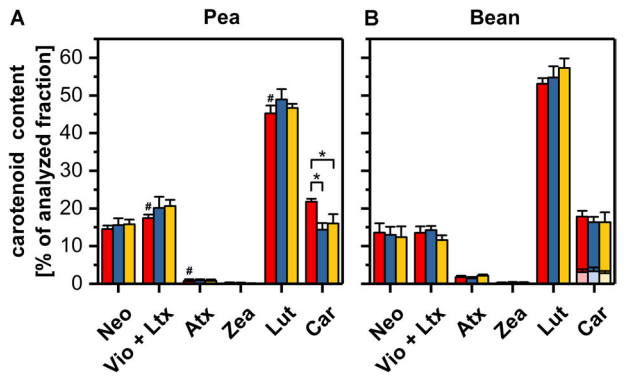

FIGURE 6 | Carotenoid compositions of pea **(A)** and bean **(B)** thylakoids isolated from control (red), dark-chilled (blue) and subsequent photo-activation (orange) leaves. The profiles present the content of neoxanthin (Neo), a sum of violaxanthin and lutheoxanthin (Vio+Ltx), antheraxanthin (Atx), zeaxanthin (Zea), Lutein (Lut) and a sum of α- and β-carotene (Car). α- and β-carotene were labeled by transparent and opaque colors, respectively. The abundance of lutheoxanthin, which is converted non-enzymatically from violaxanthin did not exceed 1 mol % and therefore is presented as a sum with violaxanthin. The data are mean values ± SD for 5–8 independent experiments. Pairs of results marked with an asterisk differ significantly at $p = 0.05$. Values marked with a hash indicate a significant difference ($p = 0.05$) between species in control samples.

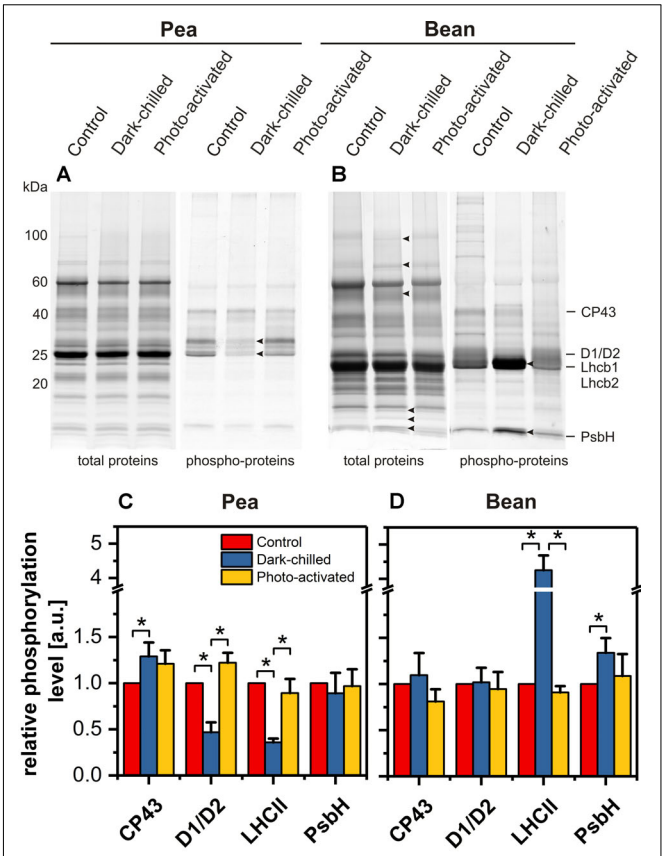

FIGURE 7 | Changes of thylakoid protein and phospho-protein composition after dark-chilling and photo-activation in pea and bean plants. SDS-PAGE gels of pea **(A)** and bean **(B)** thylakoids stained with Sypro Ruby (protein) and Pro-Q Diamond (phospho-protein). The quantitative analysis of selected phospho-proteins of pea **(C)** and bean **(D)** thylakoids. Presented data are mean values ± SD from at least three independent experiments. Pairs of results marked with an asterisk differ significantly at $p = 0.05$.

The thylakoid protein phosphorylation pattern was established using Pro-Q Diamond staining of SDS-PAGE gels (**Figures 7A,B** right panels). Four protein groups were analyzed – proteins of PSII core (CP43, D1/D2, PsbH) and LHCII antennae (Lhcb1/Lhcb2). In thylakoids isolated from control pea leaves the relative phosphorylation levels of both antenna proteins and CP43 subunit were roughly 20% higher than in bean thylakoids, suggesting differences in the kinase activity or accessibility of substrates in both species.

In pea, dark-chilling induced a significant decrease in D1, D2, Lhcb1, and Lhcb2 phosphorylation and a slight increase of CP43 phosphorylation (**Figure 7C**) compared with control conditions. Such a change in thylakoid protein phosphorylation was typical for the thylakoids isolated from plants directly after the night period. In contrast, in bean, the dark-chilling induced 4-fold increase in the phosphorylation of LHCII major antenna proteins and 1.5-fold increase in PsbH protein phosphorylation (**Figure 7D**) compared with control conditions; the CP43 and D1/D2 phosphorylation levels were stable after chilling (**Figure 7D**). In both species, photo-activation of dark-chilled caused the return of protein phosphorylation status to the values of control samples (**Figures 7C,D**).

Thylakoid Network Structure of Pea and Bean

Details of the thylakoid network structure were analyzed using both CLSM, reveling the distribution of grana stacks and their organization within the whole chloroplast (**Figure 8A**), as well as TEM showing the detailed structure of stacked grana and unstacked stroma thylakoids (**Figures 8B–D**).

In the CLSM images, visible red fluorescence spots reflect mainly grana stacks containing LHCII trimers and LHCII-PSII supercomplexes. Therefore, the spot distribution corresponds to the position of grana stacks in the chloroplast (Rumak et al., 2010, 2012). In pea, large and well-distinguished spots were registered as opposed to smaller and more blurry fluorescence discs present in bean chloroplasts (**Figure 8A**). Such differences were even more profound after the dark-chilling treatment showing a disorganized thylakoid network in bean plants. In the case of pea, no significant changes in general features of the thylakoid network structure were registered (**Figure 8A**). In both species, photo-activation did not change the chloroplast fluorescence image significantly compared to the one registered after dark-chilling (**Figure 8A**).

More structural details were revealed by electron microscopy analysis of fixed leaf samples (**Figures 8B,C**). Chloroplast cross-sections of control samples showed a significant difference in grana distribution between both analyzed species. In pea, large grana stacks (432 ± 89 nm in diameter and 238 ± 122 nm in

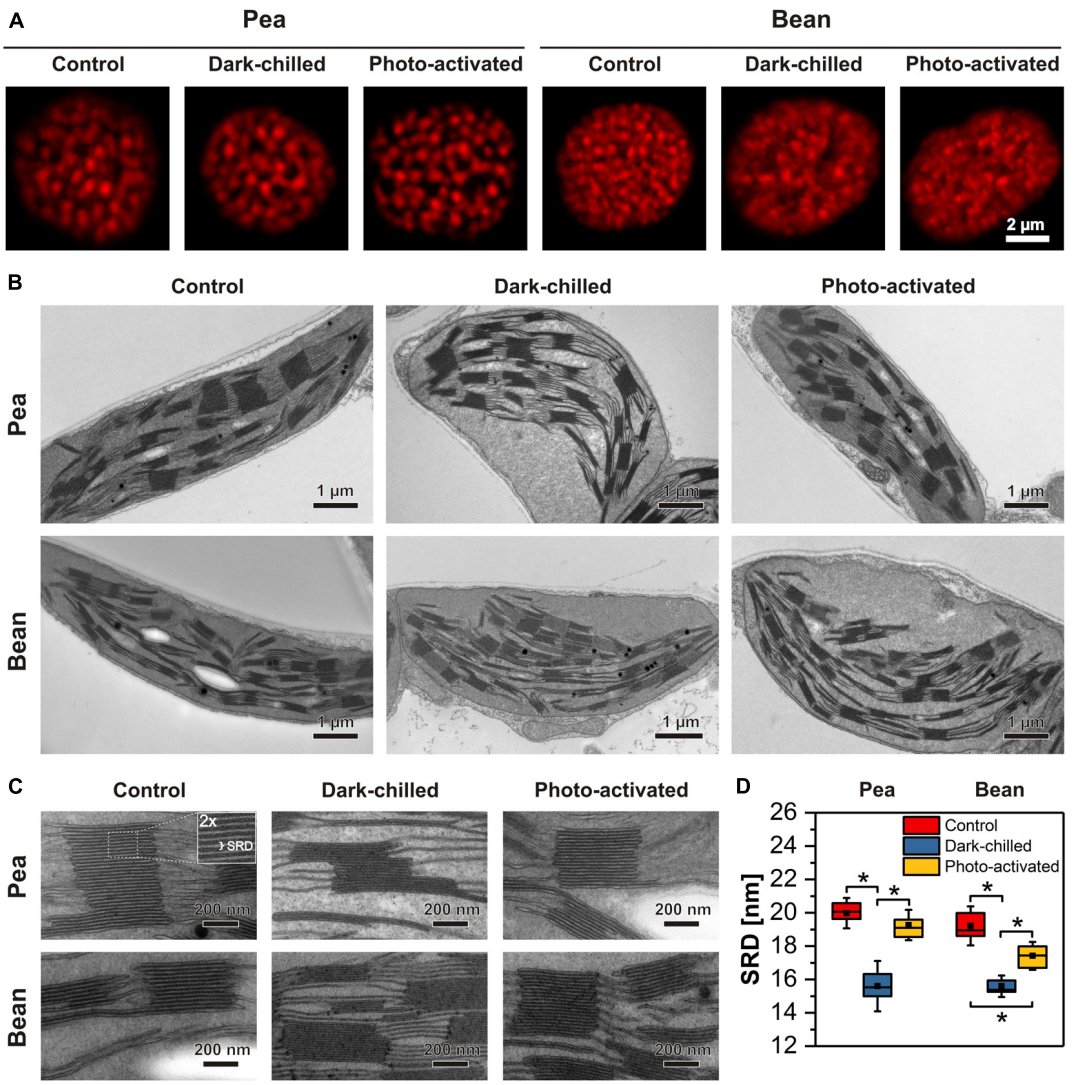

FIGURE 8 | Structural changes of thylakoid network after dark-chilling and photo-activation in pea and bean plants. The images of intact chloroplasts visualized by confocal microscopy; red fluorescence spots roughly correspond to grana size and their position inside the chloroplast **(A)**. Electron micrographs of mesophyll chloroplasts **(B)** and grana enlargement showing changes in thylakoid network regularity and fluctuation in stacking repeat distance (SRD) **(C)**. The quantitative analysis of SRD values (n = 15–20 per each variant) **(D)**. The bottom and top of each chart box represent the 25 and 75 percentile, respectively, the whiskers denote the SD; pairs of results marked with an asterisk differ significantly at p = 0.05.

height) interconnected via stroma thylakoids were distributed parallel to each other and to the long chloroplast axis (**Figure 8B**). In the case of bean, grana stacks were of similar diameter (401 ± 79 nm) as in pea but with considerably smaller height (174 ± 101 nm). Moreover, the disturbance in such regular arrangement was visible, with multiple shifts of grana stacks position. After the dark-chilling treatment, swelling of the chloroplast stroma was registered in both examined species. After the photo-activation stroma swelling was visible in bean chloroplasts only (**Figure 8B**). Low temperature did not affect the pea thylakoid network organization visible at the level of the whole chloroplast section, while in bean, the thylakoid network disorganization proceeded continuously after dark-chilling and photo-activation (**Figure 8B**).

One of the important ultrastructural grana features is the degree of thylakoid stacking, expressed by stacking repeat distance (SRD), defined as the distance between adjacent partition gaps in the stacks (Kirchhoff et al., 2011; **Figure 8C**). In control plants, no significant differences in the SRD value (around 19–20 nm) were registered between both analyzed species (**Figure 8D**). Dark-chilling treatment induced a substantial decrease in the SRD value (15–16 nm) both in pea and bean. Although photo-activation caused an increase in the SRD value in both species, full recovery of grana stacking (SRD around 19 nm) was observed in pea grana only. In the case of bean, only partial SRD increase was observed, reaching values of around 17 nm.

DISCUSSION

The diversity of the chloroplast membrane network structure organized into stacked, marginal and unstacked regions is generally explained by the presence of a lateral heterogeneity of CP complexes and in consequence, different steric and physicochemical interaction between membranes (Jia et al., 2014; Garab, 2016; Koochak et al., 2019). The role of the lipid phase and lipid-protein interactions in the determination of the thylakoid structure is less explained (Garab et al., 2017). Moreover, the relationship between the stress-induced changes in the thylakoid structure and the changes in their protein or lipid composition, as well as the arrangement of the CP complexes is unclear. Since the lipid composition of thylakoids, especially the degree of thylakoid lipids desaturation, is related to plant sensitivity to chilling (Kenchanmane Raju et al., 2018), further studies should be applied to reveal the connection between plant sensitivity to low-temperature and the lipid-protein interactions in the thylakoids of CT and CS plants.

Composition and Arrangement of CT Pea and CS Bean Thylakoid Membranes in Optimal Conditions – Background to Stress Response

We have analyzed the two plant species belonging to two separate groups due to their different responses to chilling conditions and revealing different thylakoid network structures. The observations with the use of TEM and CLSM showed that chloroplasts in pea contain larger stacked areas than in bean, in which the stacked regions are less distinguished (**Figure 8**). It was established before that observed ultrastructural differences between both species depend on the diversity of the thylakoid protein composition and arrangement, and in consequence, in different protein-protein interactions (Rumak et al., 2012).

The observed differences in the thylakoid structure and the arrangement of the CP complexes might be, moreover, partially explained by the particular lipid composition and lipid-protein interactions of the thylakoid membrane matrix of CT pea and CS bean plants analyzed in this study. Analysis of lipid profiles revealed that the MGDG and DGDG constitute more than 80% of total lipids, and their ratio is similar in pea and bean (**Figure 5** and **Supplementary Table 2**). Despite the similarities in the content of neutral lipids between both analyzed species, the lipid/protein ratio in pea thylakoids is noticeably higher than in bean (**Figure 4**). These data, together with the specific macro-domain organization of LHCII-PSII in both species (Rumak et al., 2012), point to the higher amount of lipids in the bulk phase of pea than of bean membranes and thus presumably increased membrane fluidity in this species.

Moreover, the SQDG to PG ratio is two times higher in pea than in bean thylakoids. However, the sum of these anionic lipids is similar in both analyzed species (**Figure 5** and **Supplementary Table 2**). Such results are in line with studies on lipid deficient plants pointing to the importance of the maintenance of the sum of the anionic lipids in thylakoid network formation and fitness (Yu and Benning, 2003; Kobayashi et al., 2017).

Another factor influencing thylakoid membrane fluidity is the degree of thylakoid lipid desaturation. Polyunsaturated fatty acids building acyl chain of galacto- and phospholipids stabilize the liquid-crystalline phase of the membrane. The average DBI is roughly 20% higher for pea than for bean thylakoid lipids with significant differences between lipid classes. The DBI for PG is 60% higher in pea than in bean (**Figure 5**) – PG desaturation level is frequently attributed to increased chilling tolerance (Ivanov et al., 2012).

Moreover, the 32:0 and 32:1 PG molecules are high-melting-point molecular species which, under the *in vitro* conditions, undergo the liquid-crystalline to gel phase transition at room temperature i.e., induce the rigidification of membranes. This effect is not directly observed in the thylakoid membranes because of the predominant abundance of desaturated lipids. However, the positive correlation between the amount of these PG species and sensitivity to low-temperature was found in a wide variety of plants and transgenic lines (Szalontai et al., 2003; Los et al., 2013). For example, CT Arabidopsis contains two and eight times lower amounts of the 32:0 and 32:1 PG species than CS rice (Zheng et al., 2016). Similarly, our data show five times lower abundance of high-melting-point PG species in CT pea than in CS bean thylakoids (**Supplementary Table 2**). These data indicate higher fluidity of the thylakoid membranes in CT pea compared with CS bean and agree with the observation that the higher desaturation level of lipids is correlated with the higher resistance to chilling (Los et al., 2013; Zheng et al., 2016; Kenchanmane Raju et al., 2018).

The lower value of the ACL of the total lipid pool correlates with the higher fluidity of the thylakoid membranes (Zheng et al., 2016). The ACL for MGDG and DGDG is slightly higher in pea thylakoids than in bean and their values do not change during chilling treatment (**Supplementary Table 2**), which indicates no simple correlation between the ACL values and the resistance to chilling.

Chloroplast lipid metabolism involves the activity of many types of deacylating enzymes (Matos and Pham-Thi, 2009). Significantly higher activity of galactolipase in CS than in CT species was reported previously (Kaniuga, 2008). The galactolipase isolated from bean chloroplasts had almost ten times higher activity compared with pea one (Gemel and Kaniuga, 1987), and these activities were associated with two-times higher accumulation of FFA registered in bean chloroplasts (Gemel and Kaniuga, 1987; Garstka et al., 1994). The accumulated FFA might influence the structure of thylakoids, however, the FFA undergo enzymatic and non-enzymatic peroxidation, which might decrease its detergent-like effect (Garstka et al., 1994; Mazur et al., 2018).

Free hydrophobic carotenoids, not bound to proteins, are embedded in membranes and can modify the physical properties of the lipid bilayer. Xanthophylls that contain polar groups at the two ends of the molecule and are positioned across the bilayer, cause the rigidification of membranes. On the other hand, the β-carotene embedded regardless of the orientation type within the membrane increases its fluidity. Thus, in

addition to the desaturation level of lipids, the balance between xanthophylls and β-carotene helps to maintain the optimal fluidity of thylakoid membranes under the temperature stress (Gruszecki and Strzalka, 2005; Szilagyi et al., 2008; Domonkos et al., 2013). The bean thylakoids revealed a significantly higher ratio between main xanthophyll – lutein and the β-carotene, pointing to the lower fluidity of bean membranes under control conditions compared with pea (**Figure 6** and **Supplementary Table 3**). Furthermore, both the higher ratio of lutein to the sum of β-xanthophylls and the presence of α-carotene in bean thylakoids (**Supplementary Table 3**), suggest a higher activity of the α-xanthophyll branch of the carotenoid biosynthetic pathway in bean than in pea chloroplasts (Domonkos et al., 2013).

Apart from the lipids forming the thylakoid membrane matrix, lipids are bound inside the protein scaffold of supercomplexes playing an important role in the stabilization of their structure and maintaining their photochemical functions (Jones, 2007; Domonkos et al., 2008). Based on the crystallography analyses, the abundance of integral lipids in LHCII-PSII and LHCI-PSI supercomplexes is estimated to 4.6 and 3.7% of the total pool of thylakoid lipids, respectively. Interestingly, almost 30% of the PG pool is associated with CP complexes, LHCII-PSII in particular (Kobayashi et al., 2017). Many investigations indicated that more than 50% of lipids in grana thylakoids are localized in the lipid-protein interface (Pali et al., 2003), and the "molecular dynamic simulation" showed that annular shell around PSII dimer is selectively enriched with MGDG and SQDG (Van Eerden et al., 2017). Such an ordered phase is probably larger than the bulk phase which contains lipids with higher fluidity (Azadi Chegeni et al., 2016). Therefore, it might be possible that maintaining the optimal fluidity of thylakoids depends more on lipid-protein interactions than lipid composition alone.

The relationship between the supramolecular membrane structure and the photochemical reactions can be analyzed by temperature dependencies of Chl *a* fluorescence emission measured in F_0 or steady-state (Wentworth et al., 2003; Tovuu et al., 2013; Zubik et al., 2013). The breakpoint in the linear temperature-dependent plot indicates the changes in the interactions between CP complexes due to a temperature-induced structural transformation. The temperature-dependent plot of Chl fluorescence for thylakoids isolated from control pea and bean leaves differ in the number of breakpoints; two and three phases of the fluorescence decrease in pea and bean, respectively (**Figures 2A,D**). The second and the third phase of the fluorescence decrease in bean revealed a similar slope as analogous phases for pea (**Supplementary Table 1**), indicating the similar interactions needed for the rearrangement of CP complexes.

The temperature-dependent changes in the fluorescence decrease arise from small changes in the conformation of CP complexes. Such changes may comprise alterations in the hydrogen and van der Waals interactions induced both by protein-protein and lipid-protein interactions. The breakpoint of the temperature-dependent plot might be correlated with a transition temperature of the lipid phase (Kovacs et al., 2019). Our data (**Figure 2**) showed that fluidity of bean thylakoid membranes is lower than in pea what indicates that at low temperatures, the possibility of gel phase formation is higher in bean thylakoids. Therefore, we propose that the one-breakpoint plot for pea thylakoids might be attributed to the phase transition between liquid-crystalline and disorder phases, whereas the two-breakpoint plot for bean thylakoids is related to the transition from gel-phase to liquid-crystalline and further to disorder phase (Los et al., 2013).

Species-dependent regulation of the thylakoid membrane fluidity is considered as an evolutionary adaptation mechanism to cope with high or low-temperature stress (Zheng et al., 2016; Kenchanmane Raju et al., 2018). The efficiency of photochemical reactions, among different factors, is regulated by the mobility of the electron transport chain components in the lateral plane of thylakoid membranes. To maintain appropriate transport within the lipid matrix in low temperatures its fluidity has to be preserved. Our results showed that the supramolecular organization of CP complexes, lipid composition and DBI index, lutein/β-carotene and protein/lipid ratios differ between CT pea and CS bean, indicating higher fluidity of the thylakoid membrane network in pea in optimal temperature conditions.

Effects of Dark-Chilling and Subsequent Photo-Activation on Composition and Arrangement of Thylakoid Membranes

Under dark-chilling and subsequent photo-activation at moderate light both in pea and bean, there is no decrease of the chlorophyll amount, no changes in Chl *a* to Chl *b* ratio (Garstka et al., 2005, 2007), and direct fluorescence emission from Chl *b* molecules in thylakoid samples is not observed (**Figure 3**). These data indicate that CP complexes are not degraded under applied experimental conditions. However, data obtained by mild-denaturing electrophoresis (Garstka et al., 2005, 2007) and spectroscopic measurements (**Figures 3**, **4**), revealed that under the dark-chilling conditions the arrangement of CP complexes is significantly affected in bean but not in pea thylakoids. Therefore, the lack of significant changes in the photochemical parameters and the course of the fluorescence induction curves (**Figure 1**) can be directly related to the stable behavior of pea supercomplexes under dark-chilling and subsequent photo-activation (**Figures 3**, **4**). In contrast, a decrease of F_V/F_M value, the change in the course of the fluorescence induction curves, as well as the lowered capacity of intersystem electron carrier pool (**Figure 1**) in bean thylakoids correlate with significant changes in the arrangement of CP complexes (**Figures 3**, **4**) and the increase of LHCII phosphorylation (**Figure 7**). These reorganizations of CP complexes result to some extent in LHCII-dependent energy spillover (**Figures 3**, **4**). Moreover, the presence of phosphorylated LHCII pool causes the increase of the negative charge of the stromal side of the thylakoid membrane, which changes the balance between the attractive and repulsion forces between neighboring CP complexes, and therefore alters their supramolecular organization (Puthiyaveetil et al., 2017). Furthermore, only the partial recovery of the bean

photochemical activity after photo-activation (**Figure 1**) can be related to incomplete restoration of the native structure of CP complexes (**Figures 3**, **4**) manifested mainly by the appearance of the aggregated LHCII (**Figure 3**).

Dark-chilling treatment only slightly influences the lipid phase of pea thylakoids, both in terms of values of DBI and ACL, as well as lipid composition in which some increase in the MGDG/DGDG ratio under dark-chilling is observed (**Figure 5** and **Supplementary Table 2**). Xanthophyll relative content does not change significantly, but a decline in the relative level of β-carotene is observed (**Figure 6**), probably due to the antioxidant role of β-carotene inactivating reactive oxygen species present in stress conditions (Domonkos et al., 2013). This change is also reflected in a decrease of the lutein/β-carotene ratio (**Supplementary Table 3**), attributed to the increase of membrane fluidity (Gruszecki and Strzalka, 2005; Szilagyi et al., 2008). However, in pea, the overall fluidity of thylakoid membranes remains similar to the control conditions, which is visible in the same course of the temperature-dependent plots for the control and dark-chilling plants (**Figures 2A–C** and **Supplementary Table 1**). Probably, the high level of lipid desaturation in control pea (**Figure 5C**) retains the optimal fluidity at low temperatures and prevents the loss of the CP complexes functionality in dark-chilled plants (**Figure 1**).

In contrast, the substantial changes in lipid composition are observed after dark-chilling of bean leaves. The significant decline in the MGDG and increase in the DGDG levels cause a 35% decrease in the MGDG/DGDG ratio; SQDG and PG levels remained unchanged (**Figure 5B** and **Supplementary Table 2**). In various plant species, the long-term cold-adaptation includes a decrease in the MGDG level, probably because lower level of the MGDG stabilizes the membrane bilayer phase at low temperatures (Zheng et al., 2016; Kenchanmane Raju et al., 2018).

Simultaneously, the rigidity of membranes induced by low-temperature is alleviated by the increase in the DBI index and a decrease in the ACL index (Zheng et al., 2016). It was previously proposed that the thylakoid lipids of the CT plants remain in the liquid-crystalline phase whereas thylakoids in the CS species enter the gel phase at chilling temperatures, mainly due to different levels of lipid desaturation (Szalontai et al., 2003; Los et al., 2013; Kenchanmane Raju et al., 2018). The level of lipid saturation is related to the activity of desaturases and transferases regulated directly or non-directly by factors connected with the C-repeat binding factor signaling pathway (Thomashow, 2010; Kenchanmane Raju et al., 2018). In thylakoids isolated from dark-chilled bean leaves the DBI and ACL indexes are maintained at the same level as in control thylakoids (**Figure 5** and **Supplementary Table 2**), which exclude activation of typical long-term adaptation processes during low-temperature treatment in bean.

Dark-chilling-induced changes in bean thylakoids, in lipid composition in particular, substantially alters the membrane properties, which is reflected by a drastic change in the course of the temperature-dependent plot; the three-phase plot is converted to a single-phase one (**Figures 2D,E**). The temperature-dependent plot without breakpoint indicates impairment of the lipid-protein interactions or lack of lipid phase transition in the measured temperature range. It is probably related to the detergent-like effect caused by the accumulation of FFA in thylakoids, which is typical for CS plants under dark-chilling stress (Kaniuga, 2008). Under these conditions, the FFA level in bean thylakoids increases two times and remains unchanged in pea (Garstka et al., 1994). Such variable response is correlated with higher activity of galactolipase in bean than in pea plants (Gemel and Kaniuga, 1987). Photo-activation of dark-chilled leaves of CS plants results in a decrease of FFA to the level observed in control plants (Garstka and Kaniuga, 1991; Kaniuga, 2008) probably due to the increase of peroxidative reactions (Garstka et al., 1994). This effect might be a reason why in photo-activated bean thylakoids we observed the restoration of the three-phase temperature-dependent plot with breakpoints characteristic for the control thylakoids (**Figures 2D,F**) without significant changes in the ratios of lipids and carotenoids (**Figures 5**, **6**). Moreover, changes in membrane properties of bean thylakoids during dark-chilling and photo-activation explain the reversible association of stromal proteins Rubisco and PcLOXA lipoxygenase (**Figure 7**; Mazur et al., 2018).

In contrast to pea, dark-chilling induces significant alternation in the lipid phase, thylakoid protein phosphorylation status, and arrangement of CP complexes in bean (**Figures 3**, **5**, **7**) which result in increased disorganization of the thylakoid network visible at the ultrastructural level (**Figure 8**). The photo-activation of bean leaves considerably restores the physical properties of membranes (**Figure 2**) and partially the structure and photochemical activity of CP complexes (**Figures 1**, **3**, **7**). However, the disorganized arrangement of the thylakoid network is still visible (**Figure 8**). Experiments with Mg^{2+}-induced stacking of thylakoids revealed that the protein diffusion in bean thylakoids is limited due to spatial encumbrance caused by the heterogeneous arrangement of CP complexes (Rumak et al., 2010). Such a specific supramolecular thylakoid structure in combination with the aggregation of LHCII induced by photo-activation (**Figures 3**, **4**) makes a return to initial thylakoids organization difficult.

One of the important factors that influence the thylakoid grana ultrastructure is the reversible phosphorylation of PSII proteins, LHCII antenna in particular. LHCII phosphorylation causes partial unfolding of the granum structure (reviewed in Kirchhoff, 2019). The SRD value, which is one of the parameters describing the extent of grana stacking, decreases in dark-chilled pea thylakoids which is correlated with a decrease of LHCII phosphorylation (**Figures 7**, **8**). Despite a substantial increase in LHCII phosphorylation in dark-chilled bean thylakoids, a decrease of the SRD value is observed. This indicates that there is no simple correlation between grana stacking and LHCII phosphorylation level in dark-chilling conditions. Under dark-chilling conditions, the bean thylakoid network comprises multiple small grana connected via many stroma lamellae

(**Figures 8B,C**; Rumak et al., 2012), which causes the increase of the total size of the marginal regions of the grana thylakoids and probably also the access of LHCII for the phosphorylation.

The phosphorylation of the LHCII in the darkness was described before and might be attributed to the non-photochemical PQ reduction (Nellaepalli et al., 2012a,b). The PQ reduction is essential to the activation of STN7 kinase for which LHCII is a primary target. However, the possibility of the phosphorylation of LHCII via other kinases was proposed recently (Longoni et al., 2019) and their activity in dark-chilling conditions cannot be excluded.

CONCLUSION

The direct and immediate effect of low temperature on the physical properties of the membrane is related to a decrease in mobility of the acyl chains and their stiffness. It induces activation of response mechanisms that are different in chilling sensitive and chilling tolerant plants. The direction and magnitude of this response depend on the evolutionary background of the species.

In this study, we revealed that the different susceptibility of CS bean and CT pea plants to dark-chilling treatment is mainly attributed to a particular, species-dependent, composition of their thylakoid lipid phases, manifested by specific DBI level, saturated PG content and protein/lipid ratio. The composition of the thylakoid lipid matrix of CT pea allows retaining the optimal fluidity of its chloroplast membranes under low temperatures. In contrast, the fluidity of CS bean thylakoids is drastically changed under the dark-chilling treatment which is the result of MGDG hydrolysis and in consequence, accumulation of FFA. Changes in lipid matrix properties leading to the reorganization of the supramolecular structure of photosynthetic complexes finally cause structural remodeling of the CS bean thylakoid network in dark-chilling conditions.

DATA AVAILABILITY STATEMENT

The datasets generated for this study are available on request to the corresponding author.

AUTHOR CONTRIBUTIONS

MG, RM, and KG provided conception of the manuscript. RM, KG, AK, MP, ŁK, and MG performed the experiments. MG, RM, ŁK, and AM wrote the manuscript. All authors read and approved the final manuscript, designed the experiments, and analyzed the data.

FUNDING

This work was partially financed by the National Science Centre, Poland (NCN), Grant No. 2016/23/D/NZ3/01276.

ACKNOWLEDGMENTS

TEM images were performed in the Laboratory of Electron Microscopy, Nencki Institute of Experimental Biology of PAS, Warsaw, Poland. This work was carried out with the use of CePT infrastructure financed by the European Union – the European Regional Development Fund within the Operational Programme "Innovative economy" for 2007–2013. We thank Joanna Kozioł-Lipińska from the Faculty of Biology, University of Warsaw for the technical support during TEM samples preparation.

SUPPLEMENTARY MATERIAL

The Supplementary Material for this article can be found online at: https://www.frontiersin.org/articles/10.3389/fpls.2020.00723/full#supplementary-material

REFERENCES

Asada, K., Heber, U., and Schreiber, U. (1992). Pool size of electrons that can be donated to P700+ as determined in intact leaves: donation to P700+ from stromal components via the intersystem chain. *Plant Cell Physiol.* 33, 927–932. doi: 10.1093/oxfordjournals.pcp.a078343

Azadi Chegeni, F., Perin, G., Sai Sankar, Gupta, K. B., Simionato, D., Morosinotto, T., et al. (2016). Protein and lipid dynamics in photosynthetic thylakoid membranes investigated by in-situ solid-state NMR. *Biochim. Biophys. Acta* 1857, 1849–1859. doi: 10.1016/j.bbabio.2016.09.004

Chen, M., and Thelen, J. J. (2013). ACYL-LIPID DESATURASE2 is required for chilling and freezing tolerance in *Arabidopsis*. *Plant Cell* 25, 1430–1444. doi: 10.1105/tpc.113.111179

Danielsson, R., Albertsson, P. A., Mamedov, F., and Styring, S. (2004). Quantification of photosystem I and II in different parts of the thylakoid membrane from spinach. *Biochim. Biophys. Acta* 1608, 53–61. doi: 10.1016/j.bbabio.2003.10.005

Danielsson, R., Suorsa, M., Paakkarinen, V., Albertsson, P. A., Styring, S., Aro, E. M., et al. (2006). Dimeric and monomeric organization of photosystem II. Distribution of five distinct complexes in the different domains of the thylakoid membrane. *J. Biol. Chem.* 281, 14241–14249. doi: 10.1074/jbc.M600634200

Daum, B., Nicastro, D., Austin, J. II, McIntosh, J. R., and Kuhlbrandt, W. (2010). Arrangement of photosystem II and ATP synthase in chloroplast membranes of spinach and pea. *Plant Cell* 22, 1299–1312. doi: 10.1105/tpc.109.071431

Domonkos, I., Kis, M., Gombos, Z., and Ughy, B. (2013). Carotenoids, versatile components of oxygenic photosynthesis. *Prog. Lipid Res.* 52, 539–561. doi: 10.1016/j.plipres.2013.07.001

Domonkos, I., Laczko-Dobos, H., and Gombos, Z. (2008). Lipid-assisted protein-protein interactions that support photosynthetic and other cellular activities. *Prog. Lipid Res.* 47, 422–435. doi: 10.1016/j.plipres.2008.05.003

Garab, G. (2016). Self-assembly and structural-functional flexibility of oxygenic photosynthetic machineries: personal perspectives. *Photosynth. Res.* 127, 131–150. doi: 10.1007/s11120-015-0192-z

Garab, G., Ughy, B., Waard, P., Akhtar, P., Javornik, U., Kotakis, C., et al. (2017). Lipid polymorphism in chloroplast thylakoid membranes – as revealed by (31)P-NMR and time-resolved merocyanine fluorescence spectroscopy. *Sci. Rep.* 7:13343. doi: 10.1038/s41598-017-13574-y

Garstka, M., Drozak, A., Rosiak, M., Venema, J. H., Kierdaszuk, B., Simeonova, E., et al. (2005). Light-dependent reversal of dark-chilling induced changes

in chloroplast structure and arrangement of chlorophyll-protein complexes in bean thylakoid membranes. *Biochim. Biophys. Acta-Bioenerget.* 1710, 13–23. doi: 10.1016/j.bbabio.2005.08.006

Garstka, M., and Kaniuga, Z. (1991). Reversal by light of deleterious effects of chilling on oxygen evolution, manganese and free fatty-acid content in tomato thylakoids is not accompanied by restoration of the original mambrane conformation. *Physiol. Plant.* 82, 292–298. doi: 10.1034/j.1399-3054.1991.820224.x

Garstka, M., Venema, J. H., Rumak, I., Gieczewska, K., Rosiak, M., Koziol-Lipinska, J., et al. (2007). Contrasting effect of dark-chilling on chloroplast structure and arrangement of chlorophyll – protein complexes in pea and tomato: plants with a different susceptibility to non-freezing temperature. *Planta* 226, 1165–1181. doi: 10.1007/s00425-007-0562-7

Garstka, M., Zarnowiecka, A., and Kaniuga, Z. (1994). Photosynthetic apparatus of chilling-sensitive plants.*32.* peroxidation of free fatty-acids in thylakoids of chilling-sensitive and chilling-tolerant plants. *Acta Physiol. Plant.* 16, 337–344.

Gemel, J., and Kaniuga, Z. (1987). Comparison of galactolipase activity and free fatty acid levels in chloroplasts of chill-sensitive and chill-resistant plants. *Eur. J. Biochem.* 166, 229–233. doi: 10.1111/j.1432-1033.1987.tb13506.x

Gruszecki, W. I., Grudzinski, W., Matula, M., Kernen, P., and Krupa, Z. (1999). Light-induced excitation quenching and structural transition in light-harvesting complex II. *Photosynth. Res.* 59, 175–185. doi: 10.1023/A:1006113630174

Gruszecki, W. I., and Strzalka, K. (2005). Carotenoids as modulators of lipid membrane physical properties. *Biochim. Biophys. Acta* 1740, 108–115. doi: 10.1016/j.bbadis.2004.11.015

Gu, Y., He, L., Zhao, C., Wang, F., Yan, B., Gao, Y., et al. (2017). Biochemical and transcriptional regulation of membrane lipid metabolism in maize leaves under low temperature. *Front. Plant Sci.* 8:2053. doi: 10.3389/fpls.2017.02053

Higuchi, M., Noguchi, T., and Sonoike, K. (2003). Over-reduced states of the Mn-cluster in cucumber leaves induced by dark-chilling treatment. *Biochim. Biophys. Acta (BBA) – Bioenerget.* 1604, 151–158. doi: 10.1016/s0005-2728(03)00044-6

Ivanov, A. G., Allakhverdiev, S. I., Huner, N. P., and Murata, N. (2012). Genetic decrease in fatty acid unsaturation of phosphatidylglycerol increased photoinhibition of photosystem I at low temperature in tobacco leaves. *Biochim. Biophys. Acta* 1817, 1374–1379. doi: 10.1016/j.bbabio.2012.03.010

Janik, E., Bednarska, J., Zubik, M., Puzio, M., Luchowski, R., Grudzinski, W., et al. (2013). Molecular architecture of plant thylakoids under physiological and light stress conditions: a study of lipid-light-harvesting complex II model membranes. *Plant Cell* 25, 2155–2170. doi: 10.1105/tpc.113.113076

Jia, H., Liggins, J. R., and Chow, W. S. (2014). Entropy and biological systems: experimentally-investigated entropy-driven stacking of plant photosynthetic membranes. *Sci. Rep.* 4:4142. doi: 10.1038/srep04142

Johnson, M. P., and Wientjes, E. (2019). The relevance of dynamic thylakoid organisation to photosynthetic regulation. *Biochim. Biophys. Acta-Bioenerget.* 1861:148039. doi: 10.1016/j.bbabio.2019.06.011

Jones, M. R. (2007). Lipids in photosynthetic reaction centres: structural roles and functional holes. *Prog. Lipid Res.* 46, 56–87. doi: 10.1016/j.plipres.2006.06.001

Kaniuga, Z. (2008). Chilling response of plants: importance of galactolipase, free fatty acids and free radicals. *Plant Biol. (Stuttg)* 10, 171–184. doi: 10.1111/j.1438-8677.2007.00019.x

Kenchanmane Raju, S. K., Barnes, A. C., Schnable, J. C., and Roston, R. L. (2018). Low-temperature tolerance in land plants: are transcript and membrane responses conserved? *Plant Sci.* 276, 73–86. doi: 10.1016/j.plantsci.2018.08.002

Khodakovskaya, M., McAvoy, R., Peters, J., Wu, H., and Li, Y. (2006). Enhanced cold tolerance in transgenic tobacco expressing a chloroplast omega-3 fatty acid desaturase gene under the control of a cold-inducible promoter. *Planta* 223, 1090–1100. doi: 10.1007/s00425-005-0161-4

Kirchhoff, H. (2019). Chloroplast ultrastructure in plants. *New Phytol.* 223, 565–574. doi: 10.1111/nph.15730

Kirchhoff, H., Hall, C., Wood, M., Herbstova, M., Tsabari, O., Nevo, R., et al. (2011). Dynamic control of protein diffusion within the granal thylakoid lumen. *Proc. Natl. Acad. Sci. U.S.A.* 108, 20248–20253. doi: 10.1073/pnas.1104141109

Kobayashi, K., Endo, K., and Wada, H. (2017). Specific distribution of phosphatidylglycerol to photosystem complexes in the thylakoid membrane. *Front. Plant Sci.* 8:1991. doi: 10.3389/fpls.2017.01991

Koochak, H., Puthiyaveetil, S., Mullendore, D. L., Li, M., and Kirchhoff, H. (2019). The structural and functional domains of plant thylakoid membranes. *Plant J.* 97, 412–429. doi: 10.1111/tpj.14127

Kouřil, R., Dekker, J. P., and Boekema, E. J. (2012). Supramolecular organization of photosystem II in green plants. *Biochim. Biophys. Acta* 1817, 2–12. doi: 10.1016/j.bbabio.2011.05.024

Kovacs, T., Szalontai, B., Klodawska, K., Vladkova, R., Malec, P., Gombos, Z., et al. (2019). Photosystem I oligomerization affects lipid composition in *Synechocystis* sp. PCC 6803. *Biochim. Biophys. Acta Mol. Cell. Biol. Lipids* 1864, 1384–1395. doi: 10.1016/j.bbalip.2019.06.013

Kowalewska, L., Mazur, R., Suski, S., Garstka, M., and Mostowska, A. (2016). Three-dimensional visualization of the tubular-lamellar transformation of the internal plastid membrane network during runner bean chloroplast biogenesis. *Plant Cell* 28, 875–891. doi: 10.1105/tpc.15.01053

Li, G., Knowles, P. F., Murphy, D. J., and Marsh, D. (1990). Lipid-protein interactions in thylakoid membranes of chilling-resistant and -sensitive plants studied by spin label electron spin resonance spectroscopy. *J. Biol. Chem.* 265, 16867–16872.

Longoni, P., Samol, I., and Goldschmidt-Clermont, M. (2019). The kinase state transition 8 phosphorylates light harvesting complex II and contributes to light acclimation in *Arabidopsis thaliana*. *Front. Plant Sci.* 10:1156. doi: 10.3389/fpls.2019.01156

Los, D. A., Mironov, K. S., and Allakhverdiev, S. I. (2013). Regulatory role of membrane fluidity in gene expression and physiological functions. *Photosynth. Res.* 116, 489–509. doi: 10.1007/s11120-013-9823-4

Marla, S. R., Shiva, S., Welti, R., Liu, S., Burke, J. J., and Morris, G. P. (2017). Comparative transcriptome and lipidome analyses reveal molecular chilling responses in chilling-tolerant sorghums. *Plant Genome* 10, 1–16. doi: 10.3835/plantgenome2017.03.0025

Matos, A. R., and Pham-Thi, A. T. (2009). Lipid deacylating enzymes in plants: old activities, new genes. *Plant Physiol. Biochem.* 47, 491–503. doi: 10.1016/j.plaphy.2009.02.011

Mazur, R., Trzcinska-Danielewicz, J., Kozlowski, P., Kowalewska, L., Rumak, I., Shiell, B. J., et al. (2018). Dark-chilling and subsequent photo-activation modulate expression and induce reversible association of chloroplast lipoxygenase with thylakoid membrane in runner bean (*Phaseolus coccineus* L.). *Plant Physiol. Biochem.* 122, 102–112. doi: 10.1016/j.plaphy.2017.11.015

Mizusawa, N., and Wada, H. (2012). The role of lipids in photosystem II. *Biochim. Biophys. Acta* 1817, 194–208. doi: 10.1016/j.bbabio.2011.04.008

Nellaepalli, S., Kodru, S., and Subramanyam, R. (2012a). Effect of cold temperature on regulation of state transitions in *Arabidopsis thaliana*. *J. Photochem. Photobiol. B* 112, 23–30. doi: 10.1016/j.jphotobiol.2012.04.003

Nellaepalli, S., Kodru, S., Tirupathi, M., and Subramanyam, R. (2012b). Anaerobiosis induced state transition: a non photochemical reduction of PQ pool mediated by NDH in *Arabidopsis thaliana*. *PLoS ONE* 7:e49839. doi: 10.1371/journal.pone.0049839

Orlova, I. V., Serebriiskaya, T. S., Popov, V., Merkulova, N., Nosov, A. M., Trunova, T. I., et al. (2003). Transformation of tobacco with a gene for the thermophilic acyl-lipid desaturase enhances the chilling tolerance of plants. *Plant Cell Physiol.* 44, 447–450. doi: 10.1093/pcp/pcg047

Pali, T., Garab, G., Horvath, L. I., and Kota, Z. (2003). Functional significance of the lipid-protein interface in photosynthetic membranes. *Cell Mol. Life. Sci.* 60, 1591–1606. doi: 10.1007/s00018-003-3173-x

Puthiyaveetil, S., van Oort, B., and Kirchhoff, H. (2017). Surface charge dynamics in photosynthetic membranes and the structural consequences. *Nature Plants* 3:17020. doi: 10.1038/nplants.2017.20

Ruban, A. V., and Johnson, M. P. (2015). Visualizing the dynamic structure of the plant photosynthetic membrane. *Nature Plants* 1:15161. doi: 10.1038/nplants.2015.161

Rumak, I., Gieczewska, K., Kierdaszuk, B., Gruszecki, W. I., Mostowska, A., Mazur, R., et al. (2010). 3-D modelling of chloroplast structure under (Mg2+) magnesium ion treatment. Relationship between thylakoid membrane arrangement and stacking. *Biochim. Biophys. Acta-Bioenerget.* 1797, 1736–1748. doi: 10.1016/j.bbabio.2010.07.001

Rumak, I., Mazur, R., Gieczewska, K., Koziol-Lipinska, J., Kierdaszuk, B., Michalski, W. P., et al. (2012). Correlation between spatial (3D) structure of pea and bean thylakoid membranes and arrangement of chlorophyll-protein complexes. *BMC Plant Biol.* 12:72. doi: 10.1186/1471-2229-12-72

Seiwert, D., Witt, H., Janshoff, A., and Paulsen, H. (2017). The non-bilayer lipid MGDG stabilizes the major light-harvesting complex (LHCII) against unfolding. *Sci. Rep.* 7:5158. doi: 10.1038/s41598-017-05328-7

Shen, J. R., Terashima, I., and Katoh, S. (1990). Cause for dark, chilling-induced inactivation of photosynthetic oxygen-evolving system in cucumber leaves. *Plant Physiol.* 93, 1354–1357. doi: 10.1104/pp.93.4.1354

Shikanai, T., Endo, T., Hashimoto, T., Yamada, Y., Asada, K., and Yokota, A. (1998). Directed disruption of the tobacco ndhB gene impairs cyclic electron flow around photosystem I. *Proc. Natl. Acad. Sci. U.S.A.* 95, 9705–9709. doi: 10.1073/pnas.95.16.9705

Simidjiev, I., Stoylova, S., Amenitsch, H., Javorfi, T., Mustardy, L., Laggner, P., et al. (2000). Self-assembly of large, ordered lamellae from non-bilayer lipids and integral membrane proteins in vitro. *Proc. Natl. Acad. Sci. U.S.A.* 97, 1473–1476. doi: 10.1073/pnas.97.4.1473

Skupien, J., Wojtowicz, J., Kowalewska, L., Mazur, R., Garstka, M., Gieczewska, K., et al. (2017). Dark-chilling induces substantial structural changes and modifies galactolipid and carotenoid composition during chloroplast biogenesis in cucumber (*Cucumis sativus* L) cotyledons. *Plant Physiol. Biochem.* 111, 107–118. doi: 10.1016/j.plaphy.2016.11.022

Szalontai, B., Kota, Z., Nonaka, H., and Murata, N. (2003). Structural consequences of genetically engineered saturation of the fatty acids of phosphatidylglycerol in tobacco thylakoid membranes, an FTIR study. *Biochemistry* 42, 4292–4299. doi: 10.1021/bi026894c

Szalonek, M., Sierpien, B., Rymaszewski, W., Gieczewska, K., Garstka, M., Lichocka, M., et al. (2015). Potato annexin STANN1 promotes drought tolerance and mitigates light stress in transgenic *Solanum tuberosum* L. plants. *PLoS One* 10:e0132683. doi: 10.1371/journal.pone.0132683

Szalontai, B., Nishiyama, Y., Gombos, Z., and Murata, N. (2000). Membrane dynamics as seen by fourier transform infrared spectroscopy in a cyanobacterium, Synechocystis PCC 6803. The effects of lipid unsaturation and the protein-to-lipid ratio. *Biochim. Biophys. Acta* 1509, 409–419. doi: 10.1016/s0005-2736(00)00323-0

Szilagyi, A., Selstam, E., and Akerlund, H. E. (2008). Laurdan fluorescence spectroscopy in the thylakoid bilayer: the effect of violaxanthin to zeaxanthin conversion on the galactolipid dominated lipid environment. *Biochim. Biophys. Acta* 1778, 348–355. doi: 10.1016/j.bbamem.2007.10.006

Thomashow, M. F. (2010). Molecular basis of plant cold acclimation: insights gained from studying the CBF cold response pathway. *Plant Physiol.* 154, 571–577. doi: 10.1104/pp.110.161794

Tovuu, A., Zulfugarov, I. S., and Lee, C. H. (2013). Correlations between the temperature dependence of chlorophyll fluorescence and the fluidity of thylakoid membranes. *Physiol. Plant.* 147, 409–416. doi: 10.1111/j.1399-3054.2012.01700.x

Van Eerden, F. J., Melo, M. N., Frederix, P., and Marrink, S. J. (2017). Prediction of thylakoid lipid binding sites on photosystem II. *Biophys. J.* 113, 2669–2681. doi: 10.1016/j.bpj.2017.09.039

Wentworth, M., Ruban, A. V., and Horton, P. (2003). Thermodynamic investigation into the mechanism of the chlorophyll fluorescence quenching in isolated photosystem II light-harvesting complexes. *J. Biol. Chem.* 278, 21845–21850. doi: 10.1074/jbc.M302586200

Wood, W. H. J., MacGregor-Chatwin, C., Barnett, S. F. H., Mayneord, G. E., Huang, X., Hobbs, J. K., et al. (2018). Dynamic thylakoid stacking regulates the balance between linear and cyclic photosynthetic electron transfer. *Nat. Plants* 4, 116–127. doi: 10.1038/s41477-017-0092-7

Yu, B., and Benning, C. (2003). Anionic lipids are required for chloroplast structure and function in *Arabidopsis*. *Plant J.* 36, 762–770. doi: 10.1046/j.1365-313x.2003.01918.x

Zheng, G., Li, L., and Li, W. (2016). Glycerolipidome responses to freezing- and chilling-induced injuries: examples in *Arabidopsis* and rice. *BMC Plant Biol.* 16:70. doi: 10.1186/s12870-016-0758-8

Zubik, M., Luchowski, R., Puzio, M., Janik, E., Bednarska, J., Grudzinski, W., et al. (2013). The negative feedback molecular mechanism which regulates excitation level in the plant photosynthetic complex LHCII: towards identification of the energy dissipative state. *Biochim. Biophys. Acta* 1827, 355–364. doi: 10.1016/j.bbabio.2012.11.013

Conflict of Interest: The authors declare that the research was conducted in the absence of any commercial or financial relationships that could be construed as a potential conflict of interest.

Copyright © 2020 Mazur, Gieczewska, Kowalewska, Kuta, Proboszcz, Gruszecki, Mostowska and Garstka. This is an open-access article distributed under the terms of the Creative Commons Attribution License (CC BY). The use, distribution or reproduction in other forums is permitted, provided the original author(s) and the copyright owner(s) are credited and that the original publication in this journal is cited, in accordance with accepted academic practice. No use, distribution or reproduction is permitted which does not comply with these terms.

frontiers in Plant Science

MINI REVIEW
published: 05 June 2020
doi: 10.3389/fpls.2020.00713

Responses of Membranes and the Photosynthetic Apparatus to Salt Stress in Cyanobacteria

*Wenjing Yang[1], Fang Wang[2], Lu-Ning Liu[3,4] and Na Sui[1,4]**

[1] Shandong Provincial Key Laboratory of Plant Stress, College of Life Sciences, Shandong Normal University, Jinan, China, [2] State Key Laboratory of Crop Biology, College of Life Sciences, Shandong Agricultural University, Tai'an, China, [3] College of Marine Life Sciences, and Frontiers Science Center for Deep Ocean Multispheres and Earth System, Ocean University of China, Qingdao, China, [4] Institute of Integrative Biology, University of Liverpool, Liverpool, United Kingdom

Cyanobacteria are autotrophs whose photosynthetic process is similar to that of higher plants, although the photosynthetic apparatus is slightly different. They have been widely used for decades as model systems for studying the principles of photosynthesis, especially the effects of environmental stress on photosynthetic activities. Salt stress, which is the most common abiotic stress in nature, combines ionic and osmotic stresses. High cellular ion concentrations and osmotic stress can alter normal metabolic processes and photosynthesis. Additionally, salt stress increases the intracellular reactive oxygen species (ROS) contents. Excessive amounts of ROS will damage the photosynthetic apparatus, inhibit the synthesis of photosystem-related proteins, including the D1 protein, and destroy the thylakoid membrane structure, leading to inhibited photosynthesis. In this review, we mainly introduce the effects of salt stress on the cyanobacterial membranes and photosynthetic apparatus. We also describe specific salt tolerance mechanisms. A thorough characterization of the responses of membranes and photosynthetic apparatus to salt stress may be relevant for increasing agricultural productivity.

Keywords: cyanobacteria, membranes lipids, photosynthetic apparatus, photosynthesis, salt stress

OPEN ACCESS

Edited by:
Yoshitaka Nishiyama, Saitama University, Japan

Reviewed by:
Martin Hagemann, University of Rostock, Germany
Koichiro Awai, Shizuoka University, Japan

***Correspondence:**
Na Sui
suina@sdnu.edu.cn;
suina800101@163.com

Specialty section:
This article was submitted to Plant Physiology, a section of the journal Frontiers in Plant Science

Received: *22 February 2020*
Accepted: *05 May 2020*
Published: *05 June 2020*

Citation:
Yang W, Wang F, Liu L-N and Sui N (2020) Responses of Membranes and the Photosynthetic Apparatus to Salt Stress in Cyanobacteria. Front. Plant Sci. 11:713. doi: 10.3389/fpls.2020.00713

INTRODUCTION

Salt stress is an abiotic factor that greatly influences plant survival and development. There are currently more than 1.2 billion hectares of land affected by salt, accounting for about 6% of the total global land area (Wicke et al., 2011; Yuan et al., 2016; Sui et al., 2018). Annual worldwide economic losses due to salt stress can exceed US$12 billion (Shabala, 2013; Song and Wang, 2014). Therefore, improving salt tolerance of agriculturally important plants is critical.

Cyanobacteria have a photosynthetic system similar to that of higher plants, and their cytoplasm and thylakoid membranes are similar to those of the chloroplast of higher plants in lipid composition and membrane assembly generally (Rodriguez-Ezpeleta et al., 2005; Los et al., 2010). Therefore, cyanobacteria can be used as a model system to study the mechanisms of photosynthesis, membrane lipids and signal transduction under abiotic stress (Los and Murata, 2004; Jensen and Leister, 2014), which may also provide an applicable model for higher plants. To survive in extreme or variable environment, cyanobacteria have evolved specific metabolic mechanisms and regulatory systems (Tandeau de Marsac and Houmard, 1993). For example, *Synechocystis* sp. PCC6803 (hereafter referred to as

Synechocystis 6803), a unicellular freshwater cyanobacterium, can tolerate up to 1.2 M NaCl (Desplats et al., 2005). The photosynthetic apparatus of *Synechocystis* 6803 are similar to those of higher plants and are easier to separate (Öquist et al., 1995; Allakhverdiev and Murata, 2008). And compared with higher plants, they have relatively simple genetic systems (Haselkorn, 1991). In cyanobacteria, the thylakoid membrane is the only site of photosynthesis and also the main site of respiratory electron transport in cells (Mullineaux, 2014). The growth cycle of cyanobacteria is short, making it is easy to be treated with various salt concentrations, and there are relatively few other interfering factors. These characteristics have made cyanobacteria the ideal model system for studying the photosynthetic responses to salt stress.

High NaCl concentrations are toxic to cells, ultimately resulting in a damaged photosynthetic apparatus (**Figure 1**). In cells of photosynthetic organisms, salt stress leads to a decrease in cell volume and osmotic stress, it also inhibits the photosynthetic electron transfer process (Allakhverdiev and Murata, 2008; Feng et al., 2014; Zhao et al., 2019). 0.5 M NaCl inactivated both PSII and PSI in *Synechococcus* cells due to the changes in K/Na ratio (Allakhverdiev et al., 2000). In spirulina platensis, salt stress leads to a reduction in PSII electron transport by increasing the number of Q_B-non-reduction reaction centers (Lu and Vonshak, 1999). After that, it was be found that salt stress did not directly affect the PSII activity itself in the dark, but the same salt stress combined with photosynthesis effective radiation blocked electron transport between Q_A and Q_B (primary and secondary quinone electron acceptors of PSII located in proteins D2 and D1, respectively), and the degree of inhibition was proportional to the intensity of light (Lu and Zhang, 2000; Lu and Vonshak, 2002). Sudhir et al. (2005) found that NaCl not only inhibited PSII activity by inhibiting the D1 protein, but also decreased energy transfer from light harvesting antenna to PSII by changing other thylakoid membrane proteins such as 47 kDa chlorophyll protein (CP) and 94 kDa protein in *Arthrospira platensis*. Intracellular sodium and potassium homeostasis is important for maintaining the normal activity of enzymes (Hu et al., 2016; Chen et al., 2017; Ma et al., 2019), cell membrane potential (Zhang et al., 2014; Wei et al., 2017), and normal cell volume (Serrano and Rodrigueznavarro, 2001; Zhu, 2003; Shao et al., 2014). The low concentration of Na^+ helps to regulate the pH in plants and cyanobacteria, as well as the fixation of nitrogen and carbon dioxide (Karandashova and Elanskaya, 2005; Han et al., 2012; Fan et al., 2019). Excessive Na^+ and Cl^- flows into the cell disrupted ion homeostasis, leading to accumulation of reactive oxygen species (ROS) (Scarpeci et al., 2008; Feng et al., 2015; Song et al., 2020). High ROS levels are toxic to cells, with the associated destruction of the photosynthetic apparatus and membrane lipid peroxidation (Zhang et al., 2012; Sui and Han, 2014; Yang et al., 2020), adversely affecting photosynthesis. Additionally, high NaCl concentrations inhibit the *de novo* synthesis of proteins, including many photosystem-related proteins, such as the D1 protein (Allakhverdiev et al., 2002). For example, ROS produced in cells under salt stress could inhibit transcription factor activities, resulting in downregulated *psbA* expression (Jimbo et al., 2018).

Cyanobacteria have evolved diverse physiological mechanisms to cope with salt stress. Cyanobacteria may alter the content of certain membrane proteins in order to repair or resynthesize photosynthetic complexes damaged by salt stress. For instance, salt stress results in the enhancement of the vesicle-inducing protein in plastids 1 (*Vipp1*) in *Synechocystis* 6803 (Huang et al., 2006). The *Vipp1* have been suggested to be involved in the assembly of the thylakoid membrane system by transferring lipids from the inner envelope of chloroplast (Li et al., 1994; Vothknecht et al., 2012). It has also been found that photosystem I (PSI) and photosystem II (PSII) reaction center cores are originally synthesized in the plasma membrane of cyanobacteria (Zak et al., 2001). Therefore, the increased *Vipp1* may help accelerate the transport of the reaction center cores to thylakoid membrane under salt stress (Huang et al., 2006). Marin et al. reported that the acclimation of *Synechocystis* 6803–684 mM NaCl (4%, w/v) can be divided into two phases: the initial response to salt shock and longer-term adaptation to salt (Marin et al., 2004). In the first phase, the expression levels of many genes are upregulated, whereas in the second stage, the expression levels of only a few of these genes remain upregulated, such as the genes involved in glucosylglycerol (GG) synthesis and those encoding ABC transporters (Marin et al., 2004). Kanesaki et al. revealed that the expression of many genes is induced in response to salt stress, including the genes associated with the D1 protein at the photochemical reaction center of PSII (Kanesaki et al., 2002; Qiao et al., 2013). For instance, the *rbp3* gene, which encodes a type II RNA-binding protein, helps maintain the transcript levels of acyl-lipid desaturase genes (*desA*, *desB,* and *desD*) and the substantial abundance of unsaturated membrane lipid (Tang et al., 2010). This review focuses on the effects of salt stress on membrane, the photosystem and photosynthetic activities of cyanobacteria. We also describe the mechanisms in cyanobacteria that facilitate the protection of photosystems from the detrimental effects of salinity stress.

EFFECTS OF ROS ON PHOTOSYNTHESIS UNDER SALT STRESS

The O_2 molecule has two unpaired electrons that have the same spin quantum number (Gill and Tuteja, 2010). Due to its spin restriction, molecular oxygen prefers to receive electrons from high energy level to produce the so called ROS which are toxic to cells at high concentration (Ahanger et al., 2017). ROS includes singlet oxygen ($^1O_2$), superoxide anion (O_2^-), hydrogen peroxide (H_2O_2), and the hydroxyl radical (OH·) etc. In plant, peroxisomes not only destroy ROS due to the activities of peroxidases and catalases, but also produce superoxide radicals and there are, at least, two sites of superoxide generation: one in the organelle matrix, the generating system being xanthine oxidase, and another site in the peroxisomal membranes dependent on NAD(P)H (del RÍo et al., 2002). Thus in plants, chloroplasts and peroxisomes are the main producers of ROS during the day, while mitochondria are the main producers at night (Moller, 2001; Foyer and Noctor, 2003; Gill

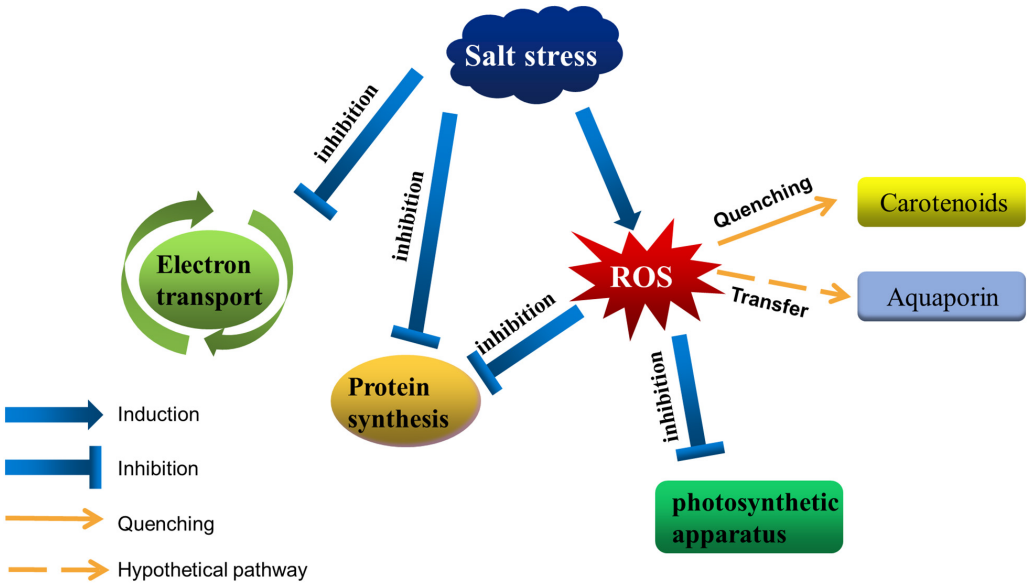

FIGURE 1 | Salt stress affects photosynthetic activities in cyanobacteria. Salt stress inhibits the electron transfer around the photosystem, as well as protein synthesis. Moreover, it disrupts intracellular ion homeostasis, resulting in the accumulation of ROS in cells. Excessive ROS destroys the photosynthetic apparatus and inhibits protein synthesis. Cyanobacteria can decrease the amount of ROS by accumulating carotenoids, and aquaporins may help transfer ROS from the photosystem to other regions.

and Tuteja, 2010). In cyanobacteria, ROS are also mainly derived from photochemical reactions and the photosynthetic electron transport (Latifi et al., 2009; Wada et al., 2013). In the process of photosynthetic electron transfer, ROS are mainly produced at three sites (Asada, 1999): (1) The oxygen-evolving complex in the water photolysis releases ROS due to state III inactivation. (2) The electrons are lost to O_2 by PQ on the reducing side of PSII to produce H_2O_2. (3) The electrons are transferred to O_2 directly or by ferredoxin (Fd) to produce $O_2^{-\cdot}$ on the reduction side of PSI. Under high light stress, due to the limited acceptors in the respiratory chain, electron leakage leads to the reduction of triplet oxygen ($^3O_2$) into $O_2^{-\cdot}$ (Mittler, 2002). Studies have shown that cyanobacteria cells under salt stress have a huge demand for ATP synthesis, which may reduce the fixation rate of CO_2 and lead to the excessive reduction of ferroredoxin pool (Van Thor et al., 2000; Latifi et al., 2009). This may be one of the reasons why salt stress result in oxidative stress.

Under abiotic stress conditions, singlet chlorophyll is transformed into triplet chlorophyll, which transfers its energy to $^3O_2$ to form $^1O_2$. $^1O_2$ has a short half-life in the cell and reacts with nearby target molecules (proteins, pigments, and lipids) immediately (Gorman and Rodgers, 1992; Latifi et al., 2009). It has been shown that $^1O_2$ and H_2O_2 can inhibit the translational elongation of *psbA* mRNA (Nishiyama et al., 2001, 2004). And H_2O_2 also interrupts the energy transfer between the core and the terminal emitter of phycobilisomes in *Synechocystis* 6803 (Liu et al., 2005). Excessive ROS will lead to membrane lipid peroxidation, which not only directly affects the normal function of cells, but also aggravates oxidative stress by producing lipid-derived free radicals (Montillet et al., 2005). ROS reacts with large molecules such as phospholipids and enzymes in the membrane to form lipid peroxidation products, resulting in decreased membrane fluidity (Gill and Tuteja, 2010). And ROS damages membrane proteins and ion channels, causing leakiness of some substance.

The scavenging of ROS in cyanobacteria cells is mainly by energy dissipation, antioxidant enzymes and non-enzymatic antioxidants. For instance, energy dissipation can be carried out by the "CP43′ protein", and this process is induced by iron deficiency in cyanobacteria (Latifi et al., 2009). Cyanobacteria can also dissipate energy through the Mehler-like reaction. Mehler first described the process of reducing O_2 to H_2O_2 by photosynthetic electron transport chain in chloroplast, and this reaction is therefore called the Mehler reaction (Mehler, 1951; Mehler and Brown, 1952). After that, H_2O_2 is rapidly detoxified to water by the ascorbate peroxidase pathway. In this process, the electrons are split from the water in oxygen releasing complex (OEC) and then flow through the PSI to produce water again. Therefore, it is called the water-water cycle, or "pseudocyclic electron flow" (Asada, 1999, 2000). Compared with plant, there is a similar reaction in cyanobacteria, known as the Mehler-like reaction. This reaction can reduce O_2 with electrons mediated by PSI by means of soluble flavoproteins 1 and flavoproteins 3 proteins (Vicente et al., 2002; Helman et al., 2003; Helman et al., 2005; Allahverdiyeva et al., 2011; Allahverdiyeva et al., 2013). It is a four-electron transfer reaction and it does not produce ROS and may protect PSI against production of O_2^- (Allahverdiyeva et al., 2013). The superoxide dismutase (SOD), most effective intracellular enzymatic antioxidant, can remove O_2^- by catalyzing its dismutation: one O_2^- being reduced to H_2O_2 and another oxidized to O_2 (Gill and Tuteja, 2010). Kanesaki et al.

demonstrated that salt stress and hyperosmotic stress induced the expression of *sodB,* which encoded an FeSOD enzyme (Kanesaki et al., 2002). Non-enzymatic antioxidant carotenoids can protect cellular structures, especially the photosystems, from the damage by scavenging $^1O_2$ and excitation energy. Carotenoids are a group of highly reductive substances that can protect cellular structures, especially the photosystems, from the damage by scavenging $^1O_2$ and excitation energy. In photosynthetic organisms, carotene mainly has three functions: harvesting light energy, acting as a light screen, and quenching singlet oxygen (Frank and Cogdell, 1996). In thylakoids, the carotenoids have two functions: harvesting light energy and photoprotection via the quenching of energy and $^1O_2$ (Sedoud et al., 2014). The orange carotenoid protein (OCP) is a soluble blue-green photoactive protein that binds a single keto-carotenoid molecule (Kirilovsky and Kerfeld, 2013, 2016; Dominguez-Martin and Kerfeld, 2019). And salt stress increases its transcripts and proteins levels (Kanesaki et al., 2002; Fulda et al., 2006). In cyanobacteria, OCP interacting with the phycobilisome, increases energy dissipation in the form of heat, thereby decreasing the amount of energy arriving at the reaction centers (Wilson et al., 2006). Kawasaki et al. (2013) found a purified astaxanthin-binding OCP from a eukaryotic microalga, named AstaP, shows high solubility in water and can quench singlet oxygen. And they found that the gene encoding AstaP was significantly up-regulated by salt stress (Kawasaki et al., 2013). A lack of β-carotene prevents cyanobacteria from generating a functional PSII, whereas a lack of almost all xanthophylls resulted in a considerable increase in the intracellular ROS content (Sozer et al., 2010; Zhu et al., 2010). Thus, in response to environmental stress, including salt stress, carotenoids are critical for maintaining the stability of photosynthesis. In addition to the above, aquaporins may also be involved in the scavenging of ROS under salt stress. Some aquaporin isoforms mediate permeation of glycerol, H_2O_2 or CO_2 in addition to water (Maurel, 2007). Some plant aquaporins expressed in yeast can transport H_2O_2 molecules (Bienert et al., 2007), implying that aquaporins may be able to maintain the stability of photosystems by transferring ROS to other regions. The Δ*aqpZ* cells of *Synechocystis* 6803 showed defects in macronutrient metabolism, pH homeostasis, and cell division under photomixotrophic conditions (Akai et al., 2011), but whether the above mechanism applies to cyanobacteria remains further experimental exploration.

In some cyanobacteria such as PCC6803 which contain polyunsaturated fatty acids, ROS would react with the acyl chains of polyunsaturated fatty acids (PUFA) or their membrane lipid residues, triggering the chain reaction of lipid peroxidation (Fryer, 1992; Yang et al., 2008). In order to maintain the normal physiological function of cells under salt stress, cyanobacteria not only need to remove excessive ROS, but also the oxidation products of ROS, such as lipid peroxides. It has been showed that tocopherol and carotenoids were very important for the scavenging of lipid peroxides in *Synechocystis* 6803 (Maeda et al., 2005). The content of tocopherol in cyanobacteria increased under high light and decreased when glucose was added to the medium (Backasch et al., 2005). This effect also showed that tocopherol takes part in protection against oxidative damage.

EFFECTS OF SALT STRESS ON POLYPEPTIDE COMPOSITION OF PHOTOSYSTEM

Salt stress could inhibit protein synthesis, with the D1 protein among the most obviously affected. In the natural environments, salt stress often occurs concomitantly with high light stress. Many studies have focused on the effects of salt stress on cyanobacterial PSII under intense light (Allakhverdiev and Murata, 2004; Allakhverdiev et al., 2005; Jantaro et al., 2005; Murata et al., 2007). A previous study revealed that exposure to 0.5 M NaCl can inhibit the repair of photodamaged PSII in *Synechocystis* 6803, but it did not directly accelerate the photodamage to PSII (Murata et al., 2007). It was also indicated that 0.5 M NaCl suppressed the synthesis of the D1 protein at the translational level (Murata et al., 2007). Allakhverdiev and Murata demonstrated that the initial rate of photoinactivation is unaffected by various NaCl concentrations, but the initial recovery rate decreases by 50 and 100% in the presence of 0.5 M and 1.0 M NaCl, respectively (Allakhverdiev and Murata, 2004). By monitoring the incorporation of [^{35}S]Met into the thylakoid membrane proteins under the recovery conditions, they observed that the synthesis of the D1 protein and many other proteins was completely impeded by 1.0 M NaCl (Allakhverdiev and Murata, 2004). Jantaro et al. (2005) determined that under severe osmotic stress conditions, the abundance of the PSII D1 protein in *Synechocystis* 6803 was decreased, whereas the protein contents of PsaA/B and NdhF3 were unaffected. They also proved that osmotic stress is more detrimental to photosynthesis than ionic stress. The D1 protein appeared to be one of the proteins targeted by osmotic stress conditions (Jantaro et al., 2005).

The repair of PSII involves the degradation of D1, transcription of *psbA* genes, translation of *psbA* transcripts, incorporation of pre-D1 into PSII, processing of pre-D1, as well as the assembly of the PSII dimer and the oxygen-evolving complex (**Figure 2**; Murata et al., 2007). Ohnishi and Murata reported that salt stress inhibited not only protein synthesis but also the degradation of the D1 protein in the photodamaged PSII of *Synechococcus elongatus* PCC 7942 (hereafter *Synechococcus* 7942), with betaine alleviating both of these inhibitory effects (Ohnishi and Murata, 2006; Nishiyama and Murata, 2014). Allakhverdiev et al. (2002) observed that the translation of mRNAs might be the primary cellular process inhibited by a decrease in the intracellular ATP level. Transcription was only partially affected by the ATP content and was likely to be a secondary target (Jantaro et al., 2005). During translation, the extension of polypeptide chains and the transfer of amino acids require energy from ATP, making ATP synthesis a potential rate-limiting step for the complete repair of photodamaged PSII (Jantaro et al., 2005).

Nishiyama et al. (2001, 2004) reported that ROS could inhibit the elongation step of the translation of *psbA* mRNA, which encodes the D1 protein in *Synechocystis* 6803. Biochemical

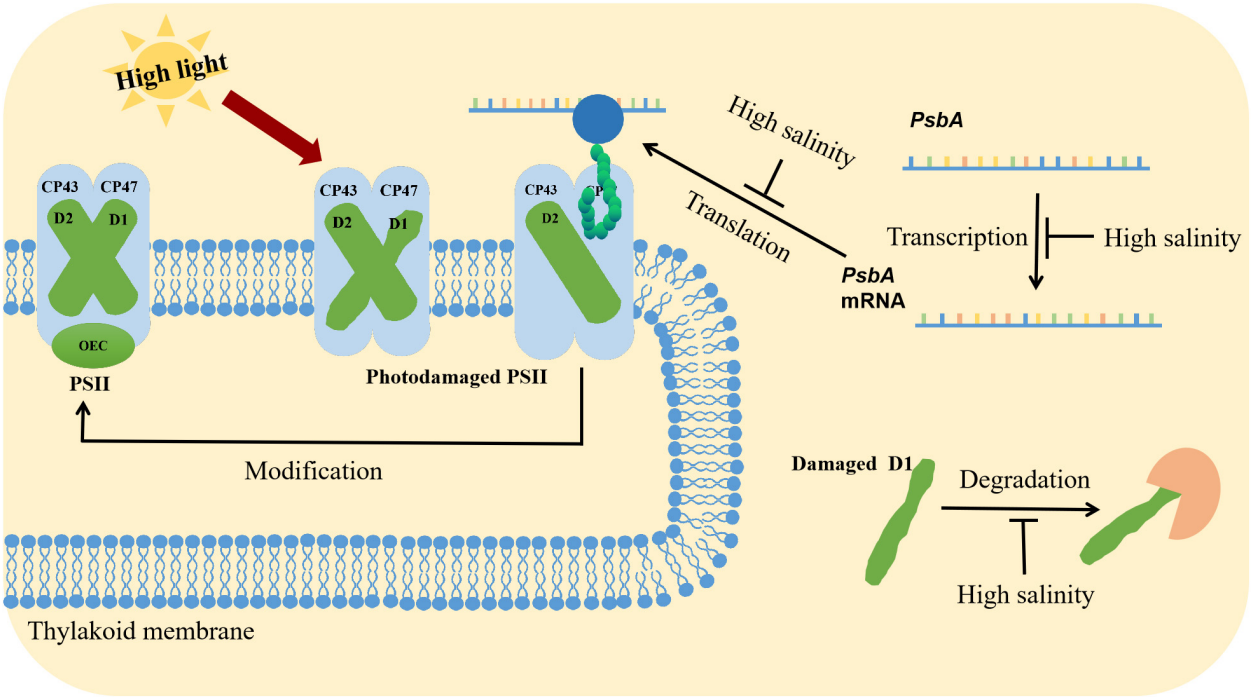

FIGURE 2 | Synergistic effects of high light and salinity stress on PSII. High light stress destroys the PSII structure. The repair of PSII involves the degradation of the D1 protein, the transcription, and translation of *psbA*, the incorporation of pre-D1 into PSII, the processing of pre-D1, and the assembly of the PSII dimer and the oxygen-evolving complex. Salt stress inhibits *psbA* transcription and translation.

studies reveal that ROS destroyed EF-G and EF-Tu, which regulates translational elongation (Kojima et al., 2007; Yutthanasirikul et al., 2016; Jimbo et al., 2018). Specifically, EF-G translocated peptidyl-tRNA from the A site to the P site of the ribosome, and it forms an intramolecular disulfide bond when inactivated by H_2O_2 (Kojima et al., 2009). In contrast, EF-Tu delivered aminoacyl-tRNA to the A site of the ribosome, and when inactivated by H_2O_2, it formed sulfenic acid and an intermolecular disulfide bond (Yutthanasirikul et al., 2016). Intense light conditions could enhance *de novo* protein synthesis of a *Synechocystis* 6803 mutant, whose Cys-82 targeted by ROS is replaced by a Ser residue (Jimbo et al., 2018). Thus, it is reasonable that excessive ROS contents induced by environmental stress can inhibit translation by disrupting transcription factor structures.

Many experiments have confirmed that salt stress inhibits *de novo* protein synthesis during the PSII repair process in cyanobacteria, but in addition to the above studies, the effects of salt stress on the synthesis of other proteins in photosynthetic apparatus remain to be studied. And besides ROS stress, the other effects of salt stress (such as ion stress and osmotic stress) on protein synthesis also need to be further studied. Three hypotheses have been proposed (Murata et al., 2007). First, the influx of NaCl into the cell may directly inhibit protein synthesis by destabilizing polysomes and ribosomes (Tester and Davenport, 2003; Murata et al., 2007). It was previously indicated that Rubisco of *Tamarix jordanis* was inactivated in response to high NaCl concentrations (Solomon et al., 1994). Thus, another hypothesis is that the primary target of salt stress is Rubisco. Salt stress inhibits the fixation of CO_2 and diminishes the regeneration of acceptors for the linear electron transport thereby inducing the generation of ROS, which subsequently inhibits protein synthesis (Murata et al., 2007; Nishiyama and Murata, 2014). The third hypothesis is that an increase in the intracellular NaCl concentration inactivates ATP synthesis, thereby decreasing the intracellular ATP content that is essential for protein synthesis (Allakhverdiev et al., 2005). In addition to these hypotheses, we speculate that salt stress may also indirectly inhibit protein synthesis by inducing ROS production.

EFFECT OF LIPID COMPOSITION AND FATTY ACID DESATURATION ON THE SALT RESISTANCE OF CYANOBACTERIA

The cell membrane is a sensor of environmental stress, which can activate a series of protective reactions by adjusting the stress perception and rigidity of cell structure (Sui et al., 2018). In cyanobacteria and plants, the thylakoid membrane structure and fluidity were affected by lipid composition and the degree of fatty acid desaturation (Mikami and Murata, 2003). The relationship between lipids and salt stress has been widely studied in plants and cyanobacteria. Sui et al. demonstrated that salt stress increases the content of unsaturated fatty acids in the euhalophyte *Suaeda salsa*, which increased the photosystem tolerance to salt stress (Sui et al., 2017). In the halophyte

Thellungiella, increasing the content of phosphatidylglycerol (PG) and sulfoquinovosyl diacylglycerol (SQDG) as well as the ratio of monogalactosyldiacylglycerols/digalactosyldiacylglycerol (MGDG/DGDG) in thylakoid membranes can alleviate PSII photoinhibition under salt stress (Sui and Han, 2014).

In response to salt stress, cyanobacteria could alter not only the composition of lipids but also the unsaturated degree of membrane lipids. The changes in lipid composition of *Synechococcus* sp. PCC6311 under salt stress include the increase of the proportion of unsaturated fatty acids and phosphatidyl glycerol (Huflejt et al., 1990). Ritter and Yopp (1993) observed that the proportion of mono/digalactosyl diacyl glycerols changes when exposed the cyanobacterium *Aphanothece halophytica* to salt stress. Changes in ion-exchange properties of the cytoplasmic membrane caused by changes in polar lipids may hamper the function of potassium ion channels (Joset et al., 1996), thereby reducing the inflow of Na^+ and reducing the damage of photosynthetic apparatus. The decrease in the protein to lipid ratio led to increased cytochrome oxidase and H^+/Na^+ antiport activities in *Synechococcus* 6301 under salt stress (Peschek et al., 1994; Srivastava et al., 2013), which also reduced the damage of photosynthetic apparatus.

The extent of the desaturation of individual fatty acids is regulated genetically and environmentally, and the content of unsaturated fatty acids will influence the photosynthetic machinery under salt stress. *Synechocystis* 6803 contains four acyl lipid desaturases, DesA, DesB, DesC, and DesD, which catalyze the desaturation at the Δ12, Δ15, Δ9, and Δ6 positions of C18 fatty acyl chains in membrane lipids, respectively (Murata and Wada, 1995; Chintalapati et al., 2006). The oxygen-evolving machinery in thylakoid membranes isolated from the $desA^-/desD^-$ cells of *Synechocystis* 6803 (the double mutant of *desA* and *desD* genes) was more sensitive to NaCl than that of the WT cells, indicating that the desaturation of membrane lipid fatty acids may directly protect the oxygen-evolving machinery against salt-induced inactivation (Allakhverdiev et al., 1999). In order to further study on the function of *desA*, Allakhverdiev et al. (2001) constructed $desA^+$ cells by overexpressing the *desA* gene in *Synechococcus* 7942 that do not have the *desA* gene. The results showed that WT cells are more sensitive to NaCl and have the reduced capacity of recovery than $desA^+$ cells (Allakhverdiev et al., 2001). These studies showed that the increase of unsaturated fatty acids in membrane lipids enhances the tolerance of the photosynthetic and Na^+/H^+ antiport systems in cyanobacteria to salt stress (Allakhverdiev et al., 2001; Singh et al., 2002).

The desaturation of fatty acids in membrane lipids may protect the oxygen-evolving machinery by stimulating the synthesis of the protein(s) in the Na^+/H^+ antiport system (Allakhverdiev et al., 1999). The energy generated by photosynthesis and respiration overcomes the inhibition of protein synthesis by NaCl, thus enabling the repair of the oxygen-releasing complex. The following scheme might explain why light or glucose can restore the oxygen-evolving activity (Allakhverdiev et al., 1999). The lack of an ATP supply under the dark and salt conditions indirectly inhibited the activities of the Na^+/H^+ antiport system and caused sodium ions to flow into the thylakoid cavity, leading to the deactivation of the oxygen-releasing complex. The presence of NaCl in the dark impeded the synthesis of certain proteins, whereas exposure to light has the opposite effect. The above-mentioned results implied that the affected proteins belong to the Na^+/H^+ antiport system. Compared with the WT Na^+/H^+ antiport system, the mutant was more sensitive to salt and its repair rate was slower (Allakhverdiev et al., 1999). Therefore, unsaturation of fatty acids might also stimulate the synthesis of protein(s) in the Na^+/H^+ antiport system.

The *rbp3* gene, which encodes a type II RNA-binding protein, is involved in maintaining the transcript levels of acyl-lipid desaturase genes (*desA*, *desB,* and *desD*) and the substantial abundance of unsaturated membrane lipids (Tang et al., 2010). It was shown that 2-day treatment with 1 M NaCl decreased the photosynthetic activity of Δ*rbp3* to 8.4% of the WT level (Wang and Xu, 2013). The complementation with *rbp3* fully restored the photosynthetic activity, whereas the overexpression of *desA* only partially restored the activity (Wang and Xu, 2013). Thus, *rbp3* may maintain the extent of unsaturated lipids in the cell membrane by enhancing the stability of *des* mRNAs, thereby stabilizing the photosynthesis of cyanobacteria under salt stress conditions.

CONCLUSION AND PERSPECTIVES

Salt stress inhibits protein synthesis, especially the D1 protein. Osmotic stress may directly inhibit protein synthesis. Moreover, it seems that the accumulated ROS caused by salt stress mainly inhibits the translation process. However, whether salt stress affects the modification processing of pre-D1 in cyanobacteria remains unclear.

Aquaporins may be able to stabilize photosystems by transferring ROS to other regions, since some plant aquaporins expressed in yeast can transport H_2O_2 molecules (Bienert et al., 2007). However, the function of aquaporins and the associated mechanisms in cyanobacteria remits further characterization.

Cyanobacteria represent an excellent model system for studying the relationship between membrane systems and photosynthesis under stress conditions. Several studies have revealed the protective effects of membrane lipids and unsaturated degree of fatty acids on photosystems under salt stress, but the protective effects of the composition of different lipids on the photosynthetic apparatus of cyanobacteria under salt stress remains to be further studied. Whether salt stress affects the lipid-assisted PSI oligomerization and affects energy transfer between phycobilisomes and the photosystem also requires further exploration. Although there is increasing interest in uncovering the effects of salt stress on photosynthetic activities in cyanobacteria, the underlying mechanism remains to be elucidated.

AUTHOR CONTRIBUTIONS

WY initiated preparation of the manuscript. NS, FW, and L-NL conceptualized the idea and revised the manuscript. All authors have read and approved the final manuscript.

FUNDING

We are grateful for the financial support from the National Key R&D Program of China (2018YFD1000700 and 2018YFD1000704), the National Natural Science Foundation of China (U1906204 and 31871538), Shandong Province Key Research and Development Program (2019GSF107079), the Development Plan for Youth Innovation Team of Shandong Provincial (2019KJE012), the Opening Foundation of Shandong Key Laboratory of Crop Genetic Improvement, Ecology and Physiology (SDKL2018008-3), Royal Society University Research Fellowship (UF120411 and URF\R\180030, L-NL), Royal Society Grants (RGF\EA\181061 and RGF\EA\180233), and Biotechnology and Biological Sciences Research Council Grant (BB/R003890/1, L-NL).

REFERENCES

Ahanger, M. A., Tomar, N. S., Tittal, M., Argal, S., and Agarwal, R. M. (2017). Plant growth under water/salt stress: ROS production; antioxidants and significance of added potassium under such conditions. *Physiol. Mol. Biol. Plants* 23, 731–744. doi: 10.1007/s12298-017-0462-7

Akai, M., Onai, K., Kusano, M., Sato, M., Redestig, H., Toyooka, K., et al. (2011). Plasma membrane aquaporin aqpz protein is essential for glucose metabolism during photomixotrophic growth of *Synechocystis* sp. pcc 6803. *J. Biol. Chem.* 286, 25224–25235. doi: 10.1074/jbc.M111.236380

Allahverdiyeva, Y., Ermakova, M., Eisenhut, M., Zhang, P., Richaud, P., Hagemann, M., et al. (2011). Interplay between flavodiiron proteins and photorespiration in *Synechocystis* sp. PCC 6803. *J. Biol. Chem.* 286, 24007–24014. doi: 10.1074/jbc.m111.223289

Allahverdiyeva, Y., Mustila, H., Ermakova, M., Bersanini, L., Richaud, P., Ajlani, G., et al. (2013). Flavodiiron proteins Flv1 and Flv3 enable cyanobacterial growth and photosynthesis under fluctuating light. *Proc. Natl. Acad. Sci. U.S.A.* 110, 4111–4116. doi: 10.1073/pnas.1221194110

Allakhverdiev, S. I., Kinoshita, M., Inaba, M., Suzuki, I., and Murata, N. (2001). Unsaturated fatty acids in membrane lipids protect the photosynthetic machinery against salt-induced damage in *Synechococcus*. *Plant Physiol.* 125, 1842–1853. doi: 10.1104/pp.125.4.1842

Allakhverdiev, S. I., and Murata, N. (2004). Environmental stress inhibits the synthesis de novo of proteins involved in the photodamage-repair cycle of photosystem II in *Synechocystis* sp. PCC 6803. *Biochim. Biophys. Acta Bioenerg.* 1657, 23–32. doi: 10.1016/j.bbabio.2004.03.003

Allakhverdiev, S. I., and Murata, N. (2008). Salt stress inhibits photosystems II and I in cyanobacteria. *Photosynth. Res.* 98, 529–539. doi: 10.1007/s11120-008-9334-x

Allakhverdiev, S. I., Nishiyama, Y., Miyairi, S., Yamamoto, H., Inagaki, N., Kanesaki, Y., et al. (2002). Salt stress inhibits the repair of photodamaged photosystem II by suppressing the transcription and translation of *psbA* Genes in *Synechocystis*. *Plant Physiol.* 130, 1443–1453. doi: 10.1104/pp.011114

Allakhverdiev, S. I., Nishiyama, Y., Suzuki, I., Tasaka, Y., and Murata, N. (1999). Genetic engineering of the unsaturation of fatty acids in membrane lipids alters the tolerance of *Synechocystis* to salt stress. *Proc. Natl. Acad. Sci U.S.A.* 96, 5862–5867. doi: 10.1073/pnas.96.10.5862

Allakhverdiev, S. I., Nishiyama, Y., Takahashi, S., Miyairi, S., Suzuki, I., and Murata, N. (2005). Systematic analysis of the relation of electron transport and ATP synthesis to the photodamage and repair of photosystem II in *Synechocystis*. *Plant Physiol.* 137, 263–273. doi: 10.1104/pp.104.054478

Allakhverdiev, S. I., Sakamoto, A., Nishiyama, Y., Inaba, M., and Murata, N. (2000). Ionic and osmotic effects of NaCl-induced inactivation of photosystem I and II in *Synechococcus* sp. *Plant Physiol.* 123, 1047–1056. doi: 10.1104/pp.123.3.1047

Asada, K. (1999). The water-water cycle in chloroplasts: scavenging of active oxygens and dissipation of excess photons. *Annu. Rev. Plant Physiol. Plant Mol. Biol.* 50, 601–639. doi: 10.1146/annurev.arplant.50.1.601

Asada, K. (2000). The water-water cycle as alternative photon and electron sinks. *Philos. Trans. R. Soc. Lond. B* 355, 1419–1431. doi: 10.1098/rstb.2000.0703

Backasch, N., Schulz-Friedrich, R., and Appel, J. (2005). Influences on tocopherol biosynthesis in the cyanobacterium *Synechocystis* sp. PCC 6803. *J. Plant Physiol.* 162, 758–766. doi: 10.1016/j.jplph.2005.04.006

Bienert, G. P., Møller, A. L. B., Kristiansen, K. A., Schulz, A., Møller, I. M., Schjoerring, J. K., et al. (2007). Specific aquaporins facilitate the diffusion of hydrogen peroxide across membranes. *J. Biol. Chem.* 282, 1183–1192. doi: 10.1074/jbc.M603761200

Chen, Y., Han, Y., Kong, X., Kang, H., Ren, Y., and Wang, W. (2017). Ectopic expression of wheat expansin gene TaEXPA2 improved the salt tolerance of transgenic tobacco by regulating Na^+/K^+ and antioxidant competence. *Physiol. Plant.* 159, 161–177. doi: 10.1111/ppl.12492

Chintalapati, S., Prakash, J. S. S., Gupta, P., Ohtani, S., Suzuki, I., Sakamoto, T., et al. (2006). A novel Δ9 acyl-lipid desaturase, DesC2, from cyanobacteria acts on fatty acids esterified to the *sn*-2 position of glycerolipids. *Biochem. J.* 398, 207–214. doi: 10.1042/BJ20060039

del RÍo, L. A., Corpas, F. J., Sandalio, L. M., Palma, J. M., GÓmez, M., and Barroso, J. B. (2002). Reactive oxygen species, antioxidant systems and nitric oxide in peroxisomes. *J. Exp. Bot.* 53, 1255–1272. doi: 10.1093/jxb/53.372.1255

Desplats, P., Folco, E., and Salerno, G. L. (2005). Sucrose may play an additional role to that of an osmolyte in *Synechocystis* sp. PCC 6803 salt-shocked cells. *Plant Physiol. Biochem.* 43, 133–138. doi: 10.1016/j.plaphy.2005.01.008

Dominguez-Martin, M. A., and Kerfeld, C. A. (2019). Engineering the orange carotenoid protein for applications in synthetic biology. *Curr. Opin. Struct. Biol.* 57, 110–117. doi: 10.1016/j.sbi.2019.01.023

Fan, Y., Yin, X., Xie, Q., Xia, Y., Wang, Z., Song, J., et al. (2019). Co-expression of SpSOS1 and SpAHA1 in transgenic Arabidopsis plants improves salinity tolerance. *BMC Plant Biol.* 19:74. doi: 10.1186/s12870-019-1680-7

Feng, Z. T., Deng, Y. Q., Fan, H., Sun, Q. J., Sui, N., and Wang, B. S. (2014). Effects of NaCl stress on the growth and photosynthetic characteristics of *Ulmus pumila* L. seedlings in sand culture. *Photosynthetica* 52, 313–320. doi: 10.1007/s11099-014-0032-y

Feng, Z. T., Deng, Y. Q., Zhang, S. C., Liang, X., Yuan, F., Hao, J. L., et al. (2015). K^+ accumulation in the cytoplasm and nucleus of the salt gland cells of Limonium bicolor accompanies increased rates of salt secretion under NaCl treatment using NanoSIMS. *Plant Sci.* 238, 286–296. doi: 10.1016/j.plantsci.2015.06.021

Foyer, C. H., and Noctor, G. (2003). Redox sensing and signalling associated with reactive oxygen in chloroplasts, peroxisomes and mitochondria. *Physiol. Plant.* 119, 355–364. doi: 10.1034/j.1399-3054.2003.00223.x

Frank, H. A., and Cogdell, R. J. (1996). Carotenoids in photosynthesis. *Photochem. Photobiol.* 63, 257–264. doi: 10.1111/j.1751-1097.1996.tb03022.x

Fryer, M. J. (1992). The antioxidant effects of thylakoid Vitamin E (α-tocopherol). *Plant Cell Environ.* 15, 381–392. doi: 10.1111/j.1365-3040.1992.tb00988.x

Fulda, S., Mikkat, S., Huang, F., Huckauf, J., and Hagemann, M. (2006). Proteome analysis of salt stress response in the cyanobacterium synechocystis sp. strain pcc 6803. *Proteomics* 6, 2733–2745. doi: 10.1002/pmic.200500538

Gill, S. S., and Tuteja, N. (2010). Reactive oxygen species and antioxidant machinery in abiotic stress tolerance in crop plants. *Plant Physiol. Biochem.* 48, 909–930. doi: 10.1016/j.plaphy.2010.08.016

Gorman, A. A., and Rodgers, M. A. (1992). Current perspectives of singlet oxygen detection in biological environments. *J. Photochem. Photobiol. B Biol.* 14, 159–176. doi: 10.1016/1011-1344(92)85095-C

Han, N., Lan, W., He, X., Shao, Q., Wang, B., and Zhao, X. (2012). Expression of a *Suaeda salsa* vacuolar H^+/Ca^{2+} transporter gene in *Arabidopsis* contributes to physiological changes in salinity. *Plant Mol. Biol. Rep.* 30, 470–477. doi: 10.1007/s11105-011-0353-y

Haselkorn, R. (1991). Genetic systems in cyanobacteria. *Methods Enzymol.* 204, 418–430. doi: 10.1016/0076-6879(91)04022-G

Helman, Y., Barkan, E., Eisenstadt, D., Luz, B., and Kaplan, A. (2005). Fractionation of the three stable oxygen isotopes by oxygen-producing and oxygen-consuming reactions in photosynthetic organisms. *Plant Physiol.* 138, 2292–2298. doi: 10.1104/pp.105.063768

Helman, Y., Tchernov, D., Reinhold, L., Shibata, M., Ogawa, T., Schwarz, R., et al. (2003). Genes encoding A-type flavoproteins are essential for photoreduction

of O_2 in cyanobacteria. *Curr. Biol.* 13, 230–235. doi: 10.1016/s0960-9822(03)00046-0

Hu, D. G., Ma, Q. J., Sun, C. H., Sun, M. H., You, C. X., and Hao, Y. J. (2016). Overexpression of MdSOS2L1, a CIPK protein kinase, increases the antioxidant metabolites to enhance salt tolerance in apple and tomato. *Physiol. Plant.* 156, 201–214. doi: 10.1111/ppl.12354

Huang, F., Fulda, S., Hagemann, M., and Norling, B. (2006). Proteomic screening of salt-stress-induced changes in plasma membranes of *Synechocystis* sp. strain PCC 6803. *Proteomics* 6, 910–920. doi: 10.1002/pmic.200500114

Huflejt, M. E., Tremolieres, A., Pineau, B., Lang, J. K., Hatheway, J., and Packer, L. (1990). Changes in membrane lipid composition during saline growth of the fresh water cyanobacterium *Synechococcus* 6311. *Plant Physiol.* 94, 1512–1521. doi: 10.1104/pp.94.4.1512

Jantaro, S., Mulo, P., Jansén, T., Incharoensakdi, A., and Mäenpää, P. (2005). Effects of long-term ionic and osmotic stress conditions on photosynthesis in the cyanobacterium *Synechocystis* sp. PCC 6803. *Funct. Plant Biol.* 32, 807–815. doi: 10.1071/FP04219

Jensen, P. E., and Leister, D. (2014). Cyanobacteria as an experimental platform for modifying bacterial and plant photosynthesis. *Front. Bioeng. Biotechnol.* 2:7. doi: 10.3389/fbioe.2014.00007

Jimbo, H., Yutthanasirikul, R., Nagano, T., Hisabori, T., Hihara, T., and Nishiyama, Y. (2018). Oxidation of translation factor EF-Tu inhibits the repair of photosystem II. *Plant Physiol.* 176, 2691–2699. doi: 10.1104/pp.18.00037

Joset, F., Jeanjean, R., and Hagemann, M. (1996). Dynamics of the response of cyanobacteria to salt stress: deciphering the molecular events. *Physiol. Plant.* 96, 738–744. doi: 10.1111/j.1399-3054.1996.tb00251.x

Kanesaki, Y., Suzuki, I., Allakhverdiev, S. I., Mikami, K., and Murata, N. (2002). Salt stress and hyperosmotic stress regulate the expression of different sets of genes in *Synechocystis* sp. PCC 6803. *Biochem. Biophys. Res. Commun.* 290, 339–348. doi: 10.1006/bbrc.2001.6201

Karandashova, I. V., and Elanskaya, I. V. (2005). Genetic control and mechanisms of salt and hyperosmotic stress resistance in cyanobacteria. *Russ. J. Genet.* 41, 1311–1321. doi: 10.1007/s11177-006-0001-z

Kawasaki, S., Mizuguchi, K., Sato, M., Kono, T., and Shimizu, H. (2013). A novel astaxanthin-binding photooxidative stress-inducible aqueous carotenoprotein from a eukaryotic microalga isolated from asphalt in midsummer. *Plant Cell Physiol.* 54, 1027–1040. doi: 10.1093/pcp/pct080

Kirilovsky, D., and Kerfeld, C. A. (2013). The Orange Carotenoid Protein: a blue-green light photoactive protein. *Photochem. Photobiol.* 12, 1135–1143. doi: 10.1039/C3PP25406B

Kirilovsky, D., and Kerfeld, C. A. (2016). Cyanobacterial photoprotection by the orange carotenoid protein. *Nat. Plants* 2:16180. doi: 10.1038/nplants.2016.180

Kojima, K., Motohashi, K., Morota, T., Oshita, M., Hisabori, T., Hayashi, H., et al. (2009). Regulation of translation by the redox state of elongation factor G in the cyanobacterium *Synechocystis* sp. PCC 6803. *J. Biol. Chem.* 284, 18685–18691. doi: 10.1074/jbc.M109.015131

Kojima, K., Oshita, M., Nanjo, Y., Kasai, K., Tozawa, Y., Hayashi, H., et al. (2007). Oxidation of elongation factor G inhibits the synthesis of the D1 protein of photosystem II. *Mol. Microbiol.* 65, 936–947. doi: 10.1111/j.1365-2958.2007.05836.x

Latifi, A., Ruiz, M., and Zhang, C. C. (2009). Oxidative stress in cyanobacteria. *FEMS Microbiol. Rev.* 33, 258–278. doi: 10.1111/j.1574-6976.2008.00134.x

Li, H. M., Kaneko, Y., and Keegstra, K. (1994). Molecular cloning of a chloroplastic protein associated with both the envelope and thylakoid membranes. *Plant Mol. Biol.* 25, 619–632. doi: 10.1007/BF00029601

Liu, X. G., Zhao, J. J., and Wu, Q. Y. (2005). Oxidative stress and metal ions effects on the cores of phycobilisomes in *Synechocystis* sp. PCC6803. *FEBS Lett.* 579, 4571–4576. doi: 10.1016/j.febslet.2005.07.020

Los, D. A., and Murata, N. (2004). Membrane fluidity and its roles in the perception of environmental signals. *Biochim. Biophys. Acta* 1666, 142–157. doi: 10.1016/j.bbamem.2004.08.002

Los, D. A., Zorina, A., Sinetova, M., Kryazhov, S., Mironov, K., and Zinchenko, V. V. (2010). Stress sensors and signal transducers in cyanobacteria[J]. *Sensors* 10, 2386–2415. doi: 10.3390/s100302386

Lu, C., and Vonshak, A. (1999). Characterization of PSII photochemistry in salt-adapted cells of cyanobacterium *Spirulina platensis*. *New Phytol.* 141, 231–239. doi: 10.1046/j.1469-8137.1999.00340.x

Lu, C., and Vonshak, A. (2002). Effects of salinity stress on photosystem II function in cyanobacterial *Spirulina platensis* cells. *Physiol. Plant.* 114, 405–413. doi: 10.1034/j.1399-3054.2002.1140310.x

Lu, C., and Zhang, J. (2000). Role of light in the response of PSII photochemistry to salt stress in the cyanobacterium *Spirulina platensis*. *J. Exp. Bot.* 51, 911–917. doi: 10.1093/jexbot/51.346.911

Ma, Q. J., Sun, M. H., Kang, H., Lu, J., You, C. X., and Hao, Y. J. (2019). A CIPK protein kinase targets sucrose transporter MdSUT2. 2 at Ser254 for phosphorylation to enhance salt tolerance. *Plant Cell Environ.* 42, 918–930. doi: 10.1111/pce.13349

Maeda, H., Sakuragi, Y., Bryant, D. A., and DellaPenna, D. (2005). Tocopherols protect *Synechocystis* sp. strain PCC 6803 from lipid peroxidation. *Plant Physiol.* 138, 1422–1435. doi: 10.1104/pp.105.061135

Marin, K., Kanesaki, Y., Los, D. A., Murata, N., Suzuki, I., and Hagemann, M. (2004). Gene expression profiling reflects physiological processes in salt acclimation of *Synechocystis* sp. strain PCC 6803. *Plant Physiol.* 136, 3290–3300. doi: 10.1104/pp.104.045047

Maurel, C. (2007). Plant aquaporins: novel functions and regulation properties. *FEBS Lett.* 581, 2227–2236. doi: 10.1016/j.febslet.2007.03.021

Mehler, A. H. (1951). Studies on reactions of illuminated chloroplasts: I. Mechanism of the reduction of oxygen and other Hill reagents. *Arch. Biochem. Biophys.* 33, 65–77. doi: 10.1016/0003-9861(51)90082-3

Mehler, A. H., and Brown, A. H. (1952). Studies on reactions of illuminated chloroplasts: III. Simultaneous photoproduction and consumption of oxygen studied with oxygen isotopes. *Arch. Biochem. Biophys.* 38, 365–370. doi: 10.1016/0003-9861(52)90042-8

Mikami, K., and Murata, N. (2003). Membrane fluidity and the perception of environmental signals in cyanobacteria and plants. *Prog. Lipid Res.* 42, 527–543. doi: 10.1016/S0163-7827(03)00036-5

Mittler, R. (2002). Oxidative stress, antioxidants and stress tolerance. *Trends Plant Sci.* 7, 405–410. doi: 10.1016/S1360-1385(02)02312-9

Moller, I. M. (2001). Plant mitochondria and oxidative stress: electron transport, nadph turnover, and metabolism of reactive oxygen species. *Annu. Rev. Plant Physiol. Plant Mol. Biol.* 52, 561–591. doi: 10.1146/annurev.arplant.52.1.561

Montillet, J. L., Chamnongpol, S., Rustérucci, C., Dat, J., van de Cotte, B., Agnel, J. P., et al. (2005). Fatty acid hydroperoxides and H_2O_2 in the execution of hypersensitive cell death in tobacco leaves. *Plant Physiol.* 138, 1516–1526. doi: 10.1104/pp.105.059907

Mullineaux, C. W. (2014). Co-existence of photosynthetic and respiratory activities in cyanobacterial thylakoid membranes. *Biochim. Biophys. Acta Bioenerg.* 1837, 503–511. doi: 10.1016/j.bbabio.2013.11.017

Murata, N., Takahashi, S., Nishiyama, Y., and Allakhverdiev, S. I. (2007). Photoinhibition of photosystem II under environmental stress. *Biochim. Biophys. Acta Bioenerg.* 1767, 414–421.

Murata, N., and Wada, H. (1995). Acyl-lipid desaturases and their importance in the tolerance and acclimatization to cold of cyanobacteria. *Biochem. J.* 308, 1–8. doi: 10.1042/bj3080001

Nishiyama, Y., Allakhverdiev, S. I., Yamamoto, H., Hayashi, H., and Murata, N. (2004). Singlet oxygen inhibits the repair of photosystem II by suppressing the translation elongation of the D1 protein in *Synechocystis* sp. PCC 6803. *Biochemistry* 43, 11321–11330. doi: 10.1021/bi036178q

Nishiyama, Y., and Murata, N. (2014). Revised scheme for the mechanism of photoinhibition and its application to enhance the abiotic stress tolerance of the photosynthetic machinery. *Appl. Microbiol. Biotechnol.* 98, 8777–8796. doi: 10.1007/s00253-014-6020-0

Nishiyama, Y., Yamamoto, H., Allakhverdiev, S. I., Inaba, M., Yokota, A., and Murata, N. (2001). Oxidative stress inhibits the repair of photodamage to the photosynthetic machinery. *EMBO J.* 20, 5587–5594. doi: 10.1093/emboj/20.20.5587

Ohnishi, N., and Murata, N. (2006). Glycinebetaine counteracts the inhibitory effects of salt stress on the degradation and synthesis of D1 protein during photoinhibition in *Synechococcus* sp. PCC 7942. *Plant Physiol.* 141, 758–765. doi: 10.1104/pp.106.076976

Öquist, G., Campbell, D., Clarke, A. K., and Gustafsson, P. (1995). The cyanobacterium *Synechococcus* modulates Photosystem II function in response to excitation stress through D1 exchange. *Photosynth. Res.* 46, 151–158. doi: 10.1007/BF00020425

Peschek, G. A., Obinger, C., Fromwald, S., and Bergman, B. (1994). Correlation between immuno-gold labels and activities of the cytochrome-c oxidase (aa3-type) in membranes of salt stressed cyanobactria. *FEMS Microbiol. Lett.* 124, 431–437. doi: 10.1111/j.1574-6968.1994.tb07320.x

Qiao, J. J., Huang, S. Q., Te, R. G., Wang, J. X., Chen, L., and Zhang, W. W. (2013). Integrated proteomic and transcriptomic analysis reveals novel genes and regulatory mechanisms involved in salt stress responses in *Synechocystis* sp. PCC 6803. *Appl. Microbiol. Biotechnol.* 97, 8253–8264. doi: 10.1007/s00253-013-5139-8

Ritter, D., and Yopp, J. H. (1993). Plasma membrane lipid composition of the halophilic cyanobacterium *Aphanothece halophytica*. *Arch. Microbiol.* 159, 435–439. doi: 10.1007/BF00288590

Rodriguez-Ezpeleta, N., Brinkmann, H., Burey, S. C., Roure, B., Burger, G., Loffelhardt, W., et al. (2005). Monophyly of primary photosynthetic eukaryotes: green plants, red algae, and glaucophytes. *Curr. Biol.* 15, 1325–1330. doi: 10.1016/j.cub.2005.06.040

Scarpeci, T. E., Zanor, M. I., Carrillo, N., Mueller-Roeber, B., and Valle, E. M. (2008). Generation of superoxide anion in chloroplasts of *Arabidopsis thaliana* during active photosynthesis: a focus on rapidly induced genes. *Plant Mol. Biol.* 66, 361–378. doi: 10.1007/s11103-007-9274-4

Sedoud, A., Lopez-Igual, R., ur Rehman, A., Wilson, A., Perreau, F., Boulay, C., et al. (2014). The cyanobacterial photoactive orange carotenoid protein is an excellent singlet oxygen quencher. *Plant Cell* 26, 1781–1791. doi: 10.1105/tpc.114.123802

Serrano, R., and Rodrigueznavarro, A. (2001). Ion homeostasis during salt stress in plants. *Curr. Opin. Cell Biol.* 13, 399–404. doi: 10.1016/S0955-0674(00)00227-1

Shabala, S. (2013). Learning from halophytes: physiological basis and strategies to improve abiotic stress tolerance in crops. *Ann. Bot.* 112, 1209–1221. doi: 10.1093/aob/mct205

Shao, Q., Han, N., Ding, T., Zhou, F., and Wang, B. (2014). SsHKT1; 1 is a potassium transporter of the C3 halophyte *Suaeda salsa* that is involved in salt tolerance. *Funct. Plant Biol.* 41, 790–802. doi: 10.1071/FP13265

Singh, S. C., Sinha, R. P., and Hader, D. P. (2002). Role of lipids and fatty acids in stress tolerance in cyanobacteria. *Acta Protozool.* 41, 297–308. doi: 10.1016/S0378-1097(02)01030-3

Solomon, A., Beer, S., Waisel, Y., Jones, G. P., and Paleg, L. G. (1994). Effects of NaCl on the carboxylating activity of Rubisco from *Tamarix jordanis* in the presence and absence of proline-related compatible solutes. *Physiol. Plant.* 90, 198–204. doi: 10.1111/j.1399-3054.1994.tb02211.x

Song, J., and Wang, B. S. (2014). Using euhalophytes to understand salt tolerance and to develop saline agriculture: *Suaeda salsa* as a promising model. *Ann. Bot.* 115, 541–553. doi: 10.1093/aob/mcu194

Song, Y., Li, J., Sui, Y., Han, G., Zhang, Y., Guo, S., et al. (2020). The sweet sorghum SbWRKY50 is negatively involved in salt response by regulating ion homeostasis. *Plant Mol. Biol.* 102, 603–614. doi: 10.1007/s11103-020-00966-4

Sozer, O., Komenda, J., Ughy, B., Domonkos, I., Laczkó-Dobos, H., Malec, P., et al. (2010). Involvement of carotenoids in the synthesis and assembly of protein subunits of photosynthetic reaction centers of *Synechocystis* sp. PCC 6803. *Plant Cell Physiol.* 51, 823–835. doi: 10.1093/pcp/pcq031

Srivastava, A. K., Rai, A. N., and Neilan, B. A. (2013). *Stress Biology of Cyanobacteria: Molecular Mechanisms to Cellular Responses*. Boca Raton, FL: CRC Press, 172–173. doi: 10.1111/jpy.12201

Sudhir, P., Pogoryelov, D., Kovacs, L., Garab, G., and Murthy, S. (2005). The effects of salt stress on photosynthetic electron transport and thylakoid membrane proteins in the cyanobacterium *Spirulina platensis*. *J. Biochem. Mol. Biol.* 38, 481–485. doi: 10.5483/BMBRep.2005.38.4.481

Sui, N., and Han, G. L. (2014). Salt-induced photoinhibition of PSII is alleviated in halophyte *Thellungiella halophila* by increases of unsaturated fatty acids in membrane lipids. *Acta Physiol. Plant.* 36, 983–992. doi: 10.1007/s11738-013-1477-5

Sui, N., Tian, S., Wang, W., Wang, M., and Fan, H. (2017). Overexpression of glycerol-3-phosphate acyltransferase from *Suaeda salsa* improves salt tolerance in Arabidopsis. *Front. Plant Sci.* 8:1337. doi: 10.3389/fpls.2017.01337/full

Sui, N., Wang, Y., Liu, S., Yang, Z., Wang, F., and Wan, S. B. (2018). Transcriptomic and physiological evidence for the relationship between unsaturated fatty acid and salt stress in peanut. *Front. Plant Sci.* 9:7. doi: 10.3389/fpls.2018.00007

Tandeau de Marsac, N., and Houmard, J. (1993). Adaptation of cyanobacteria to environmental stimuli: new steps towards molecular mechanisms. *FEMS Microbiol. Rev.* 10, 119–189. doi: 10.1111/j.1574-6968.1993.tb05866.x

Tang, Q., Tan, X. M., and Xu, X. D. (2010). Effects of a type-II RNA-binding protein on fatty acid composition in *Synechocystis* sp. PCC 6803. *Chin. Sci. Bull.* 55, 2416–2421. doi: 10.1007/s11434-010-3254-9

Tester, M., and Davenport, R. (2003). Na? tolerance and Na? transport in higher plants. *Ann. Bot.* 91, 503–527. doi: 10.1093/aob/mcg058

Van Thor, J. J., Jeanjean, R., Havaux, M., Sjollema, K. A., Joset, F., Hellingwerf, K. J., et al. (2000). Salt shock-inducible photosystem I cyclic electron transfer in Synechocystis PCC6803 relies on binding of ferredoxin: NADP(+) reductase to the thylakoidmembranes via its CpcD phycobilisome-linker homologous N-terminal domain. *Biochim. Biophys. Acta* 1457, 129–144. doi: 10.1016/s0005-2728(00)00072-4

Vicente, J. B., Gomes, C. M., Wasserfallen, A., and Teixeira, M. (2002). Module fusion in an A-type flavoprotein from the cyanobacterium Synechocystis condenses a multiple-component pathway in a single polypeptide chain. *Biochem. Biophys. Res. Commun.* 294, 82–87. doi: 10.1016/S0006-291X(02)00434-5

Vothknecht, U. C., Otters, S., Hennig, R., and Schneider, D. (2012). Vipp1: a very important protein in plastids?! *J. Exp. Bot.* 63, 1699–1712. doi: 10.1093/jxb/err357

Wada, N., Sakamoto, T., and Matsugo, S. (2013). Multiple roles of photosynthetic and sunscreen pigments in cyanobacteria focusing on the oxidative stress. *Metabolites* 3, 463–483. doi: 10.3390/metabo3020463

Wang, Y., and Xu, X. D. (2013). Effects of Rbp3 on lipid peroxidation and salt tolerance in *Synechocystis* sp. PCC 6803. *FEBS Lett.* 587, 1446–1451. doi: 10.1016/j.febslet.2013.03.028

Wei, D., Zhang, W., Wang, C., Meng, Q., Li, G., Chen, T. H., et al. (2017). Genetic engineering of the biosynthesis of glycinebetaine leads to alleviate salt-induced potassium efflux and enhances salt tolerance in tomato plants. *Plant Sci.* 257, 74–83. doi: 10.1016/j.plantsci.2017.01.012

Wicke, B., Sikkema, R., Dornburg, V., and Faaij, A. (2011). Exploring land use changes and the role of palm oil production in Indonesia and Malaysia. *Land Use Policy* 28, 193–206. doi: 10.1016/j.landusepol.2010.06.001

Wilson, A., Ajlani, G., Verbavatz, J. M., Vass, I., Kerfeld, C. A., and Kirilovsky, D. (2006). A soluble carotenoid protein involved in phycobilisome-related energy dissipation in cyanobacteria. *Plant Cell* 18, 992–1007. doi: 10.1105/tpc.105.040121

Yang, Y., Yin, C., Li, W., and Xu, X. (2008). Alpha-tocopherol is essential for acquired chill-light tolerance in the cyanobacterium *Synechocystis* sp strain PCC 6803. *J. Bacteriol.* 190, 1554–1560. doi: 10.1128/JB.01577-07

Yang, Z., Li, J. L., Liu, L. N., Xie, Q., and Sui, N. (2020). Photosynthetic regulation under salt stress and salt-tolerance mechanism of sweet sorghum. *Front. Plant Sci.* 10:1722. doi: 10.3389/fpls.2019.01722

Yuan, F., Leng, B. Y., and Wang, B. S. (2016). Progress in studying salt secretion from the salt glands in recretohalophytes: how do plants secrete salt? *Front. Plant Sci.* 7:977. doi: 10.3389/fpls.2016.00977

Yutthanasirikul, R., Nagano, T., Jimbo, H., Hihara, Y., Kanamori, T., Ueda, T., et al. (2016). Oxidation of a cysteine residue in elongation factor EF-Tu reversibly inhibits translation in the cyanobacterium *Synechocystis* sp. PCC 6803. *J. Biol. Chem.* 291, 5860–5870. doi: 10.1074/jbc.M115.706424

Zak, E., Norling, B., Maitra, R., Huang, F., Andersson, B., and Pakrasi, H. B. (2001). The initial steps of biogenesis of cyanobacterial photosystems occur in plasma membranes. *Proc. Natl. Acad. Sci. U.S.A.* 98, 13443–13448. doi: 10.1073/pnas.241503898

Zhang, D., Jiang, S., Pan, J., Kong, X., Zhou, Y., Liu, Y., et al. (2014). The overexpression of a maize mitogen-activated protein kinase gene (Z m MPK 5) confers salt stress tolerance and induces defence responses in tobacco. *Plant Biol.* 16, 558–570. doi: 10.1111/plb.12084

Zhang, Q. Y., Wang, L. Y., Kong, F. Y., Deng, Y. S., Li, B., and Meng, Q. W. (2012). Constitutive accumulation of zeaxanthin in tomato alleviates salt stress-induced photoinhibition and photooxidation. *Physiol. Plant.* 146, 363–373. doi: 10.1111/j.1399-3054.2012.01645.x

Zhao, Y. Q., Ma, Y. C., Duan, H. M., Liu, R. R., and Song, J. (2019). Traits of fatty acid accumulation in dimorphic seeds of the euhalophyte *Suaeda salsa* in saline conditions. *Plant Biosyst.* 153, 514–520. doi: 10.1080/11263504.2018.1508090

Zhu, J. K. (2003). Regulation of ion homeostasis under salt stress. *Curr. Opin. Plant Biol.* 6, 441–445. doi: 10.1016/S1369-5266(03)00085-2

Zhu, Y. H., Graham, J. E., Ludwig, M., Xiong, W., Alvey, R. M., Shen, G. Z., et al. (2010). Roles of xanthophyll carotenoids in protection against photoinhibition and oxidative stress in the cyanobacterium *Synechococcus* sp. strain PCC 7002. *Arch. Biochem. Biophys.* 504, 86–99. doi: 10.1016/j.abb.2010.07.007

Conflict of Interest: The authors declare that the research was conducted in the absence of any commercial or financial relationships that could be construed as a potential conflict of interest.

Copyright © 2020 Yang, Wang, Liu and Sui. This is an open-access article distributed under the terms of the Creative Commons Attribution License (CC BY). The use, distribution or reproduction in other forums is permitted, provided the original author(s) and the copyright owner(s) are credited and that the original publication in this journal is cited, in accordance with accepted academic practice. No use, distribution or reproduction is permitted which does not comply with these terms.

frontiers in Plant Science

ORIGINAL RESEARCH
published: 24 June 2020
doi: 10.3389/fpls.2020.00849

Photobleaching of Chlorophyll in Light-Harvesting Complex II Increases in Lipid Environment

*Mónika Lingvay[1,2], Parveen Akhtar[1], Krisztina Sebők-Nagy[3], Tibor Páli[3] and Petar H. Lambrev[1]**

[1] Institute of Plant Biology, Biological Research Centre, Szeged, Hungary, [2] Doctoral School of Physics, Faculty of Science and Informatics, University of Szeged, Szeged, Hungary, [3] Institute of Biophysics, Biological Research Centre, Szeged, Hungary

Excess light causes damage to the photosynthetic apparatus of plants and algae primarily via reactive oxygen species. Singlet oxygen can be formed by interaction of chlorophyll (Chl) triplet states, especially in the Photosystem II reaction center, with oxygen. Whether Chls in the light-harvesting antenna complexes play direct role in oxidative photodamage is less clear. In this work, light-induced photobleaching of Chls in the major trimeric light-harvesting complex II (LHCII) is investigated in different molecular environments – protein aggregates, embedded in detergent micelles or in reconstituted membranes (proteoliposomes). The effects of intense light treatment were analyzed by absorption and circular dichroism spectroscopy, steady-state and time-resolved fluorescence and EPR spectroscopy. The rate and quantum yield of photobleaching was estimated from the light-induced Chl absorption changes. Photobleaching occurred mainly in Chl *a* and was accompanied by strong fluorescence quenching of the remaining unbleached Chls. The rate of photobleaching increased by 140% when LHCII was embedded in lipid membranes, compared to detergent-solubilized LHCII. Removing oxygen from the medium or adding antioxidants largely suppressed the bleaching, confirming its oxidative mechanism. Singlet oxygen formation was monitored by EPR spectroscopy using spin traps and spin labels to detect singlet oxygen directly and indirectly, respectively. The quantum yield of Chl *a* photobleaching in membranes and detergent was found to be 3.4×10^{-5} and 1.4×10^{-5}, respectively. These values compare well with the yields of ROS production estimated from spin-trap EPR spectroscopy (around 4×10^{-5} and 2×10^{-5}). A kinetic model is proposed, quantifying the generation of Chl and carotenoid triplet states and singlet oxygen. The high quantum yield of photobleaching, especially in the lipid membrane, suggest that direct photodamage of the antenna occurs with rates relevant to photoinhibition *in vivo*. The results represent further evidence that the molecular environment of LHCII has profound impact on its functional characteristics, including, among others, the susceptibility to photodamage.

Keywords: electron paramagnetic resonance, non-photochemical quenching, photoinhibition, photosystem II, reconstituted membranes, singlet oxygen

OPEN ACCESS

Edited by:
Yoshitaka Nishiyama, Saitama University, Japan

Reviewed by:
Seiji Akimoto, Kobe University, Japan
Stefano Santabarbara, National Research Council (CNR), Italy

***Correspondence:**
Petar H. Lambrev
lambrev.petar@brc.hu

Specialty section:
This article was submitted to Plant Physiology, a section of the journal Frontiers in Plant Science

Received: *31 March 2020*
Accepted: *26 May 2020*
Published: *24 June 2020*

Citation:
Lingvay M, Akhtar P, Sebők-Nagy K, Páli T and Lambrev PH (2020) Photobleaching of Chlorophyll in Light-Harvesting Complex II Increases in Lipid Environment. Front. Plant Sci. 11:849. doi: 10.3389/fpls.2020.00849

INTRODUCTION

Plants have to cope with variable light conditions – maintaining efficient light harvesting while avoiding photodamage (Li et al., 2009). Prolonged exposure to excess light causes photoinhibition, that is decrease in photosynthetic activity, followed by chlorosis – bleaching of chlorophylls (Chl) – and ultimately death. The primary site of photoinhibition is PSII (Aro et al., 1993) and the major route of PSII photoinactivation involves ROS, especially singlet oxygen ($^1O_2$), formed by the interaction of molecular oxygen with the Chl triplet (^{3}Chl) states (Triantaphylides et al., 2008; Vass, 2011; Fischer et al., 2013). Most of the Chls are located in the light-harvesting antenna, including the core antenna, CP43 and CP47, and LHCII monomers and trimers (van Amerongen and Croce, 2013). However, it is believed that the antenna has negligible role in the production of ROS because the ^{3}Chl states are effectively quenched by carotenoids (Cars) bound to the complexes (Breton et al., 1979; Sonneveld et al., 1979; Frank and Cogdell, 1996). In contrast, ^{3}Chl states in the PSII RC are readily formed following charge recombination (Vass and Cser, 2009; Vass, 2011) and, because they are relatively far from the nearest Cars, quenching is less efficient. The formation of $^1O_2$ during light exposure of chloroplast thylakoid membranes has been directly followed by spin-trapping EPR spectroscopy and associated with the acceptor-side inhibition of PSII and the D_1 protein degradation (Hideg et al., 1994a,b).

Despite the abundance of Cars, ^{3}Chl have been detected in isolated core antenna (Carbonera et al., 1992b; Groot et al., 1995) and peripheral antenna complexes (Carbonera et al., 1992a; Peterman et al., 1995; Barzda et al., 1998) and found to sensitize the formation of ROS, including $^1O_2$ (Rinalducci et al., 2004). As a result, Chl PB has been observed in native and recombinant LHCII exposed to strong illumination in aerobic conditions (Formaggio et al., 2001; Zhang et al., 2008) and found to depend on the Car composition of the complex (Croce et al., 1999). Mozzo et al. (2008) studied the quenching capacity of individual Cars in LHCII and concluded that about 5% of Chl triplets are not quenched by Cars in contrast to the earlier results (Siefermann-Harms and Ninnemann, 1982; Peterman et al., 1995). Using optical magnetic resonance, Santabarbara et al. (2002a) detected ^{3}Chl in thylakoid membranes generated far from the PSII RC. Together with the observed inefficiency of excitation quenching to protect from the loss of PSII activity and the blue-shifted action spectrum of photoinhibition, they proposed the involvement of weakly coupled Chls in PSII photoinhibition (Santabarbara et al., 2001b, 2002b; Santabarbara, 2006).

When exposed to light, especially in the presence of oxygen, free Chls undergo PB or photomodification by a variety of mechanisms (Bonnett et al., 1999). Cars are also sensitive to oxidative photodamage and appear to be bleached faster than Chls upon irradiation of thylakoid membranes or PSII-enriched membranes (Yamashita and Butler, 1969; Yamashita et al., 1969; Klimov et al., 1990), which in turn accelerates the PB of Chls (Santabarbara, 2006). Also, Chls absorbing at longer wavelengths are bleached before those absorbing at shorter wavelengths (Zucchelli et al., 1988; Miller and Carpentier, 1991). PB of Chl *b* occurs at a much slower rate than Chl *a* – due to fast energy transfer between them (Carpentier et al., 1986; Peterman et al., 1997). These findings point toward the role of antenna Chls in photodamage. Several studies have followed the photodamage in isolated light-harvesting complexes (Zucchelli et al., 1988; Croce et al., 1999; Formaggio et al., 2001; Olszówka et al., 2003; Zhang et al., 2008; Zubik et al., 2011) but a quantitative analysis of the kinetics and quantum yield of pigment PB and its relevance to photoinhibition is lacking.

Not only the pigments but also the apoprotein is vulnerable to degradation by ROS, in addition to the proteolytic degradation of photosynthetic proteins known to occur during photoinhibition (Li et al., 2018). Zolla and Rinalducci (2002) reported the direct photodegradation of LHCII without the involvement of proteases (Rinalducci et al., 2004). Using spin trapping EPR spectroscopy, the group detected the generation of ROS in isolated LHCII upon irradiation with visible light and correlated it with fragmentation of the polypeptide. It was also pointed out that the cleavages take place in the hydrophilic portion of the N-terminal region. On the other hand, the protein secondary structure was not affected by PB of the bound pigments (Olszówka et al., 2003). Zubik et al. (2011) also followed changes in LHCII upon exposure to strong light and postulated the photoisomerization of Cars, particularly neoxanthin.

LHCII is known to have both structural and functional flexibility (Lambrev and Akhtar, 2019). It plays a crucial role in photoprotection by NPQ. The purpose of NPQ is precisely to minimize photodamage of the system by ROS generated under excess light. The reasoning is that when LHCII is in its quenched state, i.e., singlet excitations rapidly decay via thermal deactivation, the formation of ROS and the photodamage should be reduced; however, no quantitative experimental data exists to confirm this. The switch between light-harvesting and energy-dissipating mode involves changes in the molecular and supramolecular structure of the pigment–protein complexes (Ruban, 2016). This may include aggregation or clustering of LHCII (Horton et al., 2005), which is well known to induce strong excitation quenching – both in lipid-free aggregates (Ruban and Horton, 1992, 1994) and in protein-dense reconstituted membranes (Natali et al., 2016; Crisafi and Pandit, 2017; Akhtar et al., 2019). In addition, we have observed characteristic changes in the pigment–protein and protein–protein interactions in LHCII upon changing its molecular environment – in aggregates and reconstituted membranes – some of which are not associated with NPQ (Akhtar et al., 2015). It is not clear how these changes might affect the susceptibility to photodamage.

The aim of this work is to quantify Chl PB in isolated LHCII in different molecular environments – detergent-solubilized LHCII trimers, quenched LHCII-aggregates and reconstituted membranes. The effects of intense light treatment were analyzed

Abbreviations: $^1O_2$, singlet oxygen; 4-oxo-TEMPO, (4-oxo-2,2,6,6-tetramethylpiperidin-1-yl)oxyl; 5-SASL, 5-doxyl-stearic acid spin label; Car, carotenoid; CD, circular dichroism; Chl, chlorophyll; EPR, electron paramagnetic resonance; LHCII, light-harvesting complex II; NPQ, non-photochemical quenching; PAR, photosynthetically active radiation; PB, photobleaching; PFD, photon flux density; PSII, photosystem II; RC, reaction center; ROS, reactive oxygen species; TCSPC, time-correlated single-photon counting; TEMPD × H_2O, 2,2,6,6-tetramethyl-4-piperidone monohydrate; TEMPO, (2,2,6,6-tetramethylpiperidin-1-yl)oxyl; β-DDM, *n*-dodecyl-β-maltoside.

by absorption and CD spectroscopy, steady-state and time-resolved fluorescence, and EPR spectroscopy. One could naively presume that LHCII is more stable in the quenched aggregates but also in lipid membranes, which are closer to the native environment. For example, higher thermostability of the complex has been shown in reconstituted lipid membranes (Yang et al., 2006). On the contrary, the results presented here reveal a markedly increased oxidative PB of Chls when LHCII is in a lipid environment. Further, we estimated the rate and quantum yield of PB of Chl *a*, compared it with the yield of ROS formation detected by EPR spectroscopy and also with predictions from theoretical modeling.

MATERIALS AND METHODS

Preparation of LHCII

LHCII trimers were purified by solubilization of PSII-enriched membrane fragments isolated from 14-days-old greenhouse grown pea (*Pisum sativum*) leaves with 0.7% *n*-dodecyl-β-maltoside (β-DDM, Cube Biotech, Germany) followed by sucrose gradient ultracentrifugation. Reconstituted membranes of LHCII and plant thylakoid lipids (lipid:protein ratio 100:1) were prepared using the protocol described previously (Akhtar et al., 2016). LHCII aggregates were prepared by removal of the detergent from suspension of solubilized complexes with polystyrene adsorbent beads (Bio-Beads SM-2 Resin, Bio-Rad). The Chl and Car contents were determined spectrophotometrically from 80% acetone extracts using molar absorption coefficients from Lichtenthaler (1987) and are presented in **Supplementary Table 1**.

Photooxidation of LHCII Pigments

For the comparative photostability tests, samples were diluted to absorbance of 0.4 at the red maximum and placed in a glass cell of 1-cm optical pathlength. White light from a KL 2500 LED lamp (Schott, Germany) was used for irradiation, with incident PFD on the cuvette of 3000 μmol photons m^{-2} s^{-1} PAR. This PFD is equivalent to an average of ca. 2000 μmol photons m^{-2} s^{-1} in the whole sample volume. For testing the wavelength dependence of PB, the actinic light was passed through either a Schott FS red (630 nm) or a Schott FS blue (525 nm) filter, and the intensity was adjusted to obtain an equal fluorescence emission from the sample. A set of experiments was performed with light from a KL 1500 electronic lamp (Schott, Germany) passed through an SZS–22 glass cutoff filter (580 nm) to an incident PFD of 500 μmol photons m^{-2} s^{-1} PAR.

Absorption, CD and Fluorescence Spectroscopy

Absorption and CD spectra were recorded using an Evolution 500 dual-beam spectrophotometer (Thermo Scientific, United States) and a J-815 (Jasco, Japan) spectropolarimeter in the visible range, at room temperature, with spectral bandwidth of 1.5 nm and 3 nm, respectively. The absorbance of the samples was 0.4 at the red maximum in a 1-cm pathlength cuvette. Synchrotron-radiation UV CD spectra were recorded at the B23 CD beamline of the Diamond synchrotron (United Kingdom). Fluorescence emission spectra in the visible range were measured from the same samples, at room temperature, on a FP-8500 (Jasco, Japan) spectrofluorometer.

Time-Resolved Fluorescence Spectroscopy

Room temperature fluorescence decays were recorded by TCSPC using a FluoTime 200/PicoHarp 300 spectrometer (PicoQuant, Germany) as described elsewhere (Akhtar et al., 2016). A WhiteLase Micro supercontinuum fiber laser (NKT Photonics, United Kingdom) at 20 MHz repetition rate was used to generate excitation pulses. Excitation wavelength of 633 nm was selected by a monochromator, and the pulse energy was attenuated to approximately 0.1 pJ with neutral density filters. Fluorescence photons were detected by a microchannel-plate detector (R3809, Hamamatsu, Japan) and timed with 4-ps resolution. The fluorescence decays were recorded from untreated LHCII samples and after 30 min of light treatment. The samples were placed in a 1.5 mm pathlength quartz cell without further dilution. The total instrument response (IRF) width was ∼50 ps (FWHM), measured using 1% Ludox as scattering solution. The fluorescence lifetimes were determined by multiexponential fitting of the fluorescence decay kinetics combined with iterative reconvolution with the IRF. The average fluorescence lifetime was calculated as $\tau_{av} = \sum_i a_i \tau_i / \sum_i a_i$.

Electron Paramagnetic Resonance Spectroscopy

The principle of the experiments was similar to the one described by Rinalducci et al. (2004). Samples for EPR measurements were prepared under dim light and contained detergent-solubilized LHCII trimers or reconstituted LHCII membranes diluted to 0.1 mg Chl/mL in case of hydrophilic spin label and spin trap, and ca. 0.3 mg Chl/mL in case of lipophilic spin label. 5 μL sample aliquots were added to glass capillaries (with ca. 1 mm internal diameter), which were irradiated for 30 min in the EPR resonator (after tuning the instrument) with the same lamp as above, with PFD of 4800 μmol photons m^{-2} s^{-1} PAR incident on the illumination grid (front window of the resonator), directly during measurements (assuming 50% cut off by the grid and efficient reflection in the resonator (Rinalducci et al., 2004), relative PFD hitting the sample was approximately same as in the optical spectroscopy experiments). Individual scans were started at different time points of irradiation.

Singlet oxygen production upon irradiation was followed in samples with 100 mM TEMPD × H_2O (Fischer et al., 2007). TEMPD × H_2O traps $^1O_2$ resulting in the 4-oxo-TEMPO, which is paramagnetic and hence detectable by EPR. Spectra of dark and light-treated blank sample (only spin trap, no LHCII) were also measured to exclude contributions from or effects by other possible sensitizers from the buffer or impurities of the spin trap.

Indirect measurement of the production of singlet oxygen and other light-induced radicals was performed by following the consumption of spin labels in irradiated samples containing 0.5 mM TEMPO – giving signal only from the aqueous phase –

or 50 μM 5-SASL (spin label:lipid molar ratio = ∼2:100) – giving signal primarily originating from the hydrophobic region of the vesicles/micelles (Kóta et al., 2002). For reference EPR spectra, the stable nitroxide radicals (TEMPO and 5-SASL) were measured in buffer solution at same concentrations as in samples in dark and after 30 min light treatment.

All EPR spectra of the above nitroxide radicals (spin trap adducts and spin labels) were recorded with a Brucker ELEXSYS-II E580 X-band spectrometer at room temperature, with the following instrument settings: microwave frequency of 9.38 GHz; microwave power attenuation of 10 dB (12 dB in case of TEMPO); field modulation of 1 G (3 G in case of 5-SASL); scan range of 100 G, and conversion time of 40.96 s. To obtain the best possible signal-to-noise ratio, spectra in the dark were measured before and after illumination (after 10 min dark incubation), whereby the final spectra were averages of 20, 10, and 4 scans, for 4-oxo-TEMPO, 5-SASL and TEMPO, respectively.

In order to determine the concentration of the nitroxide radicals (the spin labels TEMPO and 5-SASL and the trapping adduct 4-oxo-TEMPO), reference spectra were recorded from samples lacking LHCII using the same instrument settings as for LHCII-containing samples but with known concentrations of spin labels (5-SASL or TEMPO). (It should be noted that the spectrum of TEMPO and 4-oxo-TEMPO are indistinguishable as concerns intensity calibration.) A linear fit to the plot of the integrated EPR absorptions (second integrals of the spectra) versus the known spin label concentrations served as a calibration to calculate nitroxide radical concentrations from the EPR spectra.

Data Analysis

All data processing, statistical analyses and theoretical computations were done in MATLAB using the Spectr-O-Matic toolbox (available at the MATLAB File Exchange) and homebuilt routines.

RESULTS

Photobleaching Kinetics

Photobleaching of Chls in LHCII in different molecular environments was observed by monitoring the changes in absorption in the course of irradiation with intense white light. Absorption spectra of LHCII solubilized with β-DDM and reconstituted lipid membranes before and after 30 min light exposure are shown in **Figure 1**. Upon light illumination a marked decrease in the absorption of Chl *b* and Chl *a* was observed at 652 and 675 nm, respectively, accompanied by similar changes in the Soret region. Across the visible wavelength region, the degree of PB was significantly higher in reconstituted membranes than in detergent solution (β-DDM). Qualitatively the changes are similar in all sample types (for LHCII aggregates, see **Supplementary Figure 1a**). As seen in the difference spectra, the Chl *a* bands at 675, 436 nm undergo the most bleaching, Chl *b* bands 652, 485 nm are less bleached and no appreciable PB of Cars is observed (450, 500 nm).

Figure 2 shows the degree of PB of Chls in LHCII in different molecular environments – in detergent (β-DDM), aggregates and reconstituted membranes during 30 min of irradiation. The bleaching is quantified as the relative irradiation-induced absorption difference $\Delta A/A$. The time courses reinforce the finding that reconstituted membranes are significantly more susceptible to PB than either detergent-solubilized or aggregated LHCII. The transients at 675 and 652 nm, mainly associated with the Q_y transitions of Chl *a* and *b*, respectively, fit well to monoexponential kinetics, especially for the Chl *a* band ($R^2 > 0.99$). This indicates that PB is a (pseudo) first-order process: $\Delta A/A = 1 - e^{-k_{pb}t}$, parametrized by the PB rate constant k_{pb} (Croce et al., 1999).

First-order PB rate constants and the respective quantum yields of PB, φ_{pb}, for LHCII in different environments are shown in **Table 1**. The quantum yield was calculated as the ratio $\varphi_{pb} = k_{pb}/k_{abs}$ with k_{abs} being the absorbed photon flux per Chl (at the beginning of irradiation). The latter was estimated by integrating over the entire wavelength region, taking into account the product of the wavelength-dependent light intensity and absorption cross-section (assuming it does not vary among sample types). The quantum yield φ_{pb} in detergent-solubilized trimers is more than an order of magnitude lower than that of free Chls (Aronoff and Mackinney, 1943) but comparable to the PB of various porphyrins (Spikes, 1992; Bonnett et al., 1999). In LHCII aggregates, prepared by removing the detergent from the medium, the degree of PB was about 20% higher. Even more notably, we found that the PB yield was two- to three-fold higher in reconstituted membranes than in detergent micelles. To test whether PB in membranes is oxygen-dependent, we performed experiments in anoxic environment (continuously bubbling the reaction mixture with N_2 gas) and in the presence of sodium ascorbate as an antioxidant. In both cases the PB was reduced to values comparable with those of detergent-solubilized LHCII (**Table 1**).

A separate set of experiments was conducted on all LHCII sample types listed above with a different light treatment regime – using a tungsten halogen light source through a blue colored-glass filter and an incident PFD of 500 μmol photons m^{-2} s^{-1} (**Supplementary Figure 2**). Under these conditions, PB was substantially slower but qualitatively the results were similar; more importantly, φ_{pb} was comparable as with high-intensity LED irradiation (**Supplementary Table 2**). Further, we performed treatment with red and blue actinic light with intensities adjusted to achieve identical excitation flux. The fluorescence intensity was measured from the sample excited by either red or blue light to confirm the equal absorbed photon flux. The PB rate was identical in both cases (**Supplementary Figure 3**), therefore φ_{pb} is wavelength-independent.

CD Spectral Changes

We employed CD spectroscopy to monitor the structural/conformational changes in LHCII induced by intense irradiation. The CD spectra of complexes in detergent and reconstituted membranes (**Figure 3**) show significant changes both in the Soret as well as the Chl Q_y region; the same

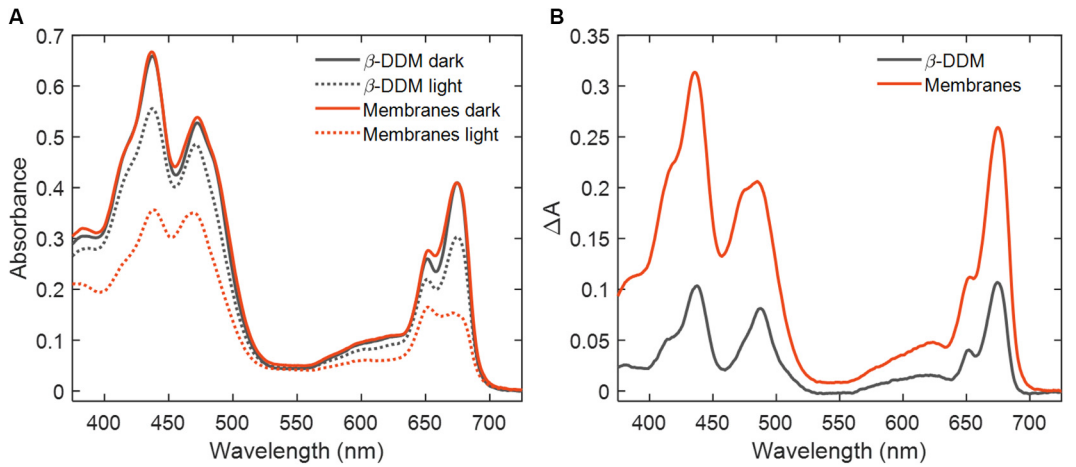

FIGURE 1 | Photobleaching in LHCII. **(A)** Absorption spectra of LHCII solubilized in detergent (β-DDM) and reconstituted membranes before (solid lines) and after 30 min of irradiation (dotted lines). **(B)** Absorption difference spectra (dark–minus–irradiated sample).

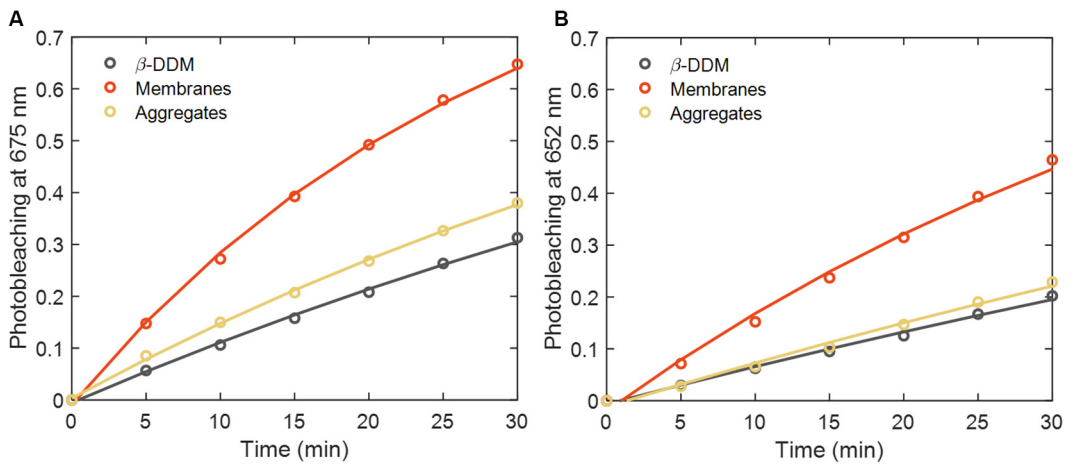

FIGURE 2 | Time course of LHCII photobleaching in detergent (β-DDM), reconstituted membranes and aggregates during 30 min of irradiation (2000 μmol photons m^{-2} s^{-1}). **(A)** Absorbance changes at 675 nm and **(B)** at 652 nm. Circles and lines represent experimental data points and monoexponential fits, respectively.

TABLE 1 | Photobleaching rate constants and quantum yields for LHCII in different environments.

LHCII environment	PB after 30 min $\Delta A_{675}/A_{675}$ (%)	PB rate constant k_{pb} (s^{-1})	Quantum yield φ_{pb}
β-DDM	29 ± 2*	(1.9 ± 0.1) × 10^{-4}	(1.4 ± 0.1) × 10^{-5}
Aggregates	34 ± 2	(2.3 ± 0.2) × 10^{-4}	(1.7 ± 0.1) × 10^{-5}
Reconstituted membranes	54 ± 2	(4.5 ± 0.3) × 10^{-4}	(3.4 ± 0.3) × 10^{-5}
Anoxic	34 ± 5	(2.3 ± 0.4) × 10^{-4}	(1.7 ± 0.3) × 10^{-5}
10 mM Na-ascorbate	32 ± 3	(2.1 ± 0.2) × 10^{-4}	(1.6 ± 0.2) × 10^{-5}
20 mM Na-ascorbate	29 ± 2	(1.8 ± 0.1) × 10^{-4}	(1.3 ± 0.1) × 10^{-5}

**Values represent standard error (n = 3–9).*

applies for LHCII aggregates (**Supplementary Figure 1b**). The CD amplitude in the Chl Q_y region decreased proportionally to the decrease in the absorption (PB) and the shape of the spectra remained unchanged – indicating that the general structure of the pigment–protein complex remains intact even though a large part of the chromophores are lost (Olszówka et al., 2003). In the Soret region, there were additional changes – especially at 494 nm in β-DDM – which were not only caused by the loss of absorbance. This is better illustrated in the spectra of the CD/A ratio (**Supplementary Figure 4**). Significant loss of CD amplitude at these wavelengths occurred already after 15 min of irradiation. The changes could be due to a disruption of excitonic couplings

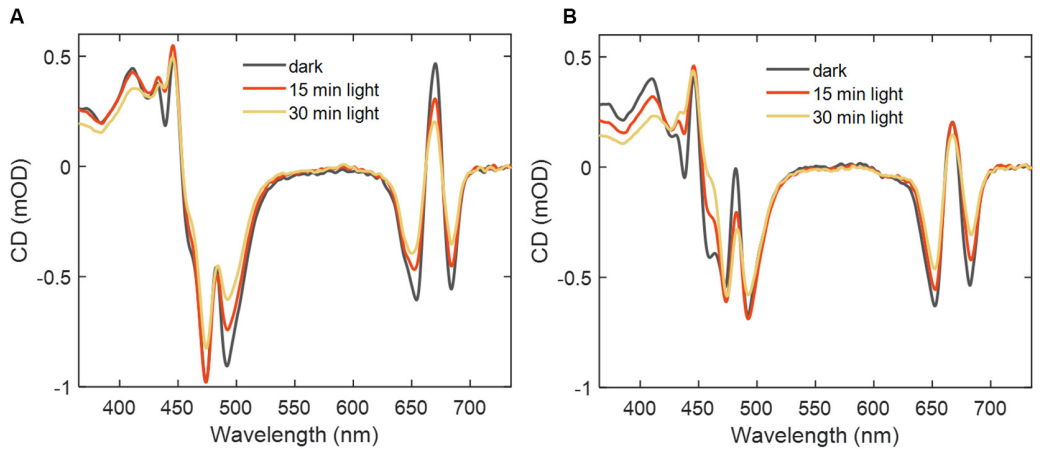

FIGURE 3 | CD spectra of LHCII before, and after 15 and 30 min of irradiation. **(A)** LHCII in detergent (β-DDM) and **(B)** in reconstituted membranes. The spectra correspond to absorbance 0.4 at 675 nm.

between (Chl and Car) transitions in the blue wavelength range or due to changes in the induced CD of Cars. The negative CD bands at 438 and 460 nm in reconstituted membranes and aggregates, which are associated with inter-trimer interactions, rapidly diminished upon irradiation.

Fluorescence Quenching

Room-temperature fluorescence emission spectra of LHCII in detergent micelles and reconstituted membranes recorded with 436 nm excitation before and after 30 min of irradiation are shown in **Figure 4**. The fluorescence emission was strongly reduced compared to the unexposed samples. Even after correcting for the loss of absorption at the excitation wavelength, the fluorescence yield was reduced by a factor of 2.2 in detergent-solubilized LHCII and 5–7 in reconstituted membranes and aggregates. In all sample types, the degree of fluorescence quenching substantially exceeded the PB (loss of absorption), suggesting that irradiation induced non-radiative dissipation in the partially photobleached complexes. Some spectral changes can also be noted. The relative fluorescence intensity in the Chl *b* region (650–660 nm) was enhanced, especially in reconstituted membranes. The shape and width of the main emission band at 680 nm remained almost the same, except for a slight (∼1 nm) red shift of the maximum. The normalized spectra of irradiated reconstituted membranes (**Figure 4B**) as well as aggregates (**Supplementary Figure 5a**) showed enhanced fluorescence emission in the far-red region (700–720 nm).

Further we performed picosecond time-resolved fluorescence measurements of the LHCII samples by TCSPC. The fluorescence recorded at 680 nm after 30 min of irradiation showed an initial phase of rapid decay in all the tested environments (**Supplementary Figures 5b**, **6**), confirming the light-induced quenching observed by steady-state fluorescence. For a quantitative analysis, the fluorescence decay curves were subjected to multiexponential fitting. The resultant decay lifetimes, their relative amplitudes and the average fluorescence lifetimes at 680 nm are shown in **Table 2**. The average lifetime $\tau_{av} = \sum_i a_i\tau_i / \sum_i a_i$ decreased by a factor of 2.3 for detergent-solubilized LHCII, in good agreement with the steady-state fluorescence data, and by a factor of 3–4 for reconstituted membranes and aggregates. The somewhat lower quenching factors estimated from time-resolved fluorescence suggest the presence of fast decay components that are below the time resolution of the measurement.

The fluorescence of LHCII in detergent decayed almost monoexponentially, as it is well known, with a lifetime of 3.8 ns and a very small (5%) contribution from a shorter, 0.8-ns component. After 30 min irradiation, at least two additional shorter decay lifetimes were observed – about 70 and 300 ps – with a combined amplitude of approximately 50%. Similar decay lifetimes (80 and 300 ps) appeared after irradiation of LHCII in reconstituted membranes, in this case having a combined amplitude of 80%, at the expense of the nanosecond decay components. In irradiated aggregates, 80% of the excitations decayed with a lifetime of 60 ps. The absence of blue-shifted emission components in the decay-associated spectra (data not shown) and long lifetimes shows that no free/uncoupled Chls were present in the irradiated samples.

Electron Paramagnetic Resonance

To identify and quantify the ROS formed during irradiation of LHCII, EPR measurements were performed at different intervals after light exposure of samples containing either the spin trap TEMPD or the spin labels TEMPO and 5-SASL. The EPR-silent spin trap 4-oxo-TEMP (TEMPD) converts to the paramagnetic nitroxide radical 4-oxo-TEMPO upon reaction with $^1O_2$ (Lion et al., 1976), yielding a specific EPR spectrum almost identical to that of the TEMPO spin label (Marshall et al., 2011). A dose-dependent EPR signal, typical for 4-oxo-TEMPO, was detected after irradiation of LHCII-containing samples (**Figure 5A**). No signal was observed in samples kept in the dark or after illumination of the spin-label-containing buffer/liposomes without LHCII (data not shown).

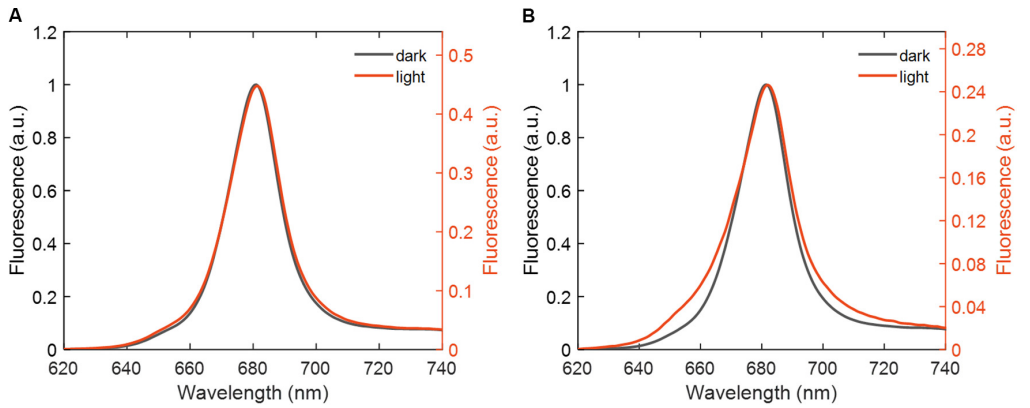

FIGURE 4 | Fluorescence emission spectra of LHCII before and after 30 min irradiation recorded with 436 nm excitation light. **(A)** LHCII in detergent (β-DDM) and **(B)** in reconstituted membranes. Note the separate intensity axes (right side) for irradiated samples.

TABLE 2 | Fluorescence lifetime analysis of LHCII in different environments.

Sample	Irradiation	τ_1 (ns)	a_1 (%)	τ_2 (ns)	a_2 (%)	τ_3 (ns)	a_3 (%)	τ_4 (ns)	a_4 (%)	τ_{av} (ns)
β-DDM	–					0.8	5	3.8	95	3.6
	30 min	0.07	27	0.27	21	1.3	16	3.6	35	1.6
Membranes	–			0.30	16	1.1	60	2.9	24	1.4
	30 min	0.08	44	0.28	35	0.9	17	2.5	4	0.4
Aggregates	–	0.11	61	0.33	33	1.0	6	3.1	1	0.26
	30 min	0.06	81	0.19	18	0.6	2	3.0	0.1	0.10

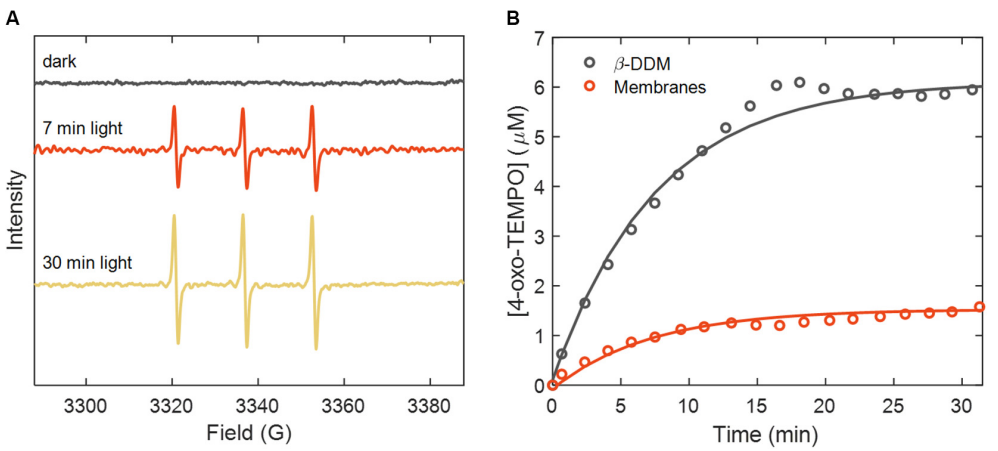

FIGURE 5 | EPR spectra of 4-oxo-TEMPO, generated during illumination of LHCII membranes in the presence of 100 mM 4-oxo-TEMP (TEMPD × H_2O). **(A)** Spectra recorded before and after 7 and 30 min of irradiation of reconstituted membranes. **(B)** Time course of singlet oxygen trapping by 4-oxo-TEMP (TEMPD × H_2O) during 30 min irradiation. Circles and lines represent experimental data points and monoexponential fits, respectively.

The dependence of the 4-oxo-TEMPO concentration on illumination time, estimated from the intensity of the central EPR band, is plotted in **Figure 5B**, along with exponential fits for LHCII in reconstituted membranes and β-DDM. The 4-oxo-TEMPO signal nearly saturated after 30 min irradiation and the total detected concentration was about 4-fold higher (6 μM) in detergent-solubilized LHCII than in reconstituted membranes (1.5 μM). On the other hand, for the initial exponential phase of the curves, the fitted time constant of radical formation was shorter for membranes than detergent (5 vs. 10 min) – thus the initial rate of $^1O_2$ generation was higher in reconstituted membranes.

Figure 6 shows the EPR spectra and illumination time course of samples containing 5-SASL. Stearic acid spin labels, such as 5-SASL, partition between the membrane and the aqueous buffer with very high preference toward membranes. The spectra of thylakoid lipid vesicles, LHCII proteoliposomes as well as of detergent-solubilized LHCII all showed features

typical for 5-SASL in membrane phase (see, e.g., Kóta et al., 2002; Páli and Kóta, 2019), whereas the aqueous-phase EPR signature was less than 1% and could be neglected. 5-SASL can react with various radicals thereby losing its EPR signal, via either one electron oxidation or reduction. As **Figure 6B** shows, after the onset of illumination, the 5-SASL concentration decayed approximately exponentially in both LHCII-containing samples but the rate of quenching was approximately double in reconstituted membranes than in detergent solution. The same result was obtained when using TEMPO instead of 5-SASL (**Supplementary Figure 7**).

DISCUSSION

The Degree of PB Does Not Correlate With the Excited-State Lifetime

The investigation of Chl PB in LHCII presented here confirms earlier observations that the light-harvesting antenna complexes are sensitive to photodamage when they are not coupled to active RCs (Siefermann-Harms, 1990; Zolla and Rinalducci, 2002; Rinalducci et al., 2004; Zhang et al., 2008). The quantum yield of Chl PB, φ_{pb}, ranges between 1×10^{-5} and 4×10^{-5}. A key experimental result is the non-trivial dependence of φ_{pb} on the molecular environment of LHCII. Firstly, higher-order aggregation of LHCII trimers leads to effective quenching of singlet excited states, diminishing the singlet lifetime by a factor of 20 in accord with numerous studies (Horton et al., 1991; Mullineaux et al., 1993; Miloslavina et al., 2008). One would expect a proportional reduction in φ_{pb}, assuming that the photosensitizer agent is Chl*. The results, however, show that φ_{pb} is slightly increased instead. In this sense LHCII aggregation, which is considered as a model of NPQ, does not seem to have a photoprotective effect on LHCII itself, although evidently any quenching mechanism will relieve the excitation pressure on PSII and have a photoprotective role *in vivo*. Lack of expected correlation between the excited-state lifetime and photoinactivation has also been noticed in thylakoid membranes. The loss of PSII activity or D1 degradation showed no or only mild correlation with the excitation quenching induced by spillover or the addition of exogeneous quenchers (Tyystjärvi et al., 1999; Santabarbara et al., 2001a, 2002a). Exogeneous quenchers exerted a modest protection from PB of Chls in light-exposed thylakoids (Santabarbara, 2006). The dose response of both photoinhibition and PB, the lack of a linear relationship, and the blue-shifted action spectrum of photoinhibition led to the suggestion that a small population of antenna complexes in which Chl–Car coupling is impaired, are mainly responsible for ROS generation and photodamage in the thylakoid membranes (Santabarbara et al., 2001b; Santabarbara, 2006). In the following sections we focus on the formation of ^{3}Chl and their quenching by Cars in LHCII.

Perhaps the most striking result of the current investigation is that LHCII in reconstituted membranes is significantly (nearly three-fold) more sensitive to photodamage than either LHCII aggregates or detergent-solubilized trimers. To understand these results, it is demanding to comprehend the specific photochemical mechanisms of photodamage.

Fluorescence Quenchers Are Generated in the Course of PB

Both steady-state and time-resolved fluorescence measurements revealed that the Chl fluorescence yield φ_F and lifetime τ_F are significantly reduced upon irradiation in all types of samples, indicating that PB is associated with the generation of quenchers. Light-induced fluorescence quenching has been known to occur in isolated LHCII and especially in lamellar LHCII aggregates (Jennings et al., 1991; Barzda et al., 1996). Quenching in irradiated LHCII liposomes has been reported by Zubik et al. (2011), who ascribed it to Car photoisomerization and formation of long-lived quencher states, particularly Chl–Car charge-transfer states, owing to the increased absorption and Stark effect around 900 nm. These results are consistent with a more general interpretation that the photoproducts, be it long-lived Chl radicals or other derivates, possibly bilinone analogs (Jose et al., 1990), may act as fluorescence quenchers in the photodamaged complexes. Upon prolonged irradiation this fluorescence quenching might have a self-protecting role; however, further quantitative analysis would be necessary to test this.

Photobleaching Is Caused by Singlet Oxygen Produced by Chl Triplets

Chlorophyll PB in LHCII in reconstituted membranes was effectively suppressed in anaerobic environment (**Table 1**) or by adding ascorbate in aerobic conditions, as has been shown for isolated LHCII (Siefermann-Harms, 1990; Croce et al., 1999), confirming that it is, for the main part, oxidative. The quantum yield φ_{pb} was independent of the intensity and wavelength of the actinic light (**Supplementary Figures 2**, **3** and **Supplementary Table 2**), indicating that the reaction is one-photon and initiated by the lowest-lying singlet-excited state of Chl. Moreover, very little PB of Chl *b* was observed, which is consistent with results on solubilized LHCII (Croce et al., 1999; Olszówka et al., 2003; Zhang et al., 2008) and the fact that Chl *b* transfers energy to Chl *a* on a much shorter timescale than the formation of triplets (Connelly et al., 1997). All these data corroborate that the PB occurs via a type II reaction photosensitized by Chl triplet states (^{3}Chl), which has been thoroughly demonstrated for Chls (Krasnovskii Jr., 1994). Moreover, the sensitizer is Chl *a* as Chl *b* triplets have not been detected in LHCII (Peterman et al., 1997). Presumably, the triplet Chl *a* reacts with molecular oxygen producing singlet oxygen ($^1O_2$) which then attacks the Chl directly or is transformed to another ROS, e.g., a hydroxyl radical.

The formation of $^1O_2$ in reconstituted LHCII membranes was confirmed directly and indirectly by EPR in agreement with the experiments of Zolla and Rinalducci (2002) and Rinalducci et al. (2004). The spin trap 4-oxo-TEMP, directly sensing $^1O_2$, produced 4-oxo-TEMPO radicals only in irradiated samples containing Chl. In principle, the EPR analysis is quantitative,

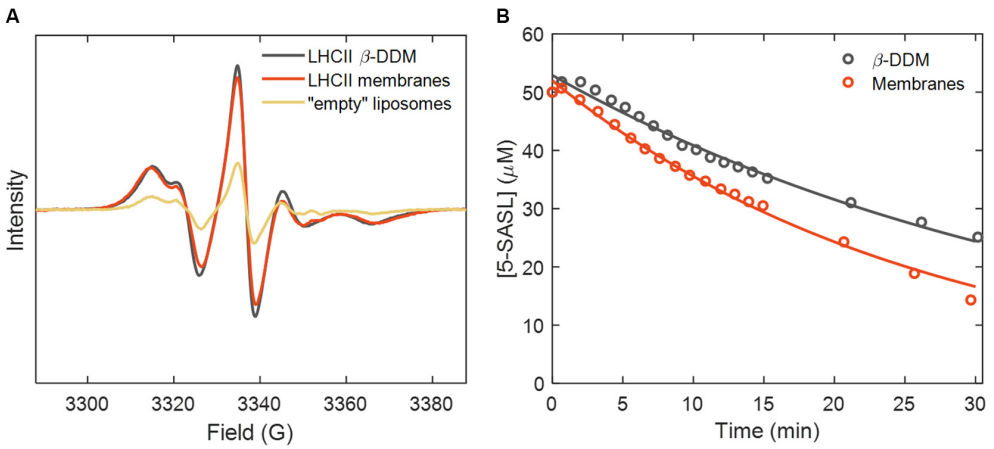

FIGURE 6 | (A) EPR spectra of 5-SASL in detergent micelles and lipid membranes. **(B)** Time course of the 5-SASL concentration estimated from the EPR signal intensity during 30 min of irradiation of the reaction mixture containing LHCII with 50 μM 5-SASL. Circles and lines represent experimental data points and monoexponential fits, respectively.

meaning that we should be able to estimate the $^1O_2$ yield from the time-dependent concentration of the spin labels. However, the hydrate form of 4-oxo-TEMP (TEMPD × H_2O) is water-soluble and partitioned entirely in the aqueous phase whereas $^1O_2$ is produced in the hydrophobic lipid/protein phase. The 4-oxo-TEMPO concentration then depends not only on the rate of $^1O_2$ formation but also on its solubility, diffusion and lifetime in the different phases. For this reason, quantifying the $^1O_2$ yield in different environments is not straightforward. The reaction mixture of LHCII–lipid membranes contains substantial amount of lipids (0.9 mM). The lipids are at the same time solvent for the oxygen and substrate for lipid peroxidation, which may explain why 4-oxo-TEMP reported less overall amount of $^1O_2$ in the reconstituted membranes than in detergent LHCII. On the other hand, the initial rate of 4-oxo-TEMPO formation was higher in reconstituted membranes but the signal saturated at a lower level. This is probably because of heterogeneity of the sample with only a fraction of the LHCII complexes exposed to the spin trap, e.g., those on the outer sheet of multilamellar vesicles.

In contrast to 4-oxo-TEMP, the EPR spectrum of the spin label 5-SASL evidenced its incorporation into the lipid phase (Kóta et al., 2002; Páli and Kóta, 2019) which is the site where ROS are formed (we observe negligible aqueous 5-SASL signal, with sharp lines). In principle, the loss of 5-SASL EPR intensity over time should reflect the ROS produced during irradiation of the samples – 0.06 and 0.11 mol/mol Chl for LHCII in detergent and membranes, respectively, after 30 min. With a large excess of free spin label, we can approximate the kinetics to be first-order with rate constants of 4.3×10^{-4} s^{-1} and 6.3×10^{-4} s^{-1}, respectively. These values correspond to quantum yields of radical formation of 2×10^{-5} (β-DDM) and 4×10^{-5} (lipid membranes), comparing well with φ_{pb}. However, these values must also be taken with caution because in detergent micelles, a large fraction of 5-SASL must be incorporated in micelles that do not contain any LHCII, whereas the majority of lipid vesicles contain more than one LHCII trimer (Tutkus et al., 2018). For a more accurate modeling of the ROS dynamics in such a heterogeneous system, the partitioning and mobility of both the ROS and the spin probe in all phases must be accounted for.

A Kinetic Model of Singlet Oxygen Formation

The rate of the photosensitization reaction is proportional to the concentration of ^{3}Chl states, which in turn depends on the ability of Cars in LHCII to quench ^{3}Chls. Several studies have shown that the triplet–triplet (T–T) energy transfer from Chls to Cars in LHCII occurs with near 100% efficiency (Siefermann-Harms and Ninnemann, 1982; Peterman et al., 1995) – which is the very reason why antenna PB should be negligible in the first place. Even if that is the case, low transient concentration of ^{3}Chl may still generate $^1O_2$. To address this question quantitatively, having in mind the considerations above, we can construct a simplified kinetic model of the PB reaction (**Scheme 1**). The relevant kinetic parameters are the rate constants of Chl singlet and triplet decay, k_D and k_T, intersystem crossing, k_{ISC}, T–T transfer to Cars, k_{T-T}, the sensitization rate constant k_{ox} and the local oxygen concentration $[O_2]$. The ^{3}Chl yield φ_T can be calculated as

$$\varphi_T = \frac{k_{ISC}}{k_D + k_{ISC}}.$$

The rate constant k_{ISC} for Chl *a* is 0.1 ns^{-1} (Bowers and Porter, 1967) and the denominator is equal to the inverse fluorescence lifetime – $(3.8\ ns)^{-1}$ for detergent-solubilized LHCII (**Table 2**). The triplet yield is then $\varphi_T = 0.38$. The $^1O_2$ yield is in turn given by the expression

$$\varphi_{ox} = \varphi_T \frac{k_{ox}[O_2]}{k_{ox}[O_2] + k_T + k_{T-T}}.$$

In anaerobic environment, k_T, which is equal to the inverse triplet lifetime, $k_T = 1/\tau_T$, is vanishingly small, in the range of 1–2.5 ms^{-1} (Peterman et al., 1997; Niedzwiedzki and Blankenship, 2010). The Car quenching rate constant

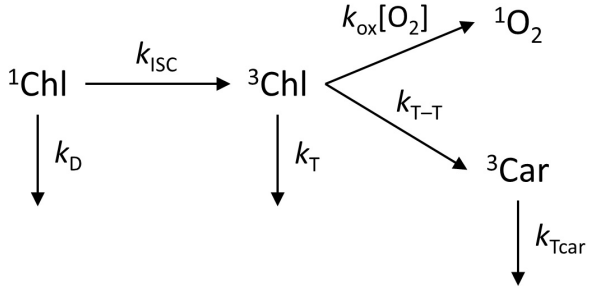

SCHEME 1 | Kinetic scheme of the photosensitization of singlet oxygen in LHCII.

k_{T-T} has been estimated in the range of 2–10 ns^{-1} (Schödel et al., 1998). Finally, for estimating k_{ox} we refer to measurements on free Chl, where we can make use of the relation

$$\tau_T = \frac{1}{k_T + k_{ox}[O_2]} .$$

In aerated organic solvents τ_T is about 0.3 μs (Drzewiecka-Matuszek et al., 2005; Niedzwiedzki et al., 2014). Consequently, $k_{ox} \approx 2 \times 10^9$ M^{-1} s^{-1} (calculating the oxygen concentration in water at 20°C to be 1.4 mM), which is consistent with the values reported for Chl *a* and its derivatives (Mathis and Kleo, 1973; Fiedor et al., 1993).

Using these rate parameters and the equations above, we calculate values of φ_{ox} in the range of 1×10^{-4} to 5×10^{-4}. The time dependence of ^{3}Chl and $^1O_2$ upon Chl excitation, obtained by solving the kinetic model, is given in **Supplementary Figure 8**. The theoretically estimated quantum yield is comparable to the yield of ROS formation reported by EPR (see above). Therefore, the calculations demonstrate that the transient concentration of ^{3}Chl, which decays with the singlet excitation lifetime, is in principle sufficient to generate ample amounts of $^1O_2$ to account for the observed PB ($\varphi_{pb} \approx 10^{-5}$). The calculations also show unequivocally that φ_{ox}, and therefore PB, should be linearly proportional to the fluorescence lifetime. Thus, the rate of PB in reconstituted LHCII membranes and in aggregates should be 3-fold and 20-fold lower, respectively, than in detergent micelles (all other parameters being constant).

Why Is LHCII More Susceptible to PB in Lipid Membranes?

The observed variation of φ_{pb} with the molecular environment can be explained with variations in either the rates k_{ISC}, k_{T-T}, or $k_{ox}[O_2]$ in the kinetic model discussed above. In principle, all of these are possible. Both φ_T and τ_T are shown to depend on the solvent environment (Hurley et al., 1980). The quenching of ^{3}Chl by Cars strongly depends on the arrangement of the pigments in the complex, with an exponential dependence on the distance between them, stemming from the Dexter exchange transfer mechanism (Siefermann-Harms, 1987). Comparatively small structural alterations, for example induced by increasing the detergent concentration, can affect the energetic coupling between pigments, reducing k_{T-T}, and in turn raising the ^{3}Chl yield (Naqvi et al., 1999). The CD spectra of LHCII, especially in the Cars region, indicate that such conformational changes occur upon aggregation and in the lipid environment (Akhtar et al., 2015). From the kinetic model it follows that a two-fold reduction in k_{T-T} will result in a corresponding two-fold increase in φ_{ox}. It may also be speculated that some Cars are destabilized or missing in the artificial reconstituted membranes; however, this seems unlikely because we do not detect a significant change in the pigment composition (**Supplementary Table 1**). Moreover, the primary quenchers of the terminal emitter Chl *a* are luteins (Dall'Osto et al., 2006) and their loss would result in protein unfolding (Formaggio et al., 2001), which has not been detected in the UV-CD of irradiated samples in our experiments (data not shown) or in previous studies (Olszówka et al., 2003). While photodegradation of the LHCII apoprotein does occur, it only involves the N-terminus (Zolla and Rinalducci, 2002).

Another potential factor affecting φ_{ox}, and hence φ_{pb} is the local O_2 concentration or the O_2 accessibility to the site of ^{3}Chl formation. This may well be a leading cause for the enhanced photosensitivity of LHCII in lipid membranes, as it has been shown that the lipid/water partitioning factor of O_2 in phospholipid liposomes and lipoproteins is up to 4, particularly in the liquid crystalline phase (Möller et al., 2005, 2016). If the O_2 concentration is higher in the vicinity of the LHCII pigments, that will also affect the Chl and Car triplet lifetimes. Careful comparison of the triplet lifetimes in LHCII in different environments might be useful to test this hypothesis.

Finally, we must consider that PB may also be indirectly caused by ROS generated in a radical chain reaction, for example by alkoxyl radicals. In that case, lipids and lipid peroxidation products may act as secondary sensitizers for the PB. In support of this, we have been able to detect, although semi-quantitatively, lipid peroxidation products in light-exposed LHCII liposomes via a malondialdehyde–thiobarbituric acid reactivity assay (data not shown). However, we did not observe significant photoprotective effect of adding α-tocopherol to the reaction mixture, in agreement with results on solubilized LHCII (Siefermann-Harms, 1990), suggesting that alcoxyl radicals are not a dominant trigger of Chl PB in the liposomes. Whether lipid peroxidation is actually involved in the photodegradation of Chls is purely a speculation but in either case our results point to an intrinsic volatility of the lipid environment with respect to photodamage that must not be overlooked. Neither the local O_2 concentration, nor lipid peroxidation readily explain the differences, or lack thereof, between the Chl PB in detergent-solubilized and aggregated LHCII. Therefore, we tend to assume that the PB dependency on the environment is due to a combination of several factors discussed above.

Is Chl PB in LHCII Relevant to Photoinhibition *in vivo*?

So far it remains unclear whether direct photodegradation of the antenna has a significant role in photoinhibition

in vivo. In comparison to the values of φ_{pb} obtained here, photoinhibition of PSII occurs with a significantly lower quantum yield, in the order of 10^{-7} (Campbell and Tyystjärvi, 2012). In active PSII, LHCII excitations are rapidly transferred to the RC and quenched by photochemistry, so the PB in the functionally connected antenna will be far less than in the isolated complexes. However, if the RCs are closed, which can be the case under prolonged excess light conditions, this photoprotective route is unavailable (Lambrev et al., 2012; Ruban, 2016). Then, considering that $\sim 10^2$ antenna Chls are connected to one PSII RC, we can expect that the rates of direct PB of antenna Chls and PSII photoinhibition will have the same order of magnitude. In native thylakoids subjected to photoinhibitory treatment, the rate of $^1O_2$ production declined by about half after the complete loss of oxygen evolution (Hideg et al., 1994b). Taken together with a report of no appreciable formation of $^1O_2$ by Photosystem I (Hideg and Vass, 1995), this invites the hypothesis that the excess $^1O_2$ is produced by the PSII antenna. However, the same authors found no $^1O_2$ formation in thylakoids upon donor-side inactivation of PSII electron transport (Hideg et al., 1994a), which either invalidates the antenna hypothesis, or it must be assumed that the oxidized RC radical, $P_{680}{}^+$, prevents the accumulation of $^1O_2$ (for example via efficient quenching).

Pigment PB associated with photoinhibition in thylakoid membranes and PSII-enriched membranes has been experimentally shown in several studies (Yamashita and Butler, 1969; Yamashita et al., 1969; Carpentier et al., 1986; Zucchelli et al., 1988; Miller and Carpentier, 1991). The PB kinetics and the sensitivity of the different pigment pools, however, appear to be markedly different in these systems compared to isolated antenna complexes. In thylakoid membranes, Cars were found to be the primary target of the photooxidation reactions (Yamashita and Butler, 1969; Yamashita et al., 1969). Cars were also the main photobleached pigments in PSII-enriched membranes lacking manganese (Klimov et al., 1990) and in the D_1–D_2–Cyt b_{559} complex (Telfer et al., 1991). In a more recent study, Santabarbara (2006) found that PB in thylakoid membranes occurred in two distinct phases – a slow initial phase, during which Cars were bleached at a rate three times higher than Chl *a*, followed by a second phase marked by rapid PB of Chls – evidently because the protective role of Cars was eliminated. These results indicate that Chl PB is a late event in photoinhibition in native thylakoid membranes and a consequence of the disruption of T–T transfer from Chl to Cars. As we do not observe substantial bleaching of Cars in isolated LHCII, similar to other results (Siefermann-Harms, 1990), it could then be postulated that T–T transfer is disrupted in the isolated antenna complexes, making the Chls more susceptible to PB (Naqvi et al., 1999). According to the kinetic model, isolated LHCII should be capable of producing enough $^1O_2$ to explain the observed Chl PB. Obviously, there is no guarantee that the model holds *in vivo*, which again exemplifies the caveats of *in vitro* experiments with a flexible protein complex such as LHCII, which is sensitive to its molecular environment (Akhtar et al., 2015).

CONCLUSION

In this work, we have shown that light exposure of isolated LHCII causes oxidative PB of Chl *a* with a quantum yield of 1×10^{-5} to 4×10^{-5}, which indicates that in excess light conditions, when the PSII RCs are predominantly closed, direct photodamage of the antenna could occur with rates comparable to the PSII RC photoinactivation. The sensitivity to photodamage depends on the molecular environment of the complex, such that PB is significantly exacerbated in reconstituted lipid membranes. Quantitative EPR spectroscopy analysis using spin labels confirms the increased light-induced generation of $^1O_2$ in the membranes. This is probably a combined effect of the solubility and diffusion of oxygen and other factors modifying the ultimate fate of the excitation energy. Regardless of what the exact underlying cause is, the increased PB susceptibility of LHCII in lipid membranes is potentially of great significance considering that this is the native environment for the majority of photosynthetic pigment–protein complexes. As direct photosensitization of ROS by the light-harvesting complexes is not negligible, ROS must be effectively scavenged in the membrane to avoid photodamage.

DATA AVAILABILITY STATEMENT

The generated datasets for this study (absorption, CD, fluorescence and EPR spectra) can be found online in the Mendeley Data repository (Lingvay et al., 2020).

AUTHOR CONTRIBUTIONS

PL designed the experiments. ML and PA isolated LHCII, prepared reconstituted membranes, and performed optical spectroscopy measurements. ML, KS-N, and TP performed EPR measurements. ML performed data analysis. PA and PL did theoretical modeling. The manuscript was written through contributions of all authors. All authors have given approval to the final version of the manuscript.

FUNDING

The work was supported by grants from the Hungarian Ministry for National Economy (GINOP-2.3.2-15-2016-00001) and the National Research, Development and Innovation Fund (NKFI NN-124904, 2018-1.2.1-NKP-2018-00009 to PL and K-112716 to TP). CD measurements at the B23 beamline of the Diamond Light Source Ltd. (session 17698) were supported by the

project CALIPSOplus under Grant Agreement 730872 from the EU Framework Programme for Research and Innovation HORIZON 2020. ML was supported by the ÚNKP-17-3 New National Excellence Program of the Hungarian Ministry of Human Capacities.

SUPPLEMENTARY MATERIAL

The Supplementary Material for this article can be found online at: https://www.frontiersin.org/articles/10.3389/fpls.2020.00849/full#supplementary-material

REFERENCES

Akhtar, P., Dorogi, M., Pawlak, K., Kovács, L., Bóta, A., Kiss, T., et al. (2015). Pigment interactions in light-harvesting complex II in different molecular environments. *J. Biol. Chem.* 290, 4877–4886. doi: 10.1074/jbc.M114.607770

Akhtar, P., Görföl, F., Garab, G., and Lambrev, P. H. (2019). Dependence of chlorophyll fluorescence quenching on the lipid-to-protein ratio in reconstituted light-harvesting complex II membranes containing lipid labels. *Chem. Phys.* 522, 242–248. doi: 10.1016/j.chemphys.2019.03.012

Akhtar, P., Lingvay, M., Kiss, T., Deák, R., Bóta, A., Ughy, B., et al. (2016). Excitation energy transfer between light-harvesting complex II and photosystem I in reconstituted membranes. *Biochim. Biophys. Acta* 1857, 462–472. doi: 10.1016/j.bbabio.2016.01.016

Aro, E.-M., Virgin, I., and Andersson, B. (1993). Photoinhibition of photosystem II. Inactivation, protein damage and turnover. *Biochim. Biophys. Acta Bioenerget.* 1143, 113–134. doi: 10.1016/0005-2728(93)90134-2

Aronoff, S., and Mackinney, G. (1943). The photo-oxidation of chlorophyll. *J. Am. Chem. Soc.* 65, 956–958. doi: 10.1021/ja01245a052

Barzda, V., Istokovics, A., Simidjiev, I., and Garab, G. (1996). Structural flexibility of chiral macroaggregates of light-harvesting chlorophyll a/b pigment-protein complexes. Light-induced reversible structural changes associated with energy dissipation. *Biochemistry* 35, 8981–8985. doi: 10.1021/bi960114g

Barzda, V., Peterman, E. J. G., van Grondelle, R., and van Amerongen, H. (1998). The influence of aggregation on triplet formation in light-harvesting chlorophyll *a/b* pigment-protein complex II of green plants. *Biochemistry* 37, 546–551. doi: 10.1021/bi972123a

Bonnett, R., Djelal, B. D., Hamilton, P. A., Martinez, G., and Wierrani, F. (1999). Photobleaching of 5, 10, 15, 20-tetrakis (m-hydroxyphenyl) porphyrin (m-THPP) and the corresponding chlorin (m-THPC) and bacteriochlorin (m-THPBC). A comparative study. *J. Photochem. Photobiol. B Biol.* 53, 136–143. doi: 10.1016/s1011-1344(99)00139-6

Bowers, P., and Porter, G. (1967). Quantum yields of triplet formation in solutions of chlorophyll. *Proc. R. Soc. Lond. Ser. A Math. Phys. Sci.* 296, 435–441. doi: 10.1098/rspa.1967.0036

Breton, J., Geacintov, N. E., and Swenberg, C. E. (1979). Quenching of fluorescence by triplet excited states in chloroplasts. *Biochim. Biophys. Acta* 548, 616–635. doi: 10.1016/0005-2728(79)90069-0

Campbell, D. A., and Tyystjärvi, E. (2012). Parameterization of photosystem II photoinactivation and repair. *Biochim. Biophys. Acta* 1817, 258–265. doi: 10.1016/j.bbabio.2011.04.010

Carbonera, D., Giacometti, G., and Agostini, G. (1992a). FDMR of carotenoid and chlorophyll triplets in light-harvesting complex LHCII of spinach. *Appl. Magn. Reson.* 3, 859–872. doi: 10.1007/bf03260117

Carbonera, D., Giacometti, G., Agostini, G., Angerhofer, A., and Aust, V. (1992b). ODMR of carotenoid and chlorophyll triplets in CP43 and CP47 complexes of spinach. *Chem. Phys. Lett.* 194, 275–281. doi: 10.1016/0009-2614(92)86051-i

Carpentier, R., Leblanc, R. M., and Bellemare, G. (1986). Chlorophyll photobleaching in pigment-protein complexes. *Zeitschrift Naturforschung C* 41, 284–290. doi: 10.1515/znc-1986-0307

Connelly, J. P., Müller, M. G., Hucke, M., Gatzen, G., Mullineaux, C. W., Ruban, A. V., et al. (1997). Ultrafast spectroscopy of trimeric light-harvesting complex II from higher plants. *J. Phys. Chem. B* 101, 1902–1909. doi: 10.1021/jp9619651

Crisafi, E., and Pandit, A. (2017). Disentangling protein and lipid interactions that control a molecular switch in photosynthetic light harvesting. *Biochim. Biophys. Acta* 1859, 40–47. doi: 10.1016/j.bbamem.2016.10.010

Croce, R., Weiss, S., and Bassi, R. (1999). Carotenoid-binding sites of the major light-harvesting complex II of higher plants. *J. Biol. Chem.* 274, 29613–29623. doi: 10.1074/jbc.274.42.29613

Dall'Osto, L., Lico, C., Alric, J., Giuliano, G., Havaux, M., and Bassi, R. (2006). Lutein is needed for efficient chlorophyll triplet quenching in the major LHCII antenna complex of higher plants and effective photoprotection in vivounder strong light. *BMC Plant Biol.* 6:32. doi: 10.1186/1471-2229-6-32

Drzewiecka-Matuszek, A., Skalna, A., Karocki, A., Stochel, G., and Fiedor, L. (2005). Effects of heavy central metal on the ground and excited states of chlorophyll. *JBIC J. Biol. Inorgan. Chem.* 10, 453–462. doi: 10.1007/s00775-005-0652-6

Fiedor, L., Gorman, A. A., Hamblett, I., Rosenbach-Belkin, V., Salomon, Y., Scherz, A., et al. (1993). A pulsed laser and pulse radiolysis study of amphiphilic chlorophyll derivatives with PDT activity toward malignant melanoma. *Photochem. Photobiol.* 58, 506–511. doi: 10.1111/j.1751-1097.1993.tb04922.x

Fischer, B. B., Hideg, E., and Krieger-Liszkay, A. (2013). Production, detection, and signaling of singlet oxygen in photosynthetic organisms. *Antioxid. Redox Signal.* 18, 2145–2162. doi: 10.1089/ars.2012.5124

Fischer, B. B., Krieger-Liszkay, A., Hideg, É, Šnyrychová, I., Wiesendanger, M., and Eggen, R. I. L. (2007). Role of singlet oxygen in chloroplast to nucleus retrograde signaling in *Chlamydomonas reinhardtii*. *FEBS Lett.* 581, 5555–5560. doi: 10.1016/j.febslet.2007.11.003

Formaggio, E., Cinque, G., and Bassi, R. (2001). Functional architecture of the major light-harvesting complex from higher plants. *J. Mol. Biol.* 314, 1157–1166. doi: 10.1006/jmbi.2000.5179

Frank, H. A., and Cogdell, R. J. (1996). Carotenoids in photosynthesis. *Photochem. Photobiol.* 63, 257–264. doi: 10.1111/j.1751-1097.1996.tb03022.x

Groot, M.-L., Peterman, E., Van Stokkum, I., Dekker, J. P., and van Grondelle, R. (1995). Triplet and fluorescing states of the CP47 antenna complex of photosystem II studied as a function of temperature. *Biophys. J.* 68, 281–290. doi: 10.1016/s0006-3495(95)80186-4

Hideg, É, Spetea, C., and Vass, I. (1994a). Singlet oxygen and free radical production during acceptor-and donor-side-induced photoinhibition: studies with spin trapping EPR spectroscopy. *Biochim. Biophys. Acta* 1186, 143–152. doi: 10.1016/0005-2728(94)90173-2

Hideg, É, Spetea, C., and Vass, I. (1994b). Singlet oxygen production in thylakoid membranes during photoinhibition as detected by EPR spectroscopy. *Photosynth. Res.* 39, 191–199. doi: 10.1007/bf00029386

Hideg, É, and Vass, I. (1995). Singlet oxygen is not produced in photosystem I under photoinhibitory conditions. *Photochem. Photobiol.* 62, 949–952. doi: 10.1111/j.1751-1097.1995.tb09162.x

Horton, P., Ruban, A. V., Rees, D., Pascal, A. A., Noctor, G., and Young, A. J. (1991). Control of the light-harvesting function of chloroplast membranes by aggregation of the LHCII chlorophyll protein complex. *FEBS Lett.* 292, 1–4. doi: 10.1016/0014-5793(91)80819-o

Horton, P., Wentworth, M., and Ruban, A. (2005). Control of the light harvesting function of chloroplast membranes: the LHCII-aggregation model for non-photochemical quenching. *FEBS Lett.* 579, 4201–4206. doi: 10.1016/j.febslet.2005.07.003

Hurley, J. K., Castelli, F., and Tollin, G. (1980). Chlorophyll photochemistry in condensed media—II. Triplet state quenching and electron transfer to quinone in liposomes. *Photochem. Photobiol.* 32, 79–86. doi: 10.1111/j.1751-1097.1980.tb03989.x

Jennings, R. C., Garlaschi, F. M., and Zucchelli, G. (1991). Light-induced fluorescence quenching in the light-harvesting chlorophyll *a/b* protein complex. *Photosynth. Res.* 27, 57–64. doi: 10.1007/bf00029976

Jose, A., Maria, G., and Michael, J. (1990). The photo-oxidation of meso-tetraphenylporphyrins. *J. Chem. Soc. Perkin Trans.* 1, 1937–1943.

Klimov, V., Shafiev, M., and Allakhverdiev, S. (1990). Photoinactivation of the reactivation capacity of photosystem II in pea subchloroplast particles after a complete removal of manganese. *Photosynth. Res.* 23, 59–65. doi: 10.1007/bf00030063

Kóta, Z., Horváth, L. I., Droppa, M., Horváth, G., Farkas, T., and Páli, T. (2002). Protein assembly and heat stability in developing thylakoid membranes during

greening. *Proc. Natl. Acad. Sci. U.S.A.* 99, 12149–12154. doi: 10.1073/pnas.192463899

Krasnovskii, A. Jr. (1994). Singlet molecular oxygen: mechanisms of formation and paths of deactivation in photosynthetic systems. *Biofizika* 39, 236–250.

Lambrev, P. H., and Akhtar, P. (2019). Macroorganisation and flexibility of thylakoid membranes. *Biochem. J.* 476, 2981–3018. doi: 10.1042/bcj20190080

Lambrev, P. H., Miloslavina, Y., Jahns, P., and Holzwarth, A. R. (2012). On the relationship between non-photochemical quenching and photoprotection of photosystem II. *Biochim. Biophys. Acta* 1817, 760–769. doi: 10.1016/j.bbabio.2012.02.002

Li, L., Aro, E.-M., and Millar, A. H. (2018). Mechanisms of Photodamage and Protein Turnover in Photoinhibition. *Trends Plant Sci.* 23, 667–676. doi: 10.1016/j.tplants.2018.05.004

Li, Z., Wakao, S., Fischer, B. B., and Niyogi, K. K. (2009). Sensing and responding to excess light. *Annu. Rev. Plant Biol.* 60, 239–260. doi: 10.1146/annurev.arplant.58.032806.103844

Lichtenthaler, H. K. (1987). Chlorophylls and carotenoids: pigments of photosynthetic biomembranes. *Methods Enzymol.* 148, 350–382. doi: 10.1016/0076-6879(87)48036-1

Lingvay, M., Akhtar, P., Sebők-Nagy, K., Páli, T., and Lambrev, P. (2020). Photobleaching of chlorophyll in light-harvesting complex II. *Mendeley Data*, V1. doi: 10.17632/fp3798tnhw.1

Lion, Y., Delmelle, M., and Van de Vorst, A. (1976). New method of detecting singlet oxygen production. *Nature* 263, 442–443. doi: 10.1038/263442a0

Marshall, D. L., Christian, M. L., Gryn'ova, G., Coote, M. L., Barker, P. J., and Blanksby, S. J. (2011). Oxidation of 4-substituted TEMPO derivatives reveals modifications at the 1-and 4-positions. *Organ. Biomol. Chem.* 9, 4936–4947. doi: 10.1039/c1ob05037k

Mathis, P., and Kleo, J. (1973). The triplet state of β-carotene and of analog polyenes of different length. *Photochem. Photobiol.* 18, 343–346. doi: 10.1111/j.1751-1097.1973.tb06431.x

Miller, N., and Carpentier, R. (1991). Energy dissipation and photoprotection mechanisms during chlorophyll photobleaching in thylakoid membranes. *Photochem. Photobiol.* 54, 465–472. doi: 10.1111/j.1751-1097.1991.tb02042.x

Miloslavina, Y., Wehner, A., Wientjes, E., Reus, M., Lambrev, P., Garab, G., et al. (2008). Far-red fluorescence: a direct spectroscopic marker for LHCII oligomers forming in non-photochemical quenching. *FEBS Lett.* 582, 3625–3631. doi: 10.1016/j.febslet.2008.09.044

Möller, M., Botti, H., Batthyany, C., Rubbo, H., Radi, R., and Denicola, A. (2005). Direct measurement of nitric oxide and oxygen partitioning into liposomes and low density lipoprotein. *J. Biol. Chem.* 280, 8850–8854. doi: 10.1074/jbc.m413699200

Möller, M. N., Li, Q., Chinnaraj, M., Cheung, H. C., Lancaster, J. R. Jr., and Denicola, A. (2016). Solubility and diffusion of oxygen in phospholipid membranes. *Biochim. Biophys. Acta* 1858, 2923–2930. doi: 10.1016/j.bbamem.2016.09.003

Mozzo, M., Dall'Osto, L., Hienerwadel, R., Bassi, R., and Croce, R. (2008). Photoprotection in the antenna complexes of photosystem II Role of individual xanthophylls in chlorophyll triplet quenching. *J. Biol. Chem.* 283, 6184–6192. doi: 10.1074/jbc.m708961200

Mullineaux, C. W., Pascal, A. A., Horton, P., and Holzwarth, A. R. (1993). Excitation-energy quenching in aggregates of the LHC II chlorophyll-protein complex: a time-resolved fluorescence study. *Biochim. Biophys. Acta* 1141, 23–28. doi: 10.1016/0005-2728(93)90184-h

Naqvi, K. R., Jávorfi, T., Melo, T. B., and Garab, G. (1999). More on the catalysis of internal conversion in chlorophyll a by an adjacent carotenoid in light-harvesting complex (Chl a/b LHCII) of higher plants: time-resolved triplet-minus-singlet spectra of detergent-perturbed complexes. *Spectrochim. Acta A* 55, 193–204. doi: 10.1016/s1386-1425(98)00179-6

Natali, A., Gruber, J. M., Dietzel, L., Stuart, M. C., van Grondelle, R., and Croce, R. (2016). Light-harvesting complexes (LHCs) cluster spontaneously in membrane environment leading to shortening of their excited state lifetimes. *J. Biol. Chem.* 291, 16730–16739. doi: 10.1074/jbc.m116.730101

Niedzwiedzki, D. M., and Blankenship, R. E. (2010). Singlet and triplet excited state properties of natural chlorophylls and bacteriochlorophylls. *Photosynth. Res.* 106, 227–238. doi: 10.1007/s11120-010-9598-9

Niedzwiedzki, D. M., Jiang, J., Lo, C. S., and Blankenship, R. E. (2014). Spectroscopic properties of the chlorophyll *a*–chlorophyll *c*2–peridinin-protein-complex (acpPC) from the coral symbiotic dinoflagellate symbiodinium. *Photosynth. Res.* 120, 125–139. doi: 10.1007/s11120-013-9794-5

Olszówka, D., Maksymiec, W., Krupa, Z., and Krawczyk, S. (2003). Spectral analysis of pigment photobleaching in photosynthetic antenna complex LHCIIb. *J. Photochem. Photobiol. B Biol.* 70, 21–30. doi: 10.1016/s1011-1344(03)00037-x

Páli, T., and Kóta, Z. (2019). "Studying lipid–protein interactions with electron paramagnetic resonance spectroscopy of spin-labeled lipids," in *Lipid-Protein Interactions*, 2nd Edn, ed. J. H. Kleinschmidt (Humana, NY: Springer), 529–561. doi: 10.1007/978-1-4939-9512-7_22

Peterman, E., Dukker, F. M., van Grondelle, R., and van Amerongen, H. (1995). Chlorophyll *a* and carotenoid triplet states in light-harvesting complex II of higher plants. *Biophys. J.* 69, 2670–2678. doi: 10.1016/S0006-3495(95)80138-4

Peterman, E. J., Gradinaru, C. C., Calkoen, F., Borst, J. C., Van Grondelle, R., and Van Amerongen, H. (1997). Xanthophylls in light-harvesting complex II of higher plants: light harvesting and triplet quenching. *Biochemistry* 36, 12208–12215. doi: 10.1021/bi9711689

Rinalducci, S., Pedersen, J. Z., and Zolla, L. (2004). Formation of radicals from singlet oxygen produced during photoinhibition of isolated light-harvesting proteins of photosystem II. *Biochim. Biophys. Acta* 1608, 63–73. doi: 10.1016/j.bbabio.2003.10.009

Ruban, A. V. (2016). Nonphotochemical chlorophyll fluorescence quenching: mechanism and effectiveness in protecting plants from photodamage. *Plant Physiol.* 170, 1903–1916. doi: 10.1104/pp.15.01935

Ruban, A. V., and Horton, P. (1992). Mechanism of ΔpH-dependent dissipation of absorbed excitation-energy by photosynthetic membranes. 1. Spectroscopic analysis of isolated light-harvesting complexes. *Biochim. Biophys. Acta* 1102, 30–38. doi: 10.1016/0005-2728(92)90061-6

Ruban, A. V., and Horton, P. (1994). Spectroscopy of non-photochemical and photochemical quenching of chlorophyll fluorescence in leaves; evidence for a role of the light harvesting complex of photosystem II in the regulation of energy dissipation. *Photosynth. Res.* 40, 181–190. doi: 10.1007/BF00019335

Santabarbara, S. (2006). Limited sensitivity of pigment photo-oxidation in isolated thylakoids to singlet excited state quenching in photosystem II antenna. *Arch. Biochem. Biophys.* 455, 77–88. doi: 10.1016/j.abb.2006.08.017

Santabarbara, S., Barbato, R., Zucchelli, G., Garlaschi, F., and Jennings, R. (2001a). The quenching of photosystem II fluorescence does not protect the D1 protein against light induced degradation in thylakoids. *FEBS Lett.* 505, 159–162. doi: 10.1016/S0014-5793(01)02796-X

Santabarbara, S., Bordignon, E., Jennings, R. C., and Carbonera, D. (2002a). Chlorophyll triplet states associated with photosystem II of thylakoids. *Biochemistry* 41, 8184–8194. doi: 10.1021/bi0201163

Santabarbara, S., Cazzalini, I., Rivadossi, A., Garlaschi, F. M., Zucchelli, G., and Jennings, R. C. (2002b). Photoinhibition *in vivo* and *in vitro* involves weakly coupled chlorophyll–protein complexes. *Photochem. Photobiol.* 75, 613–618. doi: 10.1562/0031-8655(2002)0750613PIVAIV2.0.CO2

Santabarbara, S., Neverov, K., Garlaschi, F., Zucchelli, G., and Jennings, R. (2001b). Involvement of uncoupled antenna chlorophylls in photoinhibition in thylakoids. *FEBS Lett.* 491, 109–113. doi: 10.1016/S0014-5793(01)02174-3

Schödel, R., Irrgang, K.-D., Voigt, J., and Renger, G. (1998). Rate of carotenoid triplet formation in solubilized light-harvesting complex II (LHCII) from spinach. *Biophys. J.* 75, 3143–3153. doi: 10.1016/S0006-3495(98)77756-2

Siefermann-Harms, D. (1987). The light-harvesting and protective functions of carotenoids in photosynthetic membranes. *Physiol. Plant.* 69, 561–568. doi: 10.1111/j.1399-3054.1987.tb09240.x

Siefermann-Harms, D. (1990). Protective function of the apoprotein of the light-harvesting chlorophyll-*a*/*b*—protein complex in pigment photo-oxidation. *J. Photochem. Photobiol. B Biol.* 4, 283–295. doi: 10.1016/1011-1344(90)85034-T

Siefermann-Harms, D., and Ninnemann, H. (1982). Pigment organization in the light-harvesting chlorophyll-a/b protein complex of lettuce chloroplasts. Evidence obtained from protection of the chlorophylls against proton attack and from excitation energy transfer. *Photochem. Photobiol.* 35, 719–731. doi: 10.1111/j.1751-1097.1982.tb02636.x

Sonneveld, A., Rademaker, H., and Duysens, L. N. (1979). Chlorophyll *a* fluorescence as a monitor of nanosecond reduction of the photooxidized

primary donor P-680+ of photosystem II. *Biochim. Biophys. Acta* 548, 536–551. doi: 10.1016/0005-2728(79)90063-x

Spikes, J. D. (1992). Quantum yields and kinetics of the photobleaching of hematoporphyrin, Photofrin II, tetra (4-sulfonatophenyl)-porphine and uroporphyrin. *Photochem. Photobiol.* 55, 797–808. doi: 10.1111/j.1751-1097.1992.tb08527.x

Telfer, A., De Las Rivas, J., and Barber, J. (1991). β-Carotene within the isolated photosystem II reaction centre: photooxidation and irreversible bleaching of this chromophore by oxidised P680. *Biochim. Biophys. Acta* 1060, 106–114. doi: 10.1016/S0005-2728(05)80125-2

Triantaphylides, C., Krischke, M., Hoeberichts, F. A., Ksas, B., Gresser, G., Havaux, M., et al. (2008). Singlet oxygen is the major reactive oxygen species involved in photooxidative damage to plants. *Plant Physiol.* 148, 960–968. doi: 10.1104/pp.108.125690

Tutkus, M., Akhtar, P., Chmeliov, J., Görföl, F., Trinkunas, G., Lambrev, P. H., et al. (2018). Fluorescence microscopy of single liposomes with incorporated pigment–proteins. *Langmuir* 34, 14410–14418. doi: 10.1021/acs.langmuir.8b02307

Tyystjärvi, E., King, N., Hakala, M., and Aro, E.-M. (1999). Artificial quenchers of chlorophyll fluorescence do not protect against photoinhibition. *J. Photochem. Photobiol. B Biol.* 48, 142–147. doi: 10.1016/S1011-1344(99)00022-6

van Amerongen, H., and Croce, R. (2013). Light harvesting in photosystem II. *Photosynth. Res.* 116, 251–263. doi: 10.1007/s11120-013-9824-3

Vass, I. (2011). Role of charge recombination processes in photodamage and photoprotection of the photosystem II complex. *Physiol. Plant.* 142, 6–16. doi: 10.1111/j.1399-3054.2011.01454.x

Vass, I., and Cser, K. (2009). Janus-faced charge recombinations in photosystem II photoinhibition. *Trends Plant Sci.* 14, 200–205. doi: 10.1016/j.tplants.2009.01.009

Yamashita, K., Konishi, K., Itoh, M., and Shibata, K. (1969). Photo-bleaching of carotenoids related to the electron transport in chloroplasts. *Biochim. Biophys. Acta* 172, 511–524. doi: 10.1016/0005-2728(69)90147-9

Yamashita, T., and Butler, W. L. (1969). Photooxidation by photosystem II of Tris-washed chloroplasts. *Plant Physiol.* 44, 1342–1346. doi: 10.1104/pp.44.9.1342

Yang, C., Boggasch, S., Haase, W., and Paulsen, H. (2006). Thermal stability of trimeric light-harvesting chlorophyll *a*/*b* complex (LHCIIb) in liposomes of thylakoid lipids. *Biochim. Biophys. Acta* 1757, 1642–1648. doi: 10.1016/j.bbabio.2006.08.010

Zhang, Y., Liu, C., Liu, S., Shen, Y., Kuang, T., and Yang, C. (2008). Structural stability and properties of three isoforms of the major light-harvesting chlorophyll *a*/*b* complexes of photosystem II. *Biochim. Biophys. Acta* 1777, 479–487. doi: 10.1016/j.bbabio.2008.04.012

Zolla, L., and Rinalducci, S. (2002). Involvement of active oxygen species in degradation of light-harve sting proteins under light stresses. *Biochemistry* 41, 14391–14402. doi: 10.1021/bi026 5776

Zubik, M., Luchowski, R., Grudzinski, W., Gospodarek, M., Gryczynski, I., Gryczynski, Z., et al. (2011). Light-induced isomerization of the LHCII-bound xanthophyll neoxanthin: possible implications for photoprotection in plants. *Biochim. Biophys. Acta Bioenerget.* 1807, 1237–1243. doi: 10.1016/j.bbabio.2011.06.011

Zucchelli, G., Garlaschi, F. M., and Jennings, R. C. (1988). Spectroscopic analysis of chlorophyll photobleaching in spinach thylakoids, grana and light-harvesting chlorophyll *a*/*b* protein complex. *J. Photochem. Photobiol. B Biol.* 2, 483–490. doi: 10.1016/1011-1344(88)85077-2

Conflict of Interest: The authors declare that the research was conducted in the absence of any commercial or financial relationships that could be construed as a potential conflict of interest.

Copyright © 2020 Lingvay, Akhtar, Sebők-Nagy, Páli and Lambrev. This is an open-access article distributed under the terms of the Creative Commons Attribution License (CC BY). The use, distribution or reproduction in other forums is permitted, provided the original author(s) and the copyright owner(s) are credited and that the original publication in this journal is cited, in accordance with accepted academic practice. No use, distribution or reproduction is permitted which does not comply with these terms.

frontiers in Plant Science

ORIGINAL RESEARCH
published: 07 July 2020
doi: 10.3389/fpls.2020.01030

Elevated Levels of Specific Carotenoids During Acclimation to Strong Light Protect the Repair of Photosystem II in *Synechocystis* sp. PCC 6803

Taichi Izuhara[1], *Ikumi Kaihatsu*[1], *Haruhiko Jimbo*[2], *Shinichi Takaichi*[3] *and Yoshitaka Nishiyama*[1]*

[1] Department of Biochemistry and Molecular Biology, Graduate School of Science and Engineering, Saitama University, Saitama, Japan, [2] Graduate School of Art and Sciences, The University of Tokyo, Tokyo, Japan, [3] Department of Molecular Microbiology, Faculty of Life Sciences, Tokyo University of Agriculture, Tokyo, Japan

OPEN ACCESS

Edited by:
Cornelia Spetea,
University of Gothenburg, Sweden

Reviewed by:
Josef Komenda,
Academy of Sciences of the Czech Republic, Czechia
Taina Tyystjärvi,
University of Turku, Finland

***Correspondence:**
Yoshitaka Nishiyama
nishiyama@mail.saitama-u.ac.jp

Specialty section:
This article was submitted to Plant Physiology, a section of the journal Frontiers in Plant Science

Received: 18 March 2020
Accepted: 23 June 2020
Published: 07 July 2020

Citation:
Izuhara T, Kaihatsu I, Jimbo H, Takaichi S and Nishiyama Y (2020) Elevated Levels of Specific Carotenoids During Acclimation to Strong Light Protect the Repair of Photosystem II in Synechocystis sp. PCC 6803. Front. Plant Sci. 11:1030. doi: 10.3389/fpls.2020.01030

The tolerance of photosynthesis to strong light increases in photosynthetic organisms during acclimation to strong light. We investigated the role of carotenoids in the protection of photosystem II (PSII) from photoinhibition after acclimation to strong light in the cyanobacterium *Synechocystis* sp. PCC 6803. In cells that had been grown under strong light at 1,000 μmol photons m^{-2} s^{-1} (SL), specific carotenoids, namely, zeaxanthin, echinenone, and myxoxanthophyll, accumulated at high levels, and the photoinhibition of PSII was less marked than in cells that had been grown under standard growth light at 70 μmol photons m^{-2} s^{-1} (GL). The rate of photodamage to PSII, as monitored in the presence of lincomycin, did not differ between cells grown under SL and GL, suggesting that the mitigation of photoinhibition after acclimation to SL might be attributable to the enhanced ability to repair PSII. When cells grown under GL were transferred to SL, the mitigation of photoinhibition of PSII occurred in two distinct stages: a first stage that lasted 4 h and the second stage that occurred after 8 h. During the second stage, the accumulation of specific carotenoids was detected, together with enhanced synthesis *de novo* of proteins that are required for the repair of PSII, such as the D1 protein, and suppression of the production of singlet oxygen ($^1O_2$). In the Δ*crtR*Δ*crtO* mutant of *Synechocystis*, which lacks zeaxanthin, echinenone, and myxoxanthophyll, the mitigation of photoinhibition of PSII, the enhancement of protein synthesis, and the suppression of production of $^1O_2$ were significantly impaired during the second stage of acclimation. Thus, elevated levels of the specific carotenoids during acclimation to strong light appeared to protect protein synthesis from $^1O_2$, with the resultant mitigation of photoinhibition of PSII.

Keywords: acclimation, carotenoids, singlet oxygen, photoinhibition, photosystem II

INTRODUCTION

Light is necessary for photosynthesis but excess light impairs photosynthesis. Photosystem II (PSII), which is a protein-pigment complex that converts light energy to chemical energy, is known to be particularly sensitive to strong light. Exposure of photosynthetic organisms to strong light results in the specific inactivation of PSII, and this phenomenon is referred to as photoinhibition of PSII (Aro et al., 1993b; Vass, 2012). Photoinhibition of PSII becomes apparent under strong light when the rate of photodamage to PSII exceeds the rate of repair of PSII (Murata and Nishiyama, 2018). Photodamaged PSII is repaired *via* an efficient repair system that involves proteolytic degradation of damaged D1 protein; synthesis *de novo* of the precursor to the D1 protein (pre-D1); insertion of the pre-D1 into PSII; processing of pre-D1 at the carboxy-terminal extension; and reactivation of PSII (Theis and Schroda, 2016; Li et al., 2018).

Photodamage to PSII depends on the intensity of incident light (Allakhverdiev and Murata, 2004), whereas the repair of PSII is adversely affected by various types of environmental stress and, in particular, by oxidative stress due to reactive oxygen species (ROS), such as the superoxide anion radical, hydrogen peroxide, the hydroxyl radical, and singlet oxygen ($^1O_2$: Nishiyama et al., 2001; Nishiyama et al., 2004; Allakhverdiev and Murata, 2004). These ROS are produced in abundance in the photosynthetic machinery under strong light, as a result of the transport of electrons and the transfer of excitation energy (Asada, 1999). In the cyanobacterium *Synechocystis* sp. PCC 6803 (hereafter, *Synechocystis*), the ROS-induced inhibition of the repair of PSII has been attributed to the inhibition of synthesis of pre-D1 during translational elongation (Nishiyama et al., 2001; Nishiyama et al., 2004). Biochemical studies revealed that two translation factors, EF-Tu and EF-G, key proteins that support translational elongation, are inactivated *via* oxidation by ROS of specific cysteine residues (Kojima et al., 2007; Yutthanasirikul et al., 2016). Expression, in *Synechocystis*, of mutated EF-Tu or mutated EF-G in which one of the ROS-sensitive cysteine residues had been replaced by a serine residue mitigated the photoinhibition of PSII *via* the acceleration of synthesis *de novo* of proteins, including the D1 protein, with the enhancement of the repair of PSII under strong light (Ejima et al., 2012; Jimbo et al., 2018). Thus, the sensitivity of the repair system to ROS appears to be a critical factor that determines the extent of photoinhibition of PSII.

To minimize levels of ROS, photosynthetic organisms have evolved various anti-oxidative systems, which incorporate ROS-scavenging enzymes and antioxidants. Defects in the anti-oxidative systems exacerbate the photoinhibition of PSII. For example, in mutants of *Synechocystis* that were deficient in catalase and thioredoxin peroxidase, in zeaxanthin and echinenone, and in α-tocopherol, respectively, the photoinhibition of PSII was accelerated as a consequence of the decelerated repair of PSII (Nishiyama et al., 2001; Inoue et al., 2011; Kusama et al., 2015). By contrast, in a mutant of *Synechocystis* that overexpressed superoxide dismutase and catalase, the photoinhibition of PSII was mitigated, with the accelerated repair of PSII (Sae-Tang et al., 2016). In addition, overexpression in *Synechocystis* of orange carotenoid protein, which dissipates excitation energy and depresses the production of $^1O_2$, protected the repair of PSII under strong light, with the resultant mitigation of photoinhibition of PSII (Takahashi et al., 2019). Thus, the capacity to minimize levels of ROS appears to be essential for the efficient repair of PSII under strong light.

Photosynthetic organisms exhibit enhanced tolerance of PSII to photoinhibition when they acclimate to strong light (Adams et al., 1987). This ability has been associated with the enhanced ability to repair PSII in plants (Aro et al., 1993a), in algae (Erickson et al., 2015), and in cyanobacteria (Samuelsson et al., 1987; Jimbo et al., 2019). During acclimation to strong light, various physiological changes occur (Muramatsu and Hihara, 2012). In cyanobacteria, such changes include a reduction in the size of the antenna phycobilisomes (Grossman et al., 1993), stimulation of the state transition and thermal dissipation of excitation energy (Fujimori et al., 2005), and activation of the Calvin-Benson cycle (Hihara et al., 1998) and anti-oxidative systems (Latifi et al., 2009). With respect to the repair of PSII, it seems likely that activation of anti-oxidative systems might contribute significantly to the enhanced ability to repair PSII during acclimation to strong light. It has been reported that cyanobacteria accumulate specific carotenoids, namely, zeaxanthin, echinenone, and myxoxanthophyll, at high levels when they are grown under strong light, such as 1,300 μmol photons m^{-2} s^{-1} (Masamoto and Furukawa, 1997; Steiger et al., 1999), but the roles of such carotenoids in acclimation to strong light remain to be elucidated.

In the present study, we investigated the roles of carotenoids in the protection of PSII from photoinhibition during acclimation to strong light in the Δ*crtR*Δ*crtO* mutant of *Synechocystis*. In this mutant, zeaxanthin, echinenone, and myxoxanthophyll are deficient as a result of inactivation of genes for β-carotene hydroxylase CrtR, which converts β-carotene and deoxymyxoxanthophyll to zeaxanthin and myxoxanthophyll, respectively, and β-carotene ketolase CrtO, which converts β-carotene to echinenone (Fernández-González et al., 1997; Masamoto et al., 1998; Domonkos et al., 2013). When cells were transferred from growth light to strong light, the photoinhibition of PSII was mitigated in two stages: the first stage occurred within 4 h and the second stage occurred after 8 h. The second stage of mitigation was associated with the accumulation of zeaxanthin, echinenone, and myxoxanthophyll, which contributed to the enhanced repair of PSII *via* suppression of the production of $^1O_2$ and acceleration of the synthesis *de novo* of proteins that are required for the repair of PSII, such as the D1 protein.

MATERIALS AND METHODS

Cell and Culture Conditions

Cells of a glucose-tolerant strain (hereafter referred to as wild-type) and of the Δ*crtR*Δ*crtO* mutant strain of *Synechocystis* sp. PCC 6803 (Kusama et al., 2015) were grown photoautotrophically at 32°C in liquid BG11 medium under standard growth light at 70 μmol photons m^{-2} s^{-1} (GL), moderately strong light at 200 μmol photons m^{-2} s^{-1} (ML), or strong light at 1,000 μmol photons m^{-2} s^{-1} (SL), with aeration by sterile air that contained 1% (v/v) CO_2. Cells in cultures with an optical density at 730 nm of 1.0 ± 0.1 were used for assays unless otherwise noted.

Analysis of Carotenoids

Pigments were extracted from cells with a mixture of acetone and methanol (7:2, v/v) and were analyzed by HPLC on a system equipped with a μBondapak C18 column (8 mm × 100 mm; RCM type; Waters, Milford, MA, U.S.A.), as described previously (Kusama et al., 2015), with slight modifications. Carotenoids were eluted with a linear gradient from a mixture of methanol and water (9:1, v/v) to 100% methanol for 20 min and then with isocratic 100% methanol, at a rate of 1.8 ml min^{-1}. Zeaxanthin and β-carotene were detected at 450 nm, while echinenone, myxoxanthophyll, and synechoxanthin were detected at 470 nm. Levels of individual carotenoids were normalized by the content of chlorophyll *a*.

Assay of Photoinhibition of PSII

For standard assay of photoinhibition, 30-ml aliquots of cell cultures were exposed to light at 2,000 μmol photons m^{-2} s^{-1} at 32°C for designated periods of time to induce the photoinhibition of PSII. For assays of photodamage, lincomycin was added to suspensions of cells at a final concentration of 200 μg ml^{-1} just before the onset of illumination. The activity of PSII was measured at 32°C in the terms of the evolution of oxygen in the presence of 1 mM 1,4-benzoquinone and 1 mM $K_3Fe(CN)_6$ with a Clark-type oxygen electrode (Hansatech Instruments, Norfolk, U.K.). For time-course assays after the shift from GL to SL, 30-mL suspensions of cells grown under GL with an optical density at 730 nm of 0.4 ± 0.1 were incubated under SL and aliquots of 1 mL were withdrawn at designated times for measurements of the activity of PSII. Aliquots of 1 mL were illuminated with strong light at 1,500 μmol photons m^{-2} s^{-1} for 30 min at 32°C within the chamber of the oxygen electrode and the activity of PSII was measured. The ratio, as a percentage, of the residual activity of PSII to the initial activity of PSII at each designated time point was defined as the strong-light tolerance of PSII.

Quantitation of Chlorophyll and Carotenoids

Chlorophyll *a* and carotenoids were extracted from cells with 100% methanol and the concentrations of these pigments were determined spectroscopically, as described previously (Wellburn, 1994; Ritchie, 2006).

Detection of $^1O_2$

The production of $^1O_2$ in cells was detected by measuring the rate of the light-induced uptake of oxygen in the presence of histidine, as described previously (Rehman et al., 2013; Kusama et al., 2015). Cells in cultures with an optical density at 730 nm of 0.5 ± 0.1 were exposed to light at 2,500 μmol photons m^{-2} s^{-1} at 32°C in the presence of 5 mM histidine and in its absence, and the evolution of oxygen was measured in the absence of electron acceptors. The generation of $^1O_2$ was quantitated by subtracting the rate of the evolution of oxygen in the absence of histidine from the rate in its presence. Assays were also performed in the presence of either 10 μM DCMU or 10 mM NaN_3.

Labeling of Proteins *In Vivo*

For pulse labeling of proteins, 15-ml aliquots of cell cultures were incubated at 32°C in light at 1,500 μmol photons m^{-2} s^{-1} for 15 min in the presence of 240 kBq ml^{-1} ^{35}S-labeled methionine plus cysteine (EasyTag™ EXPRE$^{35}S^{35}S$; PerkinElmer, Waltham, MA, U.S.A.), as described previously (Nishiyama et al., 2004). Labeling was terminated by the addition of non-radioactive methionine and cysteine to a final concentration of 2 mM each, with immediate cooling of samples on ice. Thylakoid membranes were isolated from cells as described previously (Nishiyama et al., 2004), and membrane proteins were separated by SDS-PAGE on a 12.5% polyacrylamide gel that contained 6 M urea. Labeled proteins on the gel were visualized with an imaging analyzer (FLA-7000; Fujifilm, Tokyo, Japan) and levels of the D1 protein were determined densitometrically, as described previously (Kojima et al., 2007).

RESULTS

Effects of Specific Carotenoids on Growth Under Strong Light

We grew cells of the wild-type strain of *Synechocystis* and the derivative Δ*crtR*Δ*crtO* strain, which is deficient in zeaxanthin, echinenone, and myxoxanthophyll (Kusama et al., 2015), under standard growth light (GL; 70 μmol photons m^{-2} s^{-1}), moderately strong light (ML; 200 μmol photons m^{-2} s^{-1}), and strong light (SL; 1,000 μmol photons m^{-2} s^{-1}). Wild-type cells grew faster under ML than under GL (**Figure 1A**). Under SL, wild-type cells grew at the almost same rate as under ML during the first 4 d and then the proliferation of cells ceased (**Figure 1A**). The growth of Δ*crtR*Δ*crtO* cells was slower than that of wild-type cells under light at the three different intensities and exhibited light dependency similar to that of wild-type cells (**Figure 1B**). Under SL, suspensions of both types of cell looked yellower in color than under GL and ML (**Figure 1C**). Spectroscopic analyses showed that under SL, the contents of chlorophyll *a* and phycocyanin decreased in both types of cell, while the contents of carotenoids increased (**Supplementary Figure S1**, **Supplementary Table S1**). The most striking difference between the two strains was that wild-type cells remained blue-green in color for 10 d under SL, whereas Δ*crtR*Δ*crtO* cells started to bleach within 8 to 10 d under SL, indicating that the mutant was sensitive to strong light.

Levels of Carotenoids in Cells Grown Under Strong Light

The major carotenoids in *Synechocystis* are β-carotene, zeaxanthin, echinenone, and myxoxanthophyll (Takaichi and Mochimaru, 2007; Kusama et al., 2015). We analyzed the levels of these carotenoids in wild-type and Δ*crtR*Δ*crtO* cells that had been grown under GL, ML, and SL for 24 h (**Figure 2**). In wild-type cells grown under SL, levels of β-carotene, zeaxanthin, echinenone, and myxoxanthophyll were much higher than those in cells grown under GL and ML. There was no detectable zeaxanthin, echinenone or myxoxanthophyll in Δ*crtR*Δ*crtO* cells.

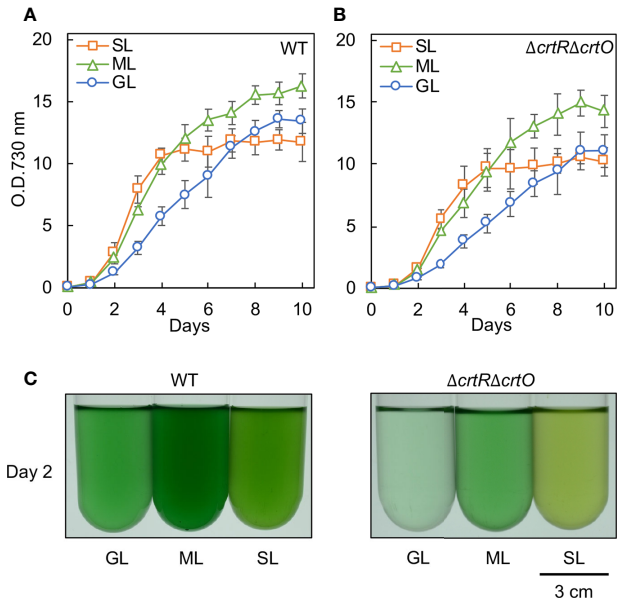

FIGURE 1 | Growth of wild-type and Δ*crtR*Δ*crtO* cells under light at three different intensities. Cells were grown photoautotrophically at 32°C under standard growth light (GL) at 70 μmol photons m^{-2} s^{-1}, under moderately strong light (ML) at 200 μmol photons m^{-2} s^{-1}, and under strong light (SL) at 1,000 μmol photons m^{-2} s^{-1}. Growth curves of wild-type **(A)** and Δ*crtR*Δ*crtO* **(B)** cells as monitored in terms of optical density at 730 nm. **(C)** Representative images of cell suspensions after culture for 2 days. Values are means ± SD (bars) of results from three independent experiments.

However, in Δ*crtR*Δ*crtO* cells grown under SL, levels of deoxymyxoxanthophyll and β-carotene were higher than those in cells grown under GL and ML. Since myxoxanthophyll is synthesized from deoxymyxoxanthophyll *via* a reaction catalyzed by β-carotene hydroxylase CrtR (Takaichi et al., 2001), it is reasonable that deoxymyxoxanthophyll accumulated in Δ*crtR*Δ*crtO* cells. The level of β-carotene in Δ*crtR*Δ*crtO* cells was about twice that in wild-type cells. Synechoxanthin, a carotenoid found specifically in cyanobacteria (Graham and Bryant, 2008), accumulated at very low levels in both types of cell under all light conditions tested.

Specific Carotenoids Protect the Repair of PSII During Acclimation to Strong Light

We examined the photoinhibition of PSII in wild-type and Δ*crtR*Δ*crtO* cells that had been grown under GL, ML, and SL to an optical density at 730 nm of 0.8 ± 0.1. When wild-type cells grown under GL were exposed to light at 2,000 μmol photons m^{-2} s^{-1}, the activity of PSII fell to 51% of the initial level in 120 min (**Figure 3A**). By contrast, the activity of PSII in cells grown under ML remained at 65% of the initial level after 120 min, and the activity of PSII in cells grown under SL remained at 88% of the initial level. However, when cells were exposed to light at 2,000 μmol photons m^{-2} s^{-1} in the presence of lincomycin, which blocks the repair of PSII, the activity of PSII in cells grown under GL, under ML, and under SL fell at similar rates (**Figure 3B**). When cells were exposed to a weaker light at 700 μmol photons m^{-2} s^{-1} in the presence of lincomycin, the activity of PSII in cells grown under GL, under ML and under SL also fell at similar rates (**Figure**

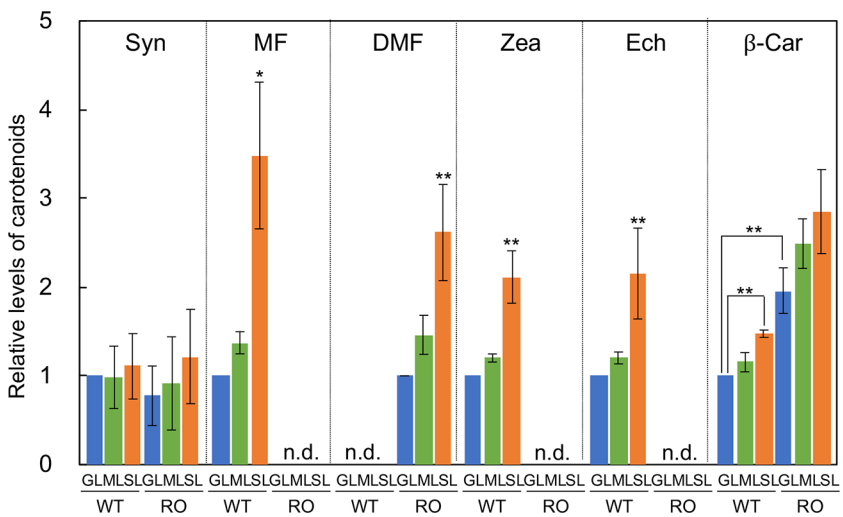

FIGURE 2 | Levels of carotenoids in wild-type (WT) and Δ*crtR*Δ*crtO* (RO) cells grown under GL, ML and SL (see legend to **Figure 1**). Syn, synechoxanthin; MF, myxoxanthophyll; DMF, deoxymyxoxanthophyll; Zea, zeaxanthin; Ech, echinenone; β-Car, β-carotene; n.d., not detected. Levels of Syn, MF, Zea, Ech, and β-Car are relative to those in wild-type cells grown under GL, respectively, while levels of DMF are relative to that in Δ*crtR*Δ*crtO* cells grown under GL. Values are means ± SD (bars) of results from three independent experiments. Asterisks indicate statistically significant differences (*$P < 0.05$; **$P < 0.01$; Student's *t* test).

3C), suggesting that increasing the intensity of the growth light did not affect photodamage but enhanced the repair of PSII. When Δ*crtR*Δ*crtO* cells that had been grown under GL were exposed to light at 2,000 μmol photons m^{-2} s^{-1}, the activity of PSII fell to 26% of the initial level within 120 min (**Figure 3D**). The activity of PSII in Δ*crtR*Δ*crtO* cells that had been grown under ML remained at 45% of initial level after 120 min, and the activity of PSII in cells in Δ*crtR*Δ*crtO* cells that had been grown under SL remained at 53% of the initial level. There were no differences in the extent of photodamage to PSII under light at 2,000 or 700 μmol photons m^{-2} s^{-1} among cells grown under GL, under ML and under SL (**Figures 3E, F**). Thus, it appeared that Δ*crtR*Δ*crtO* cells were more susceptible than wild-type cells to photoinhibition of PSII, as a consequence of the decreased ability to repair PSII. Nevertheless, the ability to enhance the repair of PSII after growth under ML and SL was retained to some extent in Δ*crtR*Δ*crtO* cells.

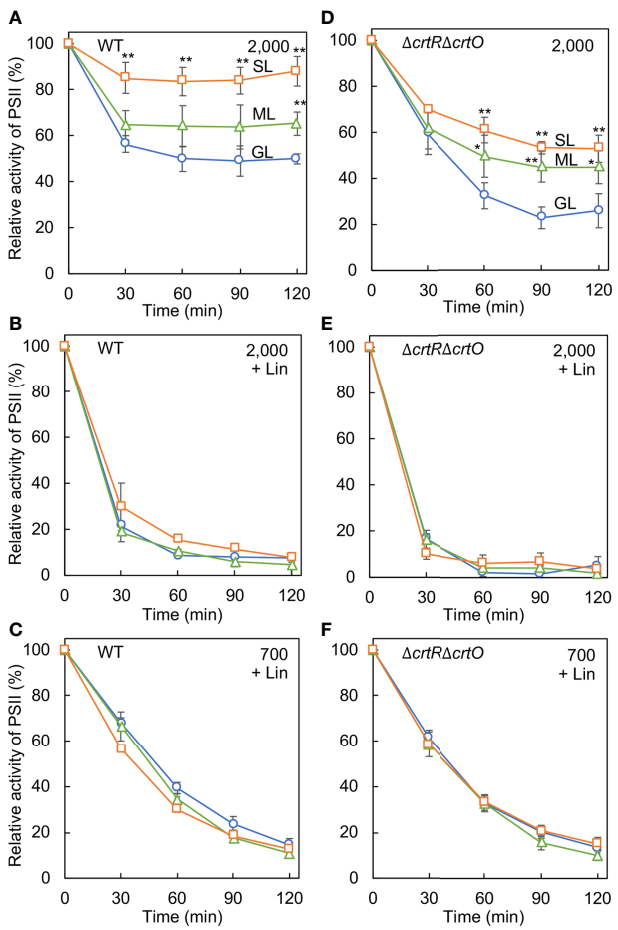

FIGURE 3 | Effects of growth light on the photoinhibition of PSII in wild-type **(A–C)** and Δ*crtR*Δ*crtO* **(D–F)** cells. Cells that had been grown under GL, ML, and SL (see legend to **Figure 1**) for 24 h were exposed to strong light at 2,000 μmol photons m^{-2} s^{-1}, with aeration by ambient air, in the absence of lincomycin (Lin; **A, D**) and in its presence **(B, E)**. Cells were also exposed to strong light at 700 μmol photons m^{-2} s^{-1} in the presence of lincomycin **(C, F)**. The activity of PSII was monitored in terms of the evolution of oxygen in the presence 1 mM 1,4-benzoquinone as the electron acceptor. The activities taken as 100% for wild-type cells grown under GL, ML, and SL were 1,075 ± 118, 1,060 ± 144, 1,006 ± 200 μmol O_2 mg^{-1} Chl h^{-1}, respectively. The activities taken as 100% for Δ*crtR*Δ*crtO* cells grown under GL, ML, and SL were 561 ± 167, 501 ± 71, 482 ± 99 μmol O_2 mg^{-1} Chl h^{-1}, respectively. Values are means ± SD (bars) of results from five independent experiments. Asterisks indicate statistically significant differences compared to cells grown under GL (*$P < 0.05$; **$P < 0.01$; Student's *t*-test).

Specific Carotenoids Mitigate the Photoinhibition of PSII During the Second Stage of Acclimation to Strong Light

We monitored the time course of changes in the activity of PSII after cells that had been grown under GL were transferred to SL. In wild-type cells, the activity of PSII dropped by 15% in 2 h and then increased to above the initial activity in 4 h (**Figure 4A**, 0 min). We also withdrew aliquots of cell suspensions at designated times during incubation under SL and exposed them to light at 1,500 μmol photons m^{-2} s^{-1} for 30 min to induce the photoinhibition of PSII. The residual activity of PSII increased during incubation under SL (**Figure 4A**, 30 min). The ratio (as a percentage) of the residual activity of PSII to the initial activity of PSII at each designated time point was defined as the strong-light tolerance of PSII. Under SL, the strong-light tolerance of PSII increased from 14% to 36% in 4 h and reached a plateau (**Figure 4B**, −Lin). Then the strong-light tolerance started to increase again after 8 h and reached 45% within 12 h. Thus, it appeared that the mitigation of photoinhibition of PSII occurred in two stages: the first stage occurred during the first 4 h and the second stage occurred after 8 h. However, when the strong-light tolerance of PSII was monitored in the presence of lincomycin, it failed to increase (**Figure 4B**, +Lin), suggesting that the repair of PSII was enhanced during transfer of cells from GL to SL. We also monitored changes in levels of chlorophyll *a* and carotenoids after the transfer of cells to SL. Levels of chlorophyll *a* fell rapidly under SL, whereas levels of carotenoids started to rise within 8 h under SL (**Figure 4C**).

In Δ*crtR*Δ*crtO* cells, the activity of PSII dropped by 21% in 2 h and then increased, albeit more slowly than that in wild-type cells, under SL (**Figure 4D**, 0 min). The residual activity of PSII after exposure of cells to light at 1,500 μmol photons m^{-2} s^{-1} for 30 min was much lower than that in wild-type cells and also increased under SL, but again more slowly than in wild-type cells (**Figure 4D**, 30 min). Under SL, the strong-light tolerance of PSII increased from 14% to 35% and then ceased to increase significantly (**Figure 4E**, −Lin). Moreover, it did not change in the presence of lincomycin (**Figure 4E**, +Lin). These results indicate that the enhancement of the repair of PSII during the second stage might have been impaired in the mutant cells. Levels of chlorophyll *a* continued to decline under SL, while levels of carotenoids remained almost unchanged (**Figure 4F**). Comparison of wild-type cells to Δ*crtR*Δ*crtO* cells suggested that the accumulation of zeaxanthin, echinenone, and myxoxanthophyll might be associated with the enhanced repair of PSII during the second stage.

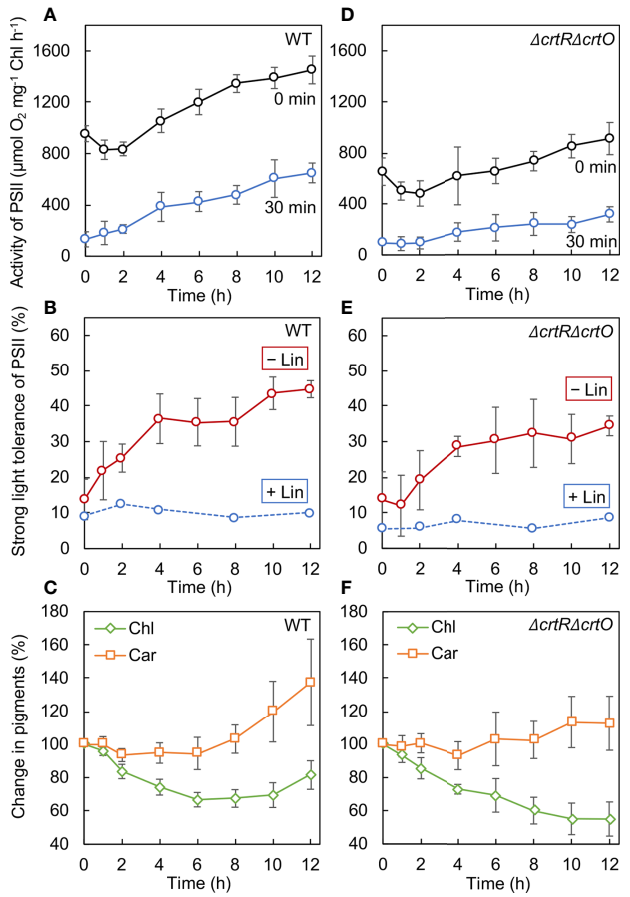

FIGURE 4 | Changes in the activity of PSII, the strong-light tolerance of PSII, and levels of pigments after transfer of wild-type **(A–C)** and Δ*crtR*Δ*crtO* **(D–F)** cells from GL to SL (see legend to **Figure 1**). **(A, D)** Changes in the activity of PSII at the indicated times (0 min) and the residual activity of PSII after cells at the indicated times had been exposed to light at 1,500 μmol photons m^{-2} s^{-1} for 30 min (30 min). **(B, E)** The strong-light tolerance of PSII, defined as the ratio (as a percentage) of the residual activity of PSII (30 min) to the initial activity of PSII (0 min) at the indicated times, as mentioned above. Photodamage to PSII was also monitored by addition of lincomycin (Lin) prior to exposure of cells to light at 1,500 μmol photons m^{-2} s^{-1} for 30 min. **(C, F)** Changes in levels of chlorophyll *a* (Chl) and carotenoids (Car). Values are means ± SD (bars) of results from five independent experiments.

Specific Carotenoids Enhance the Synthesis of the D1 Protein During Acclimation to Strong Light

The synthesis *de novo* of the D1 protein plays a vital role in the repair of PSII (Aro et al., 1993b). To examine the effects of elevated levels of carotenoids on the synthesis *de novo* of the D1 protein, we monitored the incorporation of ^{35}S-labeled methionine plus cysteine into proteins during the exposure of cells to strong light at 1,500 μmol photons m^{-2} s^{-1} for 15 min. **Figure 5A** shows the patterns of pulse-labeled proteins from thylakoid membranes of wild-type and Δ*crtR*Δ*crtO* cells after cells had been transferred from GL to SL and incubated for designated times. In wild-type cells, the rate of synthesis of the D1 protein dropped by 11% in 2 h and then increased 1.1- and 1.4-fold by 4 and 12 h, respectively, under SL (**Figure 5B**). In Δ*crtR*Δ*crtO* cells, the rate of synthesis of the D1 protein under SL was 20% lower than in wild-type cells (**Figure 5C**). The rate of synthesis dropped by 20% within 2 h, returned to the initial level at 4 h, and had increased 1.2-fold by 12 h (**Figure 5C**). In particular, the acceleration of synthesis of the D1 protein, as determined after 12 h, was much lower in Δ*crtR*Δ*crtO* cells than in wild-type cells. Note that the patterns of synthesis of almost all the thylakoid proteins were similar to that of the D1 protein, suggesting that the absence of zeaxanthin, echinenone, and

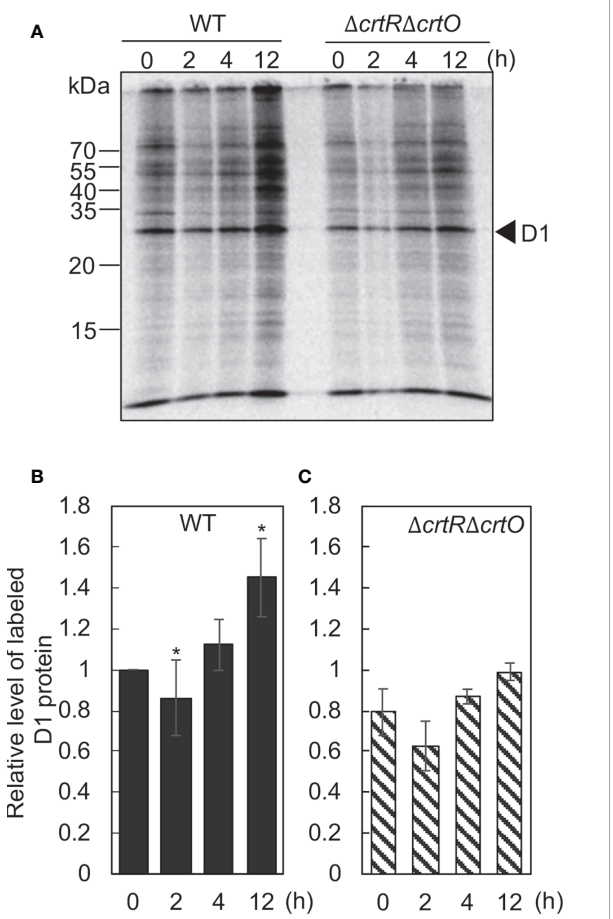

FIGURE 5 | Changes in the synthesis *de novo* of proteins in thylakoid membranes after transfer of wild-type and Δ*crtR*Δ*crtO* cells from GL to SL (see legend to **Figure 1**). Proteins from cells that had been incubated under SL for the indicated times were pulse-labeled by incubation of cells at 32°C, for 15 min, under strong light at 1,500 μmol photons m^{-2} s^{-1} in the presence of ^{35}S-labeled methionine plus cysteine. **(A)** A representative radiogram of pulse-labeled proteins from thylakoid membranes. **(B, C)** Quantitation of levels of labeled D1 protein in wild-type **(B)** and Δ*crtR*Δ*crtO* **(C)** cells. Levels of labeled D1 protein were normalized by reference to those in wild-type cells before transfer of cells to SL, namely, at zero time. Values are means ± SD (bars) of results from three independent experiments. Asterisks indicate statistically significant differences compared to the levels at zero time (*P < 0.05; Student's *t*-test).

myxoxanthophyll had an adverse effect on overall protein synthesis during incubation under SL (**Figure 5A**).

Specific Carotenoids Depress the Production of $^1O_2$ During Acclimation to Strong Light

Zeaxanthin, echinenone, and myxoxanthophyll are effective scavengers of $^1O_2$ (Young and Frank, 1996; Sandmann, 2019), and the scavenging abilities of these carotenoids are associated with the repair of PSII (Kusama et al., 2015). To monitor changes in levels of $^1O_2$ during acclimation to strong light, we measured the rates of production of $^1O_2$ by cells under strong illumination at 2,500 μmol photons m^{-2} s^{-1} in terms of the light-induced uptake of O_2 in the presence of histidine (Kusama et al., 2015). When wild-type cells were transferred to SL, the rate of production of $^1O_2$ increased 2.3-fold within 2 h; it returned to the initial level within 4 h; and it had fallen to 37% of the initial level by 12 h (**Figure 6A**). The production of $^1O_2$ was unaffected by 3-(3,4-dichlorophenyl)-1,1-dimethylurea (DCMU), which blocks the photosynthetic transport of electrons, while it was abolished in the presence of NaN_3, a quencher of $^1O_2$, confirming the accurate detection of $^1O_2$, as reported previously (Kusama et al., 2015). In Δ*crtR*Δ*crtO* cells, the rate of production of $^1O_2$ was 2.4 times higher than that in wild-type cells before the transfer of cells to SL (**Figure 6B**). After the transfer of cells from GL to SL, the rate of production of $^1O_2$ increased 1.2-fold within 2 h, returned to the initial level within 4 h, and decreased to 67% of the initial level within 12 h (**Figure 6B**). Thus, it appeared that the presence of zeaxanthin, echinenone, and myxoxanthophyll might depress the production of $^1O_2$ under strong light and, also, that the accumulation of these carotenoids during acclimation to strong light might suppress the production of $^1O_2$ to an even greater extent.

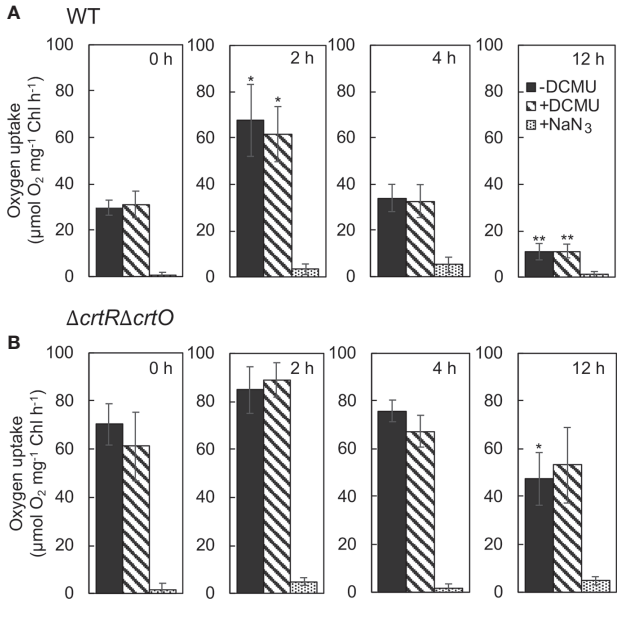

FIGURE 6 | Changes in the rate of production of $^1O_2$ in wild-type **(A)** and Δ*crtR*Δ*crtO* **(B)** cells after transfer of cells from GL to SL. The production of $^1O_2$ was monitored in terms of the difference between uptake of O_2 in the presence of histidine and in its absence under strong light at 2,500 μmol photons m^{-2} s^{-1}. The uptake of O_2 was measured in the absence of DCMU, in the presence of 10 μM DCMU, and in the presence of 10 μM DCMU plus 10 mM NaN_3. Values are means ± SD of results from three independent experiments. Asterisks indicate statistically significant differences compared to the levels at zero time (*$P < 0.05$; **$P < 0.01$; Student's *t* test).

DISCUSSION

Involvement of Specific Carotenoids in the Protection of the Repair of PSII During Acclimation to Strong Light

Earlier studies found that mitigation of the photoinhibition of PSII during acclimation to strong light is associated with the enhanced repair of PSII in plants (Aro et al., 1993a), algae (Erickson et al., 2015), and cyanobacteria (Samuelsson et al., 1987; Jimbo et al., 2019). It was also reported that carotenoids are required for the assembly and photoprotection of PSII (Sozer et al., 2010; Hakkila et al., 2013). The present study revealed that the accumulation of specific carotenoids, namely, zeaxanthin, echinenone, and myxoxanthophyll, during acclimation to strong light is involved in the enhanced repair of PSII, with the resultant mitigation of photoinhibition of PSII in *Synechocystis*. However, even in the absence of such carotenoids, Δ*crtR*Δ*crtO* cells were able to enhance the repair of PSII to some extent when grown under strong light (**Figure 3**). These results indicate that not only the accumulation of the specific carotenoids but also some other mechanism(s) might be responsible for the optimally enhanced repair of PSII during acclimation to strong light. Nevertheless, the significant decrease in the capacity for repair of PSII in Δ*crtR*Δ*crtO* cells suggests that these specific carotenoids might play a crucial role in protection of the repair of PSII from inhibition under strong light, thereby allowing cells to survive under such conditions (**Figure 1**).

Mechanism of the Mitigation of Photoinhibition of PSII During Acclimation to Strong Light

The mitigation of photoinhibition of PSII, namely, the enhancement of repair of PSII, occurred in two distinct stages: the first stage occurred during the first 4 h, and the second stage occurred after 8 h (**Figure 4**). During the second stage, specific carotenoids, namely, zeaxanthin, echinenone, and myxoxanthophyll, accumulated at high levels, while the synthesis *de novo* of proteins, including the D1 protein, was activated, and the production of $^1O_2$ was suppressed. Conversely, in the absence of these carotenoids, the second stage of mitigation of photoinhibition of PSII, the activation of protein synthesis, and the suppression of production of $^1O_2$ were significantly impaired. These observations together suggest a mechanism by which carotenoids might protect the repair of PSII during acclimation to strong light as follows. High levels of accumulation of the specific carotenoids during the second stage

of acclimation might protect protein synthesis by depressing the production of $^1O_2$, with the resultant enhanced repair of PSII.

By contrast, we detected no obvious increase in levels of carotenoids during the first stage of mitigation of photoinhibition of PSII (**Figure 4**). What mechanism might be involved in this first stage of mitigation? Within the first 2 h after cells had been transferred from growth light to strong light, both the activity of PSII and the rate of synthesis of the D1 protein decreased, while the production of $^1O_2$ rose. These features are typical of photoinhibition of PSII. During the next 2 h under strong light, by contrast, the activity of PSII and the rate of synthesis of the D1 protein rose, while the production of $^1O_2$ decreased. These changes might involve other mechanisms that protect protein synthesis from photo-oxidative stress. Recent studies of the acclimation of *Synechocystis* to strong light revealed that levels of the translation factor EF-Tu, which is sensitive to oxidation by ROS, rise during acclimation to strong light and that the elevated levels of EF-Tu help to accelerate protein synthesis and enhance the repair of PSII under strong light (Jimbo et al., 2019). It seems likely that, during the first 4 h after transfer of cells from growth light to strong light, levels of EF-Tu might increase and contribute to enhanced repair of PSII. In addition, transfer of cells to strong light should stimulate the production of ATP and reducing power, which in turn enhances the repair of PSII *via* the acceleration of the synthesis of the D1 protein at both transcriptional and translational levels (Murata and Nishiyama, 2018). Thermal dissipation of excitation energy, which is a major component of non-photochemical quenching (NPQ), might also contribute to the enhanced repair of PSII during the first 4 h of acclimation. In *Synechocystis*, exposure of cells to strong light converts orange carotenoid protein (OCP) from its inactive form to its active form, stimulating the thermal dissipation of excitation energy (Wilson et al., 2006) and enhancing the repair of PSII (Takahashi et al., 2019). The impaired mitigation of photoinhibition of PSII in *crtR*Δ*crtO* cells might also be due, in part, to the lack of 3′-hydroxyechinenone, the cofactor of OCP, and the consequent loss of active OCP. Reduction in the size of the antenna complex, the phycobilisomes, might also minimize oxidative stress and enhance the repair of PSII *via* reduction of the transfer of excitation energy to the reaction center (Grossman et al., 1993; Kopečná et al., 2012). All these mechanisms might work together to enhance the repair of PSII not only during the first stage but also during the second stage of acclimation.

The Physiological Roles of Specific Carotenoids During Acclimation to Strong Light

Zeaxanthin, echinenone, and myxoxanthophyll are effective scavengers of $^1O_2$ and free radicals (Sandmann, 2019). Their abilities to scavenge $^1O_2$ in organic solvents are higher than that of β-carotene because of the presence of hydroxyl and glycosyl groups (Sandmann, 2019). These features might explain why these three specific carotenoids accumulate in abundance during acclimation to strong light. In Δ*crtR*Δ*crtO* cells, the level of β-carotene was about twice that in wild-type cells and increased 1.5-fold after acclimation to strong light (**Figure 2**). Nonetheless, the impaired ability to repair PSII in Δ*crtR*Δ*crtO* cells suggests that β-carotene cannot substitute for these three specific carotenoids in terms of the protection of the repair of PSII under strong light.

Most carotenoids are located in thylakoid and cytoplasmic membranes, although their precise localization within these membranes remains to be elucidated (Masamoto et al., 1999; Zhang et al., 2015). It seems likely that carotenoids that are localized within and in close vicinity to the reaction center of PSII quench the triplet state of chlorophyll to prevent the formation of $^1O_2$, while other carotenoids scavenge $^1O_2$ directly. Zeaxanthin, echinenone, and myxoxanthophyll at elevated levels are likely to act in this way to depress intracellular levels of $^1O_2$, which is produced in abundance from PSII during the transfer of excitation energy under strong light.

As mentioned above, Δ*crtR*Δ*crtO* cells did retain some ability to enhance the repair of PSII. We found that, in this mutant, deoxymyxoxanthophyll, a precursor to myxoxanthophyll, accumulated, with its level increasing 2.5-fold after the transfer of cells from growth light to strong light (**Figure 2**). The accumulation of deoxymyxoxanthophyll might, in part, contribute to the enhanced repair of PSII in the absence of zeaxanthin, echinenone, and myxoxanthophyll since this carotenoid also has a glycosyl group. The roles of myxoxanthophyll and deoxymyxoxanthophyll in the protection of the repair of PSII and their localization require further clarification.

CONCLUSION

During the acclimation of *Synechocystis* to strong light, specific carotenoids, namely, zeaxanthin, echinenone, and myxoxanthophyll, accumulate in abundance and enhance the repair of PSII, with the resultant mitigation of photoinhibition of PSII. The accumulation of these carotenoids, which occurs at the late stage of acclimation, depresses the production of $^1O_2$ and thereby protects the synthesis *de novo* of proteins that are required for the repair of PSII, such as the D1 protein, under strong light.

DATA AVAILABILITY STATEMENT

The datasets generated for this study are available on request to the corresponding author.

AUTHOR CONTRIBUTIONS

TI performed most of the experiments. IK examined photoinhibition. HJ supervised the experiments. ST analyzed carotenoids. TI and YN conceived the project and wrote the article, with contributions from all the other authors.

FUNDING

This work was supported, in part, by a grant from the MIRAI Program of the Japan Science and Technology Agency (to YN); by a grant from the Japan Society for the Promotion of Science, KAKENHI (grant number JP18K06276 to YN); and by a grant from the Research Program of the "Dynamic Alliance for Open Innovation, Bridging Humans, the Environment and Materials" at the Network Joint Research Center for Materials and Devices (to YN).

ACKNOWLEDGMENTS

The authors thank Mr. Tomohisa Niimi (Saitama University) for the radioisotopic analysis of proteins.

SUPPLEMENTARY MATERIAL

The Supplementary Material for this article can be found online at: https://www.frontiersin.org/articles/10.3389/fpls.2020.01030/full#supplementary-material

REFERENCES

Adams, W. W., Osmond, C. B., and Sharkey, T. D. (1987). Responses of two CAM species to different irradiances during growth and susceptibility to photoinhibition by high light. *Plant Physiol.* 83, 213–218. doi: 10.1104/pp.83.1.213

Allakhverdiev, S. I., and Murata, N. (2004). Environmental stress inhibits the synthesis *de novo* of proteins involved in the photodamage-repair cycle of photosystem II in *Synechocystis* sp. PCC 6803. *Biochim. Biophys. Acta Bioenerg.* 1657, 23–32. doi: 10.1016/j.bbabio.2004.03.003

Aro, E. M., McCaffery, S., and Anderson, J. M. (1993a). Photoinhibition and D1 protein degradation in peas acclimated to different growth irradiances. *Plant Physiol.* 103, 835–843. doi: 10.1104/pp.103.3.835

Aro, E. M., Virgin, I., and Andersson, B. (1993b). Photoinhibition of photosystem II. Inactivation, protein damage and turnover. *Biochim. Biophys. Acta Bioenerg.* 1143, 113–134. doi: 10.1016/0005-2728(93)90134-2

Asada, K. (1999). The water-water cycle in chloroplasts: scavenging of active oxygens and dissipation of excess photons. *Ann. Rev. Plant Physiol. Plant Mol. Biol.* 50, 601–639. doi: 10.1146/annurev.arplant.50.1.601

Domonkos, I., Kis, M., Gombos, Z., and Ughy, B. (2013). Carotenoids, versatile components of oxygenic photosynthesis. *Prog. Lipid Res.* 52, 539–561. doi: 10.1016/j.plipres.2013.07.001

Ejima, K., Kawaharada, T., Inoue, S., Kojima, K., and Nishiyama, Y. (2012). A change in the sensitivity of elongation factor G to oxidation protects photosystem II from photoinhibition in *Synechocystis* sp. PCC 6803. *FEBS Lett.* 586, 778–783. doi: 10.1016/j.febslet.2012.01.042

Erickson, E., Wakao, S., and Niyogi, K. K. (2015). Light stress and photoprotection in *Chlamydomonas reinhardtii*. *Plant J.* 82, 449–465. doi: 10.1111/tpj.12825

Fernández-González, B., Sandmann, G., and Vioque, A. (1997). A new type of asymmetrically acting β-carotene ketolase is required for the synthesis of echinenone in the cyanobacterium *Synechocystis* sp. PCC 6803. *J. Biol. Chem.* 272, 9728–9733. doi: 10.1074/jbc.272.15.9728

Fujimori, T., Hihara, Y., and Sonoike, K. (2005). PsaK2 subunit in photosystem I is involved in state transition under high light condition in the cyanobacterium *Synechocystis* sp. PCC 6803. *J. Biol. Chem.* 280, 22191–22197. doi: 10.1074/jbc.M500369200

Graham, J. E., and Bryant, D. A. (2008). The biosynthetic pathway for synechoxanthin, an aromatic carotenoid synthesized by the euryhaline, unicellular cyanobacterium *Synechococcus* sp. strain PCC 7002. *J. Bacteriol.* 190, 7966–7974. doi: 10.1128/JB.00985-08

Grossman, A. R., Schaefer, M. R., Chiang, G. G., and Collier, J. L. (1993). The phycobilisome, a light-harvesting complex responsive to environmental conditions. *Microbiol. Rev.* 57, 725–749. doi: 10.1128/MMBR.57.3.725-749.1993

Hakkila, K., Antal, T., Gunnelius, L., Kurkela, J., Matthijs, H. C. P., Tyystjärvi, E., et al. (2013). Group 2 sigma factor mutant ΔsigCDE of the cyanobacterium *Synechocystis* sp. PCC 6803 reveals functionality of both carotenoids and flavodiiron proteins in photoprotection of photosystem II. *Plant Cell Physiol.* 54, 1780–1790. doi: 10.1093/pcp/pct123

Hihara, Y., Sonoike, K., and Ikeuchi, M. (1998). A novel gene, *pmgA*, specifically regulates photosystem stoichiometry in the cyanobacterium *Synechocystis* species PCC 6803 in response to high light. *Plant Physiol.* 117, 1205–1216. doi: 10.1104/pp.117.4.1205

Inoue, S., Ejima, K., Iwai, E., Hayashi, H., Appel, J., Tyystjärvi, E., et al. (2011). Protection by α-tocopherol of the repair of photosystem II during photoinhibition in *Synechocystis* sp. PCC 6803. *Biochim. Biophys. Acta* 1807, 236–241. doi: 10.1016/j.bbabio.2010.11.003

Jimbo, H., Yutthanasirikul, R., Nagano, T., Hisabori, T., Hihara, Y., and Nishiyama, Y. (2018). Oxidation of translation factor EF-Tu inhibits the repair of photosystem II. *Plant Physiol.* 176, 2691–2699. doi: 10.1104/pp.18.00037

Jimbo, H., Izuhara, T., Hihara, Y., Hisabori, T., and Nishiyama, Y. (2019). Light-inducible expression of translation factor EF-Tu during acclimation to strong light enhances the repair of photosystem II. *Proc. Natl. Acad. Sci. U. S. A.* 116, 21268–21273. doi: 10.1073/pnas.1909520116

Kojima, K., Oshita, M., Nanjo, Y., Kasai, K., Tozawa, Y., Hayashi, H., et al. (2007). Oxidation of elongation factor G inhibits the synthesis of the D1 protein of photosystem II. *Mol. Microbiol.* 65, 936–947. doi: 10.1111/j.1365-2958.2007.05836.x

Kopečná, J., Komenda, J., Bučinská, L., and Sobotka, R. (2012). Long-term acclimation of the cyanobacterium *Synechocystis* sp. PCC 6803 to high light is accompanied by an enhanced production of chlorophyll that is preferentially channeled to trimeric photosystem I. *Plant Physiol.* 160, 2239–2250. doi: 10.1104/pp.112.207274

Kusama, Y., Inoue, S., Jimbo, H., Takaichi, S., Sonoike, K., Hihara, Y., et al. (2015). Zeaxanthin and echinenone protect the repair of photosystem II from inhibition by singlet oxygen in *Synechocystis* sp. PCC 6803. *Plant Cell Physiol.* 56, 906–916. doi: 10.1093/pcp/pcv018

Latifi, A., Ruiz, M., and Zhang, C. C. (2009). Oxidative stress in cyanobacteria. *FEMS Microbiol. Rev.* 33, 258–278. doi: 10.1111/j.1574-6976.2008.00134.x

Li, L., Aro, E. M., and Millar, A. H. (2018). Mechanisms of photodamage and protein turnover in photoinhibition. *Trends Plant Sci.* 23, 667–676. doi: 10.1016/j.tplants.2018.05.004

Masamoto, K., and Furukawa, K. I. (1997). Accumulation of zeaxanthin in cells of the cyanobacterium *Synechococcus* sp. strain PCC 7942 grown under high irradiance. *J. Plant Physiol.* 151, 257–261. doi: 10.1016/S0176-1617(97)80250-7

Masamoto, K., Misawa, N., Kaneko, T., Kikuno, R., and Toh, H. (1998). β-carotene hydroxylase gene from the cyanobacterium *Synechocystis* sp. PCC 6803. *Plant Cell Physiol.* 39, 560–564. doi: 10.1093/oxfordjournals.pcp.a029405

Masamoto, K., Zsiros, O., and Gombos, Z. (1999). Accumulation of zeaxanthin in cytoplasmic membranes of the cyanobacterium *Synechococcus* sp. strain PCC 7942 grown under high light condition. *J. Plant Physiol.* 155, 136–138. doi: 10.1016/S0176-1617(99)80155-2

Muramatsu, M., and Hihara, Y. (2012). Acclimation to high-light conditions in cyanobacteria: from gene expression to physiological responses. *J. Plant Res.* 125, 11–39. doi: 10.1007/s10265-011-0454-6

Murata, N., and Nishiyama, Y. (2018). ATP is a driving force in the repair of photosystem II during photoinhibition. *Plant Cell Environ.* 41, 285–299. doi: 10.1111/pce.13108

Nishiyama, Y., Yamamoto, H., Allakhverdiev, S. I., Inaba, M., Yokota, A., and Murata, N. (2001). Oxidative stress inhibits the repair of photodamage to the photosynthetic machinery. *EMBO J.* 20, 5587–5594. doi: 10.1093/emboj/20.20.5587

Nishiyama, Y., Allakhverdiev, S. I., Yamamoto, H., Hayashi, H., and Murata, N. (2004). Singlet oxygen inhibits the repair of photosystem II by suppressing the translation elongation of the D1 protein in *Synechocystis* sp. PCC 6803. *Biochemistry* 43, 11321–11330. doi: 10.1021/bi036178q

Rehman, A. U., Cser, K., Sass, L., and Vass, I. (2013). Characterization of singlet oxygen production and its involvement in photodamage of photosystem II in

the cyanobacterium *Synechocystis* PCC 6803 by histidine-mediated chemical trapping. *Biochim. Biophys. Acta Bioenerg.* 1827, 689–698. doi: 10.1016/j.bbabio.2013.02.016

Ritchie, R. J. (2006). Consistent sets of spectrophotometric chlorophyll equations for acetone, methanol and ethanol solvents. *Photosynth. Res.* 89, 27–41. doi: 10.1007/s11120-006-9065-9

Sae-Tang, P., Hihara, Y., Yumoto, I., Orikasa, Y., Okuyama, H., and Nishiyama, Y. (2016). Overexpressed superoxide dismutase and catalase act synergistically to protect the repair of PSII during photoinhibition in *Synechococcus elongatus* PCC 7942. *Plant Cell Physiol.* 57, 1899–1907. doi: 10.1093/pcp/pcw110

Samuelsson, G., Lönneborg, A., Gustafsson, P., and Öquist, G. (1987). The susceptibility of photosynthesis to photoinhibition and the capacity of recovery in high and low light grown cyanobacterium *Anacystis nidulans*. *Plant Physiol.* 83, 438–441. doi: 10.1104/pp.83.2.438

Sandmann, G. (2019). Antioxidant protection from UV- and light-stress related to carotenoid structures. *Antioxidants* 8, 219. doi: 10.3390/antiox8070219

Sozer, O., Komenda, J., Ughy, B., Domonkos, I., Laczkó-Dobos, H., Malec, P., et al. (2010). Involvement of carotenoids in the synthesis and assembly of protein subunits of photosynthetic reaction centers of *Synechocystis* sp. PCC 6803. *Plant Cell Physiol.* 51, 823–835. doi: 10.1093/pcp/pcq031

Steiger, S., Schäfer, L., and Sandmann, G. (1999). High-light-dependent upregulation of carotenoids and their antioxidative properties in the cyanobacterium *Synechocystis* PCC 6803. *J. Photochem. Photobiol. B. Biol.* 52, 14–18. doi: 10.1016/S1011-1344(99)00094-9

Takahashi, H., Kusama, Y., Li, X., Takaichi, S., and Nishiyama, Y. (2019). Overexpression of orange carotenoid protein protects the repair of PSII under strong light in *Synechocystis* sp. PCC 6803. *Plant Cell Physiol.* 60, 367–375. doi: 10.1093/pcp/pcy218

Takaichi, S., and Mochimaru, M. (2007). Carotenoids and carotenogenesis in cyanobacteria: unique ketocarotenoids and carotenoid glycosides. *Cell. Mol. Life Sci.* 64, 2607–2619. doi: 10.1007/s00018-007-7190-z

Takaichi, S., Maoka, T., and Masamoto, K. (2001). Myxoxanthophyll in *Synechocystis* sp. PCC 6803 is myxol 2′-dimethyl-fucoside, (3R,2'S)-myxol 2′-(2,4-di-O-methyl-alpha-L-fucoside), not rhamnoside. *Plant Cell Physiol.* 42, 756–762. doi: 10.1093/pcp/pce098

Theis, J., and Schroda, M. (2016). Revisiting the photosystem II repair cycle. *Plant Signal. Behav.* 11, e1218587. doi: 10.1080/15592324.2016.1218587

Vass, I. (2012). Molecular mechanisms of photodamage in the photosystem II complex. *Biochim. Biophys. Acta Bioenerg.* 1817, 209–217. doi: 10.1016/j.bbabio.2011.04.014

Wellburn, A. R. (1994). The spectral determination of chlorophylls *a* and *b*, as well as total carotenoids, using various solvents with spectrophotometers of different resolution. *J. Plant Physiol.* 144, 307–313. doi: 10.1016/S0176-1617(11)81192-2

Wilson, A., Ajlani, G., Verbavatz, J. M., Vass, I., Kerfeld, C. A., and Kirilovsky, D. (2006). A soluble carotenoid protein involved in phycobilisome-related energy dissipation in cyanobacteria. *Plant Cell* 18, 992–1007. doi: 10.1105/tpc.105.040121

Young, A. J., and Frank, H. A. (1996). Energy transfer reactions involving carotenoids: quenching of chlorophyll fluorescence. *J. Photochem. Photobiol. B. Biol.* 36, 3–15. doi: 10.1016/S1011-1344(96)07397-6

Yutthanasirikul, R., Nagano, T., Jimbo, H., Hihara, Y., Kanamori, T., Ueda, T., et al. (2016). Oxidation of a cysteine residue in elongation factor EF-Tu reversibly inhibits translation in the cyanobacterium *Synechocystis* sp. PCC 6803. *J. Biol. Chem.* 291, 5860–5870. doi: 10.1074/jbc.M115.706424

Zhang, L., Selao, T. T., Selstam, E., and Norling, B. (2015). Subcellular localization of carotenoid biosynthesis in *Synechocystis* sp. PCC 6803. *PloS One* 10, e0130904. doi: 10.1371/journal.pone.0130904

Conflict of Interest: The authors declare that the research was conducted in the absence of any commercial or financial relationships that could be construed as a potential conflict of interest.

Copyright © 2020 Izuhara, Kaihatsu, Jimbo, Takaichi and Nishiyama. This is an open-access article distributed under the terms of the Creative Commons Attribution License (CC BY). The use, distribution or reproduction in other forums is permitted, provided the original author(s) and the copyright owner(s) are credited and that the original publication in this journal is cited, in accordance with accepted academic practice. No use, distribution or reproduction is permitted which does not comply with these terms.

frontiers in Plant Science

ORIGINAL RESEARCH
published: 14 August 2020
doi: 10.3389/fpls.2020.01257

Role of Protein-Water Interface in the Stacking Interactions of Granum Thylakoid Membranes—As Revealed by the Effects of Hofmeister Salts

Ottó Zsiros[1], Renáta Ünnep[2], Gergely Nagy[3,4,5], László Almásy[2], Roland Patai[6], Noémi K. Székely[7], Joachim Kohlbrecher[3], Győző Garab[1,8], András Dér[6]* and László Kovács[1]**

[1] Institute of Plant Biology, Biological Research Centre, Szeged, Hungary, [2] Neutron Spectroscopy Department, Centre for Energy Research, Budapest, Hungary, [3] Laboratory for Neutron Scattering and Imaging, Paul Scherrer Institute, Villigen PSI, Switzerland, [4] Institute for Solid State Physics and Optics, Wigner Research Centre for Physics, Budapest, Hungary, [5] Neutron Scattering Division, Oak Ridge National Laboratory, Oak Ridge, TN, United States, [6] Institute of Biophysics, Biological Research Centre, Szeged, Hungary, [7] Jülich Centre for Neutron Science at MLZ, Forschungszentrum Jülich GmbH, Garching, Germany, [8] Department of Physics, Faculty of Science, University of Ostrava, Ostrava, Czechia

OPEN ACCESS

Edited by:
Przemysław Malec,
Jagiellonian University, Poland

Reviewed by:
Jean-David Rochaix,
Université de Genève, Switzerland
Lorenzo Ferroni,
University of Ferrara, Italy

***Correspondence:**
Győző Garab
gyozo@brc.hu
András Dér
der.andras@brc.hu
László Kovács
kovacs.laszlo@brc.hu

Specialty section:
This article was submitted to Plant Physiology, a section of the journal Frontiers in Plant Science

Received: 17 April 2020
Accepted: 30 July 2020
Published: 14 August 2020

Citation:
Zsiros O, Ünnep R, Nagy G, Almásy L, Patai R, Székely NK, Kohlbrecher J, Garab G, Dér A and Kovács L (2020) Role of Protein-Water Interface in the Stacking Interactions of Granum Thylakoid Membranes—As Revealed by the Effects of Hofmeister Salts. Front. Plant Sci. 11:1257. doi: 10.3389/fpls.2020.01257

The thylakoid membranes of vascular plants are differentiated into stacked granum and unstacked stroma regions. The formation of grana is triggered by the macrodomain formation of photosystem II and light-harvesting complex II (PSII-LHCII) and thus their lateral segregation from the photosystem I—light-harvesting complex I (PSI-LHCI) supercomplexes and the ATP-synthase; which is then stabilized by stacking interactions of the adjacent PSII-LHCII enriched regions of the thylakoid membranes. The self-assembly and dynamics of this highly organized membrane system and the nature of forces acting between the PSII-LHCII macrodomains are not well understood. By using circular dichroism (CD) spectroscopy, small-angle neutron scattering (SANS) and transmission electron microscopy (TEM), we investigated the effects of Hofmeister salts on the organization of pigment-protein complexes and on the ultrastructure of thylakoid membranes. We found that the kosmotropic agent $(NH_4)_2SO_4$ and the Hofmeister-neutral NaCl, up to 2 M concentrations, hardly affected the macro-organization of the protein complexes and the membrane ultrastructure. In contrast, chaotropic salts, $NaClO_4$, and NaSCN destroyed the mesoscopic structures, the multilamellar organization of the thylakoid membranes and the chiral macrodomains of the protein complexes but without noticeably affecting the short-range, pigment-pigment excitonic interactions. Comparison of the concentration- and time-dependences of SANS, TEM and CD parameters revealed the main steps of the disassembly of grana in the presence of chaotropes. It begins with a rapid diminishment of the long-range periodic order of the grana membranes, apparently due to an increased stacking disorder of the thylakoid membranes, as reflected by SANS experiments. SANS measurements also allowed discrimination between the cationic and anionic effects—in stacking and disorder, respectively. This step is followed by a somewhat slower disorganization of the TEM

ultrastructure, due to the gradual loss of stacked membrane pairs. Occurring last is the stepwise decrease and disappearance of the long-range chiral order of the protein complexes, the rate of which was faster in LHCII-deficient membranes. These data are interpreted in terms of a theory, from our laboratory, according to which Hofmeister salts primarily affect the hydrophylic-hydrophobic interactions of proteins, and the stroma-exposed regions of the intrinsic membrane proteins, in particular—pointing to the role of protein-water interface in the stacking interactions of granum thylakoid membranes.

Keywords: circular dichroism, granum, Hofmeister effect, thylakoid membranes, protein-water interface, small-angle neutron scattering, ultrastructure

INTRODUCTION

In oxygenic photosynthetic organisms the light reactions of photosynthesis occur in the thylakoid membranes, which are densely packed with pigment-protein complexes of the two photosystems (PSII and PSI) and other constituents of the photosynthetic machinery. These membranes are organized in multilamellar systems, which evidently warrant efficient light capturing. During the more than 3 billion years of evolution, cyanobacteria and the chloroplasts of algae of different classes have evolved an astounding variation regarding the composition and ultrastructure of their thylakoid membranes (Solymosi, 2012; Solymosi and Keresztes, 2012).

Vascular plants evolved about 420 million years ago (Harrison and Morris, 2018). In their thylakoid membranes the PSII and PSI core complexes are associated with light-harvesting antenna complexes, LHCII and LHCI, respectively; these membranes also contain the cytochrome b6f complex and the ATP-synthase. A striking feature of their chloroplast ultrastructure is the differentiation of the thylakoid membranes into granum and stroma regions, also called stacked, or appressed, and unstacked, or non-appressed regions, respectively. The cylindrical grana stacks, of typically 10–20 layers with a diameter of 300–600 nm, are interconnected by single thylakoids of several hundred nm in length. Although PSII and LHCII reside mainly in the stacked membranes and PSI and the ATP synthase are predominantly found in the stroma thylakoids (Andersson and Anderson, 1980), the thylakoid membranes retain their continuity and enclose a single interior aqueous phase, the thylakoid lumen, and separate it from the outer, stroma aqueous phase (Mustárdy and Garab, 2003). Although many elements of this highly organized complex ultrastructure evolved earlier and can be recognized in green algae, the organization of the thylakoids into granum-stroma membrane assembly is a relatively recent and immensely successful product of the evolution (Gunning and Schwartz, 1999; Mullineaux, 2005). Its success is marked by the fact that vascular plants generate over 90% of the terrestrial photosynthetic productivity.

The tight appression of the thylakoid membranes in the grana ensures that chloroplasts contain an extremely large area-to-volume ratio, i.e. an optimized packing density of the membranes (Mustárdy and Garab, 2003; Dekker and Boekema, 2005). Evidently, this can only be warranted by a mechanism sorting the proteins according to their stroma-side protruding sizes. Whereas the protrusion of PSII and LHCII towards the stroma are small (<2 nm) (Daum et al., 2010), PSI and the ATP synthase, respectively, extend about 4 and 16 nm above the membrane surface (Miller and Staehelin, 1976; Ben-Shem et al., 2003). The lateral sorting of the complexes has been shown to be facilitated by cation-induced aggregation of PSII-LHCII supercomplexes; this step is followed by stacking of the adjacent membranes enriched in PSII-LHCII, which then stabilizes the structure (Garab et al., 1991; Garab and Mustardy, 1999; see also Garab, 2016). Evidence for the presence of PSII-LHCII macrodomains with long-range chiral order of the chromophores in the grana has been provided by circular dichorism (CD) spectroscopy (see Garab and van Amerongen, 2009; Garab, 2014; Tóth et al., 2016; Lambrev and Akhtar, 2019); ordered, semi-crystalline arrays of the supercomplexes have also been detected by electron microcopy techniques (Kouřil et al., 2012). Model calculations—using a two-dimensional matrix and cation-screened Coulomb interactions and van der Waals forces, dipole-dipole interactions, and lipid-induced protein-protein attractions—assigned the lateral segregation of the two photosystems to an interplay between electrostatic and lipid-mediated interactions (Rojdestvenski et al., 2002). With the stacking of PSII-LHCII domains in the grana regions, the interthylakoidal gap, accommodating the outer loops of two opposed PSII-LHCII supercomplexes, can be as low as 3.2 nm (Daum et al., 2010) or, in partially dehydrated thylakoid membranes, 2.6 nm (Kirchhoff et al., 2008).

Electron microscopy and tomography techniques revealed a highly organized interwoven structure of the granum and stroma thylakoid membranes, with the basic features of the stacked layers of granum thylakoids which are interconnected by stroma thylakoids wound around the grana in a quasi-helical fashion (Paolillo, 1970; Mustárdy and Garab, 2003; Mustárdy et al., 2008; Daum et al., 2010; Adam et al., 2011; Austin and Staehelin, 2011; Kowalewska et al., 2016). The most recent and highly elaborated electron tomography images have also uncovered that the entire granum-stroma thylakoid network is consolidated by arrays of right- and left-handed helical membrane structures (Bussi et al., 2019).

The robust granal ultrastructure suggests a high stability of the thylakoid membrane system, which nevertheless remains remarkably flexible in response to dynamically changing environmental conditions. Light-induced dark-reversible

reorganizations have been shown to occur in isolated plant thylakoid membranes (Murakami and Packer, 1970; Garab et al., 1988; Nagy et al., 2011; Iwai et al., 2013) and in intact leaves (Ünnep et al., 2014). In general, different structural changes have been identified and linked to different short- and long-term regulatory mechanisms (Andersson and Anderson, 1980; Horton, 1999; Johnson et al., 2011; Nevo et al., 2012; Puthiyaveetil et al., 2016; Wood et al., 2018). Thus, granal thylakoid membranes evidently possess a high propensity to undergo well discernible structural changes. The plasticity of grana appears to be based on the inherent property of lipid: LHCII macroassemblies, which are capable to self-assemble into large arrays and to undergo reversible reorganizations induced by light and/or by subtle changes in the physico-chemical environment (Barzda et al., 1996; Zer et al., 1999; Simidjiev et al., 2000; Janik et al., 2013; Hind et al., 2014; Lambrev and Akhtar, 2019).

With regard to the physical mechanisms underlying the self-assembly and structural dynamics of the granum-stroma thylakoid membrane system, we can rely on many experimental observations and a few theoretical works. Most researchers agree that, in combination with van der Waals forces, electrostatic interactions, and particularly cations play key role in the stacking of membranes (see e.g. Garab and Mustardy, 1999; Chow et al., 2005; Dekker and Boekema, 2005; Daum and Kühlbrand, 2011). Indeed, it has been shown by electron microscopic studies that upon depletion of cations the granal structure is dismantled (Izawa and Good, 1966). The classical electrostatic theory of Gouy-Chapman has also been successfully applied to describe the surface-charge density of thylakoid membranes and its role in determining the structure and function of plant thylakoid membranes (Barber, 1982; Kana and Govendjee, 2016). The formation of large, chirally ordered lamellar aggregates of LHCII also depends on the proper electrostatic conditions (Simidjiev et al., 1997); and vice versa, the light-induced reversible reorganizations of lipid-LHCII macroarrays/membrane crystals were accompanied by release of cations (Garab et al., 2002; Hind et al., 2014). (For cation release of similar origin see Garab et al., 1998). Cation release associated with the functioning of the photosynthetic electron and proton transport has earlier been thoroughly documented (Hind et al., 1974).

Concerning the structural basis of stacking interactions in the grana, it has been shown that PSII-LHCII supercomplexes stack to each other *via* physical connections of specific N-terminal regions of the light-harvesting complexes that span the stromal gap—possibly through salt bridges between negatively-charged amino acid residues (Albanese et al., 2020). This model elegantly explains the stacking of granum membranes in the presence of the most abundant, so-called C_2S_2M PSII-LHCII supercomplexes in plants. It must, however, be noted that stacking could also be induced, by increasing the cation concentration, after large sections of the outer loop segments of thylakoid proteins had been digested by trypsin (Jennings et al., 1981). Also, chiral macrodomains can be generated in thylakoids of the chlorophyll *b*-less chlorina mutants, deficient in LHCII, but it requires considerably higher concentrations of Mg^{2+} than in the wild type; further, the concentration of osmoticum also had to be increased in the absence of LHCII (Garab et al., 1991). Further, the thermal stability of the chiral macrodomains, characteristic of the macro-organization of the protein complexes in the grana, have been shown to depend both on the ionic and osmotic strengths of the medium (Cseh et al., 2000) and on the lipid composition of membranes (Krumova et al., 2010) as well on the growth-light intensity of plants (Petrova et al., 2019).

In broad terms, the structural dynamics of grana can be explained within the frameworks of a theory explaining grana stacking *via* an interplay between repulsive electrostatic and hydrostructural and attractive, van der Waals forces (Puthiyaveetil et al., 2017). It is shown that variations in the electrostatic forces, which might be modulated by ionic movements (see above) or by the phosphorylation of LHCII or other phosphoproteins, affect both the lateral organization and stability of stacking. Other theoretical calculations have also shown that charge movements exert very strong effect on stacking interaction of membranes, and thus on the structural dynamics of grana (Majee et al., 2019). Within the frameworks of a theoretical model, investigating the effect of Mg^{2+} on the entropy of the system, it has been proposed that the underlying physical mechanisms might be a combination of several events: i) the attraction between discrete, oppositely-charged areas of grana; ii) the release of loosely-bound water molecules from the interthylakoidal space; iii) variations in the orientational freedom of water dipoles; and iv) the lateral rearrangements of membrane components (Jia et al., 2014).

The major aim of our work presented here is to obtain new insight on the forces involved in the self-assembly and dynamics of the granum-stroma thylakoid membrane system. To this end, we tested the effects of Hofmeister salts on the organization of pigment-protein complexes and the ultrastructure of thylakoid membranes. Contrary to cations, mobile anions are usually not considered exerting a direct effect on the complex organization of thylakoid membranes; however, they are well-known to have a determining role in Hofmeister effects (Lo Nostro and Ninham, 2012). Hofmeister effects are related to the ability of neutral salts, of moderate and high-salt concentrations (>100 mM), to modify the aggregation and crystallization properties of proteins (and colloid particles, in general), as well as to affect protein structure, dynamics and function (Collins and Washabaugh, 1985). Salts that facilitate aggregation and stabilize closed protein conformations, as in the most common native cases, are called kosmotropes, e.g., $(NH_4)_2SO_4$, NaF, Na-acetate; while the structure-destabilizing salts are called chaotropes, e.g., NaBr, $NaClO_4$, NaSCN. At the boundary between the two groups, NaCl is considered to be "Hofmeister-neutral", or slightly chaotropic. Note that Hofmeister effects are dominated by anions but, according to their similar effects, cations can also be arranged to a Hofmeister series, as well as non-ionic compounds such as polyols (Cacace et al., 1997).

Since kosmotropic ions are also shown to be "water structure makers", while chaotropes are "water structure breakers" (Robinson and Jencks, 1965), it has been generally believed that Hofmeister effects are mediated by water structure at the interacting interfaces (Melander and Horváth, 1977; Collins and Washabaugh, 1985), although a coherent theory was missing until 2007, when a phenomenological formalism using the protein-water interfacial tension, as a key parameter, could qualitatively account for the diversity of manifestations of Hofmeister effect (Dér et al., 2007). Based on the formal match of the theory with that of hydrophobic effects (Tanford, 1979), Hofmeister effects could be interpreted as a modification of hydrophobic/hydrophilic interactions, described by the surface terms of the Gibbs free energy. Since then, a row of experimental and theoretical evidences supporting the predictions of the theory have been published (Khoroshyy et al., 2013; Szalontai et al., 2013; Bogár et al., 2014; Násztor et al., 2016; Násztor et al., 2017; Kovacs et al., 2018).

Here, we investigated the effects of chaotropic salts on the complex structure of chloroplast thylakoid membranes by structure-sensitive experimental techniques—transmission electron microscopy (TEM), CD spectroscopy and small-angle neutron scattering (SANS)—in order to reveal the possible importance of hydrophobic/hydrophilic interactions in maintaining the hierarchical organization of these paradigmatic structural units of the photosynthetic energy-transducing machinery of plants. The two non-invasive techniques, CD spectroscopy and SANS are sensitive to the macro-organization of the protein complexes and of the thylakoid membranes, respectively.

CD spectroscopy in the visible range provides information on hierarchically organized molecular assemblies (Garab and van Amerongen, 2009). Ordered arrays of the pigment-protein complexes, such as the PSII-LHCII macrodomains, give rise to giant, psi-type CD (CDψ) signal (psi, polymer or salt induced), due to long-range interactions of the chromophores, whereas the pigment-protein complexes display excitonic CD signals arising from short-range interactions between pigment dipoles. SANS carries information on the periodicity and repeat distances (RDs) of multilamellar thylakoid membranes, averaged for the entire volume of sample exposed to the neutron beam (Nagy and Garab, 2020).

We show that chaotropic salts gradually break down the structure of granum thylakoids, contrary to their kosmotropic and Hofmeister-neutral counterparts which do not have substantial effects. The time-evolution of dismantling follows the order of descending hierarchical complexity, while the kinetics and extent of structural decline correspond to the position of chaotropic ions in the Hofmeister series. These findings are interpreted as a consequence of tousling the ordered intergranal water layer by the chaotropic agents. The results call the attention to the fundamental role of water molecules between adjacent thylakoid membranes, both in maintaining stability of and providing flexibility for granum stacks, the highly organized ultrastructures in chloroplasts.

MATERIAL AND METHODS

Plant Materials and Isolation of Thylakoid Membranes

Pea, barley and tobacco plants were grown in greenhouse at 22°C under natural light conditions. Thylakoid membranes were freshly isolated from 3-week-old pea (*Pisum sativum* sp. Rajnai törpe), 2-week-old wild-type and chlorina mutant barley (*Hordeum vulgare*) and 2.5-3-months-old tobacco (*Nicotiana tabacum* L. cv. Petit Havana SR) leaves, as described earlier (Zsiros et al., 2019). Leaves were homogenized in buffer A (50 mM Tricine-KOH pH 7.5, 0.4 M sorbitol, 5 mM $MgCl_2$, 5 mM KCl). The homogenate was filtered through four layers of cheesecloth and the supernatant was centrifuged for 2 min at 300×*g*. After the centrifugation, the supernatant was further centrifuged at 5,000×*g* for 10 min. The pellet was resuspended in the hypotonic buffer B (50 mM Tricine-KOH pH 7.5, 5 mM $MgCl_2$, 5 mM KCl). After a short, 5–10 s, osmotic shock, breaking the envelope membrane, the osmolarity was returned to isotonic conditions by adding equal volume of double-osmotic medium (50 mM Tricine-KOH pH 7.5, 0.8 M sorbitol, 5 mM $MgCl_2$, 5 mM KCl) and the suspension was centrifuged at 5,000×*g* for 10 min. The pellet containing intact thylakoid membranes were resuspended in buffer A and used for further measurements. All steps of the isolation were performed at 4°C and in a dim light. Light-harvesting complexes were purified from pea leaves as previously described (Simidjiev et al., 1997).

Circular Dichroism Spectroscopy

CD spectra were measured on a Jasco J-815 CD spectropolarimeter at room temperature with a bandwidth of 2 nm and data pitch of 1.0 nm. The scan speed was set to 100 nm/min and the integration time was 1 s. Simultaneously with the CD spectra, absorption spectra were recorded as well and the CD spectra were normalized to the red absorbance maxima, at around 680 nm. 750 nm reference wavelength was used to determine the amplitude of the (+)690, (-)675 and (+)505 CDψ bands. The chlorophyll concentration of the samples was 30 μg/ml. Three to five independent biological replicates were measured. The exact number is indicated in the *Figure Legends*.

Specimen Preparation for Electron Microscopy

Thylakoid membranes were fixed in Karnovsky solution containing 2% paraformaldehyde (Sigma; St. Louis, MO, United States) and 2.5% glutaraldehyde (Polysciences; Warrington PA, United States) in phosphate buffer for overnight at 4°C. After fixation, the samples were rinsed in distilled water (pH 7.4) for 10 min followed by a 2% osmium tetroxide (in distilled water, pH 7.4) solution for 60 min. After osmification, the samples were briefly rinsed in distilled water for 10 min, then dehydrated through a graded series of ethanol (from 50% to 100%; Molar; Halasztelek, Hungary) for 10 min in each concentration and proceeded through propylene oxide. Dehydrated samples were embedded in an epoxy-based resin

(Durcupan ACM; Sigma), then polymerized at 56°C for 48 h. 50 nm ultrathin sections were cut from the resin blocks on an Ultracut UCT ultramicrotome (Leica; Wetzlar, Germany) and samples were mounted on single-hole formvar-coated copper grids (Electron Microscopy Sciences; Hatfield, PA, United States). Ultrathin sections were contrasted with 2% uranyl acetate (Electron Microscopy Sciences) in 50% ethanol (Molar) and 2% lead citrate (Electron Microscopy Sciences) in distilled water. Samples were systematically screened at 5,000× magnification to localize the membranes on the grid. Afterwards, images of thylakoid membranes were recorded at 10,000-20,000× magnification with a 16 MP Matataki Flash scientific complementary metal–oxide–semiconductor (sCMOS) camera (JEOL).

Small-Angle Neutron Scattering (SANS)

The experiments were performed on the SANS I instrument of the Paul Scherrer Institute (PSI, Villigen, Switzerland). The applied settings for the measurement of the samples were: SD, 11 m; collimation, 15 m; λ, 6 Å. (SD, sample-to-detector distance; λ, neutron wavelength). Isolated thylakoid membranes of about 1 mg/ml chlorophyll content, suspended in ^2H_2O-based buffer A (Nagy et al., 2011), were filled in quartz cuvettes with 2 mm path length and were aligned in a magnetic field, using permanent magnets of ~ 0.4 T field strength, providing a magnetic field in the horizontal direction perpendicular to the neutron beam. Data obtained with pea, spinach and tobacco thylakoid membranes were qualitatively similar to each other but tobacco displayed the most intense Bragg peak, and thus tobacco thylakoids were used for quantitative analysis. All experimental data were corrected for detector efficiency and normalized to the number of incoming neutrons; the instrumental background, recorded with the beam blocked by cadmium was subtracted. For data treatment, the "Graphical Reduction and Analysis SANS Program" package (GRASP) (developed by C. Dewhurst, ILL) was used. The recorded 2D scattering signal was radially averaged in two sectors with 75° opening angle, and the scattering intensity (I) was plotted as a function of the scattering vector, Q, and used for further analyses. RD was calculated using the formula $RD=2\pi/Q^*$, where Q^* is the position of the Bragg peak (Nagy and Garab, 2020).

Time resolved measurements were carried out to survey the structural changes in isolated thylakoid membranes upon exposure to different concentrations of NaSCN, NaCl, and $NaClO_4$, using 5 M stock solutions and different volumes of ^2H_2O-based buffer A, in order to obtain the same dilution. To minimize the dead-time (to about 1 min), the salt solutions were added directly into the cuvettes containing the untreated control.

Three independent biological replicates were measured.

RESULTS

The effect of Hofmeister salts on the macro-organization of pigment-protein complexes of thylakoid membranes was investigated by CD spectroscopy. Thylakoid membranes isolated from pea were treated with salts ranked at different positions of the Hofmeister series at various concentrations, and the changes in the amplitudes were followed as a function of time. In untreated membranes, the CD spectra are dominated by CDψ bands, originating from long-range interactions in chirally organized PSII-LHCII macrodomains, peaking at around (+)690, (-)675, and (+)505 nm (Garab and van Amerongen, 2009, see also **Figure 1**).

The kosmotropic salt, $(NH_4)_2SO_4$, did not induce any observable changes in the CD spectrum at 1 M concentration (**Figure 1B**). At the same concentration, NaCl, regarded as a Hofmeister neutral salt, caused very slight decrease in the psi-type CD bands (**Figure 1C**) while weaker and stronger chaotropic agents, $NaClO_4$ (**Figure 1D**) and NaSCN (**Figure 1E**), respectively, diminished the CDψ signals, with more pronounced effect observed with NaSCN. At the same time, no significant effects were observed on the excitonic bands at around (-)650 nm and between 400 and 460 nm. (Some losses in the excitonic band-pair of $CD_{480\text{-}470\ nm}$ originate from the monomerization of LHCII trimers (Garab and van Amerongen, 2009). The time courses of the CD-changes at different wavelengths upon chaotropic treatment showed that the different CDψ amplitudes decreased at different rates (**Figure 2**). The fastest rate was observed for the (-)675 nm band while the (+)690 and (+)505 nm bands exhibited a significantly slower kinetics.

The concentration dependence of chaotropic salts was also in good agreement with their rank in the Hofmeister series. As shown in **Figure 3**, NaCl exerted only marginal effects on the CD signals, whereas NaSCN proved to be stronger than $NaClO_4$.

It has been shown that ionic strength and osmotic potential has a role in the macro-organization of thylakoid membranes, detected by CD spectroscopy (Garab et al., 1991) and SANS measurements (Posselt et al., 2012). To assess their possible contribution to the chaotropic-salt induced changes, we recorded CD spectra of isolated thylakoid membranes exposed to different mixtures of NaCl and NaSCN, in which the ionic strength, osmotic potential and sodium ion concentration were kept constant (**Figure 4**). The gradual exchange of Cl^- to SCN^- led essentially to the same changes in the CD spectrum as NaSCN alone, indicating that the alterations in the thylakoid macro-organization were caused mainly by the Hofmeister effect of the SCN^- anion.

In order to test the chaotropic effect on membrane stacking, and to compare TEM data with CD, aliquots were taken at 0, 1, 5, and 20 min after the addition of 0.5 M NaSCN to the membranes; these aliquots were fixed immediately with 2% glutaraldehyde. By applying time-series CD measurements on glutaraldehyde-treated thylakoid membranes, we proved that glutaraldehyde fixation efficiently prevented the effect of NaSCN (**Figure 5**). Glutaraldehyde-fixed untreated and NaSCN-treated samples were subjected to further conventional fixation for subsequent TEM analysis (**Figure 6**). TEM images revealed well-defined intact grana in the control samples (**Figure 6A**), which were largely disorganized already 1 min after the addition

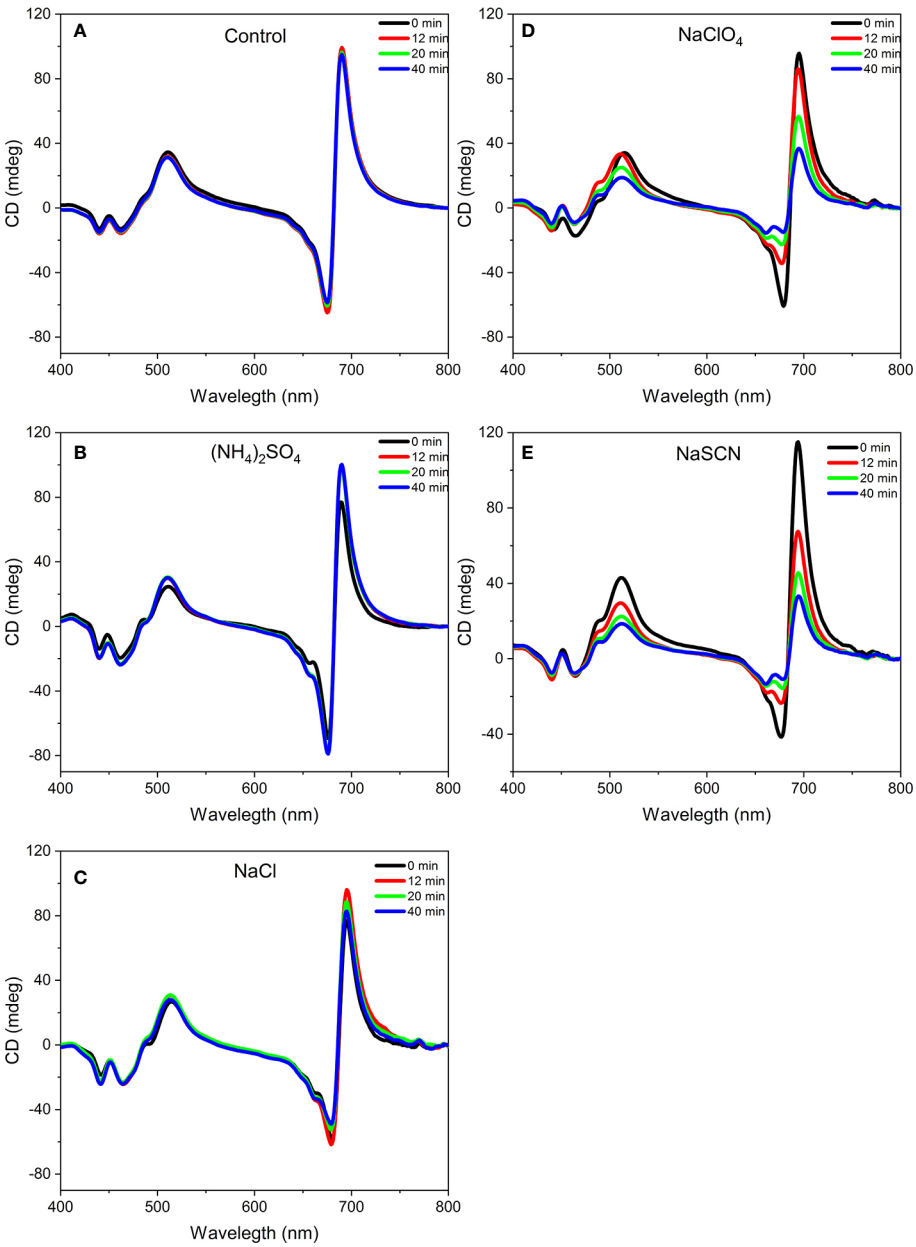

FIGURE 1 | Representative circular dichroism spectra of isolated pea thylakoid membranes without treatment **(A)** and before (0 min) and after (12, 20, and 40 min) of their treatments with 1 M $(NH_4)_2SO_2$ **(B)**, 1 M NaCl **(C)**, 1 M $NaClO_4$ **(D)**, and 1 M NaSCN **(E)**. The spectra are normalized to the corresponding red absorbance maxima [OD(680 nm)=1.0] of the untreated samples. Note that the 12, 20, 40 min traces in **(A)**, and the 0 and 12 min traces in **(B)**, largely overlap. Five independent biological replicates were measured and a typical data set is shown.

of NaSCN (**Figure 6B**). After 5 min (**Figure 6C**), the presence of grana could not be discerned but membranes with tight stacking were still present. After 20 min (**Figure 6D**), virtually only single membranes remained, which formed large vesicles, some of which appeared to contain stacked membrane regions. As shown in **Figure 6E**, the CDψ bands persisted longer than the well-defined granal ultrastructure. After 20 min of NaSCN addition, more than 60% of the CDψ bands were still present, when the grana had already disappeared (cf. **Figure 6D**).

In order to determine the chaotropic effect on the periodic organization of the thylakoid membranes, SANS experiments were performed. The effects of NaCl and NaSCN on the membrane organization were compared with each other at 0.1, 0.5, and 1.5 M concentrations, and with the untreated sample (**Figure 7**). Control thylakoid samples exhibited scattering curves with a characteristic diffraction peak, Q*, at around 0.2 $Å^{-1}$ (Nagy et al., 2011). Via fitting the curves with the sum of a power function and a Gaussian (see Nagy et al., 2013), the RD of the

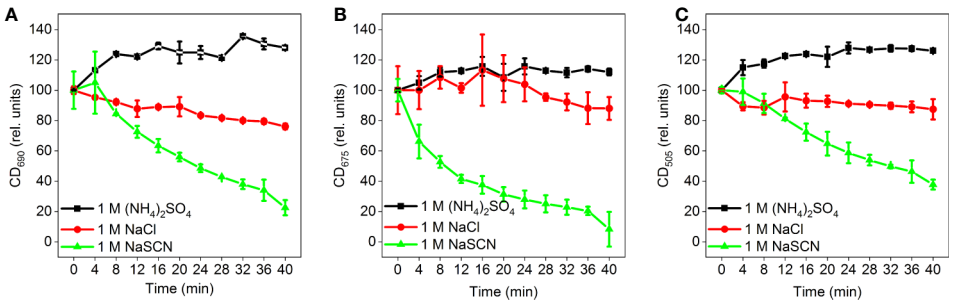

FIGURE 2 | Time-courses of the effects of different Hofmeister salts on the amplitudes of the different CD_{Ψ} bands of isolated pea thylakoid membranes: **(A)** (+)690 CD_{Ψ}, **(B)** (-)675 CD_{Ψ}, and **(C)** (+)505 CD_{Ψ}; the corresponding CD amplitudes were determined with reference to the 750 nm signals. The membranes were treated at t= 0 min with 1 M $(NH_4)_2SO_4$, 1 M NaCl, and 1 M NaSCN, as indicated. Data points are representing the mean values of five independent biological replicates ± SD.

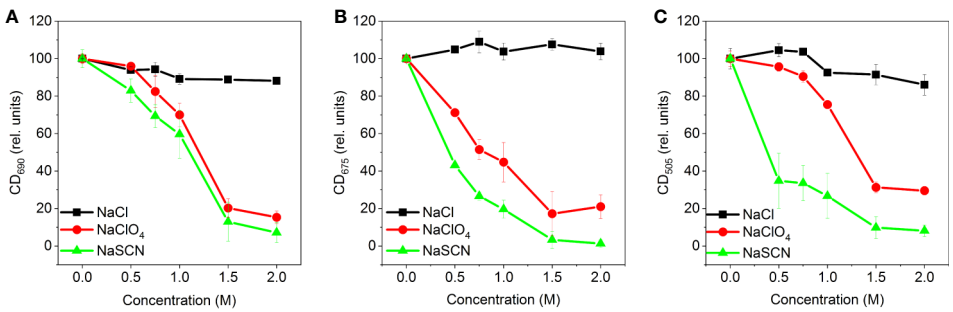

FIGURE 3 | Concentration dependences of the effects of different Hofmeister salts (NaCl, $NaClO_4$, and NaSCN) on the amplitudes of CD_{Ψ} bands of isolated pea thylakoid membranes: **(A)** (+)690 CD_{Ψ}, **(B)** (-)675 CD_{Ψ} and **(C)** (+)505 CD_{Ψ}; the amplitudes, relative to the control, were determined 20 min after the treatment, with reference to the corresponding 750 nm signal. Data points are representing the mean of three independent biological replicates ± SD.

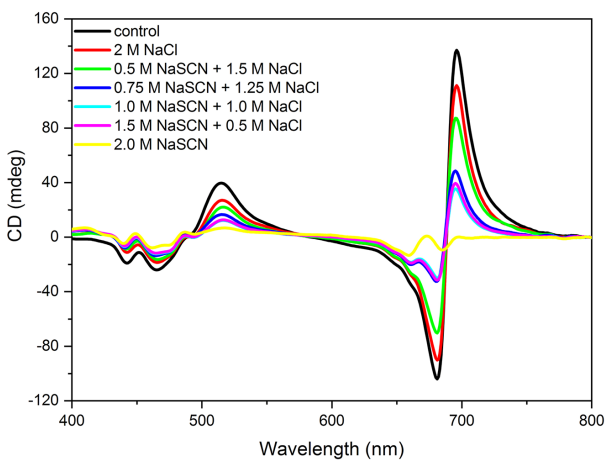

FIGURE 4 | CD spectra of isolated pea thylakoid membranes in the absence (control) and presence of 2 M Hofmeister-salt combinations composed of NaCl and NaSCN—with constant Na^+ concentration and different concentrations of Cl^- and $(SCN)^-$, as indicated. The spectra were recorded 20 min after the treatments. The spectra are normalized to the corresponding red absorbance maxima [OD(680 nm)=1.0] of the untreated samples. Three independent biological replicates were measured and a typical data set is shown.

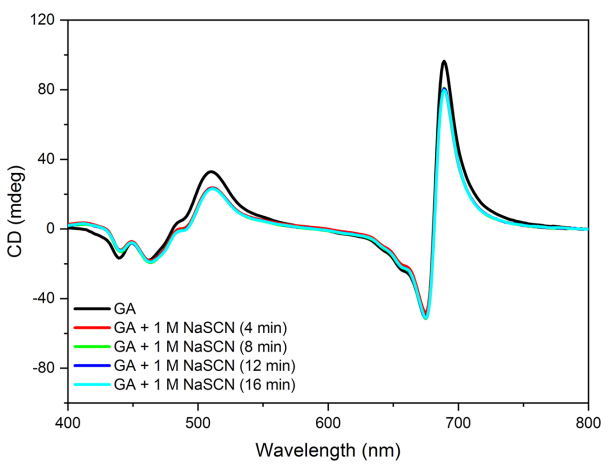

FIGURE 5 | CD spectra of isolated pea thylakoid membranes fixed for 1 min with 2% glutaraldehyde (GA) and spectra of GA-fixed membranes treated with 1 M NaSCN and recorded at different times after the GA fixation. The spectra are normalized to the red absorbance maximum [OD(680 nm)=1.0] of the GA-treated sample. Note that the 4, 8, 12, and 16 min traces overlap. Three independent biological replicates were measured and a typical data set is shown.

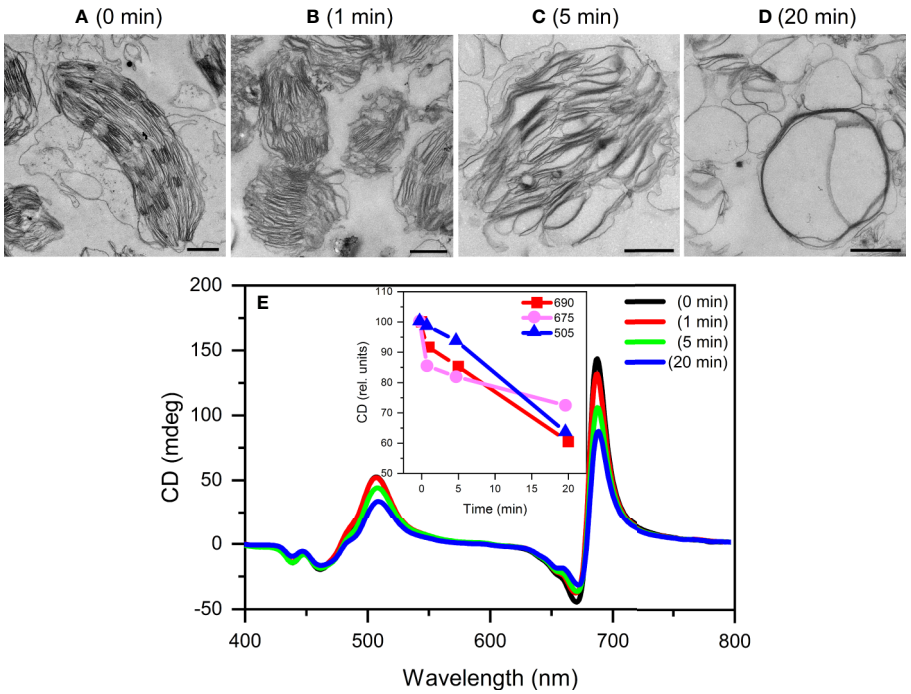

FIGURE 6 | Typical TEM images **(A–;D)** and CD spectra **(E)** of untreated (0 min) and 0.5 M NaSCN treated isolated pea thylakoid membranes obtained after different time intervals following the treatment at t=0 min. The treatments were halted at 1, 5 and 20 min by 2% glutaraldehyde and the membranes were then used for TEM and CD experiments. Inset in **(E)**, time course of the variations in the different CD_ψ bands. Scale bars in **(A–D)**, 1 μm.

thylakoid membranes was estimated to be 332 ± 2 Å (mean value ± SD from eight samples). This value is somewhat larger than the RD values obtained earlier by SANS and EM under similar experimental conditions (Ünnep et al., 2014). Upon the addition of 0.1 M NaCl, the characteristic peak shifted to higher momentumtransfer values. Similar shrinkage has earlier been reported upon increasing the concentration of the osmoticum (Posselt et al., 2012) and upon replacing sorbitol for NaCl in the suspension medium (Ünnep et al., 2014). The structural changes induced by the addition of 0.1 M NaCl were essentially completed on the time-scale of few minutes (**Figure 7A**). At 0.1 M, the effect of NaSCN treatment was very similar to that of NaCl (**Figure 7B**). This suggests that, at this relatively low concentration, the structural changes are predominantly induced by a cationic effect—leading to a decrease in the RD of the thylakoid membranes to between about 280 and 290 Å. Indeed, high concentrations of monovalent cations, in the range of some hundred millimolar concentrations, have been shown to induce stacking (Izawa and Good, 1966; Hind et al., 2014). It was also interesting to note that both with NaCl and NaSCN the integrated Bragg-peak intensities decreased to very similar extents, to about 50% compared to the control. This may originate from some contrast-losses due to a narrowing of the interthylakoidal space in the grana.

At 0.5 M, NaCl induced some further shrinkage of the thylakoid membranes to about 260 Å, a value which was reached in a few minutes (**Figure 7C**). In contrast, at this concentration, the chaotropic effect of NaSCN became clearly discernable (**Figure 7D**): in addition to the shrinkage, the amplitude of the Bragg peak dramatically decreased compared to the NaCl-treated sample and the peak was gradually smeared—a clear sign of the gradual loss of the periodic order of the thylakoid membranes. Also, $NaClO_4$ treatments caused a similar, gradual loss in the Bragg peak (data not shown), corroborating the notion that deteriorations of the membrane ultrastructure were caused by Hofmeister effect. With 1.5 M NaCl, while sufferred some further scattering intensity losses, the periodic order of the thylakoid membranes was largely retained (**Figure 7E**). In contrast, with 1.5 M NaSCN the decay of the periodic membrane ultrastructure was spectacularly accelerated; it was lost in less than 5 min (**Figure 7E**). It is to be noted here, that these agents, including even NaCl, might have also induced changes in the microscopic structure of the membranes, affecting their form factor and thus their scattering length distributions, which could, in principle, be analyzed within an advanced mathematical model recently elaborated for cyanobacteria (Jakubauskas et al., 2019). This would require a detailed and systematic approach, paying also attention to the substantial differences between the ultrastructure of thylakoid membranes in cyanobacteria and higher plants; this is outside the scope of the present study.

In order to test if and how much the Hofmeister effects depend on the macro-organization of the protein complexes, and on the LHCII content of grana, in particular, we performed experiments on wild type and chlorophyll-b-less, chlorina-f2 mutant of barley. This mutant has been reported to lack LHCs but to retain the granal structures of WT plants (Goodchild et al.,

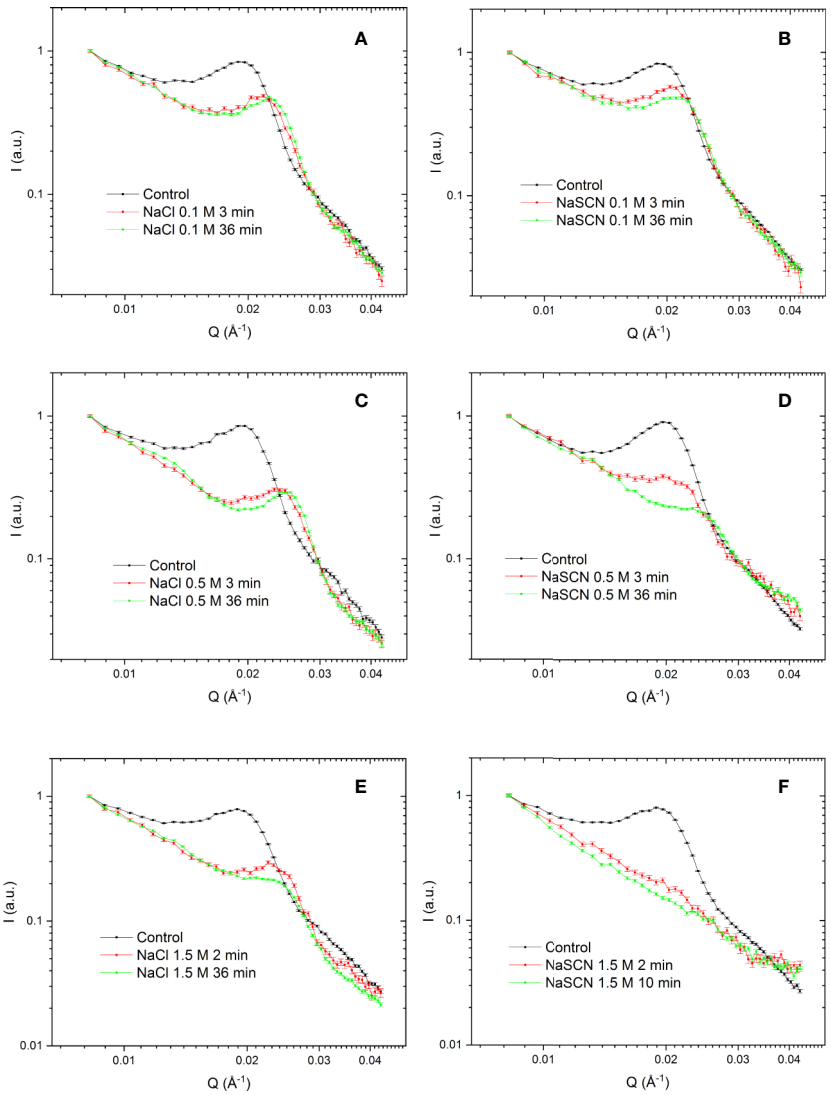

FIGURE 7 | SANS profiles of isolated tobacco thylakoid membranes in the absence (control) and presence of different concentrations of NaCl **(A**, **C**, **E)** and NaSCN **(B**, **D**, **F)** recorded at different times after the addition of salts. To optimize the S/N of the SANS curves, different data acquisition and averaging times (1-5 min) were applied, dictated by the rate of structural changes induced by NaSCN. The time-labels mark the midtimes between the start and the end of data acquisition. For better comparison all curves are normalized to 1 at Q = 0.00832 Å^{-1}. Three independent biological replicates were measured and a typical data set is shown.

1966). The CD spectra of detached leaves of the chlorina-f2 mutant has been shown to possess relatively strong (+)690 and (−)674 nm CDψ bands, but weak (+)506 nm band, indicating a different type of lateral organization of PSII supercomplexes (Tóth et al., 2016). A comparison of CD spectra of thylakoid membranes isolated from the wild type and mutant leaves in an earlier study revealed that the generation of the psi-type bands required considerably higher ionic strength to screen the negative repulsive forces, and higher concentration of the osmoticum than in the wild type (Garab et al., 1991). In accordannce with these data, compared to the wild type thylakoids (**Figure 8A**), chlorina-f2 membranes displayed weaker psi-type CD bands (**Figure 8B**). We also observed that the (+)690 nm CDψ of thylakoid membranes isolated from chlorina-f2 mutant exhibited higher sensitivity to chaotropic agents than the wild-type membranes (**Figure 8C**); data in **Figure 8** also demonstrate that Hofmeister salts on barley thylakoid membranes exert similar effects as in pea. Further, these data support the notion (Tóth et al., 2016) that LHCII plays a major role in the stabilization of the macro-organization of protein complexes in the thylakoid membranes.

We also investigated the Hofmeister effect on the structure of LHCII itself. Isolated LHCII microcrystals were exposed to 2 M NaSCN. The presence of CDψ at (-)684 nm in these tigthly stacked lamellar aggregates of isolated LHCII indicates the long-range order of the chromophores, warranted by the ordered

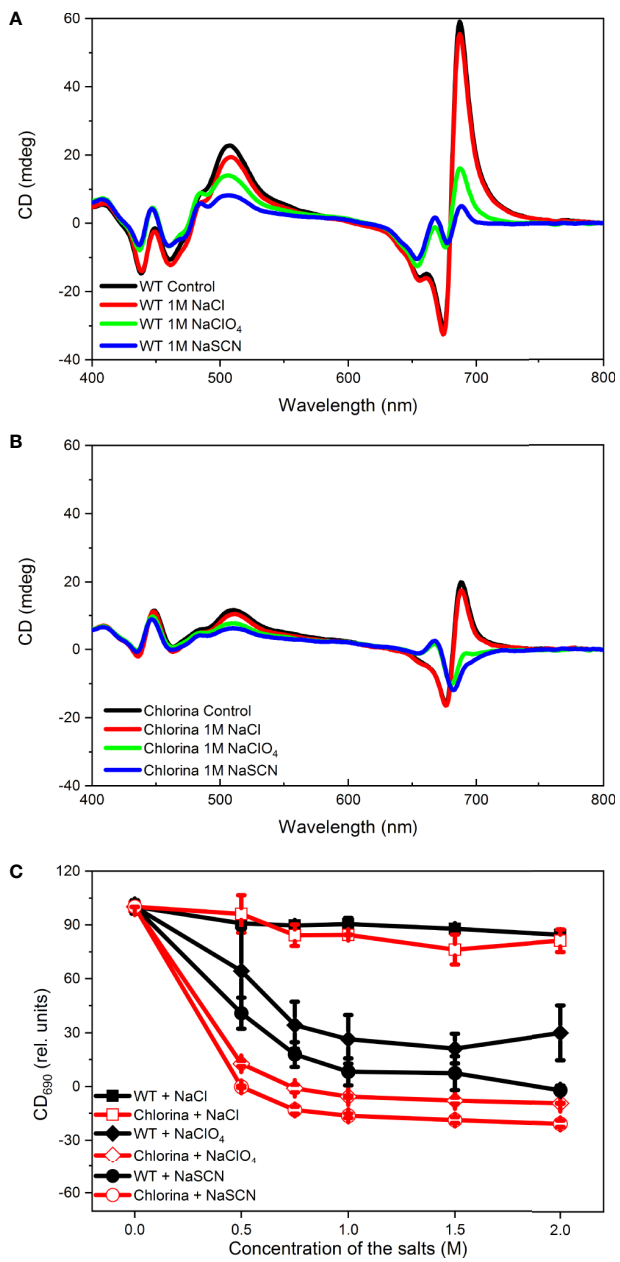

FIGURE 8 | Concentration dependence of the effects of NaCl, $NaClO_4$ and NaSCN on the CD spectra of WT **(A)** and Chl-b-less (Chlorina) mutant **(B)** barley thylakoid membranes. The amplitudes of (+)690 CD_ψ **(C)**, relative to the untreated control were determined 60 min after the addition of salts. Data points are representing the mean of 5 independent biological replicates ±SD.

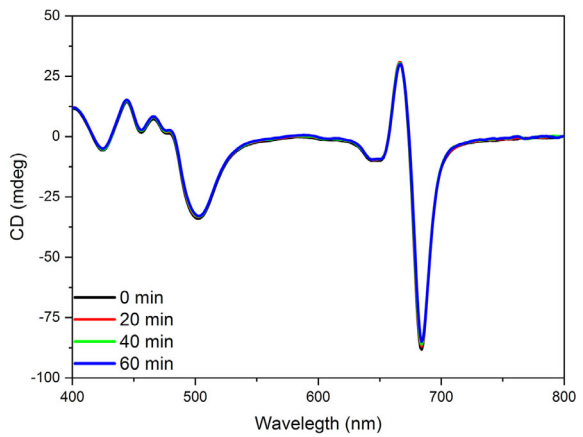

FIGURE 9 | CD spectra of untreated (0 min) and 2 M NaSCN treated LHCII microcrystals at different times after the start of the treatment, as indicated. The spectra are normalized to the red absorbance maximum [OD(680 nm) =1.0] of the untreated samples. Note that the 0, 20, 40, and 60 min traces overlap. Three independent biological replicates were measured and a typical data set is shown.

array of LHCII apoproteins (Miloslavina et al., 2012). Neither the excitonic bands, originating from the short range pigment-pigment interactions within LHCII subunits, nor the CDψ exhibited significant changes during the 1-h long incubation time, showing that NaSCN has no chaotropic effect on LHCII itself (**Figure 9**).

DISCUSSION

Understanding the physical mechanisms of the interactions stabilizing the complex, hierarchical structure of plant chloroplast thylakoid membranes is of pivotal importance in photosynthesis research. The role of electrostatic interactions (both cation-mediated attractive, and the repulsive forces) as well as the van der Waals forces (attractive) have been extensively studied and are relatively well-understood for interacting membrane surfaces (Barber, 1982; Jia et al., 2014; Puthiyaveetil et al., 2017). As concerns the narrow, densely packed interthylakoidal space in the granum, domination of steric factors, direct protein-protein contacts (Daum et al., 2010; Hind et al., 2014; Albanese et al., 2020) and the role of highly ordered proteinaceous domains (Garab, 2014; Lambrev and Akhtar, 2019) at the interface of adjacent membranes should also be considered, with special regard to the hydration forces.

Presently relatively little is known about the possible role of hydration forces in stabilizing the chloroplast structure. Based on earlier experiments on model phospholipid membranes (Cowley et al., 1978), it is generally assumed that hydration forces, emerging from layers of ordered water molecules, mediate a repulsive interaction between adjacent membrane surfaces. In fact, hydration forces tend to dominate over the van der Waals forces below separations of a few nanometers, as shown by AFM measurements (Israelachvili and Pashley, 1983; Butt, 1991) (see also Puthiyaveetil et al., 2017). Hence, an equilibrium distance in this range is expected in such cases, as, e.g., that of neighboring thylakoid membranes, as well (Chow et al., 2005). Additionally, it can also be argued that oppositely ordered water layers may give rise to an increase of flexibility of the system by facilitating the lateral sliding of neighboring thylakoid membranes (Jia et al.,

2014). A massive body of experimental evidences proves that multilevel regulatory mechanisms in the photosynthetic apparatus require a high level of structural and functional plasticity, ensured by a delicate balance between structural stability and flexibility of multilamellar membrane systems (see *Introduction*).

Our experimental results show that chaotropic Hofmeister salts decrease the stability of chloroplast structure at all levels of its hierarchical organization; at the same time the Hofmeister neutral NaCl and the kosmotropic agent $(NH_4)_2SO_4$ exerted only marginal effects (**Figure 1**). The magnitude and kinetics of the effects are in line with the position of the salts in the Hofmeister series (**Figures 2** and **3**), and can be clearly assigned to the chaotropic effect of SCN^- anions, independent or despite the strong effect of high concentrations of Na^+ cations (**Figure 4**). These marked effects of the Hofmeister salts on the protein macrodomains, and the disassembly of grana (**Figures 6** and **7**) strongly suggest the essential role of hydrophobic/hydrophilic interactions in maintaining the native structure of chloroplasts.

With regard to the sequence of events, it can be seen that the disassembly of granum follows the reverse order when compared to its assembly. Upon treatment by the chaotropic salt NaSCN, the periodicity of the stacked multilamellar array of granum thylakoid membranes was perturbed first, and was lost gradually—as reflected by the gradual weakening and loss of the Bragg diffraction peak (**Figure 7**), as well as by TEM images (**Figure 6**). At high concentrations of NaSCN this occurs virtually as a prompt effect, in less than 2 min (**Figure 7**). It is also interesting to observe that the disassembly of the grana is superimposed on the shrinkage of thylakoid membranes, evidently reflecting an increased stacking due to the high ionic strength/screening effects of Na^+ ions, possibly also combined with its osmotic effect reducing the lumenal volume. The loss of the periodic order of the thylakoid membranes is followed by the gradual diminishment of the CDψ bands, characteristic of the long-range chiral order of the chromophores in the granum stacks. The presence of CDψ bands, while also depends on the presence of the 3D ultrastructure (Keller and Bustamante, 1986; Garab and van Amerongen, 2009), is diagnostic of the long-range order of the PSII-LHCII supercomplexes. Chaotropic agents gradually dismantle the well-ordered protein macro-arrays; only marginally affecting the LHCII complexes, which, as also shown here (**Figure 8**), play a stabilizing role in the grana. In line with these observations, it was also interesting to observe that tightly stacked microcrystalline lamellar aggregates LHCII (Simidjiev et al., 1997) were not susceptible to Hofmeister effect (**Figure 9**) probably due to lack of structured water between the layers. These aggregates of LHCII with long-range chiral order probably assume the same structure as published by Standfuss et al. (2005) with very close contact between stromal-side residues. Also, in contrast to the loosely stacked LHCII membrane crystals (Hind et al., 2014), which are capable of undergoing dark-reversible light-induced reorganizations, the tightly stacked LHCII lamellar aggregates showed very high stability (Simidjiev et al., 1997).

As for the molecular interpretation of the effects, it can be argued that the highly ordered, structured water-layers between the adjacent granum membrane surfaces are prone to be disturbed by chaotropic anions. As a consequence, the spacer function of the hydration layer is destroyed, yet accompanying with an increased level of fluctuations of the interfacial structure (Dér and Ramsden, 1998; Neagu et al., 2001; Násztor et al., 2016). In fact, SANS signals show that the effects start with a decrease of the periodic order of the stacked membranes. This occurs before the further disassembly of the highly-organized membrane structure take place, as reflected by CDψ, which originate from the long-range chiral order of LHCII and LHCII : PSII supercomplexes in the grana. The most probable scenario for the subsequent events is that, following the collapse of the native interthylakoidal organization, the geometrical constraints, stabilizing the complementary charge patterns, are surpassed by conformational fluctuations. Hence, long-range repulsive forces, due to the overall negative charge of the membranes and the protein residues, start to dominate—loosening the original membrane structure, eventually leading to the destabilization of PSII-LHCII arrays and, albeit only marginally, the supercomplexes themselves.

The results highlight the primary importance of hydration forces in the stabilization of granum stacking inside chloroplasts, and are expected to have general implications for better understanding the structural dynamics of other multifolded membrane organelles, such as mitochondria, as well.

DATA AVAILABILITY STATEMENT

The original contributions presented in the study are included in the article/supplementary material; further inquiries can be directed to the corresponding authors.

AUTHOR CONTRIBUTIONS

LK, AD, and OZ conceived the study. The plants were grown and treatments on isolated thylakoid membranes were applied by OZ, who also carried out the CD spectroscopic measurements. RP carried out the electron microscopy experiments, with the data analyzed by RP, OZ, and GG. SANS measurements were configured by JK (SANS-I) and NS (KWS-2), performed and analyzed by GN, LA, and RÜ with the participation of GG. The paper was written by GG, AD, LK, GN, and OZ, with all authors contributing to the writing.

FUNDING

This work was supported by grants of the National Research Development and Innovation Office of Hungary (OTKA KH

124985 and K 128679), and of the Czech Science Foundation (GACR 19-13637S) to GG. GN was, in part, supported by the János Bolyai Research Scholarship of the Hungarian Academy of Sciences and by the ÚNKP-19-4 New National Excellence Program of the Ministry for Innovation and Technology. Infrastructural background and theoretical work was partially supported by the Ministry for National Economy of Hungary through the GINOP-2.3.2-15-2016-00001 program (RP and AD).

ACKNOWLEDGMENTS

We would like to thank the Paul Scherrer Institute (PSI), Villigen, Switzerland, for providing us beamtime for the SANS experiments on the SANS-I beam-line at the Swiss Spallation Neutron Source SINQ. This work is also based on experiments performed at the KWS2 instrument operated by JCNS at the Heinz Maier-Leibnitz Zentrum (MLZ), Garching, Germany. We also would like to thank to János Györgyey who provided us the tobacco plants.

REFERENCES

Adam, Z., Charuvi, D., Tsabari, O., Knopf, R. R., and Reich, Z. (2011). Biogenesis of thylakoid networks in angiosperms: knowns and unknowns. *Plant Mol. Biol.* 76, 221–234. doi: 10.1007/s11103-010-9693-5

Albanese, P., Tamara, S., Saracco, G., Scheltema, R. A., and Pagliano, C. (2020). How paired PSII–LHCII supercomplexes mediate the stacking of plant thylakoid membranes unveiled by structural mass-spectrometry. *Nat. Commun.* 11, 1361. doi: 10.1038/s41467-020-15184-1

Andersson, B., and Anderson, J. M. (1980). Lateral heterogeneity in the distribution of chlorophyll–protein complexes of the thylakoid membranes of spinach chloroplasts. *Biochim. Biophys. Acta* 593, 427– 440. doi: 10.1016/0005-2728(80)90078-X

Austin, J. R., and Staehelin, L. A. (2011). Three-dimensional architecture of grana and stroma thylakoids of higher plants as determined by electron tomography. *Plant Physiol.* 155, 1601–1611. doi: 10.1104/pp.110.170647

Barber, J. (1982). Influence of surface charges on thylakoid structure and function. *Ann. Rev. Plant Physiol.* 33, 261–295. doi: 10.1146/annurev.pp.33.060182.001401

Barzda, V., Garab, G., Gulbinas, V., and Valkunas, L. (1996). Evidence for long-range excitation energy migration in macroaggregates of the chlorophyll ab light-harvesting antenna complexes. *Biochim. Biophys. Acta* 1273, 231–236. doi: 10.1016/0005-2728(95)00147-6

Ben-Shem, A., Frolow, F., and Nelson, N. (2003). Crystal structure of plant photosystem I. *Nature* 426, 630–635. doi: 10.1038/nature02200

Bogár, F., Bartha, F., Násztor, Z., Fábián, L., Leitgeb, B., and Dér, A. (2014). On the Hofmeister Effect: fluctuations at the protein–water interface and the surface tension. *J. Phys. Chem. B* 118, 8496–8504. doi: 10.1021/jp502505c

Bussi, Y., Shimoni, E., Weiner, A., Kapon, R., Charuvi, D., Nevo, R., et al. (2019). Fundamental helical geometry consolidates the plant photosynthetic membrane. *Proc. Natl. Acad. Sci. U. S. A.* 116, 22366–22375. doi: 10.1073/pnas.1905994116

Butt, J.-H. (1991). Measuring electrostatic, van der Waals, and hydration forces in electrolyte solutions with an atomic force microscope. *Biophys. J.* 60, 1438–1444. doi: 10.1016/S0006-3495(91)82180-4

Cacace, M. G., Landau, E. M., and Ramsden, J. J. (1997). The Hofmeister series: salt and solvent effects on interfacial phenomena. *Q. Rev. Biophys.* 30, 241–277. doi: 10.1017/s0033583597003363

Chow, W. S., Kim, E.-H., Horton, P., and Anderson, J. M. (2005). Granal stacking of thylakoid membranes in higher plant chloroplasts: the physiochemical forces at work and the functional consequences that ensue. *Photochem. Photobiol. Sci.* 4, 1081–1090. doi: 10.1039/b507310n

Collins, K. D., and Washabaugh, M. W. (1985). The Hofmeister effect and the behavior of water at interfaces. *Q. Rev. Biophys.* 18, 323–422. doi: 10.1017/S0033583500005369

Cowley, A. C., Fuller, N. L., Rand, R. P., and Parsegian, V. A. (1978). Measurement of repulsive forces between charged Phospholipid bilayers. *Biochemistry* 17, 3163–3168. doi: 10.1021/bi00608a034

Cseh, Z., Rajagopal, S., Tsonev, T., Busheva, M., Papp, E., and Garab, G. (2000). Thermooptic effect in chloroplast thylakoid membranes. Thermal and light stability of pigment arrays with different levels of structural complexity. *Biochemistry* 39, 15250–15257. doi: 10.1021/bi001600d

Daum, B., and Kühlbrand, W. (2011). Electron tomography of plant thylakoid membranes. *J. Exp. Bot.* 62, 2393–2402. doi: 10.1093/jxb/err034

Daum, B., Nicastro, D., Austin, J., McIntosh, J. R., and Kühlbrandt, W. (2010). Arrangement of Photosystem II and ATP synthase in Chloroplast membranes of spinach and pea. *Plant Cell* 22, 1299–1312. doi: 10.1105/tpc.109.071431

Dekker, J. P., and Boekema, E. J. (2005). Supramolecular organization of thylakoid membrane proteins in green plants. *Biochim. Biophys. Acta* 1706, 12–39. doi: 10.1016/j.bbabio.2004.09.009

Dér, A., and Ramsden, J. J. (1998). Evidence for loosening of a protein mechanism. *Naturwissenschaften* 85, 353–355. doi: 10.1007/s001140050515

Dér, A., Kelemen, L., Fábián, L., Taneva, S. G., Fodor, E., Páli, T., et al. (2007). Interfacial water structure controls protein conformation. *J. Phys. Chem. B* 111, 5344–5350. doi: 10.1021/jp066206p

Garab, G., and Mustardy, L. (1999). Role of LHCII-containing macrodomains in the structure, function and dynamics of grana. *Aust. J. Plant Physiol.* 26, 647–649. doi: 10.1071/PP99069

Garab, G., and van Amerongen, H. (2009). Linear dichroism and circular dichroism in photosynthesis research. *Photosynth. Res.* 101, 135–146. doi: 10.1007/s11120-009-9424-4

Garab, G., Faludi-Daniel, A., Sutherland, J. C., and Hind, G. (1988). Macroorganization of chlorophyll a/b light-harvesting complex in thylakoids and aggregates: information from circular differential scattering. *Biochemistry* 27, 2425–2430. doi: 10.1021/bi00407a027

Garab, G., Kieleczawa, J., Sutherland, J. C., Bustamante, C., and Hind, G. (1991). Organization of pigment-protein complexes into macrodamains in the thylakoid membranes of wild-type and chlorophyll fo-less mutant of barley as revealed by circular dicroism. *Photochem. Photobiol.* 54, 273–281. doi: 10.1111/j.1751-1097.1991.tb02016.x

Garab, G., Istokovics, A., Butiuc, A., Simidjiev, I., and Dér, A. (1998). "Light-induced ion movements in thylakoid membranes and isolated LHC II," in *Photosynthesis: Mechanisms and Effects*. Ed. G. Garab (Netherlands: Springer), 341–344.

Garab, G., Cseh, Z., Kovács, L., Rajagopal, S., Várkonyi, Z., Wentworth, M., et al. (2002). Light-induced trimer to monomer transition in the main light-harvesting antenna complex of plants: Thermo-optic mechanism. *Biochemistry* 41, 15121–15129. doi: 10.1021/bi026157g

Garab, G. (2014). Hierarchical organization and structural flexibility of thylakoid membranes. *Biochim. Biophys. Acta* 1837, 481–494. doi: 10.1016/j.bbabio.2013.12.003

Garab, G. (2016). Self-assembly and structural–functional flexibility of oxygenic photosynthetic machineries: personal perspectives. *Photosynth. Res.* 127, 131–150. doi: 10.1007/s11120-015-0192-z

Goodchild, D., Highkin, H. R., and Boardman, N. K. (1966). Fine structure of chloroplasts in a barley mutant lacking chlorophyll b. *Exp. Cell Res.* 43, 684–688. doi: 10.1016/0014-4827(66)90045-0

Gunning, B. E. S., and Schwartz, O. M. (1999). Confocal microscopy of thylakoid autofluorescence in relation to origin of grana and phylogeny in green algae Aust. *J. Plant Physiol.* 26, 695–708. doi: 10.1071/PP99076

Harrison, C. J., and Morris, J. L. (2018). The origin and early evolution of vascular plant shoots and leaves. *Phil. Trans. R. Soc B* 373, 20160496. doi: 10.1098/rstb.2016.0496

Hind, G., Nakatani, H., and Izawa, S. (1974). Light-dependent redistribution of ions in suspensions of chloroplast thylakoid membranes. *Proc. Natl. Acad. Sci. U. S. A.* 71, 1484–1488. doi: 10.1073/pnas.71.4.1484

Hind, G., Wall, J. S., Várkonyi, Z., Istokovics, A., Lambrev, P. A., and Garab, G. (2014). Membrane crystals of plant light-harvesting complex II disassemble reversibly in light. *Plant Cell Physiol.* 55, 1296–1303. doi: 10.1093/pcp/pcu064

Horton, P. (1999). Are grana necessary for regulation of light harvesting? *Aust. J. Plant Physiol.* 26, 659–669. doi: 10.1071/PP99095

Iwai, M., Pack, C. G., Takenaka, Y., Sako, Y., and Nakano, A. (2013). Photosystem II antenna phosphorylation-dependent protein diffusion determined by fluorescence correlation spectroscopy. *Sci. Rep.* 3:2833. doi: 10.1038/srep02833

Izawa, S., and Good, N. E. (1966). Effect of salts and electron transport on conformation of isolated chloroplasts. 2. Electron microscopy. *Plant Physiol.* 41, 544–552. doi: 10.1104/pp.41.3.544

Jakubauskas, D., Kowalewska, Ł., Sokolova, A. V., Garvey, C. J., Mortensen, K., Jensen, P. E., et al. (2019). Ultrastructural modeling of small angle scattering from photosynthetic membranes. *Sci. Rep.* 9, 19405. doi: 10.1038/s41598-019-55423-0

Janik, E., Bednarska, J., Zubik, M., Puzio, M., Luchowski, R., Grudzinski, W., et al. (2013). Molecular architecture of plant thylakoids under physiological and light stress conditions: A study of lipid light-harvesting complex II model membranes. *Plant Cell* 25, 2155–2170. doi: 10.1105/tpc.113.113076

Jennings, R. C., Gerola, P. D., Garlaschi, F. M., and Forti, G. (1981). Effects of trypsin and cations on chloroplast membranes. *Plant Physiol.* 67, 212–215. doi: 10.1104/pp.67.2.212

Jia, H., Liggins, J., and Chow, W. (2014). Entropy and biological systems: Experimentally-investigated entropy-driven stacking of plant photosynthetic membranes. *Sci. Rep.* 4, 4142. doi: 10.1038/srep04142

Johnson, M. P., Goral, T. K., Duffy, C. D. P., Brain, A. P. R., Mullineaux, C. W., and Ruban, A. V. (2011). Photoprotective energy dissipation involves the reorganization of photosystem II light-harvesting complexes in the grana membranes of spinach chloroplasts. *Plant Cell* 23, 1468–1479. doi: 10.1105/tpc.110.081646

Kana, R., and Govindjee, (2016). Role of ions in the regulation of light-harvesting. *Front. Plant Sci.* 7, 1849. doi: 10.3389/fpls.2016.01849

Keller, D., and Bustamante, C. (1986). Theory of the interaction of light with large inhomogeneous molecular aggregates. II. Psi-type circular dichroism. *J. Chem. Phys.* 84, 2972–2980. doi: 10.1063/1.450278

Khoroshyy, P., Dér, A., and Zimányi, L. (2013). Effect of Hofmeister Cosolutes on the photocycle of photoactive yellow protein at moderately Alkaline PH. *J. Photochem. Photobiol. B Biol.* 120, 111–119. doi: 10.1016/j.jphotobiol.2012.12.014

Kirchhoff, H., Lenhert, S., Buchel, C., Chi, L., and Nield, J. (2008). Probing the organization of photosystem II in photosynthetic membranes by atomic force microscopy. *Biochemistry* 47, 431–440. doi: 10.1021/bi7017877

Kouřil, R., Dekker, J. P., and Boekema, E. J. (2012). Supramolecular organization of photosystem II in green plants. *Biochim. Biophys. Acta* 1817, 2–12. doi: 10.1016/j.bbabio.2011.05.024

Kovacs, B., Saftics, A., Biro, A., Kurunczi, S., Szalontai, B., Kakasi, B., et al. (2018). Kinetics and structure of self-assembled flagellin monolayers onhydrophobic surfaces in the presence of Hofmeister salts: experimental measurement of the protein interfacial tension at the nanometer scale. *Phys. Chem. C* 122, 21375–21386. doi: 10.1021/acs.jpcc.8b05026

Kowalewska, L., Mazur, R., Suski, S., Garstka, M., and Mostowska, A. (2016). Three-dimensional visualization of the tubular-lamellar transformation of the internal plastid membrane network during runner bean chloroplast biogenesi). *Plant Cell* 28, 875–891. doi: 10.1105/tpc.15.01053

Krumova, S. B., Laptenok, S. P., Kovács, L., Tóth, T., van Hoek, A., Garab, G., et al. (2010). Digalactosyl-diacylglycerol-deficiency lowers the thermal stability of thylakoid membranes. *Photosynth. Res.* 105, 229–242. doi: 10.1007/s11120-010-9581-5

Lambrev, P. H., and Akhtar, P. (2019). Macroorganisation and flexibility of thylakoid membranes. *Biochem. J.* 476, 2981–3018. doi: 10.1042/BCJ20190080

Lo Nostro, P., and Ninham, B. W. (2012). Hofmeister Phenomena: an update on ion specificity in Biology. *Chem. Rev.* 112, 2286. doi: 10.1021/cr200271j

lsraelachvili, J. N., and Pashley, R. M. (1983). Molecular layering of water at surfaces and origin of repulsive hydration forces. *Nature* 306, 249–250. doi: 10.1038/306249a0

Majee, A., Bier, M., Blossey, R., and Podgornik, R. (2019). Charge regulation radically modifies electrostatics in membrane stacks. *Phys. Rev.* 100, 1–6. doi: 10.1103/PhysRevE.100.050601

Melander, W., and Horváth, C. (1977). Salt Effects on Hydrophobic interactions in precipitation and chromatography of Proteins: an interpretation of the Lyotropic series. *Arch. Biochem. Biophys.* 183, 200–215. doi: 10.1016/0003-9861(77)90434-9

Miller, K. R., and Staehelin, L. A. (1976). Analysis of the thylakoid outer surface. Coupling factor is limited to unstacked membrane regions. *J. Cell Biol.* 68, 30–47. doi: 10.1083/jcb.68.1.30

Miloslavina, Y., Lambrev, P. H., Jávorfi, T., Várkonyi, Z., Karlicky, V., Wall, J. S., et al. (2012). Anisotropic circular dichroism signatures of oriented thylakoid membranes and lamellar aggregates of LHCII. *Photosynth. Res.* 111, 29–39. doi: 10.1007/s11120-011-9664-y

Mullineaux, C. W. (2005). Function and evolution of grana. *Trends Plant Sci.* 10, 521–525. doi: 10.1016/j.tplants.2005.09.001

Murakami, S., and Packer, L. (1970). Protonation and chloroplast membrane structure. *J. Cell Biol.* 47, 332–351. doi: 10.1083/jcb.47.2.332

Mustárdy, L., and Garab, G. (2003). Granum revisited. A three-dimensional model–where things fall into place. *Trends Plant Sci.* 8, 117–122. doi: 10.1016/S1360-1385(03)00015-3

Mustárdy, L., Buttle, K., Steinbach, G., and Garab, G. (2008). The three-dimensional network of the thylakoid membranes in plants: quasihelical model of the granum-stroma assembly. *Plant Cell* 20, 2552–2557. doi: 10.1105/tpc.108.059147

Nagy, G., and Garab, G. (2020). Neutron scattering in photosynthesis research. Recent advances and perspectives for testing crop plants. *Photosynt. Res.* [published online ahead of print, 2020 Jun 2]. doi: 10.1007/s11120-020-00763-6

Nagy, G., Posselt, D., Kovács, L., Holm, J. K., Szabó, M., Ughy, B., et al. (2011). Reversible membrane-reorganizations during photosynthesis *in vivo* - revealed by small-angle neutron scattering. *Biochem. J.* 436, 225–230. doi: 10.1042/BJ20110180

Nagy, G., Kovács, L., Ünnep, R., Zsiros, O., Almásy, L., Rosta, L., et al. (2013). Kinetics of structural reorganizations in multilamellar photosynthetic membranes monitored by small-angle neutron scattering. *Eur. Phys. J. E* 36, 69. doi: 10.1140/epje/i2013-13069-0

Násztor, Z., Bogár, F., and Dér, A. (2016). The interfacial tension concept, as revealed by fluctuations. *Curr. Opin. Colloid Interface Sci.* 23, 29–40. doi: 10.1016/j.cocis.2016.05.007

Násztor, Z., Dér, A., and Bogár, F. (2017). Ion-induced alterations of the local hydration environment elucidate Hofmeister effect in a simple classical model of Trp-cage miniprotein. *J. Mol. Model.* 23, 298. doi: 10.1007/s00894-017-3471-0

Neagu, A., Neagu, M., and Dér, A. (2001). Fluctuations and the Hofmeister Effect. *Biophys. J.* 81, 1285–1294. doi: 10.1016/S0006-3495(01)75786-4

Nevo, R., Charuvi, D., Tsabari, O., and Reich, Z. (2012). Composition, architecture and dynamics of the photosynthetic apparatus in higher plants. *Plant J.* 70, 157–176. doi: 10.1111/j.1365-313X.2011.04876.x

Paolillo, D. J.Jr (1970). The three-dimensional arrangement of intergranal lamellae in chloroplasts. *J. Cell Sci.* 6, 243–225.

Petrova, N., Stoichev, S., Paunov, M., Todinova, S., Taneva, S. G., and Krumova, S. (2019). Structural organization, thermal stability, and excitation energy utilization of pea thylakoid membranes adapted to low light conditions. *Acta Physiol. Plant* 41, 188. doi: 10.1007/s11738-019-2979-6

Posselt, D., Nagy, G., Kirkensgaard, J. J. K., Holm, J. K., Aagaard, T. H., Timmins, P., et al. (2012). Small-angle neutron scattering study of the ultrastructure of chloroplast thylakoid membranes — Periodicity and structural flexibility of the stroma lamellae. *Biochim. Biophys. Acta* 1817, 1220–1228. doi: 10.1016/j.bbabio.2012.01.012

Puthiyaveetil, S., Kirchhoff, H., and Höhner, R. (2016). *Structural and functional dynamics of the thylakoid membrane system in. Chloroplasts: Current Research and Future Trend*. Ed. H. Kirchhoff (Norfolk, UK: Caister Academic Press). doi: 10.21775/9781910190470.03

Puthiyaveetil, S., van Oort, B., and Kirchhoff, H. (2017). Surface charge dynamics in photosynthetic membranes and the structural consequences. *Nat. Plants* 3, 17020. doi: 10.1038/nplants.2017.20

Robinson, D. R., and Jencks, W. P. (1965). The effect of concentrated salt solutions on the activity coefficient of acetyltetraglycine ethyl ester. *J. Am. Chem. Soc* 87, 2470–2479. doi: 10.1021/ja01089a029

Rojdestvenski, I., Ivanov, A. G., Cottam, M. G., Borodich, A., Huner, N. P. A., and Öquist, G. (2002). Segregation of photosystems in thylakoid membranes as a critical phenomenon. *Biophys. J.* 82, 1719–1730. doi: 10.1016/S0006-3495(02)75524-0

Simidjiev, I., Barzda, V., Mustárdy, L., and Garab, G. (1997). Isolation of lamellar aggregates of the light-harvesting chlorophylla/b proteincomplex of photosystem II with long-range chiral order and structural flexibility. *Anal. Biochem.* 250, 169–175. doi: 10.1006/abio.1997.2204

Simidjiev, I., Stoylova, S., Amenitsch, H., Jávorfi, T., Mustárdy, L., Laggner, P., et al. (2000). Self-assembly of large, ordered lamellae from nonbilayer lipids and integral membrane-proteins *in vitro*. *Proc. Natl. Acad. Sci. U. S. A.* 97, 1473–1476. doi: 10.1073/pnas.97.4.1473

Solymosi, K., and Keresztes, Á. (2012). Plastid structure, diversification and interconversions II. Land plants. *Curr. Chem. Biol.* 6, 187–204. doi: 10.2174/2212796811206030003

Solymosi, K. (2012). Plastid structure, diversification and interconversions I. Algae. *Curr. Chem. Biol.* 6, 167–186. doi: 10.2174/2212796811206030002

Standfuss, J., van Scheltinga, A. C. T., Lamborghini, M., and Kühlbrandt, W. (2005). Mechanisms of photoprotection and nonphotochemical quenching in pea light-harvesting complex at 2.5 Å resolution. *EMBO J.* 24, 919–928. doi: 10.1038/sj.emboj.7600585

Szalontai, B., Nagy, G., Krumova, S., Fodor, E., Páli, T., Taneva, S. G., et al. (2013). Hofmeister ions control protein dynamics. *Biochim. Biophys. Acta* 1830, 4564–4572. doi: 10.1016/j.bbagen.2013.05.036

Tanford, C. (1979). Interfacial Free Energy and the Hydrophobic Effect. *Proc. Natl. Acad. Sci. U. S. A.* 76, 4175–4176. doi: 10.1073/pnas.76.9.4175

Tóth, T. N., Rai, N., Solymosi, K., Zsiros, O., Schröder, W. P., Garab, G., et al. (2016). Fingerprinting the macro-organisation of pigment–protein complexes inplant thylakoid membranes *in vivo* by circular-dichroism spectroscopy. *Biochim. Biophys. Acta* 1857, 1479–1489. doi: 10.1016/j.bbabio.2016.04.287

Ünnep, R., Nagy, G., Markó, M., and Garab, G. (2014). Monitoring thylakoid ultrastructural changes *in vivo* using small-angle neutron scattering. *Plant Physiol. Biochem.* 81, 197–207. doi: 10.1016/j.plaphy.2014.02.005

Wood, W. H. J., MacGregor-Chatwin, C., Barnett, S. F. H., Mayneord, G. E., Huang, X., Hobbs, J. K., et al. (2018). Dynamic thylakoid stacking regulates the balance between linear and cyclic photosynthetic electron transfer. *Nat. Plants* 4, 116–127. doi: 10.1038/s41477-017-0092-7

Zer, H., Vink, M., Keren, N., Dilly-Hatrwig, H., Paulsen, H., Herrmann, R. G., et al. (1999). Regulation of thylakoid protein phosphorylation at the substrate level: reversible light-induced conformational changes expose the phosphorylation site of the light-harvesting complex II. *Proc. Natl. Acad. Sci. U. S. A.* 96, 8277–8282. doi: 10.1073/pnas.96.14.8277

Zsiros, O., Nagy, V., Párducz, Á, Nagy, G., Ünnep, R., El-Ramady, H., et al. (2019). Effects of selenate and red Se-nanoparticles on the photosynthetic apparatus of Nicotiana tabacum. *Photosynth. Res.* 139, 449–460. doi: 10.1007/s11120-018-0599-4

Conflict of Interest: The authors declare that the research was conducted in the absence of any commercial or financial relationships that could be construed as a potential conflict of interest.

The handling Editor declared a past co-authorship with one of the authors LK.

Copyright © 2020 Zsiros, Ünnep, Nagy, Almásy, Patai, Székely, Kohlbrecher, Garab, Dér and Kovács. This is an open-access article distributed under the terms of the Creative Commons Attribution License (CC BY). The use, distribution or reproduction in other forums is permitted, provided the original author(s) and the copyright owner(s) are credited and that the original publication in this journal is cited, in accordance with accepted academic practice. No use, distribution or reproduction is permitted which does not comply with these terms.

frontiers in Plant Science

ORIGINAL RESEARCH
published: 21 October 2020
doi: 10.3389/fpls.2020.547818

Nonlinear Optical Investigation of Microbial Chromoproteins

Szilvia Krekic[1,2], Tomás Zakar[3†], Zoltán Gombos[3‡], Sándor Valkai[1], Mark Mero[4], László Zimányi[1], Zsuzsanna Heiner[5] and András Dér[1]**

[1] Institute of Biophysics, Biological Research Centre, Szeged, Hungary, [2] Doctoral School of Multidisciplinary Medical Sciences, University of Szeged, Szeged, Hungary, [3] Institute of Plant Biology, Biological Research Centre, Szeged, Hungary, [4] Max Born Institute for Nonlinear Optics and Short Pulse Spectroscopy, Berlin, Germany, [5] School of Analytical Sciences Adlershof, Humboldt-Universität zu Berlin, Berlin, Germany

OPEN ACCESS

Edited by:
Michael Hippler,
University of Münster, Germany

Reviewed by:
Heiko Lokstein,
Charles University, Czechia
Dimitris Petroutsos,
UMR 5168 Laboratoire de Physiologie Cellulaire Vegetale (LPCV), France

***Correspondence:**
Zsuzsanna Heiner
heinerzs@hu-berlin.de
András Dér
der.andras@brc.hu

†Present address:
Tomás Zakar,
Institute of Photonics and Electronics, The Czech Academy of Sciences, Prague, Czechia

‡Deceased

Specialty section:
This article was submitted to Plant Physiology, a section of the journal Frontiers in Plant Science

Received: 31 March 2020
Accepted: 22 September 2020
Published: 21 October 2020

Citation:
Krekic S, Zakar T, Gombos Z, Valkai S, Mero M, Zimányi L, Heiner Z and Dér A (2020) Nonlinear Optical Investigation of Microbial Chromoproteins. Front. Plant Sci. 11:547818. doi: 10.3389/fpls.2020.547818

Membrane-bound or cytosolic light-sensitive proteins, playing a crucial role in energy- and signal-transduction processes of various photosynthetic microorganisms, have been optimized for sensing or harvesting light by myriads of years of evolution. Upon absorption of a photon, they undergo a usually cyclic reaction series of conformations, and the accompanying spectro-kinetic events assign robust nonlinear optical (NLO) properties for these chromoproteins. During recent years, they have attracted a considerable interest among researchers of the applied optics community as well, where finding the appropriate NLO material for a particular application is a pivotal task. Potential applications have emerged in various branches of photonics, including optical information storage and processing, higher-harmonic and white-light continuum generation, or biosensorics. In our earlier work, we also raised the possibility of using chromoproteins, such as bacteriorhodopsin (bR), as building blocks for the active elements of integrated optical (IO) circuits, where several organic and inorganic photonic materials have been considered as active components, but so far none of them has been deemed ideal for the purpose. In the current study, we investigate the linear and NLO properties of biofilms made of photoactive yellow protein (PYP) and bR. The kinetics of the photoreactions are monitored by time-resolved absorption experiments, while the refractive index of the films and its light-induced changes are measured using the Optical Waveguide Lightmode Spectroscopy (OWLS) and Z-scan techniques, respectively. The nonlinear refractive index and the refractive index change of both protein films were determined in the green spectral range in a wide range of intensities and at various laser repetition rates. The nonlinear refractive index and refractive index change of PYP were compared to those of bR, with respect to photonics applications. Our results imply that the NLO properties of these proteins make them promising candidates for utilization in applied photonics, and they should be considered as valid alternatives for active components of IO circuits.

Keywords: Z-scan, bacteriorhodopsin, photoactive yellow protein, nonlinear refractive index, saturable absorption, photo-induced refractive index change

INTRODUCTION

Ubiquitous applications of photonics and optoelectronics are now penetrating into diverse areas from everyday life to the most advanced scientific disciplines, such as optical communication, data processing and storage, quantum computing, holography, just to mention a few. Key elements of photonic devices are the so-called nonlinear optical (NLO) materials, which can actively modify light propagation or store optical information. Examples for the use of NLO materials in photonics ranges from all-optical signal processing (Willner et al., 2014), to all-optical switching (Chai et al., 2017), optical filtering (Dini et al., 2016), with the list of applications continuously growing. To this end, one of the biggest challenges is finding materials with optimal NLO characteristics that could be applied in photonic devices. The development and characterization of NLO materials (such as nonlinear crystals or chalcogenide glasses) (Adair et al., 1989; Eggleton et al., 2011) is in current progress, because the diverse applications require special solutions. E.g., several aspects must be taken into account when selecting a material for an IO application, such as mechanical stability, re-excitability, sensitivity, but most importantly, the material has to have a large refractive index change induced by an outer stimulus of an electric field or light. Amongst others, the application of molecules possessing π-conjugated electron systems have been most favored, since they show a high (third-order) optical polarizability, usually without two-photon losses (Hales et al., 2010; Haque and Nelson, 2010; Hu et al., 2017). However, various problems concerning their robustness and incorporation into solid matrices for practical applications are still to be solved. On the other hand, natural π-conjugated materials, such as chromoproteins are readily available (Clays et al., 2001; Fábián et al., 2011). Chromoproteins have been perfected by evolution for billions of years for utilizing light as a source of energy or information. Their protein matrix stabilizes their chromophores, and fine-tunes their optical properties. At the same time, the application of proteins as NLO materials in photonics also raises non-trivial technical problems. Building up stable hybrid structures of the protein and the passive substrate (such as a thin film of chromoprotein on a photonic circuit), and a thorough characterization of their NLO properties is inevitable, as well as their optimization for a particular application, such as IO switching, or other optical information processing tasks.

One of the most investigated candidates in the field is the protein bacteriorhodopsin (bR), while other proteins, such as photoactive yellow protein (PYP) have recently also been considered as IO active materials (Krekic et al., 2019). Their molecular and bulk optical properties (e.g., linear and nonlinear polarizabilities, and their refractive index and its light-induced changes) are of high interest from the point of view of potential optoelectronic applications of chromoproteins, in general.

Bacteriorhodopsin is a membrane protein (embedded in quasi-crystalline lipid-protein patches, the so-called purple membranes) first discovered in the archaeon *Halobacterium salinarum* (Oesterhelt and Stoeckenius, 1971; Lanyi, 2004). It consists of seven-transmembrane alpha helices to which an all-trans retinal is covalently attached through a protonated Schiff base. bR is widely known to be the simplest light-driven proton pump (Oesterhelt and Stoeckenius, 1973), hence considered as a model for more complicated systems. One of the protein's most important characteristics is its photocycle. Upon light absorption, bR enters a reaction cycle, going through quasi-stable intermediate states (K, L, M, N, O) in a matter of milliseconds in solution, before returning to the initial state. Each of the intermediary states possesses characteristic absorption spectra, distinct from the initial state's spectrum. The difference in absorption spectra between the intermediate states and the initial state indicates a difference in refractive indices according to the Kramers–Kronig relations (Nussenzveig, 1972; Wooten, 2013).

Photoactive yellow protein is a water-soluble protein present in purple sulfur photosynthetic bacteria (Meyer, 1985), much smaller than bR-containing purple membrane patches (Oesterhelt and Stoeckenius, 1971; Meyer, 1985). This makes PYP a promising candidate for incorporation into IO passive structures (e.g., in porous silicon), where membrane-bound bR cannot be used due to its larger particle size. When excited with blue light, PYP enters its photocycle (Meyer et al., 1987), which standardly consists of four intermediates (pR_1, pR_2, pB_1, pB_2) and takes place in a matter of milliseconds in solution.

To fully consider a protein in IO applications, a conclusive optical characterization is needed. The utility of NLO materials for optical communication is highly dependent on the magnitude of the refractive index change that can be induced in the material at hand. The larger the associated change in the complex refractive index, the larger the amplitude and phase modulation effect will be. When combining NLO materials with passive components, the size and energy consumption also depend on the NLO response, hence a larger refractive index change is preferred (Miller, 2010; Sasikala and Chitra, 2018).

In dried films of chromoproteins the light-induced refractive index changes are orders of magnitude higher than in suspensions, where, due to the overwhelming excess of water (ca. 55 M water to a few 100 μM of protein in the densest suspensions), the refractive index of water is dominating (Heiner and Osvay, 2009). Hence, as far as photonic applications of bR utilizing light-induced optical changes are concerned, dried films (usually under controlled humidity), are used (Dér and Keszthelyi, 2001; Vsevolodov, 2012 and references therein). Exceptions are only the few applications that are based on absorption instead of refractive index changes (Stuart et al., 2001). From the point of view of technical applications, on the other hand, using dried films is convenient due to their form and stability. Combining dried films of proteins with IO passive structures is a solvable task (see the section "Materials and Methods"), and in such samples proteins maintain their optical properties for a long time (several decades) (Váró and Keszthelyi, 1983; Dér and Keszthelyi, 2001; Vsevolodov, 2012).

One should note, however, that the photocycles of both pigments do depend on the relative humidity of the films (Váró and Keszthelyi, 1983; van der Horst et al., 2005). The general rule of thumb is that at high-enough relative humidity (>80–90%), the photocycles are close to the native ones, while at moderate relative humidity (between ca. 30–50% to 80%), such transitions that accompany large-scale conformational changes (e.g., the

ones following M formation in the bR, or those after pB_1 in PYP) are hindered, hence the rate-limiting steps become slower. The reason for this phenomenon is that protein conformational flexibility is decreasing by lowering relative humidity (Fitter et al., 1999). Further lowering relative humidity values leads to more serious truncation of the photocycles (Váró and Keszthelyi, 1983; van der Horst et al., 2005). Technical applications (considered so far for bR only) normally use the higher end of moderate humidity range, as a reasonable trade-off between maximizing $\boldsymbol{\Delta n}$ and having a decent photocycle kinetics (Dér and Keszthelyi, 2001; Vsevolodov, 2012). Proteins in this range show an overall slower photocycle than native proteins, which might appear to be less favorable for some photonic applications, however, both proteins have fast (sub-picosecond to picosecond) transitions in the beginning of their photocycles, which are unaffected by humidity in bR (Colonna et al., 2005), and probably in PYP, too (see fast kinetics detected in crystallized PYP (Yeremenko et al., 2006; Schotte et al., 2012; Tenboer et al., 2014), but yet to be characterized in PYP dry samples). On the other hand, the first intermediate states of both the bR and PYP photocycles can be driven back by fast, light-induced reactions to the ground state (Balashov, 1995; Joshi et al., 2005; Tóth-Boconádi et al., 2006, 2010), allowing a rapid, light-controlled manipulation of refractive index kinetics of the films. The lifetime of various types of dried bR films is known to be in the range of several decades, appropriate for technical applications (Dér and Keszthelyi, 2001).

In the past decades, several research articles have demonstrated the dried bR film's large light-induced refractive index change ($\boldsymbol{\Delta n}$), and its utilization in optical switching experiments and light modulation (Ormos et al., 2002; Fábián et al., 2011; Mathesz et al., 2013). bR also shows a large hyperpolarizability, important in frequency-doubling experiments, investigated by NLO techniques (Naskali et al., 2014). The nonlinear refractive index value $\boldsymbol{n_2}$ of bR-containing samples has been extensively investigated previously under various experimental conditions, in most of the cases using the so-called Z-scan technique (Song et al., 1993; Aranda et al., 1995; Jeganathan et al., 2017). The spectro-kinetic properties and light-induced refractive index changes have also been discussed (van der Horst et al., 2005; Krekic et al., 2019), which further encourages investigation of the protein's NLO properties. There have been a few publications dealing with the nonlinear refractive index of different PYP samples, e.g., embedded in thick polyacrylamide matrices (Vanhanen et al., 1998; Leppanen et al., 1999) or adsorbed to poly-methyl-methacrylate microspheres (Lee et al., 2018), however, the results are hard to reconcile due to the different samples and the various methods applied (Z-scan, Michelson-interferometer, and hyperspectral quantitative phase imaging). No experiments were done so far on a thin-film PYP sample and with a pulsed Z-scan setup.

The single-beam Z-scan technique is a popular method for the characterization of the optical nonlinearities of a wide variety of materials (Sheik-Bahae et al., 1990), including organic and even protein samples. During a Z-scan, the sample is moved through the laser focus and the power or energy transmitted through an aperture placed behind the focus is measured as a function of the sample position, z. When the aperture is small, a closed-aperture trace is obtained, yielding the magnitude and sign of $\boldsymbol{n_2}$. When the aperture is removed or open, an open-aperture trace is measured, providing the magnitude of nonlinear absorption coefficients. While the experimental realization of the technique is simple, determining all the NLO mechanisms causing a particular Z-scan trace is often not possible without performing additional measurements. For example, the photocycle of bR and the related complex kinetics make the interpretation of the associated Z-scan data difficult (Kir'Yanov et al., 2000).

Here, we report on the NLO properties of a new type of thin bR and PYP films, in the light of possible optoelectronic applications of these proteins. The films were experimentally characterized through OWLS, absorption kinetics and Z-scan measurements. The linear and nonlinear refractive index, and the formation and decay times of the respective intermediate states in the photocycle of the two proteins were determined. The nonlinear refractive index was measured using the Z-scan technique with both 543-nm or 405-nm continuous wave (CW) and 514-nm pulsed laser illumination at varying repetition rates and a wide range of intensities. The determined $\boldsymbol{\Delta n}$ and $\boldsymbol{n_2}$ values of bR are compared to previously published data, as well as to the results obtained for PYP, where prior data on NLO properties are scarce. The results are considered to have important implications from the perspective of photonic applications – the future utilization of these biomaterials in film format for integrated optical switching and signal processing experiments. Compared to non-organic NLO materials currently used and researched for such purposes, biological materials, such as bR and PYP, offer a readily available, cost-effective alternative, which is also more versatile depending on the form and environment of the protein building blocks.

MATERIALS AND METHODS

Sample Preparation

Bacteriorhodopsin was prepared according to the standard procedure: purple membranes separated from strain R1M1 of *Halobacterium salinarum* were prepared as described in Oesterhelt and Stoeckenius (1971). Purple membranes contain 25% lipids and 75% bR, as the sole protein constituent in the preparation (Oesterhelt and Stoeckenius, 1974). (For the sake of simplicity, we refer to this membrane-bound form of the protein as bR, throughout the text.) Wild-type PYP apoprotein was overexpressed in *Escherichia coli (BL21DE3)* strain, isolated, and then reconstituted with freshly synthetized pCA (coumaric acid) anhydride in 4 M urea buffer (Mihara et al., 1997; Kamikubo et al., 2007). The holoprotein was purified by column chromatography (DEAE Sepharose CL6B) and concentrated/washed by 10 kDa centrifugal filters several times.

An important requirement for photonic applications is the optical quality of the films. Layering and subsequent drying of protein suspensions normally leads to highly cracked samples, inappropriate for technical applications. To prevent cracking, some ballast materials, such as gelatin or PVA are used at

relatively high concentrations (Vsevolodov, 2012), and the relative humidity is often fixed at the desired values by sandwiching and sealing the sample between glass plates (Hampp and Juchem, 2001). In our experiments, we chose to add low amounts of glycerol to the sample before drying. These treatments completely prevented crack formation, at the same time, kept the sample sufficiently humid without sandwiching, even at low relative humidity values, such as 33% humidity, the standard laboratory environment. According to our estimate based on optical multichannel analyzer experiments on bR (data not shown), the humidity inside the sample corresponded to a ca. 80–85% relative humidity value. During the Z-scan measurements and the absorption kinetic experiments, we controlled the environment to avoid any errors arising from the difference in humidity.

Each of the protein suspensions was first mixed with an 87% glycerol solution. For bR samples, glycerol constituted 10% of the mixture, while for PYP the ratio was lowered to 2% to achieve optimal homogeneity and viscosity of the film. The mixtures were first sonicated for 1–2 min to remove any microbubbles, then pipetted to a 200-μm thick microscope cover slide to form an approximately 5 mm diameter patch. The films were then left to dry under an extractor fume hood for at least 12 h. Before measurements, the protein films were sandwiched using an additional microscope cover slip. The cover slips were made of BK7 glass. For the pulsed-laser measurements, a sample thickness of 200 μm was achieved by embedding a 200-μm thick spacer between the glass slabs. Similarly, for the 405-nm CW measurement on PYP, a sample thickness of 200 μm was used. For the 543-nm CW experiment on bR, a thinner sample was made to accommodate the lowered average power of the applied laser. The environment's relative humidity was 33% during each experiment, while the sample temperature was kept at 23°C.

For the OWLS measurements, the protein-glycerol mixtures were prepared using the same methods as for the Z-scan measurements. The mixtures were pipetted to an optical slab waveguide, and left to dry for at least 12 h before measurements.

For the single-wavelength absorption kinetics experiments, the protein-glycerol mixtures, pipetted onto glass slabs, were left to dry for at least 12 h, and the slabs were then placed into cuvettes in which we set the relative humidity at 33% with a saturated solution of magnesium chloride.

OWLS Measurements

Throughout the experiments, grating-coupled (coupler grating width 1 mm, line density 2400 mm^{-1}) slab waveguides [MicroVacuum Ltd., material $Si(Ti)O_2$, n_f between 1.78 and 1.80, thickness between 195 nm and 205 nm] on glass substrate (n_s = 1.53) were used. The waveguides were mounted on a high-precision rotational turntable (DPS, Ealing Electro Optics), by which the angle of incidence of a measuring light beam (He-Ne laser, Melles Griot, 543 nm) could be adjusted with an accuracy of 10^{-4} degrees. The intensity of the coupled light was detected at the end of the waveguide by a photomultiplier tube (PMT, Hamamatsu, Japan), whose signal was amplified by a laboratory-built current-voltage converter and recorded by a digital oscilloscope (LeCroy 9310-L). Under such conditions, only two discrete modes (transversal electric, "TE" and transversal magnetic, "TM") of the guided light can propagate, with highly selective resonance conditions. From the peak positions, the refractive index of the adlayer can be determined using the mode equations of the three-layer waveguide (Ramsden, 1993).

Absorption Kinetics Measurements

Time-resolved absorption spectra of the protein samples were obtained with a home-built pump-probe apparatus on the time scale of milliseconds to seconds. The pump source was a Surelite II Nd:YAG laser with an OPO extension (Continuum, United States) and was aligned to 514 nm and 445 nm for exciting the initial state of bR and PYP, respectively. The pulse energies were 2 mJ and 2.80 mJ. The source of the unpolarized probe light was a 35-W high-pressure Xenon lamp (Hamamatsu, Japan), filtered by narrow-band interference filters at selected wavelengths. The pump and probe beams spatially overlapped on the sample, and the transmitted probe light was directed to a Hamamatsu PMT through a HR-320 monochromator (ISA Jobin–Yvon, France). The applied repetition rate of the excitation laser was chosen to be 0.1 Hz to ensure that both proteins return to the initial state during each measuring cycle. The output signals of the photomultiplier were amplified by a home-made current-voltage converter, and recorded by a National Instruments oscilloscope card. In total, 10 traces were averaged.

Light-excitation experiments were also done to measure the difference spectrum of the protein state formed after illuminating the samples with a CW laser beam for a longer period. The experimental setup was the same as in the absorption kinetics measurements, except that the measuring light was filtered by a gray-colored glass filter before reaching the sample. The measuring light was detected with a spectrograph equipped with an iStar gated ICCD detector (Andor Technology, United Kingdom). For the light-excitation of the bR film, a Nd:YAG laser (DHOM-M-532-500 mW) was used with an average power of 5 mW at 532 nm wavelength, while for PYP, 40 mW at 410 nm was applied. The samples were illuminated for 10 s before the start of the measurements. 10 spectra were averaged, and each measurement lasted for 1.30 s to complete.

Z-Scan Measurements

We utilized the Z-scan technique to characterize the nonlinear refractive index of dry bR and PYP films. Both CW and pulsed laser beams were employed to interrogate the samples. The setup used with CW illumination is shown in **Figure 1A**. The closed-aperture (CA) Z-scan traces were recorded by a PMT placed behind a circular aperture in the far-field, while the open-aperture (OA) traces were measured without an aperture in the laser beam. The light source was a 543-nm He-Ne laser delivering an average power of 0.75 mW. The power of the He-Ne laser beam was adjusted using a half-wave plate and a polarizer. A quarter-wave plate was placed between the polarizer and the sample to suppress back-reflection toward the laser. Accordingly, the laser beam incident on the samples was circularly polarized in the CW experiments.

The setup used with pulsed excitation was a modified version of the scheme described in detail elsewhere (Mero et al.,

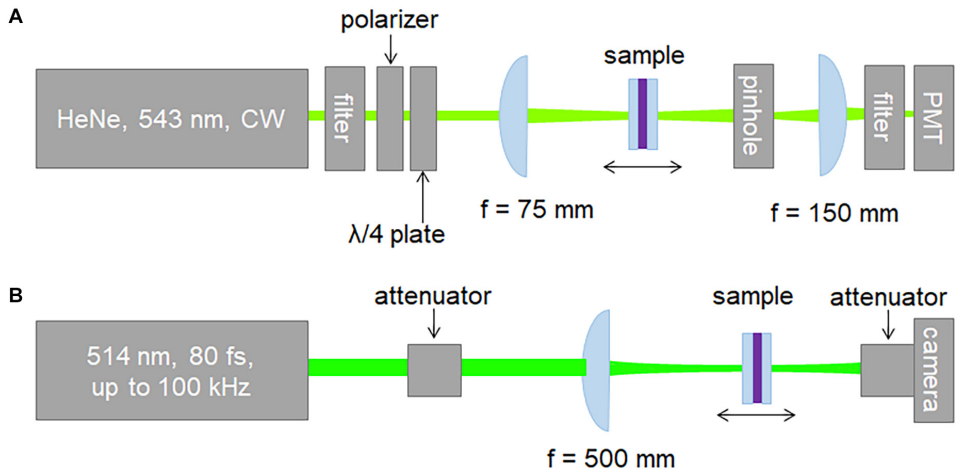

FIGURE 1 | Schematics of the experimental **(A)** CW and **(B)** pulsed-mode Z-scan setup.

2019) and is shown in **Figure 1B**. Briefly, the laser source was a commercial Yb:KGW laser oscillator-amplifier system delivering 1.028-μm pulses at adjustable repetition rates up to 100 kHz. The fundamental pulses were frequency-doubled yielding linearly polarized 82-fs, 514-nm pulses for probing the samples. The temporal intensity profile of the second-harmonic pulses was characterized using the self-diffraction frequency-resolved optical gating (SD-FROG) technique. To reduce the peak power, the pulses were attenuated by reflecting them off an uncoated wedge and sending them through neutral density filters. Further adjustment of the peak power was achieved using a half-wave plate and a thin film polarizer. An f = 500-mm singlet lens was used to focus the pulses on the sample leading to a Gaussian beam waist radius of 37 μm measured with a beam profiling camera. The minor astigmatism of the laser beam was eliminated by an appropriate tilt of the focusing lens. The M^2 values in the horizontal and vertical planes were measured to be ≤1.1. The pulsed Z-scan setup was also used to conduct CW Z-scan measurements at 405 nm, using a single longitudinal mode, TEM_{00}-spatial-mode, temperature-stabilized diode laser (not shown in **Figure 1B**). In this case, the focusing conditions were changed leading to a Gaussian beam waist radius of 36.6 μm. In contrast to the standard implementation of the Z-scan measurement scheme relying on single-pixel detectors, we employed a beam profiling camera. The open- and closed-aperture Z-scan traces were extracted from the measured beam profiles using image processing. Namely, the OA traces were determined by adding the signal counts of all pixels of the camera. The CA traces can be obtained by adding the signal counts in a predefined 2D pixel area centered on the center of gravity of the beam profile, which mimics a real hard aperture in the laser beam.

For samples with absorptive nonlinearities, the CA traces become distorted compared to those containing only refractive nonlinearities. Elimination of such distortive effects on the CA traces is often possible by dividing the CA traces by the OA traces. This procedure in turn allows the use of simple fit functions applicable to purely refractive cubic nonlinearities and a straightforward extraction of the nonlinear refractive index of the sample even in the presence of nonlinear absorption. However, we found that this procedure is not applicable for our protein samples exhibiting strong nonlinear absorption. Relying on 2D camera-based detection in our Z-scan measurements, we developed a novel procedure to remove the distortions in CA traces even in the presence of massive nonlinear absorption (see section "Procedure for Separating Refractive Nonlinearities in Closed-Aperture Z-Scan Traces"). This procedure is also useful to significantly reduce the noise in CA traces for samples exhibiting spatial inhomogeneity.

After the removal of nonlinear absorption effects, we fitted the CA traces with the expression valid for a cubic nonlinearity, negligible nonlinear absorption, thin-samples, and a peak, on-axis phase shifts below π, according to Sheik-Bahae et al. (1990):

$$T(x, \langle \Delta\phi_0 \rangle) = 1 - [4x\langle \Delta\phi_0 \rangle] / \left[(x^2+9)(x^2+1)\right]. \quad (1)$$

In Eq. 1, $\boldsymbol{x} = \frac{z}{z_0}$ is the sample position $\boldsymbol{z}$ normalized by the Rayleigh range $\boldsymbol{z_0}$, while $\langle \boldsymbol{\Delta\phi_0} \rangle$ is the time-averaged, peak, on-axis phase shift. The $\boldsymbol{n_2}$ values were calculated according to the formula,

$$n_2 \cong \langle \Delta\phi_0 \rangle (F\lambda w_0^2)/(L_{eff}P), \quad (2)$$

where $\boldsymbol{\lambda}$ is the center wavelength, $\boldsymbol{w_0}$ is the Gaussian beam waist, $\boldsymbol{L_{eff}} = (1 - \boldsymbol{e}^{-\alpha L})/\boldsymbol{\alpha}$ is the effective sample thickness, $\boldsymbol{\alpha}$ is the linear absorption coefficient and $\boldsymbol{L}$ is the sample thickness. $\boldsymbol{P}$ is the laser power inside the material. For temporally Gaussian pulses $\boldsymbol{P} = \boldsymbol{E_P}/\mathbf{1.064} \cdot \boldsymbol{\tau_P}$, or $\boldsymbol{P} = \boldsymbol{E}/\boldsymbol{T_{rep}}$, when peak or average power is considered, respectively. Here $\boldsymbol{\tau_P}$ is the pulse duration at full-width of half-maximum, and $\boldsymbol{T_{rep}}$ is the laser repetition period. The factor $\boldsymbol{F}$ is $\sqrt{2}/4$ or $1/4$ when the peak or average power aspect of the illumination is considered to be relevant, respectively. In Eq. 2, $\langle \boldsymbol{\Delta\phi_0} \rangle$ is the time-averaged peak on-axis phase shift obtained from fitting the expression in Eq. 1 to experimentally measured CA traces. We note that we tested the accuracy of the pulsed Z-scan setup by measuring the $\boldsymbol{n_2}$ value of a BK7 sample (an empty substrate without a protein film)

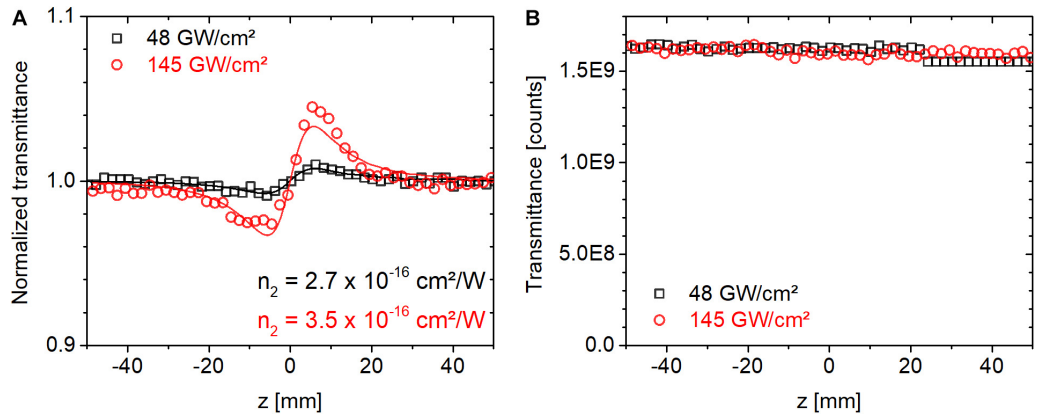

FIGURE 2 | (A) Closed and **(B)** open-aperture Z-scan traces measured for a BK7 substrate using 514-nm ultrafast laser pulses at a repetition rate of 1 kHz at peak on-axis intensities of 48 and 145 GW/cm^2.

and we obtained a value of $\sim 3 \times 10^{-16}$ cm^2/W at 514 nm in agreement with the literature (Adair et al., 1987; Nibbering et al., 1995; Boyd, 2003). **Figure 2** shows the corresponding closed and open-aperture traces. We note that the fluctuations in **Figure 2B**, characterized by a standard deviation of 0.6%, are indicative of camera noise, as BK7 exhibits negligible nonlinear absorption at our applied peak intensities. We found that camera noise had a larger impact on the open-aperture traces than the closed-aperture traces as a result of a drift of the baseline values, which strongly affects the total signal count from the entire CMOS chip.

RESULTS AND DISCUSSION

OWLS Measurements

High-resolution scans by the angle of incidence were carried out in the range of effective coupling, with the bare waveguide and, subsequently, waveguides coated with the biofilms. The recorded traces were fitted by Gaussians, in order to obtain the positions of the TE and TM modes. First, the actual refractive index and thickness values of the guiding layer were determined, then, using these data, the refractive index of the biofilms was obtained, making sure that the thickness of the adlayer was at least an order of magnitude larger than the penetration depth of the guided light (Ramsden, 1993). The measured and calculated values are summarized in **Table 1**. These refractive index data of the biofilms were used for the determination of their Δn and n_2 values from the Z-scan experiments. Adding glycerol to the protein solutions before drying them modifies the refractive indices of the thin film samples, which must be taken into account during the evaluation of the Z-scan data.

Absorption Kinetics Spectroscopy

The absorption kinetics data of both bR and PYP were measured at 33% ambient relative humidity. The photocycles of both bR and PYP are sensitive to environmental parameters, such as temperature or pH, and they are vastly different in the proteins' dry state at different relative humidity values. Therefore, we conducted all our measurements under the same relative humidity, for which we arbitrarily chose a value of 33% as stated in Materials and Methods. In the current study, glycerol was added to the protein suspensions before drying, which further modifies the photocycle, via changing the microviscosity of the medium (Beece et al., 1981), controlling water activity inside the films and enhancing hydrophobic interactions at the protein surface (Draheim and Cassim, 1985). To accurately determine the intermediates which the measured n_2 values belong to, and to see how the distinct intermediates form and decay in time, single-wavelength kinetics measurements were carried out on the proteins. The glycerol-doped films were of superior optical quality, showing reduced light scattering even for the membrane-bound bR, due to quasi-matching of its refractive index with that of bR-containing purple membranes (Ormos et al., 2002).

For bR, four wavelengths were chosen to monitor the absorption changes in time, to get a comprehensive picture of the protein's photocycle. These wavelengths were 575 nm to observe the changes corresponding to the initial state's transient bleaching, 410 nm that corresponds to the absorption maximum of the M intermediate; and additionally 500 nm and 620 nm to gain spectral information for both the red- and blue-shifted side of the initial state's maximum. We found that the dry bR-glycerol sample's photocycle had a rate-limiting step of ca. 1 s relaxation time, which is considerably shorter than the rate-limiting steps

TABLE 1 | The measured TM and TE positions and the calculated refractive index values of bR and PYP samples.

	TM position (degree)	TE position (degree)	Refractive index	Thickness
Bare waveguide 1	15.989	19.111	n_f = 1.788	205.45 nm
bR film	18.392	20.270	n_{bR} = 1.427	>5 μm
Bare waveguide 2	15.777	19.164	n_f = 1.799	195.26 nm
PYP film	18.672	20.595	n_{PYP} = 1.460	>5 μm

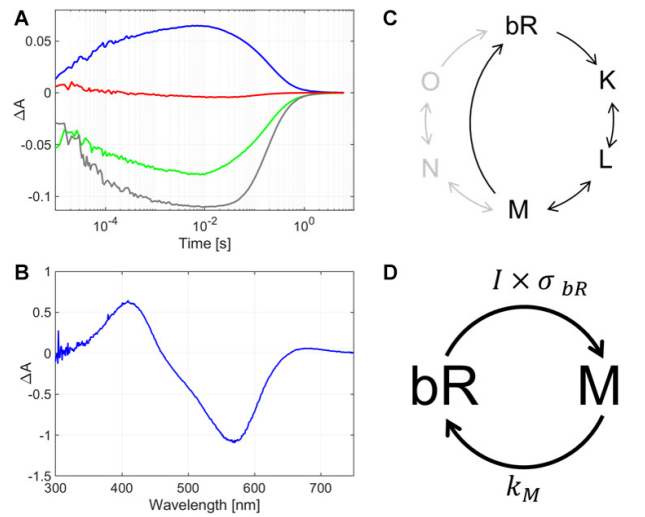

FIGURE 3 | (A) Absorption kinetics and **(B)** intermediate accumulation measurements taken on a glycerol-containing bR film. In panel **(A)**, the lines represent the change of absorption after light-excitation measured at 410 nm (blue line), 500 nm (green line), 575 nm (gray line) and at 620 nm (red line). In panel **(B)**, the difference absorption spectrum is shown, as measured after a 10-s excitation by subsequent laser pulses of a repetition rate of 2 Hz. **(C)** Schematic diagram of the full photocycle of a glycerol-containing bR film (black) and bR in water (gray). **(D)** Simplified diagram of the photocycle of the glycerol-containing bR film showing only the states relevant for our pulsed Z-scan measurements. *I* is the (average) light intensity exciting the sample, σ_{bR} is the absorption cross section of the bR molecule in the initial state, at the wavelength of excitation, and k_M is the rate constant of the M-decay.

in the dry bR film's photocycle (Tóth-Boconádi et al., 2011) (**Figure 3A**). The most probable reason for this phenomenon is that the glycerol-mediated wetting effect on the bR-conforming purple membranes dominates over viscosity effects, which were supposed to decelerate the decay of M intermediate (Beece et al., 1981). By also measuring the absorption difference spectrum after 10 s of CW excitation, we found that the majority of the bR molecules accumulate in the M intermediate state (**Figure 3B**). Compared to the flash duration and the interflash intervals of the Z-scan measurements, the decay of the photocycle is orders of magnitude slower, even at the lowest repetition rate. At 10 ms after excitation – which corresponds to the interflash interval at the lowest repetition rate in our Z-scan measurements –, the bR molecules are accumulated in the M intermediate state. Since the absorption cross section of bR in the M intermediate state is negligible at the wavelength of excitation (514 nm), and in dry samples the other long-living intermediates of the normal bR-photocycle (N and O) do not accumulate in considerable amounts (Tóth-Boconádi et al., 2011), the subsequent flashes hitting the sample will initiate photoreactions of the remaining ground-state molecules only. Hence, the exciting laser-flash train in the pulsed Z-scan experiments can be considered a quasi-CW illumination, while the sample can be considered to be in an average-intensity dependent dynamic equilibrium mixture of bR molecules in M intermediate and the initial state. **Figure 3C** shows the schematic representation of the photocycle of bR, where the most relevant part (marked with black color) corresponds to the glycerol-containing bR film. For the higher repetition rate measurements, hence the exciting laser-flash train in the pulsed Z-scan experiments can be considered quasi-CW illumination, while the sample can be considered to be in an average-intensity dependent dynamic equilibrium mixture of bR molecules in the M intermediate and the initial state. The corresponding simplified photocycle relevant for our Z-scan measurements, too, is illustrated in **Figure 3D**, indicating only the rate-limiting reactions. Here, $\boldsymbol{I}$ is the (average) light intensity exciting the sample, and $\boldsymbol{\sigma_{bR}}$ is the absorption cross section of the bR molecule in the initial state, at the wavelength of excitation. The product of the two, i.e., the probability of excitation, $\boldsymbol{I{\cdot}\sigma_{bR}}$, represents a virtual rate constant driving out the bR population from the initial state. Since the other transitions of the photocycle are much faster, practically only the M intermediate accumulates under (quasi-) steady state conditions, at an equilibrium concentration of $[\boldsymbol{bR}]_0 I\sigma_{bR}/(\boldsymbol{k_m} + I{\cdot}\sigma_{bR})$, where $\boldsymbol{[bR_0]}$ is the concentration of all the bR molecules (including the ones in the M and in the initial states), and $\boldsymbol{k_M}$ is the rate constant of the M-decay. The difference spectrum of such a sample is shown in **Figure 3B**, and the calculated $\boldsymbol{\Delta n}$ values are related to this steady state.

Similarly to bR, the wavelengths chosen for measuring the PYP's absorption kinetics represent the concentration development of different intermediates of the photocycle. The photocycle was monitored at three selected wavelengths: 430 nm, which is slightly blue-shifted from the initial state's maximum in order to limit the backscattering effect from the exciting light, while still gaining information about the initial state's concentration changes; 360 nm, to monitor the pB intermediate, and 470 nm for the pR intermediates. The rate-limiting step of the PYP-glycerol film's photocycle was found to be ca. 6 s (**Figure 4A**). Note that in PYP films devoid of glycerol, the photocycle does not take place at such low humidity, yet in our current measurements there is a clear indication of spectral changes in the wavelength range of the pR and pB intermediates, indicating a photocycle still being present in the glycerol-doped films (**Figure 4C**). Based on the glycerol concentration, the water activity in the sample was estimated to be the same as at 80% relative humidity without glycerol (Wheeler et al., 2012). Nevertheless, the photocycle is significantly slower than without glycerol (Krekic et al., 2019), which may be attributed to viscosity effects (Beece et al., 1981) rather than water-structure-mediated kosmotropic effects (Násztor et al., 2016), which should destabilize open conformations, such as pB, hence they should accelerate its decay (Kamikubo et al., 2007; Khoroshyy et al., 2013). Note that PYP is a water-soluble protein, unlike the membrane-protein, bR, so it is more exposed to solvent viscosity effects. The accumulation measurements (**Figure 4B**) are indicating a majority of the protein present in the pB state after excitation, hence, similarly to bR, we can suppose PYP is driven to a steady-state of pB and initial states, as indicated in **Figure 4D**, where their ratio is adjusted by the average exciting light intensity applied during pulsed Z-scan measurements (see similar argumentation above, for bR).

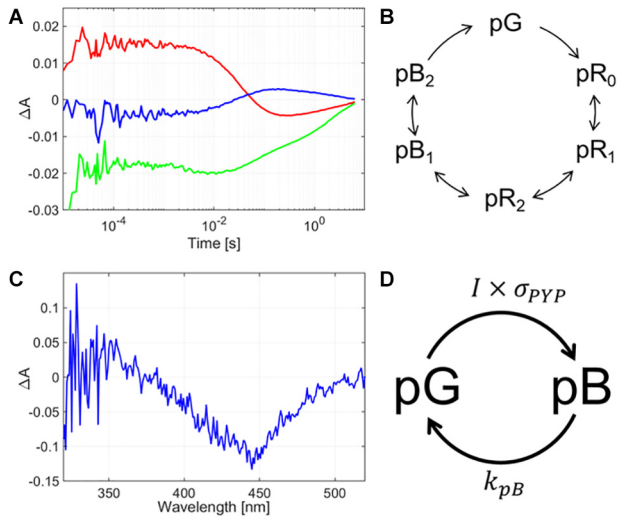

FIGURE 4 | (A) Absorption kinetics measurements and **(B)** intermediate accumulation measurements taken on a glycerol-containing PYP film. In subfigure **(A)**, the blue line represents the absorption spectrum measured at 360 nm, the green line at 430 nm, and the red line at 470 nm. In panel **(B)**, the difference absorption spectrum is shown, as measured after a 10-s excitation of the sample by a CW laser of 410 nm and 40 mW. **(C)** Schematic diagram of the full photocycle of a glycerol-containing PYP film. **(D)** Simplified diagram of the photocycle of the glycerol-containing PYP film showing only the states relevant for our pulsed Z-scan measurements. *I* is the (average) light intensity exciting the sample, σ_{PYP} is the absorption cross section of the PYP molecule in the initial state, at the wavelength of excitation, and k_{PB} is the rate constant of the pB-decay.

Z-Scan Measurements

Procedure for Separating Refractive Nonlinearities in Closed-Aperture Z-Scan Traces

Saturable absorption can drastically alter CA Z-scan traces even if the laser intensity does not significantly exceed the saturation intensity (cf. **Figure 5A**). Under such circumstances, the standard approach of dividing the CA trace by the corresponding OA trace is not sufficient to eliminate the effect of nonlinear absorption on the CA trace (cf. **Figure 5B**). Enabled by the use of a 2D camera in our Z-scan measurements, such effects can be removed using the following procedure. First, a 2D Gaussian spatial distribution is fitted on the measured beam profiles at each z position, and the position dependent beam waists, $w_x(z)$ and $w_y(z)$, and amplitudes, $A(z)$, are extracted. Then, the amplitudes are corrected assuming that the background-subtracted total signal count (E, energy) remains constant, i.e., independent of z. This constant is defined at a z position where nonlinear absorption is negligible,

$$E = A(|z| \gg z_0)\,\frac{w_x(|z| \gg z_0)\,w_y(|z| \gg z_0)\,\pi}{2} = constant. \tag{3}$$

The corrected amplitudes, $A'(z)$, constitute the corrected CA trace with an infinitesimally small aperture (cf. **Figure 5C**). In addition to separating nonlinear absorption effects from the CA traces, this correction procedure also reduces the fluctuations due to, e.g., sample inhomogeneity. All CA traces shown below are corrected traces based on this procedure.

Nonlinear Refractive Index of bR

Three laser repetition rates were used at 514 nm, 100 Hz, 1 kHz, and 100 kHz, to investigate the role of thermal effects and possible variation in the population distribution among various states in the photocycle of bR. CW measurements were also conducted at comparable intensities at 543 nm. Since the photocycle of bR is much longer than the laser repetition period (see section "Absorption Kinetics Spectroscopy"), the material is expected to be in a steady state, where a significant fraction of the molecules is in the M intermediate state (cf. **Figure 3D**). Also, the nonlinear response is expected to be driven by the average intensity rather than the peak intensity. In agreement, as shown in **Figure 6A**, we found that the magnitude of nonlinear refraction at an average intensity of 0.042 W/cm^2 was the same at a repetition rate of 100 Hz and 1 kHz despite an order of magnitude difference in peak intensity. At higher intensities, we found this to be still approximately true. The CA traces shown in **Figure 6B** were recorded at average intensities of 0.96 and 1.57 W/cm^2 at 100 Hz

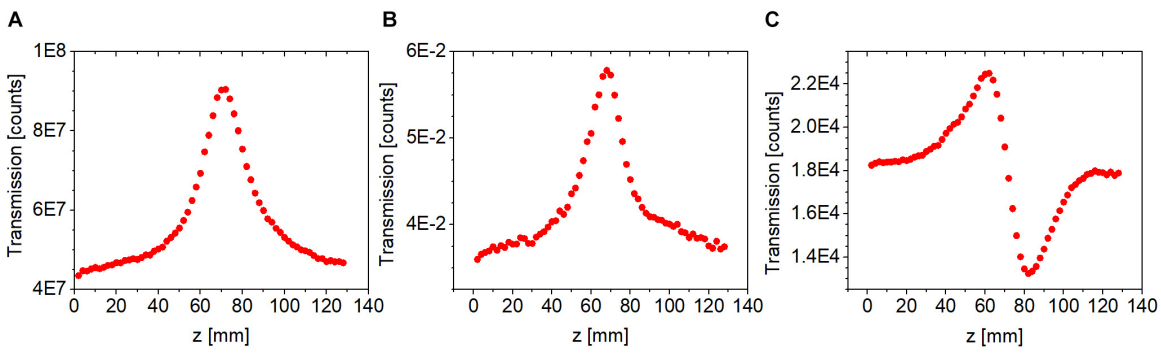

FIGURE 5 | Closed-aperture Z-scan traces measured using fs laser pulses at 514 nm for a bR sample at an average peak intensity of 0.13 W/cm^2. **(A)** Uncorrected closed-aperture trace. **(B)** Corrected closed-aperture trace obtained by dividing the uncorrected closed-aperture trace (cf. **A**) by the corresponding open-aperture trace. **(C)** Corrected closed-aperture trace obtained by applying our novel method described in Section "Procedure for Separating Refractive Nonlinearities in Closed-Aperture Z-Scan Traces."

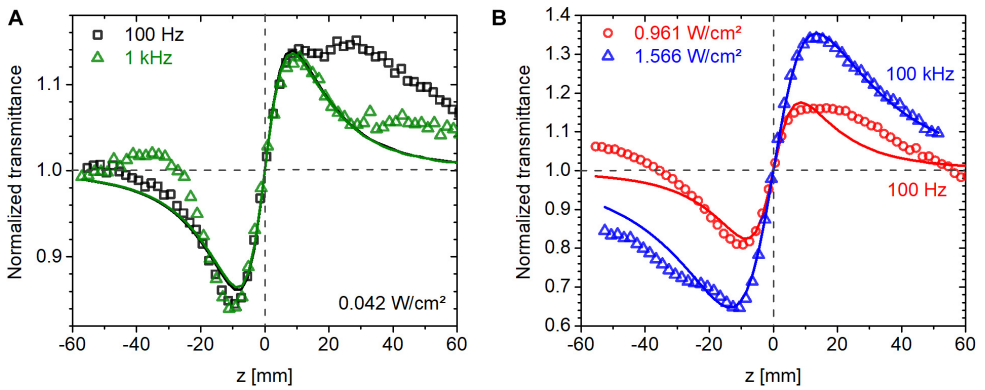

FIGURE 6 | Closed-aperture Z-scan traces measured on bR using fs laser pulses at 514 nm at average intensities of **(A)** 0.042 W/cm^2 and **(B)** around 1 W/cm^2. The symbols are measured data points obtained at various laser repetition rates, and the lines are fitted traces based on Eq. 1.

and 100 kHz, respectively. The ratio of ΔT_{P-V} (the difference between normalized peak and valley transmittance) of the 100-Hz and 100-kHz traces is 0.52, while the average intensity ratio is 0.61, i.e., only 18% higher than expected. In contrast, the ratio of peak intensities is 610.

To explore the saturable absorption behavior, we recorded open and closed-aperture Z-scan traces as a function of average intensity in the range of 0.04 and 0.42 W/cm^2 at a laser repetition rate of 1 kHz. The sample was 200 μm thick with an OD of 0.35 at 514 nm. Based on (Gu et al., 2006), we modeled the OA traces by assuming saturable absorption of a homogeneously broadened resonant transition characterized by an absorption coefficient,

$$\alpha(I) = \frac{\alpha_0}{1 + \frac{I}{I_s}}, \quad (4)$$

where $\boldsymbol{\alpha_0}$ is the linear absorption coefficient, and $\boldsymbol{I_s}$ is the saturation intensity. The results of the modeling are shown in **Figure 7A**. At the two lowest intensities, the fit is relatively good but it gets gradually worse at higher intensities. The extracted saturation intensities are shown in **Figure 7B** with a value approximately 0.1 W/cm^2 at an excitation intensity of 0.04 W/cm^2. The estimated error for the value of $\boldsymbol{I_s}$ at the lowest average intensity is ±20%, which includes uncertainty in the measured value of sample absorbance, thickness, and camera signal. The corresponding CA traces are shown in **Figure 7C**. At the two lowest intensities, the peak-to-valley distances are approximately the same with a value of $\sim\boldsymbol{2z_0}$, while at the highest intensity it is significantly larger. According to the Z-scan theory with cubic refractive nonlinearity (Sheik-Bahae et al., 1990), the peak-to-valley distance is $\sim\boldsymbol{1.7z_0}$ and it remains nearly constant at higher intensities with a small gradual decrease with increasing intensity. Therefore, at excitation intensities below 0.1 W/cm^2, we consider Eq. 1 a satisfactory model of nonlinear refraction of our bR samples.

In **Figures 8A,B**, the nonlinear refractive index, $\boldsymbol{n_2}$, is shown in a broad range of intensities. Although, we do not expect extracted $\boldsymbol{n_2}$ values to be consistent with the approximations implied by Eq. 1, our goal was to compare our measured $\boldsymbol{n_2}$ values with those in the literature and to provide for us benchmark values for the investigation of PYP (see section "Nonlinear Refractive Index of PYP"). Our measured $\boldsymbol{n_2}$ values in the average intensity range of 10^{-2} to 10^2 W/cm^2 fall in the range of 10^{-1} to 10^{-5} cm^2/W (**Figure 8A**) in agreement with the literature on bR excited in the green spectral range by CW lasers (Song et al., 1993; Kir'Yanov et al., 2000; Sifuentes et al., 2002; Banyal and Raghavendra Prasad, 2007). The increasing gap with increasing average intensity between the $\boldsymbol{n_2}$ values measured with a CW and a pulsed laser may suggest that further processes, other than a simple cubic nonlinearity are at play, such as thermal effects, thermally induced conformational changes, and refractive or absorptive nonlinearities of higher order. Our $\boldsymbol{n_2}$ data plotted as a function of peak intensity are also consistent with the literature on both bR and different retinal derivatives excited by pulsed lasers (Bezerra et al., 1997; Rakovich et al., 2013). In our peak intensity range of 10^8 to 10^{11} W/cm^2, the $\boldsymbol{n_2}$ values are in the range of 10^{-11} – 10^{-14} cm^2/W. These $\boldsymbol{n_2}$ values are many orders of magnitude smaller than the values obtained using CW lasers, which is typically not noted or discussed in the literature. As the average intensity is the main driving force behind the refractive nonlinearities of bR even at relatively low repetition rates (down to 100 Hz in our studies), we think that it is more relevant to determine and quote $\boldsymbol{n_2}$ values based on average intensities even for pulsed lasers. Interestingly, our $\boldsymbol{n_2}$ data closely follow an intensity dependence characterized by $\boldsymbol{I^{-1.075}}$, where $\boldsymbol{I}$ is the peak intensity (cf. solid line in **Figure 8B**). Importantly, the $\boldsymbol{n_2}$ data measured by our CW laser are also on this trend line. Accordingly, the corresponding change in refractive index, $\boldsymbol{\Delta n = n_2 I}$, in the whole intensity range is approximately constant with a value of 0.0009 to 0.0011 at 514 nm and around 0.0066 at 543 nm. This $\boldsymbol{\Delta n}$ value is in agreement with the refractive index change corresponding to the transition from the bR initial state to the M state (Song et al., 1993; Ormos et al., 2002; Fábián et al., 2015).

The saturable absorption behavior is also driven by average intensity rather than peak intensity. **Figure 8C** shows the relative change in the normalized transmission at $\boldsymbol{z = 0}$ as a function of average intensity approximately following the saturation behavior of a homogeneously broadened transition (solid line).

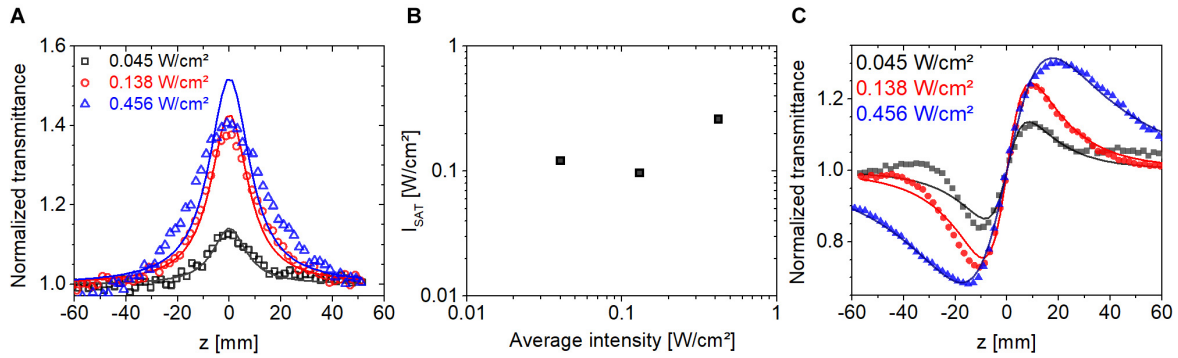

FIGURE 7 | (A) Open-aperture Z-scan traces measured on bR using fs laser pulses at 514 nm at three excitation intensities at a repetition rate of 1 kHz. **(B)** Saturation intensities extracted from the open-aperture traces in panel **(A)**. **(C)** Closed-aperture Z-scan traces obtained at 514 nm excitation corresponding to the curves in panel **(A)**. The symbols are the measured data points, and lines show the fitted traces.

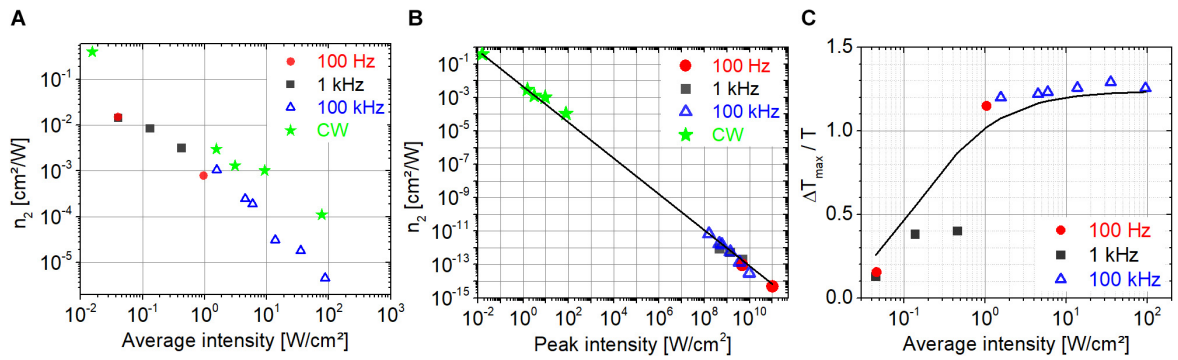

FIGURE 8 | Nonlinear refractive index of bR at 514 nm as a function of **(A)** average and **(B)** peak intensity. **(C)** The relative change in transmission as a function of average intensity. The solid line is a fit of a saturable absorption model on all measured data.

Obviously, the data do not follow a single trend when plotted as a function of peak intensity (not shown).

Nonlinear Refractive Index of PYP

In contrast to bR, excitation of the initial state of PYP (pG) at 514 nm is expected to lead to negligible linear absorption (see **Figure 4**). Therefore, the photocycle is not expected to be triggered at low excitation intensities. If the photocycle is initiated at laser repetition rates $\geq$1 kHz, it would lead to the accumulation of the pR intermediate state. Once the pR intermediate is produced, all the subsequent intermediates and also pR will linearly absorb at 514 nm.

We recorded Z-scan traces using pulsed-excitation at a repetition rate of 1 kHz and 100 kHz at 514 nm. **Figures 9A,B** show the CA traces measured at 1 kHz and 100 kHz, respectively, in the average intensity range of 10^{-1} and 10^{1} W/cm^2. Similarly to bR, the nonlinear response of PYP is also driven by the average intensity rather that peak intensity. In contrast to bR, the peak-to-valley configuration in the CA traces indicates a defocusing nonlinearity (i.e., negative $\boldsymbol{n_2}$). Note that the negative sign is in concert with the negative $\boldsymbol{\Delta n}$ measured at 633 nm in Krekic et al. (2019) and by Lee et al. (2018) between 470 nm and 570 nm. **Figure 9C** shows the CA traces measured at an average intensity of ~4.6 W/cm^2 at 1 kHz and 100 kHz. Despite of a factor of 100 larger peak intensity at 1 kHz than at 100 kHz, the $\boldsymbol{\Delta T_{P-V}}$ values are within ~30% suggesting that the excitation mechanism is not two-photon absorption but possibly a weak linear absorption process. In agreement, the OA traces show no sign of nonlinear absorption (cf. **Figure 9C** open symbols). With linear absorption, the photocycle can be started, and we expect the related refractive index changes to be larger than possible thermo-optical contributions.

The nonlinear refractive index of PYP extracted from the CA traces in **Figure 9** is shown in **Figures 10A,B**. The absolute value of our measured $\boldsymbol{n_2}$ data is also inversely proportional to the average intensity as in the case of bR (cf. **Figure 8A**), and these values fall in the range of 10^{-3} to 10^{-4} cm^2/W (**Figure 10A**) in the average intensity range of 0.1 to 1 W/cm^2. To the best of our knowledge, these are the first $\boldsymbol{n_2}$ values provided for PYP. If one extracts the $\boldsymbol{n_2}$ values from the $\boldsymbol{\Delta n}$ data provided in Vanhanen et al. (1998), the range of -2×10^{-2} to -9×10^{-3} cm^2/W is obtained for an average intensity between 3×10^{-3} and 2×10^{-2} W/cm^2 at 475-nm CW laser excitation. When plotted as a function of peak intensity, the $\boldsymbol{n_2}$ data points follow different power laws at different laser repetition rates (**Figure 10B**). The solid line was obtained by fitting the nonlinear refractive index

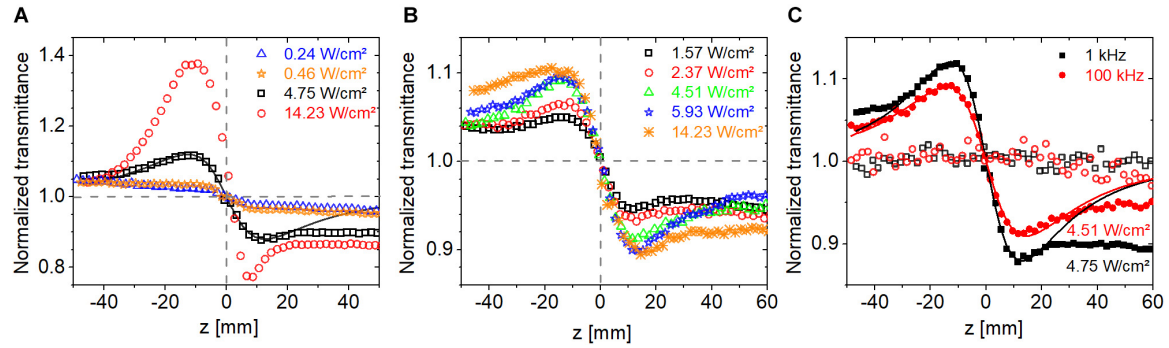

FIGURE 9 | Closed-aperture Z-scan traces measured on PYP using fs laser pulses at 514 nm at different excitation intensities at a repetition rate of **(A)** 1 kHz and **(B)** 100 kHz. **(C)** Comparison of the closed-aperture traces (filled symbols) and the open-aperture traces (hollow symbols) at a repetition rate of 1 kHz and 100 kHz, respectively, at ~4.6-W/cm^2 excitation intensity.

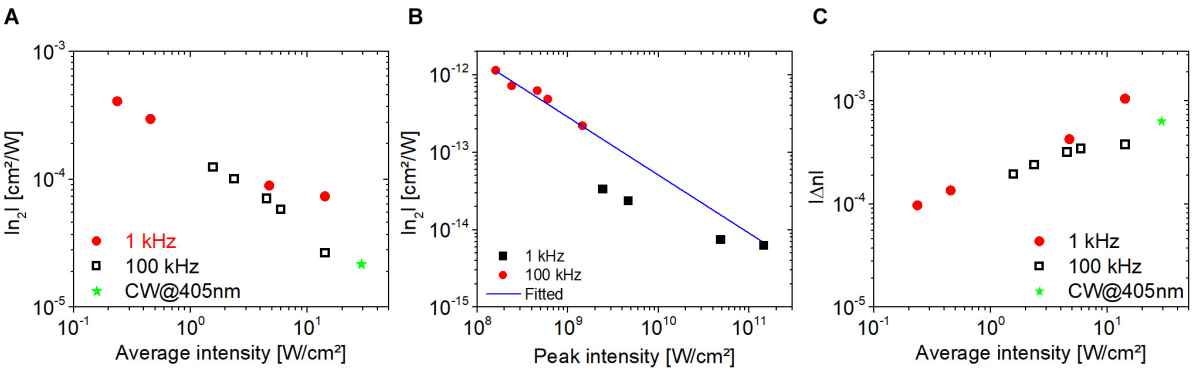

FIGURE 10 | Absolute value of the nonlinear refractive index of PYP at 514 nm as a function of **(A)** average and **(B)** peak intensity. **(C)** The absolute value of the change in the refractive index as a function of average intensity.

data points at 100 kHz. Clearly, the 1 kHz data points do not follow this trend. At both repetition rates, the dependence as a function of peak intensity is weaker than in the case of bR. The magnitude of the n_2 values of PYP in the peak intensity range of 10^8–10^{11} W/cm^2 are between 10^{-12} and 10^{-14} cm^2/W, which is a factor of 10 smaller range than that obtained with bR. Accordingly, the magnitude of the Δn values at the two repetition rates is not constant, but also increases as a function of average intensity, following a weak power law (cf. **Figure 10C**). In general, the Δn values obtained at a particular repetition rate and average intensity were of the same order of magnitude for both bR and PYP. However, in contrast to PYP, the dependence of the Δn values of bR as a function of average intensity is not monotonous and can be considered constant centered at 9×10^{-4} in a full range of 5×10^{-4} to 2×10^{-3} (not shown). The range of Δn values we obtained for PYP is in good agreement with the range obtained with 475-nm CW excitation, where the photocycle can unambiguously be initiated (Vanhanen et al., 1998).

Nonlinear Refraction as a Result of the Photocycle vs. Thermo-Optic Effects

Dealing with protein-containing samples, one should always consider the possibility of thermo-optic effects, reported for light-harvesting proteins, such as LHC complexes (Garab et al., 2002) or bR, too (Dancsházy et al., 1999). Such effects were shown to have a regulatory role in photosynthesis (Garab et al., 2002). In bR, it was demonstrated that high-energy flashes in the main absorption band of the protein can lead to permanent photobleaching of the sample. The effects were interpreted as a consequence of the transient increase of the temperature in the vicinity of the absorbing chromophore by more than 10 degrees, giving rise to temperature-induced conformational changes in the proteins. The dissipation of the heat packet was estimated to take place in the nanosecond time regime, and the effects showed a strongly nonlinear dependence on the peak intensity of the flash, attributed to a threshold phenomenon (Dancsházy et al., 1999). In the present measurements, however, we do not see such an effect as a function of peak intensity (this is why both the Δn and the n_2 dependences measured at different peak intensities could be reasonably unified to common curves on the time-averaged intensity scale), neither experienced we any photobleaching of the samples. Note, that the pulse energies were also much lower in our measurements than in Dancsházy et al. (1999). Of course, an effect of global heating of the sample at high average exciting energies cannot be excluded here, either, supporting our assumption that the

reliable values for these parameters are those in the low average power regime.

CONCLUSION

Our glycerol-doped thin films proved to be appropriate for optical applications: they allow to achieve a high protein concentration and optical quality, at the same time control the necessary water activity for the proteins to undergo a photocycle. They also show proper stability. A comprehensive study of the NLO properties of the protein-containing films was performed, by characterizing their absorption kinetics properties from the 10 μs to the 10 s time scale, and determining their linear and nonlinear refractive indices (n_0, Δn, and n_2 values).

The novel evaluation procedure we used for the Z-scan experiments could properly account for saturation effects that allows the determination of n_2 values for a Kerr material with much higher precision and reliability than before. At low average intensities, i.e., <0.1 W/cm^2, our obtained Δn values, $\sim 10^{-4}$ for PYP and $\sim 10^{-3}$ for bR, are comparable to those of the best solid-state materials. Importantly, our n_2 values, 4×10^{-4} cm^2/W for PYP and 10^{-2} cm^2/W for bR, are several orders of magnitude higher than those reported earlier for inorganic NLO materials (Adair et al., 1989; Kulagin et al., 2003; Eggleton et al., 2011), highlighting the potential utilization of these chromoproteins in special applications of photonics, where high Δn and n_2 are required. Some promising experiments have already been carried out in the fields of dynamic polarization holography (Hampp et al., 1990; Burykin et al., 2011), image filtering (Castillo et al., 2001), all-optical switching (Ormos et al., 2002; Topolancik and Vollmer, 2006; Fábián et al., 2010, 2011; Roy et al., 2010; Korposh et al., 2018) but a plethora of new applications can be envisaged in all-optical signal processing, utilizing the ultrafast transitions of the photocycle (Fábián et al., 2011), e.g., in multi-wave mixing, nonlinear mode-coupling in fibers (Xu et al., 2015), and wavelength multiplexing-demultiplexing in IO devices.

DATA AVAILABILITY STATEMENT

The raw data supporting the conclusions of this article will be made available by the authors, without undue reservation.

AUTHOR CONTRIBUTIONS

SK, ZH, MM, LZ, and AD created the research idea. ZH and MM designed the pulsed Z-scan measurements. SK, SV, LZ, and AD designed and conducted the CW Z-scan measurements, the OWLS, and kinetic experiments. TZ and ZG prepared the PYP protein while SK prepared all the thin protein film samples. The OWLS and kinetic data were analyzed by SK and AD, while the Z-scan measurements were analyzed and fitted by ZH and MM. SK, MM, ZH, and AD wrote the manuscript. All authors discussed and revised the article.

FUNDING

This study was funded by Deutsche Forschungsgemeinschaft (DFG) (GSC 1013 SALSA), National Research and Development Office, Hungary (NKFI-1 K-124922), Economic Development and Innovation Operative Programme of Hungary (GINOP-2.3.2-15-2016-00001), and German Academic Exchange Service (DAAD).

ACKNOWLEDGMENTS

ZH acknowledges funding by a Julia Lermontova Fellowship from DFG, No. GSC 1013 SALSA. We acknowledge support by the German Research Foundation (DFG) and the Open Access Publication Fund of Humboldt-Universität zu Berlin. SK acknowledges funding by the University of Szeged and the German Academic Exchange Service (DAAD). We are indebted to Prof. Hinorari Kamikubo for kindly providing the plasmid for PYP expression, and to Dr. Laszlo Fabian for helpful discussions.

REFERENCES

Adair, R., Chase, L., and Payne, S. A. (1989). Nonlinear refractive index of optical crystals. *Phys. Rev. B* 39:3337. doi: 10.1103/PhysRevB.39.3337

Adair, R., Chase, L. L., and Payne, S. A. (1987). Nonlinear refractive-index measurements of glasses using three-wave frequency mixing. *J. Optic. Soc. Am. B* 4, 875–881. doi: 10.1364/JOSAB.4.000875

Aranda, F. J., Rao, D. V., Wong, C. L., Zhou, P., Chen, Z., Akkara, J. A., et al. (1995). Nonlinear optical interactions in bacteriorhodopsin using Z-scan. *Optic. Rev.* 2, 204–206. doi: 10.1007/s10043-995-0204-x

Balashov, S. P. (1995). Photoreactions of the Photointermediates of Bacteriorhodopsin. *Israel J. Chem.* 35, 415–428. doi: 10.1002/ijch.19950 0040

Banyal, R. K., and Raghavendra Prasad, B. (2007). Measurements of photoinduced refractive index changes in bacteriorhodopsin films. *Pramana* 68, 435–441. doi: 10.1007/s12043-007-0046-0

Beece, D., Bowne, S. F., Czégé, J., Eisenstein, L., Frauenfelder, H., Good, D., et al. (1981). The effect of viscosity on the photocycle of bacteriorhodopsin. *Photochem. Photobiol.* 33, 517–522. doi: 10.1111/j.1751-1097.1981.tb05 454.x

Bezerra, A. G., Gomes, A. S. L., de Melo, C. P., and de Araújo, C. B. (1997). Z-scan measurements of the nonlinear refraction in retinal derivatives. *Chem. Phys. Lett.* 276, 445–449. doi: 10.1016/S0009-2614(97)00841-5

Boyd, R. W. (2003). "Chapter 4 - The intensity-dependent refractive index," in *Nonlinear Optics*, 2nd Edn, ed. R. W. Boyd (San Diego: Academic Press), 189–235. doi: 10.1016/b978-012121682-5/50005-5

Burykin, N., Stepanchikov, D., Dyukova, T., Savchuk, A., Balashov, S., and Korchemskaya, E. (2011). Real-time optical information processing through the use of low-saturable absorption in bacteriorhodopsin films. *Mol. Cryst. Liquid Cryst.* 535, 140–147. doi: 10.1080/15421406.2011.537966

Castillo, M. I., Sanchez-de-la-Llave, D., García, R. R., Olivos-Perez, L., Gonzalez, L. A., and Rodriguez-Ortiz, M. (2001). Real-time self-induced nonlinear optical Zernike-type filter in a bacteriorhodopsin film. *Optic. Eng. Bellingham Intern. Soc. Optic. Eng.* 40, 2367–2368. doi: 10.1117/1.1412425

Chai, Z., Hu, X., Wang, F., Niu, X., Xie, J., and Gong, Q. (2017). Ultrafast all-optical switching. *Adv. Optic. Mater.* 5:1600665. doi: 10.1002/adom.201600665

Clays, K., Van Elshocht, S., Chi, M., Lepoudre, E., and Persoons, A. (2001). Bacteriorhodopsin: a natural, efficient (nonlinear) photonic crystal. *JOSA B* 18, 1474–1482. doi: 10.1364/JOSAB.18.001474

Colonna, A., Groma, G. I., and Vos, M. H. (2005). Retinal isomerization dynamics in dry bacteriorhodopsin films. *Chem. Phys. Lett.* 415, 69–73. doi: 10.1016/j.cplett.2005.08.132

Dancsházy, Z., Tokaji, Z., and Dér, A. (1999). Bleaching of bacteriorhodopsin by continuous light. *FEBS Lett.* 450, 154–157. doi: 10.1016/S0014-5793(99)00487-1

Dér, A., and Keszthelyi, L. (2001). *Bioelectronic Applications of Photochromic Pigments*. Amsterdam: IOS Press.

Dini, D., Calvete, M. J. F., and Hanack, M. (2016). Nonlinear optical materials for the smart filtering of optical radiation. *Chem. Rev.* 116:13043. doi: 10.1021/acs.chemrev.6b00033

Draheim, J. E., and Cassim, J. Y. (1985). Effects of polyhydric alcohols on the conformational stability of the purple membrane. *J. Membr. Biol.* 86, 229–238. doi: 10.1007/BF01870602

Eggleton, B. J., Luther-Davies, B., and Richardson, K. (2011). Chalcogenide photonics. *Nat. Photon.* 5:141. doi: 10.1038/nphoton.2011.309

Fábián, L., Heiner, Z., Mero, M., Kiss, M., Wolff, E. K., Ormos, P., et al. (2011). Protein-based ultrafast photonic switching. *Optics Exp.* 19, 18861–18870. doi: 10.1364/OE.19.018861

Fábián, L., Mathesz, A., and Dér, A. (2015). New trends in biophotonics. *Acta Biol. Szegediensis* 59(Suppl. 2), 189–202.

Fábián, L., Wolff, E. K., Oroszi, L., Ormos, P., and Dér, A. (2010). Fast integrated optical switching by the protein bacteriorhodopsin. *Appl. Phys. Lett.* 97:023305. doi: 10.1063/1.3462940

Fitter, J., Lechner, R. E., and Dencher, N. A. (1999). Interactions of hydration water and biological membranes studied by neutron scattering. *J. Phys. Chem. B* 103, 8036–8050. doi: 10.1021/jp9912410

Garab, G., Cseh, Z., Kovács, L., Rajagopal, S., Várkonyi, Z., Wentworth, M., et al. (2002). Light-induced trimer to monomer transition in the main light-harvesting antenna complex of plants: thermo-optic mechanism. *Biochemistry* 41, 15121–15129. doi: 10.1021/bi026157g

Gu, B., Fan, Y.-X., Wang, J., Chen, J., Ding, J., Wang, H.-T., et al. (2006). Characterization of saturable absorbers using an open-aperture Gaussian-beam Z scan. *Phys. Rev. A* 73:065803. doi: 10.1103/PhysRevA.73.065803

Hales, J. M., Matichak, J., Barlow, S., Ohira, S., Yesudas, K., Brédas, J.-L., et al. (2010). Design of polymethine dyes with large third-order optical nonlinearities and loss figures of merit. *Science* 327, 1485–1488. doi: 10.1126/science.1185117

Hampp, N., Bräuchle, C., and Oesterhelt, D. (1990). Bacteriorhodopsin wildtype and variant aspartate-96 → aspargine as reversible holographic media. *Biophys. J.* 58, 83–93. doi: 10.1016/S0006-3495(90)82355-9

Hampp, N., and Juchem, T. (2001). Fringemaker-the first technical system based on bacteriorhodopsin. *Nato Sci. Ser. Sub. Ser. I Life Behav. Sci.* 335, 44–53.

Haque, S. A., and Nelson, J. (2010). Toward organic all-optical switching. *Science* 327, 1466–1467. doi: 10.1126/science.1188291

Heiner, Z., and Osvay, K. (2009). Refractive index of dark-adapted bacteriorhodopsin and tris (hydroxymethyl) aminomethane buffer between 390 and 880 nm. *Appl. Optics* 48, 4610–4615. doi: 10.1364/AO.48.004610

Hu, H.-J., Liu, C.-C., Zang, J.-Q., Zhu, C.-Y., and Luo, D.-B. (2017). Study the nonlinear optical property of pull/push type azo dye-doped polymer using 633 nm He-Ne laser. *J. Nonline. Optic. Phys. Mater.* 26:1750008. doi: 10.1142/S0218863517500084

Jeganathan, C., Sabari Girisun, T. C., Rao, S. V., and Thamaraiselvi, K. (2017). Variable ultrafast optical nonlinearity in bacteriorhodopsin achieved through simple chemical treatment. *J. Mater. Sci.* 52, 6866–6878. doi: 10.1007/s10853-017-0924-x

Joshi, C. P., Borucki, B., Otto, H., Meyer, T. E., Cusanovich, M. A., and Heyn, M. P. (2005). Photoreversal kinetics of the I1 and I2 intermediates in the photocycle of photoactive yellow protein by double flash experiments with variable time delay. *Biochemistry* 44, 656–665. doi: 10.1021/bi0481141

Kamikubo, H., Shimizu, N., Harigai, M., Yamazaki, Y., Imamoto, Y., and Kataoka, M. (2007). Characterization of the solution structure of the M intermediate of photoactive yellow protein using high-angle solution X-Ray scattering. *Biophys. J.* 92, 3633–3642. doi: 10.1529/biophysj.106.097287

Khoroshyy, P., Dér, A., and Zimányi, L. (2013). Effect of Hofmeister cosolutes on the photocycle of photoactive yellow protein at moderately alkaline pH. *J. Photochem. Photobiol. B Biol.* 120, 111–119. doi: 10.1016/j.jphotobiol.2012.12.014

Kir'Yanov, A., Barmenkov, Y. O., Starodumov, A., Leppanen, V.-P., Vanhanen, J., and Jaaskelainen, T. (2000). Application of the Z-scan technique to a saturable photorefractive medium with the overlapped ground and excited state absorption. *Opt. Commun.* 177, 417–423. doi: 10.1016/S0030-4018(00)00599-X

Korposh, S., James, S., Partridge, M., Sichka, M., and Tatam, R. (2018). All-optical switching based on optical fibre long period gratings modified bacteriorhodopsin. *Optics Laser Technol.* 101, 162–171. doi: 10.1016/j.optlastec.2017.11.021

Krekic, S., Nagy, D., Taneva, S. G., Fábián, L., Zimányi, L., and Dér, A. (2019). Spectrokinetic characterization of photoactive yellow protein films for integrated optical applications. *Eur. Biophys. J.* 48, 465–473. doi: 10.1007/s00249-019-01353-8

Kulagin, I. A., Ganeev, R. A., Kim, V. A., Ryasnyansky, A. I., Tugushev, R. I., Usmanov, T., et al. (2003). "Nonlinear refractive indices and third-order susceptibilities of nonlinear optical crystals," in *Proceedings of the Nonlinear Frequency Generation and Conversion: Materials, Devices, and Applications II*, San Jose, CA. doi: 10.1117/12.478999

Lanyi, J. K. (2004). Bacteriorhodopsin. *Annu. Rev. Physiol.* 66, 665–688. doi: 10.1146/annurev.physiol.66.032102.150049

Lee, K., Kim, Y., Jung, J., Ihee, H., and Park, Y. (2018). Measurements of complex refractive index change of photoactive yellow protein over a wide wavelength range using hyperspectral quantitative phase imaging. *Sci. Rep.* 8, 1–8. doi: 10.1038/s41598-018-21403-z

Leppanen, V., Haring, T., Jaaskelainen, T., Vartiainen, E., Parkkinen, S., and Parkkinen, J. (1999). The intensity dependent refractive index change of photochromic proteins. *Opt. Commun.* 163, 189–192. doi: 10.1016/S0030-4018(99)00141-8

Mathesz, A., Fábián, L., Valkai, S., Alexandre, D., Marques, P. V. S., Ormos, P., et al. (2013). High-speed integrated optical logic based on the protein bacteriorhodopsin. *Biosens. Bioelectron.* 46, 48–52. doi: 10.1016/j.bios.2013.02.022

Mero, M., Wang, L., Chen, W., Ye, N., Zhang, G., Petrov, V., et al. (2019). "Laser-induced damage of nonlinear crystals in ultrafast, high-repetition-rate, mid-infrared optical parametric amplifiers pumped at 1 μm," in *Proceedings of the Pacific Rim Laser Damage 2019 and Thin Film Physics and Applications*, Qingdao, China. doi: 10.1117/12.2540125

Meyer, T. E. (1985). Isolation and characterization of soluble cytochromes, ferredoxins and other chromophoric proteins from the halophilic phototrophic bacterium *Ectothiorhodospira halophila*. *Biochim. Biophys. Acta Bioenerget.* 806, 175–183. doi: 10.1016/0005-2728(85)90094-5

Meyer, T. E., Yakali, E., Cusanovich, M. A., and Tollin, G. (1987). Properties of a water-soluble, yellow protein isolated from a halophilic phototrophic bacterium that has photochemical activity analogous to sensory rhodopsin. *Biochemistry* 26, 418–423. doi: 10.1021/bi00376a012

Mihara, K., Hisatiomi, O., Imamoto, Y., Kataoka, M., and Tokunaga, F. (1997). Functional expression and site-directed mutagenesis of photoactive yellow protein. *J. Biochem.* 121, 876–880. doi: 10.1093/oxfordjournals.jbchem.a021668

Miller, D. A. (2010). Are optical transistors the logical next step? *Nat. Photon.* 4, 3–5. doi: 10.1038/nphoton.2009.240

Naskali, L., Huttunen, M. J., Virkki, M., Bautista, G., Deìr, A. S., and Kauranen, M. (2014). Microscopic determination of second-order nonlinear optical susceptibility tensors. *J. Phys. Chem. C* 118, 26409–26414. doi: 10.1021/jp509453b

Násztor, Z., Bogár, F., and Dér, A. (2016). The interfacial tension concept, as revealed by fluctuations. *Curr. Opin. Coll. Interf. Sci.* 23, 29–40. doi: 10.1016/j.cocis.2016.05.007

Nibbering, E. T. J., Franco, M. A., Prade, B. S., Grillon, G., Le Blanc, C., and Mysyrowicz, A. (1995). Measurement of the nonlinear refractive index of transparent materials by spectral analysis after nonlinear propagation. *Opt. Commun.* 119, 479–484. doi: 10.1016/0030-4018(95)00394-N

Nussenzveig, H. M. (1972). "Chapter 1: Casuality and dispersion relations," in *Mathematics in Science and Engineering*, ed. H. M. Nussenzveig (Amsterdam: Elsevier), 3–53. doi: 10.1016/s0076-5392(08)63161-6

Oesterhelt, D., and Stoeckenius, W. (1971). Rhodopsin-like Protein from the Purple Membrane of *Halobacterium halobium*. *Nat. New Biol.* 233, 149–152. doi: 10.1038/newbio233149a0

Oesterhelt, D., and Stoeckenius, W. (1973). Functions of a new photoreceptor membrane. *Proc. Natl. Acad. Sci. U.S.A.* 70, 2853–2857. doi: 10.1073/pnas.70.10.2853

Oesterhelt, D., and Stoeckenius, W. (1974). Isolation of the cell membrane of *Halobacterium halobium* and its fractionation into red and purple membrane. *Methods Enzymol.* 31, 667–678. doi: 10.1016/0076-6879(74)31072-5

Ormos, P., Fábián, L., Oroszi, L., Wolff, E. K., Ramsden, J. J., and Dér, A. (2002). Protein-based integrated optical switching and modulation. *Appl. Phys. Lett.* 80, 4060–4062. doi: 10.1063/1.1481197

Rakovich, A., Nabiev, I., Sukhanova, A., Lesnyak, V., Gaponik, N., Rakovich, Y. P., et al. (2013). Large enhancement of nonlinear optical response in a hybrid nanobiomaterial consisting of Bacteriorhodopsin and cadmium telluride quantum dots. *ACS Nano* 7, 2154–2160. doi: 10.1021/nn3049939

Ramsden, J. J. (1993). Review of new experimental techniques for investigating random sequential adsorption. *J. Statist. Phys.* 73, 853–877. doi: 10.1007/BF01052813

Roy, S., Prasad, M., Topolancik, J., and Vollmer, F. (2010). All-optical switching with bacteriorhodopsin protein coated microcavities and its application to low power computing circuits. *J. Appl. Phys.* 107:053115. doi: 10.1063/1.3310385

Sasikala, V., and Chitra, K. (2018). All optical switching and associated technologies: a review. *J. Optics* 47, 307–317. doi: 10.1007/s12596-018-0452-3

Schotte, F., Cho, H. S., Kaila, V. R. I., Kamikubo, H., Dashdorj, N., Henry, E. R., et al. (2012). Watching a signaling protein function in real time via 100-ps time-resolved laue crystallography. *Proc. Natl. Acad. Sci. U.S.A.* 109, 19256–19261. doi: 10.1073/pnas.1210938109

Sheik-Bahae, M., Said, A. A., Wei, T., Hagan, D. J., and Stryland, E. W. V. (1990). Sensitive measurement of optical nonlinearities using a single beam. *IEEE J. Q. Electron.* 26, 760–769. doi: 10.1109/3.53394

Sifuentes, C., Barmenkov, Y. O., and Kir'yanov, A. (2002). The intensity dependent refractive index change of bacteriorhodopsin measured by the Z-scan and phase-modulated beams techniques. *Optic. Mater.* 19, 433–442. doi: 10.1016/S0925-3467(02)00024-1

Song, Q. W., Zhang, C., Gross, R., and Birge, R. (1993). Optical limiting by chemically enhanced bacteriorhodopsin films. *Optics Lett.* 18, 775–777. doi: 10.1364/OL.18.000775

Stuart, J. A., Marcy, D. L., and Birge, R. R. (2001). Photonic and optoelectronic applications of bacteriorhodopsin. *Nato Sci. Ser. Sub. Ser. I Life Behav. Sci.* 335, 16–29.

Tenboer, J., Basu, S., Zatsepin, N., Pande, K., Milathianaki, D., Frank, M., et al. (2014). Time-resolved serial crystallography captures high-resolution intermediates of photoactive yellow protein. *Science* 346, 1242–1246. doi: 10.1126/science.1259357

Topolancik, J., and Vollmer, F. (2006). All-optical switching in the near infrared with bacteriorhodopsin-coated microcavities. *Appl. Phys. Lett.* 89:184103. doi: 10.1063/1.2372711

Tóth-Boconádi, R., Dér, A., and Keszthelyi, L. (2011). Optical and electric signals from dried oriented purple membrane of bacteriorhodopsins. *Bioelectrochemistry* 81, 17–21. doi: 10.1016/j.bioelechem.2010.12.003

Tóth-Boconádi, R., Dér, A., Taneva, S. G., and Keszthelyi, L. (2006). Excitation of the L intermediate of bacteriorhodopsin: electric responses to Test X-Ray structures. *Biophys. J.* 90, 2651–2655. doi: 10.1529/biophysj.105.068817

Tóth-Boconádi, R., Dér, A., Taneva, S. G., and Keszthelyi, L. (2010). Excitation of the M intermediates of wild-type bacteriorhodopsin and mutant D96N: temperature dependence of absorbance, electric responses and proton movements. *Theoret. Chem. Acc.* 125, 365–373. doi: 10.1007/s00214-009-0632-y

van der Horst, M. A., van Stokkum, I. H. M., Dencher, N. A., and Hellingwerf, K. J. (2005). Controlled reduction of the humidity induces a shortcut recovery reaction in the photocycle of photoactive yellow protein. *Biochemistry* 44, 9160–9167. doi: 10.1021/bi050237d

Vanhanen, J., Leppanen, V. P., Haring, T., Kettunen, V., Jaaskelainen, T., Parkkinen, S., et al. (1998). Nonlinear refractive index change of photoactive yellow protein. *Opt. Commun.* 155, 327–331. doi: 10.1016/S0030-4018(98)00395-2

Váró, G., and Keszthelyi, L. (1983). Photoelectric signals from dried oriented purple membranes of *Halobacterium halobium*. *Biophys. J.* 43, 47–51. doi: 10.1016/S0006-3495(83)84322-7

Vsevolodov, N. (2012). *Biomolecular Electronics: An Introduction via Photosensitive Proteins*. Berlin: Springer Science & Business Media.

Wheeler, M. J., Russi, S., Bowler, M. G., and Bowler, M. W. (2012). Measurement of the equilibrium relative humidity for common precipitant concentrations: facilitating controlled dehydration experiments. *Acta Crystallogr. Sect. F Struct. Biol. Crystalliz. Commun.* 68, 111–114. doi: 10.1107/S1744309111054029

Willner, A. E., Khaleghi, S., Chitgarha, M. R., and Yilmaz, O. F. (2014). All-Optical Signal Processing. *J. Lightwave Technol.* 32, 660–680. doi: 10.1109/JLT.2013.2287219

Wooten, F. (2013). *Optical Properties of Solids*. Cambridge, MA: Academic press.

Xu, J., Gordon, G. S., Wilkinson, T., and Peucheret, C. (2015). "Experimental observation of nonlinear mode conversion in few-mode fiber," in *Proceedings of the 2015 Conference on Lasers and Electro-Optics (CLEO)*, San Jose, CA. doi: 10.1364/CLEO_SI.2015.SM2L.3

Yeremenko, S., van Stokkum, I. H. M., Moffat, K., and Hellingwerf, K. J. (2006). Influence of the crystalline state on Photoinduced dynamics of photoactive yellow protein studied by ultraviolet-visible transient absorption spectroscopy. *Biophys. J.* 90, 4224–4235. doi: 10.1529/biophysj.105.074765

Conflict of Interest: The authors declare that the research was conducted in the absence of any commercial or financial relationships that could be construed as a potential conflict of interest.

Copyright © 2020 Krekic, Zakar, Gombos, Valkai, Mero, Zimányi, Heiner and Dér. This is an open-access article distributed under the terms of the Creative Commons Attribution License (CC BY). The use, distribution or reproduction in other forums is permitted, provided the original author(s) and the copyright owner(s) are credited and that the original publication in this journal is cited, in accordance with accepted academic practice. No use, distribution or reproduction is permitted which does not comply with these terms.

frontiers in Plant Science

REVIEW
published: 28 April 2021
doi: 10.3389/fpls.2021.663309

The Role of Membranes and Lipid-Protein Interactions in the Mg-Branch of Tetrapyrrole Biosynthesis

Katalin Solymosi[1†] *and Beata Mysliwa-Kurdziel*[2*†]

[1] Department of Plant Anatomy, ELTE Eötvös Loránd University, Budapest, Hungary, [2] Department of Plant Physiology and Biochemistry, Faculty of Biochemistry, Biophysics and Biotechnology, Jagiellonian University, Krakow, Poland

Chlorophyll (Chl) is essential for photosynthesis and needs to be produced throughout the whole plant life, especially under changing light intensity and stress conditions which may result in the destruction and elimination of these pigments. All steps of the Mg-branch of tetrapyrrole biosynthesis leading to Chl formation are carried out by enzymes associated with plastid membranes. Still the significance of these protein-membrane and protein-lipid interactions in Chl synthesis and chloroplast differentiation are not very well-understood. In this review, we provide an overview on Chl biosynthesis in angiosperms with emphasis on its association with membranes and lipids. Moreover, the last steps of the pathway including the reduction of protochlorophyllide (Pchlide) to chlorophyllide (Chlide), the biosynthesis of the isoprenoid phytyl moiety and the esterification of Chlide are also summarized. The unique biochemical and photophysical properties of the light-dependent NADPH:protochlorophyllide oxidoreductase (LPOR) enzyme catalyzing Pchlide photoreduction and located to peculiar tubuloreticular prolamellar body (PLB) membranes of light-deprived tissues of angiosperms and to envelope membranes, as well as to thylakoids (especially grana margins) are also reviewed. Data about the factors influencing tubuloreticular membrane formation within cells, the spectroscopic properties and the *in vitro* reconstitution of the native LPOR enzyme complexes are also critically discussed.

Keywords: chlorophyll biosynthesis, chloroplast, etioplast, NADPH:protochlorophyllide oxidoreductase, phytol, prolamellar body, protochlorophyllide, tubular complex

OPEN ACCESS

Edited by:
Yoshitaka Nishiyama, Saitama University, Japan

Reviewed by:
Ayumi Tanaka, Hokkaido University, Japan
Tatsuru Masuda, The University of Tokyo, Japan

***Correspondence:**
Beata Mysliwa-Kurdziel
b.mysliwa-kurdziel@uj.edu.pl

†These authors have contributed equally to this work

Specialty section:
This article was submitted to Plant Physiology, a section of the journal Frontiers in Plant Science

Received: *02 February 2021*
Accepted: *22 March 2021*
Published: *28 April 2021*

Citation:
Solymosi K and Mysliwa-Kurdziel B (2021) The Role of Membranes and Lipid-Protein Interactions in the Mg-Branch of Tetrapyrrole Biosynthesis. Front. Plant Sci. 12:663309. doi: 10.3389/fpls.2021.663309

INTRODUCTION

Thylakoid membranes of photosynthetic organisms have a unique and highly conserved lipid composition: in addition to the phospholipid, phosphatidylglycerol (PG), they predominantly contain galactolipids (monogalactosyldiacylglycerol—MGDG, digalactosyldiacylglycerol—DGDG, and sulfoquinovosyldiacylglycerol—SQDG). Galactolipids are major components of plastid inner membranes that play an important role in chloroplast differentiation from proplastids or etioplasts, in chlorophyll (Chl) biosynthesis, in the accumulation of light-harvesting proteins (Fujii et al., 2019a,b), and have been also identified as structural components of several major protein complexes of the photosynthetic apparatus (PSII, PSI, LHCII, and cytochrome b_6f) (Kobayashi, 2016). In this review, we provide an overview of the Mg-branch of tetrapyrrole

biosynthesis, leading to Chl biosynthesis, that occurs in plastids and is associated to plastid membranes. We focus on the reduction of protochlorophyllide (Pchlide) to chlorophyllide (Chlide), and the role of lipids and plastid inner membranes in the process. Two distinct enzymes have been evolved to catalyze this reaction step: first a nitrogenase-like, oxygen-sensitive dark-operative NADPH:Pchlide oxidoreductase enzyme (DPOR), and later a light-dependent NADPH:protochlorophyllide oxidoreductase (LPOR), which requires light for its activity (Gabruk and Mysliwa-Kurdziel, 2015; Vedalankar and Tripathy, 2019). There is very low sequence homology between these two enzymes (Gabruk et al., 2012), and in most organisms they occur simultaneously. However, angiosperms lack LPOR and became unable to synthesize Chlide and chlorophylls (Chls) in the absence of light. Due to this special feature, Chl biosynthesis has been extensively studied in dark-germinated angiosperm seedlings which also have agricultural relevance as the seeds of many crops are sown deep into the soil and thus start to germinate in the dark. Due to space limitation our focus is on data available about the role of lipids and membranes on Chl biosynthesis in angiosperms.

OVERVIEW OF THE MG-BRANCH OF TETRAPYRROLE BIOSYNTHESIS

Chlorophylls (i.e., Chl *a* and Chl *b*) are the main photosynthetic pigments in plants. Concerning their molecular structure, they belong to tetrapyrroles (Fiedor et al., 2019). Their biosynthesis takes place in plastids and shares some common steps with that of other tetrapyrroles. The tetrapyrrole biosynthesis route leading to Chl formation is often referred to as the Mg-branch (for review see Mochizuki et al., 2010; Tanaka et al., 2011; Tripathy and Pattanayak, 2012; Rebeiz, 2014; Willows, 2019; Bryant et al., 2020). Several new data indicate that galactolipids play crucial roles in Chl biosynthesis (Kobayashi et al., 2014; Fujii et al., 2019b) in addition to other factors regulating the Mg-branch at various levels and *via* different mechanisms as reviewed by Grimm (2010), Stenbaek and Jensen (2010), Zhang et al. (2011), Czarnecki and Grimm (2012), Richter and Grimm (2013), Brzezowski et al. (2015), Wang and Grimm (2015), Kobayashi and Masuda (2016), Yuan et al. (2017), and Herbst et al. (2019).

Formation of Mg-protoporphyrin IX

The incorporation of Mg^{2+} to protoporphyrin IX is the first reaction on the Mg-branch of tetrapyrrole biosynthesis and the protoporphyrin IX is the last common intermediate of both Chl and heme biosynthesis (**Figure 1**). This reaction is catalyzed by Mg-chelatase (EC 6.6.1.1) which is a large multisubunit complex composed of three subunits, CHLI, CHLD, and CHLH. Two of them, CHLD and CHLI, catalyze ATP hydrolysis, whereas the third one, CHLH, binds the substrate (protoporphyrin IX). During the two-steps reaction, first, an ATP- and Mg^{2+}-dependent activation occurs, leading to the formation of the active Mg-chelatase complex, which is then followed by the ATP-dependent chelation step (reviewed by Masuda, 2008; Bryant et al., 2020). Recent detailed analyses unraveled the conformational changes and kinetic parameters of CHLH caused by the substrate binding (Adams et al., 2020). Two CHLI isoforms, CHLI1 and CHLI2, were found in *A. thaliana*, both having similar expression profiles. The dominant CHLI1 isoform is crucial for the chelatase activity, whereas CHLI2 plays a limited role in Chl biosynthesis but certainly contributes to the assembly of the Mg-chelatase complex (Kobayashi et al., 2008).

GUN4 is a positive regulator of Mg-chelatase and is involved in plastidic retrograde signaling (Larkin et al., 2003; Davison et al., 2005). Moreover, it is a key regulator of Chl biosynthesis acting on the posttranslational level (Peter and Grimm, 2009). Together with protoporphyrin IX, it was suggested to promote interactions between CHLH and chloroplast membranes (Adhikari et al., 2009). Changes in the activity of the Mg-branch under different light conditions is probably regulated by GUN4 phosphorylation (Richter et al., 2016).

From Mg-protoporphyrin IX to Protochlorophyllide

Mg-protoporphyrin is converted to 3,8 vinyl-Pchlide (divinyl-Pchlide or DV-Pchlide) in two successive reactions. The first is the methylation of Mg-protoporphyrin IX catalyzed by Mg-protoporphyrin IX methyltransferase (EC 2.1.1.11). The second is the formation of the isocyclic ring E catalyzed by different cyclases in oxygenic and anoxygenic phototrophs, according to different mechanisms (Chen et al., 2017). In eukaryotic oxygenic phototrophs that include angiosperms, mostly discussed in this work, the formation of the E ring is catalyzed by Mg-protoporphyrin IX monomethyl ester (oxidative) cyclase (EC 1.14.13.81). This is an oxygen-dependent enzyme, composed of multiple subunits (Chereskin et al., 1982; Wong and Castelfranco, 1984, 1985; Rzeznicka et al., 2005). To keep the enzymatic activity, Mg-protoporphyrin IX monomethylester cyclase (CHL27/CRD1) (Tottey et al., 2003) requires the presence of an auxiliary factor YCF54, which is the hypothetical chloroplast open reading frame 54 (Albus et al., 2012; Chen and Hunter, 2020). Among various factors, YCF54 interacts with ferredoxin-NADPH reductase (FNR1), which may deliver electrons from the photosynthetic electron transport chain to the cyclase (Herbst et al., 2018). However, the exact mechanism of the formation of the isocyclic E ring is still not fully elucidated.

A specific reductase, 8-vinyl reductase (EC 1.3.1.75 also called divinyl reductase, i.e., DVR), can reduce one of the two vinyl groups in DV-Pchlide converting DV-Pchlide to 3-vinyl Pchlide (monovinyl-Pchlide or MV-Pchlide), a reaction observed in etiolated seedlings (Belanger and Rebeiz, 1979, 1980;

Abbreviations: Chl, chlorophyll; Chlide, chlorophyllide; DPOR, dark-operative NADPH:Pchlide oxidoreductase enzyme; DGDG, digalactosyldiacylglycerol; DV-Pchlide, divinyl-Pchlide (3;8 vinyl-Pchlide); DVR, divinyl reductase; FNR1, ferredoxin-NADPH reductase 1; GG-Chlide, geranylgeranyl chlorophyllide; LPOR, light-dependent NADPH:protochlorophyllide oxidoreductase; MEP, 2-methylerythritol-4-phosphate pathway; MGDG, monogalactosyldiacylglycerol; MV-Pchlide, protochlorophyllide; Pchlide, protochlorophyllide; PG, phosphatidylglycerol; PLB, prolamellar body; PTs, prothylakoids; SQDG, sulfoquinovosyldiacylglycerol.

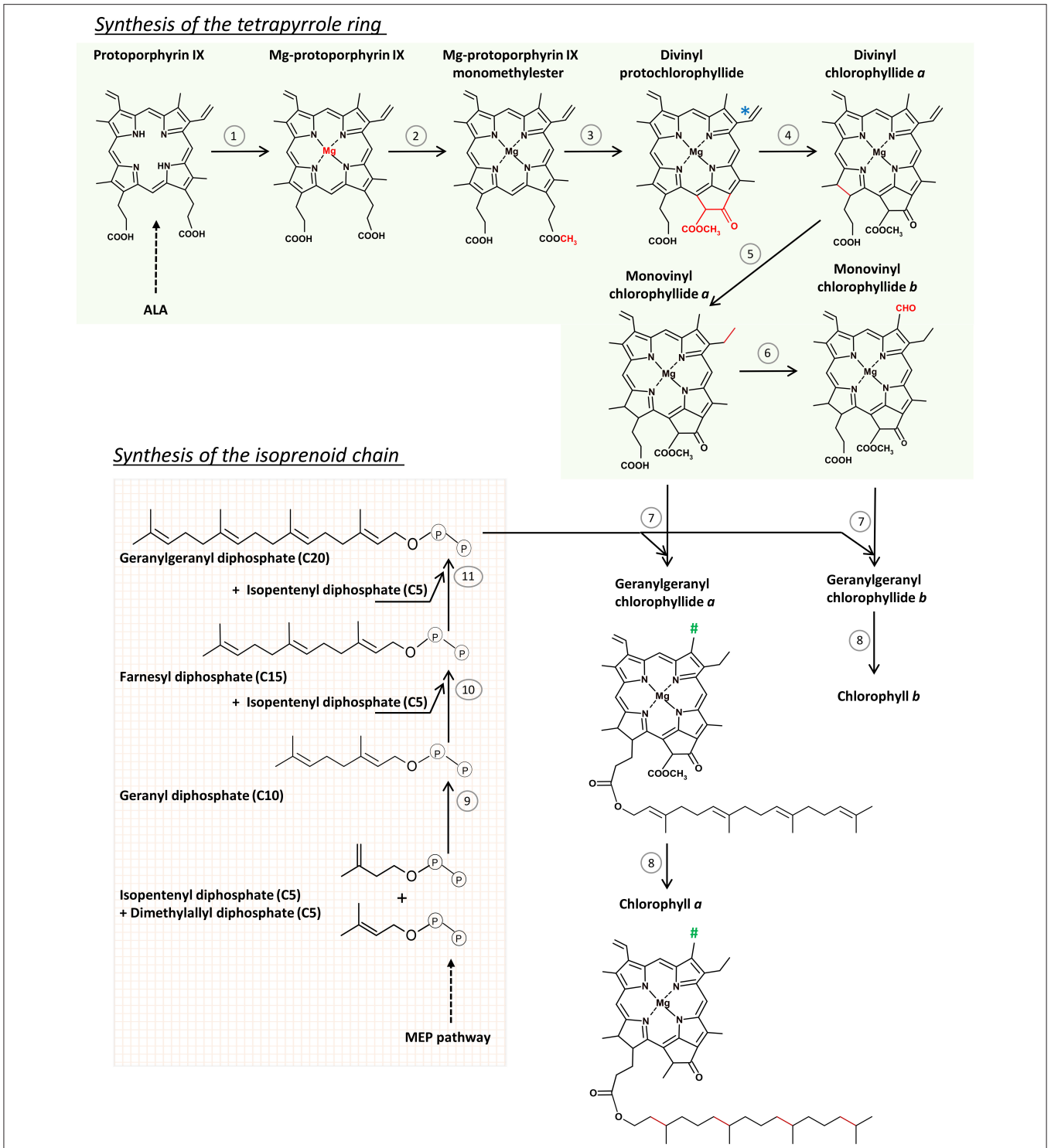

FIGURE 1 | The scheme of chlorophyll (Chl) biosynthesis in angiosperms. Reactions of the tetrapyrrole ring formation route (1–6) are catalyzed by: (1) Mg-chelatase, (2) protoporphyrin IX methyltransferase, (3) Mg protoporphyrin IX monomethyl ester (oxidative) cyclase, (4) light-dependent NADPH:protochlorophyllide oxidoreductase, (5) divinyl reductase, (6) chlorophyllide oxygenase, (7) chlorophyll synthase, (8) geranylgeranyl reductase. (*) Divinyl reductase (5) can also convert the indicated divinyl group to a monovinyl group in protochlorophyllide molecule. (#) Methyl group in Chl *a*, and formyl group in Chl *b*. Reactions of the isoprenoid chain formation (9–11) are catalyzed by geranyl diphosphate and geranylgeranyl diphosphate synthases. See text for further explanations.

Shioi and Takamiya, 1992) but also during the night phases of photoperiodic growth (Carey and Rebeiz, 1985; Carey et al., 1985; Tripathy and Rebeiz, 1988). This observation contributed to the categorization of plants depending on whether they accumulate predominantly DV-Pchlide or MV-Pchlide during daytime or nights of photoperiodic growth (Ioannides et al., 1994; Mageed et al., 1997). In particular, Arabidopsis (DDV-LDV, i.e., a dark divinyl-light divinyl plant) accumulates mainly DV-Pchlide independently on light conditions whereas wheat and rice accumulate MV-Pchlide at night and mostly DV-Pchlide at daytime and are thus considered as DMV-LDV (i.e., dark monovinyl-light divinyl) plants. Further analysis of the accumulation of other MV- and DV- tetrapyrrole intermediates and their interconversion in various plant species led to a multibranched pathway, including parallel MV and DV paths of Chl biosynthesis interconnected by DVR (Tripathy and Rebeiz, 1986; Rebeiz et al., 1999; Wang et al., 2013). Plant DVR is a NADPH-dependent enzyme (Parham and Rebeiz, 1992; Whyte and Griffiths, 1993) and shows a broad substrate specificity (Wang et al., 2013), however, it is the most active for DV-Chlide as substrate (Parham and Rebeiz, 1992; Nagata et al., 2007; Wang et al., 2013). A putative transmembrane α helix has been identified near the C terminus of DVR (Nakanishi et al., 2005; Wang et al., 2010).

Both MV-Pchlide and DV-Pchlide are accepted as substrates by the enzymes catalyzing the subsequent reactions leading finally to the formation of the Chl *a* molecule (Knaust et al., 1993; Nagata et al., 2007). What is more, most literature data dealing with the last steps of Chl biosynthesis in angiosperms did not determine the exact nature of Pchlide (e.g., MV- or DV-Pchlide) in their samples. Therefore, and for simplicity, we decided to refer to the pigment below as Pchlide. Pchlide is a key intermediate of Chl biosynthesis in angiosperms. It is a porphyrin type compound, capable of light absorption. However, its Q absorption bands are strongly blue-shifted compared to that of Chls (Fiedor et al., 2019). The photophysical properties of Pchlide in various model systems and in plastids are thoroughly discussed in section LPOR—An Enzyme Operating in Lipid Environment.

Light-Triggered Reduction of Protochlorophyllide to Chlorophyllide

DPOR (EC 1.3.7.7) is an ancestral but oxygen-sensitive enzyme catalyzing Pchlide reduction. According to a widely accepted long-held hypothesis, LPOR (EC 1.3.1.33) emerged as an evolutionary response to the increasing level of atmospheric oxygen (Fujita, 1996; Schoefs and Franck, 2003; Yamazaki et al., 2006; Reinbothe et al., 2010) caused by the emergence of oxygenic photosynthesis around 2.4 billion years ago (Suzuki and Bauer, 1995), and occurs only in oxygenic phototrophs. However, LPOR was discovered a few years ago in the aerobic anoxygenic phototrophic α-proteobacterium *Dinoroseobacter shibae* (Kaschner et al., 2014), and in other anoxygenic organisms (Chernomor et al., 2020), probably as a result of horizontal gene transfer from cyanobacteria. Further investigations are required to elucidate the evolutionary origin and distribution of LPOR. In angiosperms, the *LPOR* gene was duplicated several times, leading to the formation of LPOR isoforms in several species denoted as LPOR-A, LPOR-B, and LPOR-C (Gabruk and Mysliwa-Kurdziel, 2020) (discussed in detail in section Biochemical Characterization of LPOR).

In angiosperms, the reduction of Pchlide to Chlide is catalyzed by LPOR (for review see Scrutton et al., 2012; Gabruk and Mysliwa-Kurdziel, 2015). The photocatalytic reaction catalyzed by LPOR is the reduction of one of the conjugated double bonds in the porphyrin ring of Pchlide, thus converting it to a chlorine. The photophysical properties of the product, Chlide, are only slightly different from those of Chl (Fiedor et al., 2003, 2008). LPOR activity is induced by light and is fully inhibited in the dark. No chemical LPOR inhibitors are known. The biochemical characterization of LPOR and the reaction mechanism of the photoreduction are discussed in section LPOR—An Enzyme Operating in Lipid Environment.

From Chlorophyllide to Chlorophyll

The esterification of Chlide with an isoprenyl alcohol leads to the formation of Chl *a* molecule. Below, we'll first review the formation of the phytol chain, and then the esterification reaction itself.

Biosynthesis of the Isoprenyl Side Chain

The isoprenyl side chain of Chl is a phytyl moiety. Phytol is a 20-carbon (C20) alcohol, which is structurally related to geranylgeraniol, however, it is more saturated. The prenyl backbone of geranylgeraniol is synthesized in chloroplasts *via* the 2-methylerythritol-4-phosphate (MEP) pathway (Lichtenthaler et al., 1997), one of two pathways of isoprenoid biosynthesis present in plant cells. The characterization and detailed description of these pathways is beyond the scope of this paper and can be found in Rodriguez-Concepcion (2010), Vranová et al. (2013), Rodríguez-Concepción and Boronat (2015), and Gutbrod et al. (2019).

Geranylgeranyl diphosphate (C20) is formed from two prenyl diphosphate precursors: isopentenyl diphosphate (C5) and dimethylallyl diphosphate (C5), both produced in the MEP pathway, in sequential condensation reactions. Their condensation leads to geranyl diphosphate (C10). The condensation of geranyl diphosphate (C10) with an isopentenyl diphosphate (C5) molecule results in the formation of farnesyl diphosphate (C15), which can further condensate with another isopentenyl diphosphate (C5) molecule to form geranylgeranyl diphosphate (C20). These condensation reactions are catalyzed by the geranyl diphosphate and geranylgeranyl diphosphate synthases, EC 2.5.1.10 and EC 2.5.1.29, respectively, which are enzymes belonging to the family of isopentenyl-diphosphate synthases (prenyltransferases) (Gutbrod et al., 2019). Geranylgeranyl diphosphate (C20) is an important intermediate not only for Chl synthesis, but also for other biochemical pathways including the biosynthesis of carotenoids, prenyllipids and plant hormones (gibberellins). However, regulatory mechanisms of geranylgeranyl diphosphate consumption among these biosynthesis pathways are not yet fully understood.

Interestingly, isopentenyl diphosphate or farnesyl diphosphate formed in the cytosol by the alternative pathway of isoprenoid biosynthesis, the so-called mevalonate pathway (MVA), can contribute to the synthesis of chloroplast isoprenoids (Nagata et al., 2002; Bick and Lange, 2003; Opitz et al., 2014; Manzano et al., 2016; Pellaud and Saffrané, 2017). However, isoprenoids derived from the mevalonate pathway cannot substitute for the deficiency in the flux through the MEP pathway (Nagata et al., 2002). Geranylgeranyl diphosphate deficiency leads to overaccumulation of Chlide, which can be a source of photooxidative stress (Kim et al., 2013).

The plastid geranylgeranyl diphosphate synthase was first purified from *Capsicum* chromoplasts (Dogbo and Camara, 1987) and *Sinapsis alba* etioplasts (Laferrière and Beyer, 1991), and then cloned and further characterized (Kuntz et al., 1992). Multiple geranylgeranyl diphosphate synthase families were characterized in Arabidopsis (Beck et al., 2013) and some other plants (Wang and Dixon, 2009; Zhou et al., 2017; Wang et al., 2019). They show specific subcellular localizations and different expression patterns, which may be important for geranylgeranyl diphosphate synthesis depending on metabolic pathways, developmental stages, or specific tissues. Seven of 10 synthases found in Arabidopsis were localized to plastids. One of them (GGPPS11) mainly participates in the biosynthesis of plastid isoprenoids including Chls (Beck et al., 2013; Ruiz-Sola et al., 2016). GGPPS11 operates as a dimer with another geranylgeranyl diphosphate synthase, GGPPS12, which lacks motifs required for prenyl binding and is catalytically inactive (Beck et al., 2013; Ruiz-Sola et al., 2016). Binding of this accompanying protein regulates the enzyme specificity between the production of geranylgeranyl diphosphate and geranyl diphosphate. The accompanying protein in rice, which is called a recruiting molecule, controls the dimerization of geranylgeranyl diphosphate synthase and enhances its catalytic activity (Zhou et al., 2017). Moreover, it determines the allocation of the enzyme from the stroma to the thylakoid membranes, which is a way to control the flux of geranylgeranyl diphosphate toward Chl biosynthesis.

It is noteworthy to mention that independently from Chl biosynthesis, peculiar plastid inner membranes can be observed in plastids accumulating isoprenoids (Turner et al., 2000, 2012; reviewed e.g., in Solymosi and Schoefs, 2010) which indicates some direct or indirect interaction of these lipophilic molecules with the biomembranes.

Esterification of Chlide

Chlide is esterified with geranylgeranyl diphosphate to form geranylgeranyl Chlide (GG-Chlide). This reaction is catalyzed by chlorophyll synthase (EC 2.5.1.62) (Rüdiger et al., 1980). Pchlide is not accepted as the substrate for this enzyme (Griffiths, 1974; Rüdiger et al., 1980). However, in the two subsequent reactions, i.e., the photoreduction of Pchlide and the esterification of Chlide, the same part of the tetrapyrrole molecule is modified. Pchlide and Chlide are thus bound to the catalytic site of the respective enzymes, i.e., LPOR and chlorophyll synthase, in the same orientations (Helfrich et al., 1994, 1996; Rüdiger et al., 2005). Chlorophyll synthase binds the isoprenoid chain before binding of the second substrate, Chlide (Schmid et al., 2002).

Finally, the geranylgeranyl reductase (EC 1.3.1.83) reduces subsequently three double bonds in geranylgeranyl moiety of GG-Chlide and converts it to phytyl moiety, yielding this way Chl *a*. Observations that mainly GG-Chlide was detected shortly after illumination of etiolated seedlings (Schoch, 1978) whereas Chl *a,* having a phytyl moiety, was found in green barley seedlings (Soll et al., 1983) opened up a long-lasting discussion on the order of the esterification and reduction steps in plants. However, Schoefs and Bertrand (Schoefs and Bertrand, 2000) proved that the transformation of Chlide to Chl in developing seedlings is a four-steps process, which includes the successive formation of GG-Chlide, dihydrogeranylgeranyl Chlide and tetrahydrogeranylgeranyl Chlide as Chl *a* biosynthesis intermediates. The reduction of geranylgeranyl moiety of GG-Chlide was confirmed in tobacco cell cultures (Benz et al., 1984). Moreover, the preferential use of geranylgeranyl diphosphate than phytyl diphosphate by recombined *Arabidopsis thaliana* chlorophyll synthase was observed (Gaubier et al., 1995; Oster and Rüdiger, 1997). Chlides *a* and *b* were esterified at the same rate by recombinant chlorophyll synthase (Oster and Rüdiger, 1997).

In plastids, the same geranylgeranyl reductase may operate in different pathways of hydrogenation of geranylgeranyl moiety. The hydrogenation of GG-Chlide for Chl biosynthesis occurs in thylakoids whereas the reduction of geranylgeranyl diphosphate to phytyl diphosphate during the synthesis of tocopherols takes place in the envelopes (Soll et al., 1983; Keller et al., 1998). In etiolated seedlings the hydrogenation process is slowed down making it easier to observe than in green leaves. The activity of geranylgeranyl reductase is more affected by low temperature (273 K) than that of chlorophyll synthase (Schoefs and Bertrand, 2000). Cycloheximide is an inhibitor of the hydrogenation of geranylgeranyl to phytyl moiety in the irradiated etiolated seedlings, whereas it has no effect on Chlide esterification with geranylgeranyol (Rassadina et al., 2004).

Chlorophyll *b* Formation

Chl *b* is formed from Chlide in two reactions (**Figure 1**). The first is the two-step oxygenation of the side methyl group at the C7 in the ring B to a formyl group using molecular oxygen, which is catalyzed by chlorophyllide a oxygenase (CAO; EC 1.14.13.122) (Tanaka et al., 1998; for review see Rüdiger, 2002, 2006; Tanaka and Tanaka, 2007). Chlide *a* was shown to be the sole substrate for CAO activity, because neither Chl *a* nor Pchlide were accepted as the substrates of CAO *in vitro* (Oster et al., 2000; Rüdiger, 2002). The CAO is a membrane-bound protein, localized in thylakoid and envelope membranes (Eggink et al., 2004). The biosynthesis of Chl *b* plays an important regulatory role in the assembly and stabilization of light harvesting antennae (LHC) and as a consequence in granum stacking, which rely on the presence of this pigment (Espineda et al., 1999; Tanaka et al., 2001; Harper et al., 2004; Reinbothe et al., 2006). Judging from the low activity of the recombinant CAO *in vitro* it was suggested that additional accessory proteins might be required to reach

the optimal catalytic oxygenase activity (Eggink et al., 2004), but these are yet unidentified.

Esterification of the D ring of Chlide, a reaction which is described in section Esterification of Chlide for Chl *a* formation, converts Chlide *b* into Chl *b*. The Chl *a/b* ratio in plants is regulated using the reversible conversion of Chlide *a*—Chl *b*—Chl(ide) *a*, which is known as "the chlorophyll cycle" (for a review see Rüdiger, 2002; Tanaka and Tanaka, 2019). Keeping the optimal level of Chl *a/b* ratio which correlates with the amount of the LHC complexes and supramolecular structure of photosynthetic complexes enables plant adaptation to changing environmental conditions (for a review see Tanaka and Tanaka, 2011; Voitsekhovskaja and Tyutereva, 2015).

Late Chlorophyll Biosynthesis Is Associated With Plastid Membranes

The Mg-branch occurs at the plastid membranes and some enzymes are organized into macromolecular complexes. For example, LIL3, a protein belonging to LHC family, plays an essential role in the organization of complexes involved in Chl biosynthesis and in the delivery of Chls to photosynthetic complexes. By linking tetrapyrrole and terpenoid biosynthesis, LIL3 plays a critical role in the organization of later steps in Chl biosynthesis (Hey et al., 2017). Studies on the Arabidopsis mutant lacking LIL3 revealed the importance of this protein for Chl biosynthesis and in the stabilization of geranylgeranyl reductase (Tanaka et al., 2010). A direct interaction of geranylgeranyl reductase with LIL3 was demonstrated using a split ubiquitin assay, bimolecular fluorescence complementation as well as combined blue-native and SDS polyacrylamide gel electrophoresis (Tanaka et al., 2010). LIL3 was also shown to stabilize LPOR, and the direct LIL3-LPOR interaction was also confirmed using multiple analysis of protein-protein interactions (Hey et al., 2017). In addition to that, fluorescence *in vitro* analysis showed high binding affinity of LIL3 to Pchlide—the substrate of LPOR. However, no interactions with chlorophyll synthase were reported in this study. Similar complexes were detected in etio-chloroplasts and etioplasts of barley, using native gel electrophoresis with autofluorescence detection and mass spectrometry (Reisinger et al., 2008; Mork-Jansson et al., 2015). In these experiments, LIL3 formed complexes with LPOR, geranylgeranyl reductase and chlorophyll synthase. However, using split ubiquitin assay, the interaction between LIL3, LPOR and chlorophyll synthase was demonstrated, whereas no interaction with gerenylgeranyl reductase was proven (Mork-Jansson et al., 2015). Studies performed on thylakoids of rice (Zhou et al., 2017) revealed an additional protein called geranylgeranyl reductase recruiting protein, regulating the binding of geranylgeranyl reductase in the complexes clustered around LIL3.

Membrane complexes composed of Mg-protoporphyrin IX monomethylester cyclase, CHL27, LPOR (i.e., LPOR-B, LPOR-C), geranylgeranyl reductase and the FLU protein were identified in isolated thylakoids of Arabidopsis (Kauss et al., 2012). FLU is a negative regulator of Chl biosynthesis operating at the step of delta aminolevulinic acid (ALA) formation (Meskauskiene et al., 2001; Meskauskiene and Apel, 2002). In the absence of light, glutamyl-tRNA reductase is bound to FLU in these complexes and ALA formation is inhibited (Zhang et al., 2015). Formation of complexes of FLU with enzymes catalyzing the final steps of Chl biosynthesis was demonstrated using native electrophoresis, immunoprecipitation and mass spectrometry (Kauss et al., 2012).

It was also shown that, Mg-protoporphyrin IX monomethylester cyclase forms complexes with YCF54 and FNR1. However, YCF54 is probably a scaffold protein for a multi-subunit enzymatic complex, including other enzymes of late Chl biosynthesis, namely LPOR as well as the DVR and geranylgeranyl reductases (Kong et al., 2016; Herbst et al., 2018). Formation of such multi-subunit complexes favors the flow of intermediates during the Chl synthesis in light as well as the inhibition of the process in the dark. Taking into account that FNR1 provides the electrons for the cyclase activity, it is hypothesized that it might also deliver electrons for LPOR and DVR in the multi-enzymatic complex (Herbst et al., 2018, 2019). Nevertheless, the direct interaction of YCF54-FNR1 with LPOR and DVR has not yet been shown until now. Moreover, the question about the regulation of the electron flow in thylakoids remains open. Finally, it has not been elucidated how the late Chl synthesis is orchestrated at the beginning of angiosperm greening.

Another question which also remains open till date concerns the coexistence of CHL27-YCF54-FLU-LPOR-geranylgeranyl reductase complex with the LIL3-LPOR-geranylgeranyl reductase-geranylgeranyl diphosphate synthase-chlorophyll synthase complex in thylakoid membranes. LPOR and geranylgeranyl reductase were found in both type of complexes in thylakoid membranes. However, it remains unknown whether these complexes are somehow associated or stay separated. Recent analyses revealed that in Arabidopsis LPOR, curvature Thy1 (CURT1), the Mg^{2+}-chelatase subunit 1 (CHLI) and Mg^{2+} protoporphyrin IX methyl transferase (CHLM) are also located to the granum margins (Wang et al., 2020). Further research is required to elucidate the exact localization, organization and regulation of the last steps of Chl biosynthesis. Answering these questions is important for the understanding of the regulatory mechanisms of the delivery of prenyl intermediates for Chl and tocopherol synthesis (Gutbrod et al., 2019).

Dual Localization of the Mg-branch in Plastids and the Role of Lipids in It

Dual localization of enzymes involved in the Mg-branch in both chloroplast envelope and plastid inner membranes were documented based on biochemical studies (Joyard et al., 1990; Block et al., 2002; Tottey et al., 2003; Eggink et al., 2004; Tanaka and Tanaka, 2007), and later confirmed by proteomics (for review see Joyard et al., 2009; Bruley et al., 2012; Salvi et al., 2018). Dual localization was suggested to supply Chl to different Chl-binding proteins (PS core complexes and LHC) (Tottey et al., 2003). Additional research is required to elucidate the functional meaning of the dual localization and its relation to protein import mechanisms of plastids. Some yet unsolved problems that need to be mentioned: (i) interactions among enzymes and regulatory

factors, (ii) structure and functioning of enzyme complexes, and (iii) their interaction with lipid membrane components, as well as (iv) the MV and DV heterogeneity of the biosynthesis route.

An interesting research area is the understanding of the regulatory networks connecting the biosynthesis of Chls, of protein components of photosynthetic complexes as well as lipids with the formation of the thylakoid membranes typical for chloroplasts. These processes need to be orchestrated to enable the proper assembly of the photosynthetic apparatus and to avoid the overaccumulation of unbound tetrapyrroles which may lead among others to photooxidative damage (Erdei et al., 2005; Hideg et al., 2010; Kim et al., 2013). It is nowadays known that the expression of Mg-chelatase and Mg-protoporphyrin IX monomethyl ester cyclase is linked to the synthesis of galactolipids (Fujii et al., 2014; Kobayashi et al., 2014; Kobayashi, 2016, 2018; Kobayashi and Masuda, 2016). Coordination of Chl and galactolipid biosyntheses goes through cytokinin and light signaling pathways (Kobayashi et al., 2014), however, further studies are needed to understand the molecular background of this regulation.

It has been shown that in etioplasts, the Mg-branch is sensitive to the membrane lipid environment, namely the MGDG and DGDG levels. Deficiency of any of these galactolipids in *A. thaliana* mutants resulted in overaccumulation of Mg-protoporphyrin IX pointing to the impairment of the following enzymes in the biosynthetic pathway (**Figure 1**) and leading to the accumulation of Pchlide intermediates and low Pchlide content (Fujii et al., 2017, 2018). On the contrary, the Mg-branch was reconstituted in *E. coli* cells from recombined *Synechocystis* proteins: Mg-chelatase, Mg-protoporphyrin IX methyltransferase, Mg-protoporphyrin IX monomethyl ester cyclase, LPOR, DVR, Chl synthase, and geranylgeranyl reductase without galactolipids (Chen et al., 2018). Thus, galactolipids rather enhance the activity of the enzymes, however, the regulatory mechanisms are yet unknown. Functioning of Mg-protoporphyrin IX methyltransferase, Mg-protoporphyrin IX monomethyl ester cyclase in barley etioplasts was also affected in the absence of carotenoids (La Rocca et al., 2007).

LPOR—AN ENZYME OPERATING IN LIPID ENVIRONMENT

Among all reaction steps of Chl biosynthesis, the photoreduction of Pchlide is probably the most studied. This may be a result of several factors including (i) the unique catalytic activity of the enzyme involving an ultrafast light-activated photochemical reaction interesting from the biophysical and biochemical points of view, (ii) its important role in the regulation of tetrapyrrole biosynthesis, (iii) its association with arrested chloroplast differentiation and the formation of peculiar etioplast inner membranes, and (iv) the fact that dark-grown angiosperm seedlings represent a convenient plant material to study the last steps of the biosynthetic pathway in a synchronized way after illumination. Spectroscopy is also a useful tool to study this topic because there is a 30–40 nm difference in the spectral properties of the substrate, Pchlide (a porphyrin containing 11 double bonds in the tetrapyrrole ring) and the product, Chlide (a chlorine with 10 double bonds). This way and due to the high sensitivity of the delocalized electron system of the porphyrin ring to alterations in the molecular environment of the pigment, the reaction as well as the different populations of the pigments can be easily studied and characterized by relatively simple steady-state spectroscopic methods, which is summarized in the section Spectroscopic Properties of Pchlide *in vivo*. Pigments involved in similar molecular interactions and located in similar molecular micro-environments within the plastids exhibit similar spectral properties and thus represent a subpopulation of the entire pigment pool denoted as a pigment "form." Pigment forms are often referred to by using the wavelength of their spectral maxima, but most of them have been also characterized from the biochemical and physiological points of view.

However, it is important to mention, that in green leaves containing significant amounts of Chls in the form of the various Chl-protein complexes of the photosynthetic apparatus, the fluorescence emission signal of Chl hinders the detection of its precursors such as e.g., Pchlide, which are present in much lower quantities (i.e., three order of magnitude lower amounts). Similarly, in green plants, the level of enzymes required for the steady-state Chl synthesis that produces Chl molecules to replace the pigments damaged during photosynthesis or stress conditions is very low and is hard to detect with classical biochemical or spectroscopic methods. Therefore, most studies related to the last steps of Chl biosynthesis have been performed on dark-germinated angiosperm seedlings in which the light-dependent LPOR enzyme is accumulating along with its substrate Pchlide, while Chl is absent.

When deprived from light during the early stages of their development, proplastids differentiate into a peculiar plastid type called etioplast in the photosynthetic tissues of dark-grown plants. The inner membranes of etioplasts consist of flat, sac-like membranes called prothylakoids, i.e., lipid bilayers encircling an inner aqueous phase called lumen, and a unique non-lamellar, but cubic phase inner membrane structure, the prolamellar body (PLB). Due to the inhibition of other light-signaling pathways [e.g., those involving phytochrome and cryptochrome (Sineshchekov and Belyaeva, 2019)] in darkness, the development of such dark-grown seedlings is also peculiar and is called skotomorphogenesis. When etiolated plants get illuminated, photomorphogenesis proceeds in them in parallel with the light-induced conversion of Pchlide to Chlide, resulting in the etioplast-to-chloroplast conversion which includes major reorganization of the plastid inner membranes, and active synthesis of the components of the photosynthetic apparatus (reviewed in Solymosi and Aronsson, 2013; Armarego-Marriott et al., 2020; Hernández-Verdeja et al., 2020).

Data about LPOR and its native structure and activity are reviewed below with emphasis on the lipid-protein interactions in them.

Biochemical Characterization of LPOR

LPOR belongs to the short-chain dehydrogenase/reductase (SDR) protein superfamily (Yang and Cheng, 2004). It is a nuclear encoded protein which is then post-translationally imported to

plastids (Aronsson et al., 2003b; Kim et al., 2005). Based on its amino acid sequence it is considered as a soluble and globular protein with surprisingly high contents of basic and hydrophobic amino acids (Schoefs and Franck, 2003; Masuda and Takamiya, 2004; Heyes and Hunter, 2005; Gabruk and Mysliwa-Kurdziel, 2015). Circular dichroism studies and bioinformatic tools predicted its secondary and tertiary structure (Schulz et al., 1989; Darrah et al., 1990; Birve et al., 1996; Dahlin et al., 1999; Townley et al., 2001; Buhr et al., 2008; Gabruk et al., 2012, 2015; Menon et al., 2016; Gholami et al., 2018), but hydropathy plots did not identify potential hydrophobic transmembrane segments in it (Benli et al., 1991; Spano et al., 1992). This is surprising as 98% of LPOR present in etioplasts has been localized to PLB membranes (Ryberg and Sundqvist, 1982a; Ikeuchi and Murakami, 1983), and it represents the major protein of isolated PLB fractions (Ryberg and Sundqvist, 1982a; Selstam and Sandelius, 1984; von Zychlinski et al., 2005; Blomqvist et al., 2008; Kanervo et al., 2008). Several *in vitro* and *in vivo* experiments involving washing and directed mutagenesis tried to identify the membrane association mechanism of LPOR. It has been shown that NADPH and ATP are required for its proper binding to plastid inner membranes such as PLBs, PTs and thylakoids (Dahlin et al., 1995; Engdahl et al., 2001). Washing experiments with various salts, detergents (Grevby et al., 1989; Selstam and Widell-Wigge, 1989) and proteases (Lütz and Tönissen, 1984; Dahlin et al., 1995; Engdahl et al., 2001) also revealed that LPOR binds more strongly to etioplast inner membranes (PLBs and PTs) than to thylakoid membranes. In chloroplasts, LPOR was predominantly found in the granum margins (Wang et al., 2020) which are, similarly to PLBs, also highly curved membranes with special lipid composition and special membrane organization. Based on its amino acid sequence LPOR is not an integral transmembrane protein, but because of its strong attachment to PLBs and PTs due to which it is difficult to solubilize it, it is probably not a peripheral membrane protein but an integral monotopic membrane protein which is permanently attached to one side of the plastid inner membrane. Using mutagenesis experiments, some amino acid residues (Cys) and the C-terminal have been shown to be involved in membrane association of LPOR (Dahlin et al., 1999; Aronsson et al., 2001), and recently a Chaperone-like Protein of POR1 (CPP1) has been identified which may be involved in anchoring LPOR to the PLBs (Lee et al., 2013b).

LPOR has a central β-sheet comprised of β-strands surrounded by α-helices, forming a typical dinucleotide binding Rossmann fold (Rossmann et al., 1974). The catalytic YxxxK and the NADPH-bounding G-rich (GxxxGxG) motifs are conservative (Wilks and Timko, 1995; Schoefs and Franck, 2003; Gabruk and Mysliwa-Kurdziel, 2020). LPOR crystal structure remained unknown for a long time; the structures of two cyanobacterial LPOR enzymes have been published only recently (Zhang et al., 2019; Dong et al., 2020). In general, both structures are compatible with the homology models, however, due to slightly different protocols there were some differences between these two works.

Most SDR proteins have tendency to form dimers and oligomers (Jörnvall et al., 1995), a property which was also found in LPOR macrocomplexes isolated from PLBs pre-treated with chemical cross-linkers (Wiktorsson et al., 1993), or isolated in fully photoactive native state from PLBs after mild solubilization and gel chromatography (Ouazzani Chahdi et al., 1998). Circular dichroism spectra (Mathis and Sauer, 1972; Böddi et al., 1989, 1990) and energy transfer studies (Kahn et al., 1970) also revealed that dimers or oligomers of the pigments are involved in the photoreduction of Pchlide. Cross-linking and subsequent mass spectrometric analysis of recombinant LPOR suggested that after substrate binding, structural changes occur in the LPOR oligomers which bring the catalytic motifs and the Pchlide molecules bound to the active site closer together (Gabruk et al., 2016). Similar observations were done in case of the analyses of cyanobacterial LPOR in which substrate binding induced oligomerization (Zhang et al., 2019) or monomers were observed in solution but homodimerization was observed during crystal formation (Dong et al., 2020). Experiments with recombinant pea LPOR also showed that it can form photoactive dimers in solution (Martin et al., 1997). A close distance between catalytic motifs brings the Pchlide molecules bound within the oligomers into close proximity, which enables energy transfer between them and also influences their spectral properties (Kahn et al., 1970). It has to be noted that the enzymatically active LPOR complexes have unique spectral and biochemical properties that are hardly reconstituted *in vitro*, especially in the absence of lipids (Gabruk et al., 2017). However, recent *in vitro* reconstitution studies successfully yielded crystal structures of oligomers: in case of cyanobacterial LPOR octamers were reported (Zhang et al., 2021) while in case of Arabidopsis LPOR helical structures associated with lipids were observed (Nguyen et al., 2021).

Data indicate the role of carotenoids [zeaxanthin and violaxanthin (Ouazzani Chahdi et al., 1998); neoxanthin and violaxanthin (Bykowski et al., 2020); the accumulation of poly-cis xanthophylls (Park et al., 2002; Cuttriss et al., 2007)] and lipids [MGDG (Aronsson et al., 2008; Fujii et al., 2017); and MGDG, PG, and SQDG (Gabruk et al., 2017; Nguyen et al., 2021)] in the formation of the photoactive enzyme complexes and the PLBs. Similarly, carotenoids (Denev et al., 2005) were suggested to be involved in the membrane association of LPOR. Lipid biosynthesis mutants had hindered LPOR activity, no LPOR oligomerization and abnormal PLB formation (Fujii et al., 2017, 2018, 2019b) which again outlines the strong relation between the LPOR oligomers, plastid lipids and inner membrane structures. Cryo electron microscopic investigations on *in vitro* reconstituted LPOR revealed that LPOR oligomers form helical filaments around lipid bilayer tubes and are inserted in the outer leaflet of the membranes (Nguyen et al., 2021).

LPOR gene probably appeared ∼1.36 billion years ago, and since then it underwent several duplication events and mutations (**Figure 2**) (Gabruk and Mysliwa-Kurdziel, 2020). As a result, few organisms contain only one LPOR gene and thus one isoform [e.g., pea (Spano et al., 1992) and cucumber (Fusada et al., 2000)], but several organisms contain at least two different isoforms (termed in general or historically as LPOR-A and LPOR-B—barley, rice, tobacco, and wheat, see later for references) or even more than that [e.g., Arabidopsis also has LPOR-C (Oosawa et al., 2000; reviewed in Gabruk and Mysliwa-Kurdziel, 2020)]. The isoforms share ∼75% sequence homology, but according

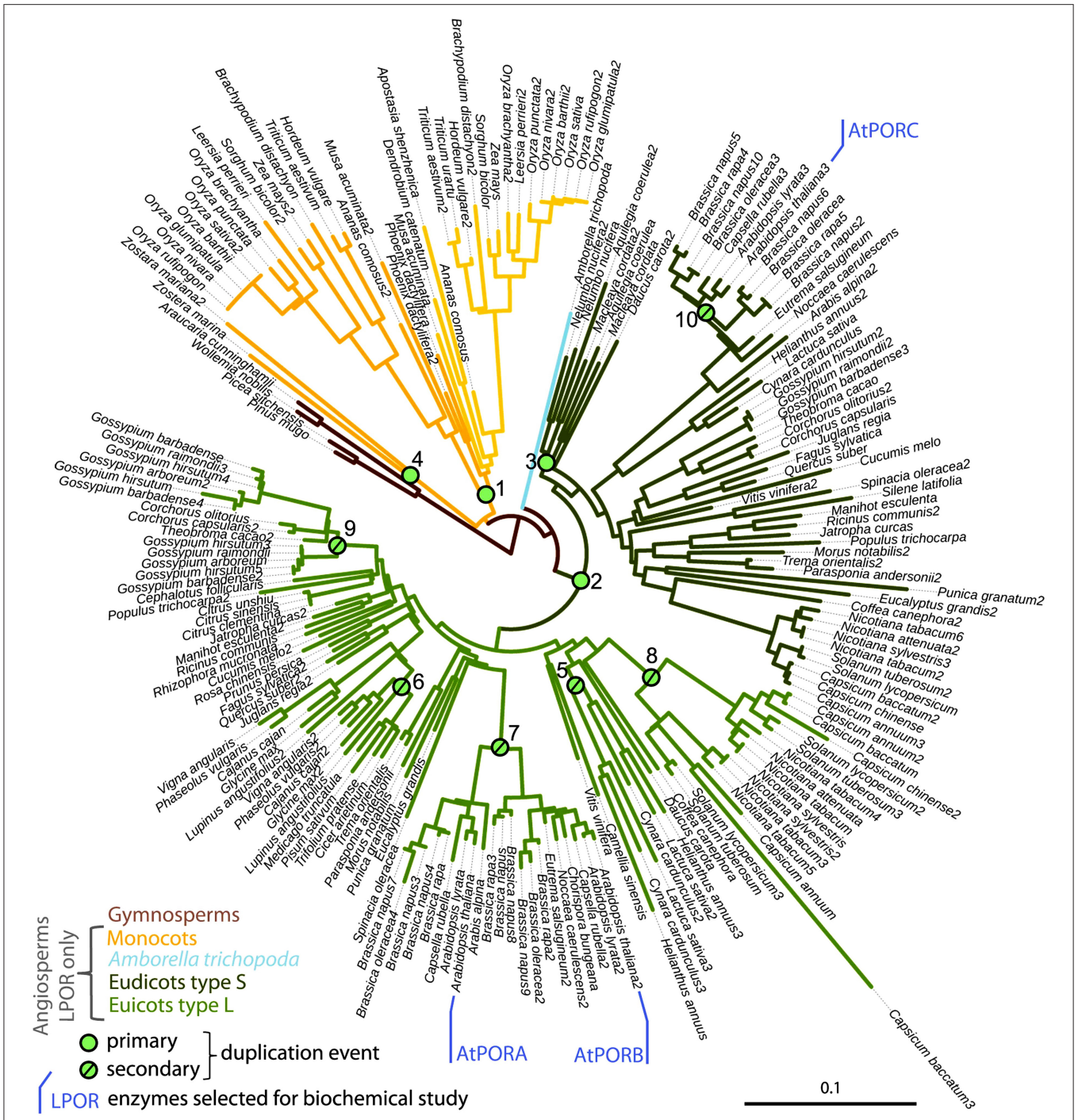

FIGURE 2 | Subtree of LPOR sequences from seed plants, with *Arabidopsis thaliana*'s isoforms AtPORA, AtPORB, and AtPORC being marked, and green dots indicating duplication events. Republished with permission of Portland Press Ltd., from The origin, evolution and diversification of multiple isoforms of light-dependent protochlorophyllide oxidoreductase (LPOR): Focus on angiosperms; Gabruk and Mysliwa-Kurdziel (2020), permission conveyed through Copyright Clearance Center, Inc.

to detailed functional analyses performed on a few species—barley (Holtorf et al., 1995; Garrone et al., 2015), Arabidopsis (Armstrong et al., 1995), tobacco (Masuda et al., 2002), wheat (Blomqvist et al., 2008), and rice (Kwon et al., 2017)—they have different expression patterns, substrate binding affinities, different plastid import mechanisms, different localization within the plastid membranes and different gene regulation patterns also depending on the developmental stage, temperature and

light conditions (reviewed in Solymosi and Schoefs, 2008, 2010; Gabruk and Mysliwa-Kurdziel, 2020). The transport of the different isoforms into the plastids is peculiar as it shows a large substrate, cell, tissue, and organ specificity (Aronsson et al., 2003b; Kim et al., 2005), the detailed discussion of which is beyond the scope of this review.

LPOR-A and LPOR-B are present in etiolated material, while LPOR-C is expressed typically in green tissues (Oosawa et al., 2000; Aronsson et al., 2003a; Masuda et al., 2003; reviewed in Solymosi and Schoefs, 2010; Gabruk and Mysliwa-Kurdziel, 2015). LPOR-A is transiently expressed during early phases of development when large amounts of pigments need to be synthesized quickly, while LPOR-B and LPOR-C are thought to be responsible for the bulk Chl synthesis of adult or green plants (Paddock et al., 2010, 2012). Arabidopsis double mutants lacking LPOR-B and -C were shown to be unable to produce enough Chl under light conditions, indicating the importance of these isoforms in the biogenesis of the photosynthetic apparatus and also its membrane structures such as grana (Frick et al., 2003). Some ancestral LPOR genes (like that of *Synechocystis*) may even have different catalytic activity as they operate in lipid independent manner in contrast with other LPORs analyzed so far in angiosperms or gymnosperms (Gabruk and Mysliwa-Kurdziel, 2020). Taking into account the biochemical characteristics of LPOR isoforms, their interaction with lipids, as well as their phylogenetic relationships, Gabruk and Mysliwa-Kurdziel (Gabruk and Mysliwa-Kurdziel, 2020) proposed a new classification of LPOR family consisting of three LPOR types (**Figure 2**). The first one includes bacterial LPORs, termed "Z-type," which are lipid-independent. Two other categories, termed L-type and S-type LPOR isoforms, are lipid-driven and present in angiosperms. L-type isoforms preferentially form complexes on the lipid membranes (like *A. thaliana* LPOR-A and LPOR-B), while the S-type ones (like *A. thaliana* LPOR-C) are active both with and without lipids. Further biochemical investigation is required to characterize the effect of lipids on LPOR isoforms from other angiosperm species.

Spectroscopic Properties of Pchlide *in vivo*

Native spectral properties of Pchlide complexes in etiolated seedlings, and the spectral changes following the light-induced reduction of photoactive Pchlide were described already in the 50's (**Figure 3**) (Shibata, 1957). Photoreduction of Pchlide can take place at 203 K and reversible intermediates can be observed already at 77 K (Sironval and Brouers, 1970; Heyes et al., 2002, 2003; Belyaeva and Litvin, 2011, 2014), therefore, low temperature (typically 77 K) spectroscopic methods are needed to characterize the native state of the pigments. The absorption and fluorescence emission spectra of etiolated leaves contain two major spectral bands, each attributed to a specific pigment form also characterized at the biochemical level. Since low temperature absorption spectroscopy is less frequently used, we will refer to 77 K fluorescence properties of the pigments in this work.

The short-wavelength band with fluorescence emission maximum at 633 nm represents a pool of monomeric Pchlide pigments bound either to the membrane surface or to a yet unidentified protein or to LPOR, but not in the active site of

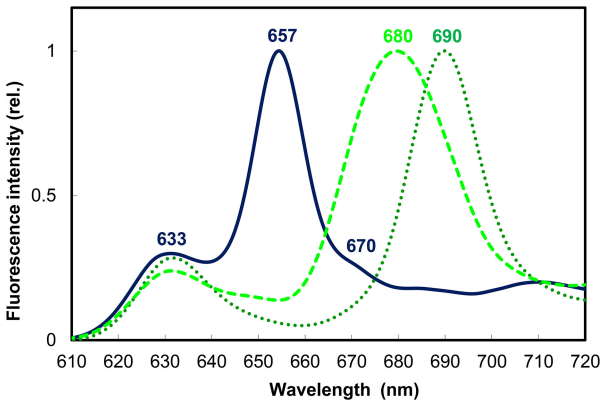

FIGURE 3 | Normalized 77 K fluorescence emission spectra of 10-day-old dark-grown wheat (*Triticum aestivum*) leaves before (solid line) and after illumination with white light of 100 μmol s^{-1} m^{-2} photon flux density for 10 s (dotted line) and a subsequent 15 min dark incubation to reach the end stage of Shibata shift (broken line). Experimental conditions were as in Solymosi et al. (2002) and Smeller et al. (2003).

the enzyme or not to the active form of the enzyme (**Figure 3**). These pigments were primarily localized to the prothylakoid membranes of the etioplasts (Ryberg and Sundqvist, 1982a,b) and to the cytosolic side of the outer envelope (Joyard et al., 1990). They are not directly photoconvertible with a flash, and thus belong to the so-called "non-photoactive" Pchlide pool.

Another major band located at 655–657 nm belongs to the so-called "photoactive" Pchlide pool, i.e., Pchlide pigments bound to the active site of LPOR macrodomains, which correspond to oligomers of Pchlide:LPOR:NADPH ternary complexes and are strongly associated with the PLB membranes of the etioplasts (**Figure 3**) (Ryberg and Sundqvist, 1982a,b). Gaussian deconvolution and further spectral and biochemical analyses of isolated and fractionated etioplast inner membranes revealed the presence of other minor Pchlide forms, like for instance smaller oligomers (probably dimers) of Pchlide:LPOR:NADPH ternary complexes with emission maximum at 644 nm which are also photoactive and are suggested to be located to the edge of the PLB membranes (Böddi et al., 1990, 1991, 1992). In addition, a non-photoactive Pchlide molecular subpopulation hypothetically located to the central regions of PLBs and having fluorescence emission maximum at around 670 nm was also described (**Figure 3**) (Böddi et al., 1990; Bykowski et al., 2020). Upon short (already μs-long) illumination the fluorescence emission of Pchlide:LPOR:NADPH oligomers with emission maxima at 655 nm disappears, and that of the freshly produced Chlide:LPOR:$NADP^+$ oligomers appears at 690 nm (**Figure 3**) (Böddi et al., 1990). After 10–15 min these oligomers and the pigments located in them undergo conformational changes and disaggregation as reflected by the blue shift of their emission maximum toward 680 nm, referred to as the so-called Shibata shift (**Figure 3**) (Shibata, 1957; Smeller et al., 2003; Solymosi et al., 2007a).

After the ultrafast transformation of the LPOR-bound, so-called "photoactive" Pchlide molecules into Chlide, and the

subsequent slower conformational changes and reorganizations of LPOR oligomers including the dissociation of Chlide, the so-called "non-photoactive" Pchlide molecules can bind to the active site of LPOR and can be then also directly transformed into Chlide in the same ultrafast photochemical reaction step.

Depending on the oxidation state of NADPH in the ternary complexes, and also on the studied species and organs (e.g., leaves or stems) other spectral forms have been also characterized but discussion about them, as well as about developmental and other species-specific factors determining the ratios of the different forms is beyond the scope of this review, and can be found e.g., in Schoefs (2005), Belyaeva and Litvin (2007), and Solymosi and Schoefs (2008, 2010). Below we summarize knowledge about the molecular background of Pchlide photoreduction and the membrane association of LPOR.

Understanding the Photophysical and Spectral Properties and Molecular Organization of Pchlide and LPOR

The major hurdle in understanding LPOR structure and its exact molecular interaction with PLB membranes is the fact that the *in vivo* crystal structure of photoactive LPOR complexes is not available so far. In addition, photoactive dimeric and oligomeric complexes of LPOR are also hard to be isolated and fully purified from etiolated tissues because they often undergo disaggregation and dissociation during these processes. As stated earlier, it is even harder to detect or isolate them from fully green plant material. On the other hand, photoactive LPOR is also hard to reconstitute *in vitro*. Below we'll review some key spectral and structural features of Pchlide and LPOR, and also discuss how various *in vitro* experiments and reconstitution studies helped us to better understand the native structure of LPOR.

Photophysical and Spectral Properties of Pchlide in Solvents and Lipid Model Systems

The key role of Pchlide in the light-triggered biosynthesis of Chl is related to its electronic properties. The Pchlide molecule captures sunlight and uses the absorbed energy to power the enzymatic reduction of its C17–C18 double bond. Data for understanding Pchlide photochemistry were collected from numerous studies of Pchlide in various model systems. It is now well-documented that Pchlide is an intrinsically reactive molecule. After light absorption, an electronically excited Pchlide molecule undergoes deexcitation using two parallel pathways (Dietzek et al., 2004, 2006b, 2009; Colindres-Rojas et al., 2011). The first one, called the reactive pathway, goes through an intramolecular charge-transfer state (S_{ICT}), which is non-fluorescent. The other, called the non-reactive pathway, goes through the lowest excited singlet state (S_1), which then decays *via* fluorescence or by intersystem crossing to the long-lived Pchlide triplet state. Charge separation across Pchlide molecule in the S_{ICT} state depends on solvent polarity and is more stable in polar solvents (Dietzek et al., 2006a, 2010). A carbonyl group (C13) in the Pchlide isopentanone ring is of special importance for this charge separation (Sytina et al., 2010; Heyes et al., 2017), and the formation of the S_{ICT} state is important for Pchlide photocatalysis (Dietzek et al., 2006b, 2010; Heyes et al., 2015).

Fluorescence emission spectra of Pchlide in organic solvents have the maximum between 626 and 641.5 nm (Mysliwa-Kurdziel et al., 2004). The photophysical properties of Pchlide S_1 state only weakly depend on non-specific solvation, as revealed from the small Stokes shifts (between 50 and 300 cm^{-1}) observed in organic solvents (Mysliwa-Kurdziel et al., 2004). Specific solvation in protic (methanol, ethanol) and coordinating solvents (pyridine) enlarges the Stokes shift due to the lowering of the S_1 state energy, and shortens the fluorescence lifetime. The site-specific solvation in Pchlide excited state *via* hydrogen bonding was confirmed experimentally (Mysliwa-Kurdziel et al., 2004; Sytina et al., 2010) and by theoretical calculation (Zhao and Han, 2008). DV-Pchlide has slightly red-shifted absorption and fluorescence maxima and differs in fluorescence lifetime when compared to MV-Pchlide (Kotzabasis et al., 1990; Kruk and Mysliwa-Kurdziel, 2004; Mysliwa-Kurdziel et al., 2008). The prenyl moiety, present in protochlorophyll molecule, only slightly changes the spectral and photophysical properties of the tetrapyrrole ring of Pchlide (Mysliwa-Kurdziel et al., 2004, 2008).

Pchlide in aqueous solutions forms aggregates even at low concentrations, which is manifested by a significant red shift of the absorption and emission maxima, and in strong fluorescence quenching (Mysliwa-Kurdziel et al., 2004, 2013b; Sytina et al., 2011a,b). Aggregation of the pigments was also observed in organic solvents at high Pchlide concentrations (Kotzabasis et al., 1990; Kruk and Mysliwa-Kurdziel, 2004; Mysliwa-Kurdziel et al., 2013b).

Liposomes composed of thylakoid lipids were used to model interactions of free Pchlide molecules with etioplast inner membranes (Mysliwa-Kurdziel et al., 2013a,b). Pchlide molecules were found at the interface area of the liposomes and/or the head-group area of the lipid bilayer. In the case of high Pchlide contents, aggregate formation was observed, which was facilitated in galactolipid liposomes. Pchlide aggregates had similar fluorescence emission to aggregated Pchlide:LPOR:NADPH complexes *in vivo* (i.e., at 656 nm), however, the excitation maximum was red-shifted to 480 nm. Experiments performed for Pchlide in reversed micelles from dioctyl sulfosuccinate sodium salt (AOT)/isooctane mixture showed that the molecular dynamics of water bound at the hydrophylic core of micelles is also important for Pchlide monomer-aggregate equilibrium (Mysliwa-Kurdziel et al., 2013b).

As observed in the experiments performed with *in vitro* enzyme-free model systems, the Pchlide chromophore is very sensitive to changes in its molecular environment. In the monomeric state its fluorescence emission varies between 626 and 641.5 nm, fluorescence emission maxima of Pchlide pigment forms above 641.5 nm can only be obtained when two or more Pchlide molecules are in close proximity, have overlapping delocalized electron systems and thus form aggregates *in vitro* (see above, and Mysliwa-Kurdziel et al., 2004, 2013a,b; Sytina et al., 2011a,b). A model summarizing the spectral properties and the molecular interactions of Pchlide *in vitro* is presented in **Figure 4**.

Spectral Properties of *in vitro* Reconstituted Pchlide:LPOR:NADPH Complexes

Based on data obtained from *in vitro* model systems as well as other experimental evidence including CD spectroscopy of etioplast inner membrane fractions isolated from etiolated leaves (Böddi et al., 1989, 1990), it seems clear that the photoactive Pchlide complexes contain Pchlide pigments in at least dimeric or aggregated forms. This can be probably achieved by the distinct conformation of the LPOR dimers or oligomers in which the delocalized electron systems of neighboring Pchlide molecules overlap. Below we'll briefly review the latest *in vitro* reconstitution experiments of photoactive LPOR complexes. Again, we should mention that important pioneering observations have been done on isolated and partially purified photoactive complexes (in early works referred to as holochromes) from plants, but detailed discussion of these complexes and early data is provided elsewhere (e.g., Schoefs and Franck, 2003; Solymosi and Schoefs, 2010). Similarly, we only discuss data on *in vitro* reconstitution experiments of photoactive plant LPOR complexes, and not those about cyanobacterial LPOR (reviewed e.g., in Heyes and Hunter, 2005), because the peculiar membrane structures (prolamellar bodies) and direct LPOR-lipid and LPOR-membrane interactions have been only scarcely studied in such organisms (Schneidewind et al., 2019; Yamamoto et al., 2020).

Martin et al. (1997) successfully reconstituted photoactive complexes from recombinant pea LPOR with absorption maximum at around 630 nm, which were—based on their molecular mass—assigned to LPOR dimers. However, plant LPOR complexes with fluorescence emission maximum at 655 nm were reconstituted for the first time using a mixture of LPOR isoforms from barley (i.e., LPOR-A and LPOR-B), two different zinc derivatives of Pchlide as well as lipids extracted from isolated PLBs (Reinbothe et al., 1999). Later *in vitro* experiments using Pchlide and recombinant LPOR-A from *Arabidopsis thaliana* demonstrated that the formation of ternary LPOR complexes with fluorescence emission maximum at 655 nm requires the presence of MGDG and a negatively charged plant lipid (either PG or SQDG) (**Figure 4**) (Gabruk et al., 2017; Nguyen et al., 2021). Lipids did not only play a kind of structural role but also influenced the enzyme activity. Negatively charged lipids (PG and SQDG) did not influence the spectral properties of the complexes but affected their NADPH binding properties. When only PG was present, much lower concentrations of NADPH were required by the enzyme to form photoactive complexes, suggesting that these LPOR-A complexes are preferably associated to the lipid membranes, especially under low NADPH concentrations which are common in etiolated tissues (Gabruk et al., 2017).

Interestingly, the conical shaped, non-bilayer lipid, MGDG had a strong effect on the spectral properties of LPOR-A complexes *in vitro*. In the presence of MGDG, the fluorescence emission maximum of *in vitro* reconstituted LPOR complexes was shifted up to 652 nm, but the formation of complexes with native-like fluorescence properties (i.e., emission maximum at 655 nm) were only induced in the simultaneous presence of MGDG and PG (**Figure 4**) (Gabruk et al., 2017). Successful cryo electron microscopic analyses of *in vitro* assembled LPOR, NADPH, Pchlide in a mixture of lipids revealed that LPOR and Pchlide are inserted into the outer leaflet of the membranes, and LPOR forms oligomers arranged in helical filaments which are strongly associated with the membranes and have an important role in inducing and shaping their tubular organization (Nguyen et al., 2021).

Interaction of Pchlide-LPOR Complexes With Plastid Inner Membranes

As stated above, in etioplasts the photoactive LPOR proteins and their oligomers are mostly located to the PLBs and are only present in minor amounts in isolated prothylakoid fractions, in which monomeric, non-photoactive Pchlide complexes are dominating (Ryberg and Sundqvist, 1982b). LPOR (and especially LPOR-A) accounts for the vast majority of the proteins of the PLBs (Ryberg and Sundqvist, 1982a; Blomqvist et al., 2008).

On the other hand, it has to be added that fluorescence emission typical for monomeric Pchlide has been described in the cytosolic side of the outer envelope membranes of chloroplasts in spinach (Joyard et al., 1990). On the long term (i.e., after 10 min) and in the presence of glycerol slow transformations of the Pchlide pigments was observed in such isolated envelope membrane fractions upon illumination. This indicates that Pchlide-Chlide transformation may take place in the envelope membrane when the LPOR protein conformation is influenced by glycerol (Joyard et al., 1990) which is a component that stabilizes and maybe preferentially favors oligomerization (Zhong et al., 1996; Klement et al., 2000; Solymosi et al., 2002, 2007a; Smeller et al., 2003).

Information about the transport of the LPOR protein from the envelope membranes where they were located (Joyard et al., 1990) toward the internal parts of the plastids is scarce. On the other hand, Dahlin et al. (1995) did not observe accumulation of LPOR in the stroma and the envelope membranes, but have shown that LPOR is a peripheral protein associated with the stromal side of the thylakoid membranes of chloroplasts where it is bound more loosely to the membranes than to PLBs or PTs. Other authors located them to grana margins (Wang et al., 2020). Concerning the import of LPOR from the envelope toward the membranes, it may use plastid vesicle trafficking pathways (Lindquist et al., 2016; Lindquist and Aronsson, 2018).

The Unique Membrane Structure of the PLBs

PLBs represent a highly peculiar membrane structure, in which the lipids do not form bilayers, but special cubic phase structures. Such special membranes termed tubular complexes or tubuloreticular inclusions were observed within various intracellular compartments of several organisms including animals, humans or plants. In the former, these are thought to represent the modification of the (rough) endoplasmic reticulum, are in general located inside its cisternae or in the perinuclear space (e.g., Boor et al., 1979) and are rich in acidic glycoproteins. Tubuloreticular complexes have been observed in the cytoplasm of various animal [e.g., dog (Krohn and Sandholm, 1975; Madewell and Munn, 1990), Rhesus monkey (Feldman et al., 1986), cynomolgus monkey (Geisbert et al., 1992), horse

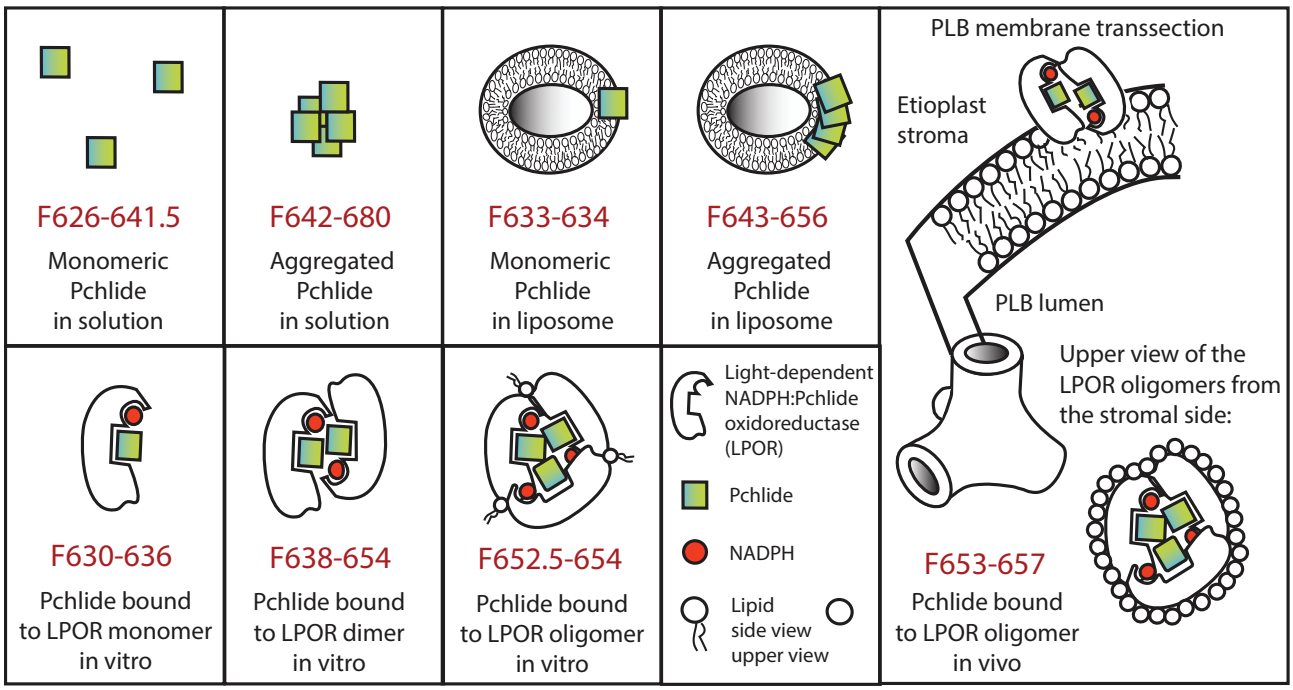

FIGURE 4 | Model representing spectral properties and molecular interactions of protochlorophyllide in various *in vitro* model systems as well as *in vivo* in case of the major photoactive protochlorophyllide form located to the prolamellar bodies. In case of oligomers for simplicity trimers are represented, although larger aggregates (e.g., tetramers and octamers) have been also reported. For further details see the text.

and mule (Madewell and Munn, 1989), chicken (Schaff et al., 1976), rat (Datsis, 1993)] and human cells [e.g., lymphoid cells, lymphocytes (Schaff et al., 1972, 1973; Grimley et al., 1973, 1985; Splinter et al., 1975; Kang et al., 1984), monocytes (Luu et al., 1989; Kostianovsky et al., 2016), brain endothelial cells (Lee et al., 1988), liver endothelial cells (Geisbert et al., 1992), heart endothelial cells (Boor et al., 1979), renal cells (Hurd et al., 1969; Grimley et al., 1973; Krohn and Sandholm, 1975; Lee et al., 1988, 2013a, 2017; Datsis, 1993; Elmaghrabi et al., 2017), fibroblasts (Boor et al., 1979; Feldman et al., 1986)] where they were often associated with various, first of all immunological disorders or viral diseases [lupus erythematosus (Hurd et al., 1969; Grimley et al., 1973; Schaff et al., 1973), AIDS (Maturi and Font, 1996), AIDS-associated Kaposi's sarcoma (Marquart, 2005), cytomegalovirus infection (Lee et al., 1988), Sjögren's syndrome (Daniels et al., 1974), SARS (Almsherqi et al., 2005), many other types of virus infections (Deng et al., 2010; reviewed in Grimley and Schaff, 1976; Luu et al., 1989; Almsherqi et al., 2006; Deng et al., 2010) or certain neoplasms [e.g., pituitary tumors (Landolt et al., 1976), connective tissue neoplasms (Madewell and Munn, 1989), plasmacytoma (Madewell and Munn, 1990), intracranial germinomas (Matsumura et al., 1984), lung carcinomas (Schaff et al., 1976), hepatomas (Schaff et al., 1976), Burkitt's type lymphoma (Popoff and Malinin, 1976)].

Tubuloreticular membrane organization has been also observed inside mitochondria and plastids (Almsherqi et al., 2009; Almsherqi, 2010). In the former, cubic membrane formation was induced by starvation and/or autophagy processes of the amoeba cells, during which they were slowing the degradation of the organelle and thus contributed to the survival of the cell upon stress conditions (Chong et al., 2017). In case of plastids, they occurred either in etioplasts or etio-chloroplasts in the form of PLBs and were thus strongly associated with intensive Chl biosynthesis and accumulation of LPOR (**Figure 5**) (Solymosi and Schoefs, 2008, 2010; Solymosi and Aronsson, 2013) or in secretory plastids having active isoprenoid biosynthesis involving the plastid located MEP-pathway or biosynthesis of hydrophobic molecules such as cutin or suberin (Solymosi and Schoefs, 2010; Böszörményi et al., 2020). Rarely, such tubuloreticular membrane organizations could be interpreted as vesicle clusters (Lindquist et al., 2016) or as structures that appeared under various stress conditions [e.g., UV irradiation (Kovács and Keresztes, 2002)].

Secretory plastids containing tubuloreticular membranes were observed in various taxa and secretory tissues including extrafloral nectaries of *Passiflora* (Schnepf, 1961), plastids of various glandular hairs [e.g., *Cannabis* (Hammond and Mahlberg, 1978; Kim and Mahlberg, 1997; Solymosi and Köfalvi, 2017), *Artemisia* (Ascensao and Pais, 1982), *Chrysanthemum* (Vermeer and Peterson, 1979), *Centrolobium* (Matos and Paiva, 2012), *Platanthera* (Stpiczyńska et al., 2005)], *Mentha piperita* (Amelunxen, 1965; Turner et al., 2000, 2012), *Perilla ocymoides* (Kashina and Danilova, 1993) and *Rosmarinus officinalis* (Böszörményi et al., 2020). Some authors suggested that light may play a role in the formation of these peculiar membrane structures in secretory cells (Kashina and Danilova, 1993), while

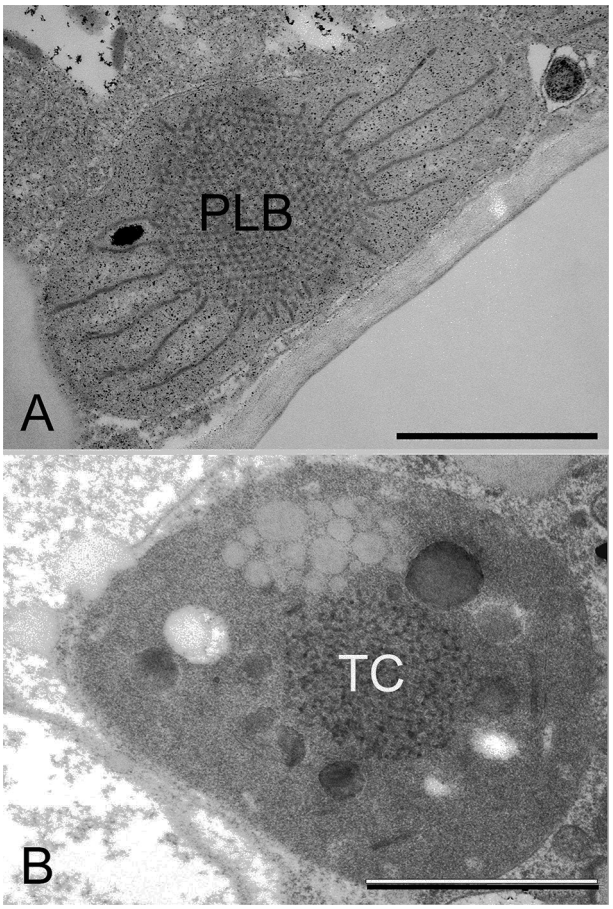

FIGURE 5 | Transmission electron micrographs of the prolamellar body (PLB) present in the etioplast of the cotyledon of a 2-week-old dark-germinated rosemary (*Rosmarinus officinalis*) seedling **(A)**, and tubular complex (TC) of a leucoplast of the neck cell of a peltate glandular hair on the surface of a light-grown adult rosemary plant **(B)**. Scale bar: 1 μm. Sample preparation was as described in Böszörményi et al. (2020).

others observed identical structures in the neck cells of the peltate glandular hairs of both light-grown and dark-forced shoots (Böszörményi et al., 2020). Detailed comparative analyses about these peculiar non-bilayer membranes of *Rosmarinus officinalis* plastids have clearly demonstrated important structural differences. The PLBs of etioplasts represented a highly ordered and symmetrical membrane organization when compared with the loose and irregular tubuloreticular membranes of the secretory plastids (**Figure 5**) (Böszörményi et al., 2020).

The PLB should be thus considered as a highly regular subtype of tubular complexes, in which membrane tubules are arranged into tetrahedral (**Figure 4**) or hexapodel units, which are then joined into a paracrystalline 3D spatial network of membranes (**Figure 5**) (Gunning, 1965, 2001; Solymosi and Schoefs, 2008; Rudowska et al., 2012; Solymosi and Aronsson, 2013; Kowalewska et al., 2019; Bykowski et al., 2020). The different PLB types observed in different species and plastids, at different stages of development are beyond the scope of this review.

In spite of their widespread occurrence, it is still unclear whether tubuloreticular membranes have any specific function (e.g., in the production of secreted compounds of plastids or storage or accumulation of some metabolites) or they simply reflect some disturbance in the membrane homeostasis. The latter possibility may be outlined by the fact that such structures in animals or humans are mostly associated with stressful or diseased conditions [in case of AIDS tubuloreticular membranes have even been suggested to represent an ultrastructural pathological marker of the disease (Almsherqi et al., 2006)] and may be induced by exogenous or endogenous interferon (Grimley et al., 1985; Feldman et al., 1986; Orenstein et al., 1987), halogenated pyrimidines (Hulanicka et al., 1977) or even pyridoxine deficiency (Datsis, 1993). Stressful conditions such as starvation (Chong et al., 2017) or UV-irradiation (Kovács and Keresztes, 2002) also led to the formation of tubuloreticular complexes in amoeba mitochondria and apple plastids, respectively. On the other hand, some works suggest that such structures may be involved in regeneration processes of endothelial cells in wounded tissues (Eady and Odland, 1975), or in viral DNA or RNA uptake procedures (Almsherqi et al., 2006; Almsherqi, 2010).

In case of the PLBs, several data clearly indicate that due to their very high surface-to-volume ratio, these membranes represent a kind of membrane depot from which the photosynthetic membranes of the chloroplasts can be formed very fast upon illumination (reviewed in Solymosi and Schoefs, 2010; Solymosi and Aronsson, 2013). Thus, the etioplast-to-chloroplast transformation is much faster than the proplastid-to-chloroplast transformation pathway (Liebers et al., 2017), because during the latter important *de novo* synthesis of membrane lipids is required in parallel with protein and pigment biosynthesis. In addition, the PLBs and the proper organization and oligomerization of LPOR as well as the presence of carotenoids clearly play a role in photoprotection of the porphyrin pigments upon illumination, while in the absence of them, often photooxidative stress is induced (Sperling et al., 1997; Erdei et al., 2005; Hideg et al., 2010; reviewed by Solymosi and Schoefs, 2010). Similarly, cubic membranes efficiently prevented lipid peroxidation and RNA damage under oxidative stress conditions (Almsherqi, 2010).

There is no consensus on the factors inducing the formation of tubuloreticular membrane organization. Some authors suggested that they are the result of altered lipid (cholesterol) homeostasis, lipid and fatty acid composition induced by for instance viral infection (Almsherqi, 2010; Deng et al., 2010), others suggested that they may be associated with altered carotenoid composition (Park et al., 2002; Cuttriss et al., 2007), membrane symmetry (Larsson and Larsson, 2014), special protein-protein interactions or lipid-to-protein ratio (Almsherqi et al., 2009) or low divalent ion concentrations (Almsherqi et al., 2006; Brasnett et al., 2017). Such membrane organization was also observed in the aqueous lipid-protein film of lung surfactants (Larsson and Larsson, 2014). Therefore, it might be possible that a kind of specific water-lipid-protein composition is responsible for the formation of such structures. Similarly, we may speculate that the accumulation of lipophilic compounds (isoprenoids, terpenes,

carotenoids, fatty acids, etc.) within the membranes could be involved in the formation of the PLBs. In the next section, we'll briefly discuss data about factors influencing PLB structure in etioplasts.

The Role of Lipid-Protein Interactions in the Formation of the Prolamellar Bodies

The lipid composition of the PLBs of etioplasts and chloroplast thylakoids is basically similar (Selstam and Sandelius, 1984; Selstam, 1998; Fujii et al., 2018, 2019a,b; Yu et al., 2020) with slightly lower amount of unsaturated (18:3) fatty acids being present in the PLB membranes than in the thylakoids (Selstam and Sandelius, 1984; Selstam, 1998). The ratio of the non-bilayer lipid MGDG to DGDG is slightly higher (1.6–1.8) in purified PLBs and in chloroplast thylakoids (1.7) than in prothylakoids (1.1–1.4) (Ryberg et al., 1983; Sandelius and Selstam, 1984; Selstam and Sandelius, 1984). Data on chloroplast structure of different lipid biosynthesis mutants revealed that minor alterations in the MGDG:DGDG ratio may have important effect on plastid structure (Mazur et al., 2019; Yu et al., 2020) and that dynamic local changes of the neutral/anionic lipid ratios may have important role in thylakoid arrangement (Kobayashi and Wada, 2016).

It is also evident from studies using lipid biosynthesis mutants (Fujii et al., 2017) and from *in vitro* reconstitution experiments (Gabruk et al., 2017) that some lipids (MGDG, DGDG and SQDG) are crucial for the proper assembly of PLBs and also for their transformation into thylakoids upon illumination (Fujii et al., 2018). Fujii et al. (2019b) have reviewed in detail the role of different plastid lipids on the Mg-branch of porphyrin biosynthesis, therefore, we prefer not to discuss these data in detail in this work.

In spite of the similar lipid composition, major differences are observed in the protein composition of chloroplast thylakoids and PLBs (Ryberg and Sundqvist, 1982a; Selstam and Sandelius, 1984; von Zychlinski et al., 2005; Blomqvist et al., 2008; Kanervo et al., 2008) with the latter containing much less proteins (and thus a relatively high lipid to protein ratio) and among them predominantly LPOR.

The lipid-dependent formation of the photoactive oligomers was proposed to be a mechanism inducing the formation of the PLBs (Gabruk et al., 2017), and correlations were found between PLB formation and proper lipid composition and accumulation, and proper amounts of LPOR in other works as well (reviewed in Fujii et al., 2019b). Similarly, a clear relationship was found between the formation and accumulation of LPOR oligomers (especially LPOR-A) and the occurrence and size of PLBs in etioplasts (Sperling et al., 1997; Franck et al., 2000; Frick et al., 2003; Paddock et al., 2010, 2012). Studies using *Arabidopsis thaliana* mutants showed that the amounts of LPOR-A and LPOR-B correlate with PLB size. Inhibition of LPOR-A expression led to reduced PLB size (Frick et al., 2003; Paddock et al., 2010, 2012), while its overexpression resulted in larger PLBs (Sperling et al., 1997; Franck et al., 2000; Paddock et al., 2010, 2012).

Similar data were observed in pea with overexpressed or antisense-LPOR (Seyedi et al., 2001). Furthermore, in organs with low LPOR levels, proplastids are present and PLBs are scarce or small [e.g., in non-leaf organs of pea (Böddi et al., 1994)]. Recent data on cyanobacterial LPOR indicated that it is present in dimerized form *in vivo* (Schneidewind et al., 2019) and its overexpression induced the formation of tubuloreticular membranes slightly resembling PLBs within the cells accumulating LPOR and Pchilde but being deficient in NADPH (Yamamoto et al., 2020).

Similarly, the disaggregation of the LPOR oligomers or the degradation of LPOR are also strongly associated with the disruption of the regular structure of the PLBs (e.g., Ryberg and Sundqvist, 1988) both under dark conditions (and induced by stress factors, e.g., Solymosi et al., 2006b) or during the light-induced greening of etiolated leaves, during which the PLB is fully reorganized and transformed into developing thylakoids (Kowalewska et al., 2016; reviewed in Solymosi and Schoefs, 2010; Solymosi and Aronsson, 2013; Kowalewska et al., 2019). These large-scale membrane reorganizations occur in parallel with important spectral changes (e.g., the Shibata shift—**Figure 3**, Shibata, 1957) which reflect the disaggregation of Chlide pigments and further outline the strong structural connection between LPOR macrodomains and PLB membranes. The Shibata shift is strongly inhibited by low temperature, high pressure as well as protein cross-linkers, or glycerol and sugars (Wiktorsson et al., 1993; Zhong et al., 1996; Solymosi et al., 2002, 2007a; Smeller et al., 2003), i.e., factors and conditions which stabilize the oligomeric structure, inhibit its conformational changes, disaggregation or the dissociation of peripheral proteins from membranes. However, under normal conditions, in parallel with the disruption of the PLB structure, the LPOR oligomers also undergo disaggregation and release Chlide from their active site. After this, the photoactive LPOR oligomers are again regenerated by binding Pchlide (Granick and Gassman, 1970; Amirjani and Sundqvist, 2004; Rassadina et al., 2004; Schoefs and Franck, 2008) from the pool of non-photoactive Pchlide molecules, and they again catalyze Pchlide photoreduction in them. Several authors reported that until Chl biosynthesis is still active in organs, because their final Chl content has not been reached, PLBs (Ikeda, 1970, 1971) and LPOR oligomers persist in their plastids and may even accumulate under special light conditions (e.g., Solymosi et al., 2006a,b; Schoefs and Franck, 2008; Solymosi et al., 2012). The plastids of such low-light-grown or partially etiolated or young tissues contain simultaneously developing grana and PLBs, thus an important spatial and structural heterogeneity can be clearly observed in the organization of the plastid inner membranes in these so-called etio-chloroplasts. Unfortunately, the PLBs of etio-chloroplasts seem to be versatile structures hard to isolate, therefore, we have not much information about the lipid and protein composition of these membranes.

CONCLUDING REMARKS

Most data on Chl biosynthesis and especially about Pchlide photoreduction and its molecular details were obtained using etiolated seedlings. The use of etiolated systems to study these processes were often criticized because the major chloroplast

differentiation pathway under natural light conditions is the proplastid-to-chloroplast pathway occurring in most seeds germinating on the soil surface or in new leaves produced by the shoot apical meristem (Charuvi et al., 2012; Yadav et al., 2019). However, several data indicate that etioplasts and accumulation of Pchlide and LPOR ternary complexes occur also under natural conditions in seedlings germinating in the soil (e.g., Vitányi et al., 2013; Kakuszi et al., 2017), in tissues partially covered by other organs (e.g., Solymosi et al., 2007b), in inner leaf primordia developing inside closed bud structures (e.g., Solymosi et al., 2004, 2006a, 2012), and in other systems (water plants, etc., reviewed in Solymosi and Aronsson, 2013; Armarego-Marriott et al., 2020). In such tissues or organs Chl biosynthesis and etioplast-to-chloroplast transformation may be similar to those described in completely etiolated seedlings, but the processes and their regulation still need to be elucidated in such naturally etiolated tissues.

In addition, photosynthesis requires a constant supply of Chls especially in plants under fluctuating or stressful conditions. Several data indicate that for instance after recovery from desiccation or drought stress (e.g., Solymosi et al., 2013; Liu et al., 2018, 2020), Chl synthesis genes are upregulated and an intensive biosynthesis occurs. So far only limited amount of information is available about LPOR catalytic activity and macromolecular organization in chloroplasts. Taken together, a better understanding of the Mg-branch of Chl biosynthesis, especially of LPOR activity, structure and location, and factors involved in its regulation in chloroplasts and etio-chloroplasts of various green (crop) plants may be also important for agriculture. The recent breakthroughs in molecular biology (e.g., next generation sequencing and tremendous developments in various omics techniques which enable the identification of different isoforms and their expression and translational patterns in various plant species and plastid subcompartments) and microscopic methods, as well as the use of various novel model systems (i.e., dark-forced tobacco shoots—Armarego-Marriott et al., 2019, duckweed—Monselise et al., 2015) will probably provide novel and interesting data on the exact molecular regulation of these processes and the role of lipids in them.

A large step into the understanding of LPOR-lipid interactions has been achieved by the *in vitro* reconstitution of photoactive LPOR macrodomains in the presence of lipids (Nguyen et al., 2021). These data demonstrate for the first time directly the role of LPOR and LPOR-lipid interactions in the formation of a special membrane phase and helical organization. In addition to analyses on different mutants, similar *in vitro* reconstitution experiments and membrane and lipid binding assays of various LPOR isoforms as well as other Chl biosynthesis enzymes of different species should be performed to increase our understanding of the membrane association and localization of Chl biosynthesis. It is also important to outline, that at the moment our data are mostly related to the 3 LPOR isoforms of Arabidopsis, and the 2 isoforms present in few crop species (rice, barley), but further experiments with other crops with less or more isoforms are necessary to understand LPOR activity and its universal or specific regulation in case of the various isoforms and species. The same applies to other enzymes of Chl biosynthesis. Due to its major and central role in autotrophic plant metabolism, we believe that an increased understanding of Chl biosynthesis may be crucial to breed plants with improved quality, e.g., higher yield or performance under adverse environmental conditions.

AUTHOR CONTRIBUTIONS

KS and BM-K equally contributed to the conceptualization, writing, and discussion about the manuscript's content. Both authors edited and approved the submitted version.

FUNDING

KS acknowledges the support from the Bolyai János Research Scholarship of the Hungarian Academy of Sciences and from the National Research, Development and Innovation Office (Grant OTKA FK 124748). BM-K acknowledges the support from the Polish National Science Centre (NCN; https://www.ncn.gov.pl) as a part of Grant UMO-2013/10/E/NZ3/00748.

ACKNOWLEDGMENTS

KS acknowledges ERASMUS+ Training Staff Mobility for financing her short trip to Krakow in June 2019.

REFERENCES

Adams, N. B. P., Bisson, C., Brindley, A. A., Farmer, D. A., Davison, P. A., Reid, J. D., et al. (2020). The active site of magnesium chelatase. *Nat. Plants* 6, 1491–1502. doi: 10.1038/s41477-020-00806-9

Adhikari, N. D., Orler, R., Chory, J., Froehlich, J. E., and Larkin, R. M. (2009). Prophyrins promote the association of GENOMES UNCOUPLED 4 and a Mg-chelatase subunit with chloroplast membranes. *J. Biol. Chem.* 284, 24783–24796. doi: 10.1074/jbc.M109.025205

Albus, C. A., Salinas, A., Czarnecki, O., Kahlau, S., Rothbart, M., Thiele, W., et al. (2012). LCAA, a novel factor required for magnesium protoporphyrin monomethylester cyclase accumulation and feedback control of aminolevulinic acid biosynthesis in tobacco. *Plant Physiol.* 160, 1923–1939. doi: 10.1104/pp.112.206045

Almsherqi, Z. A. (2010). *The Missing Dimension of Cell Membrane Organization. Study on Cubic Membrane Structure and Function*. Available online at: https://scholarbank.nus.edu.sg/handle/10635/22981.

Almsherqi, Z. A., Kohlwein, S. D., and Deng, Y. (2006). Cubic membranes: a legend beyond the flatland of cell membrane organization. *J. Cell Biol.* 173, 839–844. doi: 10.1083/jcb.200603055

Almsherqi, Z. A., Landh, T., Kohlwein, S. D., and Deng, Y. (2009). Chapter 6 cubic membranes. The missing dimension of cell membrane organization. *Int. Rev. Cell Mol. Biol.* 274, 275–342. doi: 10.1016/S1937-6448(08)02006-6

Almsherqi, Z. A., McLachlan, C. S., Mossop, P., Knoops, K., and Deng, Y. (2005). Direct template matching reveals a host subcellular membrane gyroid cubic structure that is associated with SARS virus. *Redox Rep.* 10, 167–171. doi: 10.1179/135100005X57373

Amelunxen, F. (1965). Elektronenmikroskopische Untersuchungen an den Drüsenshuppen von *Mentha piperita* L. *Planta Med.* 13, 457–453. doi: 10.1055/s-0028-1100141

Amirjani, M. R., and Sundqvist, C. (2004). Regeneration of protochlorophyllide in green and greening leaves of plants with varying proportions of protochlorophyllide forms in darkness. *Physiol. Plant.* 121, 377–390. doi: 10.1111/j.1399-3054.2004.00340.x

Armarego-Marriott, T., Kowalewska, Ł., Burgos, A., Fischer, A., Thiele, W., Erban, A., et al. (2019). Highly resolved systems biology to dissect the etioplast-to-chloroplast transition in tobacco leaves. *Plant Physiol.* 180, 654–681. doi: 10.1104/pp.18.01432

Armarego-Marriott, T., Sandoval-Ibañez, O., and Kowalewska, Ł. (2020). Beyond the darkness: recent lessons from etiolation and de-etiolation studies. *J. Exp. Bot.* 71, 1215–1225. doi: 10.1093/jxb/erz496

Armstrong, G. A., Runge, S., Frick, G., Sperling, U., and Apel, K. (1995). Identification of NADPH:protochlorophyllide oxidoreductases A and B: a branched pathway for light-dependent chlorophyll biosynthesis in *Arabidopsis thaliana*. *Plant Physiol.* 108, 1505–1517. doi: 10.1104/pp.108.4.1505

Aronsson, H., Schöttler, M. A, Kelly, A. A, Sundqvist, C., Dörmann, P., Karim, S., et al. (2008). Monogalactosyldiacylglycerol deficiency in Arabidopsis affects pigment composition in the prolamellar body and impairs thylakoid membrane energization and photoprotection in leaves. *Plant Physiol.* 148, 580–592. doi: 10.1104/pp.108.123372

Aronsson, H., Sundqvist, C., and Dahlin, C. (2003a). POR - import and membrane association of a key element in chloroplast development. *Physiol. Plant.* 118, 1–9. doi: 10.1034/j.1399-3054.2003.00088.x

Aronsson, H., Sundqvist, C., and Dahlin, C. (2003b). POR hits the road: import and assembly of a plastid protein. *Plant Mol. Biol.* 51, 1–7. doi: 10.1023/A:1020795415631

Aronsson, H., Sundqvist, C., Timko, M. P., and Dahlin, C. (2001). The importance of the C-terminal region and Cys residues for the membrane association of the NADPH:protochlorophyllide oxidoreductase in pea. *FEBS Lett.* 502, 11–15. doi: 10.1016/S0014-5793(01)02595-9

Ascensao, L., and Pais, M. S. S. (1982). Secretory trichomes from *Artemisia crithmifolia*: some ultrastructural aspects. *Bull. la Société Bot. Fr.* 129, 83–87. doi: 10.1080/01811789.1982.10826552

Beck, G., Coman, D., Herren, E., Ruiz-Sola, M. Á., Rodríguez-Concepción, M., Gruissem, W., et al. (2013). Characterization of the GGPP synthase gene family in *Arabidopsis thaliana*. *Plant Mol. Biol.* 82, 393–416. doi: 10.1007/s11103-013-0070-z

Belanger, F. C., and Rebeiz, C. A. (1979). Chloroplast biogenesis XXVII detection of novel chlorophyll and chlorophyll precursors in higher plants. *Biochem. Biophys. Res. Commun.* 88, 365–372. doi: 10.1016/0006-291X(79)92057-6

Belanger, F. C., and Rebeiz, C. A. (1980). Chloroplast biogenesis. Detection of divinyl protochlorophyllide in higher plants. *J. Biol. Chem.* 255, 1266–1272. doi: 10.1016/S0021-9258(19)86024-6

Belyaeva, O. B., and Litvin, F. F. (2007). Photoactive pigment-enzyme complexes of chlorophyll precursor in plant leaves. *Biochemistry* 72, 1458–1477. doi: 10.1134/S0006297907130044

Belyaeva, O. B., and Litvin, F. F. (2011). Advances in understanding of the primary reactions of protochlorophyll(ide) photoreduction in cells and model systems. *J. Biophys. Chem.* 02, 1–9. doi: 10.4236/jbpc.2011.21001

Belyaeva, O. B., and Litvin, F. F. (2014). Mechanisms of phototransformation of protochlorophyllide into chlorophyllide. *Biochem. Biokhimiia* 79, 337–348. doi: 10.1134/S0006297914040038

Benli, M., Schulz, R., and Apel, K. (1991). Effect of light on the NADPH-protochlorophyllide oxidoreductase of *Arabidopsis thaliana*. *Plant Mol. Biol.* 16, 615–625. doi: 10.1007/BF00023426

Benz, J., Lempert, U., and Rüdiger, W. (1984). Incorporation of phytol precursors into chlorophylls of tobacco cell cultures. *Planta* 162, 215–219. doi: 10.1007/BF00397442

Bick, J. A., and Lange, B. M. (2003). Metabolic cross talk between cytosolic and plastidial pathways of isoprenoid biosynthesis: unidirectional transport of intermediates across the chloroplast envelope membrane. *Arch. Biochem. Biophys.* 415, 146–154. doi: 10.1016/S0003-9861(03)00233-9

Birve, S. J., Selstam, E., and Johansson, L. B. (1996). Secondary structure of NADPH: protochlorophyllide oxidoreductase examined by circular dichroism and prediction methods. *Biochem. J.* 317, 549–555. doi: 10.1042/bj3170549

Block, M. A., Tewari, A. K., Albrieux, C., Maréchal, E., and Joyard, J. (2002). The plant S-adenosyl-L-methionine:Mg-protoporphyrin IX methyltransferase is located in both envelope and thylakoid chloroplast membranes. *Eur. J. Biochem.* 269, 240–248. doi: 10.1046/j.0014-2956.2001.02643.x

Blomqvist, L. A., Ryberg, M., and Sundqvist, C. (2008). Proteomic analysis of highly purified prolamellar bodies reveals their significance in chloroplast development. *Photosynth. Res.* 96, 37–50. doi: 10.1007/s11120-007-9281-y

Böddi, B., Lindsten, A., Ryberg, M., and Sundqvist, C. (1989). On the aggregational states of protochlorophyllide and its protein complexes in wheat etioplasts. *Physiol. Plant.* 76, 135–143. doi: 10.1111/j.1399-3054.1989.tb05622.x

Böddi, B., Lindsten, A., Ryberg, M., and Sundqvist, C. (1990). Phototransformation of aggregated forms of protochlorophyllide in isolated etioplast inner membranes. *Photochem. Photobiol.* 52, 83–87. doi: 10.1111/j.1751-1097.1990.tb01759.x

Böddi, B., McEwen, B., Ryberg, M., and Sundqvist, C. (1994). Protochlorophyllide forms in non-greening epicotyls of dark-grown pea (*Pisum sativum*). *Physiol. Plant.* 92, 160–170. doi: 10.1111/j.1399-3054.1994.tb06667.x

Böddi, B., Ryberg, M., and Sundqvist, C. (1991). The formation of a short-wavelength chlorophyllide form at partial phototransformation of protochlorophyllide in etioplast inner membranes. *Photochem. Photobiol.* 53, 667–673. doi: 10.1111/j.1751-1097.1991.tb08495.x

Böddi, B., Ryberg, M., and Sundqvist, C. (1992). Identification of four universal protochlorophyllide forms in dark-grown leaves by analyses of the 77 K fluorescence emission spectra. *J. Photochem. Photobiol. B Biol.* 12, 389–401. doi: 10.1016/1011-1344(92)85043-T

Boor, P. J., Ferrans, V. J., Jones, M., Kawanami, O., Thiedemann, K. U., Herman, E. H., et al. (1979). Tubuloreticular structures in myocardium: an ultrastructural study. *J. Mol. Cell. Cardiol.* 11, 977–979. doi: 10.1016/0022-2828(79)90388-2

Böszörményi, A., Dobi, A., Skribanek, A., Pávai, M., and Solymosi, K. (2020). The effect of light on plastid differentiation, chlorophyll biosynthesis, and essential oil composition in rosemary (*Rosmarinus officinalis*) leaves and cotyledons. *Front. Plant Sci.* 11:196. doi: 10.3389/fpls.2020.00196

Brasnett, C., Longstaff, G., Compton, L., and Seddon, A. (2017). Effects of cations on the behaviour of lipid cubic phases. *Sci. Rep.* 7:8229. doi: 10.1038/s41598-017-08438-4

Bruley, C., Dupierris, V., Salvi, D., Rolland, N., and Ferro, M. (2012). AT_CHLORO: a chloroplast protein database dedicated to sub-plastidial localization. *Front. Plant Sci.* 3:205. doi: 10.3389/fpls.2012.00205

Bryant, D. A., Hunter, C. N., and Warren, M. J. (2020). Biosynthesis of the modified tetrapyrroles—the pigments of life. *J. Biol. Chem.* 295, 6888–6925. doi: 10.1074/jbc.REV120.006194

Brzezowski, P., Richter, A. S., and Grimm, B. (2015). Regulation and function of tetrapyrrole biosynthesis in plants and algae. *Biochim. Biophys. Acta* 1847, 968–985. doi: 10.1016/j.bbabio.2015.05.007

Buhr, F., El Bakkouri, M., Valdez, O., Pollmann, S., Lebedev, N., Reinbothe, S., et al. (2008). Photoprotective role of NADPH:protochlorophyllide oxidoreductase A. *Proc. Natl. Acad. Sci. U.S.A.* 105, 12629–12634. doi: 10.1073/pnas.0803950105

Bykowski, M., Mazur, R., Buszewicz, D., Szach, J., Mostowska, A., and Kowalewska, Ł. (2020). Spatial nano-morphology of the prolamellar body in Etiolated *Arabidopsis thaliana* plants with disturbed pigment and polyprenol composition. *Front. Cell Dev. Biol.* 8:586628. doi: 10.3389/fcell.2020.586628

Carey, E., and Rebeiz, C. (1985). Chloroplast biogenesis 49: differences among angiosperms in the biosynthesis and accumulation of monovinyl and divinyl protochlorophyllide during photoperiodic greening. *Plant Physiol.* 79, 1–6. doi: 10.1104/pp.79.1.1

Carey, E. E., Tripathy, B. C., and Rebeiz, C. A. (1985). Chloroplast biogenesis 51. *Plant Physiol.* 79, 1059–1063. doi: 10.1104/pp.79.4.1059

Charuvi, D., Kiss, V., Nevo, R., Shimoni, E., Adam, Z., and Reich, Z. (2012). Gain and loss of photosynthetic membranes during plastid differentiation in the shoot apex of arabidopsis. *Plant Cell* 24, 1143–1157. doi: 10.1105/tpc.111.094458

Chen, G. E., Canniffe, D. P., Barnett, S. F. H., Hollingshead, S., Brindley, A. A., Vasilev, C., et al. (2018). Complete enzyme set for chlorophyll biosynthesis in *Escherichia coli*. *Sci. Adv.* 4:eaaq1407. doi: 10.1126/sciadv.aaq1407

Chen, G. E., Canniffe, D. P., and Neil Hunter, C. (2017). Three classes of oxygen-dependent cyclase involved in chlorophyll and

bacteriochlorophyll biosynthesis. *Proc. Natl. Acad. Sci. U.S.A.* 114, 6280–6285. doi: 10.1073/pnas.1701687114

Chen, G. E., and Hunter, C. N. (2020). Protochlorophyllide synthesis by recombinant cyclases from eukaryotic oxygenic phototrophs and the dependence on Ycf54. *Biochem. J.* 477, 2313–2325. doi: 10.1042/BCJ20200221

Chereskin, B. M., Wong, Y. S., and Castelfranco, P. A. (1982). *In vitro* synthesis of the chlorophyll isocyclic ring: transformation of magnesium-protoporphyrin IX and magnesium-protoporphyrin IX monomethyl ester into magnesium-2,4-divinyl pheoporphyrin A(5). *Plant Physiol.* 70, 987–993. doi: 10.1104/pp.70.4.987

Chernomor, O., Peters, L., Schneidewind, J., Loeschcke, A., Knieps-Grünhagen, E., Schmitz, F., et al. (2020). Complex evolution of light-dependent protochlorophyllide oxidoreductases in aerobic anoxygenic phototrophs: origin, phylogeny, and function. *Mol. Biol. Evol.* 38, 819–837. doi: 10.1093/molbev/msaa234

Chong, K., Almsherqi, Z. A., Shen, H., and Deng, Y. (2017). Cubic membrane formation supports cell survival of amoeba Chaos under starvation-induced stress. *Protoplasma* 255, 517–525. doi: 10.1007/s00709-017-1169-x

Colindres-Rojas, M., Wolf, M. M. N., Grob, R., Seidel, S., Dietzek, B., Schmitt, M., et al. (2011). Excited-state dynamics of protochlorophyllide revealed by subpicosecond infrared spectroscopy. *Biophys. J.* 100, 260–267. doi: 10.1016/j.bpj.2010.11.054

Cuttriss, A. J., Chubb, A. C., Alawady, A., Grimm, B., and Pogson, B. J. (2007). Regulation of lutein biosynthesis and prolamellar body formation in Arabidopsis. *Funct. Plant Biol.* 34, 663–672. doi: 10.1071/FP07034

Czarnecki, O., and Grimm, B. (2012). Post-translational control of tetrapyrrole biosynthesis in plants, algae, and cyanobacteria. *J. Exp. Bot.* 63, 1675–1687. doi: 10.1093/jxb/err437

Dahlin, C., Aronsson, H., Wilks, H. M., Lebedev, N., Sundqvist, C., and Timko, M. P. (1999). The role of protein surface charge in catalytic activity and chloroplast membrane association of the pea NADPH: protochlorophyllide oxidoreductase (POR) as revealed by alanine scanning mutagenesis. *Plant Mol. Biol.* 39, 309–323. doi: 10.1023/A:1006135100760

Dahlin, C., Sundqvist, C., and Timko, M. P. (1995). The *in vitro* assembly of the NADPH-protochlorophyllide oxidoreductase in pea chloroplasts. *Plant Mol. Biol.* 29, 317–330. doi: 10.1007/BF00043655

Daniels, T. E., Sylvester, R. A., Silverman, S., Polando, V., and Talal, N. (1974). Tubuloreticular structures within labial salivary glands in sjögren's syndrome. *Arthritis Rheum.* 17, 593–597. doi: 10.1002/art.1780170514

Darrah, P. M., Kay, S. A., Teakle, G. R., and Griffiths, W. T. (1990). Cloning and sequencing of protochlorophyllide reductase. *Biochem. J.* 265, 789–798. doi: 10.1042/bj2650789

Datsis, A. G. S. (1993). Tubuloreticular structures in pyridoxine deficiency. *Exp. Toxicol. Pathol.* 45, 55–59. doi: 10.1016/S0940-2993(11)80458-6

Davison, P. A., Schubert, H. L., Reid, J. D., Iorg, C. D., Heroux, A., Hill, C. P., et al. (2005). Structural and biochemical characterization of Gun4 suggests a mechanism for its role in chlorophyll biosynthesis. *Biochemistry* 44, 7603–7612. doi: 10.1021/bi050240x

Denev, I. D., Yahubyan, G. T., Minkov, I. N., and Sundqvist, C. (2005). Organization of protochlorophyllide oxidoreductase in prolamellar bodies isolated from etiolated carotenoid-deficient wheat leaves as revealed by fluorescence probes. *Biochim. Biophys. Acta Biomembr.* 1716, 97–103. doi: 10.1016/j.bbamem.2005.09.001

Deng, Y., Almsherqi, Z. A., Ng, M. M. L., and Kohlwein, S. D. (2010). Do viruses subvert cholesterol homeostasis to induce host cubic membranes? *Trends Cell Biol.* 20, 371–379. doi: 10.1016/j.tcb.2010.04.001

Dietzek, B., Kiefer, W., Hermann, G., Popp, J., and Schmitt, M. (2006a). Solvent effects on the excited-state processes of protochlorophyllide: a femtosecond time-resolved absorption study. *J. Phys. Chem. B* 110, 4399–4406. doi: 10.1021/jp0556456

Dietzek, B., Kiefer, W., Yartsev, A., Sundström, V., Schellenberg, P., Grigaravicius, P., et al. (2006b). The excited-state chemistry of protochlorophyllide a: a time-resolved fluorescence study. *ChemPhysChem* 7, 1727–1733. doi: 10.1002/cphc.200600172

Dietzek, B., Maksimenka, R., Siebert, T., Birckner, E., Kiefer, W., Popp, J., et al. (2004). Excited-state processes in protochlorophyllide a - a femtosecond time-resolved absorption study. *Chem. Phys. Lett.* 397, 110–115. doi: 10.1016/j.cplett.2004.08.075

Dietzek, B., Tschierlei, S., Hanf, R., Seidel, S., Yartsev, A., Schmitt, M., et al. (2010). Dynamics of charge separation in the excited-state chemistry of protochlorophyllide. *Chem. Phys. Lett.* 492, 157–163. doi: 10.1016/j.cplett.2010.04.027

Dietzek, B., Tschierlei, S., Hermann, G., Yartsev, A., Pascher, T., Sundström, V., et al. (2009). Protochlorophyllide a: a comprehensive photophysical picture. *ChemPhysChem* 10, 144–150. doi: 10.1002/cphc.200800536

Dogbo, O., and Camara, B. (1987). Purification of isopentenyl pyrophosphate isomerase and geranylgeranyl pyrophosphate synthase from Capsicum chromoplasts by affinity chromatography. *Biochim. Biophys. Acta Lipids Lipid Metab.* 920, 140–148. doi: 10.1016/0005-2760(87)90253-0

Dong, C. S., Zhang, W. L., Wang, Q., Li, Y. S., Wang, X., Zhang, M., et al. (2020). Crystal structures of cyanobacterial light-dependent protochlorophyllide oxidoreductase. *Proc. Natl. Acad. Sci. U.S.A.* 117, 8455–8461. doi: 10.1073/pnas.1920244117

Eady, R. A. J., and Odland, G. F. (1975). Intraendothelial tubular aggregates in experimental wounds. *Br. J. Dermatol.* 93, 165–173. doi: 10.1111/j.1365-2133.1975.tb06736.x

Eggink, L. L., LoBrutto, R., Brune, D. C., Brusslan, J., Yamasato, A., Tanaka, A., et al. (2004). Synthesis of chlorophyll b: localization of chlorophyllide a oxygenase and discovery of a stable radical in the catalytic subunit. *BMC Plant Biol.* 4:5. doi: 10.1186/1471-2229-4-5

Elmaghrabi, A., Brown, E., Khin, E., Hassler, J., and Hendricks, A. R. (2017). Tubuloreticular inclusions in the absence of systemic lupus erythematosus and HIV infection: a report of three pediatric cases. *Case Rep. Nephrol. Dial.* 7, 91–101. doi: 10.1159/000477661

Engdahl, S., Aronsson, H., Sundqvist, C., Timko, M. P., and Dahlin, C. (2001). Association of the NADPH:protochlorophyllide oxidoreductase (POR) with isolated etioplast inner membranes from wheat. *Plant J.* 27, 297–304. doi: 10.1046/j.1365-313x.2001.01094.x

Erdei, N., Barta, C., Hideg, É., and Böddi, B. (2005). Light-induced wilting and its molecular mechanism in epicotyls of dark-germinated pea (*Pisum sativum* L.) seedlings. *Plant Cell Physiol.* 46, 185–191. doi: 10.1093/pcp/pci012

Espineda, C. E., Linford, A. S., Devine, D., and Brusslan, J. A. (1999). The AtCAO gene, encoding chlorophyll a oxygenase, is required for chlorophyll b synthesis in *Arabidopsis thaliana*. *Proc. Natl. Acad. Sci. U.S.A.* 96, 10507–10511. doi: 10.1073/pnas.96.18.10507

Feldman, D., Hoar, R. M., Niemann, W. H., Valentine, T., Cukierski, M., and Hendrickx, A. G. (1986). Tubuloreticular inclusions in placental chorionic villi of rhesus monkeys after maternal treatment with interferon. *Am. J. Obstet. Gynecol.* 155, 413–424. doi: 10.1016/0002-9378(86)90844-6

Fiedor, L., Kania, A., Mysliwa-Kurdziel, B., Orzeł, Ł., and Stochel, G. (2008). Understanding chlorophylls: central magnesium ion and phytyl as structural determinants. *Biochim. Biophys. Acta Bioenerg.* 1777, 1491–1500. doi: 10.1016/j.bbabio.2008.09.005

Fiedor, L., Stasiek, M., Mysliwa-Kurdziel, B., and Strzałka, K. (2003). Phytol as one of the determinants of chlorophyll interactions in solution. *Photosynth. Res.* 78, 47–57. doi: 10.1023/A:1026042005536

Fiedor, L., Zbyradowski, M., and Pilch, M. (2019). "Tetrapyrrole pigments of photosynthetic antennae and reaction centers of higher plants: structures, biophysics, functions, biochemistry, mechanisms of regulation, applications," in *Advances in Botanical Research*, Vol. 90, ed B. Grimm (London: Academic Press), 1–33. doi: 10.1016/bs.abr.2019.04.001

Franck, F., Sperling, U., Frick, G., Pochert, B., Van Cleve, B., Apel, K., et al. (2000). Regulation of etioplast pigment-protein complexes, inner membrane architecture and protochlorophyllide a chemical heterogeneity by light-dependent I NADPH:protochlorophyllide oxidoreductases A and B. *Plant Physiol.* 124, 1678–1696. doi: 10.1104/pp.124.4.1678

Frick, G., Su, Q., Apel, K., and Armstrong, G. A. (2003). An Arabidopsis porB porC double mutant lacking light-dependent NADPH:protochlorophyllide oxidoreductases B and C is highly chlorophyll-deficient and developmentally arrested. *Plant J.* 35, 141–153. doi: 10.1046/j.1365-313X.2003.01798.x

Fujii, S., Kobayashi, K., Nagata, N., Masuda, T., and Wada, H. (2017). Monogalactosyldiacylglycerol facilitates synthesis of photoactive protochlorophyllide in etioplasts. *Plant Physiol.* 174, 2183–2198. doi: 10.1104/pp.17.00304

Fujii, S., Kobayashi, K., Nagata, N., Masuda, T., and Wada, H. (2018). Digalactosyldiacylglycerol is essential for organization of the membrane structure in etioplasts. *Plant Physiol.* 177, 1487–1497. doi: 10.1104/pp.18.00227

Fujii, S., Kobayashi, K., Nakamura, Y., and Wada, H. (2014). Inducible knockdown of monogalactosyldiacylglycerol synthase1 reveals roles of galactolipids in organelle differentiation in arabidopsis cotyledons. *Plant Physiol.* 166, 1436–1449. doi: 10.1104/pp.114.250050

Fujii, S., Nagata, N., Masuda, T., Wada, H., and Kobayashi, K. (2019a). Galactolipids are essential for internal membrane transformation during etioplast-to-chloroplast differentiation. *Plant Cell Physiol.* 60, 1224–1238. doi: 10.1093/pcp/pcz041

Fujii, S., Wada, H., and Kobayashi, K. (2019b). Role of galactolipids in plastid differentiation before and after light exposure. *Plants* 8, 1–17. doi: 10.3390/plants8100357

Fujita, Y. (1996). Protochlorophyllide reduction: a key step in the greening of plants. *Plant Cell Physiol.* 37, 411–421. doi: 10.1093/oxfordjournals.pcp.a028962

Fusada, N., Masuda, T., Kuroda, H., Shiraishi, T., Shimada, H., Ohta, H., et al. (2000). NADPH-protochlorophyllide oxidoreductase in cucumber is encoded by a single gene and its expression is transcriptionally enhanced by illumination. *Photosynth. Res.* 64, 147–154. doi: 10.1023/A:1006418608647

Gabruk, M., Grzyb, J., Kruk, J., and Mysliwa-Kurdziel, B. (2012). Light-dependent and light-independent protochlorophyllide oxidoreductases share similar sequence motifs -in silico studies. *Photosynthetica* 50, 529–540. doi: 10.1007/s11099-012-0057-z

Gabruk, M., and Mysliwa-Kurdziel, B. (2015). Light-dependent protochlorophyllide oxidoreductase: phylogeny, regulation, and catalytic properties. *Biochemistry* 54, 5255–5262. doi: 10.1021/acs.biochem.5b00704

Gabruk, M., and Mysliwa-Kurdziel, B. (2020). The origin, evolution and diversification of multiple isoforms of light-dependent protochlorophyllide oxidoreductase (LPOR): focus on angiosperms. *Biochem. J.* 477, 2221–2236. doi: 10.1042/BCJ20200323

Gabruk, M., Mysliwa-Kurdziel, B., and Kruk, J. (2017). MGDG, PG and SQDG regulate the activity of lightdependent protochlorophyllide oxidoreductase. *Biochem. J.* 474, 1307–1320. doi: 10.1042/BCJ20170047

Gabruk, M., Nowakowska, Z., Skupien-Rabian, B., Kędracka-Krok, S., Mysliwa-Kurdziel, B., and Kruk, J. (2016). Insight into the oligomeric structure of PORA from *A. thaliana*. *Biochim. Biophys. Acta Proteins Proteomics* 1864, 1757–1764. doi: 10.1016/j.bbapap.2016.09.015

Gabruk, M., Stecka, A., Strzałka, W., Kruk, J., Strzałka, K., and Mysliwa-Kurdziel, B. (2015). Photoactive protochlorophyllide-enzyme complexes reconstituted with PORA, PORB and PORC proteins of *A. thaliana*: fluorescence and catalytic properties. *PLoS ONE* 10:e0116990. doi: 10.1371/journal.pone.0116990

Garrone, A., Archipowa, N., Zipfel, P. F., Hermann, G., and Dietzek, B. (2015). Plant protochlorophyllide oxidoreductases A and B: catalytic efficiency and initial reaction steps. *J. Biol. Chem.* 290, 28530–28539. doi: 10.1074/jbc.M115.663161

Gaubier, P., Wu, H. J., Laudié, M., Delseny, M., and Grellet, F. (1995). A chlorophyll synthetase gene from *Arabidopsis thaliana*. *MGG Mol. Gen. Genet.* 249, 58–64. doi: 10.1007/BF00290236

Geisbert, T. W., Jahrling, P. B., Hanes, M. A., and Zack, P. M. (1992). Association of Ebola-related Reston virus particles and antigen with tissue lesions of monkeys imported to the United States. *J. Comp. Pathol.* 106, 137–152. doi: 10.1016/0021-9975(92)90043-T

Gholami, S., Nenov, A., Rivalta, I., Bocola, M., Bordbar, A. K., Schwaneberg, U., et al. (2018). Theoretical model of the protochlorophyllide oxidoreductase from a hierarchy of protocols. *J. Phys. Chem. B* 122, 7668–7681. doi: 10.1021/acs.jpcb.8b04231

Granick, S., and Gassman, M. (1970). Rapid regeneration of protochlorophyllide650. *Plant Physiol.* 45, 201–205. doi: 10.1104/pp.45.2.201

Grevby, C., Engdahl, S., Ryberg, M., and Sundqvist, C. (1989). Binding properties of NADPH-protochlorophyllide oxidoreductase as revealed by detergent and ion treatments of isolated and immobilized prolamellar bodies. *Physiol. Plant.* 77, 493–503. doi: 10.1111/j.1399-3054.1989.tb05382.x

Griffiths, W. T. (1974). Protochlorophyll and protochlorophyllide as precursors for chlorophyll synthesis *in vitro*. *FEBS Lett.* 49, 196–200. doi: 10.1016/0014-5793(74)80510-7

Grimley, P., Davis, G., Kang, Y., Dooley, J., Strohmaier, J., and Hoofnagle, J. (1985). Tubuloreticular inclusions in peripheral blood mononuclear cells related to systemic therapy with alpha-interferon. *Lab Invest.* 52, 638–649.

Grimley, P., and Schaff, Z. (1976). Significance of tubuloreticular inclusions in the pathobiology of human diseases. *Pathobiol Annu.* 6, 221–257.

Grimley, P. M., Decker, J. L., Michelitch, H. J., and Frantz, M. M. (1973). Abnormal structures in circulating lymphocytes from patients with systemic lupus erythematosus and related diseases. *Arthritis Rheum.* 16, 313–323. doi: 10.1002/art.1780160305

Grimm, B. (2010). "Chapter 3: Control of the metabolic flow in tetrapyrrole biosynthesis: regulation of expression and activity of enzymes in the Mg branch of tetrapyrrole biosynthesis," in *The Chloroplast, Advances in Photosynthesis and Respiration,* Vol. 31, eds C. A. Rebeiz, C. Benning, H. Bohnert, H. Daniell, J. K. Hoober, H. K. Lichtenthaler, et al. (Dordrecht: Springer), 39–54.

Gunning, B. (2001). Membrane geometry of "open" prolamellar bodies. *Protoplasma* 215, 4–15. doi: 10.1007/BF01280299

Gunning, B. E. S. (1965). The greening process in plastids - 1. The structure of the prolamellar body. *Protoplasma* 60, 111–130. doi: 10.1007/BF01248133

Gutbrod, K., Romer, J., and Dörmann, P. (2019). Phytol metabolism in plants. *Prog. Lipid Res.* 74, 1–17. doi: 10.1016/j.plipres.2019.01.002

Hammond, C. T., and Mahlberg, P. G. (1978). Ultrastructural development of capitate glandular hairs of *Cannabis sativa* L. (Cannabaceae). *Am. J. Bot.* 65, 140–151. doi: 10.1002/j.1537-2197.1978.tb06051.x

Harper, A. L., Von Gesjen, S. E., Linford, A. S., Peterson, M. P., Faircloth, R. S., Thissen, M. M., et al. (2004). Chlorophyllide a oxygenase mRNA and protein levels correlate with the chlorophyll a/b ratio in *Arabidopsis thaliana*. *Photosynth. Res.* 79, 149–159. doi: 10.1023/B:PRES.0000015375.40167.76

Helfrich, M., Schoch, S., Schäfer, W., Ryberg, M., and Rüdiger, W. (1996). Absolute configuration of protochlorophyllide a and substrate specificity of NADPH-protochlorophyllide oxidoreductase. *J. Am. Chem. Soc.* 118, 2606–2611. doi: 10.1021/ja953440c

Helfrich, M., Schoch, S., Ulrika, L., Cmiiel, E., and Rudiger, W. (1994). Chlorophyll synthetase cannot synthesize chlorophyll a′. *Eur. J. Biochem.* 219, 267–275. doi: 10.1111/j.1432-1033.1994.tb19938.x

Herbst, J., Girke, A., Hajirezaei, M. R., Hanke, G., and Grimm, B. (2018). Potential roles of YCF54 and ferredoxin-NADPH reductase for magnesium protoporphyrin monomethylester cyclase. *Plant J.* 94, 485–496. doi: 10.1111/tpj.13869

Herbst, J., Hey, D., and Grimm, B. (2019). "Posttranslational control of tetrapyrrole biosynthesis: interacting proteins, chaperones, auxiliary factors," in *Advances in Botanical Research*, Vol. 91, ed B. Grimm (London: Academic Press), 163–194. doi: 10.1016/bs.abr.2019.01.001

Hernández-Verdeja, T., Vuorijoki, L., and Strand, Å. (2020). Emerging from the darkness: interplay between light and plastid signaling during chloroplast biogenesis. *Physiol. Plant.* 169, 397–406. doi: 10.1111/ppl.13100

Hey, D., Rothbart, M., Herbst, J., Wang, P., Müller, J., Wittmann, D., et al. (2017). LIL3, a light-harvesting complex protein, links terpenoid and tetrapyrrole biosynthesis in *Arabidopsis thaliana*. *Plant Physiol.* 174, 1037–1050. doi: 10.1104/pp.17.00505

Heyes, D. J., Hardman, S. J. O., Hedison, T. M., Hoeven, R., Greetham, G. M., Towrie, M., et al. (2015). Excited-state charge separation in the photochemical mechanism of the light-driven enzyme protochlorophyllide oxidoreductase. *Angew. Chemie Int. Ed.* 54, 1512–1515. doi: 10.1002/anie.201409881

Heyes, D. J., Hardman, S. J. O., Mansell, D., Ní Cheallaigh, A., Gardiner, J. M., Johannissen, L. O., et al. (2017). Excited-state properties of protochlorophyllide analogues and implications for light-driven synthesis of chlorophyll. *J. Phys. Chem. B* 121, 1312–1320. doi: 10.1021/acs.jpcb.7b00528

Heyes, D. J., and Hunter, C. N. (2005). Making light work of enzyme catalysis: protochlorophyllide oxidoreductase. *Trends Biochem. Sci.* 30, 642–649. doi: 10.1016/j.tibs.2005.09.001

Heyes, D. J., Ruban, A. V., and Hunter, C. N. (2003). Protochlorophyllide oxidoreductase: "dark" reactions of a light-driven enzyme. *Biochemistry* 42, 523–528. doi: 10.1021/bi0268448

Heyes, D. J., Ruban, A. V., Wilks, H. M., and Hunter, C. N. (2002). Enzymology below 200 K: the kinetics and thermodynamics of the photochemistry catalyzed by protochlorophyllide oxidoreductase. *Proc. Natl. Acad. Sci. U.S.A.* 99, 11145–11150. doi: 10.1073/pnas.182274199

Hideg, É., Vitányi, B., Kósa, A., Solymosi, K., Bóka, K., Won, S., et al. (2010). Reactive oxygen species from type-I photosensitized reactions contribute to the light-induced wilting of dark-grown pea (*Pisum sativum*) epicotyls. *Physiol. Plant.* 138, 485–492. doi: 10.1111/j.1399-3054.2009.01329.x

Holtorf, H., Reinbothe, S., Reinbothe, C., Bereza, B., and Apel, K. (1995). Two routes of chlorophyllide synthesis that are differentially regulated by light in barley (*Hordeum vulgare* L.). *Proc. Natl. Acad. Sci. U.S.A.* 92, 3254–3258. doi: 10.1073/pnas.92.8.3254

Hulanicka, B., Barry, D. W., and Grimley, P. M. (1977). Induction of tubuloreticular inclusions in human lymphoma cells (Raji line) related to S-phase treatment with halogenated pyrimidines. *Cancer Res.* 37, 2105–2113.

Hurd, E., Eigenbrodt, E., Ziff, M., and Strunk, S. (1969). Cytoplasmic tubular structures in kidney biopsies in systemic lupus erythematosus. *Arthritis Rheum.* 12, 541–542. doi: 10.1002/art.1780120517

Ikeda, T. (1970). Changes in Fine Structure of prolamellar body in relation to the formation of the chloroplast. *Bot. Mag. Tokyo* 83, 1–9. doi: 10.15281/jplantres1887.83.1

Ikeda, T. (1971). Prolamellar body formation under different light and temperature conditions. *Shokubutsugaku Zasshi* 84, 363–375. doi: 10.15281/jplantres1887.84.363

Ikeuchi, M., and Murakami, S. (1983). Separation and characterization of prolamellar bodies and prothylakoids from squash etioplasts. *Plant Cell Physiol.* 24, 71–80. doi: 10.1093/oxfordjournals.pcp.a076515

Ioannides, I. M., Fasoula, D. A., Robertson, K. R., and Rebeiz, C. A. (1994). An evolutionary study of chlorophyll biosynthetic heterogeneity in green plants. *Biochem. Syst. Ecol.* 22, 211–220. doi: 10.1016/0305-1978(94)90010-8

Jörnvall, H., Persson, B., Krook, M., Atrian, S., Gonzàlez-Duarte, R., Jeffery, J., et al. (1995). Short-chain dehydrogenases/reductases(SDR). *Biochemistry* 34, 6003–6013. doi: 10.1021/bi00018a001

Joyard, J., Block, M., Pineau, B., Albrieux, C., and Douce, R. (1990). Envelope membranes from mature spinach chloroplasts contain a NADPH:protochlorophyllide reductase on the cytosolic side of the outer membrane. *J. Biol. Chem.* 265, 21820–21827. doi: 10.1016/S0021-9258(18)45813-9

Joyard, J., Ferro, M., Masselon, C., Seigneurin-Berny, D., Salvi, D., Garin, J., et al. (2009). Chloroplast proteomics and the compartmentation of plastidial isoprenoid biosynthetic pathways. *Mol. Plant* 2, 1154–1180. doi: 10.1093/mp/ssp088

Kahn, A., Boardman, N. K., and Thorne, S. W. (1970). Energy transfer between protochlorophyllide molecules: evidence for multiple chromophores in the photoactive protochlorophyllide-protein complex *in vivo* and *in vitro*. *J. Mol. Biol.* 48, 85–101. doi: 10.1016/0022-2836(70)90220-2

Kakuszi, A., Solymosi, K., and Böddi, B. (2017). Transformation of plastids in soil-shaded lowermost hypocotyl segments of bean (*Phaseolus vulgaris*) during a 60-day cultivation period. *Physiol. Plant.* 159, 483–491. doi: 10.1111/ppl.12519

Kanervo, E., Singh, M., Suorsa, M., Paakkarinen, V., Aro, E., Battchikova, N., et al. (2008). Expression of protein complexes and individual proteins upon transition of etioplasts to chloroplasts in pea (*Pisum sativum*). *Plant Cell Physiol.* 49, 396–410. doi: 10.1093/pcp/pcn016

Kang, Y. H., Yaffe, L., and Grimley, P. M. (1984). Immunoelectron microscopic application of monoclonal antibodies for identification of lymphocyte subsets bearing tubuloreticular inclusions or parallel tubular arrays. *J. Exp. Pathol.* 1, 157–173.

Kaschner, M., Loeschcke, A., Krause, J., Minh, B. Q., Heck, A., Endres, S., et al. (2014). Discovery of the first light-dependent protochlorophyllide oxidoreductase in anoxygenic phototrophic bacteria. *Mol. Microbiol.* 93, 1066–1078. doi: 10.1111/mmi.12719

Kashina, T. K., and Danilova, M. F. (1993). Ultrastructure of glandular hair plastids and nictophylness of *Perilla ocymoides* L. *Russ. J. Plant Physiol.* 40, 785–790.

Kauss, D., Bischof, S., Steiner, S., Apel, K., and Meskauskiene, R. (2012). FLU, a negative feedback regulator of tetrapyrrole biosynthesis, is physically linked to the final steps of the Mg ++ -branch of this pathway. *FEBS Lett.* 586, 211–216. doi: 10.1016/j.febslet.2011.12.029

Keller, Y., Bouvier, F., D'Harlingue, A., and Camara, B. (1998). Metabolic compartmentation of plastid prenyllipid biosynthesis - evidence for the involvement of a multifunctional geranylgeranyl reductase. *Eur. J. Biochem.* 251, 413–417. doi: 10.1046/j.1432-1327.1998.2510413.x

Kim, C., Ham, H., and Apel, K. (2005). Multiplicity of different cell- and organ-specific import routes for the NADPH-protochlorophyllide oxidoreductases A and B in plastids of Arabidopsis seedlings. *Plant J.* 42, 329–340. doi: 10.1111/j.1365-313X.2005.02374.x

Kim, E.-S., and Mahlberg, P. G. (1997). Plastid development in disc cells of glandular trichomes of Cannabis (Cannabaceae). *Mol. Cells* 7, 352–359.

Kim, S., Schlicke, H., Van Ree, K., Karvonen, K., Subramaniam, A., Richter, A., et al. (2013). Arabidopsis chlorophyll biosynthesis: an essential balance between the methylerythritol phosphate and tetrapyrrole pathways. *Plant Cell* 25, 4984–4993. doi: 10.1105/tpc.113.119172

Klement, H., Oster, U., and Rüdiger, W. (2000). The influence of glycerol and chloroplast lipids on the spectral shifts of pigments associated with NADPH:protochlorophyllide oxidoreductase from *Avena sativa* L. *FEBS Lett.* 480, 306–310. doi: 10.1016/S0014-5793(00)01887-1

Knaust, R., Seyfried, B., Schmidt, L., Schulz, R., and Senger, H. (1993). Phototransformation of monovinyl and divinyl protochlorophyllide by NADPH:protochlorophyllide oxidoreductase of barley expressed in *Escherichia coli*. *J. Photochem. Photobiol. B Biol.* 20, 161–166. doi: 10.1016/1011-1344(93)80146-Z

Kobayashi, K. (2016). Role of membrane glycerolipids in photosynthesis, thylakoid biogenesis and chloroplast development. *J. Plant Res.* 129, 565–580. doi: 10.1007/s10265-016-0827-y

Kobayashi, K. (2018). Correction to: role of membrane glycerolipids in photosynthesis, thylakoid biogenesis and chloroplast development (Journal of Plant Research, (2016), 129, 4, (565-580), 10.1007/s10265-016-0827-y). *J. Plant Res.* 131:563. doi: 10.1007/s10265-018-1011-3

Kobayashi, K., Fujii, S., Sasaki, D., Baba, S., Ohta, H., Masuda, T., et al. (2014). Transcriptional regulation of thylakoid galactolipid biosynthesis coordinated with chlorophyll biosynthesis during the development of chloroplasts in Arabidopsis. *Front. Plant Sci.* 5:272. doi: 10.3389/fpls.2014.00272

Kobayashi, K., and Masuda, T. (2016). Transcriptional regulation of tetrapyrrole biosynthesis in *Arabidopsis thaliana*. *Front. Plant Sci.* 7:1811. doi: 10.3389/fpls.2016.01811

Kobayashi, K., Mochizuki, N., Yoshimura, N., Motohashi, K., Hisabori, T., and Masuda, T. (2008). Functional analysis of *Arabidopsis thaliana* isoforms of the Mg-chelatase CHLI subunit. *Photochem. Photobiol. Sci.* 7, 1188–1195. doi: 10.1039/b802604c

Kobayashi, K., and Wada, H. (2016). "Role of lipids in chloroplast biogenesis," in *Lipids in Plant and Algae Development. Subcellular Biochemistry*, Vol. 86, eds Y. Nakamura, and Y. Li-Beisson (Cham: Springer). doi: 10.1007/978-3-319-25979-6_5

Kong, W., Yu, X., Chen, H., Liu, L., Xiao, Y., Wang, Y., et al. (2016). The catalytic subunit of magnesium-protoporphyrin IX monomethyl ester cyclase forms a chloroplast complex to regulate chlorophyll biosynthesis in rice. *Plant Mol. Biol.* 92, 177–191. doi: 10.1007/s11103-016-0513-4

Kostianovsky, M., Kang, Y. H., and Grimley, P. M. (2016). Disseminated tubuloreticular inclusions in acquired immunodeficiency syndrome (AIDS). *Ultrastruct. Pathol.* 4, 331–336. doi: 10.3109/01913128309140585

Kotzabasis, K., Senge, M., Seyfried, B., and Senger, H. (1990). Aggregation of monovinyl- and divinyl-protochlorophyllide in organic solvents. *Photochem. Photobiol.* 52, 95–101. doi: 10.1111/j.1751-1097.1990.tb01761.x

Kovács, E., and Keresztes, A. (2002). Effect of gamma and UV-B/C radiation on plant cells. *Micron* 33, 199–210. doi: 10.1016/S0968-4328(01)00012-9

Kowalewska, Ł., Bykowski, M., and Mostowska, A. (2019). Spatial organization of thylakoid network in higher plants. *Bot. Lett.* 166, 326–343. doi: 10.1080/23818107.2019.1619195

Kowalewska, L., Mazur, R., Suski, S., Garstka, M., and Mostowska, A. (2016). Three-dimensional visualization of the tubular-lamellar transformation of the internal plastid membrane network during runner bean chloroplast biogenesis. *Plant Cell.* 28, 875–891. doi: 10.1105/tpc.15.01053

Krohn, K., and Sandholm, M. (1975). Myxovirus-like structures in the glomerular endothelial cell cytoplasm in canine nephritis. *Acta Pathol Microbiol. Scand. A* 83, 355–359. doi: 10.1111/j.1699-0463.1975.tb01883.x

Kruk, J., and Mysliwa-Kurdziel, B. (2004). Separation of monovinyl and divinyl protochlorophyllides using C-30 reverse phase high performance liquid chromatography column: analytical and preparative applications. *Chromatographia* 60, 117–123. doi: 10.1365/s10337-004-0320-y

Kuntz, M., Römer, S., Suire, C., Hugueney, P., Weil, J. H., Schantz, R., et al. (1992). Identification of a cDNA for the plastid-located geranylgeranyl pyrophosphate synthase from *Capsicum annuum*: correlative increase in enzyme activity and transcript level during fruit ripening. *Plant J.* 2, 25–34. doi: 10.1046/j.1365-313X.1992.t01-47-00999.x

Kwon, C. T., Kim, S. H., Song, G., Kim, D., and Paek, N. C. (2017). Two NADPH: protochlorophyllide oxidoreductase (POR) isoforms play distinct roles in environmental adaptation in rice. *Rice* 10, 1–14. doi: 10.1186/s12284-016-0141-2

La Rocca, N., Rascio, N., Oster, U., and Rüdiger, W. (2007). Inhibition of lycopene cyclase results in accumulation of chlorophyll precursors. *Planta* 225, 1019–1029. doi: 10.1007/s00425-006-0409-7

Laferrière, A., and Beyer, P. (1991). Purification of geranylgeranyl diphosphate synthase from *Sinapis alba* etioplasts. *Biochim. Biophys. Acta Protein Struct. Mol.* 1077, 167–172. doi: 10.1016/0167-4838(91)90054-4

Landolt, A., Ryffel, U., Hosbach, H., and Wyler, R. (1976). Ultrastructure of tubular inclusions in endothelial cells of pituitary tumors associated with acromegaly. *Virchows Arch. A Path. Anat. Histol.* 370, 129–140. doi: 10.1007/BF00430809

Larkin, R. M., Alonso, J. M., Ecker, J. R., and Chory, J. (2003). GUN4, a regulator of chlorophyll synthesis and intracellular signaling. *Science* 299, 902–906. doi: 10.1126/science.1079978

Larsson, M., and Larsson, K. (2014). Periodic minimal surface organizations of the lipid bilayer at the lung surface and in cubic cytomembrane assemblies. *Adv. Colloid Interface Sci.* 205, 68–73. doi: 10.1016/j.cis.2013.07.003

Lee, C., Suh, K., and Kim, K. (2013a). The clinicopathologic significance of endothelial tubuloreticular inclusions in glomerular diseases. *Ultrastruct. Pathol.* 37, 386–394. doi: 10.3109/01913123.2013.814738

Lee, J. Y., Lee, H. S., Song, J. Y., Jung, Y. J., Reinbothe, S., Park, Y., et al. (2013b). Cell growth defect factor1/CHAPERONE-LIKE PROTEIN OF POR1 plays a role in stabilization of light-dependent protochlorophyllide oxidoreductase in *Nicotiana benthamiana* and Arabidopsis. *Plant Cell* 25, 3944–3960. doi: 10.1105/tpc.113.111096

Lee, J. Y., Song, S. H., Kim, Y. S., Lim, B. J., Il Kim, S., Kim, M. S., et al. (2017). Tubuloreticular inclusions in peritubular capillaries of renal allografts. *Pathol. Res. Pract.* 213, 1185–1190. doi: 10.1016/j.prp.2017.06.009

Lee, S., Harris, C., Hirschfeld, A., and Dickson, D. W. (1988). Cytomembranous inclusions in the brain of a patient with the acquired immunodeficiency syndrome. *Acta Neuropathol.* 76, 101–106. doi: 10.1007/BF00687686

Lichtenthaler, H. K., Schwender, J., Disch, A., and Rohmer, M. (1997). Biosynthesis of isoprenoids in higher plant chloroplasts proceeds via a mevalonate-independent pathway. *FEBS Lett.* 400, 271–274. doi: 10.1016/S0014-5793(96)01404-4

Liebers, M., Grübler, B., Chevalier, F., Lerbs-Mache, S., Merendino, L., Blanvillain, R., et al. (2017). Regulatory shifts in plastid transcription play a key role in morphological conversions of plastids during plant development. *Front. Plant Sci.* 8:23. doi: 10.3389/fpls.2017.00023

Lindquist, E., and Aronsson, H. (2018). Chloroplast vesicle transport. *Photosynth. Res.* 138, 361–371. doi: 10.1007/s11120-018-0566-0

Lindquist, E., Solymosi, K., and Aronsson, H. (2016). Vesicles are persistent features of different plastids. *Traffic* 17, 1125–1138. doi: 10.1111/tra.12427

Liu, X., Li, L., Li, M., Su, L., Lian, S., Zhang, B., et al. (2018). AhGLK1 affects chlorophyll biosynthesis and photosynthesis in peanut leaves during recovery from drought. *Sci. Rep.* 8:2250. doi: 10.1038/s41598-018-20542-7

Liu, X., Li, L., Zhang, B., Zeng, L., and Li, L. (2020). AhHDA1-mediated AhGLK1 promoted chlorophyll synthesis and photosynthesis regulates recovery growth of peanut leaves after water stress. *Plant Sci.* 294:110461. doi: 10.1016/j.plantsci.2020.110461

Lütz, C., and Tönissen, H. (1984). Effects of enzymatic cleavage on prolamellar bodies and prothylakoids prepared from oat ehoplasts. *Isr. J. Bot.* 33, 195–209.

Luu, J., Bockus, D., Remington, F., Bean, M. A., and Hammar, S. P. (1989). Tubuloreticular structures and cylindrical confronting cisternae: a review. *Hum. Pathol.* 20, 617–627. doi: 10.1016/0046-8177(89)90148-2

Madewell, B., and Munn, R. (1989). Tubuloreticular inclusions in equine connective tissue neoplasms. *J. Comp. Pathol.* 100, 449–452. doi: 10.1016/0021-9975(89)90011-X

Madewell, B. R., and Munn, R. J. (1990). Canine lymphoproliferative disorders. *J. Vet. Intern. Med.* 4, 63–70. doi: 10.1111/j.1939-1676.1990.tb03105.x

Mageed, H. A. A., El, El Sahhar, K. F., Robertson, K. R., Parham, R., and Rebeiz, C. A. (1997). Chloroplast biogenesis 77: two novel monovinyl and divinyl light-dark greening groups of plants and their relationship to the chlorophyll a biosynthetic heterogeneity of green plants. *Photochem. Photobiol.* 66, 89–96. doi: 10.1111/j.1751-1097.1997.tb03143.x

Manzano, D., Andrade, P., Caudepón, D., Altabella, T., Arró, M., and Ferrer, A. (2016). Suppressing farnesyl diphosphate synthase alters chloroplast development and triggers sterol-dependent induction of jasmonate- and Fe-related responses. *Plant Physiol.* 172, 93–117. doi: 10.1104/pp.16.00431

Marquart, K. H. (2005). Occurrence of tubuloreticular structures and intracisternal paracrystalline inclusions in endothelial cells of tissue from different epidemiological types of Kaposi's sarcoma. *Ultrastruct. Pathol.* 29, 85–93. doi: 10.1080/01913120590912205

Martin, G. E., Timko, M. P., and Wilks, H. M. (1997). Purification and kinetic analysis of pea (*Pisum sativum* L.) NADPH:protochlorophyllide oxidoreductase expressed as a fusion with maltose-binding protein in *Escherichia coli*. *Biochem. J.* 325, 139–45. doi: 10.1042/bj3250139

Masuda, T. (2008). Recent overview of the Mg branch of the tetrapyrrole biosynthesis leading to chlorophylls. *Photosynth. Res.* 96, 121–143. doi: 10.1007/s11120-008-9291-4

Masuda, T., Fusada, N., Oosawa, N., Takamatsu, K., Yamamoto, Y. Y., Ohto, M., et al. (2003). Functional analysis of isoforms of NADPH: protochlorophyllide oxidoreductase (POR), PORB and PORC, in *Arabidopsis thaliana*. *Plant Cell Physiol.* 44, 963–974. doi: 10.1093/pcp/pcg128

Masuda, T., Fusada, N., Shiraishi, T., Kuroda, H., Awai, K., Shimada, H., et al. (2002). Identification of two differentially regulated isoforms of protochlorophyllide oxidoreductase (POR) from tobacco revealed a wide variety of light- and development-dependent regulations of POR gene expression among angiosperms. *Photosynth. Res.* 74, 165–172. doi: 10.1023/A:1020951409135

Masuda, T., and Takamiya, K. I. (2004). Novel insights into the enzymology, regulation and physiological functions of light-dependent protochlorophyllide oxidoreductase in angiosperms. *Photosynth. Res.* 81, 1–29. doi: 10.1023/B:PRES.0000028392.80354.7c

Mathis, P., and Sauer, K. (1972). Circular dichroism studies on the structure and the photochemistry of protochlorophyllide and chlorophyllide holochrome. *Biochim. Biophys. Acta Bioenerg.* 267, 498–511. doi: 10.1016/0005-2728(72)90178-8

Matos, E., and Paiva, E. (2012). Structure, function and secretory products of the peltate glands of *Centrolobium tomentosum* (Fabaceae, Faboideae). *Aust. J. Bot.* 60, 301–309. doi: 10.1071/BT12009

Matsumura, H., Setoguti, T., Mori, K., Ross, E. R., and Koto, A. (1984). Endothelial tubuloreticular structures in intracranial germinomas. *Pathol. Int.* 34, 1–9. doi: 10.1111/j.1440-1827.1984.tb02176.x

Maturi, R. K., and Font, R. L. (1996). Ultrastructural features and prevalence of tubuloreticular structures in the ocular vasculature of patients with AIDS: a study of 23 cases. *Br. J. Ophthalmol.* 80, 252–255. doi: 10.1136/bjo.80.3.252

Mazur, R., Mostowska, A., Szach, J., Gieczewska, K., Wójtowicz, J., Bednarska, K., et al. (2019). Galactolipid deficiency disturbs spatial arrangement of the thylakoid network in *Arabidopsis thaliana* plants. *J. Exp. Bot.* 70, 4689–4703. doi: 10.1093/jxb/erz219

Menon, B. R. K., Hardman, S. J. O., Scrutton, N. S., and Heyes, D. J. (2016). Multiple active site residues are important for photochemical efficiency in the light-activated enzyme protochlorophyllide oxidoreductase (POR). *J. Photochem. Photobiol. B Biol.* 161, 236–243. doi: 10.1016/j.jphotobiol.2016.05.029

Meskauskiene, R., and Apel, K. (2002). Interaction of FLU, a negative regulator of tetrapyrrole biosynthesis, with the glutamyl-tRNA reductase requires the tetratricopeptide repeat domain of FLU. *FEBS Lett.* 532, 27–30. doi: 10.1016/S0014-5793(02)03617-7

Meskauskiene, R., Nater, M., Goslings, D., Kessler, F., op den Camp, R., and Apel, K. (2001). FLU: a negative regulator of chlorophyll biosynthesis in *Arabidopsis thaliana*. *Proc. Natl. Acad. Sci. U.S.A.* 98, 12826–12831. doi: 10.1073/pnas.221252798

Mochizuki, N., Tanaka, R., Grimm, B., Masuda, T., Moulin, M., Smith, A. G., et al. (2010). The cell biology of tetrapyrroles: a life and death struggle. *Trends Plant Sci.* 15, 488–498. doi: 10.1016/j.tplants.2010.05.012

Monselise, E. B. I., Levkovitz, A., and Kost, D. (2015). Ultraviolet radiation induces stress in etiolated Landoltia punctata, as evidenced by the presence of alanine, a universal stress signal: a 15N NMR study. *Plant Biol.* 1, 101–107. doi: 10.1111/plb.12198

Mork-Jansson, A., Bue, A. K., Gargano, D., Furnes, C., Reisinger, V., Arnold, J., et al. (2015). Lil3 assembles with proteins regulating chlorophyll synthesis in barley. *PLoS ONE* 10:e133145. doi: 10.1371/journal.pone.0133145

Mysliwa-Kurdziel, B., Kruk, J., and Strzałka, K. (2004). Fluorescence lifetimes and spectral properties of protochlorophyllide in organic solvents in relation to the respective parameters *in vivo*. *Photochem. Photobiol.* 79, 62–67. doi: 10.1562/0031-8655(2004)79<62:FLASPO>2.0.CO;2

Mysliwa-Kurdziel, B., Kruk, J., and Strzałka, K. (2013a). Protochlorophyllide and protochlorophyll in model membranes - an influence of hydrophobic side chain moiety. *Biochim. Biophys. Acta* 1828, 1075–1082. doi: 10.1016/j.bbamem.2012.12.007

Mysliwa-Kurdziel, B., Kruk, J., and Strzałka, K. (2013b). Protochlorophyllide in model systems - an approach to *in vivo* conditions. *Biophys. Chem.* 175–176, 28–38. doi: 10.1016/j.bpc.2013.02.002

Mysliwa-Kurdziel, B., Solymosi, K., Kruk, J., Böddi, B., and Strzałka, K. (2008). Solvent effects on fluorescence properties of protochlorophyll and its derivatives with various porphyrin side chains. *Eur. Biophys. J.* 37, 1185–1193. doi: 10.1007/s00249-008-0288-x

Nagata, N., Suzuki, M., Yoshida, S., and Muranaka, T. (2002). Mevalonic acid partially restores chloroplast and etioplast development in Arabidopsis lacking the non-mevalonate pathway. *Planta* 216, 345–350. doi: 10.1007/s00425-002-0871-9

Nagata, N., Tanaka, R., and Tanaka, A. (2007). The major route for chlorophyll synthesis includes [3,8-divinyl]- chlorophyllide a reduction in *Arabidopsis thaliana*. *Plant Cell Physiol.* 48, 1803–1808. doi: 10.1093/pcp/pcm153

Nakanishi, H., Nozue, H., Suzuki, K., Kaneko, Y., Taguchi, G., and Hayashida, N. (2005). Characterization of the *Arabidopsis thaliana* mutant pcb2 which accumulates divinyl chlorophylls. *Plant Cell Physiol.* 46, 467–473. doi: 10.1093/pcp/pci053

Nguyen, H. C., Melo, A. A., Kruk, J., Frost, A., and Gabruk, M. (2021). Photocatalytic LPOR forms helical lattices that shape membranes for chlorophyll synthesis. *Nat. Plants*. doi: 10.1038/s41477-021-00885-2

Oosawa, N., Masuda, T., Awai, K., Fusada, N., Shimada, H., Ohta, H., et al. (2000). Identification and light-induced expression of a novel gene of NADPH-protochlorophyllide oxidoreductase isoform in *Arabidopsis thaliana*. *FEBS Lett.* 474, 133–136. doi: 10.1016/S0014-5793(00)01568-4

Opitz, S., Nes, W. D., and Gershenzon, J. (2014). Both methylerythritol phosphate and mevalonate pathways contribute to biosynthesis of each of the major isoprenoid classes in young cotton seedlings. *Phytochemistry* 98, 110–119. doi: 10.1016/j.phytochem.2013.11.010

Orenstein, J. M., Olivia, T., Kind, P., and Washington, G. (1987). The relationship of serum alpha-interferon and ultrastructural markers in HIV-seropositive individuals. *Ultrastruct. Pathol.* 11, 673–679. doi: 10.3109/01913128709048453

Oster, U., and Rüdiger, W. (1997). The G4 gene of *Arabidopsis thaliana* encodes a chlorophyll synthase of etiolated plants. *Bot. Acta* 110, 420–423. doi: 10.1111/j.1438-8677.1997.tb00658.x

Oster, U., Tanaka, R., Tanaka, A., and Rüdiger, W. (2000). Cloning and functional expression of the gene encoding the key enzyme for chlorophyll b biosynthesis (CAO) from *Arabidopsis thaliana*. *Plant J.* 21, 305–310. doi: 10.1046/j.1365-313x.2000.00672.x

Ouazzani Chahdi, M. A., Schoefs, B., and Franck, F. (1998). Isolation and characterization of photoactive complexes of NADPH:protochlorophyllide oxidoreductase from wheat. *Planta* 206, 673–680. doi: 10.1007/s004250050446

Paddock, T., Lima, D., Mason, M. E., Apel, K., and Armstrong, G. A. (2012). Arabidopsis light-dependent NADPH: protochlorophyllide oxidoreductase A (PORA) is essential for normal plant growth and development: an addendum. *Plant Mol. Biol.* 80, 237–240. doi: 10.1007/s11103-012-9944-8

Paddock, T. N., Mason, M. E., Lima, D. F., and Armstrong, G. A. (2010). Arabidopsis protochlorophyllide oxidoreductase A (PORA) restores bulk chlorophyll synthesis and normal development to a porB porC double mutant. *Plant Mol. Biol.* 72, 445–457. doi: 10.1007/s11103-009-9582-y

Parham, R., and Rebeiz, C. (1992). Chloroplast biogenesis: [4-vinyl] chlorophyllide a reductase is a divinyl chlorophyllide a-specific, NADPH-dependent enzyme. *Biochemistry* 31, 8460–8464. doi: 10.1021/bi00151a011

Park, H., Kreunen, S. S., Cuttriss, A. J., DellaPenna, D., and Pogson, B. J. (2002). Identification of the carotenoid isomerase provides insight into carotenoid biosynthesis, prolamellar body formation, and photomorphogenesis. *Plant Cell* 14, 321–332. doi: 10.1105/tpc.010302

Pellaud, S., and Saffrané, L. M. (2017). Metabolic origins and transport of vitamin E biosynthetic precursors. *Front. Plant Sci.* 8:1959. doi: 10.3389/fpls.2017.01959

Peter, E., and Grimm, B. (2009). GUN4 is required for posttranslational control of plant tetrapyrrole biosynthesis. *Mol. Plant* 2, 1198–1210. doi: 10.1093/mp/ssp072

Popoff, A., and Malinin, T. (1976). Cytoplasmic tubular arrays in cells of American Burkitt's type lymphoma. *Cancer* 37, 275–284. doi: 10.1002/1097-0142(197601)37:1<275::AID-CNCR2820370138>3.0.CO;2-V

Rassadina, V., Domanskii, V., Averina, N. G., Schoch, S., and Rüdiger, W. (2004). Correlation between chlorophyllide esterification, Shibata shift and regeneration of protochlorophyllide650 in flash-irradiated etiolated barley leaves. *Physiol. Plant.* 121, 556–567. doi: 10.1111/j.1399-3054.2004.00362.x

Rebeiz, C. A. (2014). "The Chl a carboxylic biosynthetic routes: reactions between Mg-Protoporphyrin IX and protochlorophyllide a," in *Chlorophyll Biosynthesis and Technological Applications* (Berlin: Springer), 197–214. doi: 10.1007/978-94-007-7134-5_7

Rebeiz, C. A., Ioannides, I. M., Kolossov, V., and Kopetz, K. J. (1999). Chloroplast biogenesis 80. Proposal of a unified multibranched chlorophyll a/b biosynthetic pathway. *Photosynthetica* 36, 117–128. doi: 10.1023/A:1007027005903

Reinbothe, C., Buhr, F., Bartsch, S., Desvignes, C., Quigley, F., Pesey, H., et al. (2006). *In vitro*-mutagenesis of NADPH:protochlorophyllide oxidoreductase B: two distinctive protochlorophyllide binding sites participate in enzyme catalysis and assembly. *Mol. Genet. Genomics* 275, 540–552. doi: 10.1007/s00438-006-0109-9

Reinbothe, C., El Bakkouri, M., Buhr, F., Muraki, N., Nomata, J., Kurisu, G., et al. (2010). Chlorophyll biosynthesis: spotlight on protochlorophyllide reduction. *Trends Plant Sci.* 15, 614–624. doi: 10.1016/j.tplants.2010.07.002

Reinbothe, C., Lebedev, N., and Reinbothe, S. (1999). A protochlorophyllide light-harvesting complex involved in de-etiolation of higher plants. *Nature* 397, 80–84. doi: 10.1038/16283

Reisinger, V., Plöscher, M., and Eichacker, L. A. (2008). Lil3 assembles as chlorophyll-binding protein complex during deetiolation. *FEBS Lett.* 582, 1547–1551. doi: 10.1016/j.febslet.2008.03.042

Richter, A. S., and Grimm, B. (2013). Thiol-based redox control of enzymes involved in the tetrapyrrole biosynthesis pathway in plants. *Front. Plant Sci.* 4:371. doi: 10.3389/fpls.2013.00371

Richter, A. S., Hochheuser, C., Fufezan, C., Heinze, L., Kuhnert, F., and Grimm, B. (2016). Phosphorylation of GENOMES UNCOUPLED 4 alters stimulation of Mg chelatase activity in angiosperms. *Plant Physiol.* 172, 1578–1595. doi: 10.1104/pp.16.01036

Rodriguez-Concepcion, M. (2010). Supply of precursors for carotenoid biosynthesis in plants. *Arch. Biochem. Biophys.* 504, 118–122. doi: 10.1016/j.abb.2010.06.016

Rodríguez-Concepción, M., and Boronat, A. (2015). Breaking new ground in the regulation of the early steps of plant isoprenoid biosynthesis. *Curr. Opin. Plant Biol.* 25, 17–22. doi: 10.1016/j.pbi.2015.04.001

Rossmann, M. G., Moras, D., and Olsen, K. W. (1974). Chemical and biological evolution of a nucleotide-binding protein. *Nature* 250, 194–199. doi: 10.1038/250194a0

Rüdiger, W. (2002). Biosynthesis of chlorophyll b and the chlorophyll cycle. *Photosynth. Res.* 74, 187–193. doi: 10.1023/A:1020959610952

Rüdiger, W. (2006). "Biosynthesis of chlorophylls a and b: the last steps," in *Chlorophylls and Bacteriochlorophylls. Advances in Photosynthesis and Respiration*, Vol. 25, eds B. Grimm, R. J. Porra, W. Rüdiger, and H. Scheer (Dordrecht: Springer), 189–200. doi: 10.1007/1-4020-4516-6_14

Rüdiger, W., Benz, J., and Guthoff, C. (1980). Detection and partial characterization of activity of chlorophyll synthetase in etioplast membranes. *Eur. J. Biochem.* 109, 193—200. doi: 10.1111/j.1432-1033.1980.tb04784.x

Rüdiger, W., Böhm, S., Helfrich, M., Schulz, S., and Schoch, S. (2005). Enzymes of the last steps of chlorophyll biosynthesis: modification of the substrate structure helps to understand the topology of the active centers. *Biochemistry* 44, 10864–10872. doi: 10.1021/bi0504198

Rudowska, Ł., Gieczewska, K., Mazur, R., Garstka, M., and Mostowska, A. (2012). Chloroplast biogenesis - Correlation between structure and function. *Biochim. Biophys. Acta Bioenerg.* 1817, 1380–1387. doi: 10.1016/j.bbabio.2012.03.013

Ruiz-Sola, M. Á., Coman, D., Beck, G., Barja, M. V., Colinas, M., Graf, A., et al. (2016). Arabidopsis GERANYLGERANYL DIPHOSPHATE SYNTHASE 11 is a hub isozyme required for the production of most photosynthesis-related isoprenoids. *New Phytol.* 209, 252–264. doi: 10.1111/nph.13580

Ryberg, M., Sandelius, A. S., and Selstam, E. (1983). Lipid composition of prolamellar bodies and prothylakoids of wheat etioplasts. *Physiol. Plant.* 57, 555–560. doi: 10.1111/j.1399-3054.1983.tb02785.x

Ryberg, M., and Sundqvist, C. (1982a). Characterization of prolamellar bodies and prothylakoids fractionated from wheat etioplasts. *Physiol. Plant.* 56, 125–132. doi: 10.1111/j.1399-3054.1982.tb00313.x

Ryberg, M., and Sundqvist, C. (1982b). Spectral forms of protochlorophyllide in prolamellar bodies and prothylakoids fractionated from wheat etioplasts. *Physiol. Plant.* 56, 133–138. doi: 10.1111/j.1399-3054.1982.tb00314.x

Ryberg, M., and Sundqvist, C. (1988). The regular ultrastructure of isolated prolamellar bodies depends on the presence of membrane- bound NADPH-protochlorophyllide oxidoreductase. *Physiol. Plant.* 73, 218–226. doi: 10.1111/j.1399-3054.1988.tb00589.x

Rzeznicka, K., Walker, C. J., Westergren, T., Kannangara, C. G., Von Wettstein, D., Merchant, S., et al. (2005). Xantha-I encodes a membrane subunit of the aerobic Mg-protoporphyrin IX monomethyl ester cyclase involved in chlorophyll biosynthesis. *Proc. Natl. Acad. Sci. U.S.A.* 102, 5886–5891. doi: 10.1073/pnas.0501784102

Salvi, D., Bournais, S., Moyet, L., Bouchnak, I., Kuntz, M., Bruley, C., et al. (2018). AT_CHLORO: the first step when looking for information about subplastidial localization of proteins. *Methods Mol. Biol.* 1829, 395–406. doi: 10.1007/978-1-4939-8654-5_26

Sandelius, A. S., and Selstam, E. (1984). Localization of galactolipid biosynthesis in etioplasts isolated from dark-grown wheat (*Triticum aestivum* L.). *Plant Physiol.* 76, 1041–1046. doi: 10.1104/pp.76.4.1041

Schaff, Z., Barry, D. W., and Grimley, P. M. (1973). Cytochemistry of tubuloreticular structures in lymphocytes from patients with systemic lupus erythematosus and in cultured human lymphoid cells. Comparison to a paramyxovirus. *Lab. Investig.* 29, 577–586.

Schaff, Z., Heine, U., and Dalton, A. J. (1972). Ultramorphological and ultracytochemical studies on tubuloreticular structures in lymphoid cells. *Cancer Res.* 32, 2696–2706.

Schaff, Z., Lapis, K., and Grimley, P. (1976). Undulating membraneous structures associated with the endoplasmic reticulum in tumour cells. *Int. J. Cancer* 18, 697–702. doi: 10.1002/ijc.2910180519

Schmid, H. C., Rassadina, V., Oster, U., Schoch, S., and Rüdiger, W. (2002). Pre-loading of chlorophyll synthase with tetraprenyl diphosphate is an obligatory step in chlorophyll biosynthesis. *Biol. Chem.* 383, 1769−1778. doi: 10.1515/BC.2002.198

Schneidewind, J., Krause, F., Bocola, M., Stadler, A. M., Davari, M. D., Schwaneberg, U., et al. (2019). Consensus model of a cyanobacterial light-dependent protochlorophyllide oxidoreductase in its pigment-free apo-form and photoactive ternary complex. *Commun. Biol.* 2:351. doi: 10.1038/s42003-019-0590-4

Schnepf, E. (1961). Piastidenstrukturen bei passiflora. *Protoplasma* 54, 310–313. doi: 10.1007/BF01260360

Schoch, S. (1978). The esterification of chlorophyllide a in greening bean leaves. *Zeitschrift für Naturforsch. C* 33, 712–714. doi: 10.1515/znc-1978-9-1018

Schoefs, B. (2005). Protochlorophyllide reduction - what is new in 2005? *Photosynthetica* 43, 329–343. doi: 10.1007/s11099-005-0056-4

Schoefs, B., and Bertrand, M. (2000). The formation of chlorophyll from chlorophyllide in leaves containing proplastids is a four-step process. *FEBS Lett.* 486, 243–246. doi: 10.1016/S0014-5793(00)02309-7

Schoefs, B., and Franck, F. (2003). Protochlorophyllide reduction: mechanisms and evolutions. *Photochem. Photobiol.* 78, 543–557. doi: 10.1562/0031-8655(2003)078<0543:PRMAE>2.0.CO;2

Schoefs, B., and Franck, F. (2008). The photoenzymatic cycle of NADPH: protochlorophyllide oxidoreductase in primary bean leaves (*Phaseolus vulgaris*) during the first days of photoperiodic growth. *Photosynth. Res.* 96, 15–26. doi: 10.1007/s11120-007-9274-x

Schulz, R., Steinmüller, K., Klaas, M., Forreiter, C., Rasmussen, S., Hiller, C., et al. (1989). Nucleotide sequence of a cDNA coding for the NADPH-protochlorophyllide oxidoreductase (PCR) of barley (*Hordeum vulgare* L.) and its expression in *Escherichia coli*. *MGG Mol. Gen. Genet.* 217, 355–361. doi: 10.1007/BF02464904

Scrutton, N. S., Louise Groot, M., and Heyes, D. J. (2012). Excited state dynamics and catalytic mechanism of the light-driven enzyme protochlorophyllide oxidoreductase. *Phys. Chem. Chem. Phys.* 14, 8818–8824. doi: 10.1039/c2cp23789j

Selstam, E. (1998). "Development of thylakoid membranes with respect to lipids," in *Lipids in Photosynthesis: Structure, Function and Genetics. Advances in Photosynthesis and Respiration*, eds S. Paul-André and M. Norio (Dordrecht: Springer), 209–224.

Selstam, E., and Sandelius, A. S. (1984). A comparison between prolamellar bodies and prothylakoid membranes of etioplasts of dark-grown wheat concerning lipid and polypeptide composition. *Plant Physiol.* 76, 1036–1040. doi: 10.1104/pp.76.4.1036

Selstam, E., and Widell-Wigge, A. (1989). Hydrophobicity of protochlorophyllide oxidoreductase, characterized by means of Triton X-114 partitioning of isolated etioplast membrane fractions. *Physiol. Plant.* 77, 401–406. doi: 10.1111/j.1399-3054.1989.tb05660.x

Seyedi, M., Timko, M. P., and Sundqvist, C. (2001). The distribution of protochlorophyllide and chlorophyll within seedlings of the lip1 mutant of Pea. *Plant Cell Physiol.* 42, 931–941. doi: 10.1093/pcp/pce118

Shibata, K. (1957). Spectroscopic studies on chlorophyll formation in intact leaves. *J. Biochem.* 44, 147–173. doi: 10.1093/oxfordjournals.jbchem.a126741

Shioi, Y., and Takamiya, K. (1992). Monovinyl and divinyl protochlorophyllide pools in etiolated tissues of higher plants. *Plant Physiol.* 100, 1291–1295. doi: 10.1104/pp.100.3.1291

Sineshchekov, V. A., and Belyaeva, O. B. (2019). Regulation of chlorophyll biogenesis by phytochrome A. *Biochemistry* 84, 491–508. doi: 10.1134/S0006297919050043

Sironval, C., and Brouers, M. (1970). The reduction of protochlorophyllide into chlorophyllide. II. The temperature dependence of the P657-647-P688-676 phototransformation. *Photosynthetica* 4, 38–47.

Smeller, L., Solymosi, K., Fidy, J., and Böddi, B. (2003). Activation parameters of the blue shift (Shibata shift) subsequent to protochlorophyllide phototransformation. *Biochim. Biophys. Acta Proteins Proteomics* 1651, 130–138. doi: 10.1016/S1570-9639(03)00261-9

Soll, J., Schultz, G., Rüdiger, W., and Benz, J. (1983). Hydrogenation of geranylgeraniol. Two pathways exist in spinach chloroplasts. *Plant Physiol.* 71, 849–854. doi: 10.1104/pp.71.4.849

Solymosi, K., and Aronsson, H. (2013). "Etioplasts and their significance in chloroplast biogenesis," in *Plastid Development in Leaves During Growth and Senescence: Advances in Photosynthesis and Respiration*, eds B. Biswal, K. Krupińska, and A. K. Biswal (Dordrecht: Springer), 39–71.

Solymosi, K., Bóka, K., and Böddi, B. (2006a). Transient etiolation: protochlorophyll(ide) and chlorophyll forms in differentiating plastids of closed and breaking leaf buds of horse chestnut (*Aesculus hippocastanum*). *Tree Physiol.* 26, 1087–1096. doi: 10.1093/treephys/26.8.1087

Solymosi, K., and Köfalvi, A. (2017). Cannabis: a treasure trove or Pandora's box? *Mini Rev. Med. Chem.* 17, 1223–1291. doi: 10.2174/1389557516666161004162133

Solymosi, K., Martinez, K., Kristóf, Z., Sundqvist, C., and Böddi, B. (2004). Plastid differentiation and chlorophyll biosynthesis in different leaf layers of white cabbage (*Brassica oleracea* cv. *capitata*). *Physiol. Plant.* 121, 520–529. doi: 10.1111/j.0031-9317.2004.00349.x

Solymosi, K., Morandi, D., Bóka, K., Böddi, B., and Schoefs, B. (2012). High biological variability of plastids, photosynthetic pigments and pigment forms of leaf primordia in buds. *Planta* 235, 1035–1049. doi: 10.1007/s00425-011-1559-9

Solymosi, K., Mysliwa-Kurdziel, B., Bóka, K., Strzałka, K., and Böddi, B. (2006b). Disintegration of the prolamellar body structure at high concentrations of Hg2+. *Plant Biol.* 8, 627–635. doi: 10.1055/s-2006-924110

Solymosi, K., and Schoefs, B. (2008). "Prolamellar body: a unique plastid compartment, which does not only occur in dark-grown leaves," in *Plant Cell Compartments - Selected Topics*, ed B. Schoefs (Trivandrum: Research Signpost), 151–202.

Solymosi, K., and Schoefs, B. (2010). Etioplast and etio-chloroplast formation under natural conditions: the dark side of chlorophyll biosynthesis in angiosperms. *Photosynth. Res.* 105, 143–166. doi: 10.1007/s11120-010-9568-2

Solymosi, K., Smeller, L., Böddi, B., and Fidy, J. (2002). Activation volumes of processes linked to the phototransformation of protochlorophyllide determined by fluorescence spectroscopy at high pressure. *Biochim. Biophys. Acta Bioenerg.* 1554, 1–4. doi: 10.1016/S0005-2728(02)00209-8

Solymosi, K., Smeller, L., Ryberg, M., Sundqvist, C., Fidy, J., and Böddi, B. (2007a). Molecular rearrangement in POR macrodomains as a reason for the blue shift of chlorophyllide fluorescence observed after phototransformation. *Biochim. Biophys. Acta Biomembr.* 1768, 1650–1658. doi: 10.1016/j.bbamem.2007.02.022

Solymosi, K., Tuba, Z., and Böddi, B. (2013). Desiccoplast-etioplast-chloroplast transformation under rehydration of desiccated poikilochlorophyllous Xerophyta humilis leaves in the dark and upon subsequent illumination. *J. Plant Physiol.* 170, 583–590. doi: 10.1016/j.jplph.2012.11.022

Solymosi, K., Vitányi, B., Hideg, É., and Böddi, B. (2007b). Etiolation symptoms in sunflower (Helianthus annuus) cotyledons partially covered by the pericarp of the achene. *Ann. Bot.* 99, 857–867. doi: 10.1093/aob/mcm034

Spano, A. J., He, Z., Michel, H., Hunt, D. F., and Timko, M. P. (1992). Molecular cloning, nuclear gene structure, and developmental expression of NADPH:protochlorophyllide oxidoreductase in pea (*Pisum sativum* L.). *Plant Mol. Biol.* 18, 967–972. doi: 10.1007/BF00019210

Sperling, U., van Cleve, B., Frick, G., Apel, K., and Armstrong, G. A. (1997). Overexpression of light-dependent PORA or PORB in plants depleted of endogenous POR by far-red light enhances seedling survival in white light and protects against photooxidative damage. *Plant J.* 12, 649–658. doi: 10.1046/j.1365-313X.1997.d01-11.x

Splinter, T., Helder, A., Lucas, C., and Feltkamp-Vroom, T. (1975). Spontaneous occurrence of TRS The available lymphoid cell lines were It is very remarkable that all 4 cell patients are negative and all 5 cell lines. *Br. J. Exp. Path.* 56, 124–132.

Stenbaek, A., and Jensen, P. E. (2010). Redox regulation of chlorophyll biosynthesis. *Phytochemistry* 71, 853–859. doi: 10.1016/j.phytochem.2010.03.022

Stpiczyńska, M., Milanesi, C., Faleri, C., and Cresti, M. (2005). Ultrastructure of the nectary spur of *Platanthera chlorantha* (Custer) Rchb. (Orchidaceae) during successive stages of nectar secretion. *Acta Biol. Cracoviensia Ser. Bot.* 47, 111–119.

Suzuki, J. Y., and Bauer, C. E. (1995). A prokaryotic origin for light-dependent chlorophyll biosynthesis of plants. *Proc. Natl. Acad. Sci. U.S.A.* 92, 3749–3753. doi: 10.1073/pnas.92.9.3749

Sytina, O. A., Novoderezhkin, V. I., Van Grondelle, R., and Groot, M. L. (2011a). Modeling of multi-exciton transient absorption spectra of protochlorophyllide aggregates in aqueous solution. *J. Phys. Chem. A* 115, 11944–11951. doi: 10.1021/jp204395z

Sytina, O. A., van Stokkum, I. H. M., Heyes, D. J., Hunter, C. N., van Grondelle, R., and Groot, M. L. (2010). Protochlorophyllide excited-state dynamics in organic solvents studied by time-resolved visible and mid-infrared spectroscopy. *J. Phys. Chem. B* 114, 4335–4344. doi: 10.1021/jp9089326

Sytina, O. A., Van Stokkum, I. H. M., Van Grondelle, R., and Groot, M. L. (2011b). Single and multi-exciton dynamics in aqueous protochlorophyllide aggregates. *J. Phys. Chem. A* 115, 3936–3946. doi: 10.1021/jp108317u

Tanaka, A., Ito, H., Tanaka, R., Tanaka, N. K., Yoshida, K., and Okada, K. (1998). Chlorophyll a oxygenase (CAO) is involved in chlorophyll b formation from chlorophyll a. *Proc. Natl. Acad. Sci. U.S.A.* 95, 12719–12723. doi: 10.1073/pnas.95.21.12719

Tanaka, A., and Tanaka, R. (2019). "Chapter Six - The biochemistry, physiology, and evolution of the chlorophyll cycle," in *Metabolism, Structure and Function of Plant Tetrapyrroles: Introduction, Microbial and Eukaryotic Chlorophyll Synthesis and Catabolism*, Vol. 90, ed B. Grimm (London: Academic Press), 183–212. doi: 10.1016/bs.abr.2019.03.005

Tanaka, R., Kobayashi, K., and Masuda, T. (2011). Tetrapyrrole metabolism in *Arabidopsis thaliana*. *Arab. B.* 9, e0145. doi: 10.1199/tab.0145

Tanaka, R., Koshino, Y., Sawa, S., Ishiguro, S., Okada, K., and Tanaka, A. (2001). Overexpression of chlorophyllide a oxygenase (CAO) enlarges the antenna size of photosystem II in *Arabidopsis thaliana*. *Plant J.* 26, 365–373. doi: 10.1046/j.1365-313X.2001.2641034.x

Tanaka, R., Rothbart, M., Oka, S., Takabayashi, A., Takahashi, K., Shibata, M., et al. (2010). LIL3, a light-harvesting-like protein, plays an essential role in chlorophyll and tocopherol biosynthesis. *Proc. Natl. Acad. Sci. U.S.A.* 107, 16721–16725. doi: 10.1073/pnas.1004699107

Tanaka, R., and Tanaka, A. (2007). Tetrapyrrole biosynthesis in higher plants. *Annu Rev Plant Biol.* 58, 321–346. doi: 10.1146/annurev.arplant.57.032905.105448

Tanaka, R., and Tanaka, A. (2011). Biochimica et biophysica acta chlorophyll cycle regulates the construction and destruction of the light-harvesting complexes. *Biochim. Biophys. Acta Bioenerg.* 1807, 968–976. doi: 10.1016/j.bbabio.2011.01.002

Tottey, S., Block, M. A., Allen, M., Westergren, T., Albrieux, C., Scheller, H. V., et al. (2003). Arabidopsis CHL27, located in both envelope and thylakoid membranes, is required for the synthesis of protochlorophyllide. *Proc. Natl. Acad. Sci. U.S.A.* 100, 16119–16124. doi: 10.1073/pnas.2136793100

Townley, H. E., Sessions, R. B., Clarke, A. R., Dafforn, T. R., and Trevor Griffiths, W. (2001). Protochlorophyllide oxidoreductase: a homology model examined by site-directed mutagenesis. *Proteins Struct. Funct. Genet.* 44, 329–335. doi: 10.1002/prot.1098

Tripathy, B., and Pattanayak, G. (2012). "Chlorophyll biosynthesis in higher plants," in *Photosynthesis: Plastid Biology, Energy Conversion and Carbon Assimilation, Advances in Photosynthesis and Respiration*, Vol. 34, eds J. J. Eaton-Rye, B. C. Tripathy, and T. D. Sharkey (Springer Science+Business Media B.V.), 63–94.

Tripathy, B. C., and Rebeiz, C. A. (1986). Chloroplast biogenesis. Demonstration of the monovinyl and divinyl monocarboxylic routes of chlorophyll biosynthesis in higher plants. *J. Biol. Chem.* 261, 13556–13564. doi: 10.1016/S0021-9258(18)67055-3

Tripathy, B. C., and Rebeiz, C. A. (1988). Chloroplast biogenesis 60. *Plant Physiol.* 87, 89–94. doi: 10.1104/pp.87.1.89

Turner, G. W., Davis, E. M., and Croteau, R. B. (2012). Immunocytochemical localization of short-chain family reductases involved in menthol biosynthesis in peppermint. *Planta* 235, 1186–1195. doi: 10.1007/s00425-011-1567-9

Turner, G. W., Gershenzon, J., and Croteau, R. B. (2000). Development of peltate glandular trichomes of peppermint. *Plant Physiol.* 124, 665–680. doi: 10.1104/pp.124.2.665

Vedalankar, P., and Tripathy, B. C. (2019). Evolution of light-independent protochlorophyllide oxidoreductase. *Protoplasma* 256, 293–312. doi: 10.1007/s00709-018-1317-y

Vermeer, J., and Peterson, R. L. (1979). Glandular trichomes on the inflorescence of *Chrysanthemum morifolium* cv dramatic (Compositae). 1. Development and morphology. *Can. J. Bot.* 57, 705–713. doi: 10.1139/b79-090

Vitányi, B., Kósa, A., Solymosi, K., and Böddi, B. (2013). Etioplasts with protochlorophyll and protochlorophyllide forms in the under-soil epicotyl segments of pea (*Pisum sativum*) seedlings grown under natural light conditions. *Physiol. Plant.* 148, 307–315. doi: 10.1111/j.1399-3054.2012.01714.x

Voitsekhovskaja, O. V., and Tyutereva, E. V. (2015). Chlorophyll b in angiosperms: functions in photosynthesis, signaling and ontogenetic regulation. *J. Plant Physiol.* 189, 51–64. doi: 10.1016/j.jplph.2015.09.013

von Zychlinski, A., Kleffmann, T., Krishnamurthy, N., Sjölander, K., Baginsky, S., and Gruissem, W. (2005). Proteome analysis of the rice etioplast: metabolic and regulatory networks and novel protein functions. *Mol. Cell. Proteomics* 4, 1072–1084. doi: 10.1074/mcp.M500018-MCP200

Vranová, E., Coman, D., and Gruissem, W. (2013). Network analysis of the MVA and MEP pathways for isoprenoid synthesis. *Annu. Rev. Plant Biol.* 64, 665–700. doi: 10.1146/annurev-arplant-050312-120116

Wang, G., and Dixon, R. A. (2009). Heterodimeric geranyl(geranyl)diphosphate synthase from hop (*Humulus lupulus*) and the evolution of monoterpene biosynthesis. *Proc. Natl. Acad. Sci. U.S.A.* 106, 9914–9919. doi: 10.1073/pnas.0904069106

Wang, J., Lin, H. X., Su, P., Chen, T., Guo, J., Gao, W., et al. (2019). Molecular cloning and functional characterization of multiple geranylgeranyl pyrophosphate synthases (ApGGPPS) from Andrographis paniculata. *Plant Cell Rep.* 38, 117–128. doi: 10.1007/s00299-018-2353-y

Wang, L., Leister, D., Guan, L., Zheng, Y., Schneider, K., Lehmann, M., et al. (2020). The Arabidopsis SAFEGUARD1 suppresses singlet oxygen-induced stress responses by protecting grana margins. *Proc. Natl. Acad. Sci. U.S.A.* 117, 6918–6927. doi: 10.1073/pnas.1918640117

Wang, P., Gao, J., Wan, C., Zhang, F., Xu, Z., Huang, X., et al. (2010). Divinyl chlorophyll(ide) a can be converted to monovinyl chlorophyll(ide) a by a divinyl reductase in rice. *Plant Physiol.* 153, 994–1003. doi: 10.1104/pp.110.158477

Wang, P., and Grimm, B. (2015). Organization of chlorophyll biosynthesis and insertion of chlorophyll into the chlorophyll-binding proteins in chloroplasts. *Photosynth. Res.* 126, 189–202. doi: 10.1007/s11120-015-0154-5

Wang, P., Wan, C., Xu, Z., Wang, P., Wang, W., Sun, C., et al. (2013). One divinyl reductase reduces the 8-vinyl groups in various intermediates of chlorophyll biosynthesis in a given higher plant species, but the isozyme differs between species. *Plant Physiol.* 161, 521–534. doi: 10.1104/pp.112.208421

Whyte, B. J., and Griffiths, W. T. (1993). 8-Vinyl reduction and chlorophyll a biosynthesis in higher plants. *Biochem. J.* 291, 939–944. doi: 10.1042/bj2910939

Wiktorsson, B., Engdahl, S., Zhong, L. B., Boddi, B., Ryberg, M., and Sundqvist, C. (1993). The effect of cross-linking of the subunits of nadph- protochlorophyllide oxidoreductase on the aggregational state of protochlorophyllide. *Photosynthetica* 29, 205–218.

Wilks, H. M., and Timko, M. P. (1995). A light-dependent complementation system for analysis of NADPH:protochlorophyllide oxidoreductase: identification and mutagenesis of two conserved residues that are essential for enzyme activity. *Proc. Natl. Acad. Sci. U.S.A.* 92, 724–728. doi: 10.1073/pnas.92.3.724

Willows, R. D. (2019). "The Mg branch of chlorophyll synthesis: biosynthesis of chlorophyll a from protoporphyrin IX," in *Advances in Botanical Research*, Vol. 90, ed B. Grimm (London: Academic Press Inc.), 141–182. doi: 10.1016/bs.abr.2019.03.003

Wong, Y.-S., and Castelfranco, P. A. (1984). Resolution and reconstitution of Mg-protoporphyrin IX monomethyl ester (oxidative) cyclase, the enzyme system responsible for the formation of the chlorophyll isocyclic ring. *Plant Physiol.* 75, 658–661. doi: 10.1104/pp.75.3.658

Wong, Y.-S., and Castelfranco, P. A. (1985). Properties of the Mg-protoporphyrin IX monomethyl ester (oxidative) cyclase system. *Plant Physiol.* 79, 730–733. doi: 10.1104/pp.79.3.730

Yadav, D., Zemach, H., Belausov, E., and Charuvi, D. (2019). Initial proplastid-to-chloroplast differentiation in the developing vegetative shoot apical meristem of Arabidopsis. *Biochem. Biophys. Res. Commun.* 519, 391–395. doi: 10.1016/j.bbrc.2019.09.019

Yamamoto, H., Kojima-Ando, H., Ohki, K., and Fujita, Y. (2020). Formation of prolamellar-body-like ultrastructures in etiolated cyanobacterial cells overexpressing light-dependent protochlorophyllide oxidoreductase in Leptolyngbya boryana. *J. Gen. Appl. Microbiol.* 66, 129–139. doi: 10.2323/jgam.2020.01.009

Yamazaki, S., Nomata, J., and Fujita, Y. (2006). Differential operation of dual protochlorophyllide reductases for chlorophyll biosynthesis in response to environmental oxygen levels in the cyanobacterium *Leptolyngbya boryana*. *Plant Physiol.* 142, 911–922. doi: 10.1104/pp.106.086090

Yang, J., and Cheng, Q. (2004). Origin and evolution of the light-dependent protochlorophyllide oxidoreductase (LPOR) genes. *Plant Biol.* 6, 537–544. doi: 10.1055/s-2004-821270

Yu, C.-W., Lin, Y.-T., and Li, H. (2020). Increased ratio of galactolipid MGDG: DGDG induces jasmonic acid overproduction and changes chloroplast shape. *New Phytol.* 228, 1327–1335. doi: 10.1111/nph.16766

Yuan, M., Zhao, Y. Q., Zhang, Z. W., Chen, Y. E., Ding, C. B., and Yuan, S. (2017). Light regulates transcription of chlorophyll biosynthetic genes during chloroplast biogenesis. *CRC. Crit. Rev. Plant Sci.* 36, 35–54. doi: 10.1080/07352689.2017.1327764

Zhang, M., Zhang, F., Fang, Y., Chen, X., Chen, Y., Zhang, W., et al. (2015). The non-canonical tetratricopeptide repeat (TPR) domain of fluorescent (FLU) mediates complex formation with glutamyl-tRNA reductase. *J. Biol. Chem.* 290, 17559–17565. doi: 10.1074/jbc.M115.662981

Zhang, S., Godwin, A. R. F., Taylor, A., Hardman, S. J. O., Jowitt, T. A., Johannissen, L. O., et al. (2021). Dual role of the active site 'lid' regions of protochlorophyllide oxidoreductase in photocatalysis and plant development. *FEBS J.* 288, 175–189. doi: 10.1111/febs.15542

Zhang, S., Heyes, D. J., Feng, L., Sun, W., Johannissen, L. O., Liu, H., et al. (2019). Structural basis for enzymatic photocatalysis in chlorophyll biosynthesis. *Nature* 574, 722–725. doi: 10.1038/s41586-019-1685-2

Zhang, Z. W., Yuan, S., Feng, H., Xu, F., Cheng, J., Shang, J., et al. (2011). Transient accumulation of Mg-protoporphyrin IX regulates expression of PhANGs - new evidence for the signaling role of tetrapyrroles in mature Arabidopsis plants. *J. Plant Physiol.* 168, 714–721. doi: 10.1016/j.jplph.2010.10.016

Zhao, G.-J., and Han, K.-L. (2008). Site-specific solvation of the photoexcited protochlorophyllide a in methanol: formation of the hydrogen-bonded intermediate state induced by hydrogen-bond strengthening. *Biophys. J.* 94, 38–46. doi: 10.1529/biophysj.107.113738

Zhong, L. B., Wiktorsson, B., Ryberg, M., and Sundqvist, C. (1996). The Shibata shift; effects of *in vitro* conditions on the spectral blue-shift of chlorophyllide in irradiated isolated prolamellar bodies. *J. Photochem. Photobiol. B Biol.* 36, 263–270. doi: 10.1016/S1011-1344(96)07394-0

Zhou, F., Wang, C. Y., Gutensohn, M., Jiang, L., Zhang, P., Zhang, D., et al. (2017). A recruiting protein of geranylgeranyl diphosphate synthase controls metabolic flux toward chlorophyll biosynthesis in rice. *Proc. Natl. Acad. Sci. U.S.A.* 114, 6866–6871. doi: 10.1073/pnas.1705689114

Conflict of Interest: The authors declare that the research was conducted in the absence of any commercial or financial relationships that could be construed as a potential conflict of interest.

Copyright © 2021 Solymosi and Mysliwa-Kurdziel. This is an open-access article distributed under the terms of the Creative Commons Attribution License (CC BY). The use, distribution or reproduction in other forums is permitted, provided the original author(s) and the copyright owner(s) are credited and that the original publication in this journal is cited, in accordance with accepted academic practice. No use, distribution or reproduction is permitted which does not comply with these terms.

Advantages of publishing in Frontiers

OPEN ACCESS
Articles are free to read for greatest visibility and readership

FAST PUBLICATION
Around 90 days from submission to decision

HIGH QUALITY PEER-REVIEW
Rigorous, collaborative, and constructive peer-review

TRANSPARENT PEER-REVIEW
Editors and reviewers acknowledged by name on published articles

Frontiers
Avenue du Tribunal-Fédéral 34
1005 Lausanne | Switzerland

Visit us: www.frontiersin.org
Contact us: frontiersin.org/about/contact

REPRODUCIBILITY OF RESEARCH
Support open data and methods to enhance research reproducibility

DIGITAL PUBLISHING
Articles designed for optimal readership across devices

FOLLOW US
@frontiersin

IMPACT METRICS
Advanced article metrics track visibility across digital media

EXTENSIVE PROMOTION
Marketing and promotion of impactful research

LOOP RESEARCH NETWORK
Our network increases your article's readership